THE UNIVERSITY OF QUEENSLAND

AUSTRALIA

Zinc oxide-centred deterioration of modern artists' oil paint and implications for the conservation of twentieth century paintings

Gillian Ilena Osmond

Bachelor of Applied Science (Conservation of Cultural Materials)

A thesis submitted for the degree of Doctor of Philosophy at

The University of Queensland in 2014

Australian Institute for Bioengineering and Nanotechnology

Abstract

Zinc oxide is a prevalent industrial age pigment which readily reacts with fatty acids in oil-based paints to form zinc carboxylates. It is present in many paintings from the late nineteenth century through until the present day. This thesis examines the reactivity of zinc oxide in the context of serious aesthetic and structural deterioration in paintings linked to formation and aggregation of zinc soaps of C_{16} and C_{18} straight chain saturated fatty acids. It extends current understanding of how zinc soaps form, why they aggregate and the conditions that promote deterioration. This knowledge is important for effective long term management of contemporary painting collections.

Historical aspects of zinc oxide pigment production and paint formulation are reviewed. Pigment particle properties, fatty acid profiles, paint additives and environmental conditions are all significant factors influencing the reactive tendencies of zinc oxide in oil-based paints.

Approaches to the characterisation of oil paint are reviewed. Techniques are emphasised which are appropriate for samples from unique paintings with implicit limitations on size and availability, particularly complementary techniques applicable to embedded paint cross-sections. Fourier transform infrared microspectroscopy (FTIR) is a highly sensitive technique for characterisation of metal carboxylates and a key tool in determining the progression of the formation of zinc soaps. Synthesis of zinc carboxylates of the common fatty acids found in mature paints is described and reference spectra are produced. The systematic application of FTIR and scanning electron microscopy (SEM) and elemental analysis (EDX) throughout this thesis identifies trends to assist interpretation of deterioration in historic paint samples. Correlation of backscatter electron (BSE) images, elemental analysis and synchrotron FTIR (SR-µFTIR) mapping of paint cross-sections suggests saponification of zinc oxide is distinguishable within paint cross sections at an early stage. Individual spectra extracted from SR-µFTIR maps allow discrimination between metal carboxylates present in a single sample based on high spatial and spectral resolution.

Naturally aged oil-based artists' commercial and custom control reference paints containing zinc oxide are investigated to consider links between compositional factors and zinc carboxylate formation. Paints are prepared with linseed, safflower and soybean oils and pigmented with zinc oxide alone or in combination with lead or titanium whites or within Naples yellow hue formulations. Results establish the significance of aluminium stearate as a component in paint formulations in combination with zinc oxide; its presence is more significant than oil or pigment composition in influencing zinc stearate formation and metal carboxylate distributions in paints of otherwise similar

composition and exposure history. Paints with zinc oxide as a secondary pigment are also susceptible to zinc stearate formation and segregation in the presence of a stearic acid source.

Interactions between zinc oxide and stearic acid are examined within a solvent model designed to reduce and control variables impacting the study of paint films. Rapid reactions in solvent models using nano-sized zinc oxide are comparable to those observed longer term in reference paints with larger artist grade pigment. The products of reactions are characterised. A suspension which forms in the toluene model comprises zinc oxide particles surrounded by zinc stearate in characteristic bilayer structures with comparable morphology to that observed in samples from paintings.

Paint cross-sections from zinc oxide-containing paintings by expatriate Australian artist E. Phillips Fox (1865-1915) and Vietnamese artist Nguyễn Trọng Kiệm (1933-1991) are examined in detail. Fox's paintings are typically painted on hygroscopic glue-based ground layers and/or have been subject to heat-based lining procedures or exposed to uncontrolled, sometimes extreme environments and are visibly affected by zinc carboxylate aggregation. The morphology and chemical signature of circular formations rich in zinc, carbon and oxygen common to the paintings are examined in detail using SEM-EDX and SR-µFTIR imaging. Crystallisation of basic zinc carbonate is observed within aggregates.

Kiệm's paintings have been exposed to hot, humid, polluted conditions and extensive hydrolysis of the oil medium is indicated. The presence of unusual zinc and sulphur containing lumps in one work has been investigated previously and the proposed mechanism of formation is reassessed. X-ray microdiffraction allows a tentative hypothesis of formation of multifunctional layered basic zinc salts. Preferential dissolution of zinc oxide over lead white, lithopone and a range of coloured pigments is observed in backscatter electron images, interpreted in conjunction with elemental and FTIR analysis. Structural consequences are indicated for affected paints. Zinc lactate is characterised in samples from paintings by both profiled artists; zinc lactate has been reported previously as a disfiguring surface accretion but these are the first known instances of zinc lactate identified within the paint.

Unique paintings are chemically complex and infinitely variable. This complexity coupled with interactions occurring over long timescales is challenging to replicate experimentally, and fundamental mechanisms are difficult to establish. This thesis combines results from simple models, reference paints and actual paintings and contributes important new detail to the continuing study of zinc soap formation in paintings.

Declaration by author

This thesis is composed of my original work, and contains no material previously published or written by another person except where due reference has been made in the text. I have clearly stated the contribution by others to jointly-authored works that I have included in my thesis.

I have clearly stated the contribution of others to my thesis as a whole, including statistical assistance, survey design, data analysis, significant technical procedures, professional editorial advice, and any other original research work used or reported in my thesis. The content of my thesis is the result of work I have carried out since the commencement of my research higher degree candidature and does not include a substantial part of work that has been submitted to qualify for the award of any other degree or diploma in any university or other tertiary institution. I have clearly stated which parts of my thesis, if any, have been submitted to qualify for another award.

I acknowledge that an electronic copy of my thesis must be lodged with the University Library and, subject to the General Award Rules of The University of Queensland, immediately made available for research and study in accordance with the *Copyright Act 1968*.

I acknowledge that copyright of all material contained in my thesis resides with the copyright holder(s) of that material. Where appropriate I have obtained copyright permission from the copyright holder to reproduce material in this thesis.

Publications during candidature

Peer reviewed papers

Osmond, G, 2011. Zinc white: a review of zinc oxide pigment properties and implications for stability in oil-based paintings, *AICCM Bulletin* vol 33 pp 20-29

Osmond, G, Boon, JJ, Puskar, L and Drennan, J, 2012. Metal stearate distributions in modern artists' oil paints: surface and cross-sectional investigation of reference paint films using conventional and synchrotron infrared microspectroscopy, *Applied Spectroscopy* 66(10) pp 1136-1144

Osmond, G, Ebert, B and Drennan, J, 2014. Zinc oxide-centred deterioration in 20th century Vietnamese paintings by Nguyen Trọng Kiệm *AICCM Bulletin* vol 34 pp 4-14

Osmond, G 2014. Zinc white and the influence of paint composition for stability in oil-based media In: van den Berg KJ, Burnstock A, Keijzer M, Kruger J, Learner T, de Tagle A, Heydenreich G (eds) *Issues in contemporary oil paint*. Springer International Publishing 2014: 263-281.

Conference Presentations (abstracts)

Osmond, G *Deterioration processes of modern oil-based paints and implications for the conservation of 20th century paintings: the significance of zinc*. The 20th Century in Paint: Production, Deterioration and Works of Art, Melbourne, 20 April 2010

Osmond, G, Monteiro, M and Drennan, J *The role of zinc oxide in deterioration of modern oil based paintings*. 21st Australian Conference on Microscopy and Microanalysis, Brisbane, 11-15 July 2010

Osmond, G *The role of zinc oxide in deterioration of modern oil based paintings.* 12th AICCM Paintings Group Symposium (Dialogues with artists), Adelaide, 21-22 October 2010

Osmond, G, Drennan, J, Jack, K, Monteiro, M and Kozak, D *Nanometre sized zinc oxide particles and the formation of 'zinc soaps' in paintings*. 1st International Conference on BioNano Innovation, Brisbane, 19-20 July 2012

Osmond, G, Ebert, B and Drennan, J, *Zinc oxide centred deterioration in 20th century Vietnamese paintings by Nguyen Trọng Kiệm*. The Meaning of Materials in Modern and Contemporary Art, Brisbane, 10-11 December 2012

Osmond, G, *Zinc white and the influence of paint composition for stability in oil based media*. Issues in Contemporary Oil Paint, Amersfoort, The Netherlands, 28-29 March 2013

Poster presentations

Glasson, M, Tse, N, Dredge, P, Osmond, G, Heasman, C, Sloggett, R, Chayabutra, S and Best, S *IR-Microspectroscopy and Conservation*. Australian Synchrotron Users Meeting, 23 November 2010

Osmond, G, Dredge, P, and Best, S *IR Microscopy of zinc carboxylate distributions in paintings*. Australian Synchrotron Users Meeting, 8-9 December 2011

Osmond, G, Ives, S, Dredge, P, Drennan, J and Puskar, L. *From porcelain to pimples: a study of synchrotron-sourced infrared spectroscopy for understanding the localised aggregation of zinc soaps in a painting by Sir Frederick Leighton*. 7th International Workshop on Infrared Microscopy and Spectroscopy with Accelerator Based Sources, Lorne, 10-14 November 2013

Osmond, G, Ives, S, Dredge, P, Drennan, J and Puskar, L. *From porcelain to pimples: a study of synchrotron-sourced infrared spectroscopy for understanding the localised aggregation of zinc soaps in a painting by Sir Frederick Leighton*. Australian Synchrotron Users Meeting, 21-22 November 2013

Press and Media

Masterpieces under the microscope. Research feature article, Australian Microscopy and Microanalysis Research Facility (AMMRF) News 19, September 2012

http://www.ammrf.org.au/featured/masterpieces-under-the-microscope/

Impact Art. Australian Microscopy & Microanalysis Research Facility, Profile 2012, p 23

http://www.ammrf.org.au/wp-content/uploads/2012/11/Profile2012_AMMRFweb.pdf

20th century paintings conservation - zinc oxide and aluminium stearate.

Australian Synchrotron Research Highlights 2010-12 pp 80-81

Publications included in this thesis

Osmond G, 2011. Zinc white: a review of zinc oxide pigment properties and implications for stability in oil-based paintings, *AICCM Bulletin* 33 pp 20-29 – incorporated as part of Chapter 1

Osmond G, Boon JJ, Puskar L and Drennan J, 2012. Metal stearate distributions in modern artists' oil paints: surface and cross-sectional investigation of reference paint films using conventional and synchrotron infrared microspectroscopy, *Applied Spectroscopy* 66(10) pp 1136-1144 – incorporated as part of Chapter 3

Contributor	Statement of contribution
Osmond (Candidate)	Designed experiments (100%) Analysed samples (95%), Interpreted data (90%) Wrote the paper (90%)
Boon	Interpreted data (10%) Wrote and edited paper (5%)
Puskar	Assisted with acquisition and reporting of synchrotron data: Analysed samples (5%) Wrote and edited paper (5%)
Drennan	Supervision and critical review of the text

Osmond G, Ebert B and Drennan J, 2014. Zinc oxide centred deterioration in 20th century Vietnamese paintings by Nguyen Trọng Kiệm *AICCM Bulletin* 34 pp 4-14 – incorporated as part of Chapter 5

Contributor	Statement of contribution
Osmond (Candidate)	Designed experiments (95%) Analysed samples (95%), Interpreted data (100%) Wrote the paper (95%)
Ebert	Provided painting samples and contextual

	information
	Wrote and edited paper (5%)
Drennan	Designed experiments (5%)
	Supervision and critical review of the text

Osmond, G 2014. Zinc white and the influence of paint composition for stability in oil based media. In: van den Berg KJ, Burnstock A, de Tagle M et al. (eds) *Issues in Contemporary Oil Paint*, Springer International Publishing, Chapter 18 pp 263-281 – incorporated as part of Chapter 3

Contributions by others to the thesis

No contributions by others.

Statement of parts of the thesis submitted to qualify for the award of another degree

None

Acknowledgements

Keywords

zinc oxide, zinc stearate, zinc carboxylate, zinc soap, metal soap, aluminium stearate, painting conservation, Fourier transform infrared spectroscopy, Nguyen Trọng Kiệm, E Phillips Fox

Australian and New Zealand Standard Research Classifications (ANZSRC)

ANZSRC code: 210203 Materials Conservation	50%
ANZSRC code: 030301 Chemical Characterisation of Materials	40%
ANZSRC code: 030606 Structural Chemistry and Spectroscopy	10%

Fields of Research (FoR) Classification

FoR code: 2102 Curatorial and Related Studies	50%
FoR code: 0303 Macromolecular and Materials Chemistry	40%
FoR code: 0306 Physical Chemistry (incl. Structural)	10%

Contents

List of tables

List of figures

Abbreviations

AIBN	Australian Institute for Bioengineering and Nanotechnology
AIC	American Institute for Conservation of Historic and Artistic Works
AICCM	Australian Institute for the Conservation of Cultural Materials
APTCCARN	Asia Pacific Twentieth Century Conservation Art Research Network
ARC	Australian Research Council
ATR	attenuated total reflection
BET	Brunauer-Emmett-Teller
BSE	backscatter electron
CCD	charge-couple device
CCMC	Centre for Cultural Materials Conservation
CSIRO	Commonwealth Scientific and Industrial Research Organisation
DDSA	dodecenylsuccinic anhydride
DMP	2,4,6-Tris(dimethylaminomethyl)phenol
EBAI	L'Ecole des Beaux-Artes de l'Indochine
FA	fatty acid
FTIR	Fourier transform infrared spectroscopy
GADDS	general area diffraction detector system
GCMS	gas chromatography – mass spectrometry
HCO	hydrogenated castor oil
HRTEM	high resolution transmission electron microscopy
HSt	stearic acid
ICDD	International Centre for Diffraction Data

ICOM-CC	International Council of Museums - Committee for Conservation
ICOP	Issues in Contemporary Oil Paint
IFT	interfacial tension
IIC	International Institute for Conservation of Historic and Artistic Works
IR	infrared
IRUG	Infrared and Raman Users Group
LALLS	low angle laser light scattering
MCT	mercury cadmium telluride
MOLART	Molecular aspects on ageing in painted works of art (NWO Prioriteit project)
NMA	nadic methyl anhydride
NMR	nuclear magnetic resonance spectroscopy
NWO	Netherlands Organisation for Scientific Research
OCA	optical contact angle
PET	polyethylene terephthalate
PTFE	polytetrafluoroethylene
QAGOMA	Queensland Art Gallery | Gallery of Modern Art
SAED	selected area electron diffraction
SAXS	small angle X-ray scattering
SEM	scanning electron microscopy
SEM-EDX	scanning electron microscopy with energy dispersive X-ray analysis
SIMS	secondary ion mass spectrometry
SMCI	Smithsonian Museum Conservation Institute
SR-µFTIR	synchrotron Fourier transform infrared microspectroscopy
TEM	transmission electron microscopy

UV   ultraviolet

UVF   ultraviolet fluorescence

μXRD   X-ray microdiffraction

W&N   Winsor and Newton

XRD   X-ray diffraction

XPS   X-ray photoelectron spectroscopy

XRF   X-ray fluorescence

1 Introduction

1.1 Research aims

This research aims to investigate zinc oxide-centred deterioration of oil-based paintings with particular focus on zinc carboxylate formation and segregation. A fundamental goal is to determine compositional and environmental factors contributing to the incidence of zinc carboxylate formation and migration. Outcomes will be an improved understanding of the vulnerabilities of paintings known to contain, or with potential to develop, zinc carboxylate aggregates, enabling design of appropriate conservation strategies for storage or treatment. There are significant implications for painting collections nationally and internationally where this condition is of increasing prevalence and concern.

A significant body of work in this chapter has been published and is included as section 1. 3:

Osmond G. 2012. Zinc white: a review of zinc oxide pigment properties and implications for stability in oil-based paintings. *AICCM Bulletin*, 33: 20-29

1.2 Background

Recognition of the incidence of metal soap aggregation as a cause of paint defects in oil-based paintings has been evolving over the past fifteen years. Initial research stemmed from a need to explain disfiguring protrusions observed in seventeenth century Dutch paintings, notably Rembrandt's *The anatomy lesson of Dr Nicolaes Tulp* (Noble et al. 2000; Noble et al. 2002). Although similar protrusions have been observed in paintings over centuries, it was really only with the advent of concerted research supported over a decade by the Netherlands Organisation for Scientific Research under the MOLART and de Mayerne programs that our understanding of the causes has developed. Launched in 1995, the objective of MOLART was the development of a scientific framework for the conservation of painted art on the molecular level, focused on determination of the present chemical and physical condition of works of art produced since the 15th century (Clarke and Boon 2003). The de Mayerne program provided funding for a second 5 year period to build on knowledge gained through MOLART and collectively have produced many theses and publications relating to the phenomenon of metal soap aggregation, for example (Boon et al. 2002b; Noble et al. 2002; van der Weerd et al. 2002a; van der Weerd et al. 2003; Keune 2005; Boon and Ferreira 2006; Keune and Boon 2007; Shimadzu et al. 2008). Related investigations and collaborations have also been undertaken in France (Cotte et al. 2006; Cotte et al. 2007), Canada (Corbeil and Robinet 2002;

Robinet and Corbeil 2003; Corbeil et al. 2011), the UK (Higgitt et al. 2003; Plater et al. 2003) and Australia (Osmond et al. 2005). A survey questionnaire distributed following the International Council of Museums Committee for Conservation (ICOM-CC) 2002 Triennial Meeting and reported at the following meeting served to highlight the incidence of the phenomenon (Noble et al. 2005). A half-day program of presentations on Metal Soaps in Paint Layers was held in Amsterdam in 2005 in conjunction with the Users' Group for Mass Spectrometry and Chromatography meeting, and the annual meeting of the American Institute for Conservation in 2006 devoted a large part of its Paintings Specialty Group program to the topic, with papers summarising understanding to date of the chemical processes (Boon et al. 2007), physical/aesthetic implications for paintings (Noble and Boon 2007) and case studies of lead soap formation and paint film defects in specific schools of painting (nineteenth century American works from the Hudson River school (Zucker and Boon 2007), and 16th -17th century British (Townsend et al. 2007)). More recently the Dutch have resumed their focus in this field through the establishment of a 'Paint alterations in time' research team (PAinT) at the University of Amsterdam, with a mission to investigate ageing, deterioration and migration processes in oil paints related to pigment-binding medium interactions (Iedema et al. 2014).

A related phenomenon of 'efflorescence' or appearance of crystalline surface deposits has also been of interest and concern to conservators over a number of decades with sporadic research to characterise and attempt identification of the cause and implications of this disfiguring condition (Williams 1988; Koller and Burmester 1990; Singer et al. 1995; Ordonez and Twilley 1997; Rimer et al. 1999; Schilling et al. 1999; Lau et al. 2007; van Loon 2008).

1.2.1 Oil-based paint formation and degradation

Common to the degradation phenomena of interest are mobile fractions within paint films which have long been considered cured or dry. The 'drying' of oil-based paints is a complex process which continues over many years, indeed the life of the painting, and which has been extensively researched. A comprehensive review of the processes can be found in a 2002 PhD thesis prepared early in the MOLART program (van den Berg 2002). Competing bond forming and degradation reactions are involved, influenced by the components of the paint and the exposure environment. Central to the defects under consideration in this study is the presence of free fatty acids which are capable of migrating within the paint matrix (Boon et al. 1997; Schilling et al. 1999; Boon et al. 2007). Typical drying oils comprise mixtures of saturated and unsaturated fatty acids in varying proportions dependent on source and predominantly bound in triglyceride structures. Straight chain acids with eighteen carbon atoms predominate. An indicative triglyceride is represented in Figure 1.1.
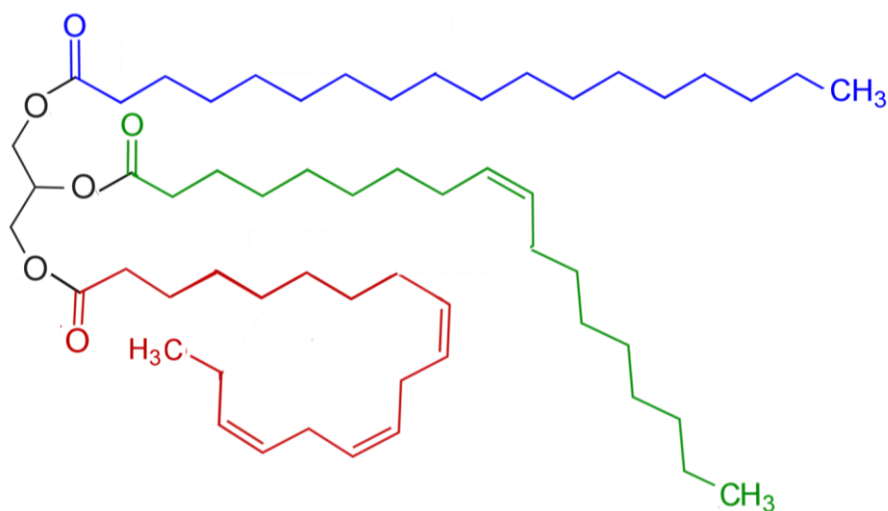
Figure 1.1 A triglyceride incorporating C$_{18:0}$ (stearic), C$_{18:1}$ (oleic) and C$_{18:3}$ (linolenic) fatty acid moieties

Representative fatty acids tend to be randomly distributed over many triglycerides, meaning the triglyceride structures are complex and varied, even though the range of constituent fatty acids in typical oils is relatively small (Mills and White 1987). Typical fatty acid compositions of common modern oil media are shown in Table 1.1.

Table 1.1 Typical fatty acid compositions of common twentieth century oil media (adapted from (Mills and White 1987; Schilling et al. 2007)

OIL	FATTY ACID WEIGHT PERCENTAGES						
	Palmitic C16:0	Stearic C18:0	Oleic C18:1	Linoleic C18:2	Linolenic C18:3	Other	
Castor	1	1	7	3		Ricinoleic	87
Coconut	48	15	29	9			
Cotton	23	3	25	45	1		
Linseed	6	4	19	24	47		
Oiticica	6	10	14	21		Licanic	48
Poppy	10	2	11	72	5		
Rapeseed	1	1	15	15	8	Erucic	60
Safflower	7	3	18	69	4		
Soybean	11	4	23	54	8		
Sunflower	7	5	23	65			
Tall oil			46	41	3	Rosin	8
Tung	2	2	5	3		Eleostearic	87

Polyunsaturated fatty acids in the oil undergo autocatalytic oxidative polymerisation to form a three-dimensional network and ultimately a solid film. Various comprehensive studies exist, including a series of articles reviewing various mechanisms and influences by which formation and decomposition of hydroperoxides occur in unpigmented films (Mallégol et al. 1999, 2000b, a; Mallégol et al. 2000c; Mallégol et al. 2001). The catalysing role of various driers in hydroperoxide formation, leading to formation of peroxy and alkoxy radicals and their recombination to form cross linked dimers prone to radical addition reactions is reviewed in relation to oils in alkyd paint binders (van Gorkum and Bouwman 2005). Metal ions from pigments and other additives also strongly influence the curing process, as does the prevailing exposure environment. Van den Berg considers a range of possible reaction pathways to take into account the catalysing role of transition metal ions (van den Berg 2002). These studies show that β-scission degradation reactions simultaneously occur, and that hydrolysis and oxidative cleavage of glycerol ester bonds produce low molecular weight products within the cross linked structure. Release of free glycerol requires hydrolysis of all three glyceride bonds and as such is unlikely to be substantial other than in extreme cases (Erhardt et al. 2005).

Relative humidity levels above 50% have been associated with increased susceptibility to photolytically induced cleavage of fatty acid side chains (Saunders and Kirby 2004). Higher saturated fatty acid yields can also be expected at elevated temperatures (Schilling et al. 1999); (Rimer et al. 1999), although extreme or prolonged exposure will reduce detectable levels via evaporation, most pronounced for palmitic acid (Schilling and Khanjian 1996; Schilling et al. 1999; Keune et al. 2008). Palmitic and stearic acids are preferentially located in triglyceride positions 1 and 3 which are more readily hydrolysed than second-position acids (Erhardt et al. 2005).

The MOLART working model on ageing oil paint proposes a transition from a cross-linked oil to a metal-coordinated paint system as a way of explaining why extensive hydrolysis now known to occur in oil paint films over time does not lead to complete loss of paintings (Boon et al. 2007); metal ions react rapidly with acid groups formed by 'degrouping' of cross linked oil components and, in the case of diacids (most commonly azelaic acid formed by oxidation of unsaturated fatty acid ester groups at the C9 double bond position (Plater et al. 2003; Tumosa et al. 2005)), enable links between the metal soap and to the network via original ester bonds (Boon et al. 2007). In mono and divalent salts of another ionomeric structure, methacrylic acid, redistribution of metal ions under heat and shear suggest that there is no permanent association of those ions with any particular carboxyl group (Bonotto and Bonner 1968). The idea of competition between cations in the formation of carboxylate complexes has also been postulated as the mechanism by which secondary calcium or zirconium-

based paint driers increase the effectiveness of primary cobalt based driers (Mallégol et al. 2000c). Monocarboxylic acids can only act as chain-terminating units and are therefore more vulnerable to separation from the network by competing anions, enabling migration to the surface where they precipitate as crystalline efflorescence, or reformation and aggregation with other mobile apolar soaps (Boon et al. 2007).

1.2.2 Modern oil-based paints

In addition to traditional artists' oil paints based on linseed, walnut and poppy oils, and safflower oil more recently, twentieth century oil-based paints and paintings may derive from a much wider range of oils or combinations of oils, include many more additives to modify working/handling properties and storage/shelf life of mixed paints, and also include oil-modified paints such as those in the alkyd class (Schilling et al. 2007). Even for paints still based on traditional oils, large scale production led to changes in processing with attendant impact on properties (van den Berg 2002; Burnstock et al. 2007). Economising on oil content in paint formulations during World War II was also required due to rationing and shortages or requestioning of materials for the war effort, requiring substitutions to be found (Faucett 1943; Standeven 2003). Additionally, fatty acids and their metal soaps are themselves frequently used in modern paints formulations, for example, to regulate acidity, to improve mixing, gloss and levelling properties, or to reduce the volume of oil required or enable substitution of cheaper oils (Barnett 1949; Wendt and Wagner 1954; Rinse 1967; Tumosa 2001). At times pigments have been precoated with metal soaps to facilitate dispersion and overcome settling problems associated with use of modern organic pigments with poor wetting ability or formulations using alkali refined linseed oil which have reduced capacity for independent soap formation (Ordonez and Twilley 1997; Tumosa 2001).

Twentieth century artists also commonly chose to work with paints not specifically produced for the artist market (Crook and Learner 2000; Standeven 2003; Dredge 2012), meaning an even wider range of oil-based paints is possible in paintings originating since the advent of premixed industrial paints.

1.3 Zinc white: a review of zinc oxide pigment properties and implications for stability in oil-based paintings

Zinc white: a review of zinc oxide pigment properties and implications for stability in oil-based paintings

Gillian Osmond
Contact: gillian.osmond@qagoma.qld.gov.au

Abstract
Zinc oxide became a frequent component of 20th century paints following its first commercial availability the previous century. Aspects of zinc oxide pigment production and paint formulation which influence the reactive tendencies of zinc oxide in oil based paints are reviewed. Particular attention is given to the formation and aggregation of zinc soaps which have been linked to deterioration in paintings. Pigment particle properties, fatty acid profiles, paint additives and environmental conditions are all significant factors.

Keywords
Zinc oxide, zinc white, oil paint, paintings conservation, zinc soap, zinc stearate

Introduction

The advent of zinc oxide as a white pigment for oil painting introduced an alternative to the traditional toxic lead white in both the artist and industrial paint markets. From its commercial origins in the 19th century and for much of the 20th century the beneficial properties of zinc oxide led to its frequent incorporation in both white and coloured paints. However, the reactivity of zinc oxide in oil based media posed industrial challenges for managing shelf life and durability of house paints. Zinc soaps readily form in oil based paints in the presence of zinc oxide. Zinc soaps have also recently been associated with deterioration of various paintings from the 19th and 20th centuries. The prevalence of zinc oxide in paintings from throughout this period creates a clear imperative to improve understanding of the degradation phenomena. This paper reviews aspects of zinc oxide production and paint formulation with significance for stability in oil based paintings.

Industry development

Pigment production
The early history of zinc oxide pigment development is well covered in the literature and is not repeated in detail here (e.g. Gardner 1917; Brown 1957; Kühn 1986; Carlyle 2001). Although known since ancient times, its popularity as a white pigment was not possible until commencement of industrial scale zinc oxide production during the 19th century.

The majority of zinc oxide pigment is produced via one of two pyrolytic processes: the Direct (American) Process which involves smelting ore in a furnace, and the Indirect (French) Process which produces the oxide via burning zinc metal in air. In France there was early concern surrounding the toxicity of lead based pigments, so attempts to introduce zinc white as a pigment for paint there date from 1780 (Kühn 1986). Development of the metallurgical Indirect Process and commercialisation of production in the 1840s then facilitated a rapid and wider adoption of zinc

oxide to protect the health of French pigment manufacturers and painters (Heckel 1934; Bomford et al. 1990).

Direct Process zinc oxide was developed in 1852 to take advantage of large Franklinite (lead-free ore) deposits in the U.S.A. and as a more economical form of production than Indirect Process (Gardner 1917; Brown 1957). Abundant sources of ore ensured that Direct Process pigment dominated American industrial paint production consistently from the late 19th century until the second half of the 20th century (Jolly 1993). Direct Process pigment, however, was of inferior purity and contained heavy metal contaminants deriving from the ores, especially those predating development of flotation methods of separation (Cocks and Walters 1968). Zinc oxide containing from between 5 and 35% basic lead sulphate (up to 50% prior to 1910), obtained from mixed lead and zinc ores and known as 'leaded zinc' was also intentionally produced for the housepaint market (Gardner 1917; Heckel 1934).

In Australia large ore deposits at Broken Hill ensured an active local zinc oxide industry from the first decades of the 20th century which, in addition to domestic production, supplied zinc concentrates for European markets (Cocks and Walters 1968). Mascot Smelting Company, Botany began producing Direct Process zinc oxide in 1917, rapidly increasing domestic consumption (*The decorator and painter for Australia and New Zealand* 1925). The Australian product claimed to be heavier and denser, with superior covering power to any imported zinc oxide due to an innovative 'concentrating plant' (*The decorator and painter for Australia and New Zealand* 1925), and contemporary sources state that 'practically all the zinc oxide used in the Australian paint industry is prepared in Australia' (Farquharson Boan 1924, p. 96). Production of French Process zinc oxide commenced in Sydney in 1947 following Durham Chemicals acquisition of Mascot Smelting (*The Argus* Melbourne, 23 July 1947, 'Durham Chemicals for Australia'), introducing technology from the English parent company.

Uptake by the paint industry
There is reference to 'extensive' use of zinc oxide in artists' paints in France as early as 1784 (Gardner 1917). In Britain, zinc white watercolour paints appeared in 1834 following an improvement in pigment density by Winsor and Newton via mechanical compression while 'red hot' (Carlyle 2001). The first appearance of zinc white in oil tubes was significantly later, listed in a British catalogue (Reeves) in 1860, although mixtures containing zinc oxide with lead white or barium sulfate appear to have been available a decade or so earlier (Carlyle 2001). There is documentary evidence that zinc oxide was progressively being incorporated in prepared paints and pigment supplies, often not declared but in addition to or substituted for more traditional materials (Townsend et al. 1995; Carlyle 2001). An 1899 German text mentions use of zinc oxide for brightening lake pigments in preference to barium sulfate (Josef Bersch, *Lexikon der Farben-Technik* 1899, cited in Pilz 2005), and investigations of paintings suggest its presence as a component in coloured paints possibly more than in whites (Kühn 1986).

In the house paint industry zinc oxide is said to have transformed the early production of ready mixed paints due to its good suspension properties in oil based media (Brown 1957). It was a component in the first patented 'prepared' paint in America in 1867 (Heckel 1934). By the early 20th century Gardner (1917, pp 27-28) states that 'the use of zinc oxide is universal with the paint

manufacturers of the United States and it is rapidly becoming standard practice with the painting craft to use zinc oxide in nearly all interior and exterior paints'. Australia's 1925 range of *Mascot Zinc in Oil* and *Ready Mixed Zinc Paints* included 30 different tints and shades and 3 different whites (*The decorator and painter for Australia and New Zealand* 1925). Generally used in combination with lead based pigment and later titanium dioxide, zinc oxide improved strength and mould resistance of exterior house paints (Nicholson and Mastin 1942; Salvin 1944). It afforded paints protection from ultraviolet radiation, found to be optimal at 30% pigment concentration in mixtures of basic lead carbonate or rutile titanium dioxide (Elm 1957), at which percentage it was routinely used in exterior paints for much of the early-mid 20th century (Brown 1957). For interior applications, zinc oxide was valued for minimising yellowing of paints (Elm 1957; Kühn 1986).

Zinc oxide remained popular until the mid 20th century by which time titanium white had come to dominate. However, titanium based paints often incorporated zinc oxide to improve film strength (Kühn 1986). Today, zinc oxide is no longer routinely used in general purpose alkyd paints because of its reactivity (Dixon 2009). Zinc oxide does, however, remain a common component in artists' paints (Mecklenburg et al. 2005; O'Hanlon 2007) and special purpose industrial paint formulations (Dixon 2009).

Artist uptake

Although typically of inferior hiding and drying power and substantially higher cost than lead white, zinc white paints had little tendency to yellow and did not blacken in the polluted sulfurous air common to many 19th century cities (Harley 1970; Kühn 1986; Bomford et al. 1990). Before widespread incorporation in artists' paint formulations, zinc white was consciously sought and used by some artists including Camille Pissaro (Bomford et al. 1990) and some of the Pre-Raphaelites working in mid 19th century Britain who included zinc white in special primings or in localised ground applications as a reflective base for the bright transparent palette they favoured (Hackney et al. 2002; 2004). An 1870 painting by American Thomas Eakins shows alternating layers of lead and zinc based paint (Currie and Smith 1994), and Australian artist J.P. Russell, based in France, is known to have replaced lead white with zinc oxide for uppermost paint layers in at least one painting, with a likely aim to avoid future deleterious darkening (Dredge 1996). Paintings by other artists working in France including van Gogh (Kühn 1986; Roy 1987) and Australian E. Phillips Fox are also found to commonly include zinc white (Osmond 2010). Joan Miró writes of his preference for incorporating zinc oxide into plaster grounds to attenuate its absorbency, a technique reportedly based on the practice of Henri Matisse (O'Donoghue et al. 2006).

Paintings by artists who were early adopters of house paints are also likely to contain significant amounts of zinc oxide. Pre- and post-WWII Ripolin® paints much favoured by artists including Picasso and Sidney Nolan have been found to widely include zinc oxide (Gautier et al. 2009; Dredge et al. 2012).

Pigment properties

Pure zinc oxide crystals have complex surface chemistry. This is in part due to electrostatic instability arising from the two opposing polar surfaces Zn-ZnO and O-ZnO. Recent experimental and theoretical research on the topic has been comprehensively reviewed (Wöll 2007). The

properties of zinc oxide and its behaviour in oil based paints will vary according to the individual properties of the pigment particle.

Particle size

Direct Process zinc oxide particles typically have larger particle size and are more acicular (needle-shaped) than the finer, nodular Indirect pigment (Oil and Colour Chemists' Association 1966). Acicular boule-shaped crystals can be formed with slow burning of zinc vapour (Kühn 1986), while increased airflow accelerates oxidation and cooling and favours fine particle formation (Oil and Colour Chemists' Association 1966). Reheating crystals enables particle size to be increased (Brown 1957). Larger particle size typically reduces surface area for a given measure of pigment and is associated with reduced oil absorption (Kühn 1986). Studies on particle size effects, however, describe zinc oxide pigment as forming stable aggregates in the dry state. These aggregates essentially function as a kinetic unit, translating primary particle sizes of 0.25-1um to effective particle sizes of 1-5um, and typically of more spherical shape (Princen and Devena-Peplinski 1964). The presence of coarse aggregates in a pigment mix is given as possible explanation for a lack of correlation between paint properties and notional particle size in some studies (Barnett 1949).

Crystal structure

Zinc oxide belongs to the hexagonal crystal system. Zinc and oxygen centred tetrahedra join at a common zinc atom forming a nucleus for additional tetrahedra, developing crystal lattice of the wurtzite type (Brown 1957) (Figure 1). Alternate layers of zinc and oxygen atoms in the 'c' (longitudinal) axis of the crystal promote the formation of needle shaped crystals. Zn-O distance along the 'c' axis is shorter than the other 2 axes; this departure from tetrahedral symmetry is considered to be due to a covalent bond along the 'c' axis (Brown 1957).
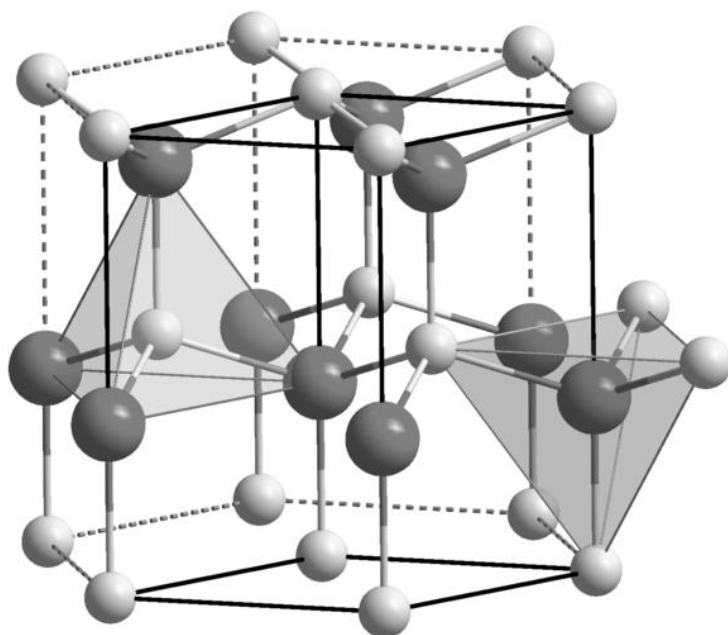
Figure 1 Crystal structure of zinc oxide (wurtzite) with coordination tetrahedral. Zinc atoms are represented by the smaller white balls and oxygen by grey. Image: Wikimedia Commons, http://en.wikipedia.org/wiki/File:Wurtzite _polyhedra.png, accessed 11 August 2011

Many metal atoms can enter a zinc oxide crystal at elevated temperatures (such as in the course of production) and introduce marked change in properties (Brown 1957). Direct Process pigment is associated with stoichiometric proportions of zinc and oxygen. French Process pigment is more likely to contain interstitial zinc (Morley-Smith 1958). One consequence is the effect on ultraviolet (UV) fluorescence properties. Stoichiometric zinc oxide is associated with bright green fluorescence in contrast to lower purple-blue fluorescence associated with interstitial zinc (Morley-Smith 1958).

Photostability
Zinc oxide absorbs UV radiation. In paints this may help the pigment protect an organic binder from destructive radiation, but may also 'be the source of troublesome photochemical reactions' (Barnett 1949). Zinc oxide with interstitial zinc or other lattice irregularities is considered more likely to dissipate energy capable of initiating photochemical reactions in adjacent materials (Winter and Whittem 1950; Morley-Smith 1958). Degradation of binding media and fading of organic pigments (Kühn 1986), and weakening of supports including paper (Kemp et al. 2004) and textiles (Kühn 1986) have been associated with zinc oxide.

Consistent with typical stoichiometry, paint films containing Direct Process pigment were found to be more resistant to surface degradation than French Process (Hoffmann and Saracz 1969). Stability issues also arose in Australia following introduction of French Process pigment into local house paint formulations (Morley-Smith 1950). Zinc oxide paints previously produced with Direct Process pigment had claimed superior durability to lead based paints even in Queensland, 'where the semi-tropical environment is severe upon light painted surfaces' (*The decorator and painter for Australia and New Zealand* 1925). Conditions in Australia evidently initiated degradation in paints formulated with the French Process oxide which had not been significant in milder British and European climates. Research led to pigment modifications, effectively increasing particle size, which improved the performance of paints (Morley-Smith 1950). However, it appears Direct Process zinc oxide was quickly resumed for use in exterior paint applications (Morley-Smith 1958).

Subsequent studies of zinc oxide in a variety of synthetic resin binders found that radiation in the range 385-415nm was the most significant in film decomposition, compared to shorter wavelengths for titanium dioxide pigmented films (Hoffmann and Saracz 1971). Decomposition was also accelerated by increasing relative humidity (RH), without affecting wavelength sensitivity, however the weathering of Direct Process pigmented films was more dependent on RH, and lead content in the Direct grade was considered a possible factor in addition to particle size (Hoffmann and Saracz 1969).

Today, high purity French Process zinc oxide dominates international production (Shelton 2010), however Direct Process pigment still has a market in the paint industry where its lower reactivity is advantageous (International Zinc Association 2009). Features distinguishing Direct and Indirect grades are likely to be less certain in modern zinc oxide samples given the greater production control now possible over crystal and particle properties.

Reactivity of zinc oxide in oil

The prevalence of zinc oxide in paintings becomes significant when its reactivity in oil based media is considered. Zinc oxide is amphoteric and is capable of neutralising both acids and alkalis (Oil and Colour Chemists' Association 1966). In oil based paints this manifests in reaction with fatty acid components of the paint medium to form zinc soaps. Zinc carboxylate based lumps may form in paint either during storage or in the film (Bell 1970). The house paint industry directed considerable research over many decades towards managing the interaction in order to retain the beneficial properties of the pigment. In addition to generic stability issues associated with pigment grade, the fatty acid composition of paint and environmental conditions are significant for reactivity in oil.

Temperature
Temperature influences the solubility of zinc soaps in the oil medium in accordance with concentration, with separation occurring when the temperature drops below that corresponding to the solubility limit at the prevailing concentration (Hansen and Klauss 1971). Elm (1957) found that during paint production, crystalline 'seeds' of zinc stearate and palmitate may form on cooling following paint grinding, with rapid cooling producing small soap crystals and slower cooling favouring larger soap crystals more likely to affect texture. Aggregation of soaps has been shown to occur under extreme fluctuations, especially in warmer climates based on cycling tests to 60° C which yielded seeded paints at approximately half the time of those cycled to 47° C (Hansen and Klauss 1971). This tendency led to the concept of temperature cycling to determine seeding propensity of different paint formulations (55-60° C for 48 hours, cooled over 48 hours, repeated (Elm 1957); 60° C for 5 days, followed by slow cooling and standing at room temperature for 2 days (Hansen and Klauss 1971)). Variations are still used by paint manufacturers today with one local producer reporting that paints are expected to remain stable in the wet state during a month of daily temperature cycling between 20 and 50° C (Dixon 2009).

Fatty acid composition and formulation
Control of acid level is important for minimising zinc oxide reactivity (Elm 1957; Bell 1970). Different oils comprise triglyceride structures based on different types and relative proportions of saturated and unsaturated fatty acids. Oil processing methods also influence triglyceride composition and inherent reactivity (van den Berg et al. 2004). Experiments have shown that all straight chain saturated fatty acids yield zinc salts capable of forming seeds (Elm 1957). Zinc soaps produced from a standard grade of zinc oxide pigment in combination with different fatty acids showed that as chain length increased, rates of reaction decreased (Morley-Smith 1958). A rapid increase in soap formation was observed with zinc oxide in linseed oil of acid no. 12 in comparison with linseed oil of lower acid group concentration (acid no. 4) (Jacobsen and Gardner 1941); acid number indicates the milligrams of potassium hydroxide required to neutralise the free fatty acids in one gram of oil. Alkyds containing oils with high proportions of saturated or mono-unsaturated fatty acids such as soya or tall oils have been found to be more prone to film disruption caused by zinc soap protruberances, however distillation or segregation of the oil to reduce the proportion of saturated fatty acids was found to reduce susceptibility (Elm 1957; Bell 1970).

Fatty acids may also derive from other sources in the paint. Aluminium stearate is one common additive likely to be a potential source of stearic acid (Elm 1957; Ordonez and Twilley 1997;

Tumosa 2001; Burnstock et al. 2007; Hoogland et al. 2007). Propionic acid has been used to form zinc propionate at the surface of zinc oxide pigment to modify oil-pigment interaction and properties in the wet state (Barnett 1949). Metal salts of organic acids are the form of many driers developed for the paint industry, including those prompted by the poor drying properties of zinc oxide in oil (Kastens and Hansen 1949; Taylor and Marks 1969). Additives such as calcium napthenate and cobalt driers, as well as resin acids from another early additive, rosin, were found to increase the solubility, dispersion and concentration of zinc soaps in oil, so paint in the tin would become progressively thicker but without skinning or separation (Ware and Christman 1916; Finnie et al. 1936; Hansen and Klauss 1971). In the applied film, high fatty acid concentration appeared to restrict oxygen absorption and drying; large zinc soap masses formed and enveloped portions of the cobalt drier, preventing the intended increase in oxygen uptake (Nicholson 1940). The opposite effect was observed when acidity was increased in films pigmented with titanium dioxide or zinc sulfide, shortening the induction period. An earlier study determined that zinc oxide has a reducing effect on cobalt driers, while titanium dioxide oxidises, influencing oxygen absorption (Finnie et al. 1936).

Water and relative humidity
Moisture has long been recognised as a factor in reducing the shelf life of mixed paints (Ware and Christman 1916). As little as 0.25% water was found to favour zinc based seeding, with water facilitating liberation of fatty acids in oil based paints via hydrolysis (Hansen and Klauss 1971). Addition of water caused zinc oxide pigmented alkyd paints to thicken in storage and to have reduced opacity, however, was also found to improve the gloss retention of paint films, the postulate being that soaps formed in milling improved dispersion in the paint (Bell 1970). Water was similarly found to catalyse saponification in reconstructed recipes for lead soaps (Cotte et al. 2006) and high relative humidity levels had a similar effect (Keune et al. 2009). This sensitivity is significant given that oil based paints pigmented with zinc oxide have been found to be strongly moisture absorbing with accompanying volumetric swelling (Browne 1955) and to have high permeability to water vapour relative to paints pigmented with titanium dioxide or a variety of iron oxide pigments (Suryanarayana 1970).

Co-pigmentation
Zinc oxide has most commonly been used as a co-pigment in oil based paints to confer various desirable properties both in artist and industrial paint formulations. Other metal ions with potential to influence paint film chemistry may also be present deriving from components other than pigments, for example lead present in zinc paints as an impurity or via addition as a drier in traditional formulations.

Studies of zinc related deterioration of paintings show that incidences commonly occur in the presence of lead white (Osmond et al. 2005; Shimadzu and van den Berg 2006; Maor and Murray 2008; Shimadzu et al. 2008). Zinc carboxylate aggregation in van Gogh's painting, *Les Alyscamps*, occurred in a zinc oxide containing lead chromate layer (Van der Weerd et al. 2003). Additionally, zinc oxide present in a Naples yellow (lead antimonite) linseed oil paint reconstruction resulted in rapid zinc carboxylate formation under conditions of high humidity and light intensity (Keune et al. 2009). Research into settling of pigments in linseed oil house paints revealed that addition of zinc

oxide (at almost any ratio) to lead based oil paint produced a thinner paint more prone to settling, with both pigments settling in proportion consistent with original composition (Beakes 1928).

Zinc and titanium oxides also interact strongly due to oppositely charged colloidal particles and mutual flocculation tendencies. These vary with particle size and relative proportions of the two pigments and can strongly influence the viscosity of water based paint formulations and the stability of the resulting film (Princen and Devena-Peplinski 1964; Diebold et al. 2003). In oil based alkyds addition of zinc oxide to rutile titanium paints also has an effect, with one study finding that lowering zinc oxide content with aim to reduce zinc soap protuberances may actually result in fewer larger aggregates disrupting the paint film (Bell 1970).

Paint films based on lead or titanium whites which independently demonstrate quite distinct physical/mechanical responses behave more like zinc oxide pigmented films in stress/strain tests when mixed with even small percentages of zinc oxide (Mecklenburg 2008). Similarly, addition of zinc oxide to oil films pigmented with basic lead carbonate or titanium dioxide was found to increase their water absorbency and swelling closer to that recorded for films pigmented with zinc oxide alone (Browne 1956).

Consequences for paintings conservation

Reactivity of zinc oxide in premixed paints 'on the shelf' and following exposure to relatively extreme environments such as paints used in exterior applications has not had immediate apparent consequences for easel paintings containing zinc oxide, although some early sources do remark on the brittleness of zinc oxide based paints, (e.g. Arthur Herbert Church: *The Chemistry of Paints and Painting*. London 1890 cited in Carlyle 2001), supported by a body of anecdotal evidence and more recently articulated concerns (O'Hanlon 2007). A recent study links widespread structural instability in a group of mid 20th century abstract expressionist paintings to the presence of preparatory layers of zinc oxide based house paint (Rogala et al. 2010). A similar phenomenon is identified in a 1938 painting by Joan Miró where additions of the relatively slow drying poppy oil are suggested as a contributing factor (O'Donoghue et al. 2006). And flaking of zinc containing oil paints from acrylic ground layers has been attributed to accumulation of zinc soaps at the interface (Maor and Murray 2008).

It is only in the past decade that deterioration of some paintings has been linked to the aggregation of zinc soaps. One example includes a work by Vincent van Gogh where lumps have erupted through the surface of the painting (Van der Weerd et al. 2003). Other studies have also identified zinc carboxylate aggregates within paintings, apparently similar to the phenomenon of lead carboxylate protrusions responsible for deterioration of earlier paintings (Boitelle and van den Berg 2005; Osmond et al. 2005; O'Donoghue et al. 2006; Shimadzu and van den Berg 2006; Zümbuhl and Fuesers 2006). Impacts of zinc oxide saponification on surface appearance have also been considered (Shimadzu et al. 2008); increased transparency of paints affected by lead soap formation is now recognised to be responsible for devastating changes in appearance of some paintings (Zucker 1999; Noble et al. 2005; Noble and Boon 2007; Townsend et al. 2007; Zucker and Boon 2007). Remineralisation within zinc soap aggregates has also been observed, typically zinc carbonate (Keune 2005) but also zinc sulfate precipitation in two 1950s paintings from Hanoi,

Vietnam, which implies a link between environment and manifestation given the relatively humid, polluted environment to which these paintings have been exposed (MacMillan 2007; Ebert 2008). Formation of zinc carbonate was also found by German researchers in association with hardening and cracking of early 20th century zinc based house paints (H.W. 1925).

Related research and insights

Substantial research has been undertaken in relation to deterioration of paintings associated with lead soap aggregation, and indications are that similar mechanisms are involved when the more reactive zinc oxide is present. Both lead and zinc based aggregates have been shown to comprise soaps of the saturated C16 and C18 monocarboxylic fatty acids, palmitic and stearic acid, rather than of the more reactive and prevalent unsaturated $C_{18:1-3}$ carboxylic acids originally present in the oil (Higgitt et al. 2003; Keune and Boon 2007). Problematic crystalline lumps forming in paint stock have been characterised as zinc salts of the same fatty acids (Elm 1957; Hansen and Klauss 1971). In paintings, azelaic acid, a common product of oxidative degradation of unsaturated C18 fatty acids predominant in drying oils, is frequently found around the perimeter of aggregates (Boon et al. 2005). A phase separation appears to occur, possibly explained by differences in polarity or unfavourable chain packing configurations (Plater et al. 2003). The presence of two phases within an aggregate has been taken to suggest that the compounds were present and mobile at the same time, implying soap formation occurred during the drying of the oil (Keune and Boon 2007). In other paintings monocarboxylic fatty acids appear to have separated from the mature crosslinked network and reacted with lead-containing pigment, causing localised volume expansion and deformation of surrounding paint (Keune and Boon 2007). Monocarboxylic lead soaps have also been implicated in the formation of white crusts on 17th century paintings; moisture gradients and capillary forces are discussed as possible drivers of migration to the surface (van Loon 2008). This is in contrast to findings in relation to efflorescence on modern paintings, where colours containing pigments capable of forming soaps tend not to be affected, and the formation of fatty acid soaps is thought to immobilise and prevent migration of stearic and palmitic acids to the surface (Ordonez and Twilley 1997).

Oleic acid levels may be a significant indicator of the predisposition for paints based on zinc oxide to be brittle and subject to flaking. Recent research has identified high levels of oleic acid in mid-20th century paintings exhibiting structural weakness (Rogala et al. 2010). These levels are unusual for paintings of this age as oleic acid ($C_{18:1}$) would normally oxidise to azelaic acid in the course of paint cure. The particular crystal lattice orientation of zinc carboxylate molecules within paint layers is postulated to lock oleic and other unsaturated fatty acids acid in place, restricting oxidation and cross linking reactions (Rogala et al. 2010). The result is a hard, brittle film. Mechanical testing of paints containing zinc oxide confirms a high modulus with extremely low breaking strain (Suryanarayana 1970; Mecklenburg 2008).

Conclusion

Zinc oxide is a prevalent pigment in oil based paintings from the late nineteenth century through until the present day. Developments and variety in pigment production and paint formulation, and artists' use of paints intended for both artist and industrial applications mean that a range of properties can be expected in these paints. The reactivity of zinc oxide in oil based media has

implications for the stability of paintings containing the pigment. Knowledge of specific pigment properties, fatty acid composition and the influence of additives and environmental conditions on component interactions is critical to our interpretation of the appearance, condition and chemical analysis of these works. Greater understanding of the circumstances likely to favour development of associated degradation phenomena will improve our capacity to identify the most vulnerable paintings and to implement appropriate conservation strategies.

Acknowledgements

References

Barnett, CE 1949, 'Physics and Chemistry of Pigments', *Industrial & Engineering Chemistry* vol. 41, no. 2, pp. 272-279.

Beakes, HL 1928, 'Settling of Pigments in House Paints', *Industrial & Engineering Chemistry* vol. 21, no. 7, pp. 732-734.

Bell, SH 1970, 'Zinc oxide hazing', *Paint and Varnish Production* April 1970 pp. 55-60.

Boitelle, R and van den Berg, KJ 2005, 'A technical examination of Odilon Redon's paintings from the Bonger Collection, Van Gogh Museum', *ArtMatters: Netherlands technical studies in art* vol. 3 pp. 66-81.

Bomford, D, Kirby, J, Leighton, J and Roy, A 1990, *Art in the making: Impressionism*, London, National Gallery Publications Limited.

Boon, J, Keune, K and Zucker, J 2005, 'Imaging analytical studies of lead soaps aggregating in preprimed canvas used by the Hudson River School painter F.E. Church', *Microscopy and Microanalysis* vol. 11(Supplement 2), pp. 444-445.

Brown, HE 1957, *Zinc oxide rediscovered*, New York, New Jersey Zinc Company.

Browne, FL 1955, 'Swelling of paint films in water III: Absorption and volumetric swelling of bound and free films from air of different relative humidities', *Forest Products Journal* vol. 5 pp. 92-96.

Browne, FL 1956, 'Swelling of paint films in water VIII: Swelling of linseed oil paints in water and organic liquids', *Forest Products Journal* vol. 6, pp. 312-318.

Burnstock, A, van den Berg, KJ, de Groot, S and Wijnberg, L 2007, 'An investigation of water sensitive oil paints in twentieth century paintings', in Learner, TJS, Smithen, P, Krueger, JW, and Schilling MR (eds), *Modern Paints Uncovered: Proceedings from the modern paints uncovered symposium,Tate Modern, London, May 16-19, 2006*, The Getty Conservation Institute pp.177-188.

Carlyle, L 2001, *The artist's assistant: oil painting instruction manuals and handbooks in Britain 1800-1900 with reference to selected eighteenth-century sources*, London, Archetype Publications.

Cocks, EJ and Walters, B 1968, *A history of the zinc smelting industry in Britain*, London, George G. Harrap & Co. Ltd.

Cotte, M, Checroun, E, Susini, J, Dumas, P, Tchoreloff, P, Besnard, M and Walter, P 2006, 'Kinetics of oil saponification by lead salts in ancient preparations of pharmaceutical lead plasters and painting lead mediums', *Talanta* vol. 70 pp. 1136-1142.

Currie, C and Smith, J 1994, ''The Biglin brothers turning the stake boat' by Thomas Eakins: a technical study reveals surprising techniques', *AIC Paintings Specialty Group Postprints: papers presented at the 22nd annual meeting of the AIC, Nashville Tennessee, 10 June 1994*, AIC pp. 18-23.

Diebold, MP, Bettler, CR and Mukoda, DM 2003, 'Mechanism of TiO2/ZnO instability in latex paints', *Journal of Coatings Technology* vol. 75 no. 942 pp. 29-36.

Dixon, J 2009, Personal communication with Technical Services Manager, Wattyl Australia P/L, email 12 September 2009.

Dredge, P 1996, 'John Russell: a study of his Impressionist technique' in S-A Wallace, J Macnaughtan and J Parvey (eds), *The articulate surface: dialogues on paintings between conservators, curators and art historians*, Canberra, The humanities research centre, Australian National University/National Gallery of Australia pp. 265-277.

Dredge, P, Schilling, MR, Gautier, G, Mazurek, J and Learner, T 2012, 'Lifting the lids off Ripolin®. A collection of paint from Sidney Nolan's studio', *Proceedings: From Can to Canvas. Early uses of housepaint by Picasso and his contemporaries in the first half of the 20th century, Marseille, May 25-26 and Antibes, May 27 2011, Journal of the American Institute for Conservation*, special issue in press.

Ebert, B 2008, *Volume II: A scientific investigation into the degradation processes of zinc-based paints together with art historical research*, MA thesis (Conservation of Fine Art), Northumbria University, Newcastle.

Elm, AC 1957, 'Reevaluation of the function of pigments in paints', *Official Digest* (April) pp. 351-385.

Farquharson Boan, R 1924, 'The manufacture of mixed paints', *The Australasian Decorator and Painter*, Melbourne, J.E. Bishop, January 1 pp. 94-99.

Finnie, W, Grant, R and McColm, K 1936, 'The adsorption of metallic driers by pigments', *American Paint Journal* vol.21 no. 8 pp. 7-10.

Gardner, HA 1917, *Paint researches and their practical application*, Press of Judd and Detweiler, Inc., Washington D.C.

Gautier, G, Bezur, A, Muir, K, Casadio, F and Fiedler, I 2009, 'Chemical Fingerprinting of Ready-Mixed House Paints of Relevance to Artistic Production in the First Half of the Twentieth Century. Part I: Inorganic and Organic Pigments', *Applied Spectroscopy* vol. 63 no. 6 pp. 597-603.

H.W. 1925, 'Notes on the durability and manipulation of zinc paints', *The decorator and painter for Australia and New Zealand*, Sydney, Bishop Bros., 1 October pp. 7-8.

Hackney, S, Ridge, J and Townsend, JH 2002, 'Pre-Raphaelite technique and its consequences', *Preprints of the ICOM-CC 13th Triennial Meeting, Rio de Janeiro*, James and James pp. 426-431.

Hackney, S, Townsend, JH and Ridge, J 2004, 'Pre-Raphaelite methods and materials' in JH Townsend, J Ridge and S Hackney (eds) *Pre-Raphaelite painting techniques 1848-1856*, London, Tate Publishing pp. 51-75.

Hansen, CM and Klauss, HC 1971, 'Mechanism of paint seeding', *Industrial and Engineering Chemistry Product Research and Development* vol 10 no. 2. pp 189-192.

Harley, RD 1970, *Artists' pigments c.1600-1835*, London, Butterworths and IIC.

Heckel, GB 1934, 'A century of progress in the paint industry', *Journal of Chemical Education* vol. 11 no. 9 pp. 487-93.

Higgitt, C, Spring, M and Saunders, D 2003, 'Pigment-medium interactions in oil paint films containing red lead or lead-tin yellow', *National Gallery Technical Bulletin* vol. 24 pp. 75-95.

Hoffmann, E and Saracz, A 1969, 'Weathering of Paint Films I. Chalking Caused by Zinc Oxide in Latex Paints', *Journal of the Oil & Colour Chemists Association* vol. 52 no. 2 pp.113-132.

Hoffmann, E and Saracz, A 1971, 'Weathering of paint films III. Influence of wavelength of radiation and temperature on the chalking of latex paints', *Journal of the Oil & Colour Chemists Association* vol. 54 pp. 450-470.

Hoogland, FG, van der Horst, J and Boon, JJ 2007, 'Liquefying oil paint in some late twentieth-century paintings' in Learner, TJS, Smithen, P, Krueger, JW and Schilling MR (eds), *Modern Paints Uncovered: Proceedings from the modern paints uncovered symposium,* Tate Modern, London, *May 16-19, 2006*, The Getty Conservation Institute**:** 282-283.

International Zinc Association 2009, *Commercial grades of zinc oxide*, Viewed 7 June 2010, <http://www.znoxide.org/commercial_grades.html>.

Jacobsen, AE and Gardner, WH 1941, 'Zinc soaps in paints: zinc oleates', *Industrial and Engineering Chemistry* vol. 33 no. 10 pp. 1254-1256.

Jolly, JH 1993, 'Materials flow of zinc in the United States 1850-1990', *Resources, Conservation and Recycling* vol. 9 nos. 1-2 pp. 1-30.

Kastens, ML & Hansen, FR 1949, 'Drier soap manufacture', *Industrial & Engineering Chemistry* vol. 41 no. 10 pp. 2080-90.

Kemp, F, Wise, A and Hamilton, B 2004, 'Re-inventing Diddy: The examination and treatment of a pastel drawing on paper by Grace Cossington Smith', *Collaboration and Connections: Postprints of the AICCM Paper, Books and Photographic Materials Special Interest Group Symposium, Sydney 1-3 April 2004*, AICCM pp. 115-124.

Keune, K 2005, *Binding medium, pigments and metal soaps characterised and localised in paint cross-sections*, PhD thesis, University of Amsterdam, Amsterdam.

Keune, K and Boon, JJ 2007, 'Analytical imaging studies of cross-sections of paintings affected by lead soap aggregate formation', *Studies in Conservation* vol. 52 no. 3 pp. 161-176.

Keune, K, Hoogland, F, Boon, JJ, Peggie, D and Higgitt, C 2009, 'Evaluation of the "added value" of SIMS: A mass spectrometric and spectroscopic study of an unusual Naples yellow oil paint reconstruction', *International Journal of Mass Spectrometry* vol. 284 nos. 1-3 pp. 22-34.

Kühn, H 1986, 'Zinc white', in Feller, RL (ed) *Artists' pigments*, Cambridge University Press, vol. 1 pp. 169-186.

MacMillan, S 2007 *A report on the art historical investigation, condition, technical examination and initial investigations into the conservation treatment of two paintings on canvas by Vietnamese artist Nguyen Trong Kiem (1933-1991) dated 1963; in conjunction with scientific investigation of various tube paints used by Vietnamese artists during the mid C20th, and the materials, degradation mechanisms and conservation issues regarding the two paintings*, MA thesis (Conservation of Fine Art), Northumbria University, Newcastle.

Maor, Y and Murray, A 2008, 'Delamination of Oil Paints on Acrylic Grounds', *Materials issues in art and archaeology VIII*, Materials Research Society, Symposia Proceedings, vol.1047 pp. 127-136.

Mecklenburg, MF 2008, *Meccanismi di cedimento nei dipinti su tela: approcci per lo sviluppo di protocolli di consolidamento - Failure Mechanisms in Canvas Supported Paintings: Approaches for Developing Consolidation Protocols*, I Talenti. Metodologie, tecniche e formazione nel mondo del restauro, Il Prato, Padova

Mecklenburg, MF, Tumosa, CS and Erhardt, D 2005, 'The changing mechanical properties of aging oil paints', *Materials Issues in Art and Archaeology VII*, Materials Research Society Symposium Proceedings vol. 85 pp 23-24.

Morley-Smith, CT 1950, 'The development of anti-chalking French Process zinc oxides', *Journal of the Oil & Colour Chemists' Association* vol 33 pp 484-501.

Morley-Smith, CT 1958, 'Zinc oxide - a reactive pigment', *Journal of the Oil & Colour Chemists' Association* vol. 41(January) pp. 85-97.

Nicholson, DG 1940, 'Drying of Linseed Oil Paint Effect of Acidity upon Rate of Oxygen Absorption', *Industrial & Engineering Chemistry* vol. 32 no. 9 pp. 1259-1261.

Noble, P and Boon, JJ 2007, 'Metal soap degradation of oil paintings: aggregates, increased transparancy and efflorescence', *AIC Paintings Specialty Group Postprints*: *papers presented at the 34th Annual Meeting of the AIC, Providence, Rhode Island, June 16-19 2006*, AIC pp. 1-15.

Noble, P, van Loon, A and Boon, JJ 2005, 'Chemical changes in old master paintings II: darkening due to increased transparency as a result of metal soap formation', *Preprints of the ICOM Committee for Conservation 14th Triennial meeting, The Hague 12-16 September 2005*, James and James pp. 496-503.

O'Donoghue, E, Johnson, AM, Mazurek, J, Preusser, FD, Schilling, MR and Walton, MS 2006, 'Dictated by media: conservation and technical analysis of a 1938 Joan Miro canvas painting', *The object in context: Crossing Conservation Boundaries: Contributions to the Munich Congress 28 August - 1 September 2006*, IIC pp. 62-68.

O'Hanlon, G, 2007, '*Zinc white: problems in oil paint*', viewed 24 October 2007, <www.naturalpigments.com/education/article.asp?ArticleID=127>.

Oil and Colour Chemists' Association 1966, '*Pigments, dyestuffs and lakes*', Paint technology manuals, London, Chapman and Hall for the Oil and Colour Chemists' Association.

Ordonez, E and Twilley, J 1997, 'Clarifying the haze: efflorescence on works of art' ~~in~~ WAAC Newsletter vol. 20 no. 1 reproduced from *Analytical Chemistry* 69(13): A416-A422, viewed 14 October 2009, < http://cool.conservation-us.org/waac/wn/wn20/wn20-1/wn20-108.html>.

Osmond, G, Keune, K and Boon, J 2005, 'A study of zinc soap aggregates in a late 19th century painting by R.G. Rivers at the Queensland Art Gallery', *AICCM Bulletin* vol. 29 pp. 37-46.

Osmond, G 2010, Unpublished results of SEM-EDX analysis of samples from 6 paintings by E. Phillips Fox, reports dated 30.07.10, 06.08.10, 25.08.10, 02.09.10, 23.09.10.

Pilz, K 2005, '*Zinc white*', Student report (Department of Restoration and Conservation Studies), University of Applied Sciences, Cologne.

Plater, MJ, De Silva, B, Gelbrich, T, Hursthouse, MB, Higgitt, CL and Saunders, DR 2003, 'The characterisation of lead fatty acid soaps in 'protrusions' in aged traditional oil paint', *Polyhedron* vol. 22 no. 24 pp. 3171-3179.

Princen, LH and Devena-Peplinski, M 1964, 'Effect of particle size on the mutual flocculation between zinc oxide and titanium dioxide', *Journal of Colloid Science* vol. 19 no. 9 pp. 786-797.

Rogala, D, Lake, S, Maines, C and Mecklenburg, M 2010, 'Condition problems related to zinc oxide underlayers: examination of selected Abstract Expressionist paintings from the collection of

the Hirschhorn Museum and Sculpture Garden, Smithsonian Institution', *Journal of the American Institute for Conservation* vol. 49 no. 2 pp. 96-113.

Roy, A 1987 'The materials of van Gogh's 'A cornfield, with cypresses', *National Gallery Technical Bulletin* vol. 11, pp. 50-59.

Salvin, SB 1944, 'Influence of zinc oxide on paint molds', *Industrial and Engineering Chemistry* vol. 36, pp. 336-340.

Shelton, R 2010, Personal communication between Umicore Australia Ltd. via John Dixon (Wattyl Paints), email 28 June 2010.

Shimadzu, Y, Keune, K and van den Berg, KJ 2008, 'The effects of lead and zinc white saponification on surface appearance of paint', *Preprints of the ICOM Committee for Conservation: Preprints of the 15th Triennial Meeting, New Delhi, 22-26 September 2008*, New Delhi, Allied Publishers Pvt Ltd, vol. II, pp. 626-632.

Shimadzu, Y and van den Berg, KJ 2006, 'On metal soap related colour and transparency changes in a 19th century painting by Millais', *Reporting Highlights of the de Mayerne Programme*, JJ Boon and ESB Ferreira, The Hague, Netherlands Organisation for Scientific Research (NWO) pp. 43-52.

Suryanarayana, NP 1970, 'Critical pigment volume concentration of some oxide pigments', *Journal of the Colour Society* vol. 9, no.2, pp. 2-6.

Taylor, CJA and Marks, S, (eds.) 1969, *Solvents, oils, resins and driers*, Paint technology manuals, London, Chapman and Hall on behalf of the Oil and Colour Chemists' Association.

The decorator and painter for Australia and New Zealand 1925, 'The Mascot Smelting Works', Sydney, Bishop Bros. April 1 pp. 187-188.

Townsend, J, Carlyle, L, Khandekar, N and Woodcock, S 1995 'Later nineteenth century pigments: evidence for additions and substitutions' *The Conservator* vol. 19, pp. 65-78.

Townsend, JH, Jones, R and Stoner, K 2007, 'Lead soap aggregates in sixteenth- and seventeenth-century British paintings', *AIC Paintings specialty group postprints*: *papers presented at the 34th Annual Meeting of the AIC*, Providence, Rhode Island, June 16-19 2006, AIC pp. 24-32.

Tumosa, CS 2001, 'A brief history of aluminium stearate as a component of paint', *WAAC Newsletter* vol. 23, no.3, viewed 14 October 2009, <http://cool.conservation-us.org/waac/wn/wn23/wn23-3/wn23-304.html>.

van den Berg, JDJ, Vermist, ND, Carlyle, L and Holčapek, M 2004, 'Effects of traditional processing methods of linseed oil on the composition of its triacylglycerols', *Journal of Separation Science* vol. 27, pp. 181-199.

Van der Weerd, J, Gelddof, M, van der Loeff, LS, Heeren, R and Boon, J 2003, 'Zinc soap aggregate formation in 'Falling leaves (Les Alyscamps)' by Vincent van Gogh' *Zeitschrift für Kunsttechnologie und Konservierung* vol. 17, no. 2, pp. 407-416.

van Loon, A 2008, *Color changes in chemical reactivity in seventeenth century oil paintings*, PhD thesis, University of Amsterdam, Amsterdam.

Ware, EE and Christman, RE 1916, 'A study of the effect of storage on mixed paints', *The Journal of Industrial and Engineering Chemistry* October 1916, pp. 879-883.

Winter, G and Whittem, RN 1950, 'Fluorescence and photo-chemical activity of zinc oxides', *Journal of the Oil & Colour Chemists' Association* vol. 33 (November) pp. 477-483.

Wöll, C 2007, 'The chemistry and physics of zinc oxide surfaces', *Progress in Surface Science* vol. 82 pp. 55-120.

Zucker, J 1999, 'From the ground up: the ground in 19th-century American pictures' *Journal of the American Institute for Conservation* vol 38, pp. 3-20.

Zucker, J and Boon, J 2007, 'Opaque to transparent: paint film defects in the work of Frederick Church and the Hudson River School', *AIC Paintings Specialty Group Postprints: papers presented at the 34th Annual Meeting of the AIC, Providence, Rhode Island, June 16-19 2006*, AIC pp. 33-41.

Zümbuhl, S and Fuesers, O 2006, 'The formation of protrusions in the later works of Alexej von Jawlensky', *The object in context: crossing conservation boundaries: contributions to the Munich Congress 28 August - 1 September 2006*, Munich, IIC pp. 309.

1.4   Conservation science and technical art history

Conservators of cultural heritage occupy an unusual and privileged professional space bridging the worlds of art and science. Often perceived as the scientists of the art world or as intriguing novelties within the scientific community, conservators require sound knowledge of both fields without necessarily being expert in either, while remaining highly specialised in their own discipline. The conservation field is infinitely varied and offers fascinating opportunities for interdisciplinary collaboration together with enormously complex challenges. Within art history conservators assist interpretation by contributing valuable information derived from physical study of the object itself. Understanding of the physical object is greatly assisted by scientific enquiry and analysis applied to address specific questions. The evolution of the interdisciplinary study of art is considered in a focussed issue of the Getty Conservation Institute newsletter (Ainsworth 2005; Considine 2005; Levin et al. 2005). The Twentieth Century in Paint ARC Linkage Project is a large scale collaboration combining the expertise and research capabilities and interests of art museums, conservation organisations and scientific research groups. Although a small number of dedicated conservation research organisations exist internationally and various major collecting institutions in the UK/Europe and North America employ conservation scientists on a permanent basis, this is not the case in Australia or the Asia Pacific Region (Lau 2008). This ARC Project is therefore of great significance in this country and regionally, not only for its intended research aims but also for its establishment role in building cross-disciplinary partnerships and facilitating collaborative research with potential to deliver ongoing benefits for all parties.

1.5   Scope of this thesis

The research contained in this thesis concentrates on the reaction of zinc oxide with stearic acid in the context of artists' oil paint and associated structural or optical deterioration. Zinc oxide will react with other fatty acids present in oil paint, however soaps formed from the longer chain C_{18} and C_{16} saturated carboxylic acids, stearic and palmitic acids, are most implicated in deterioration identified in paintings. For the purposes of this research, stearic acid has been selected as representative of both. A focus of the study is the examination of paint cross-sections which allow results from complementary methods to be correlated and interpreted in the context of painting structure. A primary aim of the research is to improve understanding of compositional factors influencing formation and distribution of zinc carboxylates within a paint film. Factors considered include:

- the presence of other metal ions from pigments with which zinc oxide is frequently combined, notably lead and titanium whites;

- the relationship between metal soaps present as original components in paint formulations and zinc carboxylate phases forming *in situ*, with a particular focus on aluminium stearate;

- the significance of painting stratigraphy and the presence of hygroscopic or medium rich layers as facilitators of hydrolysis or potential sources of fatty acid.

The research methodology incorporates four strands:

- historical research of technological developments in zinc oxide pigment and paint production affecting pigment-oil interactions;

- analysis of naturally aged reference paints comprising cast films of control and commercially prepared artists' paints which incorporate zinc oxide in different oils and in combination with various pigments and additives;

- investigation of specific interactions under controlled conditions within a model system;

- investigation of paint samples from actual paintings affected by zinc carboxylate formation and aggregation.

This thesis contributes important new insights to the growing body of international research on pigment-medium interactions and more specifically the saponification of oil mediums by metal ions present in paintings. Selected results have been published in peer review journals or proceedings and, as such, three chapters of the thesis incorporate research in published form:

Chapter 1

Osmond G. 2012. Zinc white: a review of zinc oxide pigment properties and implications for stability in oil-based paintings. *AICCM Bulletin*, 33: 20-29

Chapter 3

Osmond G, Boon JJ, Puskar L, Drennan J. 2012. Metal stearate distributions in modern artists' oil paints: surface and cross-sectional investigation of reference paint films using conventional and synchrotron infrared microspectroscopy. *Applied spectroscopy*, 66(10): 1136-1144

Osmond G 2014. Zinc white and the influence of paint composition for stability in oil based media. In: van den Berg KJ, Burnstock A, de Tagle M et al. (eds) *Issues in Contemporary Oil Paint*, Springer International Publishing, Chapter 18: 263-281

Chapter 5

Osmond G, Ebert B, Drennan J. 2014. Zinc oxide-centred deterioration in 20th century Vietnamese paintings by Nguyễn Trọng Kiệm (1933-1991). *AICCM Bulletin*, 34: 4-14

1.5.1 Chapter overviews

Chapter 2 reviews approaches to the characterisation of oil paint and in particular the capacity for analytical distinction between fatty acids in free, ester or soap-bound forms. Discussion concentrates on techniques which are appropriate for samples from unique paintings with implicit limitations on size and availability, particularly complementary techniques applicable to embedded paint cross-sections. The sensitivity and advantages of Fourier transform infrared spectroscopy for the study of metal carboxylates present and forming in oil-based paints are presented. Synthesis of zinc carboxylates of the common fatty acids found in mature paints is described and reference spectra produced. Experimental conditions are detailed for techniques applied through subsequent chapters of the thesis.

Chapter 3 involves a detailed study of naturally aged oil-based artists' commercial and custom control reference paints containing zinc oxide. Conventional and synchrotron FTIR techniques are used in conjunction with optical microscopy and scanning electron microscopy with energy dispersive X-ray analysis to consider links between compositional factors and zinc carboxylate formation. Results establish the significance of the presence of aluminium stearate as a component in paint formulations in combination with zinc oxide, with broader implications for metal carboxylate distributions.

Chapter 4 examines interactions between zinc oxide and stearic acid in a solvent model designed to reduce and control variables impacting the study of paint films. In response to the results of reference paint film studies described in Chapter 3, the model additionally allows reactivity of zinc oxide in the presence of aluminium stearate to be investigated. The products of reactions are characterised. Experiments involving interfacial tension measurements within the model attempt to elucidate further detail about the interaction between zinc oxide and stearic acid and the mechanism of zinc stearate formation.

Chapter 5 investigates paint cross-sections from five paintings dated between 1963 and 1980 by Vietnamese artist Nguyễn Trọng Kiệm exposed to hot, humid, polluted conditions. The presence of unusual zinc and sulphur containing lumps in one early work has been investigated previously and the proposed mechanism of formation is reassessed. X-ray microdiffraction allows a tentative hypothesis

of formation of multifunctional layered basic zinc salts. Preferential dissolution of zinc oxide over lead white and lithopone is observed in backscatter electron images, interpreted in conjunction with elemental and FTIR analysis. Structural consequences are indicated for inter- and intra-layer stability of affected paints.

Chapter 6 focuses on early twentieth century paintings by Australian artist E. Phillips Fox which are visibly affected by zinc carboxylate aggregation. A majority are painted on hygroscopic glue-based ground layers and/or have been subject to heat-based lining procedures and exposure to uncontrolled, sometimes extreme environments. These conditions appear deleterious for the paintings in which zinc oxide is prevalent. Nine paint samples from five paintings are investigated in cross-section. The morphology and chemical signature of circular formations rich in zinc, carbon and oxygen common to the paintings are examined in detail using SEM-EDX and SR-µFTIR imaging. Crystallisation of basic zinc carbonate, and incidences of zinc lactate are examined, demonstrating the complexity of potential interactions.

1.6   References

Ainsworth MW (2005) From Connoisseurship to Technical Art History: The Evolution of the Interdisciplinary Study of Art. *The Getty Conservation Institute Newsletter* 20 (1):4-10

Barnett CE (1949) Physics and Chemistry of Pigments. *Industrial & Engineering Chemistry* 41 (2):272-279. doi:10.1021/ie50470a015

Bonotto S, Bonner EF (1968) Effect of Ion Valency on the Bulk Physical Properties of Salts of Ethylene-Acrylic Acid Copolymers. *Macromolecules* 1 (6):510-515. doi:10.1021/ma60006a011

Boon J, van der Weerd K, Keune K, Noble P, Wadum J (2002b) Mechanical and chemical changes in Old Master paintings: dissolution, metal soap formation and remineralization processes in lead pigmented ground/intermediate paint layers of 17th century paintings. In: Vontobel R (ed) *Preprints of the ICOM Committee for Conservation 13th Triennial Meeting*, Rio de Janeiro, 2002. James and James, London, pp 401-406

Boon JJ, Ferreira ESB (eds) (2006) *Reporting highlights of the De Mayerne Program, research program on molecular studies in conservation and technical studies in art history* NWO, The Hague

Boon JJ, Hoogland F, Keune K (2007) Chemical processes in aged oil paints affecting metal soap migration and aggregation. In: Mar Parkin H (ed) *AIC Paintings Specialty Group Postprints*, Providence, Rhode Island, 16-19 June 2006. AIC, pp 16-23

Boon JJ, Peulvé SL, van den Brink OF, Duursma MC, Rainford D (1997) Molecular aspects of mobile and stationary phases in ageing tempera and oil paint films. In: Bakkenist T, Hoppenbrouwers R, Dubois H (eds) *Early Italian paintings: techniques and analysis, Symposium*, Maastricht, 1996. Limburg Conservation Institute, pp 35-56

Burnstock A, van den Berg KJ, de Groot S, Wijnberg L (2007) An investigation of water sensitive oil paints in twentieth century paintings. In: Learner T, Smithen P, Krueger JW, Schilling MR (eds) *Modern Paints Uncovered*, Tate Modern, London, 16-19 May 2006. The Getty Conservation Institute, pp 177-188

Clarke M, Boon JJ (eds) (2003) *Molart: a multidisciplinary NWO Prioriteit project on molecular aspects on ageing in painted works of art. Final report and highlights 1995-2002*. FOM Institute AMOLF, Amsterdam

Considine B (2005) Recent initiatives in technical art history. *The Getty Conservation Institute Newsletter* 20 (1):21-24

Corbeil MC, Helwig K, Poulin J (2011) *Jean Paul Riopelle: the artist's materials*. Getty Conservation Institute, Los Angeles

Corbeil MC, Robinet L (2002) X-ray powder diffraction data for selected metal soaps. *Powder Diffr* 17 (1):52-60. doi:10.1154/1.1431950

Cotte M, Checroun E, Susini J, Dumas P, Tchoreloff P, Besnard M, Walter P (2006) Kinetics of oil saponification by lead salts in ancient preparations of pharmaceutical lead plasters and painting lead mediums. *Talanta* 70:1136-1142. doi:10.1016/j.talanta.2006.03.007

Cotte M, Checroun E, Susini J, Walter P (2007) Micro-analytical study of interactions between oil and lead compounds in paintings. *Appl Phys A* 89:841-848. doi:10.1007/s00339-007-4213-4

Crook J, Learner T (2000) *The impact of modern paints*. Tate Gallery Publishing, London

Dredge P (2012) A history of Australian housepaint technology from the 1920s to the 1950s, with reference to its use by Australian artists, particularly Sidney Nolan. *AICCM Bulletin* 33:53-61

Erhardt D, Tumosa CS, Mecklenburg MF (2005) Long-term chemical and physical processes in oil paint films. *Stud Conserv* 50 (2):143-150

Faucett PH (1943) Conserving oils in paints. *Paint, oil and chemical review* 105 (8):9-10

Higgitt C, Spring M, Saunders D (2003) Pigment-medium interactions in oil paint films containing red lead or lead-tin yellow. *National Gallery Technical Bulletin* 24:75-95

Iedema P, van Loon A, Keune K (2014) *PAinT - Paint alterations in time*. University of Amsterdam. http://www.s4a-paint.uva.nl/. Accessed 10 July 2014

Keune K (2005) *Binding medium, pigments and metal soaps characterised and localised in paint cross-sections*. PhD thesis, University of Amsterdam, Amsterdam

Keune K, Boon JJ (2007) Analytical imaging studies of cross-sections of paintings affected by lead soap aggregate formation. *Stud Conserv* 52 (3):161-176

Keune K, Hoogland F, Boon JJ, Peggie D, Higgitt C (2008) Comparative study of the effect of traditional pigments on artificially aged paint systems using complementary analytical techniques. In: Bridgland J (ed) *Preprints of the ICOM Committee for Conservation 15th Triennial Meeting* New Delhi, 2008. Allied Publishers Pvt Ltd, New Delhi, pp 833-842

Koller J, Burmester A (1990) Blanching of unvarnished modern paintings: a case study on a painting by Serge Poliakoff In: Mills JS, Smith P (eds) *Cleaning, retouching and coatings,*

Preprints of the contributions to the Brussels Congress, 3-7 September 1990. IIC, London, pp 138-143

Lau D (2008) Conservation science in Australia: a space between places. In: Villis C, Ellem A (eds) *Paintings conservation in Australia from the nineteenth century to the present day: Connecting the past to the future. 11th AICCM Paintings Group Symposium*, National Gallery of Victoria, Melbourne 9-10 October, 2008. AICCM, pp 143-148

Lau D, Brunoro K, Varcoe-Cocks M (2007) Preliminary investigations into crystalline efflorescence on Australian and Indigenous paintings in the NGA and NGV collections - research in progress. In: Pagliarino A, Osmond G (eds) *Contemporary collections: AICCM National Conference*, Brisbane, 17-19 October 2007. AICCM, p 57

Levin J, Considine B, Lechtman H, Stone R, Walch-von Miller K (2005) A discussion about technical studies in art history. *The Getty Conservation Institute Newsletter* 20 (1):11-16

Mallégol J, Gardette J-L, Lemaire J (1999) Long-term behavior of oil-based varnishes and paints I. Spectroscopic analysis of curing drying oils. *J Am Oil Chem Soc* 76 (8):967-976. doi:10.1007/s11746-999-0114-3

Mallégol J, Gardette J-L, Lemaire J (2000a) Long-term behaviour of oil-based varnishes and paints. Fate of hydroperoxides in drying oils. *Journal of the Amercian Oil Chemists' Society* 77 (3):249-255. doi:10.1007/s11746-000-0041-5

Mallégol J, Gardette J-L, Lemaire J (2000b) Long-term behaviour of oil-based varnishes and paints. Photo- and thermooxidation of cured linseed oil. *Journal of the Amercian Oil Chemists' Society* 77 (3):257-263

Mallégol J, Gonon L, Lemaire J, Gardette J-L (2001) Long-term behaviour of oil based varnishes and paints 4. Influence of film thickness on the photooxidation. *Polym Degrad Stab* 72:191-197

Mallégol J, Lemaire J, Gardette J-L (2000c) Drier influence on the curing of linseed oil. *Prog Org Coat* 39:107-113. doi:10.1016/S0300-9440(00)00126-0

Mills JS, White R (1987) *The organic chemistry of museum objects* Butterworths Series in Conservation and Museology. Butterworths, London

Noble P, Boon J, Wadum J (2002) Dissolution aggregation and protrusion: lead soap formation in 17th century grounds and paint layers. *Art Matters: Netherlands technical studies in art* 1:46-61

Noble P, Boon JJ (2007) Metal soap degradation of oil paintings: aggregates, increased transparency and efflorescence. In: Mar Parkin H (ed) *AIC Paintings Specialty Group Postprints*, Providence, Rhode Island, 16-19 June 2006. AIC, pp 1-15

Noble P, van Loon A, Boon JJ (2005) Chemical changes in old master paintings II: darkening due to increased transparency as a result of metal soap formation. In: Verger I (ed) *Preprints of the ICOM Committee for Conservation 14th Triennial meeting*, The Hague, 12-16 September 2005. James and James, London, pp 496-503

Noble P, Wadum J, Groen K, Heeren R, van den Berg KJ (2000) Aspects of 17th century binding medium: inclusions in Rembrandt's 'Anatomy lesson of Nicolaes Tulp'. In: *Art et chimie, La couleur, Actes du Congrès*, Paris, 1998. pp 126-129

Ordonez E, Twilley J (1997) Clarifying the haze: efflorescence on works of art in WAAC Newsletter 20(1) 11pp reproduced from *Anal Chem* 69 (13):A416-A422

Osmond G, Keune K, Boon J (2005) A study of zinc soap aggregates in a late 19th century painting by R.G. Rivers at the Queensland Art Gallery. *AICCM Bulletin* 29:37-46

Plater MJ, De Silva B, Gelbrich T, Hursthouse MB, Higgitt CL, Saunders DR (2003) The characterisation of lead fatty acid soaps in 'protrusions' in aged traditional oil paint. *Polyhedron* 22 (24):3171-3179. doi:10.1016/s0277-5387(03)00461-3

Rimer B, Fiedler I, Miller M, Cunningham M, van den Berg J (1999) Investigation of fatty acid migration in alizarin crimson oil paint in two works by Frank Stella In: Wallace FA (ed) *AIC Paintings Specialty Group Postprints*, St. Louis, Missouri, 8-13 June 1999. AIC, pp 1-14

Rinse J (1967) Metal soaps. *American Paint Journal* (March 13):22-28

Robinet L, Corbeil MC (2003) The characterization of metal soaps. *Stud Conserv* 48 (1):23-40

Saunders D, Kirby J (2004) The effect of relative humidity on artists' pigments. *National Gallery Technical Bulletin* 25:62-72

Schilling MR, Carson DM, Khanjian H, P. (1999) Gas chromatographic determination of the fatty acid and glycerol content of lipids. IV. Evaporation of fatty acids and the formation of ghost images by framed oil paintings In: Bridgland J, Brown J (eds) *Preprints of the ICOM Committee for Conservation12th Triennial Meeting*, Lyon, 1999. James and James, London, pp 242-247

Schilling MR, Khanjian H, P. (1996) Gas chromatographic determination of the fatty acid and glycerol content of lipids I. The effects of pigments and aging on the composition of oil paints. In: Bridgland J (ed) *Preprints of the ICOM Committee for Conservation 11th Triennial meeting*, Edinburgh, Scotland. James and James, London, pp 220-227

Schilling MR, Mazurek J, Learner TJS (2007) Studies of modern oil-based artists' paint media by gas chromatography/mass spectrometry. In: Learner TJS, Smithen P, Krueger JW, Schilling MR (eds) *Modern paints uncovered*, Tate Modern, London, 16-19 May 2006. The Getty Conservation Institute, pp 129-139

Shimadzu Y, Keune K, van den Berg KJ (2008) The effects of lead and zinc white saponification on surface appearance of paint. In: Bridgland J (ed) *Preprints of the ICOM Committee for Conservation: Preprints of the 15th Triennial Meeting*, New Delhi, 22-26 September 2008. Allied Publishers Pvt Ltd, pp 626-632

Singer B, Devenport J, Wise D (1995) Examination of a blooming problem in a collection of unvarnished oil paintings. *The Conservator* 19:3-9

Standeven H (2003) *The historical and technical development of gloss housepaints, with reference to their use by twentieth century artists*. PhD thesis, Royal College of Art, London

Townsend JH, Jones R, Stoner K (2007) Lead soap aggregates in sixteenth- and seventeenth-century British paintings. In: Mar Parkin H (ed) *AIC Paintings specialty group postprints*, Providence, Rhode Island, 16-19 June 2006. AIC, pp 24-32

Tumosa CS (2001) A brief history of aluminum stearate as a component of paint. *WAAC Newsletter* 23 (3)

Tumosa CS, Erhardt D, Mecklenburg MF, Su X (2005) Linseed oil paint as ionomer: synthesis and characterization. In: Vandiver PB (ed) *Materials issues in art and archaeology VII*, Boston, Massachusetts, 2004. Materials Research Society, pp 25-31

van den Berg JJD (2002) *Analytical chemical studies on traditional linseed oil paints*. PhD thesis, University of Amsterdam, Amsterdam

van der Weerd J, Boon JJ, Gelddof M, Heeren RMA, Noble P (2002a) Chemical changes in old master paintings: dissolution, metal soap formation and remineralisation processes in lead pigmented paint layers of 17th century paintings. *Zeitschrift für Kunsttechnologie und Konservierung* 16:36-51

van der Weerd J, Gelddof M, van der Loeff LS, Heeren R, Boon J (2003) Zinc soap aggregate formation in 'Falling leaves (Les Alyscamps)' by Vincent van Gogh *Zeitschrift für Kunsttechnologie und Konservierung* 17 (2):407-416

van Gorkum R, Bouwman E (2005) The oxidative drying of alkyd paint catalysed by metal complexes. *Coord Chem Rev* 249:1709-1728. doi:10.1016/j.ccr.2005.02.002

van Loon A (2008) *Color changes and chemical reactivity in seventeenth century oil paintings*. PhD thesis, University of Amsterdam, Amsterdam

Wendt R, Wagner E (1954) Applications of fatty acids in metallic soaps. *J Am Oil Chem Soc* 31 (11):590-593

Williams RS (1988) Blooms, blushes, transferred images and mouldy surfaces: what are these distracting accretions on art works? In: *Proceedings of the 14th annual IIC-Canadian Group conference* Toronto, Canada, 27-30 May 1988. pp 65-84

Zucker J, Boon J (2007) Opaque to transparent: paint film defects in the work of Frederick Church and the Hudson River School. In: Mar Parkin H (ed) *AIC Paintings Specialty Group Postprints*, Providence, Rhode Island, 16-19 June 2006. AIC, pp 33-41

2 Characterisation, FTIR studies and Experimental

2.1 Introduction

Characterisation of samples from paintings relies on a general understanding of the complex drying and ageing processes in oil paint. In simple terms fresh oils comprise polyunsaturated fatty acids in triglyceride structures which undergo oxidative polymerization to form a solid film. Concurrent with polymerization are β-scission degradation reactions and oxidative cleavage of the double bonds in the fatty acyl moieties and hydrolysis of glycerol ester bonds producing low molecular weight products within the cross-linked structure (van den Berg et al. 1999). Hydrolysis may produce unsaturated fatty acids which are yet to react, acid groups attached to the polymerised matrix, and saturated fatty acids and shorter chain products of scission notably mono- and di-carboxylic acids (Erhardt et al. 2005). Cross-linking and photo-oxidation reactions reduce the amounts of unsaturated fatty acids to such an extent that they cannot be detected in aged oil films (Schilling and Khanjian 1996). Gas chromatography – mass spectrometry (GCMS) has shown that three acids comprise the bulk of monomeric content of aged paint, the stable saturated C_{16} and C_{18} straight chain monocarboxylic fatty acids, palmitic and stearic, and the saturated C_9 dicarboxylic acid, azelaic (Plater et al. 2003). This is despite saturated monocarboxylic acids typically comprising only 7% of the fatty acid component in fresh linseed oil (Keune and Boon 2007). Azelaic acid is the main oxidative degradation product of the polyunsaturated C_{18} fatty acids found in drying oils (Mills 1966). Shorter chain diacids are typically present in much lower quantities, the abundance and diversity influenced by pigment composition in addition to exposure conditions (Keune et al. 2008).

Interpretation of factors contributing to metal soap-related defects in paintings relies on determining whether carboxyl moieties are present in free, ester or metal-bound form. Fourier transform infrared spectroscopy (FTIR) is a technique widely applicable in the field of conservation science (Derrick et al. 1999) and metal carboxylates conveniently have distinctive infrared absorption due to COO^- stretching enabling clear distinction from protonated acid forms (Robinet and Corbeil 2003). Together with elemental analysis to establish the metal ion with which carboxylates are associated, FTIR has played a critical role in the characterisation of metal soaps implicated in deterioration of paintings (Boon et al. 2002b; van der Weerd et al. 2002a; Higgitt et al. 2003; van der Weerd et al. 2003; Keune 2005; Noble et al. 2005; Cotte et al. 2007).

It is the case, however, that contributions from other components in a paint sample may mask sensitive lower frequency FTIR bands which in isolated soap samples enable discrimination of fatty

acid based on length of carbon chain (Robinet and Corbeil 2003). The carbon chain signal is stronger in Raman spectra and it has recently been proposed that Raman spectroscopy more effectively enables stearate and palmitate chains to be distinguished based on a single C-C stretch difference producing a peak at 1098 (stearate) and 1104 cm^{-1} (palmitate) (Otero et al. 2014); Robinet and Corbeil (2003), however, note that instruments may not always have sufficient resolution to distinguish this small difference in frequency. Complementary chromatographic procedures are therefore usually necessary to conclusively characterise fatty acid composition (Derrick et al. 1999).

GCMS has been usefully applied to characterisation of oil-based paint media in conservation science since the 1960s (Mills 1966), however typical sample preparation involves hydrolysis of the sample and conversion of fatty acids to methyl esters prior to analysis (Schilling and Khanjian 1996) and so does not allow distinction between moieties originating from free or bound form. There is continuing debate about the mechanisms involved in typical oil-based paint ageing, the resultant structures and how these influence properties in the mature film. A model which has gained increasing acceptance in recent years is that of ionomer. Ionomer is a term used to describe a polymer containing both covalent and ionic bonds, in typical oil paint encompassing that part of the film comprising metal salts of carboxylic acid groups bound to a glyceride backbone or the cross-linked polymer network (van den Berg 2002; Tumosa et al. 2005; Boon et al. 2007). Various studies have attempted to analytically determine the degree of hydrolysis of paints (van den Berg et al. 2001; Erhardt et al. 2005). Adaptations in derivatisation have been developed to assist analytical distinction between fatty acids in different forms, including transethylation of esterified fatty acids followed by a trimethylsilylation of free fatty acids and their salts (van den Berg et al. 2001). A three-step process involving solvent extraction of free acids followed by sequential treatment of the sample to allow extraction of soap and finally esterified acid groups for individual trimethylsilyation and GCMS was applied to investigate relative amounts of fatty acids present in each form (Erhardt et al. 2005). Electrospray ionisation mass spectrometry was applied with results interpreted in conjunction with GCMS analysis to allow discrimination between metal- and ester-bound fatty acids (Keune et al. 2008). A desorption event in direct temperature resolved mass spectrometry has been used to distinguish fatty acids in metal bound form (van Loon 2008; Keune et al. 2009). Solid state nuclear magnetic resonance spectroscopy (NMR) studies were also able to distinguish between the carbonyl groups of an ester, acid, its conjugated base and metal carboxylates in reconstructed paint systems undergoing ageing based on chemical shifts producing a broad NMR signal in the associated regions (Verhoeven et al. 2006); free acid states are suggested to only be transiently present, reacting rapidly in the presence of basic lead carbonate pigment.

NMR requires relatively large amounts of sample and so is not directly applicable to material sampled from actual paintings. Secondary ion mass spectrometry (SIMS) in positive mode was able to detect lead and potassium soaps in paints, but not zinc soaps which had previously been characterised using Fourier transform infrared spectroscopy (FTIR), due to instability in the SIMS conditions (Keune et al. 2008).

X-ray diffraction (XRD) is frequently used to confirm the assignment or elucidate crystal structures of synthesised metal carboxylates (Corkery 1998; Corbeil and Robinet 2002; Plater et al. 2003; Corkery 2004; Otero et al. 2014). Crystallographic data of long chain saturated metal carboxylates has typically been obtained using powder diffraction, possibly because of difficulties in isolating pure single crystals (Plater et al. 2003). One consequence has been that reference data attributed to specific carboxylates has on occasion been found to reflect mixtures, for example when metal stearates have inadvertently been synthesised from stearic acid contaminated with palmitic acid (Corbeil and Robinet 2002). Corkery (1998) provides a comprehensive review of XRD as a technique to elicit details pertaining to the in-plane and long axis structures of metal soaps. The long spacings derive from the splayed-chain conformation of the soaps, where chains extend either side of a metal-carboxylate headgroup. A plot of the layer spacings (d) versus number of carbons in the chain for a homologous set of long chain compounds enables determination of the tilt angle and headgroup thickness of a lamella soap (Corkery 1998). Robinet and Corbeil (2003) summarise key features of saturated and unsaturated C_{18} zinc carboxylates which share seven well resolved peaks with comparable relative intensity below 20° 2θ. Similar d-spacings occur in the vicinity of 4.2, 2.1, 1.4, 1.1 and 0.9 nm for the five most intense peaks. The introduction of one or two double bonds can technically be distinguished by the shape of a peak cluster between 20 and 30° 2θ although these peaks are very weak. A slight shift in low angle peaks with smaller d-spacing values is observed for C_{16} zinc palmitate consistent with a shorter carbon chain (Robinet and Corbeil 2003). The potential for applying XRD to characterisation of metal carboxylates in paint samples is uncertain, although development of micro-XRD instruments and capabilities have enabled characterisation of crystal structure of pigments from paint cross-sections (Hochleitner et al. 2003; Cotte et al. 2009; Monico et al. 2011b; Lluveras-Tenorio et al. 2012).

2.2 Analytical imaging

Paintings are structurally and chemically complex and heterogeneous in nature which complicates interpretation of analysis derived from small samples and has implications for correlating data obtained by complementary techniques if obtained from different samples. Analysis is most reliably interpreted when results are derived from a single sample, with the added benefit of maximising data obtained from paintings where opportunities for sampling are necessarily limited. Cross-

sections of tiny samples taken from paintings are a widely used form of determining structural and compositional information (Derrick et al. 1994a; Khandekar 2003; Townsend and Keune 2006). Samples are typically embedded in a resin and cut or polished to expose a cross-section of all layers contained in the sample. These samples can then be examined using a range of non-destructive techniques beginning with optical microscopy, where visible light and ultraviolet (UV)-autofluorescence images provide complementary information. Scanning electron microscopy (SEM) in backscatter mode provides detailed images based on atomic contrast, enabling visualisation of particle shape and morphology and often helpful for distinguishing degradation products within the original pigment matrix (Keune et al. 2011). Coupled with energy dispersive X-ray analysis (EDX), SEM enables elemental information to be determined both via spot analyses and full spectrum area mapping to highlight lateral distributions, although EDX quantification software has been found to be unreliable based on measurements of binary mixtures at known proportions (Carlyle and Witlox 2005). Transmission electron microscopy (TEM) of thin sections enabling determination of crystal structure by electron diffraction has had limited application (Barba et al. 1995; Colombini and Grauby 2011), while focussed ion beam extraction of individual pigment particles from cross-sections for analysis (Haswell et al. 2008) or to expose underlying microstructure (van der Snickt et al. 2009) has also been attempted. High-resolution 3D-imaging techniques using synchrotron radiation sources are evolving for study of paint samples and have been applied to metal carboxylate aggregates in studies involving X-ray tomographic microscopy (Ferreira et al. 2011) and X-ray fluorescence analysis (XRF) (Faubel et al. 2011). Spatially resolved characterisation is important for distinguishing zinc carboxylates in distributed/dispersed or aggregated form and for monitoring diffusion over time.

In situ analysis of organic components is more problematic. FTIR microscopy has been investigated as a means of obtaining spectra from discrete regions of a sample (Tsang and Cunningham 1991; Pilc and White 1995; Langley and Burnstock 1999; Rizzo 2008) and there have been substantial improvements in applying various techniques in recent years, including FTIR-ATR imaging (Derrick et al. 1994b; Heeren et al. 2000; van der Weerd et al. 2002b; van der Weerd et al. 2004; Mazzeo et al. 2007; Goodall et al. 2008; Mazzeo et al. 2008; Spring et al. 2008; Joseph et al. 2010b; Prati et al. 2012; Prati et al. 2013) and SIMS (Heeren et al. 1999; Boon et al. 2002a; Keune and Boon 2004; Boon et al. 2005; Keune and Boon 2007; Keune et al. 2009; Sanyova et al. 2011). Surface presentation is critical to the quality of data obtained, with optimum results achieved with dry polishing and use of a sample holder to maintain uniform pressure (van Loon 2008), cutting with an ultra-microtome (Cotte et al. 2009), or argon ion polishing (Boon and van der Horst 2008). Data quality can be improved by transmission FTIR experiments of paint thin-sections, however

these are notoriously difficult to obtain from historic paint samples, and attempts are ongoing to optimise embedding techniques which effectively support fragile paint fragments for microtoming while simultaneously avoiding infiltration and contamination of the sample (Derrick et al. 1994a; Pilc and White 1995; Martin de Fonjaudran et al. 2008; Cotte et al. 2009; Joseph et al. 2010a; Mulvihill 2012; Pouyet et al. 2014). Increasing accessibility of synchrotron facilities has also seen emerging application of FTIR microspectroscopy (Smith 2003; Sloggett et al. 2010), often in conjunction with complementary beam lines including X-ray absorption near edge microspectroscopy, XRF spectrometry, electron energy loss spectrometry and X-ray diffraction (Cotte et al. 2007; Cotte et al. 2009; Casadio et al. 2011; Monico et al. 2011a; Lluveras-Tenorio et al. 2012).

2.3 Fourier transform infrared spectroscopy studies

2.3.1 Oil-based paint

The sensitivity of FTIR for distinguishing metal soaps, its requirement for only very small sample sizes necessary for analysis of unique cultural items, coupled with its applicability to both static and imaging measurements, make the technique an obvious choice around which to centre investigations in the present study. In conjunction with complementary methods of analysis, FTIR is an established and accessible technique for broad characterisation of paints and for monitoring changes in functionality over time such as those which occur during the complex drying and ageing processes in oil paint (Meilunas et al. 1990; Derrick et al. 1999; Mallégol et al. 1999; van der Weerd et al. 2005). A review of the FTIR spectral features of linseed oil is provided by van der Weerd et al (2005). Although not individually distinguishable from other oils, the FTIR spectrum of linseed oil incorporates features common to the class of materials dominated by fatty acid chains and glycerol ester bonds. This includes significant CH_2 stretches (2926, 2855 cm^{-1}), aliphatic C-H bands at 1464, 1379 and 725 cm^{-1}, a strong, sharp carbonyl band ca 1740-1750 cm^{-1} and three C-O (triester) bands at 1240, 1165 and 1100 cm^{-1} – strongest at the centre of the triplet (Derrick et al. 1999). Vibrations associated with carbon double bonds are rarely significant in well-dried oils. As oil paint ages, carboxylic acids present or formed produce a shoulder at wavenumber ca 1708 cm^{-1} to the v C=O glycerol ester absorption, accompanied by broad O-H stretch centred 3400 cm^{-1} and δ CH_2 peak at 1414 cm^{-1}, and deformation of the ester triplet (van der Weerd et al. 2005). Ionisation of the carbonyl groups as occurs in many metal-organic acid compounds enables clear distinction from protonated acid forms (Mehrotra et al. 1995; Corkery 1998). Metal carboxylates have distinctive infrared absorption due to COO$^-$ stretching which varies within a range depending on metal cation and acid group. Soap formation is characterised by disappearance of the O-H stretch

and replacement of acid v C=O and C-O (1300 cm^{-1}) bands with COO^{-} asymmetric and symmetric stretching at *ca* 1550 cm^{-1} and 1400 cm^{-1} (Robinet and Corbeil 2003; Corkery 2004).

Pigments and additives present in paint not only influence FTIR spectra through their own characteristic absorptions but also via their influence on short and long term reactions occurring in the oil paint medium. Zinc oxide itself has no absorption signal in the mid-infrared range between 4000 and 600 cm^{-1}, but oil-based paints containing zinc oxide are among the most likely to develop strong carboxylate absorption (van der Weerd et al. 2005). Infrared (IR) absorptions of key relevance to metal carboxylate (zinc stearate) formation are summarised in Table 2.1 (Robinet and Corbeil 2003; Corkery 2004; van der Weerd et al. 2005).

Table 2.1 Summary of characteristic infrared bands (cm^{-1}) and assignments related to the presence and formation of metal carboxylates in oil-based paints.

Linseed oil	Stearic acid[a]	Zinc stearate[a]	Attribution
	3400 (broad)		v OH
2956	2954	2952	v_{as} CH$_3$
2926	2917	2918	v CH2
	2871		v_s CH3
2855	2850	2848	v CH2
1740	1703 (strong)		v C=O
		1540 (strong)	v_{as} COO
	1472/1463	1465	δ CH$_2$
	1411		
		1398	v_s COO
1240/1165/1100	1298		v C-O

[a] stearic acid and zinc stearate are virtually indistinguishable from palmitic acid and zinc palmitate using the specified peaks

For a given metal ion, carboxylate spectra are similar except for an increase in the number of regularly spaced progression of narrow bands in the region 1150-1350 cm^{-1} as the carbon chain length increases, associated with wagging or twisting motions of CH$_2$ groups in the hydrocarbon chain (Mesubi 1982). It is therefore more difficult to distinguish between carboxylates of similar chain length and saturation with the same cation, e.g. between zinc salts of the saturated palmitate and stearate ligands, with only subtle differences in the IR spectra of the two (Robinet and Corbeil 2003). Similarly the spectra of zinc salts of the unsaturated oleate and linoleate chains are very similar. Decreasing intensity of progression bands relative to carboxylate vibrations has been

associated with a decrease in crystallinity (Corkery 1998). Broad asymmetric metal carboxylate vibrations in paint samples, in comparison with the same band in spectra of pure metal soaps, is taken to suggest coordination of the metal to different types of carboxylate-containing compounds, incorporation of the metal compound in diverse and complex chemical or physical environments and/or metal carboxylate compounds with more than one type of metal (Keune et al. 2008). Variation between the FTIR spectra of synthesised soaps and the same soaps characterised in paintings has been attributed to structural distortion (Helwig et al. 2014). Metal soaps often crystallise from solution with large amounts of disorder compared to smaller molecules (Corkery 2008), while different crystalline modifications and impurities may dramatically affect chain packing (Akanni et al. 1992).

2.3.2 Coordination structure of zinc carboxylates

Zinc(II) has d^{10} electron configuration more like alkaline earth metals which influences coordination chemistry (Corkery 1998). Zinc compounds are electrophilic with a pronounced capacity for complex formation. Tetra-coordination is favoured by means of sp^3 hybridization involving unoccupied 4s and 4p valence shell orbitals (van der Kerk 1972). There is a strong condensation effect compared to other divalent cations (Sakai and Umemura 2002) and the small size of the zinc ion leaves open the possibility of covalency between metal and oxygen (Corkery 1998). The principal modes of coordination between COO^- group and metal ion are monodentate, chelating bidentate and bridging bidentate (the carboxylate bridging between two metal ions (Mesubi 1982; Akanni et al. 1992; Marques et al. 1998) (Figure 2.1).
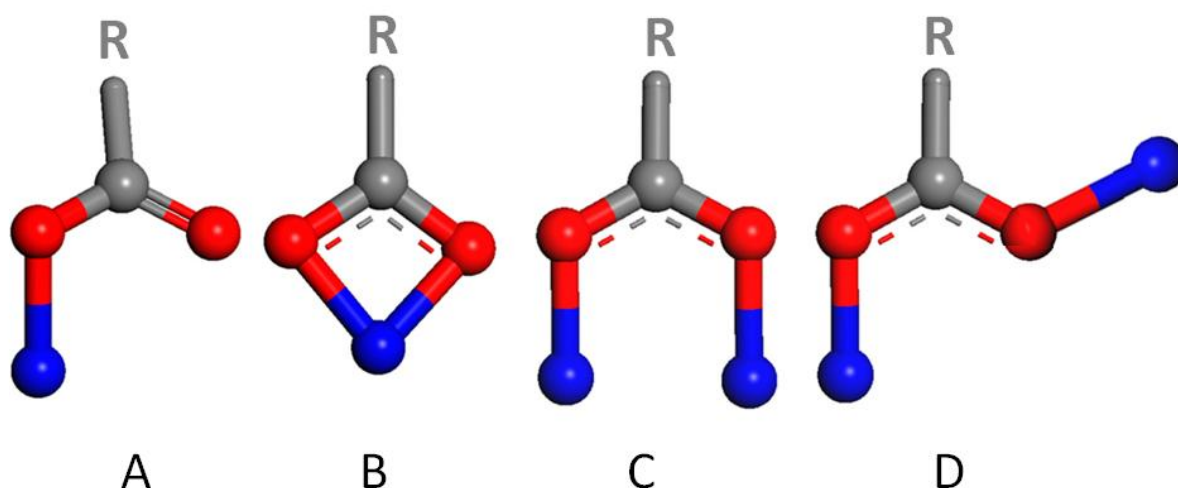
Figure 2.1 Possible coordination modes for carboxylates bound directly to surface metal atoms in (A) monodentate, (B) chelating bidentate; and bridging bidentate: (C) *syn-syn* and (D) *syn-anti* configurations. Grey: C, red: O, blue: metal atom. Adapted from (Clegg et al. 1988; Greathouse et al. 2014)

Various studies have been reviewed which establish that the separation between, and shifts in the antisymmetric and symmetric stretching modes of the COO$^-$ stretching vibration are indicative for coordination structure (Marques et al. 1998). Coupled with molar mass calculations from measured densities and molar volume, zinc carboxylates of even numbered chain length from C_6-C_{18} were deduced to involve a combination of the two bidentate structures, or asymmetric chelating bidentate coordination based on $100 < \Delta v < 150$ cm^{-1}; Δv (v_a COO$^-$ and v_s COO$^-$) ranging from 136 (C_6) and 144 cm^{-1} (C_{18}) (Mesubi 1982). The higher frequency difference for zinc stearate brings it closer to that expected for bridging bidentate (Ishioka et al. 2000). X-ray absorption fine structure analysis of Zn-O distance in zinc stearate coupled with COO$^-$ rocking vibration supports bridging bidentate structure and all-*trans* conformation of alkyl chains with parallel subshell packing (Ishioka et al. 2000). The same conclusion is reached with FTIR and XRD studies for a homologous series of C_4-C_{20} zinc alkanoates indicating a similar structure across the range where each zinc atom is tetrahedrally coordinated to oxygen atoms from four different carboxylate groups and each ligand forms a bidentate bridge with two tetrahedral zinc atoms resulting in a *syn–anti* arrangement (Taylor and Ellis 2007). Splitting of v_a and v_s COO$^-$ vibrations is observed in shorter chain carboxylates ($n_C < 10$) and is taken to reflect stronger Zn-O binding than occurs in longer chain homologues, where van der Waals interactions become more dominant, weakening the metal-ligand bond (Taylor and Ellis 2007). Overlapping bilayers have been hypothesised to form methyl–methylene carbon–carbon interactions from opposite layers in a lamellar for $n_C > 9$ which are stronger in even chain homologues as a consequence of better orientation, conformation and packing of end terminal methyl groups in the molecular lattice, when compared with the odd chains (Nelson et al. 2011), however the validity of these proposed structures has recently been challenged (Hermans and Iedema 2014).

Wavenumbers of v_a CH$_2$ and v_s CH$_2$ bands have been shown to be sensitive to the state of molecular conformation in studies of zinc stearate monolayers at the air/water interface (Simon-Kutscher et al. 1996; Sakai and Umemura 2002). Higher frequencies (2924 2854 cm^{-1}) and peak broadening are associated with the gauche conformer while lower frequencies (2917 2850 cm^{-1}) imply the all-*trans* conformer is predominant. The lowest frequencies in zinc stearate are linked to highly ordered *trans*-zigzag conformation of methylene chains packed parallel with a fixed hydrophilic part (Figure 2.2).
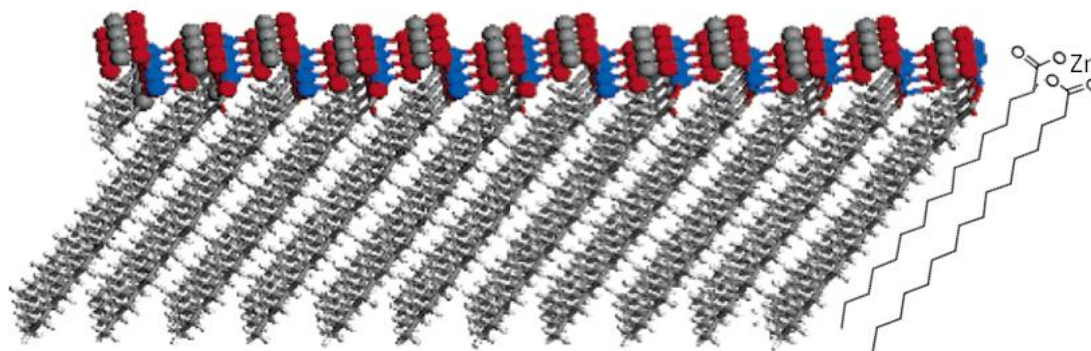
Figure 2.2 Schematic structure of a saturated fatty acid zinc soap with highly ordered *trans*-zigzag conformation of methylene chains. Blue: Zn, red: O, grey: C, white: H. Adapted from (Barman and Vasudevan 2006b)

Differences in hydrocarbon chain conformation indicated by IR spectroscopy in mixtures of zinc stearate and zinc oleate have enabled explanation of how solid solutions of the two are able to exist across all compositional ratios (Barman and Vasudevan 2007). Spectra indicate the introduction of gauche defects into a fraction of stearate chains enables solid solutions of the zinc salts; zinc coordination allows sufficient space between alkyl chains to accommodate conformational freedom not possible in the respective acids. Mixtures were not distinguishable by carboxylate stretching modes with the difference between v_s and v_a COO$^-$ band frequencies remaining constant at 142 cm^{-1}, indicative of bridging bidentate coordination, but IR progression bands enabled quantitative information regarding concentration of each type of ordered chain (Barman and Vasudevan 2007). C-H progression bands have similarly been used to distinguish the simultaneous presence of palmitate and stearate lead salts which have combined to form inclusions in paintings (Higgitt et al. 2003), and have very recently been documented for both physical mixtures of zinc stearate and zinc palmitate as well as for binary salts of zinc with palmitate and stearate ligands (Helwig et al. 2014).

Carboxylate and methylene scissoring bands have been used to demonstrate the pH dependency of metal – carboxylate coordination structures within a stearic acid monolayer/Zn^{2+} system at an air/water interface; elucidation of the transformation mechanism shows asymmetric bridging bidentate coordination is replaced by increasingly ionic interaction below pH 6.1 until the undissociated fatty acid comes to dominate at pH 5 (Simon-Kutscher et al. 1996). Carbonyl stretching vibrations for stearic acid have been shown to shift from 1703 cm^{-1} in Langmuir-Blodgett films compared to 1709 cm^{-1} in chloroform, attributed to the dimer of the carboxylic group formed by intermolecular hydrogen bonds (Li et al. 2001). Overlapping in this peak *ca* 1700 cm^{-1} was attributed to a stearic acid dimer with *cis* and *trans* configuration (Marshbanks et al. 1994).

2.4   Scope of the present study

This thesis draws primarily on the technique of FTIR in complement with optical microscopy and SEM imaging and elemental analysis for interpretation and characterisation of zinc carboxylate phases in paint samples. When applied to investigation of paint cross-sections, these techniques provide compelling insights into zinc oxide-centred deterioration and zinc carboxylate formation. The techniques are suitable for application to samples from unique paintings and can be applied to existing samples and paint cross-sections. Results are produced in formats which are broadly familiar to the Australian and international conservation community, and involve instrumentation which is locally available and for which personal mastery was feasible. No systematic attempt has been made to acquire supporting chromatographic or mass spectrometric data. The optimisation of GCMS instruments suitable for paint analysis for conservation science investigations remains underdeveloped in Australia and pursuit of options for accessing facilities internationally or for local customisation was considered beyond the scope of the present study. While the absence of corroborating fatty acid assignments is acknowledged as a limitation, particularly with respect to characterisation of complex samples from paintings in the final chapters of the thesis, it remains the case that vibrational spectroscopy with supporting elemental assignment of the specific metal ion/s involved can provide detailed information regarding carboxylate structures. For the purposes of reference paint film studies and model systems discussed in Chapters 3 and 4, spectral interpretation is assisted to some extent by the presence of limited and known components. Results are further supported by use of synchrotron source FTIR imaging which enables laterally resolved chemical signatures at high resolution to be combined with elemental analysis in the form of SEM-EDX of the same sample. It is also the case that options for analysis of complex paint samples obtained from unique works of art is necessarily limited by availability of sample material. Mass spectrometric techniques typically applicable to paintings are destructive in nature and require relatively large sample sizes or samples large enough to support multiple complementary approaches to derivatisation which preclude their routine employment. FTIR is a widely applied and effective method for sample characterisation; improved understanding of the significance of subtleties in spectral features when carefully interpreted in conjunction with complementary techniques provides a useful addition to the repertoire available to researchers of historic paint samples.

2.5   Synthesis of zinc carboxylates as reference compounds

Obtaining reliable reference data for metal soaps is critical for basing characterisation of incidences in paintings. Commercially available supplies are frequently mixtures of soaps (Ordonez and Twilley 1997; Tumosa 2001; Corbeil and Robinet 2002), so synthesis is typically preferred for

acquisition of baseline reference data and for structural determination (Corbeil and Robinet 2002; Corkery 2004; Taylor and Ellis 2007; Nelson et al. 2011).

2.5.1 Overview of synthesis methods

Early paint industry studies on the reactivity of zinc oxide in linseed oil used X-ray diffraction (XRD) to characterise reaction products of salts formed with oleic acid and determined that a hydrated soap (coordinated compound) formed when zinc oxide was used in excess, in contrast with the normal salt, $(RCO_2)_nM$, if stoichiometric quantities were used (Ware and Christman 1916; Jacobsen and Gardner 1941). An excess of acid or metal may lead to formation of basic $(M(OH)_x(RCO_2)_y)$ or acidic soaps $((RCO_2)_nM \cdot RCO_2H)$ such as can be found in commercially produced samples (Akanni et al. 1992). Zinc, as a (post-) transition metal, is most likely to form basic soaps (Corkery 1998). No difference was found to soaps produced by direct combination of zinc oxide with oleic acid to soaps produced via zinc sulfate and sodium oleate (Jacobsen and Gardner 1941). Both reaction products were dissolved, centrifuged and allowed to dry by evaporation forming crystals. Combining zinc oxide pigment with 'pharmaceutical white oil' adjusted to acid value 10 by addition of the relevant fatty acid also produced zinc soaps, but practical challenges were encountered in separating the solids of unsaturated soaps due to the limited solubility of excess acid and soap (Morley-Smith 1958). Lead soaps have been successfully formed by mixture of palmitic acid and lead white pigment in chloroform, while mixtures of the same pigment with glyceryl tripalmitate did not react (Boon et al. 2007).

General methods for preparing carboxylates of polyvalent metal ions have been summarised as precipitation, ligand exchange, fusion, or direct reaction between metal and molten fatty acid (Akanni et al. 1992; Corkery 1998). Synthesis of zinc soaps has most commonly used variations on the precipitation method, where neutral zinc carboxylates are produced via reaction of a sodium soap of the relevant fatty acid and a slight stoichiometric excess of zinc salt (chloride or sulfate) (Nelson and Pink 1952; Pilpel 1963; Corbeil and Robinet 2002; Corkery 2004). Resulting soaps were found to contain a small percentage of unreacted fatty acid. Zinc was the only metal among lead and copper to form a crystalline solid with linoleic ($C_{18:2}$) acid when synthesised according to the precipitation method, in contrast to synthesis with oleic $C_{18:1}$ acid and with saturated C_{16} and C_{18} fatty acids where crystalline soaps were obtained for all three metals (Corbeil and Robinet 2002). Hydrothermal synthesis is advocated for preparation of crystals of cross-linked polymeric solids suitable for characterisation by single crystal XRD (Plater et al. 2003). Single crystals were produced for selected zinc carboxylates to validate powder XRD data for a larger range of soaps prepared by refluxing zinc oxide with an excess of carboxylic acid in ethanol for approximately 2 hours before filtering, rinsing and drying (Taylor and Ellis 2007).

2.5.2 Experimental

For the present study, zinc carboxylates were synthesised as reference compounds representing soaps of the fatty acids most frequently encountered in aged oil paint or which have been implicated in association with deterioration in paintings. In addition to zinc stearate, zinc soaps were synthesised from azelaic acid, the main oxidative degradation product of the polyunsaturated C_{18} fatty acids found in drying oils, and oleic acid, unusually high levels of which have been linked to zinc oxide-based paints (Rogala et al. 2010; Maines et al. 2011). Zinc palmitate is structurally very similar to zinc stearate with almost indistinguishable major IR stretching bands as discussed in section 2.3.1 and so was not specifically synthesised.

2.5.2.1 Zinc stearate

A zinc stearate reference was synthesised using a published one-step precipitation technique (Corbeil and Robinet 2002). In summary, an aqueous mix of stearic acid (octadecanoic acid, $CH_3(CH_2)_{16}COOH$, Sigma Aldrich reagent grade $\geq 95\%$), sodium hydroxide and zinc chloride ($ZnCl_2$, Aldrich anhydrous powder, $\geq 99.995\%$ trace metals basis) were combined at 2:2:1 stoichiometry, with a slight excess of the zinc salt to facilitate final rinsing. The mixture was stirred and heated to 70°C using an oil bath for 20 minutes. The resulting precipitate was filtered and washed with sequential rinses of ethanol and warm water before drying in a vacuum oven overnight. An FTIR spectrum of the synthesised soap is shown in Figure 2.3, and with progression bands detailed in Figure 2.4.
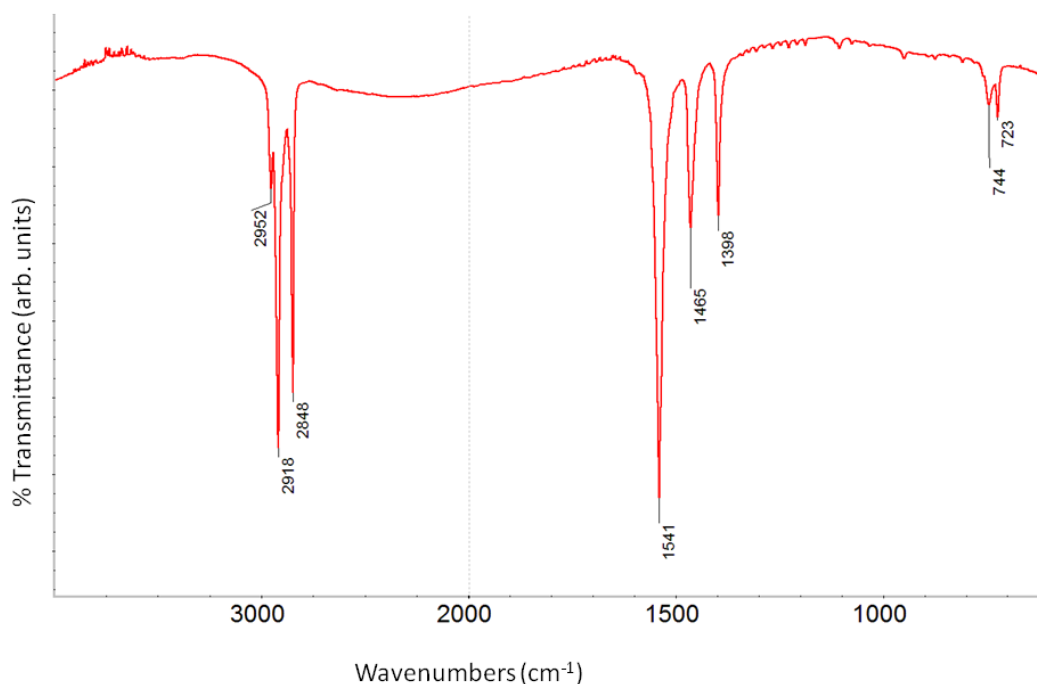
Figure 2.3 FTIR spectrum of zinc stearate as synthesised

Strong, sharp peaks at 1541, 1465 and 1398 cm^{-1} are characteristic of v_a COO^{-}, v CH$_2$ and v_s COO^{-} vibrations for zinc stearate with other peaks also in agreement with published references (Robinet and Corbeil 2003). The absence of an acid carbonyl peak at 1703 cm^{-1} gives no indication of residual stearic acid. However, traces were detected by subsequent powder X-ray diffraction which has a sensitivity of approx 0.3 wt% (Corkery 1998). Some residual sodium chloride was also found, indicating a minor deficiency in the rinse stage of synthesis. At low levels these impurities were considered acceptable for the purposes of this research.
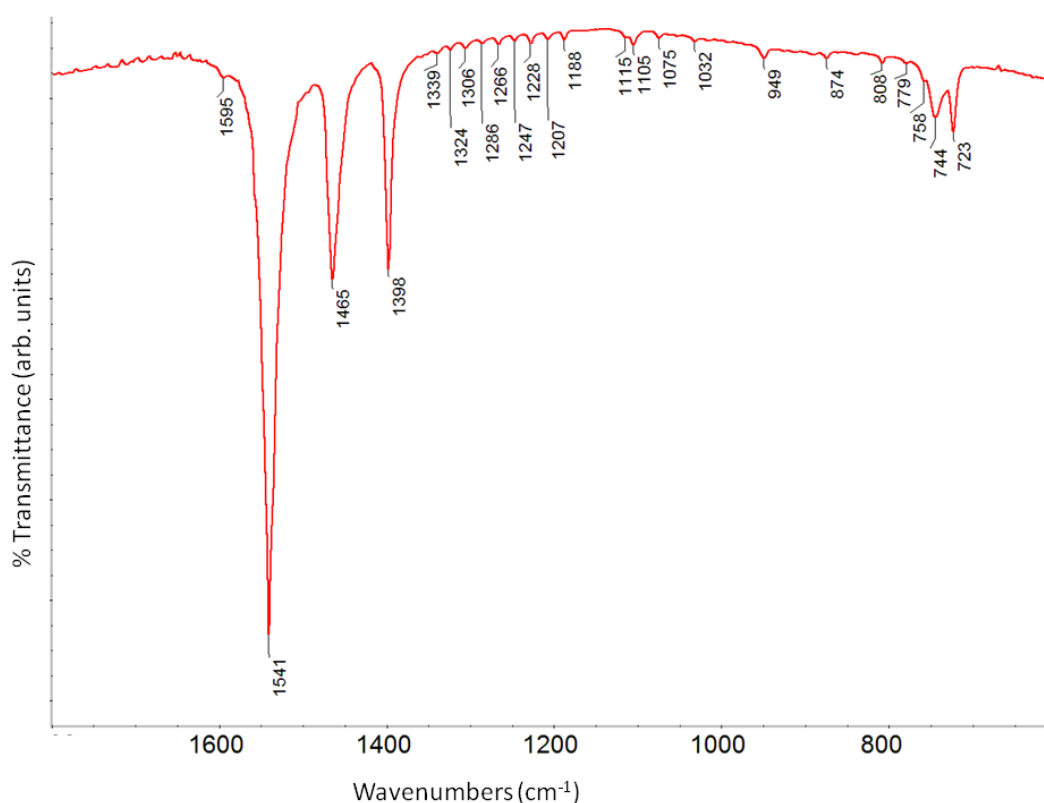
Figure 2.4 Spectrum detail of zinc stearate as synthesised showing peak positions 600-1800 cm^{-1}

2.5.2.2 Other zinc carboxylate reference compounds

The same procedure outlined for zinc stearate was used to synthesise samples of zinc oleate - prepared using oleic acid (*cis*-9-octadecenoic acid, CH$_3$(CH$_2$)$_7$CH=CH(CH$_2$)$_7$COOH) ≥99.0% (GC) analytical standard obtained from Fluka; and zinc azelate - prepared using azelaic acid (nonanedioic acid, HOOC(CH$_2$)$_7$COOH) 98% obtained from Aldrich. Their characteristic spectra are shown in Figures 2.5-2.8.
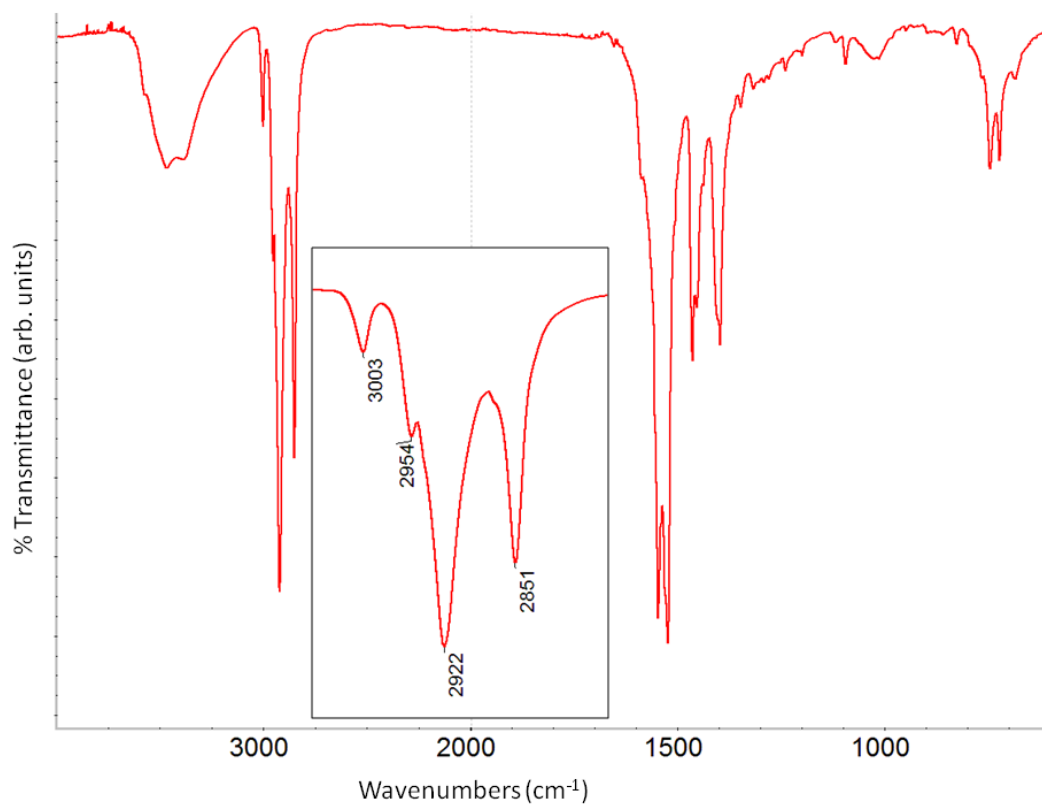
Figure 2.5 FTIR spectrum of zinc oleate as synthesised, with inset detailing peak frequencies 2800-3100 cm^{-1}
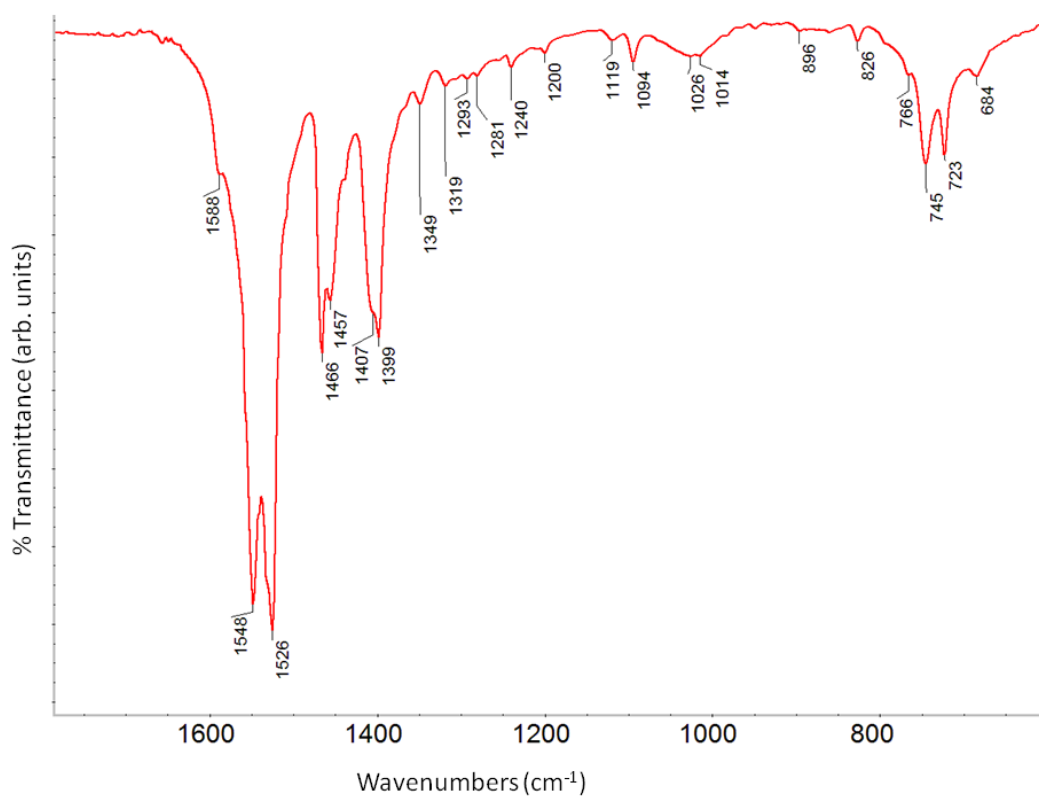
Figure 2.6 FTIR spectrum detail of zinc oleate as synthesised showing peak positions 600-1800 cm^{-1}
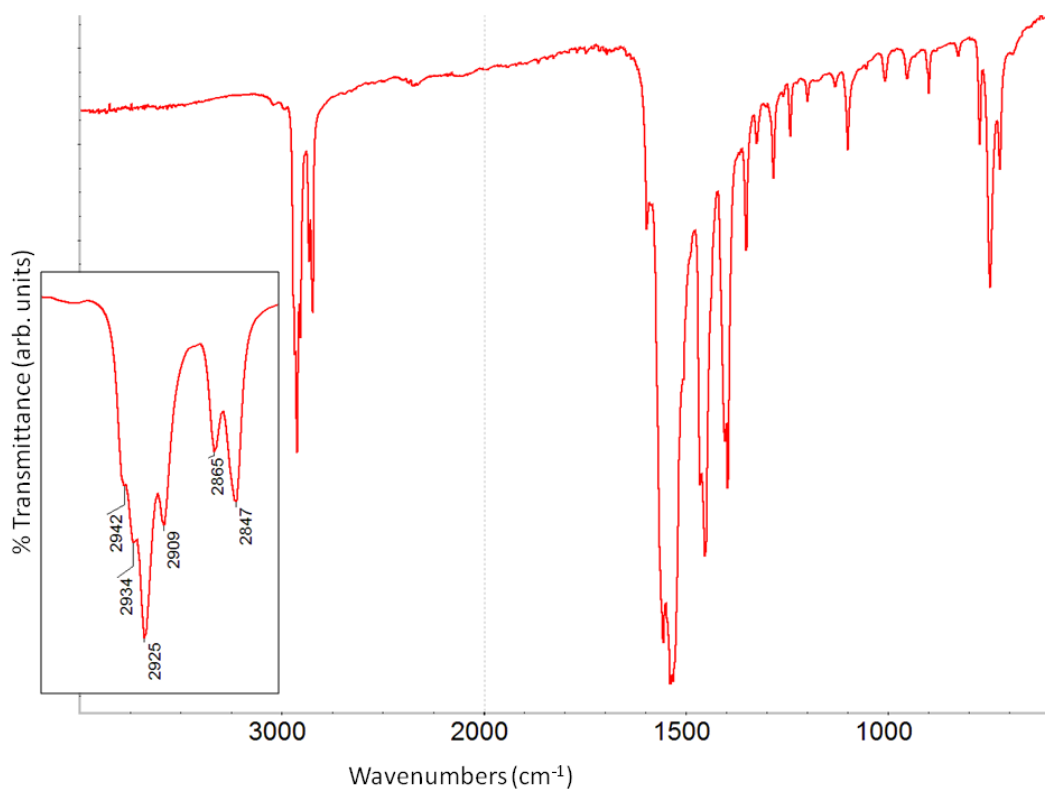
Figure 2.7 FTIR spectrum of zinc azelate as synthesised, with inset detailing peak frequencies 2800-3000 cm^{-1}
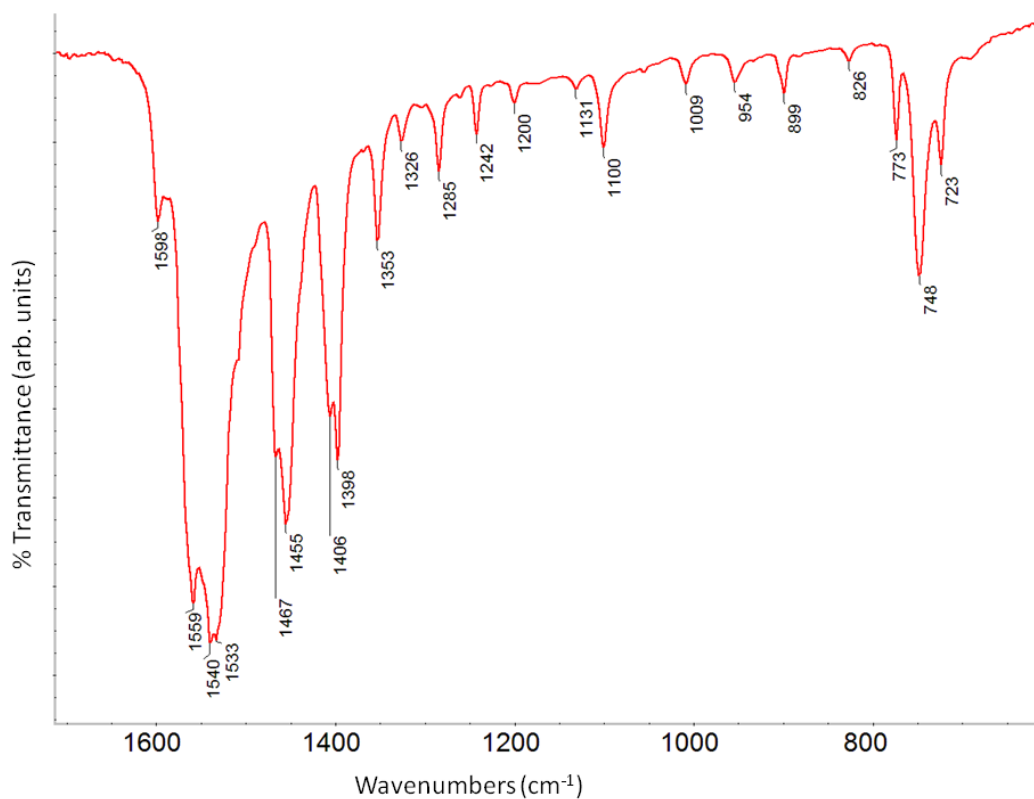
Figure 2.8 FTIR spectrum detail of zinc azelate as synthesised showing peak positions 600-1700 cm^{-1}

Zinc oleate frequencies correlate very well to those published (Robinet and Corbeil 2003) with the exception of an absent band at 1160 cm^{-1} (also absent in a more recently published spectrum (Helwig et al. 2014)) and an additional absorption at 1014/1026 cm^{-1} (possibly linked to the broad OH stretch at c. 3400 cm^{-1} suggesting bulk water of hydration, Marshbanks 1994). The presence of a carbon double bond is evident by the C=CH vibration at 3003 cm^{-1} and twisting-rocking in the methylene chain (Barman and Vasudevan 2006a) which reduce the regularity of progression bands relative to the stearate. Peak splitting of the dominant carboxylate and CH$_2$ vibrations between 1390 and 1560 cm^{-1} are evident in the oleate and the azelate, although the ν_a COO$^-$ peak for the azelate is broader with additional complexity. The shorter chain diacid structure of zinc azelate produces a spectrum which is distinct from the stearate and oleate, reflected in the CH$_2$ and CH$_3$ bands 2840-2960 cm^{-1} and a noticeably different pattern of peaks below 1360 cm^{-1}.

2.6 Experimental

2.6.1 Cross-section preparation

Samples were obtained from reference paint film draw-downs from the Smithsonian Museum Conservation Institute reference paint collection (discussed in Chapter 3) and from paintings by Vietnamese artist Nguyễn Trọng Kiệm (1933-1991) (Chapter 5) and Australian artist E. Phillips Fox (1865-1915) (Chapter 6). Fragments typically less than 1 mm in width from each reference paint and painting were embedded in polyester resin (Volksglas, MEKP, cured at room temperature) and microtomed with a tungsten knife to expose a cross-section normal to the paint surface. Cross-sections revealed paint films typically 150-450 µm in thickness. Final (dry) polishing of sections was undertaken with Micro-Mesh™ cloth backed abrasives (12000 grit) where required. Samples of selected reference paints were additionally embedded in epoxy resin (Procure 812, DDSA, NMA, DMP cured at 60 °C). Embedded samples were microtomed with a glass or histo diamond knife to obtain 5 µm thin-sections for transmission measurements.

2.6.2 Optical microscopy (OM)

Microscopy was conducted with a Leica DMLP microscope using N plan objectives and an external halogen fibre optic illuminator. Ultraviolet fluorescence (UVF) was observed using an EL6000 compact light source with mercury short arc reflector lamp and Leica 'A' filter with excitation range BP 340-380 and suppression BP 425. Cross-sections were photographed under incident light and fluorescence conditions using a Leica DFC500 camera.

2.6.3 Fourier transform infrared spectroscopy (FTIR)

FTIR spectroscopy was conducted using a Nicolet 5700 FTIR spectrometer and Continuum microscope. Data was collected using Omnic 7 software over wavenumber range 4000-600 cm^{-1}. Spectra are the sum of 32 or 64 scans at a resolution of 4 cm^{-1}. Spectra were collected from multiple points on each sample with an aperture of 100x100 μm^2. Spectra obtained were interpreted and compared to published or personal reference spectra and are shown in absorbance or transmittance with an offset scale (arbitrary units) and x-axis split at 2000 cm^{-1}.

Spectra of paints prior to embedding were acquired by applying a scraping to a single diamond window of a micro-compression cell, flattened using a stainless steel roller. Samples were analysed in transmission mode.

Spectra of paint film or cross-section surfaces were acquired without preparation using a Nicolet 5700 FTIR spectrometer and Continuum microscope using an ATR accessory with germanium crystal. Samples were analysed in reflectance mode.

2.6.4 Synchrotron Fourier transform infrared microspectroscopy (SR-μFTIR)

Selected samples were prepared for measurements at the Infrared Microspectroscopy beamline at the Australian Synchrotron. The beamline is equipped with a Bruker Hyperion 2000 microscope with a liquid nitrogen-cooled narrow-band MCT detector coupled to a Vertex V80v FTIR spectrometer. The samples were analysed following custom-defined grid points, saved as 2D IR map files. Data collection and analysis were done using Bruker Opus software. Spectra are the sum of 32 co-added scans at a resolution of 4 cm^{-1} for both sample and background measurements, collected over wavenumber range 3800-750 cm^{-1}. Chemical maps show absorbance intensity as a function of an integrated area under a spectral band defined by the two frequency points after subtraction of the local baseline defined by the same two points.

Thin-sections were placed on a single 1 mm diamond window of a ThermoFisher (Waltham, MA, USA) microcompression cell and flattened using a stainless steel roller to ensure contact. The samples were analysed in transmission mode using 5x5 μm^2 apertures and 5 μm steps following custom-defined grid points (typically a band spanning top to bottom through each sample).

Spectra from the surface of embedded cross-sections were acquired using a 250 μm tip germanium crystal ATR (Attenuated Total Reflection) accessory. Cross sections were positioned using a custom sample holder to ensure a horizontal surface presentation and analysed using 20x20 μm^2 apertures and 10 or 20 μm steps which due to the high refractive index of Ge (n=4) corresponds to 5x5 μm^2 aperture and 2.5 or 5 μm steps on the sample.

2.6.5 Scanning electron microscopy (SEM)

Embedded cross-sections of selected paints were carbon coated using a JEOL JEE-4X vacuum evaporator to enable scanning electron microscopy imaging with energy dispersive X-ray analysis (EDX) using either a Philips LaB6 XL30 or JEOL JSM-6460 LA thermionic emission scanning electron microscope. Both EDX spectrometers used SiLi crystals with approximate resolution of 130 eV, polymer light element windows and matrix-correction software (Phoenix V3.10 or JEOL Analysis Station V3.8). Samples were examined in high-vacuum mode at 16-20 kV accelerating voltage. Backscatter electron images were captured. EDX of points of interest on the specimen were acquired in spot mode. Larger regions of the sample were full-spectrum X-ray mapped to elucidate elemental distribution.

2.6.6 Raman spectroscopy

Raman spectroscopy of paint samples was undertaken using a Renishaw inVia Raman Microscope. The microscope is a Leica DM2500M with 50X reflected light illuminated objectives, and a trinocular head with colour video camera. A Renishaw near infrared diode laser at 785 nm with 300 mW nominal power at the source was calibrated on a silicon standard. The spatial resolution for the $50\times$ objective is 2 μm. The spectrometer is a near infrared-enhanced, deep depletion charge-couple device (CCD) array detector with 576 x 384 pixels and Peltier cooling, and fitted with 785 nm Rayleigh edge filters and a 1200 lines per mm dispersive grating. Data was collected using Windows-based Raman environment software WiRE version 3.0. Spectra were obtained with extended scans (3200-100 cm^{-1}) and 10 s dwell time at 10% laser power with pin hole inserted.

2.6.7 X-ray microdiffraction (μXRD)

XRD microdiffraction was conducted using a Bruker GADDS (General Area Diffraction Detector System), utilising CuKα radiation from a conventional long fine focus tube operating at 40 mA, 40 kV. The emergent beam was focussed with crossed mirror optics to a fine, parallel high-brilliance source and directed through collimating pinholes to the surface of the embedded paint cross-section. The point of incidence of the beam on the sample surface was monitored by a carefully aligned optical video microscope component. The detector is a Bruker "Hi-Star" area detector, which enables a segment of approximately 40° of the diffracted Debye cones to be sampled. By integration around these sampled segments, the counting statistics are significantly improved over a spot or linear arc detector. Crystalline phases in the recorded diffraction patterns were identified using Bruker EVA software, along with the ICDD Powder Diffraction File database.

Initial measurements indicated that, even with significantly long counting times, the use of a 50 μm collimated beam gave extremely poor counting statistics, with very low signal to background ratios. Thus all measurements were made using a collimated beam of 100 μm diameter. Counting times varied to a maximum of 2400 s for each recorded spot.

In addition to single spot analyses, the instrument was used for two linear maps along the length of the sample. In each case the starting and finishing points were in the embedding medium beyond the paint sample, and a total of 18 equi-spaced patterns were measured. The spacing between each measurement was 50 μm (0.05 mm) which gave an overlap of 50 μm in measured patterns (i.e. the collimator size was 100 μm).

2.7   References

Akanni MS, Okoh EK, Burrows HD, Ellis HA (1992) The thermal behaviour of divalent and higher valent metal soaps: a review. *Thermochim Acta* 208:1-41

Barba C, san Andrés M, Peinado J, Báez MI, Baldonedo JL (1995) A note on the characterization of paint layers by transmission electron microscopy. *Stud Conserv* 40:194-200

Barman S, Vasudevan S (2006a) Contrasting Melting Behavior of Zinc Stearate and Zinc Oleate. *The Journal of Physical Chemistry B* 110 (2):651-654. doi:10.1021/jp055814m

Barman S, Vasudevan S (2006b) Melting of Saturated Fatty Acid Zinc Soaps. *The Journal of Physical Chemistry B* 110 (45):22407-22414. doi:10.1021/jp064306p

Barman S, Vasudevan S (2007) Mixed Saturated-Unsaturated Alkyl-Chain Assemblies: Solid Solutions of Zinc Stearate and Zinc Oleate. *The Journal of Physical Chemistry B* 111 (19):5212-5217. doi:10.1021/jp068675x

Boon J, Keune K, Learner T (2002a) Identification of pigments and media from a paint cross-section by direct mass spectrometric and microspectrometric techniques In: Vontobel R (ed) *Preprints of the ICOM Committee for Conservation 13th Triennial Meeting*, Rio de Janeiro, 2002. James and James, London, pp 223-230

Boon J, Keune K, Zucker J (2005) Imaging analytical studies of lead soaps aggregating in preprimed canvas used by the Hudson River School painter F.E. Church. *Microsc Microanal* 11 (Supplement 2):444-445

Boon J, van der Weerd K, Keune K, Noble P, Wadum J (2002b) Mechanical and chemical changes in Old Master paintings: dissolution, metal soap formation and remineralization processes in lead pigmented ground/intermediate paint layers of 17th century paintings. In: Vontobel R (ed) *Preprints of the ICOM Committee for Conservation 13th Triennial Meeting*, Rio de Janeiro, 2002. James and James, London, pp 401-406

Boon JJ, Hoogland F, Keune K (2007) Chemical processes in aged oil paints affecting metal soap migration and aggregation. In: Mar Parkin H (ed) *AIC Paintings Specialty Group Postprints*, Providence, Rhode Island, 16-19 June 2006. AIC, pp 16-23

Boon JJ, van der Horst J (2008) Remarkably improved spatial resolution in SEM images of paint cross-sections after argon ion polishing. In: Townsend J, Doherty T, Heydenreich G (eds) *Preparation for painting: the artist's choice and its consequences*, London, 2007. Archetype Books, pp 42-49

Carlyle L, Witlox M (2005) Historically accurate reconstructions of artists' oil painting materials. In: Clarke M, Townsend J, Stijnman A (eds) *Art of the past: sources and reconstructions. Proceedings of the first symposium of the Art Technolgical Source Research study group*, Amsterdam, 2004. Archteype Publications Ltd, London, pp 53-59

Casadio F, Xie S, Rukes S, Myers B, Gray K, Warta R, Fiedler I (2011) Electron energy loss spectroscopy elucidates the elusive darkening of zinc potassium chromate in Georges Seurat's 'A Sunday on La Grande Jatte-1884'. *Anal Bioanal Chem* 399 (9):2909-2920. doi:10.1007/s00216-010-4264-9

Clegg W, Little IR, Straughan BP (1988) Zinc carboxylate complexes: structural characterization of the mixed-metal linear trinuclear complexes $MZn_2(crot)_6(base)_2$ (M = Mn, Co, Ni, Zn, Cd, Mg, Ca, Sr; $crot^-$ = crotonate(1-); base = quinoline, 6-methylquinoline). *Inorg Chem* 27 (11):1916-1923. doi:10.1021/ic00284a020

Colombini A, Grauby O (2011) Morpholgy and chemical investigations of zinc soaps by scanning electron microscopy and transmission electron microscopy: case study of Picasso paintings. In: *From Can to Canvas. Early uses of housepaint by Picasso and his contemporaries in the first half of the 20th century (poster session)*, Marseille and Antibes, 25-27 May 2011.

Corbeil MC, Robinet L (2002) X-ray powder diffraction data for selected metal soaps. *Powder Diffr* 17 (1):52-60. doi:10.1154/1.1431950

Corkery RW (1998) *Artificial biomineralisation and metallic soaps*. PhD thesis, Australian National University, Canberra

Corkery RW (2004) A variation on Luzzati's soap phases. Room temperature thermotropic liquid crystals. *PCCP* 6:1534-1546. doi:10.1039/B315595C

Corkery RW (2008) Metal organic framework (MOF) liquid crystals. 1D, 2D and 3D ionic coordination polymer structures in the thermotropic mesophases of metal soaps, including alkaline earth, transition metal and lanthanide soaps. *Current Opinion in Colloid and Interface Science* 13:288-302

Cotte M, Checroun E, Mazel V, Sole VA, Richardin P, Taniguchi Y, Walter P, Susini J (2009) Combination of FTIR and X-rays synchrotron-based micro-imaging techniques for the study of ancient paintings. A practical point of view. *e-Preservation Science* 6:1-9

Cotte M, Checroun E, Susini J, Walter P (2007) Micro-analytical study of interactions between oil and lead compounds in paintings. *Appl Phys A* 89:841-848. doi:10.1007/s00339-007-4213-4

Derrick M, Douza L, Kieslich T, Florsheim H, Stulik D (1994a) Embedding paint cross-section samples in polyester resins: problems and solutions *Journal of the American Institute for Conservation* 33:227-245

Derrick M, Stulik D, Landry J (1999) *Infrared spectroscopy in conservation science* The Getty Conservation Institute Los Angeles

Derrick MR, Doehne EF, Parker AE, Stulik DC (1994b) Some new analytical techniques for use in conservation. *Journal of the American Institute for Conservation* 33 (2):171-184

Erhardt D, Tumosa CS, Mecklenburg MF (2005) Long-term chemical and physical processes in oil paint films. *Stud Conserv* 50 (2):143-150

Faubel W, Simon R, Heissler S, Friedrich F, Weidler PG, Becker H, Schmidt W (2011) Protrusions in a painting by Max Beckmann examined with confocal µ-XRF. *J Anal At Spectrom* 26 (5). doi:10.1039/C0JA00178C

Ferreira ESB, Boon JJ, Stampanoni M, Marone F (2011) Study of the mechanism of formation of calcium soaps in an early 20th-century easel painting with correlative 2D and 3D microscopy. In: Bridgland J, Antomarchi C (eds) *Preprints of the ICOM Committee for Conservation 16th Triennial Conference*, Lisbon, 2011. ICOM-CC p1604

Goodall RA, Hall J, Sharer RJ, Traxler L, Rintoul L, Fredericks PM (2008) Micro-Attenuated Total Reflection Spectral Imaging in Archaeology: Application to Maya Paint and Plaster Wall Decorations. *Appl Spectrosc* 62 (1):10-16

Greathouse JA, Johnson KL, Greenwell HC (2014) Interaction of natural organic matter with layered minerals: recent developments in computational methods at the nanoscale. *Minerals* 4 (2):519-540. doi:10.3390/min4020519

Haswell R, Zeile U, Mensch K (2008) Van Gogh's painting grounds: an examination of barium sulphate extender using analytical electron microscopy – SEM/FIB/TEM/EDX. *Microchimica Acta* 161 (3):363-369

Heeren R, Boon J, Noble P, Wadum J (1999) Integrating imaging FTIR and secondary ion mass spectrometry for the analysis of embedded paint cross-sections In: Bridgland J, Brown J (eds) *Preprints of the ICOM Committee for Conservation 12th Triennial Meeting* Lyon, 1999. James and James, London, pp 228-233

Heeren R, van der Weerd J, Boon J (2000) FTIR imaging spectroscopy for organic surface analysis of embedded paint cross-sections In: Fotakis C, Papazoglou TG, Kalpouzos C (eds) *Optics and lasers in biomedicine and culture: contributions to the Fifth International Conference on Optics within Life Sciences*, 1998. Springer, pp 179-182

Helwig K, Poulin J, Corbeil M-C, Moffatt E, Duguay D (2014) Conservation issues in several 20th-century Canadian oil paintings: the role of zinc carboxylate reaction products. In: van den Berg KJ, Burnstock A, de Tagle M et al. (eds) *Issues in Contemporary Oil Paint*. Springer International Publishing, Switzerland, p Chapter 11. In press. doi:10.1007/978-3-319-10100-2__11

Hermans JJ, Iedema PD (2014) Comment on the paper "Odd–even alternation in a homologous series of Zn(II) n-alkanoates" by P.N. Nelson, H.A. Ellis and R.A. Taylor [J. Mol. Struc. 986 (2011) 10–15]. *J Mol Struct* 1070 (0):43-44. doi:http://dx.doi.org/10.1016/j.molstruc.2014.04.026

Higgitt C, Spring M, Saunders D (2003) Pigment-medium interactions in oil paint films containing red lead or lead-tin yellow. *National Gallery Technical Bulletin* 24:75-95

Hochleitner B, Schreiner M, Drakopoulos M, Snigireva I, Snigirev A (2003) Analysis of paint layers by light microscopy, scanning electron microscopy and synchrotron induced X-ray micro-diffraction. In: *Proceedings of Art 2002*, Antwerp, Belgium, 2-6 June 2002.

Ishioka T, Maeda K, Watanabe I, Kawauchi S, Harada M (2000) Infrared and XAFS study on structure and transition behaviour of zinc stearate. *Spectrochimica Acta Part A* 56:1731-1737

Jacobsen AE, Gardner WH (1941) Zinc soaps in paints: zinc oleates. *Ind Eng Chem* 33 (10):1254-1256

Joseph E, Prati S, Sciutto G, Ioele M, Santopadre P, Mazzeo R (2010a) Performance evaluation of mapping and linear imaging FTIR microspectroscopy for the characterisation of paint cross sections. *Anal Bioanal Chem* 396 (2):899-910. doi:10.1007/s00216-009-3269-8

Joseph E, Ricci C, Kazarian SG, Mazzeo R, Prati S, Ioele M (2010b) Macro-ATR-FT-IR spectroscopic imaging analysis of paint cross-sections. *Vib Spectrosc* 53 (2):274-278

Keune K (2005) *Binding medium, pigments and metal soaps characterised and localised in paint cross-sections*. PhD thesis, University of Amsterdam, Amsterdam

Keune K, Boon JJ (2004) Imaging secondary ion mass spectrometry of a paint cross section taken from an early Netherlandish painting by Rogier van der Weyden. *Anal Chem* 76 (5):1374-1385. doi:10.1021/ac035201a

Keune K, Boon JJ (2007) Analytical imaging studies of cross-sections of paintings affected by lead soap aggregate formation. *Stud Conserv* 52 (3):161-176

Keune K, Hoogland F, Boon JJ, Peggie D, Higgitt C (2008) Comparative study of the effect of traditional pigments on artificially aged paint systems using complementary analytical techniques. In: Bridgland J (ed) *Preprints of the ICOM Committee for Conservation 15th Triennial Meeting* New Delhi, 2008. Allied Publishers Pvt Ltd, New Delhi, pp 833-842

Keune K, Hoogland F, Boon JJ, Peggie D, Higgitt C (2009) Evaluation of the "added value" of SIMS: A mass spectrometric and spectroscopic study of an unusual Naples yellow oil paint reconstruction. *Int J Mass spectrom* 284 (1-3):22-34. doi:10.1016/j.ijms.2008.10.016

Keune K, van Loon A, Boon JJ (2011) SEM Backscattered-Electron Images of Paint Cross Sections as Information Source for the Presence of the Lead White Pigment and Lead-Related Degradation and Migration Phenomena in Oil Paintings. *Microsc Microanal* 17 (05):696-701. doi:10.1017/S1431927610094444

Khandekar N (2003) Preparation of cross-sections from easel paintings *Reviews in Conservation* 4:52-64

Langley A, Burnstock A (1999) The analysis of layered paint samples from moden paintings using FTIR microscopy. In: Bridgland J, Brown J (eds) *Preprints of the ICOM Committee for Conservation 12th Triennial Meeting*, Lyon, 1999. James and James, London, pp 234-241

Li C, Zhao B, Lu Y, Liang Y (2001) Microstructure and Ion Exchange in Stearic Acid Langmuir–Blodgett Films Studied by Fourier Transform Infrared-Attenuated Total Reflection Spectroscopy. *J Colloid Interface Sci* 235 (1):59-65. doi:10.1006/jcis.2000.7343

Lluveras-Tenorio A, Andreotti A, Bonaduce I, Boularand S, Cotte M, Roqué J, Colombini MP, Vendrell-Saz M (2012) Mass Spectrometric and Synchrotron Radiation based techniques for the identification and distribution of painting materials in samples from paints of Josep Maria Sert. *Chemistry Central Journal* 6. doi:http://dx.doi.org/10.1186/1752-153X-6-45

Maines CA, Rogala D, Lake S, Mecklenburg MF (2011) Deterioration in Abstract Expressionist paintings: analysis of zinc oxide paint layers in works from the collection of the Hirshhorn Museum and Sculpture Garden, Smithsonian Institution. *Materials Research Society Proceedings* 1319:275-284. doi:10.1557/opl.2011.733

Mallégol J, Gardette J-L, Lemaire J (1999) Long-term behavior of oil-based varnishes and paints I. Spectroscopic analysis of curing drying oils. *J Am Oil Chem Soc* 76 (8):967-976. doi:10.1007/s11746-999-0114-3

Marques EF, Burrows HD, da Graça Miguel M (1998) The structure and thermal behaviour of some long chain cerium carboxylates. *Journal of the Chemical Society, Faraday Transactions* 94 (12):1729-1736

Marshbanks TL, Ahn DJ, Franses EI (1994) Transport and ion exchange in Langmuir-Blodgett films: water transport and film microstructure by attenuated total reflectance Fourier transform infrared spectroscopy. *Langmuir* 10 (1):276-285. doi:10.1021/la00013a041

Martin de Fonjaudran C, Nevin A, Piqué F, Cather S (2008) Stratigraphic analysis of organic materials in wall painting samples using micro-FTIR attenuated total reflectance and a novel sample preparation technique. *Anal Bioanal Chem* 392 (1):77-86. doi:10.1007/s00216-008-2111-z

Mazzeo R, Joseph E, Prati S, Millemaggi A (2007) Attenuated total reflection-fourier transform infrared microspectroscopic mapping for the characterisation of paint cross-sections. *Anal Chim Acta* 599 (1):107-117. doi:10.1016/j.aca.2007.07.076

Mazzeo R, Prati S, Quaranta M, Joseph E, Kendix E, Galeotti M (2008) Attenuated total reflection micro FTIR characterisation of pigment-binder interaction in reconstructed paint films. *Anal Bioanal Chem* 392 (1-2):65-76. doi:10.1007/s00216-008-2126-5

Mehrotra KN, Shukla RK, Chauhan M (1995) Spectroscopic and Conductometric Studies of Lanthanide Soaps. *Bull Chem Soc Jpn* 68 (7):1825-1831

Meilunas R, Bentsen J, Steinberg A (1990) Analysis of aged paint binders by FTIR spectroscopy. *Stud Conserv* 35:33-51

Mesubi MA (1982) An infrared study of zinc, cadmium, and lead salts of some fatty acids. *J Mol Struct* 81:61-71

Mills JS (1966) The gas chromatographic examination of paint media. Part I. Fatty acid composition and identification of dried oil films. *Stud Conserv* 11:92-107

Monico L, Van der Snickt G, Janssens K, De Nolf W, Miliani C, Dik J, Radepont M, Hendriks E, Geldof M, Cotte M (2011a) Degradation Process of Lead Chromate in Paintings by Vincent van Gogh Studied by Means of Synchrotron X-ray Spectromicroscopy and Related Methods. 2. Original Paint Layer Samples. *Anal Chem* 83 (4):1224-1231. doi:10.1021/ac1025122

Monico L, Van der Snickt G, Janssens K, De Nolf W, Miliani C, Verbeeck J, Tian H, Tan H, Dik J, Radepont M, Cotte M (2011b) Degradation Process of Lead Chromate in Paintings by Vincent van Gogh Studied by Means of Synchrotron X-ray Spectromicroscopy and Related Methods. 1. Artificially Aged Model Samples. *Anal Chem* 83 (4):1214-1223. doi:10.1021/ac102424h

Morley-Smith CT (1958) Zinc oxide - a reactive pigment. *Journal of the Oil & Colour Chemists' Association* 41 (January):85-97

Mulvihill E (2012) *Analysing paint cross-sections with FTIR microspectroscopy: developing alternative sample preparation methodologies*. Minor Thesis, Master of Cultural Material Conservation, University of Melbourne, Melbourne

Nelson PN, Ellis HA, Taylor RA (2011) Odd–even alternation in a homologous series of Zn (II) n-alkanoates. *J Mol Struct* 986 (1–3):10-15. doi:http://dx.doi.org/10.1016/j.molstruc.2010.11.014

Nelson SM, Pink RC (1952) 322. Solutions of metal soaps in organic solvents. Part III. The aggregation of metal soaps in toluene, isobutyl alcohol, and pyridine. *Journal of the Chemical Society (Resumed)*:1744-1750

Noble P, van Loon A, Boon JJ (2005) Chemical changes in old master paintings II: darkening due to increased transparency as a result of metal soap formation. In: Verger I (ed) *Preprints of the ICOM Committee for Conservation 14th Triennial meeting*, The Hague, 12-16 September 2005. James and James, London, pp 496-503

Ordonez E, Twilley J (1997) Clarifying the haze: efflorescence on works of art in WAAC Newsletter 20(1) 11pp reproduced from *Anal Chem* 69 (13):A416-A422

Otero V, Sanches D, Montagner C, Vilarigues M, Carlyle L, Lopes JA, Melo MJ (2014) Characterisation of metal carboxylates by Raman and infrared spectroscopy in works of art. *Journal of Raman Spectroscopy*:n/a-n/a. doi:10.1002/jrs.4520

Pilc J, White R (1995) The application of FTIR-microscopy to the analysis of paint binders in easel paintings *National Gallery Technical Bulletin* 16:73-84

Pilpel N (1963) Properties of Organic Solutions of Heavy Metal Soaps. *Chem Rev* 63 (3):221-234. doi:10.1021/cr60223a001

Plater MJ, De Silva B, Gelbrich T, Hursthouse MB, Higgitt CL, Saunders DR (2003) The characterisation of lead fatty acid soaps in 'protrusions' in aged traditional oil paint. *Polyhedron* 22 (24):3171-3179. doi:10.1016/s0277-5387(03)00461-3

Pouyet E, Lluveras-Tenorio A, Nevin A, Saviello D, Sette F, Cotte M (2014) Preparation of thin-sections of painting fragments: Classical and innovative strategies. *Anal Chim Acta* 822 (0):51-59. doi:http://dx.doi.org/10.1016/j.aca.2014.03.025

Prati S, Rosi F, Sciutto G, Mazzeo R, Magrini D, Sotiropoulou S, Van Bos M (2012) Evaluation of the effect of six different paint cross section preparation methods on the performances of Fourier Transformed Infrared microscopy in attenuated total reflection mode. *Microchem J* 103 (0):79-89. doi:http://dx.doi.org/10.1016/j.microc.2012.01.007

Prati S, Sciutto G, Catelli E, Ashashina A, Mazzeo R (2013) Development of innovative embedding procedures for the analyses of paint cross sections in ATR FITR microscopy. *Anal Bioanal Chem* 405 (2-3):895-905. doi:10.1007/s00216-012-6435-3

Rizzo A (2008) Progress in the application of ATR-FTIR microscopy to the study of multi-layered cross-sections from works of art. *Anal Bioanal Chem* 392 (1):47-55. doi:10.1007/s00216-008-2064-2

Robinet L, Corbeil MC (2003) The characterization of metal soaps. *Stud Conserv* 48 (1):23-40

Rogala D, Lake S, Maines C, Mecklenburg M (2010) Condition problems related to zinc oxide underlayers: examination of selected Abstract Expressionist paintings from the collection of the

Hirschhorn Museum and Sculpture Garden, Smithsonian Institution. *Journal of the American Institute for Conservation* 49 (2):96-113

Sakai H, Umemura J (2002) Evaluation of molecular structure in Langmuir monolayers of zinc stearate and zinc 12-hydroxystearate by IR external reflection spectroscopy. *Colloid Polym Sci* 280 (4):316-321. doi:10.1007/s003960100581

Sanyova J, Cersoy S, Richardin P, LapreÌ•vote O, Walter P, Brunelle A (2011) Unexpected Materials in a Rembrandt Painting Characterized by High Spatial Resolution Cluster-TOF-SIMS Imaging. *Anal Chem* 83 (3):753-760. doi:10.1021/ac1017748

Schilling MR, Khanjian H, P. (1996) Gas chromatographic determination of the fatty acid and glycerol content of lipids I. The effects of pigments and aging on the composition of oil paints. In: Bridgland J (ed) *Preprints of the ICOM Committee for Conservation 11th Triennial meeting*, Edinburgh, Scotland. James and James, London, pp 220-227

Simon-Kutscher J, Gericke A, Hühnerfuss H (1996) Effect of bivalent Ba, Cu, Ni, and Zn cations on the structure of octadecanoic acid monolayers at the air-water interface as determined by external Infrared reflection-absorption spectroscopy. *Langmuir* 12 (4):1027-1034. doi:10.1021/la950731q

Sloggett R, Kyi C, Tse N, Tobin MJ, Puskar L, Best SP (2010) Microanalysis of artworks: IR microspectroscopy of paint cross-sections. *Vib Spectrosc* 53 (1):77-82

Smith G (2003) Infrared microspectroscopy using a synchrotron source for arts-science research *Journal of the American Institute for Conservation* 42:399-406

Spring M, Ricci C, Peggie D, Kazarian S (2008) ATR-FTIR imaging for the analysis of organic materials in paint cross sections: case studies on paint samples from the National Gallery, London. *Anal Bioanal Chem* 392 (1):37-45. doi:10.1007/s00216-008-2092-y

Taylor RA, Ellis HA (2007) Room temperature molecular and lattice structures of a homologous series of anhydrous zinc(II) n-alkanoate. *Spectrochimica Acta Part A: Molecular and Biomolecular Spectroscopy* 68 (1):99-107. doi:http://dx.doi.org/10.1016/j.saa.2006.11.007

Townsend JH, Keune K (2006) Microscopical techniques applied to traditional paintings. *infocus: Magazine of the Royal Microscopical Society* 1 (March):53-65

Tsang J, Cunningham R (1991) Some improvements in the study of cross sections. *Journal of the American Institute for Conservation* 30 (2):163-177

Tumosa CS (2001) A brief history of aluminum stearate as a component of paint. *WAAC Newsletter* 23 (3)

Tumosa CS, Erhardt D, Mecklenburg MF, Su X (2005) Linseed oil paint as ionomer: synthesis and characterization. In: Vandiver PB (ed) *Materials issues in art and archaeology VII*, Boston, Massachusetts, 2004. Materials Research Society, pp 25-31

van den Berg J, van den Berg K, Boon J (1999) Chemical changes in curing and ageing oil paints. In: Bridgland J (ed) *Preprints of the ICOM Committee for Conservation 12th Triennial Meeting, Lyon*. pp 248-253

van den Berg JDJ, van den Burg KJ, Boon JJ (2001) Determination of the degree of hydrolysis of oil paint using a two-step derivatisation method and on-column GC/MS. *Prog Org Coat* 41:143-155

van den Berg JJD (2002) *Analytical chemical studies on traditional linseed oil paints*. PhD thesis, University of Amsterdam, Amsterdam

van der Kerk GJM (1972) Organozinc coordination chemistry and catalytic effects of organozinc coordination compounds. *Pure Appl Chem* 30 (3-4):389-408. doi:10.1351/pac197230030389

van der Snickt G, Dik J, Cotte M, Janssens K, Jaroszewicz J, de Nolf W, Groenewegen J, van der Loeff L (2009) Characterization of a degraded cadmium yellow (CdS) pigment in an oil painting by means of synchrotron radiation based X-ray techniques. *Anal Chem* 81 (7):2600-2610. doi:10.1021/ac802518z

van der Weerd J, Boon JJ, Gelddof M, Heeren RMA, Noble P (2002a) Chemical changes in old master paintings: dissolution, metal soap formation and remineralisation processes in lead pigmented paint layers of 17th century paintings. *Zeitschrift für Kunsttechnologie und Konservierung* 16:36-51

van der Weerd J, Brammer H, Boon JJ, Heeren RMA (2002b) Fourier Transform Infrared Microscopic Imaging of an Embedded Paint Cross-Section. *Appl Spectrosc* 56 (3):275-283

van der Weerd J, Gelddof M, van der Loeff LS, Heeren R, Boon J (2003) Zinc soap aggregate formation in 'Falling leaves (Les Alyscamps)' by Vincent van Gogh *Zeitschrift für Kunsttechnologie und Konservierung* 17 (2):407-416

van der Weerd J, Heeren RMA, Boon JJ (2004) Preparation methods and accessories for the infrared spectroscopic analysis of multi-layer paint films. *Stud Conserv* 49:193-210

van der Weerd J, van Loon A, Boon JJ (2005) FTIR studies of the effects of pigments on the aging of oil. *Stud Conserv* 50 (1):3-22

van Loon A (2008) *Color changes and chemical reactivity in seventeenth century oil paintings*. PhD thesis, University of Amsterdam, Amsterdam

Verhoeven MA, Carlyle L, Reeddijk J, Haasnoot JG (2006) Exploring the application of solid-state Nuclear Magnetic Resonance to the study of the deterioration of paintings. In: Boon JJ, Ferreira ESB (eds) *Reporting highlights of the De Mayerne Programme*. Netherlands Organisation for Scientific Research (NWO), The Hague, pp 34-42

Ware EE, Christman RE (1916) A study of the effect of storage on mixed paints. *Ind Eng Chem* 8 (10):879-883

3 Reference paint film draw-downs: surface and cross sectional investigation of metal stearate distributions in modern artists' oil paints

3.1 Abstract

Zinc oxide is a prevalent industrial age pigment which readily reacts with fatty acids in oil-based paints to form zinc carboxylates. Zinc stearate aggregates are associated with deterioration in late nineteenth and twentieth century paintings. The current study investigates metal carboxylate composition within naturally aged artists' oil paints and reference paint film draw-downs using optical and scanning electron microscopy, conventional attenuated total reflectance and synchrotron transmission Fourier transform infrared spectroscopy. The paints contain zinc oxide alone or in combination with lead white, titanium white and within Naples yellow hue formulations, and are prepared with linseed, safflower and soybean oils with and without addition of aluminium stearate. Attenuated total reflectance-FTIR using the conventional source identifies marked differences in carboxylate profiles between exposed and protected surfaces in a significant number of samples. Scanning electron microscopy of paint cross-sections reveals morphological variation enabling distinction between aluminium stearate present as an additive and zinc stearate which has formed *in situ*. Reduced particle density and atomic brightness is associated with saponification. Synchrotron FTIR microspectroscopy of thin paint cross-sections maps metal carboxylate distributions at high spatial resolution and resolves broad concentration gradients and micron scale phase separation of carboxylate species. Aluminium stearate is found to influence the formation and distribution of zinc carboxylates more strongly than pigment composition or oil type. Preliminary results suggest hydrogenated castor oil has a similar effect. Soybean and linseed oil paints are more reactive than safflower. Zinc stearate concentration is linked to the amount of zinc oxide present, but the distribution pattern is consistent; higher concentrations of saturated C_{16} and C_{18} chain zinc carboxylates occur in the margin of the paint film closest to the polyester substrate. The presence of aluminium stearate in association with zinc oxide has a clear influence on zinc carboxylate formation, with potential implications for long term stability of vulnerable paintings.

A substantial body of work in this chapter has been published and two papers are included as sections 3.2 and 3.3:

Osmond G, Boon JJ, Puskar L, Drennan J. 2012. Metal stearate distributions in modern artists' oil paints: surface and cross-sectional investigation of reference paint films using conventional and synchrotron infrared microspectroscopy. *Applied spectroscopy*, 66(10): 1136-1144.

My contributions to the paper include experiment design, analysis of samples, data interpretation, pattern recognition and preparation of the manuscript and figures, refined in conjunction with contributing authors. JJ Boon assisted with interpretation of data, L Puskar assisted with acquisition and reporting of synchrotron data, and J Drennan was responsible for supervision and critical review of the text.

Additional content is published as Chapter 18 within a peer reviewed book of conference proceedings, a paper which incorporates results from both the current and following chapter (Model system):

Osmond G 2014. Zinc white and the influence of paint composition for stability in oil-based media In: van den Berg KJ, Burnstock A, de Tagle M et al. (eds) *Issues in contemporary oil paint*. Springer International Publishing pp 263-281.

In addition to publications this chapter presents supplementary data which relates findings to an expanded range of reference paint samples. Emphasis is placed on the significance of SEM imaging and elemental analysis in support of vibrational spectroscopic data forming the basis of published material.

3.2   Introduction

Analysis and interpretation of deterioration phenomena in paintings is complicated by the large range of variables unique to each piece. Artist technique, paint composition, age, environmental history and conservation interventions each have potential to substantially influence paint film chemistry. A further difficulty for investigation of significant works of art is the extremely limited capacity for sampling and the priority for applying non-destructive analytical techniques. Study of reference paint films offers an opportunity to examine specific aspects of paint ageing with less restriction on sample material and fewer variables than unique works of art. There is also scope for potential analytical techniques to be trialled and refined on multiple relatively reproducable samples which have structural and chemical similarities to unique samples from paintings.

Film age is a perennial issue for any paint reconstruction; accelerated ageing techniques are widely applied to enable testing of reference material within reasonable timeframes but results remain tempered by the possibility deterioration pathways do not accurately represent those occurring longer term under ambient conditions. Fortunately for the present research it was possible to access naturally aged reference paint formulations of direct relevance from the Smithsonian Museum Conservation Institute (SMCI) reference paint collection. Initiated by Senior Conservation Scientist,

Dr Marion Mecklenburg, paint films were prepared between 1978 and 1999 and have been stored under stable, interior ambient conditions. The collection includes cast films of a range of commercially available artists' paints in addition to custom produced control paints prepared using specified pigment and oil combinations. A range of paint samples in which zinc oxide is present either as a primary or secondary pigment was generously made available.

In addition to reference paints combining zinc oxide with the widely used lead and titanium white pigments and in coloured formulations, the SMCI reference collection also represents paints produced with different oils and frequently used additives. These control paints allow for useful correlation with the relatively complex formulations of commercially produced paints also contained in the collection. Represented oils include variations of linseed oil - the drying oil most frequently used in traditional oil paint - and the semi-drying safflower and soybean oils. Safflower oil is preferred over linseed in modern white paint formulations because of its lesser tendency to yellow. Soybean oil has been widely used in paint manufacture since the 1930s in the United States and in the United Kingdom by the 1960s, initially as an adulterant with linseed oil, and later as an important oil for alkyd paint production (Standeven 2011). All remain in current usage.

Metal soaps as original components in paints are of particular interest in terms of the present study. Aluminium stearate became a common rheology modifier during the 20th century, and continues to be used in paint formulations along with stearates of other metals including zinc. Aluminium stearate is the metal soap represented in SMCI control paint formulations, its metal ion and characteristic FTIR absorption conveniently enabling a distinction between stearates intentionally added to the paint and those of zinc which form *in situ* via reaction between zinc oxide pigment and fatty acids deriving from the triglyceride based oil medium.

This chapter involves a detailed study of paint films which differ only with respect to pigment composition in association with zinc oxide, oil type, the presence of specific additives, commercial origin or casting date. FTIR is used in conjunction with optical microscopy and scanning electron microscopy with energy dispersive X-ray analysis to investigate oil-based artists' commercial and custom made reference paints containing zinc oxide to determine any link between compositional factors and zinc carboxylate distributions. Attenuated total reflectance (ATR)-FTIR measurement mode is used to investigate the carboxylate profiles of both exposed and protected surfaces of the paints. Additionally, metal stearate distributions within selected paint films are resolved with cross-sectional mapping acquired via synchrotron FTIR microspectroscopy (SR-μFTIR). The paints investigated are detailed in Table 3.1.

Table 3.1 Reference paints with composition as specified by manufacturers with additional pigmentation determined using optical microscopy, FTIR and SEM-EDX (italicised).

Square brackets indicate minor/trace amounts. Ratios indicate relative proportion by weight of zinc oxide to other pigments combined where known

Paint Manufacturer/ Product name/ Date of film casting	Composition Pigment	Oil, additive	Cross-section analysis
Zinc whites linseed-based			
Grumbacher Zinc white 1978	Zinc oxide	Linseed alkali refined + aluminium stearate	SEM-EDX SR-µFTIR
Custom control *Zinc white* 1998	Zinc oxide	Linseed + Al stearate	SEM-EDX SR-µFTIR
Custom control *Zinc white* 1990	Zinc oxide	Linseed boiled	
Custom control *Zinc white* 1990	Zinc oxide	Linseed cold pressed	SEM-EDX SR-µFTIR
Custom control *Zinc white* 1990	Zinc oxide	Linseed with litharge	
Zinc whites safflower-based			
Winsor and Newton Zinc white 1978	Zinc oxide	Safflower	SEM-EDX SR-µFTIR
Custom control *Zinc white* 1998	Zinc oxide	Safflower alkali refined + Al stearate	SEM-EDX SR-µFTIR
Zinc whites soybean-based			
Custom control *Zinc white* 1998	Zinc oxide	Soya modified + Al stearate	SEM-EDX SR-µFTIR
Titanium whites linseed-based			
Grumbacher Titanium white 1978	Titanium dioxide, zinc oxide 1:2; *[Al-silicate]*	Linseed alkali refined + Al stearate	SEM-EDX SR-µFTIR
Grumbacher Titanium white 1999	Titanium dioxide, zinc oxide; *Ca*	Linseed alkali refined + *Al stearate*	SEM-EDX
Custom control *Titanium white* 1998	Titanium dioxide, zinc oxide 12:1, Al silicate	Linseed + Al stearate	SEM-EDX SR-µFTIR

Colorlab Titanium white 1981	Titanium dioxide, zinc oxide, barium sulfate 5:1:10; *[Al, S, Cl]*	Linseed + Al stearate	SEM-EDX
Gamblin Titanium white 1999	Titanium dioxide, zinc oxide; *CaCO$_3$, [Al silicate]*	Linseed alkali refined	SEM-EDX

Titanium whites safflower-based

Winsor and Newton Titanium white 1978	Titanium dioxide, [barium sulfate]; *ZnO, dolomite*	Safflower *(+ HCO?)*	SEM-EDX
Colorlab Titanium white 1981	Titanium dioxide, zinc oxide, barium sulfate 5:1:10	Safflower + Al stearate	SEM-EDX SR-µFTIR
Winsor and Newton Titanium dioxide APermanent white 1980	*Titanium dioxide, zinc oxide, BaSO$_4$, MgCO$_3$, [Al, S]*	Safflower	SEM-EDX
Winsor and Newton Titanium white 1999	*TiO$_2$, BaSO$_4$, MgCO$_3$, [ZnO]*	Not specified (safflower assumed)	SEM-EDX
Custom control *Titanium white* 1998	Titanium dioxide, zinc oxide 12:1, Al silicate	Safflower alkali refined + Al stearate	SEM-EDX SR-µFTIR

Titanium whites soybean-based

Speedball *Titanium white* 1981	Titanium dioxide, zinc oxide	Soya + *Al stearate*	SR-µFTIR
Custom control *Titanium white* 1998	Titanium dioxide, zinc oxide 12:1, Al silicate	Soya modified + Al stearate	SR-µFTIR

Lead whites linseed-based

Grumbacher Flake white 1978	Basic lead carbonate, zinc oxide 20:1	Linseed alkali refined + Al stearate	SEM-EDX SR-µFTIR
Grumbacher Flake white 1999	Basic lead carbonate, zinc oxide	Linseed alkali refined + *aluminium stearate*	SEM-EDX

Lead whites safflower-based

Winsor and Newton Flake white 1978	Basic lead carbonate; *zinc oxide, barium sulfate, [Al, C]*	Safflower	SEM-EDX SR-µFTIR
Winsor and Newton Flake white no.1 ASilver white 1980	Basic lead carbonate; *ZnO, Al silicate, CaCO$_3$*	Safflower	SEM-EDX
Winsor and Newton Flake white 1999	*Basic lead carbonate, zinc oxide*	Not specified (safflower assumed)	SEM-EDX

Naples Yellow hue linseed-based

Gamblin Naples yellow hue 1999	cadmium sulfide, natural hydrated iron oxide, red iron oxide, zinc oxide; *Al silicate, chalk, Ti*	Linseed, alkali refined	SEM-EDX
Grumbacher Naples yellow hue 1999	zinc oxide, calcined natural iron oxide, cadmium selenium sulfide, cadmium zinc sulfide co-precipitated with barium sulfate (6:1)	Linseed alkali refined + *Al stearate*	
Winsor and Newton Naples yellow (London oil colour series 2) 1978	Basic lead carbonate, cadmium sulfide, iron oxide; *ZnO, dolomite*	Linseed	SEM-EDX
Winsor and Newton Naples yellow1999	basic lead carbonate, iron oxide, zinc oxide	Not specified (linseed assumed)	SEM-EDX

3.3　Metal stearate distributions in modern artists' oil paints

Metal Stearate Distributions in Modern Artists' Oil Paints: Surface and Cross-Sectional Investigation of Reference Paint Films Using Conventional and Synchrotron Infrared Microspectroscopy

Gillian Osmond,[a,b,*] Jaap J. Boon,[c] Ljiljana Puskar,[d] John Drennan[a]

[a] *Australian Institute for Bioengineering and Nanotechnology, The University of Queensland, Brisbane 4072, Australia*

[b] *Queensland Art Gallery, Centre for Contemporary Art Conservation, South Brisbane 4101, Australia*

[c] *JAAP Enterprise for MOLART Advice, Nieuwendammerdijk 79, 1025LD Amsterdam, The Netherlands*

[d] *Australian Synchrotron, 800 Blackburn Rd, Clayton, Victoria 3168, Australia*

Zinc oxide is a prevalent industrial-age pigment that readily reacts with fatty acids in oil-based paints to form zinc carboxylates. Zinc stearate aggregates are associated with deterioration in late nineteenth and twentieth century paintings. The current study uses both conventional and synchrotron Fourier transform infrared spectroscopy (FT-IR) to investigate metal carboxylate composition in a range of naturally aged artists' oil paints and reference paint film draw-downs. The paints contain zinc oxide alone or in combination with lead white, titanium white, and aluminum stearate and are prepared with linseed and safflower oils. Attenuated total reflectance (ATR)-FT-IR using the conventional source identifies marked differences in carboxylate profiles between exposed and protected surfaces in a large number of samples. Synchrotron FT-IR microspectroscopy of thin paint cross-sections maps metal carboxylate distributions at high spatial resolution and resolves broad concentration gradients and micrometer-scale phase separation of carboxylate species. Aluminum stearate, a common paint additive, is found to influence the distribution of zinc carboxylates more strongly than pigment composition or oil type. The presence of aluminum stearate results in higher concentrations and more pronounced separation of saturated C16 and C18 chain zinc carboxylates in the margin of paint nearest the polyester substrate. The presence of aluminum stearate in association with zinc oxide has a clear influence on zinc carboxylate formation and distribution, with potential implications for long term stability of vulnerable paintings.

Index Headings: Zinc oxide; Zinc stearate; Zinc soap; Aluminum stearate; Metal carboxylate; Fourier transform infrared spectroscopy; FT-IR spectroscopy; Synchrotron; Oil paint; Art conservation.

INTRODUCTION AND BACKGROUND

In the conservation of paintings, metal soaps, notably palmitates and stearates of lead and zinc, have come to attention in recent years as a result of their involvement in serious deterioration of significant paintings.[1–5] The various phenomena responsible for associated structural and optical changes in the paintings all indicate that metal soaps are capable of mobility within the paint after the paint has dried to form a solid film.[6–9] However, understanding of the precise circumstances in which metal carboxylates form, migrate, and aggregate within a painting remains limited, with potentially serious implications for art collections worldwide.

Metal salts of organic acids have a long history of use in oil-based industrial and artist paint formulations to modify production, storage, working, and drying properties.[10,11] Aluminum stearate in particular became a common rheology modifier during the 20th century, effectively increasing the body and suspension properties of the paint via gel formation with the oil, enabling economies in oil and pigment use.[11–14]

Metal soaps may additionally form in situ in the paint via reaction between metal ions deriving from components in the paint, typically pigments, and fatty acids deriving from the triglyceride based oil medium. Zinc oxide is one such reactive pigment. Zinc oxide became a common component in oil-based paints following commencement of commercial production in the 1840s, peaking in popularity during the first half of the 20th century.[15] Valued as a white pigment in its own right, it has most frequently been used in combination with both lead white (basic lead carbonate, for many centuries the white pigment of choice) and titanium white pigments (predominantly synthetic titanium dioxides of anatase or rutile form), and as a component in colored paint formulations.[16,17] The formation of zinc soaps in paint contributes to some of the advantages conferred by the pigment but is also implicated in undesirable changes affecting shelf life and stability in the film. This was quickly apparent in the harsh exposure environments of the house paint industry, prompting considerable research throughout the early to mid-20th century into managing the inherent reactivity.[18] In artists' paints there was early concern for the apparent brittleness of zinc based paints;[19] however, broader concern over the stability of zinc oxide in paintings has evolved only recently. Aggregated masses of zinc stearate and palmitate have erupted through the surface of paintings by artists including van Gogh[4] and Miro[20] and the accumulation of zinc soaps at the interface between paint layers has been implicated in adhesive failure and flaking.[20,21] Although now rarely used in industrial oil modified paints, zinc oxide remains a common component in artists' paints and grounds.[22,23] Its prevalence in paintings throughout the 20th century creates a clear imperative to understand its long-term behavior. The current study considers the influence of paint composition on formation, distribution, and phase separation of zinc carboxylates in oil-based paints in the presence of zinc oxide.

Metal soaps have been characterized by various techniques including X-ray diffraction and a range of vibrational spectroscopic and mass spectrometric techniques.[7,9,24–28] Of these, Fourier transform infrared spectroscopy (FT-IR), in conjunction with complementary methods of analysis, is an established technique for broad characterization of paints and for monitoring changes in functionality over time such as those

APPLIED SPECTROSCOPY

TABLE I. Summary of characteristic infrared bands (cm^{-1}) and assignments related to the presence and formation of metal carboxylates in oil-based paints.[24,27,32]

Linseed oil	Stearic acid[a]	Zn stearate[a]	Al stearate[b]	Attribution
			3690 (sharp)	ν OH
	3400 (broad)		3400 (broad)	ν OH
2956	2954	2952	2955	ν_{as} CH$_3$
2926	2917	2918	2918	ν CH$_2$
	2871			ν_s CH$_3$
2855	2850	2848	2850	ν CH$_2$
1740	1703 (strong)			ν C=O
		1540 (strong)	1588 (strong)	ν_{as} COO$^-$
	1472/1463	1465	1469	δ CH$_2$
	1411		1433/1411 (shoulder)	
		1398		ν_s COO$^-$
1240/1165/1100	1298			ν C–O
			990	Al–O

[a] Stearic acid and zinc stearate are virtually indistinguishable from palmitic acid and zinc palmitate using the specified peaks.
[b] The IR absorption of Al stearate incorporates features of stearic acid and Al hydroxide.

that occur during the complex drying and aging processes in oil paint.[29–32] In simple terms, fresh oils comprise polyunsaturated fatty acids in triglyceride structures, which undergo oxidative polymerization to form a solid film. Concurrent with polymerization are β-scission degradation reactions and oxidative cleavage of the double bonds in the fatty acyl moieties and hydrolysis of glycerol ester bonds producing low molecular weight products within the cross-linked structure.[33] These include monocarboxylic acids, which are vulnerable to separation from the network, enabling migration to the surface or reaction with metal ions to form soaps.[6,34]

A number of publications discuss infrared (IR) absorptions of key relevance to metal carboxylate formation, as summarized in Table I.[24,27,32] Carboxylic acids that are present or formed produce a shoulder at wavenumber ~1705 cm^{-1} to the ν C=O glycerol ester absorption (~1740 cm^{-1}), accompanied by a broad O–H stretch centered at ~3400 cm^{-1} and peaks at ~1415 cm^{-1} and 915 cm^{-1}. Soap formation is characterized by disappearance of the O–H stretch and replacement of ν C=O

and C–O (1300 cm^{-1}) bands with COO$^-$ antisymmetric and symmetric stretch at ~1550 cm^{-1} and 1400 cm^{-1}, reflecting the ionized structure of the COO–metal bond.[35] Zinc stearate and palmitate have the same characteristic peaks at ~1540 cm^{-1} and 1398 cm^{-1} and CH$_2$ bend at 1465 cm^{-1}.[27] Aluminum stearate has characteristic absorptions at ~1588 cm^{-1} and shoulder peaks at ~1433 and 1411 cm^{-1} below the δ CH$_2$ band at ~1469 cm^{-1}.[24,36]

The presence of pigments and additives not only influences IR absorption spectra through their own characteristic absorptions but also via their influence on short- and long-term reactions occurring in the oil paint medium. Zinc oxide itself has no absorption signal in the mid-infrared range between 4000 and 600 cm^{-1}, but oil-based paints containing zinc oxide are among the most likely to develop strong carboxylate absorption.[32]

The current study uses FT-IR in conjunction with optical microscopy (OM) and scanning electron microscopy with energy dispersive X-ray analysis (SEM-EDX) to investigate oil-based artists' commercial and custom-made reference paints containing zinc oxide to determine any link between compositional factors and zinc carboxylate distributions. Attenuated total reflection (ATR)-FT-IR measurement mode is used to investigate the zinc carboxylate distributions of both exposed and protected surfaces of the paints. Additionally, metal stearate distribution within paint films is resolved with cross-sectional mapping acquired via synchrotron FT-IR microspectroscopy (SR-μFT-IR).

EXPERIMENTAL

Oil-based artists' paint film draw-downs containing zinc oxide either as the primary pigment (coded Z) or as a secondary component in combination with lead or titanium whites (coded L and T, respectively) were sourced from the Smithsonian's Museum Conservation Institute reference collection. Paints had been cast onto Melinex® film (DuPont, PET) between 1978 and 1999 and stored under stable interior ambient conditions for between 11 and 32 years at the time of testing. The 22 draw-downs discussed here included commercial artists' paints and custom control paints produced using only specified pigment and oil combinations (Tables II and III). Of the

TABLE II. Paints with a pronounced difference between ATR-FT-IR spectra obtained from exposed and protected surfaces, characterized by strong, defined underside absorption at ~1540 cm^{-1} in contrast to broad surface carboxylate absorption. Composition is as specified by manufacturers with additional details regarding pigmentation determined using optical microscopy, FT-IR, and SEM-EDX. Paints with zinc oxide as the primary pigment (coded Z). Paints with zinc oxide as a minor pigment: lead based (coded L); titanium based (coded T) with relative proportions by weight where known.

Reference code	Paint manufacturer/product name/ date of film casting	Composition	
		Pigment[a]	Oil
L1	Grumbacher Flake white 1978	Basic lead carbonate, zinc oxide 20:1	Linseed alkali refined + Al stearate
T1	Grumbacher Titanium white 1978	Titanium dioxide, zinc oxide 1:2; *trace Al silicate*	Linseed alkali refined + Al stearate
Z1	Grumbacher Zinc white 1978	Zinc oxide; *[Al, S, Cl]*	Linseed alkali refined + Al stearate
L4	Grumbacher Flake white 1999	Basic lead carbonate, zinc oxide	Linseed alkali refined + *Al stearate*
T7	Grumbacher Titanium white 1999	Titanium dioxide, zinc oxide	Linseed alkali refined + *Al stearate*
T9	Custom control *Titanium white* 1998	Titanium dioxide (rutile), zinc oxide 12:1, Al silicate	Linseed grinding + Al stearate
Z6	Custom control *Zinc white* 1998	Zinc oxide	Linseed grinding + Al stearate
Z7	Custom control *Zinc white* 1998	Zinc oxide	Safflower alkali refined + Al stearate
T2	Winsor and Newton Titanium white 1978	Titanium dioxide, barium sulfate; *ZnO, CaCO$_3$, [Al(OH)$_3$]*	Safflower
T4	Colorlab Titanium white 1981	Titanium dioxide, zinc oxide, barium sulfate 5:1:10	Safflower + Al stearate
T5	Colorlab Titanium white 1981	Titanium dioxide, zinc oxide, barium sulfate 5:1:10; *[Al, S, Cl]*	Linseed + Al stearate

[a] Italicized text indicates compositional information inferred from analysis in addition to that specified.

TABLE III. Paints with broad underside carboxylate IR absorption with a small or no defined peak at ~1540 cm^{-1}.

Reference code	Paint manufacturer/product name/ date of film casting	Composition	
		Pigment[a]	Oil
Z2	Winsor and Newton Zinc white 1978	Zinc oxide	Safflower
L2	Winsor and Newton Flake white 1978	Basic lead carbonate; *ZnO, BaSO$_4$ [Al, C]*	Safflower
L3	Winsor and Newton Flake white no.1 ASilver white 1980	Basic lead carbonate; *ZnO, Al silicate, CaCO$_3$*	Safflower
L5	Winsor and Newton Flake white 1999	*Basic lead carbonate, zinc oxide*	Not specified
T3	Winsor and Newton Titanium dioxide APermanent white 1980	*TiO$_2$, ZnO, BaSO$_4$, MgCO$_3$, [Al, S]*	Safflower
T8	Winsor and Newton Titanium white 1999	*TiO$_2$, BaSO$_4$, MgCO$_3$, ZnO (trace)*	Not specified
T6	Gamblin Titanium white 1999	Titanium dioxide, zinc oxide; *CaCO$_3$, trace Al silicate*	Linseed alkali refined
T10	Custom control *Titanium white* 1998	Titanium dioxide (rutile), zinc oxide 12:1, Al silicate	Safflower alkali refined + Al stearate
Z3	Custom control *Zinc white* 1990	Zinc oxide	Linseed boiled
Z4	Custom control *Zinc white* 1990	Zinc oxide	Linseed cold pressed
Z5	Custom control *Zinc white* 1990	Zinc oxide	Linseed with litharge (PbO)

[a] Italicized text indicates compositional information inferred from analysis in addition to that specified.

commercial paints only Grumbacher and Colorlab samples contain added aluminum stearate. Control paints include sets with and without addition of aluminum stearate. Zinc stearate was not an ingredient in any of the paint formulations. Removal of paint samples from the casting supports enabled the characteristics of protected (underside) paint surfaces to be compared to those at the top with long-term exposure to air, i.e., water, oxygen, and carbon dioxide.

In addition to the bulk films, samples from each paint were prepared by embedding millimeter-sized fragments in polyester resin (Volksglas, MEKP, cured at room temperature) and microtoming to expose a cross-section normal to the paint surface. Cross-sections revealed paint films ranging in thickness from 150 to 450 μm. Final (dry) polishing of sections was undertaken with Micro-Mesh™ cloth backed abrasives (12 000 grit) where required. Samples of selected paints were additionally embedded in epoxy resin (Procure 812, DDSA, NMA, DMP cured at 60 °C). Embedded samples were microtomed with a glass or histo diamond knife to obtain 5 μm thin sections for transmission measurements.

The different sample presentations enabled surface analysis of bulk films at the paint/air interface, and cross-sectional analysis of component distribution through film thickness using a variety of instrumental techniques.

Optical Microscopy. Microscopy was conducted with a Leica DMLP microscope using N-plan objectives and an external halogen fiber-optic illuminator. Ultraviolet fluorescence (UVF) was observed using an EL6000 compact light source with mercury short arc reflector lamp and Leica 'A' filter with excitation range BP 340-380 and suppression BP 425. Cross-sections were photographed under incident light and fluorescence conditions using a Leica DFC500 camera.

Fourier Transform Infrared Spectroscopy. Spectra of paints were acquired using a Nicolet 5700 FT-IR spectrometer and Continuum microscope using an ATR accessory with germanium crystal. Data was collected using Omnic 7 software over wavenumber range 4000–600 cm^{-1}. Spectra are the sum of 32 or 64 scans at a resolution of 4 cm^{-1}. Spectra were collected from multiple points on the exposed surface and protected underside of each paint film. Spectra obtained were interpreted and compared to published or personal reference spectra and are shown in absorbance units.

Synchrotron Fourier Transform Infrared Microspectroscopy. Microtomed thin sections of selected samples were prepared for transmission measurements at the Infrared Microspectroscopy beamline at the Australian Synchrotron. The beamline is equipped with a Bruker Hyperion 2000 microscope with a liquid nitrogen cooled narrow-band mercury cadmium telluride (MCT) detector coupled to a Vertex V80v FT-IR spectrometer. Thin sections were placed on a single 1 mm diamond window of a ThermoFisher (Waltham, MA, USA) microcompression cell and flattened using a stainless steel roller to ensure contact. The samples were analyzed in transmission mode using 5×5 μm apertures and 5 μm steps following custom-defined grid points (typically a band spanning top to bottom through each sample), saved as two-dimensional (2D) IR map files using Bruker Opus software. Spectra are the sum of 32 co-added scans at a resolution of 4 cm^{-1} for both sample and background measurements, collected over the wavenumber range 3800–750 cm^{-1}. Chemical maps show absorbance intensity as a function of an integrated area under a spectral band defined by the two frequency points after subtraction of the local baseline defined by the same two points.

Scanning Electron Microscopy. Embedded cross-sections of selected paints were carbon coated using a JEOL JEE-4X vacuum evaporator to enable SEM imaging with EDX analysis using either a Philips LaB6 XL30 or JEOL JSM-6460 LA thermionic emission scanning electron microscope. Both EDX spectrometers used SiLi crystals with approximate resolution of 130 eV, polymer light element windows and matrix correction software (Phoenix V3.10 or JEOL Analysis Station V3.8). Samples were examined in high vacuum mode at 18 or 20 kV accelerating voltage. Backscatter electron images were captured. EDX of points of interest on the specimen were acquired in spot mode. Larger regions of the sample were full spectrum X-ray mapped to elucidate elemental distribution.

RESULTS AND DISCUSSION

Surface Paint Film Analysis. Paint samples were removed from the PET supports and both the exposed top and protected underside surfaces of the bulk films were surveyed using conventional ATR-FT-IR microscopy. Strong metal carboxylate absorption occurred in all films as expected for oil-based
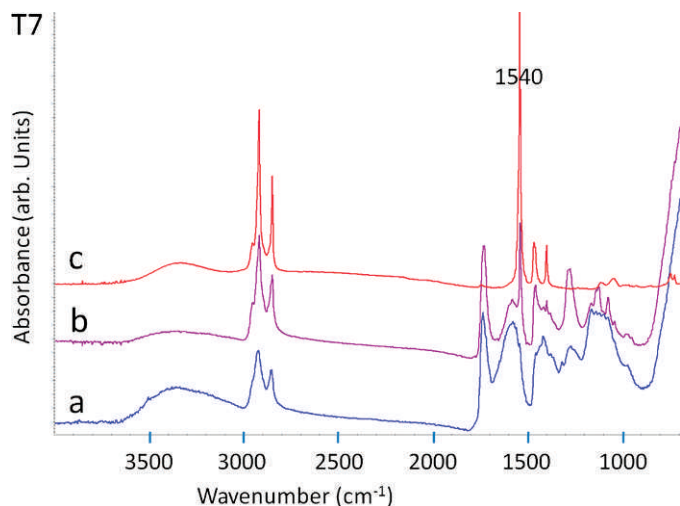
FIG. 1. T7 Grumbacher Titanium white 1999: ATR-FT-IR spectra showing differences recorded from exposed top (*a*) and protected (*b*) surfaces in comparison to a reference spectrum for Zn stearate (*c*). The underside (b) shows a strong contribution from Zn stearate, a key feature being the v_{as} COO$^-$ peak at 1540 cm^{-1}.

paints containing zinc oxide. Significantly, pronounced differences were observed in spectra acquired from the two surfaces in many samples, despite deriving from a single paint film. Spectra from exposed top surfaces consistently showed broad carboxylate absorption in the range 1640–1505 cm^{-1}. This suggests coordination of zinc ions to a range of different carboxylate moieties, or carboxylates coordinated to different metals or involving different coordination structures, including the possibility of ZnO surfaces functionalized with carboxylic acid monolayers.[26,27,32,37] In contrast, spectra from the underside of a significant number of paints included a strong, sharp peak at 1540 cm^{-1}, characteristic of the asymmetric COO$^-$ stretch for zinc stearate/palmitate (Fig. 1).

This difference was most pronounced in the paints known to contain Al stearate; comparison of the top and underside surface spectra of zinc oxide/linseed control paints with and
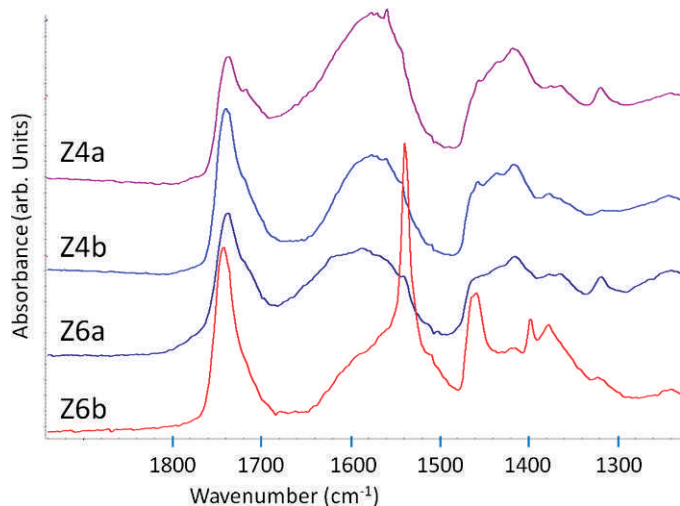
FIG. 2. ATR-FT-IR spectra comparing carboxylate absorption obtained from zinc based linseed control paints formulated with Al stearate (Z6 1998) and without (Z4 1990): (*a*) top surface; (*b*) underside. Only the paint containing Al stearate shows a defined underside peak at 1540 cm^{-1}.
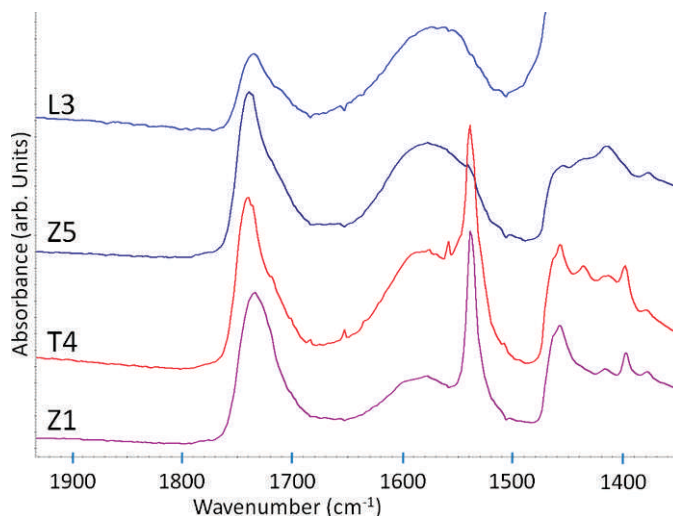
FIG. 3. ATR-FT-IR underside spectra comparing paints incorporating zinc oxide with a variety of pigment and oil combinations. Carboxylate absorption in paints formulated with Al stearate consistently includes a defined peak at 1540 cm^{-1}: T4 Colorlab Titanium white safflower 1981; Z1 Grumbacher Zinc white linseed 1978. Commercial and custom control paints without Al stearate show broad carboxylate absorption: L3 W&N Flake white safflower 1980; Z5 Zinc oxide linseed (litharge) control 1990.

without Al stearate shows that distinct and strong zinc stearate absorption at 1540 cm^{-1} is only evident at the underside of the formulation containing Al stearate (Fig. 2).

This trend was observed in other Al stearate containing controls and also in the Grumbacher paints (irrespective of primary pigment type) and the Colorlab titanium based paints (irrespective of oil type) (Table II and Fig. 3, T4, Z1). One exception was custom control T10 (titanium dioxide/zinc oxide with safflower oil and Al stearate). Despite incorporating Al stearate, the underside of this paint did not absorb strongly at 1540 cm^{-1}. Possible factors include the combination of safflower oil, which is less reactive than linseed oil (T9) as a result of a composition dominated by C$_{18:2}$ as opposed to C$_{18:3}$ fatty acids, and less than half the period of aging in comparison to the other similarly formulated reference paint, T4.

Paints with little or no defined underside peak at 1540 cm^{-1} include all but one of the Winsor and Newton (W&N) paints and zinc based control paints without added Al stearate (Table III).[†] Broad carboxylate absorption is observed at both exposed and protected surfaces, contracted towards lower wavenumber at undersides (Fig. 3, L3, Z5).

Other differences observed in spectra acquired from the top and bottom of paint films generally include a reduced intensity of C–O stretching frequency (1300/1320 cm^{-1}) at the exposed top surface. In addition, stronger C=O absorption slightly broadened to lower wavenumbers and a more pronounced O–H stretch at ~3400 cm^{-1} are consistent with higher surface concentration of carboxylic acid moieties. Variation in fatty acid composition at the top and bottom of a zinc oxide containing reference paint film has also been observed in a previous study using static secondary ion mass spectrometry (SIMS).[25] Negative ion counts corresponding to deprotonated

---

† Although W&N have included stearates in some of their artists' oil colors, none have been used in formulating the paints discussed here. (Private communication Phil Jones, Group Innovation and Development Director, ColArt International Holdings, Ltd. London, email 8 March 2011.)
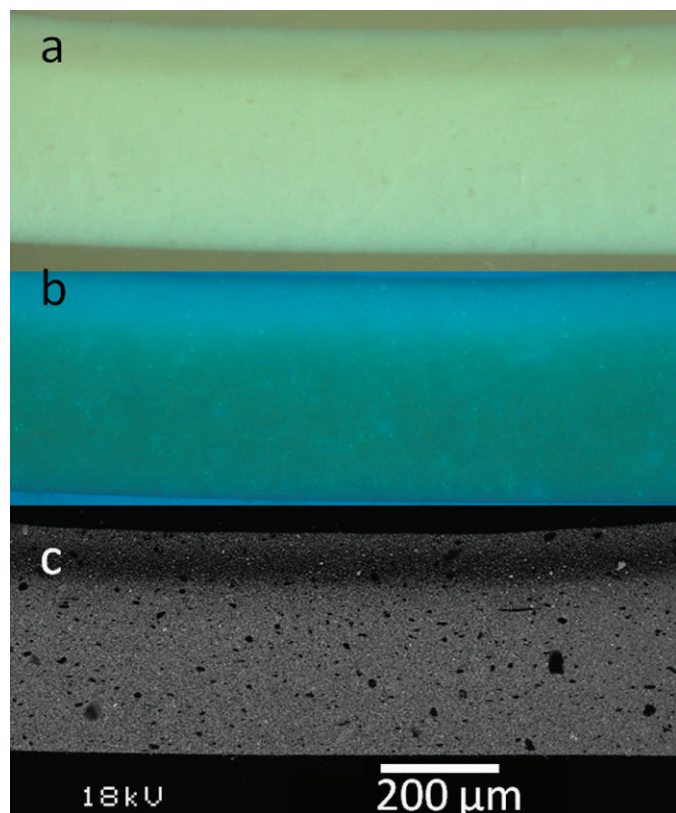
FIG. 4. Embedded cross-section of Z6 Zinc white control paint with linseed oil and Al stearate 1998 shown as (**a**) visible light, (**b**) ultraviolet fluorescence, and (**c**) back scatter electron images. The surface margin appears darker, more UV-fluorescent, and of lower electron density than the bulk of the film.

palmitic and stearic acids were found to be approximately twice as high at the top surface relative to the bottom surface of a two-year-old paint film. Curiously, in cross-section imaging mode, the same paper reports depleted carboxylic acid concentrations in the upper margin of the paint, attributed to evaporative loss associated with a more advanced state of aging. In the present study, comparison of zinc oxide control paints produced with linseed oils of differing preparation shows the sample with boiled linseed oil to have the least variation between surfaces. Oil processing methods are known to influence the initial triglyceride composition of the oil, with heat treatment reducing the proportion of unsaturated triglycerides via formation of oligomers.[38] The spectrum of the boiled linseed paint shows a relatively small carboxylate absorption which, coupled with a strong glyceride ester stretching band at ~ 1740 cm^{-1} suggests a lower reactivity than the other oil preparations. This is supported by the physical condition of this paint, which remains soft more than 20 years from the date of casting.

Analysis of Embedded Paint Cross-Sections. Embedded cross-sections were used to obtain additional information on variations between and within paint films. Sections were imaged using optical and electron microscopies, the latter coupled with EDX analysis to confirm elemental composition. Various individual paints exhibited significant differences in visible, ultraviolet fluorescence (UVF), and backscatter electron (BSE) density distributions (Fig. 4).

Paints studied with SR-μFT-IR contained zinc oxide in three different preparations within the same commercial range. This enabled comparison of zinc stearate distribution between paints of similar formulation but with different primary pigmentation, in this case zinc, lead, and titanium based whites from the 1978 Grumbacher range (Z1, L1, T1). Zinc and titanium/zinc control paints with and without Al stearate (Z4, Z6, Z7; T9, T10) and
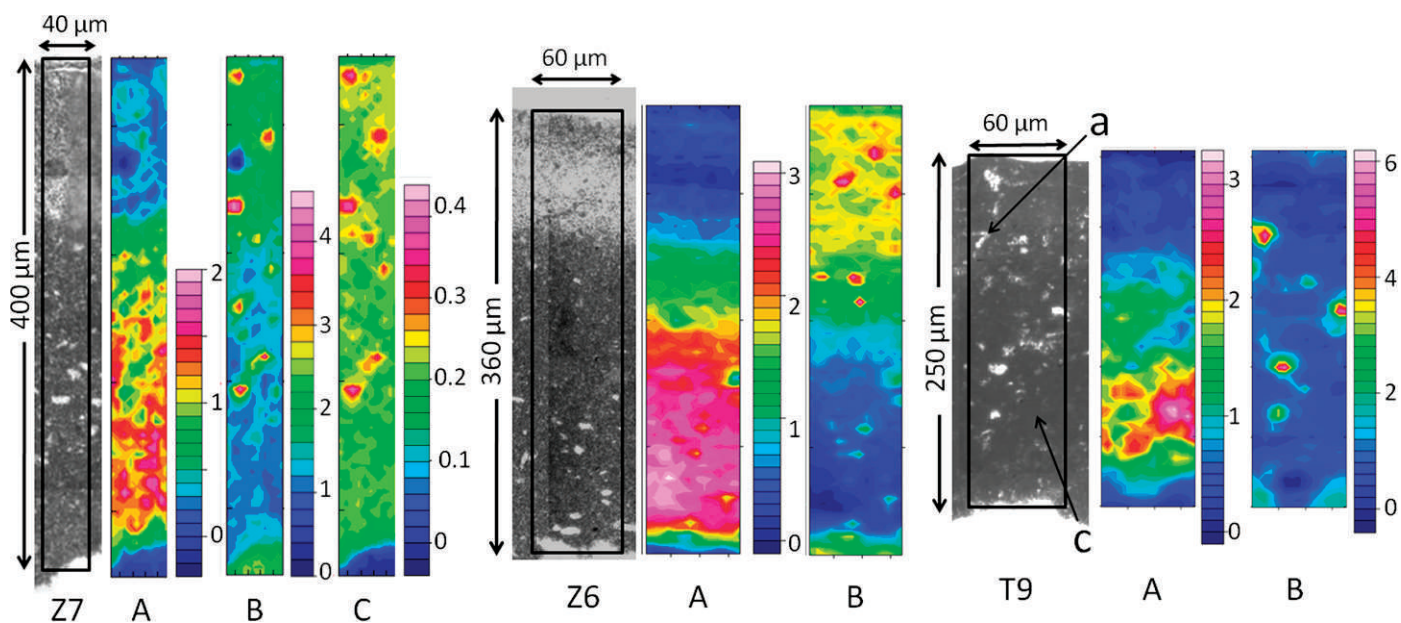
FIG. 5. Selection of paints investigated using SR-μFT-IR. Boxed optical images of thin sections indicate regions mapped. Integrated absorption intensity maps are shown for wavenumber range A: 1525–1555 cm^{-1}, B: 1560–1620 cm^{-1}, and C: 1585–1595 cm^{-1}. Al stearate concentration is closely aligned with hot spots in the maps for broad carboxylate absorption. Zinc stearate is at highest concentration in the lower margin of the paints. From L-R: Z7 Zinc white safflower control with Al stearate 1998; Z6 Zinc white linseed control with Al stearate 1998; T9 Titanium white (containing zinc oxide) linseed control with Al stearate 1998 (*a* and *c* denote location of extracted spectra shown in Fig. 6).
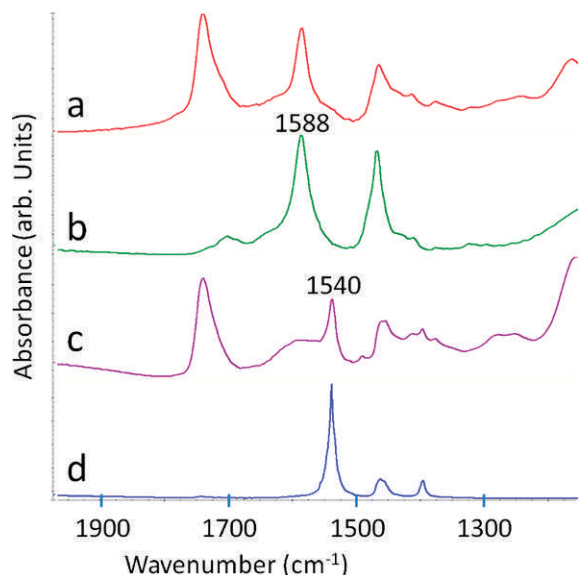
FIG. 6. Spectra (*a*) and (*c*) extracted from SR-μFT-IR map of paint T9 contain metal carboxylate peaks with close agreement to reference spectra for aluminum stearate (*b*) and zinc stearate (*d*), respectively.

one Winsor and Newton paint (Z2) were also included for comparison.

Chemical maps were produced by integrating absorbance intensities corresponding to specific functional groups within the carboxylate region. Integration ranges were selected to reflect the features of typical spectra represented in the samples, either a single broad peak in the range 1560–1620 cm^{-1} or a defined side peak at 1540 cm^{-1}. Characteristic peaks for Al stearate were rarely discernible over the broad carboxylate absorption. Maps showed a marked positional separation of absorptions between 1535–1545 cm^{-1} (v_{as} COO$^-$ zinc stearate/palmitate), and the broader range between 1560–1620 cm^{-1} in most paints, consistent with ATR-FT-IR measurements of paint

surfaces (Fig. 5). Integration of the narrow band 1585–1595 cm^{-1} (v_{as} COO$^-$ Al stearate) produced maps showing a strong correlation with high intensity areas in the maps of broader range. Zinc stearate was most concentrated in the lower half of the majority of paint films, with broader carboxylate absorption evident in upper margins or within small, visibly defined regions distributed through the sample.

Individual spectra extracted from high intensity spots in these maps reflect the presence of discrete metal carboxylate species (Fig. 6).

The concentration of zinc stearate in the bottom half of the film was observed for all three Grumbacher paints and the control paints containing Al stearate. The zinc white control without aluminum stearate, Z4, has negligible levels of zinc stearate, and broad carboxylate absorption occurs throughout the paint.

Broad carboxylate absorption is also seen throughout the only other sample without Al stearate, Z2. Unfortunately this paint was affected by embedding, compromising spectra acquired from the sample periphery. Mapping of an area in the intact lower part of the section resolved small defined areas with a pronounced peak at ~1540 cm^{-1}. These regions correlate well with optical features and suggest the presence of small (~5 μm) distributed clusters of zinc stearate/palmitate (Fig. 7). However, the paint does not contain corresponding defined areas of low atomic mass in BSE images as is the case for paints containing Al stearate. It is possible that the Zn stearate phase has emerged from within the microstructure and spread to the cross-section surface, a phenomenon that has been previously reported.[39] In comparison, high intensity features present in maps of the 1560–1620 cm^{-1} region in Al stearate containing paints are visible both optically in thin section and as defined regions of low atomic mass in BSE images. SEM-EDX confirms the association of Al with these features (Fig. 8). The carboxylate absorption in spectra extracted from these regions is typically broad and is comparable to that observed in upper margins of the same paints (Fig. 9). Small side peaks at 1540 cm^{-1} suggest a small
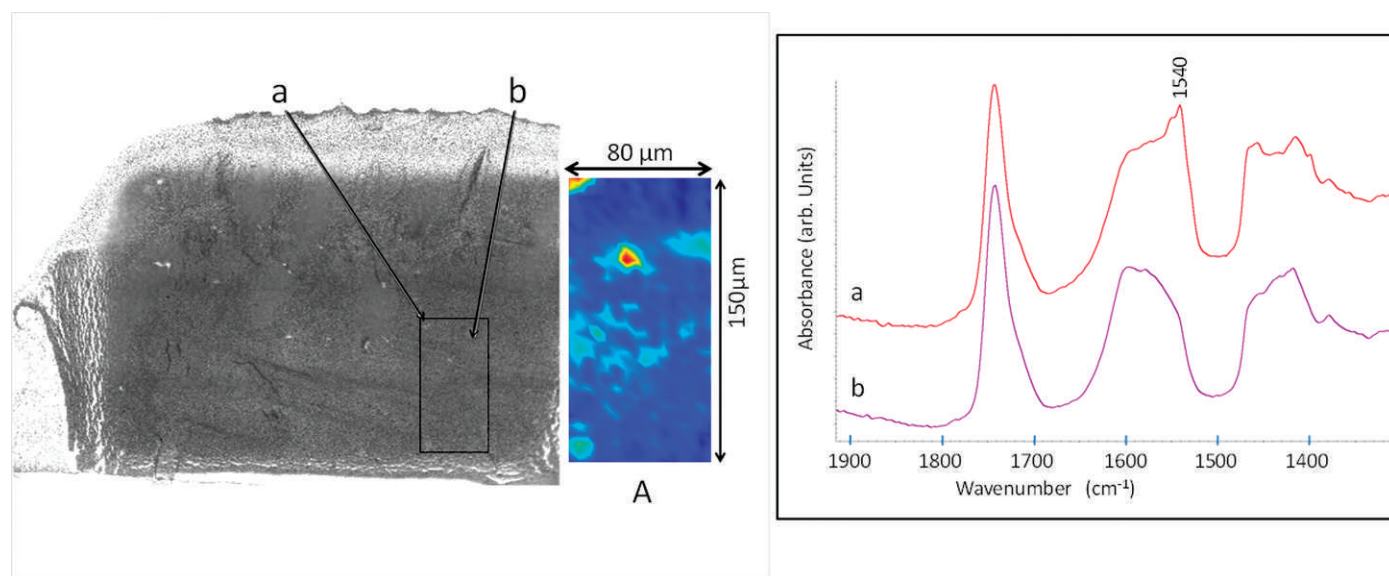
FIG. 7. Z2 W&N Zinc white safflower 1978: optical image of thin section investigated using SR-μFT-IR; box denotes region mapped and the image at center shows integrated absorption intensity for wavenumber range 1535–1545 cm^{-1}. Arrows designate location of extracted spectra shown at right corresponding to (*a*) high intensity (red) and (*b*) low intensity (blue) regions. The peak at 1540 cm^{-1} is only present in small micrometer-sized features in the sample.
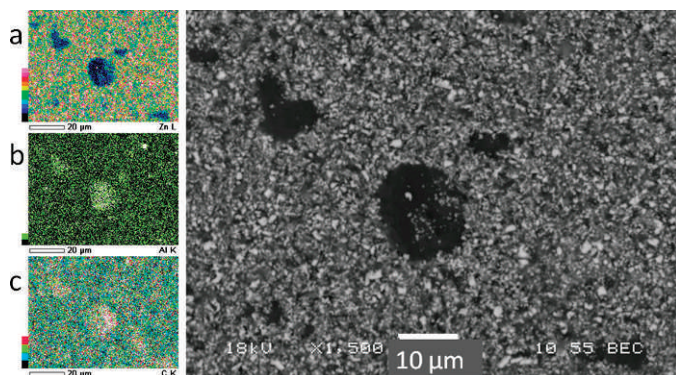
FIG. 8. Z6 Zinc white control paint with linseed oil and Al stearate 1998: Embedded cross-section detail shown as SEM backscatter electron image and elemental intensity maps of the same area for (**a**) Zn, (**b**) Al, and (**c**) C. Areas with low Zn and low electron density have high concentrations of Al and C and are consistent with high intensity points in IR absorption map 1560–1620 cm^{-1} (Fig. 5). The combined results point to the presence of Al stearate.

amount of Zn stearate remains associated with more polar soap species.

The conversion of zinc oxide to Zn carboxylate is facilitated by exposure to atmospheric moisture. The significance of water on kinetics of lead soap formation has been demonstrated in reconstructions of historic paint media and pharmaceutical recipes.[40] Exposure of paints to high relative humidity has also been shown to increase formation of zinc carboxylates.[25] In addition to increased availability of carboxylic acids following hydrolysis reactions, ready availability of water will enable surface conversion of zinc oxide to zinc hydroxide, facilitating formation of Zn carboxylates and producing additional water (Eqs. 1 and 2).

$$ZnO + H_2O \rightarrow Zn(OH)_2 \qquad (1)$$

$$Zn(OH)_2 + 2FAH \rightarrow Zn(FA)_2 + 2H_2O \qquad (2)$$
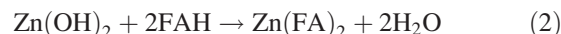
The presence of Al stearate as an original component increases the concentration and availability of stearic acid as a result of its presence in free form in typical commercial grades of Al stearate.[41] Al stearate has a high capacity for hydration attributable to the small radius of the Al^{3+} ion with capability for H-bonding through the OH groups of the hydrate water molecules[36] and is readily hydrolyzed, releasing further stearic acid (Eq. 3). Relatively polar molecules of Al mono- or di-stearate and Al hydroxide Al(OH)$_3$ may therefore be present or formed (Eq. 4). This contrasts with the formation of apolar zinc stearate.

$$Al(FA)_3 + H_2O \rightarrow Al(FA)_2OH + FAH \qquad (3)$$

$$Al(FA)_2OH + 2H_2O \rightarrow Al(OH)_3 + 2FAH \qquad (4)$$

It has recently been demonstrated that in oil, nano-sized micelles of Al soap molecules aggregate into jammed networks; however, over time configuration energy is minimized by rearranging particles into more closely packed forms.[42] In the current study, paint films containing Al stearate appear to contain small dispersed clusters of the additive. FT-IR spectra extracted from these areas in paints with Al stearate show comparable absorption to spectra obtained from upper margins of the same paint, suggesting a preferential concentration of relatively polar hydrated soap forms and hydrolysis-derived carboxylic acid moieties towards the air interface. At the same time, the apolar zinc stearate appears to phase separate and preferentially occupy the lower margins of the film. The tendency for Zn stearate to migrate towards the protected surface is in this case possibly influenced by the properties of the PET substrate on which the paints were cast. PET film is commonly used in the preparation of reference paint films because of its chemical stability. It does, however,
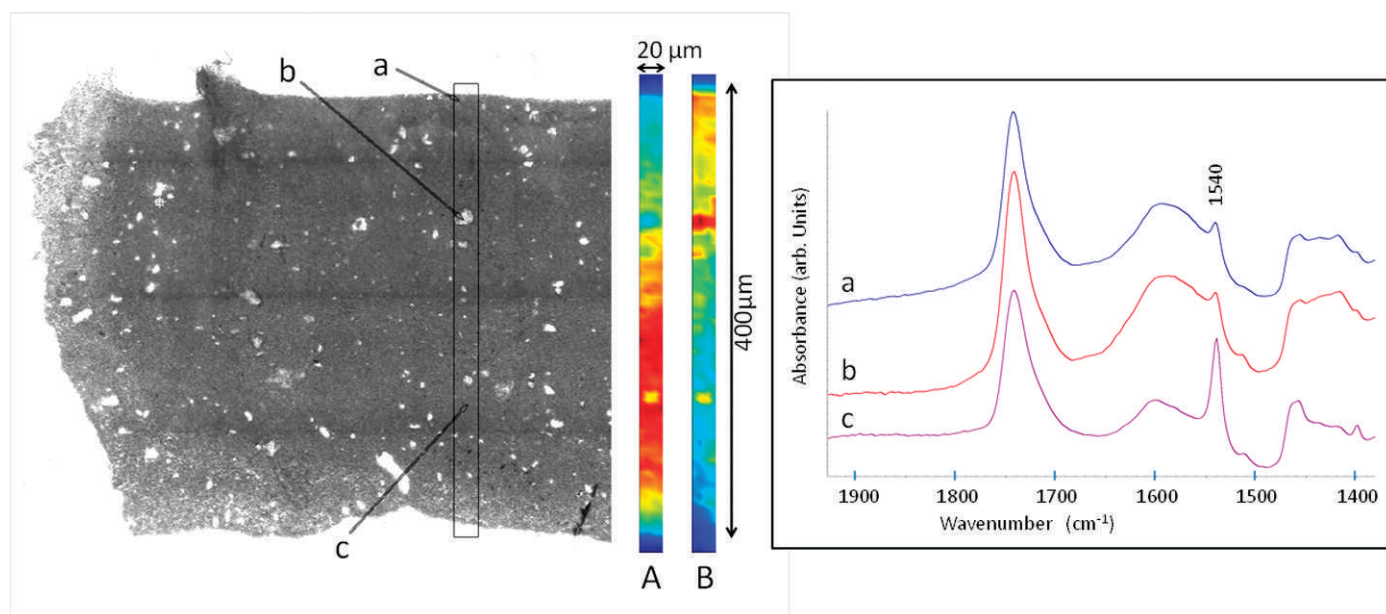
FIG. 9. Z1 Grumbacher Zinc white 1978: optical image of thin section investigated using SR-μFT-IR; box denotes region mapped and the images (center) show integrated absorption intensities for wavenumber range A: 1535–1545 cm^{-1} and B: 1560–1620 cm^{-1} (blue/low to red/high). Arrows designate location of extracted spectra shown at right showing strong correlation between spectra obtained from the surface margin (**a**) and from small, distributed features visible in the optical image (**b**) both with broad carboxylate peaks encompassing the characteristic absorption for Al stearate. In contrast, a strong defined peak at 1540 cm^{-1} is evident in the spectrum from the lower margin of the paint (**c**).

prevent passage of water, oxygen, and carbon dioxide. This differs from typical painting supports, which are open at a molecular level. However, while the lateral organization of carboxylate species may vary in paint films applied to different substrates, it is nonetheless significant that the polar and apolar carboxylate phases are observed to separate.

In zinc oxide pigmented paints without Al stearate, the longer chain saturated zinc carboxylates appear to be in lower concentration. Discrete micrometer-sized aggregates of zinc stearate/palmitate are discerned within these paints by synchrotron source IR microspectroscopy; however, these remain distributed throughout the film. IR carboxylate absorption is generally broad, consistent with the presence of a range of zinc soaps. The W&N paint, T9, which does not contain Al stearate but which exhibits variation in Zn stearate distribution more in keeping with paints which do, is also seen to contain low atomic mass features in BSE images. At ~2 μm these regions are clearly discernible, but smaller than the 5–10 μm micelles of Al stearate. Aluminum hydroxide is a likely component in this paint,[‡] which would share some of the functionality of hydrolyzed forms of Al stearate and may help explain the preferential concentration of Zn stearate away from the air interface.

CONCLUSION

Fourier transform infrared spectroscopy of reference paint films has shown that zinc carboxylate distribution within a paint film is influenced by additional components present in combination with zinc oxide, in this case by Al stearate as an original component of the paint. The influence of Al stearate on zinc saponification and aggregation is more significant than either different pigment combinations or oil types present in association with zinc oxide. Substantial differences in IR absorption spectra obtained from exposed and protected surfaces in paints containing Al stearate were revealed by the use of ATR-FT-IR measurements, most notably a broad COO^- stretching frequency at the exposed top surface in contrast to a strong, sharp peak at 1540 cm^{-1} characteristic for zinc stearate at the surface adjacent to the PET substrate. These observations are supported by SR-μFT-IR, which revealed gradients in metal carboxylate distribution and preferential concentrations of C16/C18 chain saturated Zn carboxylates within lower margins of paints incorporating Al stearate. In zinc oxide containing paints without Al stearate, carboxylate absorption is broad with minimal variation through film thickness. Small, dispersed clusters of zinc stearate were discerned with SR-μFT-IR.

In all paints, zinc stearates and palmitates that have formed over relatively short timescales in films exposed only to stable interior ambient conditions appear to have phase separated. The presence of Al stearate in combination with zinc oxide appears to favor more pronounced separation due to higher concentrations of stearic acid and due to its influence on film chemistry creating less favorable chain packing configurations for longer chain C16 and C18 saturated zinc carboxylates. The phase separation of zinc stearate in paints has potentially severe implications for long-term stability of paintings, whether manifesting as aggregated masses that compromise appearance and structure, or as concentrations at an interface with potential to cause adhesive failure. This study contributes to our understanding of and capacity to manage factors influencing associated deterioration in collections.

1. C. Higgitt, M. Spring, D. Saunders. "Pigment-medium interactions in oil paint films containing red lead or lead-tin yellow". National Gallery Technical Bulletin. 2003. 24: 75-95.
2. P. Noble, J.J. Boon. "Metal soap degradation of oil paintings: aggregates, increased transparency and efflorescence". In: AIC Annual Meeting: Paintings Specialty Group Postprints. 2007. Pp. 1-15.
3. G. Osmond, K. Keune, J. Boon. "A study of zinc soap aggregates in a late 19th century painting by R.G. Rivers at the Queensland Art Gallery". AICCM Bulletin. 2005. 29: 37-46.
4. J. Van der Weerd, M. Gelddof, L.S. van der Loeff, R. Heeren, J. Boon. "Zinc soap aggregate formation in 'Falling leaves (Les Alyscamps)' by Vincent van Gogh". Zeitschrift für Kunsttechnologie und Konservierung, 2003. 17(2): 407-416.
5. J. Zucker, J. Boon. "Opaque to transparent: paint film defects in the work of Frederick Church and the Hudson River School". In: AIC Annual Meeting: Paintings Specialty Group Postprints. 2007. Pp. 33-41.
6. J.J. Boon, F. Hoogland, K. Keune. "Chemical processes in aged oil paints affecting metal soap migration and aggregation". In: AIC Annual Meeting: Paintings Specialty Group Postprints. AIC, 2007. Pp. 16-23.
7. M. Cotte, E. Checroun, J. Susini, P. Walter. "Micro-analytical study of interactions between oil and lead compounds in paintings". Appl. Phys. A. 2007. 89: 841-848. doi: 10.1007/s00339-007-4213-4.
8. K. Keune, J.J. Boon. "Analytical imaging studies of cross-sections of paintings affected by lead soap aggregate formation". Stud. Conserv. 2007. 52(3): 161-176.
9. M.J. Plater, B. De Silva, T. Gelbrich, M.B. Hursthouse, C.L. Higgitt, D.R. Saunders. "The characterisation of lead fatty acid soaps in 'protrusions' in aged traditional oil paint". Polyhedron. 2003. 22(24): 3171-3179. doi: 10.1016/s0277-5387(03)00461-3.
10. M.L. Kastens, F.R. Hansen. "Drier soap manufacture". Ind. Eng. Chem. 1949. 41(10): 2080-2090. doi: 10.1021/ie50478a008.
11. J. Rinse. "Metal soaps". Am. Paint J. 1967. (March 13): 22-28.
12. C.S. Tumosa. "A brief history of aluminum stearate as a component of paint". WAAC Newsletter. 2001. 23(3).
13. J.H.W. Turner, S.G. Kemp, S.E. Harson. "The function of aluminium complexes as structure modifiers for paint". J. Oil Colour Chem. Assoc. 1958. 41(11): 769-779. doi.
14. J. Weiss. "Organic aluminium compounds in drying oils". J. Oil Colour Chem. Assoc. 1957. 40: 863-879. 976-989.
15. H.E. Brown. "Zinc oxide rediscovered". New York: New Jersey Zinc Company, 1957.
16. G. Gautier, A. Bezur, K. Muir, F. Casadio, I. Fiedler. "Chemical Fingerprinting of Ready-Mixed House Paints of Relevance to Artistic Production in the First Half of the Twentieth Century. Part I: Inorganic and Organic Pigments". Appl. Spectrosc. 2009. 63(6): 597-603.
17. H. Kühn. "Zinc white". In: R.L. Feller, editor. Artists' pigments. Cambridge University Press, 1986. Pp. 169-186.
18. G. Osmond. "Zinc white: a review of zinc oxide pigment properties and implications for stability in oil-based paintings". AICCM Bulletin. 2011. 33: paper in press.
19. A.H. Church. "The chemistry of paints and painting". London: Seeley, Service and Co., 1915. Limited, Fourth edition, revised and enlarged.
20. E. O'Donoghue, A.M. Johnson, J. Mazurek, F.D. Preusser, M.R. Schilling, M.S. Walton. "Dictated by media: conservation and technical analysis of a 1938 Joan Miro canvas painting". In: The object in context: Crossing Conservation Boundaries: Contributions to the Munich Congress 28 August - 1 September 2006. IIC, 2006. Pp. 62-68.
21. Y. Maor, A. Murray. "Delamination of Oil Paints on Acrylic Grounds". In: Materials issues in art and archaeology VIII. Warrendale, PA: Materials Research Society, 2008. Pp. 127-136.
22. M.F. Mecklenburg, C.S. Tumosa, D. Erhardt. "The changing mechanical properties of aging oil paints". In: Materials Issues in Art and Archaeology VII. Warrendale, PA: Materials Research Society, 2005. Pp. 13-24.

‡ Private communication, Phil Jones, Group Innovation and Development Director, ColArt International Holdings, Ltd. London, email 15 May 2012.

23. G. O'Hanlon. "Zinc white: problems in oil paint". Natural Pigments LLC, 2007. www.naturalpigments.com/education/article.asp?ArticleID=127 [accessed 24 October 2011].

24. R.W. Corkery. "A variation on Luzzati's soap phases. Room temperature thermotropic liquid crystals". Phys. Chem. Chem. Phys. 2004. 6: 1534-1546. doi: 10.1039/B315595C.

25. K. Keune, F. Hoogland, J.J. Boon, D. Peggie, C. Higgitt. "Evaluation of the added value of SIMS: A mass spectrometric and spectroscopic study of an unusual Naples yellow oil paint reconstruction". Int. J. Mass Spectrom. 2009. 284(1-3): 22-34. doi: 10.1016/j.ijms.2008.10.016.

26. M.A. Mesubi. "An infrared study of zinc, cadmium, and lead salts of some fatty acids". J. Mol. Struct. 1982. 81: 61-71.

27. L. Robinet, M.C. Corbeil. "The characterization of metal soaps". Stud. Conserv. 2003. 48(1): 23-40.

28. W. Faubel, R. Simon, S. Heissler, F. Friedrich, P.G. Weidler, H. Becker, W. Schmidt. "Protrusions in a painting by Max Beckmann examined with confocal μ-XRF". J. Anal. At. Spectrom. 2011. 26(5): doi: 10.1039/C0JA00178C.

29. M. Derrick, D. Stulik, J. Landry. "Infrared spectroscopy in conservation science". Los Angeles, CA: The Getty Conservation Institute, 1999.

30. J. Mallégol, J. Gardette, J. Lemaire. "Long-term behavior of oil-based varnishes and paints I. Spectroscopic analysis of curing drying oils". J. Am. Oil Chem. Soc. 1999. 76(8): 967-976. doi: 10.1007/s11746-999-0114-3.

31. R. Meilunas, J. Bentsen, A. Steinberg. "Analysis of aged paint binders by FT-IR spectroscopy". Stud. Conserv. 1990. 35: 33-51.

32. J. van der Weerd, A. van Loon, J.J. Boon. "FTIR studies of the effects of pigments on the aging of oil". Stud. Conserv. 2005. 50(1): 3-22.

33. J. Van den Berg, K. van den Berg, J. Boon. "Chemical changes in curing and ageing oil paints". In: J. Bridgland, J. Brown, editors. Preprints of the ICOM Committee for Conservation 12th Triennial Meeting, Lyon, France. London, UK: James and James, 1999. Pp. 248-253.

34. C.S. Tumosa, D. Erhardt, M.F. Mecklenburg, X. Su. "Linseed oil paint as ionomer: synthesis and characterization". In: Materials issues in art and archaeology VII symposium. Warrendale, PA: Materials Research Society, 2005. Pp. 25-31.

35. K.N. Mehrotra, R.K. Shukla, M. Chauhan. "Spectroscopic and Conductometric Studies of Lanthanide Soaps". Bull. Chem. Soc. Jpn. 1995. 68(7): 1825-1831.

36. Y.N. Shekhter, T.I. Bogdanova, L.N. Teterina, I.G. Fuks, I.R. Zaslavskaya. "Polarity and functional properties of soaps of stearic acid". Chem. Technol. Fuels Oils. 1975. 11(9): 734-737. doi: 10.1007/bf00730325.

37. A. Lenz, L. Selegård, F. Söderlind, A. Larsson, P.O. Holtz, K. Uvdal, L. Ojamäe, P.-O. Käll. "ZnO Nanoparticles Functionalized with Organic Acids: An Experimental and Quantum-Chemical Study". J. Phys. Chem. C. 2009. 113(40): 17332-17341. doi: 10.1021/jp905481v.

38. J.D.J. van den Berg, N.D. Vermist, L. Carlyle, M. Holčapek, J.J. Boon. "Effects of traditional processing methods of linseed oil on the composition of its triacylglycerols". J. Sep. Sci. 2004. 27: 181-199. doi: 10.1002/jssc.200301610.

39. K. Keune. Binding medium, pigments and metal soaps characterised and localised in paint cross-sections. [PhD thesis]. Amsterdam: University of Amsterdam, 2005.

40. M. Cotte, E. Checroun, J. Susini, P. Dumas, P. Tchoreloff, M. Besnard, P. Walter. "Kinetics of oil saponification by lead salts in ancient preparations of pharmaceutical lead plasters and painting lead mediums". Talanta. 2006. 70: 1136-1142. doi: 10.1016/j.talanta.2006.03.007.

41. E.S. Lower. "The properties of aluminium stearate and its uses in the coatings and allied industries. Pigment". Resin Technol. 1982. 11(2): 13-18.

42. X. Wang, M. Rackaitis. "Gelling nature of aluminum soaps in oils". J. Colloid Interface Sci. 2009. 331(2): 335-342. doi: 10.1016/j.jcis.2008.11.032.

3.4 Zinc white and the influence of paint composition for stability in oil-based media

Zinc white and the influence of paint composition for stability in oil based media

Gillian Osmond

Queensland Art Gallery│Gallery of Modern Art and Australian Institute for Bioengineering and Nanotechnology, University of Queensland, Brisbane, Australia
gillian.osmond@qagoma.qld.gov.au

Abstract

Zinc oxide is a prevalent pigment in 20th Century oil based paints. Its reactivity with fatty acids has consequences for paint film properties and stability. Resulting zinc carboxylates are implicated in a variety of deterioration phenomena affecting late 19th and 20th Century paintings. Naturally aged artists' oil paints and reference paint film draw downs are investigated using scanning electron microscopy, and conventional attenuated total reflectance and synchrotron transmission Fourier transform infrared spectroscopy. This study reports results for soybean oil paints and Naples yellow hue pigment mixtures with zinc oxide in addition to previously reported findings for linseed and safflower oil based paints involving zinc oxide alone and in combination with lead and titanium whites. A solvent model examining interactions between zinc oxide and stearic acid or aluminium stearate supports observations made in paint films. The significance of aluminium stearate as a stearic acid source in paint formulations is corroborated and is more significant than oil type or pigment combination for formation of high concentrations and more pronounced separation of saturated C16 and C18 chain zinc carboxylates.

18.1 Introduction

Zinc oxide became a frequent component of modern oil based paints following developments in industrial scale production during the 19th Century. Modern zinc white history and pigment properties have recently been reviewed (Osmond 2012). Zinc oxide was particularly valued in the housepaint industry for its good suspension properties in oil. Although some 19th Century artists specifically sought zinc white for its resistance to yellowing and blackening, artists generally were less enthusiastic about zinc white oil paint. However, zinc oxide was progressively incorporated into many artists' paints and in both the decorator and artists' paint markets it has typically been used to modify the properties of paints based on other white pigments or colours. Straight zinc white oil paints are less common, although the oil based Ripolin® gloss range much favoured by artists was substantially based on zinc oxide (Dredge et al. 2013; Gautier et al. 2009). Research indicates that even as a minor component zinc oxide strongly influences mechanical responses and water absorbency of paints (Browne 1956; Mecklenburg 2008).

Zinc oxide's effect on paint film properties makes its prevalence in 20th Century paints significant. An emerging body of evidence links zinc oxide to a variety of deterioration phenomena including formation of lumps based on zinc soaps of stearic and palmitic acids, and brittle paint films subject to cracking or cleavage between layers. The reactivity of zinc oxide with fatty acids in oil based paints to form zinc carboxylates appears implicated in each case.

The factors which determine whether zinc carboxylates aggregate to form lumps, migrate to interfaces, or remain dispersed throughout a paint film are the subject of ongoing research. Potential influences on zinc oxide reactivity have recently been reviewed (Osmond 2012). The zinc oxide particle is one variable, with different grades representing a range of particle and crystal properties. Zinc oxide is electrostatically unstable because it has two polar facets at opposing ends of the crystal, one terminating in zinc atoms and one with oxygen (Wöll 2007). Particle size and shape may emphasise the influence of one facet over another, and lattice variations will also influence pigment properties, particularly interactions with light with implications for fluorescence characteristics and photostability (Winter and Whittem 1950). Production method may influence properties; French (Indirect) Process is typically of higher purity, while American (Direct) process pigment is considered less reactive for paint applications because of its larger particle size and stoichiometry (Morley-Smith 1950, International Zinc Association 2009).

Other significant variables include availability and profile of fatty acids in the paint. Mid 20th Century paint producers focussed on reducing acid level and proportion of saturated fatty acids in oils (Elm 1957; Jacobsen and Gardner 1941). Various additives were found to influence solubility and dispersion of zinc soaps in prepared paints, with implications for shelf life (Ware and Christman 1916). More recently in studies of paintings, the significance of co-pigmentation has been raised with many incidences of deterioration being observed in the presence of other metal ions (Osmond 2012).

Isolating the most critical factors for paint stability is difficult given the complexity of typical formulations. Analysis and interpretation of samples from paintings is further complicated by external variables arising from artist technique, painting age, environmental history and conservation interventions, each with potential to influence paint film chemistry. The study of reference paint films and models offers the opportunity to examine specific aspects of paint ageing with fewer variables than unique works of art.

This paper involves a detailed study of paint films which differ only with respect to pigment composition in association with zinc oxide, oil type, the presence of specific additives, commercial brand or casting date. It expands on previously reported results indicating aluminium stearate in paint strongly influences formation and distribution of zinc carboxylates (Osmond et al. 2012). Interactions between pigment and fatty acid source alone are further examined in model systems.

18.2 Experimental

18.2.1 Reference paints

Paints containing zinc oxide (ZnO) were sourced from the Smithsonian's Museum Conservation Institute reference collection. Paints were cast on Melinex substrates between 1978 and 1999 and have aged naturally under stable interior ambient conditions. Cast films include a range of commercially available artists' paints and custom produced controls prepared using specified pigment and oil combinations. Samples discussed include artists' oil paints from Grumbacher, Winsor & Newton and Gamblin, and custom produced control paints containing ZnO alone or in combination with lead white, titanium white or within Naples yellow hue formulations. A variety of linseed oils, safflower and soybean oils, and preparations with and without aluminium stearate are represented. Optical microscopy of paint surfaces was followed by acquisition of spectra from exposed top and protected bottom surfaces using attenuated total reflectance - Fourier transform infrared spectroscopy (ATR-FTIR). Paint cross sections were prepared and examined using optical and scanning electron microscopies with elemental analysis (OM and SEM-EDX) while synchrotron-FTIR (SR-µFTIR) of thin paint cross sections enabled mapping of metal carboxylate distributions at high spatial resolution. Experimental conditions have been detailed previously (Osmond et al. 2012).

18.2.2 Model system

Model experiments were designed to support observations made in paint films by investigating specific component interactions under controlled conditions. A solvent model was chosen and toluene selected on the basis of trials and observed in-vial behaviour in conjunction with published solubility parameters and graphic models charting oil paint film solubility according to swelling response to specific solvents. The solvent was intended to model a 'typical' paint film based on an observed affinity implying comparable intermolecular forces. Toluene has been categorised as high-moderate swelling for a representative paint film (10 year old lead white and yellow ochre in linseed oil) (Phenix 2002). Sensitivity of the representative paint film to toluene was consistent between light- and dark-aged paint samples, indicating its applicability as a model has validity for paints at varying states of oxidation.

Zinc oxide pigment samples were obtained from Kremer Pigmente (Germany), also the source of ZnO used in formulating control paints in the Smithsonian reference collection. Tight particle size distribution was important to remove size as a variable, so ZnO grades not specifically produced for the pigment market were additionally obtained. Sample compositions were confirmed with X-ray diffraction and particle characteristics investigated using transmission electron microscopy (TEM) and particle sizing techniques. The International Zinc Association (2009) advocates ZnO with specific surface area 5 m^2/g as the preferred 'standard' for paint, corresponding to maximum opacity. Potential model candidates with comparable average particle size were sought, however only nano grades had sufficiently narrow size distributions. 30 nm ZnO, MKN-ZnO-030 (M K Impex Corp., Canada) was selected. Both Kremer and MKN samples comprise ZnO of wurtzite structure. TEM shows Kremer pigment has highly variable size and shape including acicular particles (**Fig. 18.1**). MKN particles are nodular and regularly sized with diameters consistently around 30 nm; particle shape is similar to an industrial paint grade pigment, Umicore White seal. Kremer ZnO has specific surface area 5.5-6.5 m^2/g (specified) compared with 16.6 m^2/g for MKN (measured). The larger surface area of 30 nm ZnO will enhance surface activity and reduce time

required for reactions of interest to proceed. To ensure comparable interactions occur with paint grade ZnO, selected experiments were conducted simultaneously using Kremer pigment.
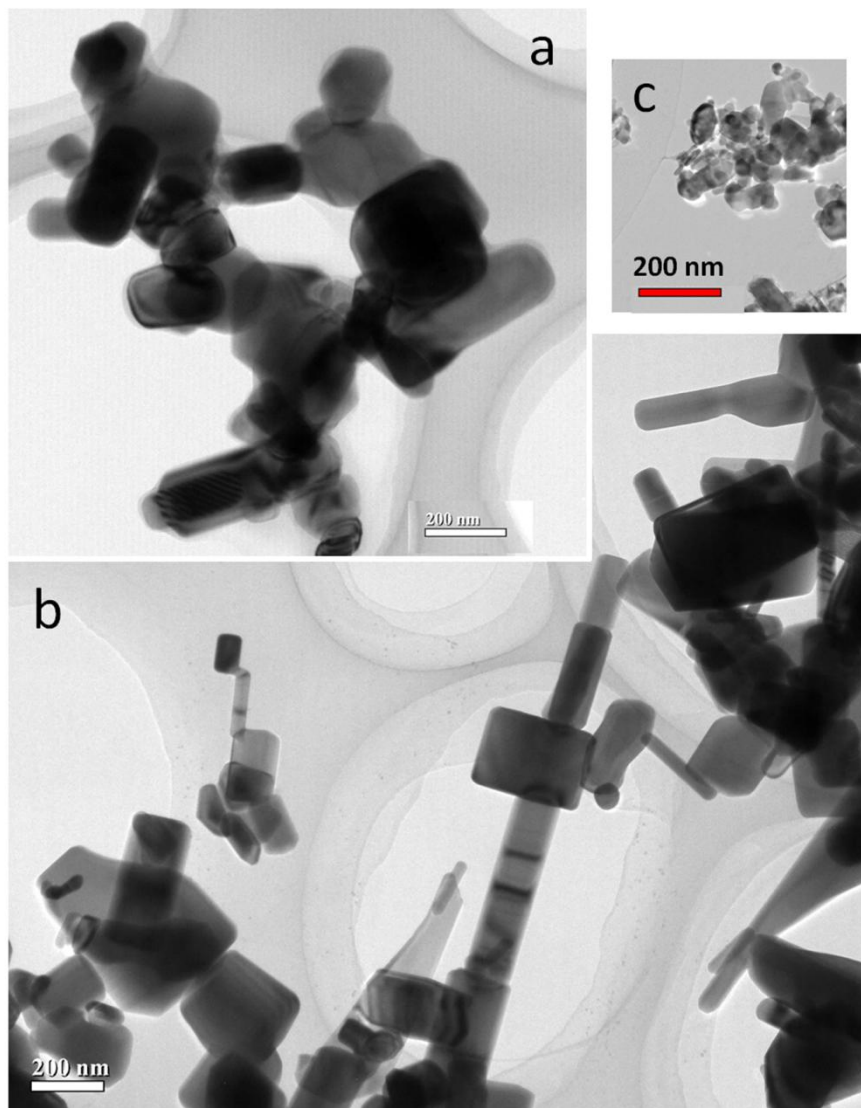
Fig. 18.1 TEM images of zinc oxide shown at equivalent magnification **a** Umicore 'White seal' **b** Kremer Pigmente 46300 **c** MKN-ZnO-030 (Images: Yanan Guo and John Drennan)

Reagent grade stearic acid ≥95% (octadecanoic acid) was obtained from Sigma Aldrich and its composition confirmed with FTIR.

Aluminium stearate was synthesised from sodium stearate and aqueous solution of aluminium sulfate (3:1 stoichiometry) using the modified double decomposition technique described by Corkery (2004). Transmission FTIR confirmed the presence of the intended soap, the absence of reactants and the extent of any free acid. Retention of some stearic acid in the synthesised soap was considered acceptable as it reflects industrial grades of aluminium stearate typically used in paint production.

Zinc oxide and stearic acid or aluminium stearate were combined with toluene in capped glass vials with Teflon liners. Reactants were combined in two ratios representing an excess of stearic acid (HSt) or ZnO assuming

$$ZnO + 2HSt \rightarrow ZnSt_2 + H_2O \qquad (18.1)$$
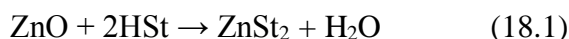
Zinc oxide is essentially insoluble in toluene, while stearic acid solubility was calculated as 42 g/L. In each vial the amount of stearic acid was at or below the solubility limit for the measure of toluene. Vials were manually shaken then left to stand. After five minutes, and subsequent intervals extending from minutes to hours and then days and weeks, each solution was shaken and a drop pipetted from the vial onto a glass slide to dry for in situ OM and FT-Raman, and sampling of solids for transmission FTIR.

18.3 Results and Discussion

18.3.1 Reference paint films

18.3.1.1 General observations

Microscopy
Magnified surface details of paint films reveal differences in physical appearance. Control paints prepared with ZnO and linseed oil of different preparations have features reflecting expected variation in rheology and drying rate, including strong retention of casting features in linseed + litharge formulations, consistent with rapid drying. Paints formulated with ZnO in different oils with aluminium stearate demonstrate the yellowing tendency of linseed oil, while fatty acid efflorescence is notable on the surface of soybean oil based paint (**Fig. 18.2**).

These distinctions are not apparent in comparable reference paints where titanium white is combined with ZnO, which have consistent appearance and pronounced granular texture. Of the commercially produced paints, surface texture varies according to pigment mix within Grumbacher paints and later Winsor & Newton paints but is less pronounced in 1978 Winsor & Newton samples which reflect an earlier formulation. More information is obtained through cross sections. Differences between 1978 and 1980 Winsor & Newton titanium paints are apparent both in OM (ultraviolet fluorescence - UVF) and backscatter electron (BSE) images. The later paint has a more perceptible fluorescent band at the top surface which has correspondingly lower electron density in BSE images. Differences apparent in cross sections from the range of Naples yellow paints are shown in **Fig. 18.3**.
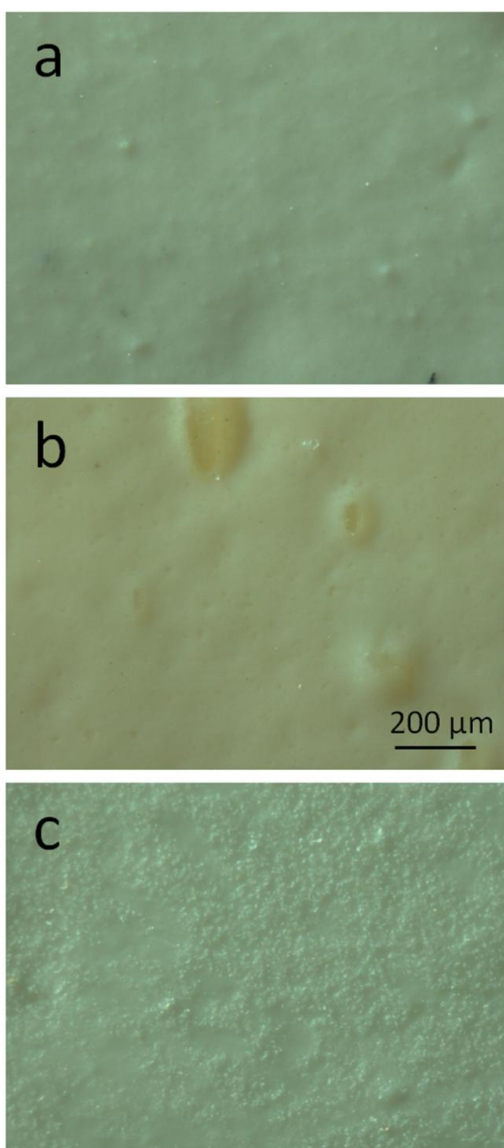
Fig. 18.2 Macro surface details of zinc white control paints with aluminium stearate cast 1998: **a** safflower, **b** linseed and **c** soybean oils

FTIR

Zinc oxide has no absorption signal in the mid infrared range between 4000 and 600 cm^{-1}, but oil based paints containing ZnO are among the most likely to develop strong carboxylate absorption (van der Weerd et al. 2005), reflecting formation of zinc soaps. Carboxylic acids present or formed produce a shoulder at wavenumber ca. 1705 cm^{-1} to the v C=O glycerol ester absorption (ca. 1740 cm^{-1}), accompanied by broad O-H stretch centred 3400 cm^{-1} and peaks at 1415 cm^{-1} and 915 cm^{-1}. Soap formation is characterised by disappearance of the O-H stretch and replacement of v C=O and C-O (1300 cm^{-1}) bands with COO$^-$ asymmetric and symmetric stretching at ca. 1550 cm^{-1} and 1400 cm^{-1}, reflecting the ionised structure of the COO-metal bond (Mehrotra et al. 1995). Broad carboxylate absorption reflects coordination of zinc ions to a range of carboxylate moieties. Individually, zinc stearate and palmitate have the same characteristic sharp peaks at 1540 cm^{-1} and 1398 cm^{-1}, and CH$_2$ bend at 1465 cm^{-1} (Robinet and Corbeil 2003). Aluminium stearate has characteristic absorptions at 1588 and 1469 cm^{-1}.

SR- μFTIR enables chemical maps to be produced by integrating absorbance intensities corresponding to specific vibrational frequencies and characteristic features of spectra represented

in the samples. Synchrotron source maps are of higher spatial and spectral resolution than those obtained by conventional FTIR mapping techniques. Zinc oxide pigment is of fine particle size (typically <1micron diameter, or 1-5 micron aggregated effective particle size), so high spatial resolution is critical to characterisation of the chemical signature of reactive sites at an early stage and allows correlation with high resolution backscatter electron images and elemental maps.

Across the range of ZnO-containing paints, ATR-FTIR measurement of exposed surfaces show varying intensity of carboxylate absorption but a broad peak 1560-1620 cm^{-1} is consistent irrespective of commercial origin, pigment combination, oil type, film age or presence of additives. The presence of specific zinc soaps is not indicated other than a small side peak at 1540 cm^{-1} in spectra from soybean oil based paint.

Previously reported results for white paints based on linseed and safflower oils showed a significant number of samples recorded unexpected differences in carboxylate profiles between exposed top and protected underside surfaces (Osmond et al. 2012). Upper surfaces invariably absorbed broadly while the underside of paints incorporating aluminium stearate recorded a defined peak at 1540 cm^{-1}, surprisingly not indicative of aluminium stearate but rather zinc stearate. In cross sections, SR-μFTIR integrated absorption intensity maps confirmed a preferential accumulation of zinc stearate in the lower margins of paints. Characteristic peaks for aluminium stearate were less frequently discernible over more general broad carboxylate absorption, but integration of the narrow band 1585-1595 cm^{-1} (v_a COO$^-$ aluminium stearate) produced maps showing a correlation with high intensity areas in maps of broader range, typically dispersed 5-10 μm diameter masses.

Paints without aluminium stearate recorded more subtle differences between surfaces. The presence of aluminium stearate influenced zinc carboxylate distribution more strongly than pigment composition or oil type. Here, results are presented for an expanded range of ZnO containing paints including whites produced with soybean oil and several commercial Naples Yellow hue formulations with varied and more complex pigmentation than paints previously discussed. Previously reported paints and the current selection are detailed in **Table 18.1**.

18.3.1.2 Naples yellow hue, linseed and safflower oil based paints

Winsor & Newton Naples yellow hue paints from 1978 and 1999 include lead white, ZnO and iron oxides, the older film additionally incorporates dolomite and neither contains aluminium stearate. FTIR spectra obtained from top and underside surfaces are similar although the generally broad carboxylate soap peak and oil carbonyl and triglyceride ester peaks appear smaller in underside spectra with a small side peak at 1540 cm^{-1}. Both paints are dominated by lead carbonate and ATR-FTIR reveals little difference in carboxylate absorption irrespective of the presence of dolomite; spectra are comparable to those obtained from similarly dated Winsor & Newton lead white paints. Spectra are also similar for Gamblin Naples yellow hue which includes ZnO and iron oxides but is otherwise formulated differently with cadmium sulphide, chalk and no lead carbonate (**Fig. 18.3**). UVF cross section images (supported by SEM-EDX) suggest Gamblin paint incorporates more ZnO than Winsor & Newton counterparts. Grumbacher paint similarly has a high proportion of ZnO which, with added aluminium stearate results in an intense underside peak at 1540 cm^{-1} consistent with underside spectra from zinc oxide/ aluminium stearate containing white paints.
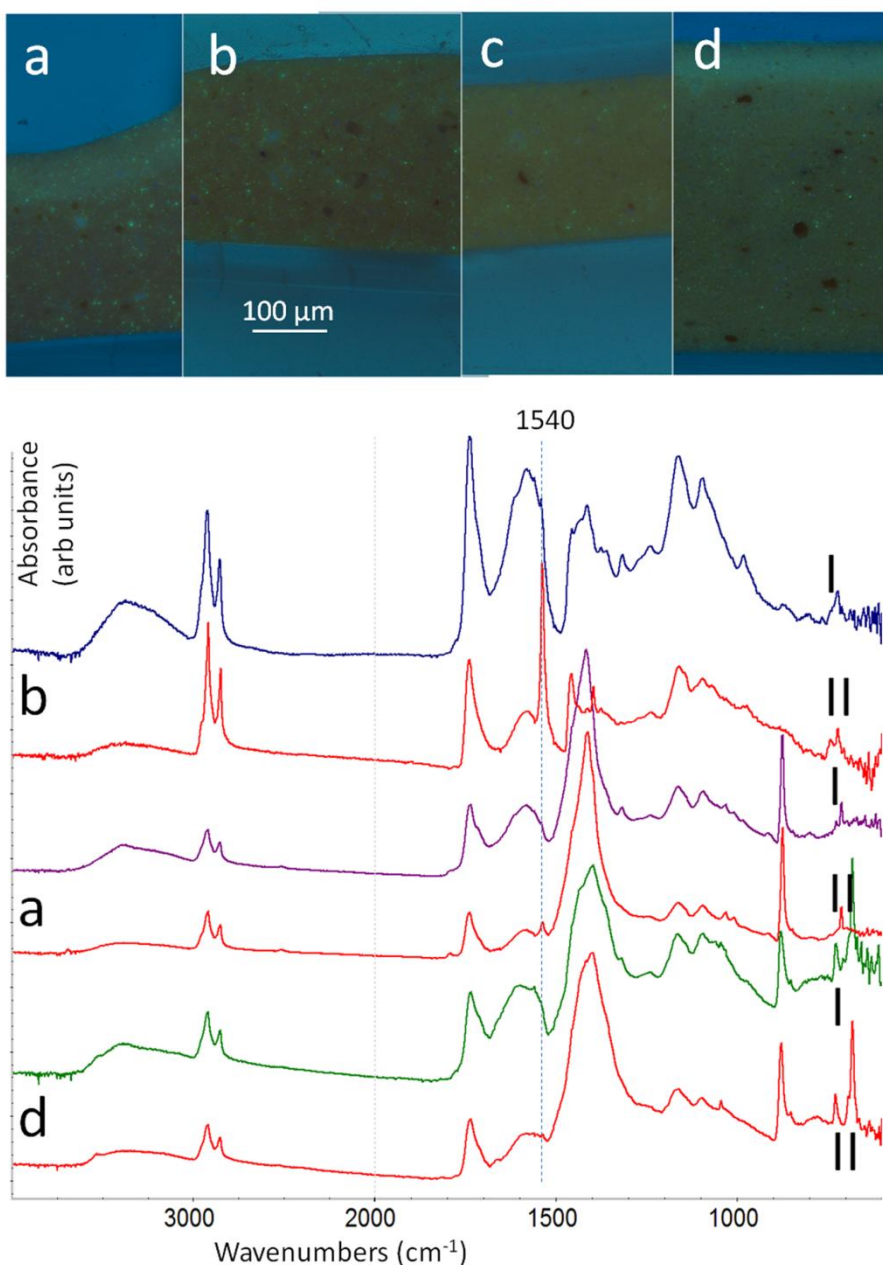
Fig. 18.3 UVF cross section images and ATR-FTIR spectral pairs from exposed surface (I) and protected underside spectra (II) of Naples yellow hue paints: **a** Gamblin 1999, **b** Grumbacher 1999, **c** Winsor & Newton 1999 and **d** Winsor & Newton 1978. Characteristic cross section fluorescence suggests more zinc oxide is present in Gamblin and Grumbacher paints. Differences in IR absorption between surfaces do not correlate with fluorescent surface bands. v_a COO$^-$ zinc stearate/palmitate (1540 cm^{-1}) features strongly in the Grumbacher underside spectrum which contains aluminium stearate.

UV fluorescent, low BSE density masses in Grumbacher paints have been previously shown to comprise aluminium stearate. Similar features in Gamblin paint are calcium based but have not been further characterised. In addition to large masses, calcium is also found in association with micron-sized carbon rich halos surrounding dispersed zinc based particles. Calcium driers function by competing for formation of carboxylate complexes, reducing mobility of fatty acid carboxylates with which they coordinate (Mallégol et al. 2000). Their alkalinity enables formation of stable salts

with acid groups (Soucek et al. 2012). Although no drier is present (R. Gamblin, personal communication, email 21 September 2013), it is curious that calcium is detected in close association with zinc based particles in paint with moderate and dispersed general carboxylate absorption despite a high concentration of ZnO.

Winsor & Newton Titanium white (1978) also has small (ca. 2 μm) dispersed low BSE intensity points but without the bright centres of Gamblin paint. These spots are carbon rich with trace contributions from elements generally present in the paint. The anomalous behaviour of this sample in recording strong underside zinc stearate FTIR absorption had been attributed to the likely inclusion of aluminium hydroxide in the formulation (Osmond et al. 2012). However there is less evidence for its presence in the 1978 paint than in later Winsor & Newton formulations which incorporate relatively large (10-20 μm) fluorescent inclusions high in carbon, aluminium and sulphur, in addition to similar magnesium based areas. A feature of the early Winsor & Newton paint not present in later titanium whites from Winsor & Newton or other manufacturers is a high proportion of dolomite. Dolomite has been used by Winsor & Newton in *Winton* Titanium white in conjunction with hydrogenated castor oil (HCO), an alternative rheology modifier to stearates (I. Garrett, personal communication, email 20 September 2013). HCO principally comprises glycerides of 12-hydroxystearic acid and stearic acid (Maskaev et al. 1971) and its presence could explain both the small carbon rich masses and the higher stearic acid concentration available for soap formation in this paint than comparable paints without HCO.

The strongest zinc stearate underside peak occurs in Grumbacher paints where similarities with control formulations with aluminium stearate indicate the additive contributes significantly to availability of stearic acid. Dissolution of ZnO to form zinc stearate is indicated in BSE images by irregular regions of reduced atomic density with less defined pigment particles. These regions are most prevalent in the lower margin of the film.

18.3.1.3 Soybean oil paints

Previously reported results indicate reactivity of oil in paint formulations has some relationship to the rapidity and extent of zinc soap formation. Comparably pigmented paints prepared with safflower oil had lower carboxylate absorption than those produced with linseed oil, and the processing of linseed oil also influenced reactivity with ZnO. However, addition of aluminium stearate contributed generically to zinc stearate formation, diminishing the significance of oil type. Unfortunately it is not possible to compare soybean oil paints with and without aluminium stearate as only controls with the additive are represented, and analysis of Speedball Titanium white suggests it is similarly formulated. Control soybean paint surface spectra unusually have a small 1540 cm^{-1} side peak adjacent to broad carboxylate absorption in addition to a stronger underside peak. Speedball paint has strong surface carboxyl doublets (oil plus acid) and negligible carboxylate absorption, in contrast with underside readings, consistent with high fatty acid concentration. Zinc stearate formation in the soybean + aluminium stearate range appears linked to ZnO concentration with the strongest 1540 cm^{-1} peak at the protected underside of paint with ZnO as the primary pigment.

SR-µFTIR of three soybean based paints was undertaken to determine spectral variation through film thickness. The zinc and titanium/zinc controls displayed distribution patterns consistent with previously reported results for the same pigment combinations with linseed and safflower oils, with zinc stearate concentrated in the lower margin of films (**Fig. 18.4**). Aluminium stearate is localised within small spots although none is detected in the single pigment film; its absence coincides with the highest zinc stearate concentration. Integration of the ester carbonyl peak above 1720 cm^{-1} (excluding that attributable to fatty acids) indicates levels of intact triglycerides are reduced where zinc stearate dominates.
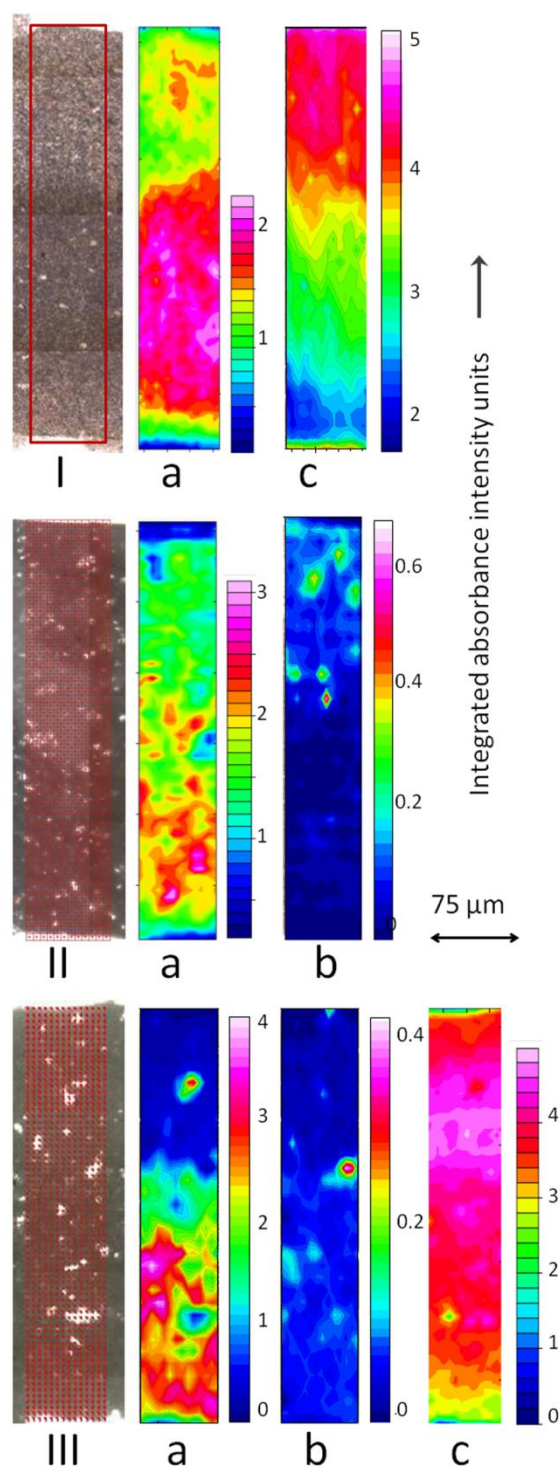
SR-µFTIR of Speedball (Titanium/ZnO) soybean paint resolved more complex zinc carboxylate distributions including areas with split carboxylate vibrations. In these instances carboxylate peaks are comparable to doublets expected for zinc oleate (Robinet and Corbeil 2003) but other characteristic bands are not visible and spectra are otherwise indistinguishable from those assigned to zinc stearate/palmitate (**Fig. 18.5**). Similar spectra have been observed in paintings which GCMS analysis indicates are mixed zinc soaps with zinc palmitate predominant (Helwig et al 2014). Another possible attribution includes hydrated stearates (Tachibana et al. 1970). Soybean oil has a higher combined percentage of palmitic, stearic and oleic acids than either linseed or safflower oils (typically 38% versus 28-29%) (Schilling et al. 2007).

Fig. 18.4 Transmission SR-µFTIR integrated absorption intensity maps for wavenumber range **a** 1525-1555, **b** 1580-1600, **c** 1720-1760 cm^{-1} for soybean based paints with aluminium stearate **I** zinc white control; **II** titanium + zinc white and aluminium silicate control; **III** Speedball titanium + zinc white. Boxed optical image details of thin sections indicate regions mapped
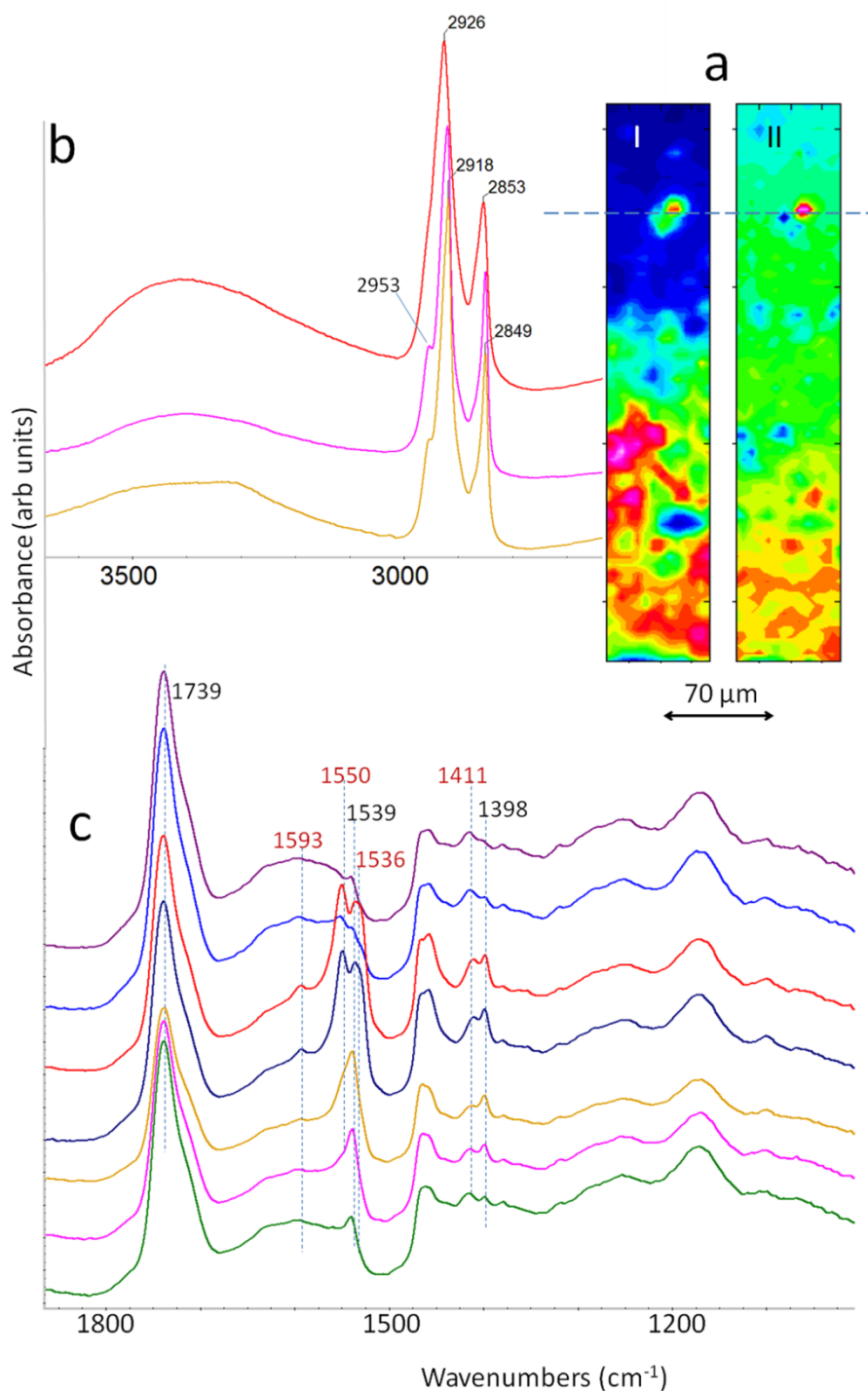
Fig. 18.5 Speedball titanium + ZnO soybean paint transmission SR-μFTIR **a** integrated absorption intensity maps for wavenumber range **I** 1525-1560 and **II** 2947-2960cm^{-1}; **b-c** spectra extracted from a line though the hotspot indicated centre top. Hotspots in map I include spectra with both singlet v_a COO$^-$ (1539) and doublet (1536 1550 cm^{-1}) (**a**). C-H stretching region (**b**) shows singlets are distinguished by CH$_2$ peaks at lower wavenumbers and a v_a CH$_3$ 2953 cm^{-1} shoulder, localised in map II.

Chemical maps show the single and split peak 'stearates' broadly occupy the same region although are distinguished as adjacent when individual spectra (5x5 μm apertures) are interrogated. Split peak spectra are associated with stronger carbonyl and ester C-O absorptions through the upper half of the paint film, where hydration is greatest. CH_2 vibrations also occur at higher wavenumbers (2926, 2853 cm^{-1}) than single peak spectra (2918, 2849 cm^{-1}), consistent with a relatively polar molecular environment (Derrick et al. 1999). The low values applicable to single peak soap structures are characteristic of highly compact trans-zigzag conformation of stearate chains with parallel packing (Sakai and Umemura 2002). Carboxylate doublets are also found in safflower Titanium/ZnO/aluminium silicate control paint with aluminium stearate, associated with spectra combining features of zinc and aluminium soaps where mixed structures may prevent compact packing.

18.3.2 Solvent model

Over the experimental time frame of several months, the initial small volume of solids in individual vials was observed to increase significantly and form a partial suspension. This was most apparent with MKN ZnO and stearic acid in excess. Very limited changes were observed for Kremer models over the same period. For the purposes of accelerating timelines, the results discussed below refer to solvent models prepared with MKN ZnO.

Droplets sampled from models with ZnO in excess indicate that available stearic acid reacts quickly to form zinc stearate, even with minimal agitation. Microscopy shows stearic acid has greatly diminished after 5 hours and is no longer present at 24 hours. Fine, irregular waxy aggregates are the only solid evident in droplets sampled at 24 hours. The FTIR spectrum of this substance is characteristic of zinc stearate, while FT-Raman and X-ray diffraction indicate ZnO is also present.

Zinc stearate formation is apparent in droplets sampled after 15 minutes from the aluminium stearate model. The characteristic 1541 cm^{-1} COO^{-} peak accompanies disappearance of the small C=O acid peak in the spectrum (**Fig. 18.6**) suggesting zinc stearate initially forms by reaction with the most readily available free acid, a reaction producing water (Eq. 18.1).

There is little to visually distinguish aluminium and zinc soaps within dried droplets as both solids comprise irregularly sized white lumps. After 1 hour, a fine perimeter ring dries separately to the bulk which FTIR characterises as stearic acid. Solids sampled from the centre of the droplet contain both zinc and aluminium soaps and spectra include peaks for Al-O/OH at ca. 986 and 3694 cm^{-1} consistent with hydrolysis of aluminium stearate (Eq. 18.2):

$$AlSt_2OH + H_2O \rightarrow AlSt(OH)_2 + HSt \qquad (18.2)$$

By 24 hours, there is little evidence of stearic acid; the purest zinc stearate phase dries at the centre of each droplet, while spectra from perimeter solids indicate a mixture of zinc and aluminium soaps. Insoluble gel lumps also form in the toluene and adhere to the vial walls following agitation. These comprise soaps with stronger Al-O contribution (Eq. 18.3):

$$2ZnO + 3AlSt_2OH + 2H_2O \rightarrow 2ZnSt_2 + 2AlSt(OH)_2 + Al(OH)_3 \qquad (18.3)$$
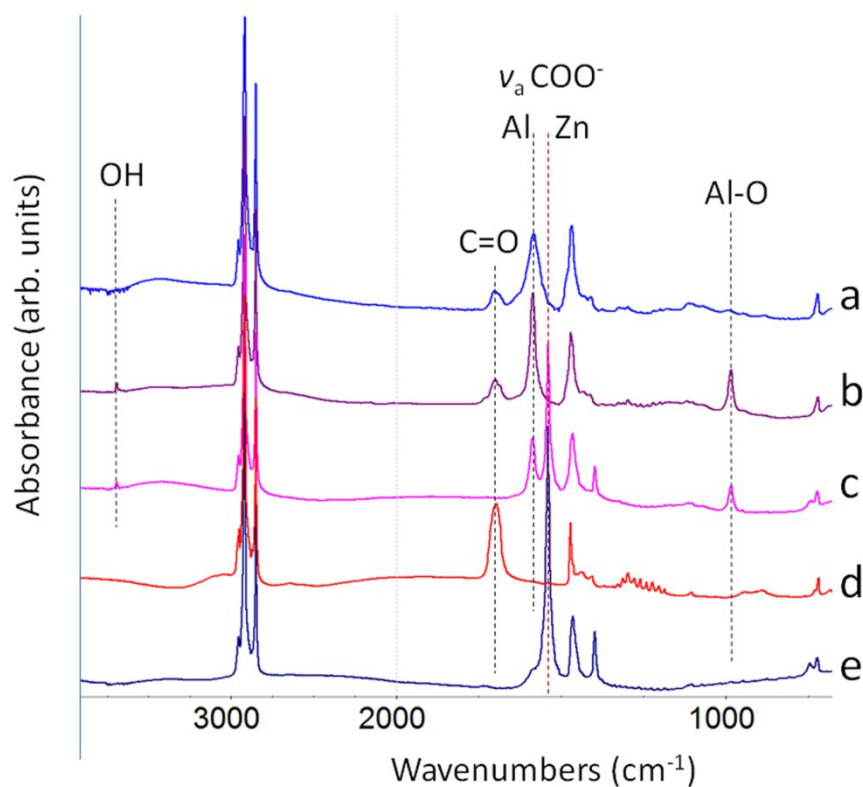
Fig. 18.6 Transmission FTIR spectral sequence obtained from ZnO and aluminium stearate in toluene. Aluminium stearate before mixing includes **a** free acid and **b** OH groups which have replaced stearate chains. Within minutes of combining zinc stearate peaks appear **c**, and after several hours purer phases of stearic acid **d** and zinc stearate **e** are obtained

The 24 hour aluminium stearate-model reaction sequence closely resembles what is observed in decade old reference paints. Incorporation of aluminium stearate increases concentration and availability of stearic acid typically released through hydrolysis. Additions of hydrogenated castor oil may function similarly. Hydroxyl groups replace stearate chains to form relatively polar molecules of aluminium mono- or di-stearate or aluminium hydroxide. In a paint film, increasing concentration of zinc stearate and contrasting polarity with Al-OH groups encourages phase separation. Zinc stearate is capable of highly efficient molecular conformation when associated with other similar molecules.

Beyond the presence of aluminium stearate, current and previously reported results indicate differences in ZnO reactivity are attributable to pigmentation and oil medium. Films pigmented solely with ZnO have higher surface area of zinc ions available to react with sources of stearic acid than comparable mixed pigment formulations. However only mixed-pigment control paints *with* aluminium stearate are available to compare with commercial formulations, where proprietary differences make it difficult to isolate possible influences of co-pigmentation on reactivity or propensity for phase separation.

Different oils have different fatty acid profiles influencing rate of reaction. Control paint prepared with ZnO and boiled linseed oil remains soft 20 years after casting with no discernible variation in FTIR absorbance between surfaces. Zinc stearate is less concentrated in decade-old Titanium/zinc/safflower oil control paint with aluminium stearate than comparable older films or films formulated with linseed oil. Paints with soybean oil and aluminium stearate are distinguished by accumulation of fatty acids and some zinc stearate at exposed surfaces.

Possible influences on carboxylate migration within reference paints cast onto Melinex have been discussed previously. Despite differences with typical painting supports, concentration of zinc soaps at interfaces between layers is implicated in instability, including a recent study of flaking paintings dated 1962-1980 by Vietnamese artist Nguyễn Trọng Kiệm (Osmond et al. 2013). Zinc oxide containing paintings are vulnerable to both intra- and interlayer failure.

18.4 Conclusion

Paint composition has implications for the reactivity of zinc oxide in oil based media. Rapid reactions in solvent models using nano-sized zinc oxide are comparable to those observed longer term in reference paints with larger artist grade pigment. Aluminium stearate is unequivocally shown to be a source of stearic acid which in the presence of zinc oxide will progressively be replaced by zinc stearate. Its inclusion in paints dominates more subtle differences in reactivity apparent between different oils. The availability of stearic acid from aluminium stearate or fatty acids released by oil hydrolysis facilitates formation of zinc soaps according to the amount of zinc oxide present. The influence of specific pigment combinations on carboxylate distributions has not been conclusively determined. Soaps with split carboxylate peaks revealed by high resolution SR-μFTIR may be indicative of mixed or hydrated soaps preventing compact packing configurations. Progressive reorganisation and aggregation of similar soap molecules is energetically favourable for C16 and C18 chain saturated zinc soaps as film chemistry increases in polarity with age. For zinc oxide containing paintings, specific pigment properties, fatty acid composition, additives and environmental history all influence component interactions with a range of aesthetic and structural consequences.

Table 18.1 Reference paints with composition as specified by manufacturers with additional pigmentation determined using optical microscopy, FTIR and SEM-EDX (italicised). Ratios indicate relative proportion by weight of zinc oxide to other pigments combined where known

Paint Manufacturer/Product name/Date of film casting	Composition Pigment	Oil, additive	Underside FTIR 1540 cm^{-1} peak
Naples Yellow hue			
Gamblin Naples yellow hue 1999	cadmium sulphide, natural hydrated iron oxide, red iron oxide, zinc oxide; *aluminium silicates, chalk*	Linseed, alkali refined	small
Grumbacher Naples yellow hue 1999	zinc oxide, calcined natural iron oxide, cadmium selenium sulphide, cadmium zinc sulphide co-precipitated with barium sulfate (6:1)	Linseed alkali refined + aluminium stearate	strong
Winsor and Newton Naples yellow (London oil colour series 2) 1978	Basic lead carbonate, cadmium sulphide, iron oxide; *zinc oxide, dolomite*	Linseed	negligible
Winsor and Newton Naples yellow1999	*basic lead carbonate, iron oxide, zinc oxide, chromium titanium yellow*	Not specified (linseed assumed)	small
Titanium whites soybean oil based			
Speedball *Titanium white* 1981	Titanium dioxide, zinc oxide	Soybean + *aluminium stearate*	strong
Custom control *Titanium white* 1998	Titanium dioxide, zinc oxide 12:1, aluminium silicate	Soybean modified + aluminium stearate	medium
Custom control *Zinc white* 1998	Zinc oxide	Soybean modified + aluminium stearate	strong
Titanium whites safflower oil based			
Winsor and Newton Titanium white 1978	Titanium dioxide, barium sulphate *(trace)*; *ZnO, dolomite*	Safflower *(+ HCO?)*	medium
Colorlab Titanium white 1981	Titanium dioxide, zinc oxide, barium sulphate 5:1:10	Safflower + aluminium stearate	strong

Winsor and Newton Titanium dioxide APermanent white 1980	*Titanium dioxide, zinc oxide, barium sulphate, magnesium carbonate, [Al, S]*	Safflower	negligible
Winsor and Newton Titanium white 1999	*Titanium dioxide, barium sulphate, magnesium carbonate, zinc oxide (trace)*	Not specified (safflower assumed)	negligible
Custom control *Titanium white* 1998	Titanium dioxide, zinc oxide 12:1, aluminium silicate	Safflower alkali refined + aluminium stearate	small

Titanium whites linseed based

Grumbacher Titanium white 1978	Titanium dioxide, zinc oxide 1:2; *trace aluminium silicate*	Linseed alkali refined + aluminium stearate	strong
Grumbacher Titanium white 1999	Titanium dioxide, zinc oxide	Linseed alkali refined + *aluminium stearate*	strong
Custom control *Titanium white* 1998	Titanium dioxide, zinc oxide 12:1, aluminium silicate	Linseed + aluminium stearate	strong
Colorlab Titanium white 1981	Titanium dioxide, zinc oxide, barium sulfate 5:1:10; *[Al, S, Cl]*	Linseed + aluminium stearate	strong
Gamblin Titanium white 1999	Titanium dioxide, zinc oxide; *chalk, trace aluminium silicate*	Linseed alkali refined	very small

Lead whites safflower based

Winsor and Newton Flake white 1978	Basic lead carbonate; *zinc oxide, barium sulphate, [Al, C]*	Safflower	small
Winsor and Newton Flake white no.1 ASilver white 1980	Basic lead carbonate; *zinc oxide, aluminium silicate, chalk*	Safflower	negligible
Winsor and Newton Flake white 1999	*Basic lead carbonate, zinc oxide*	Not specified (safflower assumed)	small

Lead whites linseed based

Grumbacher Flake white 1978	Basic lead carbonate, zinc oxide 20:1	Linseed alkali refined + aluminium stearate	strong
Grumbacher Flake white 1999	Basic lead carbonate, zinc oxide	Linseed alkali refined + *aluminium stearate*	strong

Zinc whites safflower based

Winsor and Newton Zinc white 1978	Zinc oxide	Safflower	small
Custom control *Zinc white* 1998	Zinc oxide	Safflower alkali refined + aluminium stearate	strong

Zinc whites linseed based

Grumbacher Zinc white 1978	Zinc oxide	Linseed alkali refined + aluminium stearate	strong
Custom control *Zinc white* 1998	Zinc oxide	Linseed + aluminium stearate	strong
Custom control *Zinc white* 1990	Zinc oxide	Linseed boiled	negligible
Custom control *Zinc white* 1990	Zinc oxide	Linseed cold pressed	negligible
Custom control *Zinc white* 1990	Zinc oxide	Linseed with litharge	very small

References

Browne FL (1956) Swelling of paint films in water VIII: Swelling of linseed oil paints in water and organic liquids. Forest Products Journal 6:312-318

Corkery RW (2004) A variation on Luzzati's soap phases. Room temperature thermotropic liquid crystals. PCCP 6:1534-1546. doi:10.1039/B315595C

Derrick M, Stulik D, Landry J (1999) Infrared spectroscopy in conservation science. The Getty Conservation Institute Los Angeles

Dredge P, Schilling MR, Gautier G, Mazurek J, Learner T, Wuhrer R (2013) Lifting the Lids Off Ripolin: A Collection of Paint from Sidney Nolan's Studio. Journal of the American Institute for Conservation 52 (4)

Elm AC (1957) Reevaluation of the function of pigments in paints. Official Digest (April):351-385

Gautier G, Bezur A, Muir K, Casadio F, Fiedler I (2009) Chemical Fingerprinting of Ready-Mixed House Paints of Relevance to Artistic Production in the First Half of the Twentieth Century. Part I: Inorganic and Organic Pigments. Appl Spectrosc 63 (6):597-603

Helwig K, Poulin J, Corbeil M-C, Moffat E, Duguay D (2014) Using analysis to shed light on conservation issues in several 20th-century Canadian oil paintings. This proceedings, Chapter 11

International Zinc Association (2009) Commercial grades of zinc oxide. International Zinc Association. http://www.znoxide.org/commercial_grades.html. Accessed 7 June 2010

Jacobsen AE, Gardner WH (1941) Zinc soaps in paints: zinc oleates. Ind Eng Chem 33 (10):1254-1256

Mallégol J, Lemaire J, Gardette J-L (2000) Drier influence on the curing of linseed oil. Prog Org Coat 39:107-113

Maskaev AK, Man'kovskaya NK, Lend'el IV, Fedorovskii VT, Simurova EI, Terent'eva VN (1971) Preparation of 12-hydroxystearic acid, the raw material for plastic greases. Chem Technol Fuels Oils 7 (2):109-112. doi:10.1007/bf00718698

Mecklenburg MF (2008) Meccanismi di cedimento nei dipinti su tela: approcci per lo sviluppo di protocolli di consolidamento - Failure Mechanisms in Canvas Supported Paintings: Approaches for Developing Consolidation Protocols. I Talenti. Metodologie, tecniche e formazione nel mondo del restauro Il Prato, Padova

Mehrotra KN, Shukla RK, Chauhan M (1995) Spectroscopic and Conductometric Studies of Lanthanide Soaps. Bull Chem Soc Jpn 68 (7):1825-1831

Osmond G (2012) Zinc white: a review of zinc oxide pigment properties and implications for stability in oil-based paintings. AICCM Bulletin 33:20-29

Osmond G, Boon JJ, Puskar L, Drennan J (2012) Metal stearate distributions in modern artists' oil paints: surface and cross-sectional investigation of reference paint films using conventional and synchrotron infrared microspectroscopy. Appl Spectrosc 66 (10):1136-1144. doi:10.1366/12-06659

Osmond G, Ebert B, Drennan J (2013) Zinc oxide centred deterioration in 20th century Vietnamese paintings by Nguyễn Trọng Kiệm. AICCM Bulletin 34 (in press)

Phenix A (2002) Building Models: Comparative swelling powers of organic solvents on oil paint and the cleaning of paintings. V&A Conservation Journal 40 (Spring)

Robinet L, Corbeil MC (2003) The characterization of metal soaps. Stud Conserv 48 (1):23-40

Sakai H, Umemura J (2002) Evaluation of molecular structure in Langmuir monolayers of zinc stearate and zinc 12-hydroxystearate by IR external reflection spectroscopy. Colloid Polym Sci 280 (4):316-321. doi:10.1007/s003960100581

Schilling MR, Mazurek J, Learner TJS (2007) Studies of modern oil-based artists' paint media by gas chromatography/mass spectrometry. Modern paints uncovered. The Getty Conservation Institute Los Angeles:129-139

Soucek MD, Khattab T, Wu J (2012) Review of autoxidation and driers. Prog Org Coat 73 (4):435-454. doi: 10.1016/j.porgcoat.2011.08.021

Tachibana T, Kitazawa S, Takeno H (1970) Studies of Helical Aggregates of Molecules. II. The Sense of Twist in the Fibrous Aggregates from the Alkali Metal Soaps of Optically Active 12-Hydroxystearic Acid. Bull Chem Soc Jpn 43 (8):2418-2421

van der Weerd J, van Loon A, Boon JJ (2005) FTIR studies of the effects of pigments on the aging of oil. Stud Conserv 50 (1):3-22

Ware EE, Christman RE (1916) A study of the effect of storage on mixed paints. Ind Eng Chem 8 (10):879-883

Winter G, Whittem RN (1950) Fluorescence and photo-chemical activity of zinc oxides. Journal of the Oil & Colour Chemists' Association 33 (November):477-483

Wöll C (2007) The chemistry and physics of zinc oxide surfaces. Prog Surf Sci 82:55-120

3.5 Supplementary information

3.5.1 Surface paint film analysis

3.5.1.1 Microscopy

Magnified surface details of paint films reveal differences in physical appearance. Control paints prepared with zinc oxide and linseed oil of different preparations have features reflecting expected variation in rheology and drying rate, including strong retention of casting features in formulations of linseed oil with litharge, consistent with rapid drying (Figure 3.1).
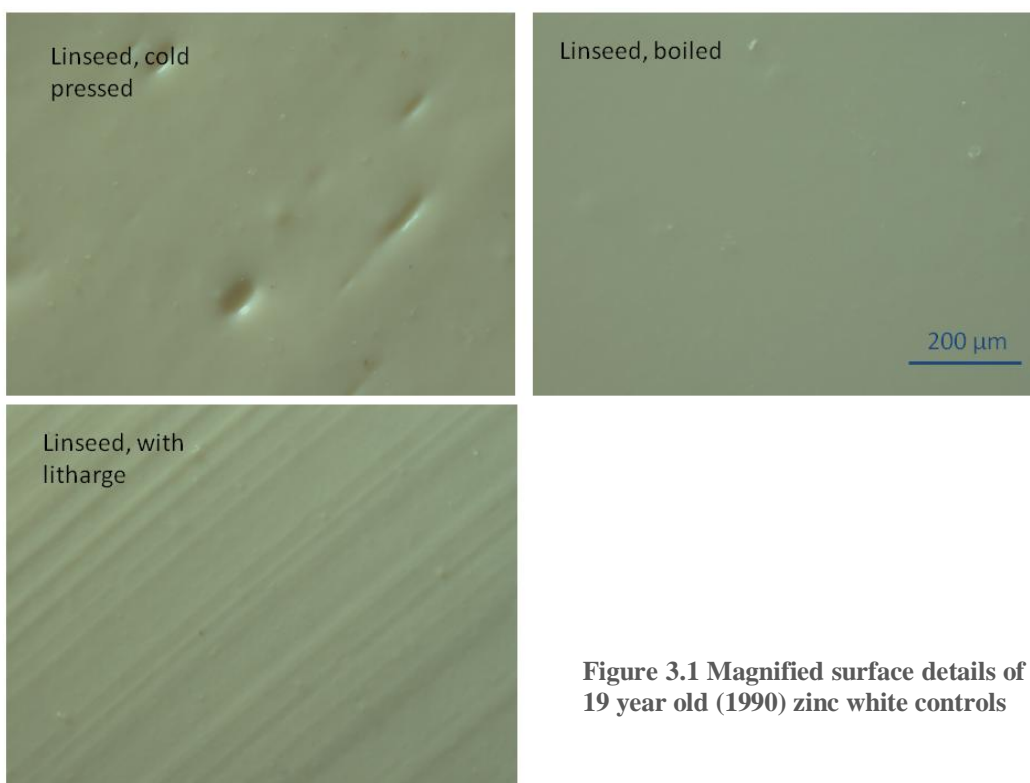
Figure 3.1 Magnified surface details of 19 year old (1990) zinc white controls

Paints formulated with zinc oxide in different oils with aluminium stearate demonstrate the greater yellowing tendency of linseed oil, while fatty acid efflorescence is notable on the surface of soybean oil-based paint (Figure 3.2). These distinctions are not apparent in comparable reference paints where titanium white is combined with zinc oxide, which have relatively consistent appearance and a pronounced granular texture (Figure 3.3).

safflower

linseed

200 µm

soya
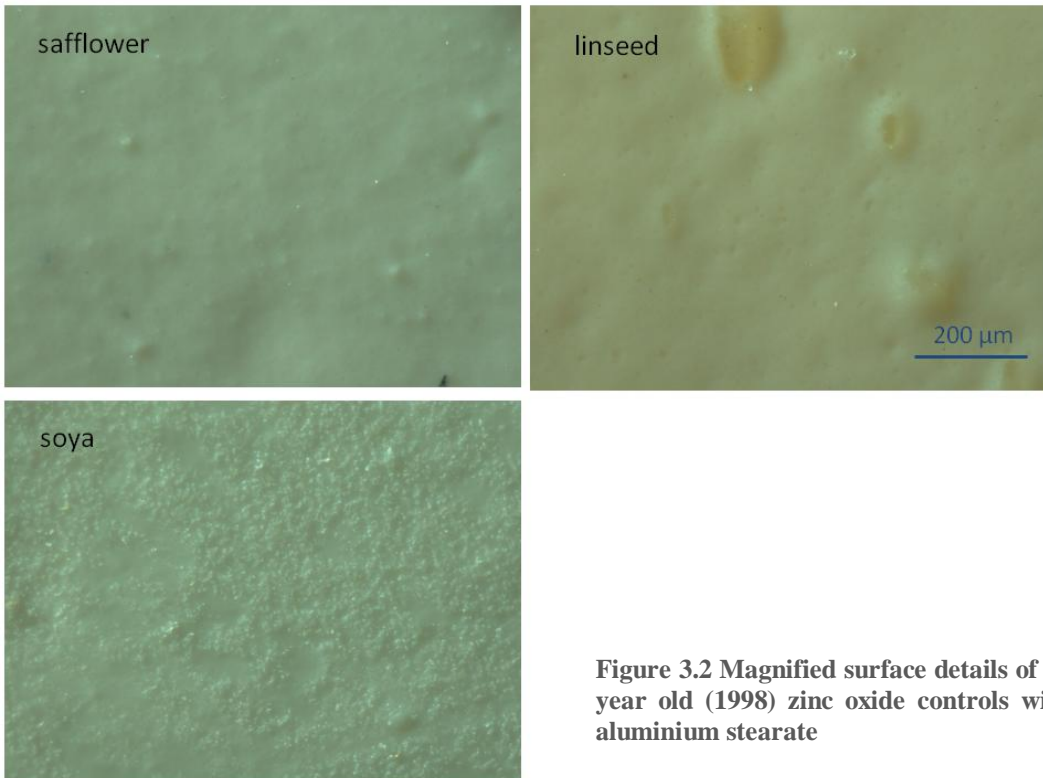
Figure 3.2 Magnified surface details of 11 year old (1998) zinc oxide controls with aluminium stearate

safflower

linseed

200 µm

soya
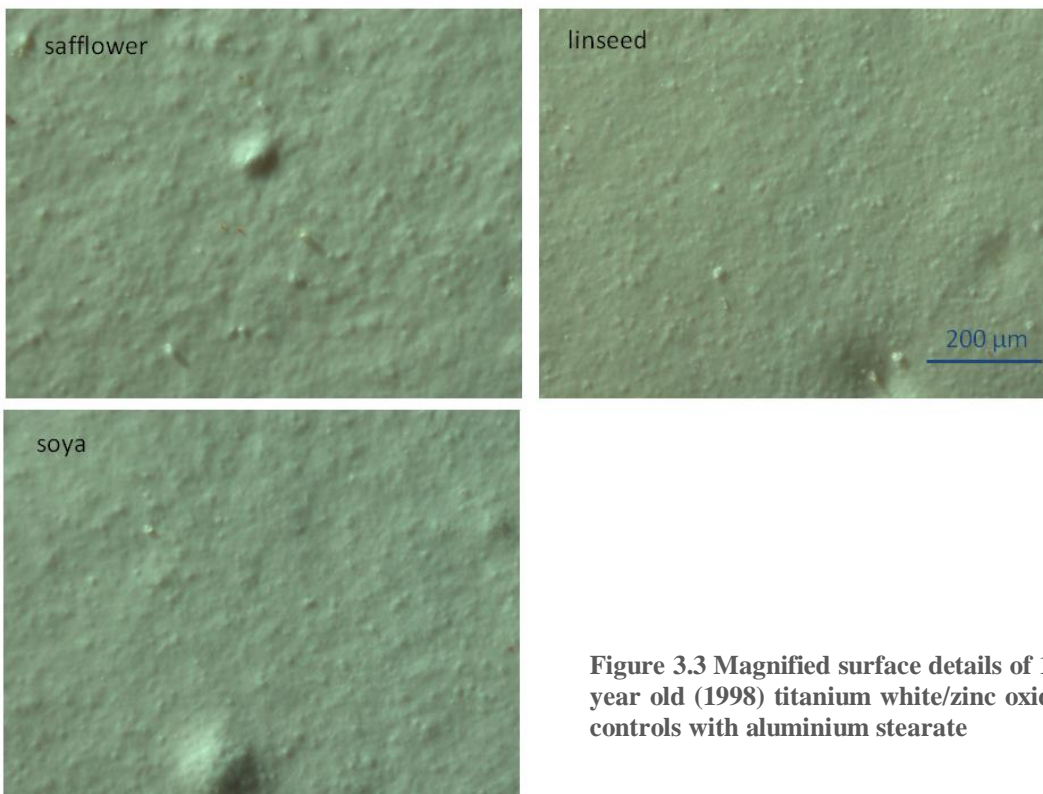
Figure 3.3 Magnified surface details of 11 year old (1998) titanium white/zinc oxide controls with aluminium stearate

Of the commercially produced paints, surface texture varies according to pigment mix within Grumbacher paints (Figure 3.4) and later W&N paints but is less pronounced in 1978 W&N samples which reflect an earlier formulation (Figure 3.5).

Titanium

Flake (lead)

200 μm
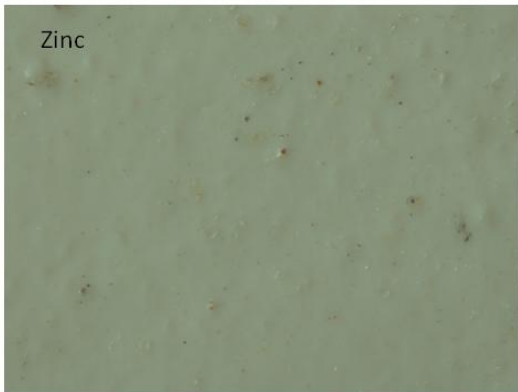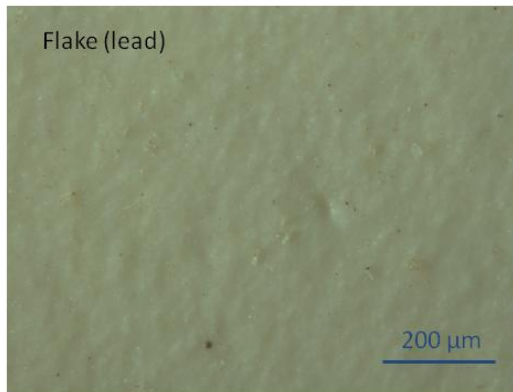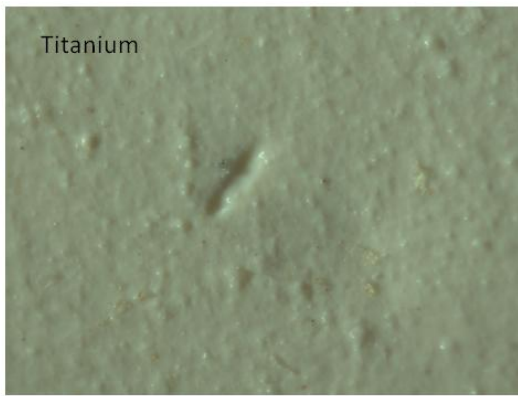
Zinc

Figure 3.4 Magnified surface details of 31 year old (1978) Grumbacher linseed whites (all containing zinc oxide with aluminium stearate)

Titanium

Flake (lead)

200 μm
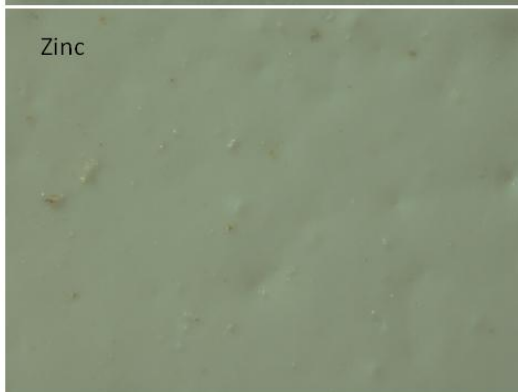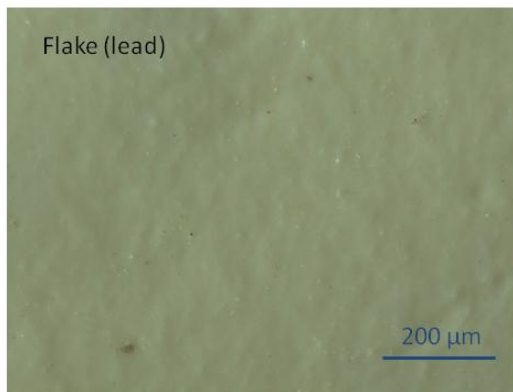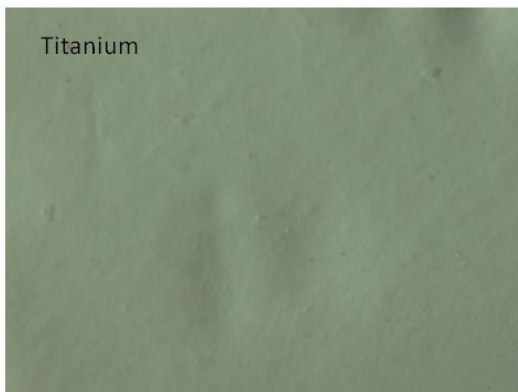
Zinc

Figure 3.5 Magnified surface details of 31 year old (1978) Winsor and Newton safflower whites (all containing zinc oxide)
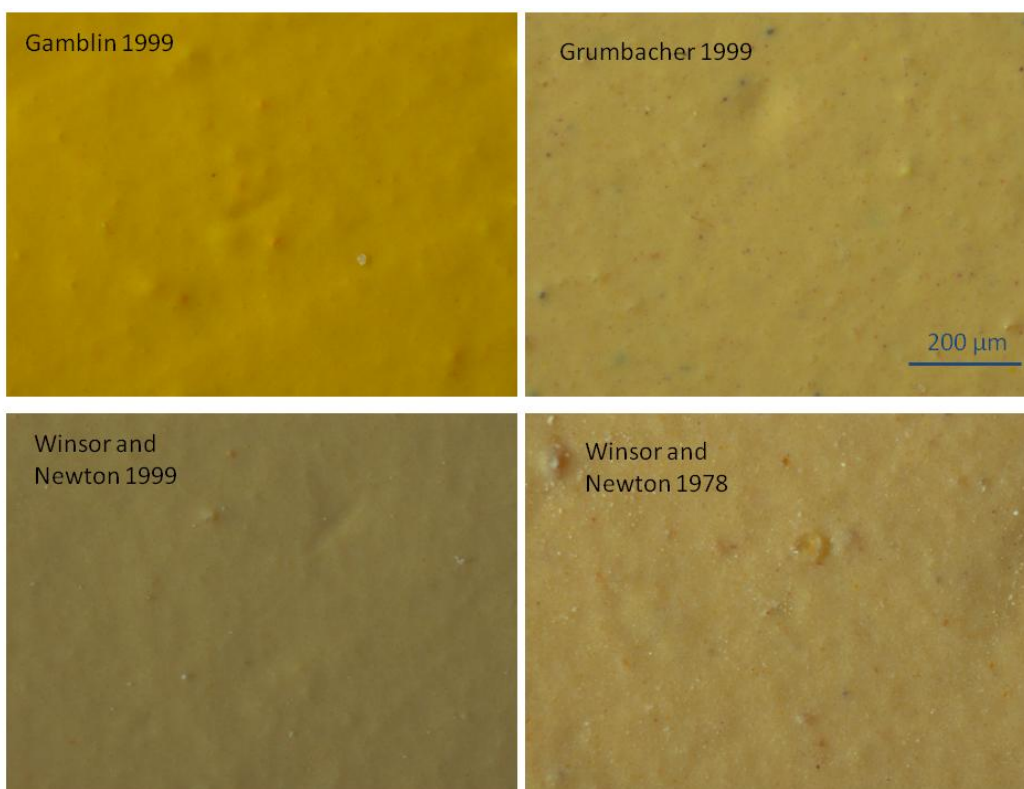
Figure 3.6 Magnified surface details of commercial Naples yellow hue paint films comprising various pigment combinations but all including zinc oxide

3.5.1.2 FTIR

ATR-FTIR spectra obtained from the exposed top surfaces of a representative range of the paints are shown in Figure 3.7. Significant variation is attributable to differences in pigmentation, reflected most strongly in spectral features below 1500 cm^{-1}. However, absorption in the asymmetric metal carboxylate band 1520-1630 cm^{-1}, while varying in intensity, is otherwise remarkably consistent across the compositional range, forming a broad, rounded peak. Only the titanium soybean-based control paint spectrum includes a discernible small side peak at 1540 cm^{-1}.

Spectra obtained from protected undersides of a representative range of paints are shown in Figure 3.8. While many spectra are similar to those obtained from the top surfaces, more variation within the carboxylate band is apparent across the compositional range. An intense sharp side peak at 1540 cm^{-1} is evident in several spectra, most notably the 1978 Grumbacher zinc white sample, shown in more detail in Figure 3.9.
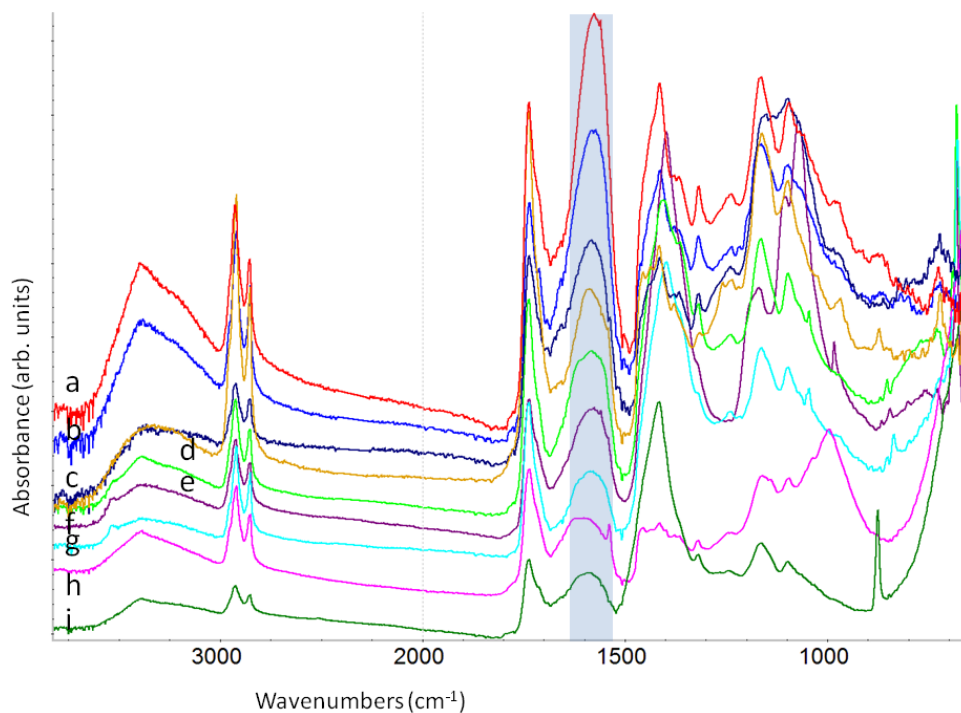
Figure 3.7 ATR-FTIR spectra from exposed top surfaces

(a) Zn control linseed litharge 1990; (b) W&N Zn safflower 1978; (c) Grumbacher Zn linseed 1978; (d) Zn control linseed boiled 1990; (e) W&N Pb 1999; (f) W&N Pb safflower 1978; (g) W&N Naples yellow linseed 1978; (h) Ti/Zn/aluminium stearate soybean control 1998; (i) Gamblin Ti linseed 1999. Highlighted band corresponds to wavenumber range 1520-1630 cm^{-1}
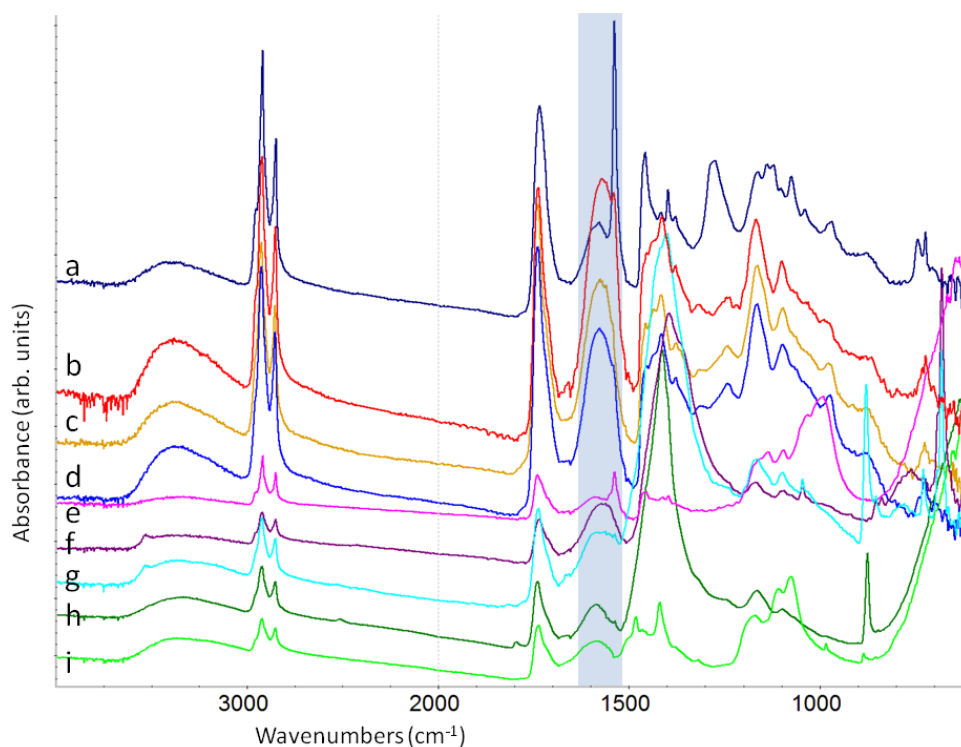
Figure 3.8 ATR-FTIR spectra from protected underside surfaces

(a) Grumbacher Zn linseed 1978; (b) W&N Zn safflower 1978; (c) Zn control linseed cold press 1990; (b) (d) Zn control linseed litharge 1990; (e) Ti/Zn/aluminium stearate soybean control 1998; (f) W&N Pb safflower 1980; (g) W&N Naples yellow linseed 1978; (h) Gamblin Ti linseed 1999; (i) W&N Ti safflower 1980. Highlighted band corresponds to wavenumber range 1520-1630 cm^{-1}
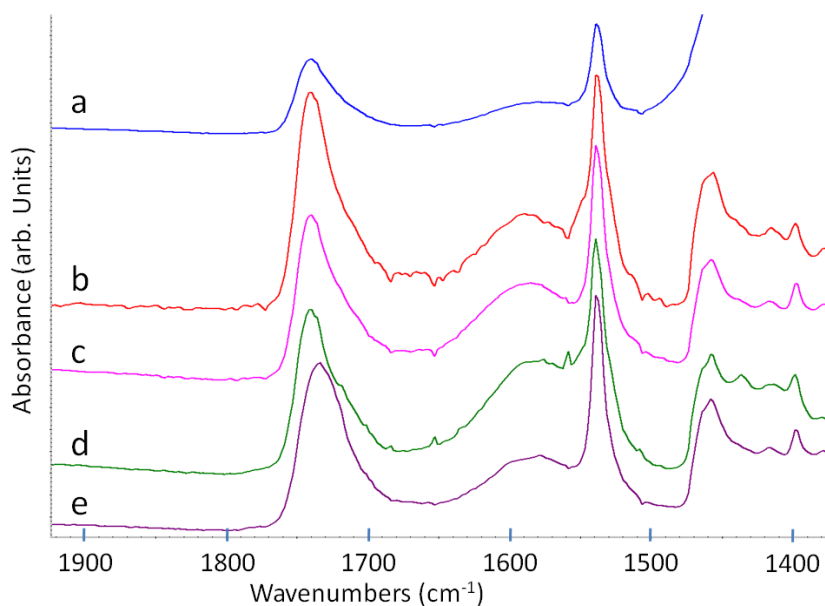
Figure 3.9 ATR-FTIR spectra from protected underside surfaces detailing carboxylate region of paints with a defined peak *ca* 1540 cm^{-1} (a) Grumbacher Pb 1999; (b) Ti/Zn/aluminium stearate linseed control 1998; (c) Grumbacher Ti 1999; (d) Colorlab Ti 1981; (e) Grumbacher Zn 1978

The intensity of the underside spectral peak in these examples is in sharp contrast to the broad, rounded carboxylate absorption obtained from the exposed top surfaces of the same paints. The incidence and intensity of the 1540 cm^{-1} underside peak shows little correlation to primary pigmentation or oil type, but suggests a strong correlation between this peak and formulations containing aluminium stearate. The least variation between surfaces occurs in zinc oxide control paint produced with boiled linseed oil (Figure 3.10).
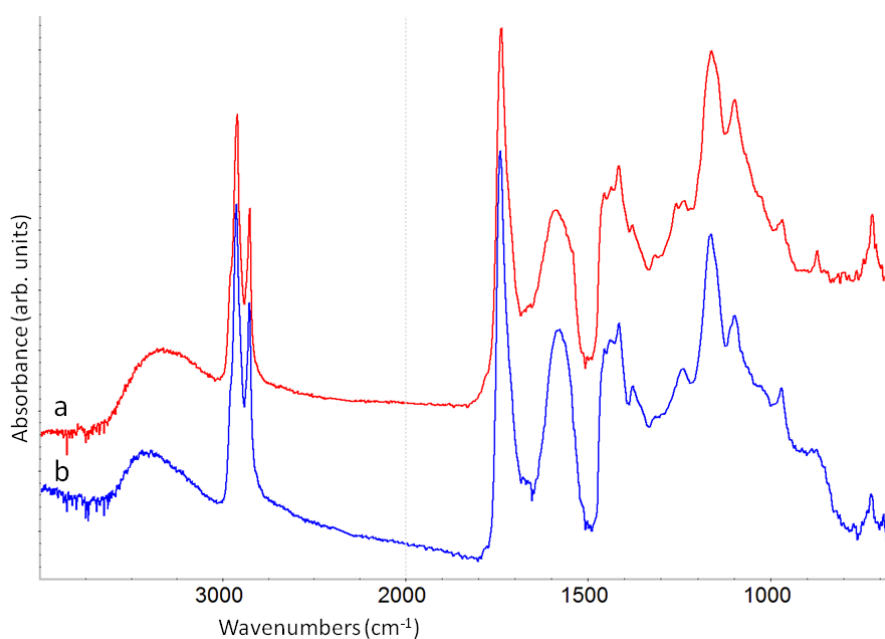
Figure 3.10 ATR-FTIR spectra from Zn linseed boiled 1990 control (a) exposed top (b) protected underside. Very little variation is apparent between the two surfaces consistent with low reactivity

One exception to the occurrence of strong underside absorption at 1540 cm^{-1} in paints formulated with aluminium stearate was titanium white safflower custom control with zinc oxide. Despite incorporating aluminium stearate the underside of this paint did not record a defined 1540 cm^{-1} peak. Figure 3.11 shows its spectrum in comparison to that from the underside of the equivalent linseed control paint and an older titanium white safflower paint film (Colorlab) also with zinc oxide and aluminium stearate.
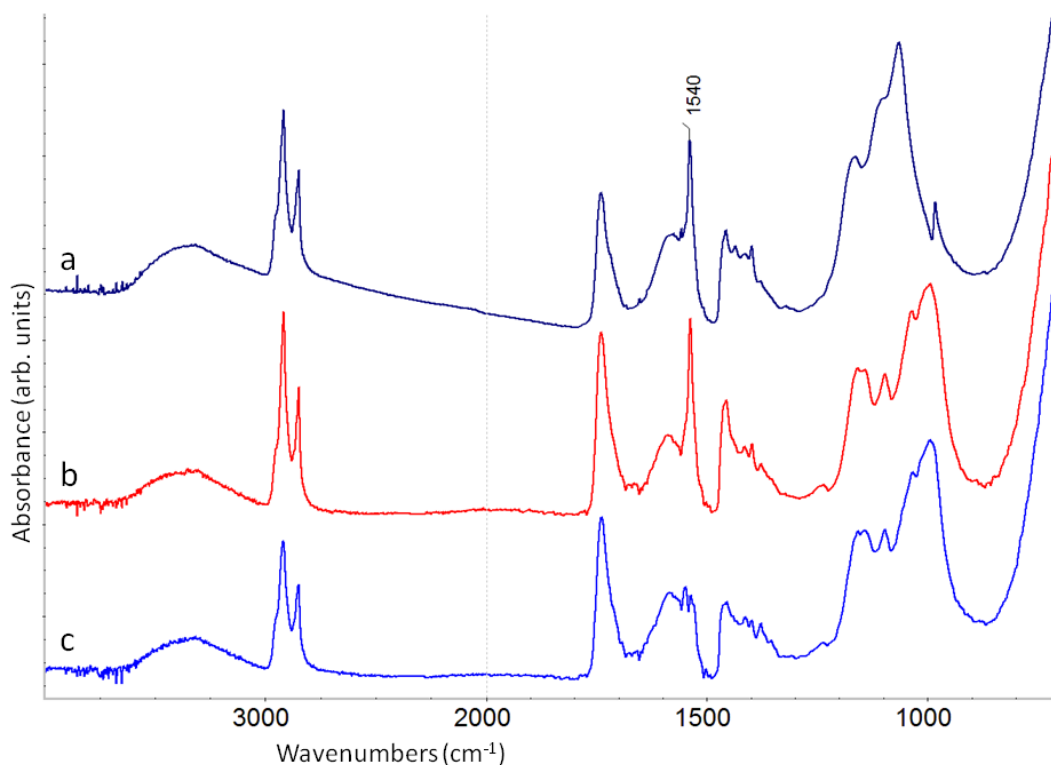
Figure 3.11 ATR-FTIR spectra from protected underside surfaces of Ti paints

(a) Colorlab 1981; (b) linseed control + aluminium stearate 1998; (c) safflower control + aluminium stearate 1998. The absence of a defined 1540 cm^{-1} peak in (c) is an anomaly, possibly reflecting the combination of lower reactivity and younger film age than counterparts

Possible explanations for the absence of a distinct 1540 cm^{-1} absorption in the titanium white safflower control despite the inclusion of aluminium stearate include the lower reactivity of safflower oil relative to linseed oil as a result of a composition dominated by $C_{18:2}$ as opposed to $C_{18:3}$ fatty acids, in combination with less film age than its similarly formulated counterpart (11 years versus 28 years at the time of measurement).

Spectra from commercially produced titanium white paints containing zinc oxide of comparable film age (all cast 1999 and 10 years of age when measured) but different fillers and additives are shown in Figure 3.12. Broad carboxylate absorption is observed at both exposed and protected

surfaces contracted towards lower wavenumber at undersides except in the case of Grumbacher paint - formulated with aluminium stearate. Carbonate absorptions (calcium: 1415, 874 cm^{-1} and magnesium: 1483, 1420 cm^{-1}) are also stronger in spectra measured at underside surfaces while the intensity of barium sulfate peaks (1174, 1118, 1072, 983) appears more consistent.
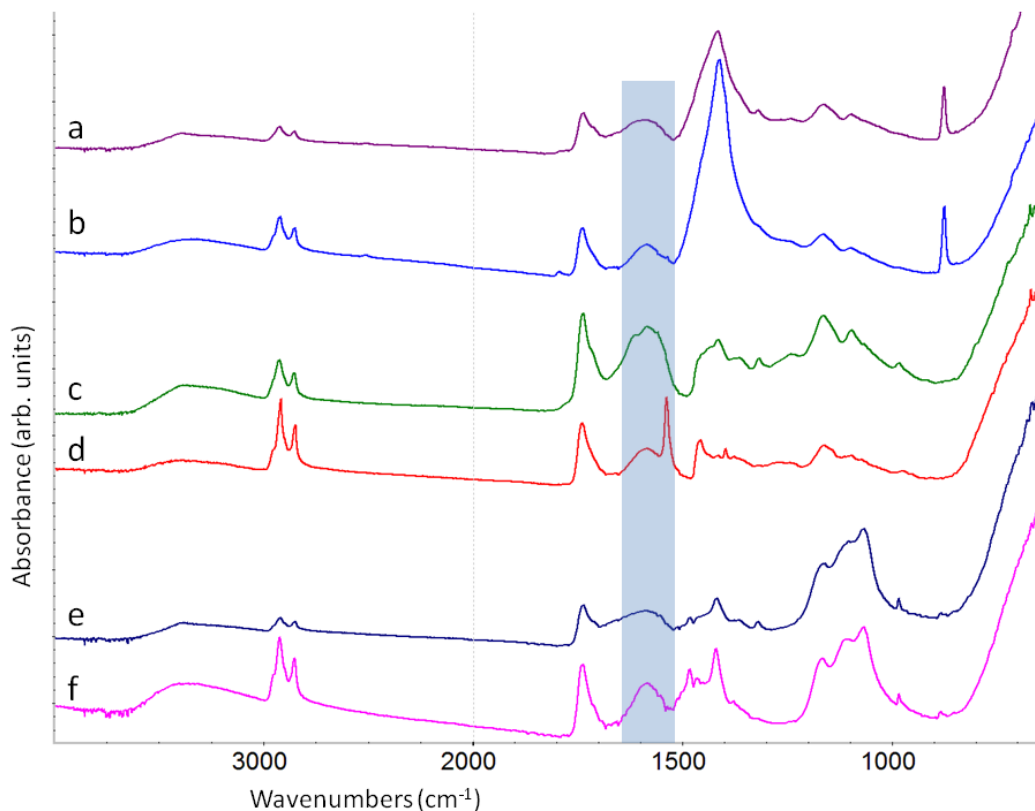
Figure 3.12 ATR-FTIR spectra from various Ti/Zn paints of same film age (1999, or 10 years when measured) but different additives

Gamblin (a) top and (b) underside with calcium carbonate; Grumbacher (c) top and (d) underside with aluminium stearate; W&N (e) top and (f) underside with barium sulfate + magnesium carbonate. A clear distinction in carboxylate absorption is apparent in the formulation with aluminium stearate. Highlighted band corresponds to wavenumber range 1520-1630 cm^{-1}

The incidence of a 1540 cm^{-1} peak in paints containing aluminium stearate invites the assumption that this peak is characteristic of that additive. However overlay with reference spectra indicates no distinct aluminium stearate absorptions are evident, and the 1540 cm^{-1} peak is instead consistent with the asymmetric COO^{-} stretch for zinc stearate (Figure 3.13). Zinc stearate is itself a known paint additive, however has not been used in formulating any of the paints included in this study [proprietary information made available by Marion Mecklenburg, Smithsonian Museum Conservation Institute (email 23 February 2011) and Phil Jones, Group Innovation and Development Director, ColArt International Holdings, Ltd. London (email 8 March 2011)]. In these paints zinc stearate is inferred to have formed following reaction with zinc oxide.
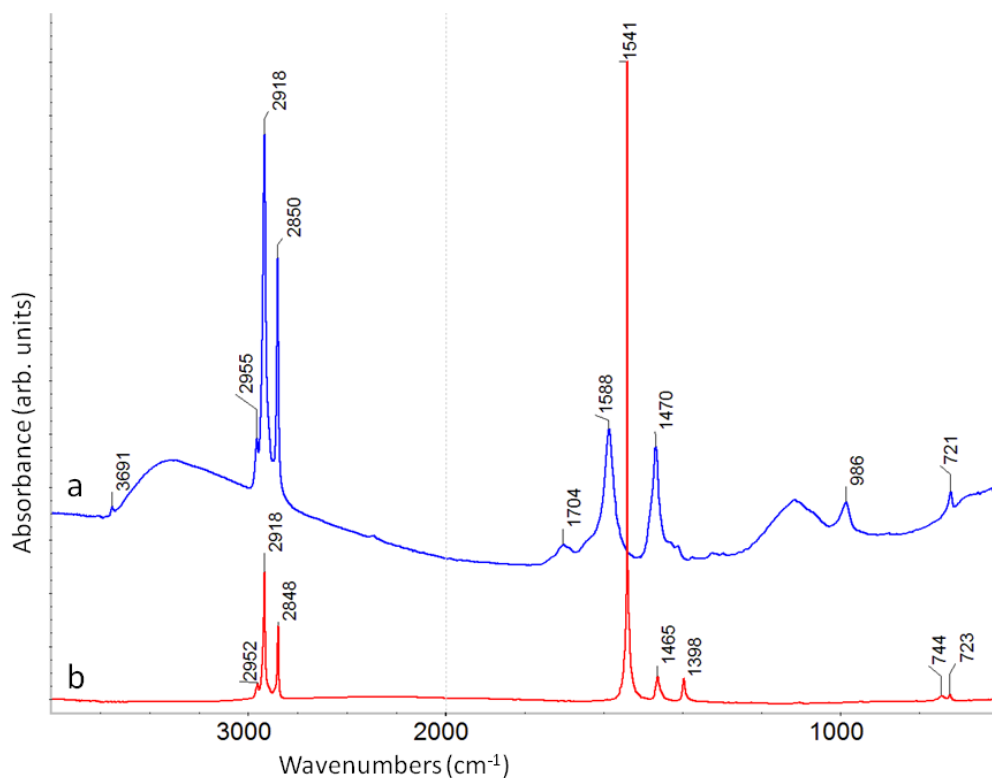
Figure 3.13 Transmission FTIR reference spectra for (a) aluminium stearate and (b) zinc stearate

Pigment variation among otherwise similarly formulated paints produces surprisingly little variation in carboxylate absorption. Paints with little or no defined underside peak at 1540 cm^{-1} include zinc-based control paints without added aluminium stearate and all but one of the W&N paints (Figure 14).
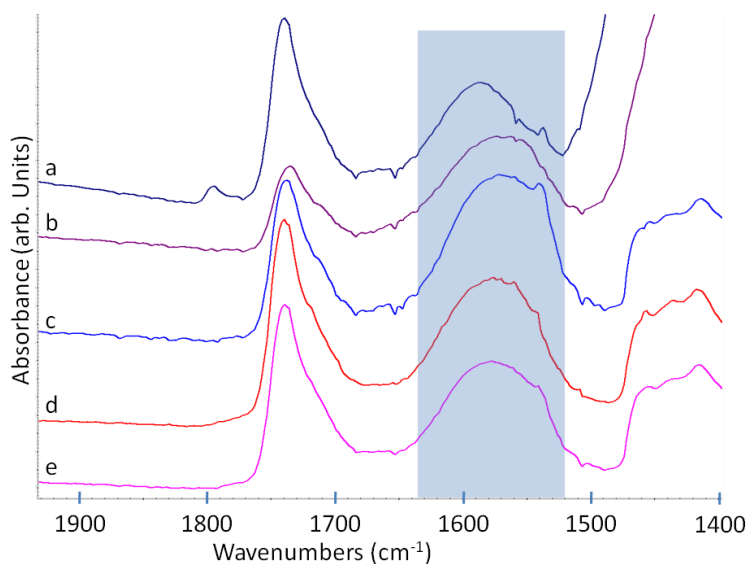
Figure 3.14 ATR-FTIR spectra from protected underside surfaces detailing carboxylate region

(a) Gamblin Ti 1999; (b) W&N Pb 1980; (c) W&N Zn 1978; (d) Zn control linseed, cold pressed 1990; (e) Zn control linseed + litharge 1990. Absorption in the metal carboxylate band is generally broad. Highlighted band corresponds to wavenumber range 1520-1630 cm^{-1}

Details from protected underside spectra including W&N Naples yellow hue samples from 1978 and 1999 are shown in Figure 3.15. Both W&N paints are based on lead white but the younger film is without dolomite. Spectra from each are dominated by lead carbonate and are comparable to those obtained from similarly dated W&N Flake (lead) white paints. Little difference in carboxylate absorption is apparent irrespective of the presence of dolomite.
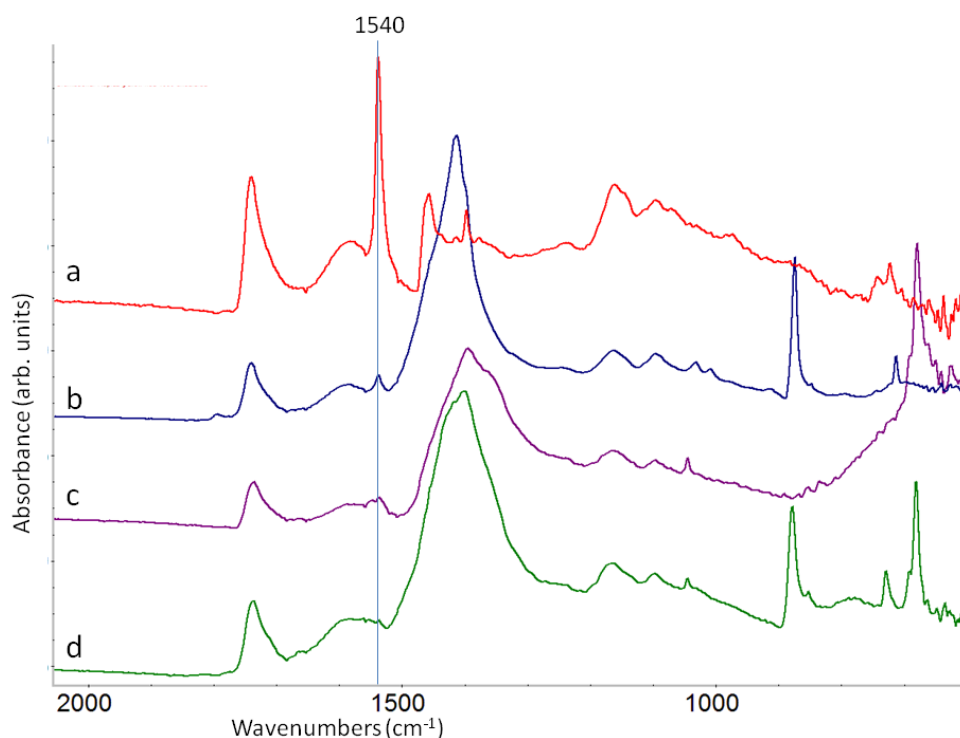
Figure 3.15 ATR-FTIR underside spectral detail from Naples yellow hue varieties

(a) Grumbacher 1999; (b) Gamblin 1999; (c) W&N 1999; (d) W&N 1978 showing typically low carboxylate absorption with a small side peak *ca* 1540 cm^{-1}

3.5.1.2.1 Soybean oil paints

Unfortunately it was not possible to compare soybean paints with and without aluminium stearate as all soybean controls contain the additive, and analysis of Speedball Titanium white suggests it is similarly formulated. Spectra are shown in Figure 3.16. Exposed surface spectra from control soybean paint with aluminium stearate unusually have small 1540 cm^{-1} side peaks adjacent to broad carboxylate absorption in addition to stronger underside peaks. It was difficult to obtain well resolved spectra from the top surfaces, and strong carboxyl doublets in some (*ca* 1710/1740 cm^{-1}) (not shown) suggest high fatty acid concentration. This is consistent with visible surface efflorescence evident on the zinc oxide soybean control paint in Figure 3.2. The intensity of

protected underside 1540 cm^{-1} peaks in the soybean range with aluminium stearate appears linked to zinc oxide concentration, with the strongest peak recorded in paint with zinc oxide as the primary pigment, formulated without titanium dioxide or aluminium silicate fillers.
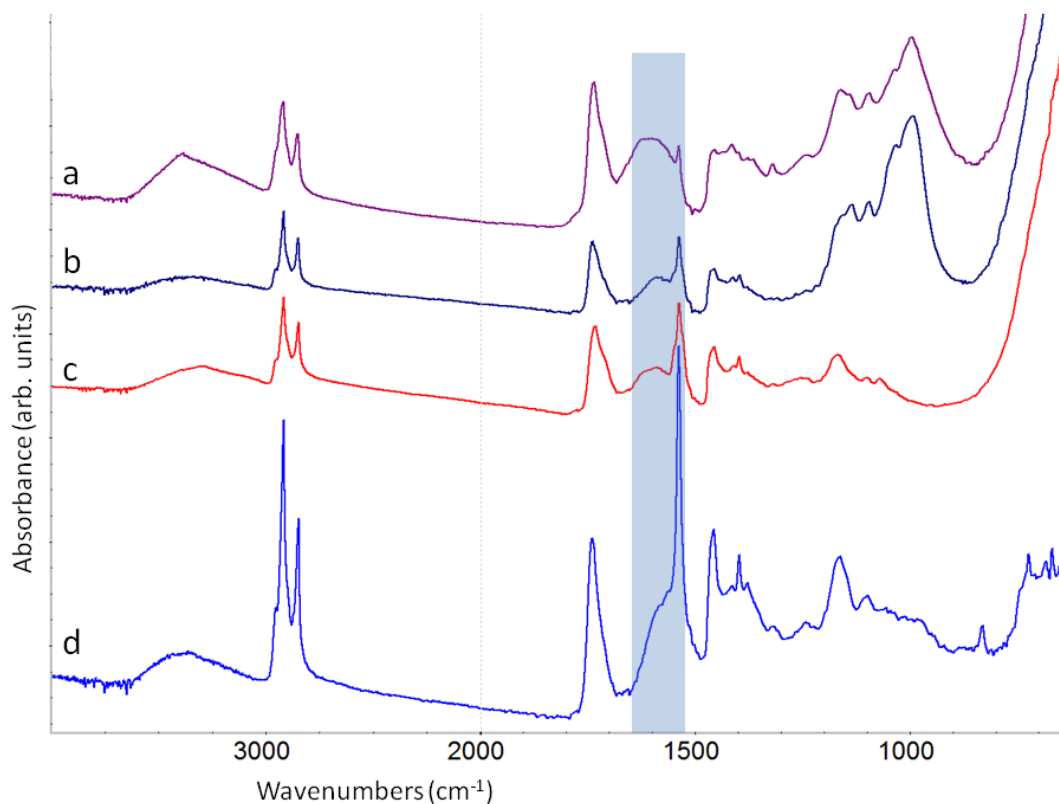
Figure 3.16 ATR-FTIR spectra from soybean oil paint range, all including aluminium stearate

Ti/Zn 1998 control (a) top and (b) underside; (c) Speedball Ti/Zn 1981 underside; (d) Zn control 1998 underside. A peak at 1540 cm^{-1} is apparent in each, strongest at the underside of the paint formulated with zinc oxide without Ti white or silicate fillers. Highlighted band corresponds to wavenumber range 1520-1630 cm^{-1}

3.5.2 Analysis of embedded paint cross-sections

3.5.2.1 Microscopy and microanalysis

Embedded cross-sections were used to obtain additional information on variations between and within paint films.

3.5.2.1.1 Zinc white paints

Figure 3.17 shows UVF and BSE images of four paint samples primarily pigmented with zinc oxide, two of which incorporate aluminium stearate.
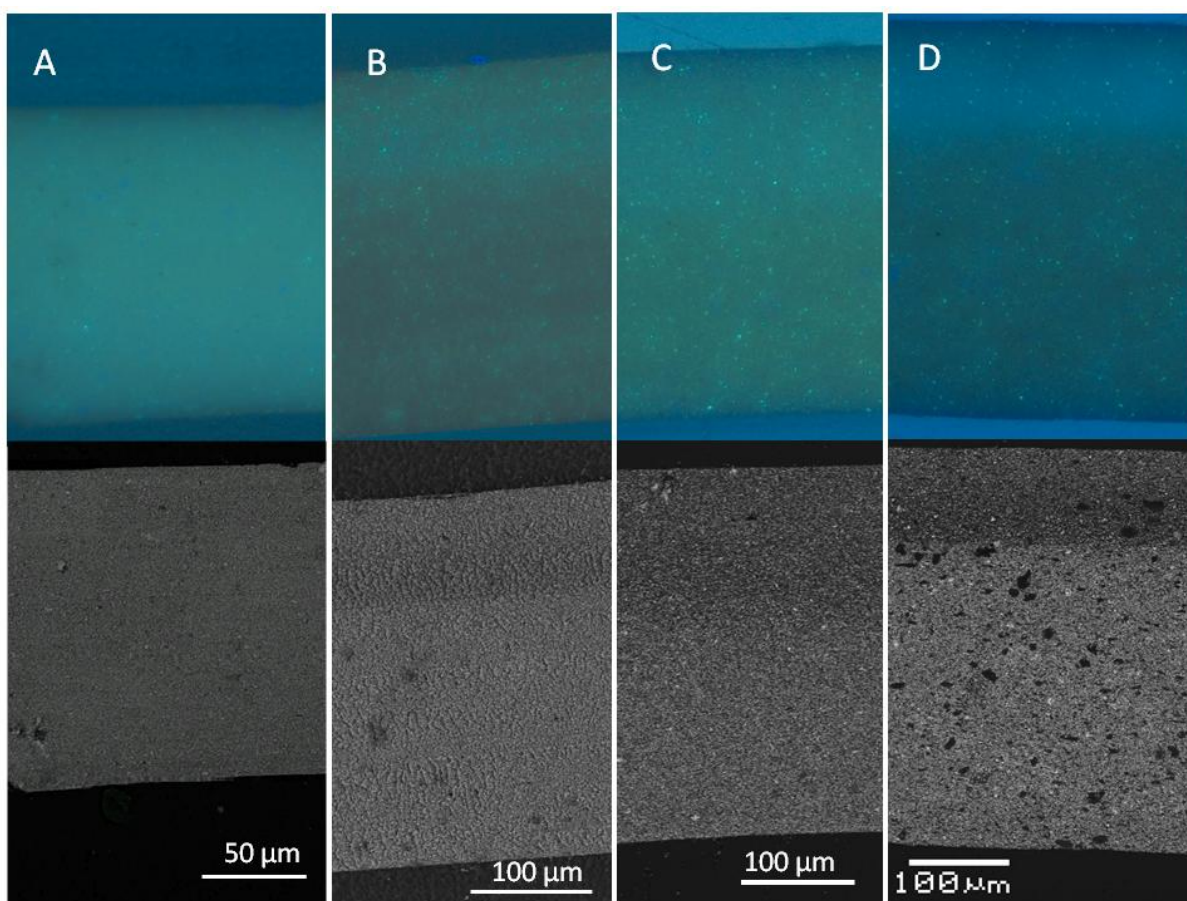
Figure 3.17 UVF (top) and BSE (bottom) cross-section images of (A) Zn linseed cold pressed control 1990; (B) W&N Zn safflower 1978; (C) Zn soybean control with aluminium stearate 1998; (D) Zn safflower control with aluminium stearate 1998.

UV fluorescent bands with corresponding reduced electron density are visible at the upper margin of three of the four paint films. The incidence occurs in both controls and one commercially produced paint and is not connected to the presence of aluminium stearate. Across the range of paints there is no apparent correlation between surface fluorescence and pronounced differences in carboxylate IR absorption between surfaces. Of the paints with aluminium stearate, one contains dispersed 5-20 µm diameter low electron density features which are not apparent in the paints without, nor so obvious in the soybean-based paint with aluminium stearate. Elemental mapping confirms high concentrations of aluminium and carbon in association with these features (Figure 3.18). The absence of similar inclusions in the soybean-based zinc oxide paint with aluminium stearate is interesting and is investigated further using SR-µFTIR in the following section.
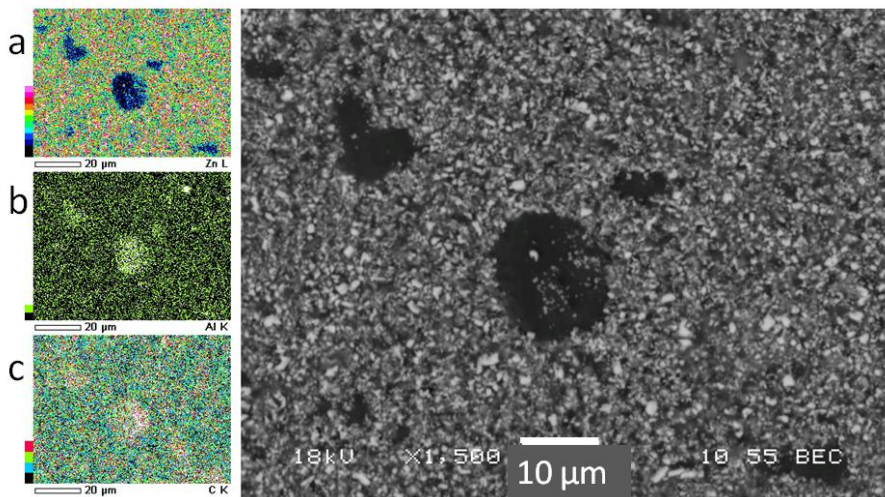
Figure 3.18 Zn safflower control with aluminium stearate 1998 BSE cross-section detail and corresponding elemental maps for (a) Zn, (b) Al and (c) C

3.5.2.1.2 Titanium white paints with zinc oxide

Paints formulated with titanium dioxide as the primary pigment are characteristically more UV absorbent than those pigmented only with zinc oxide. In cross-sections this translates to a darker appearance in UVF images (Figure 3.19). Various pigment and extender particles can be resolved in BSE images at higher magnification as illustrated by images from titanium white safflower control paint with zinc oxide and aluminium stearate (Figure 3.20).
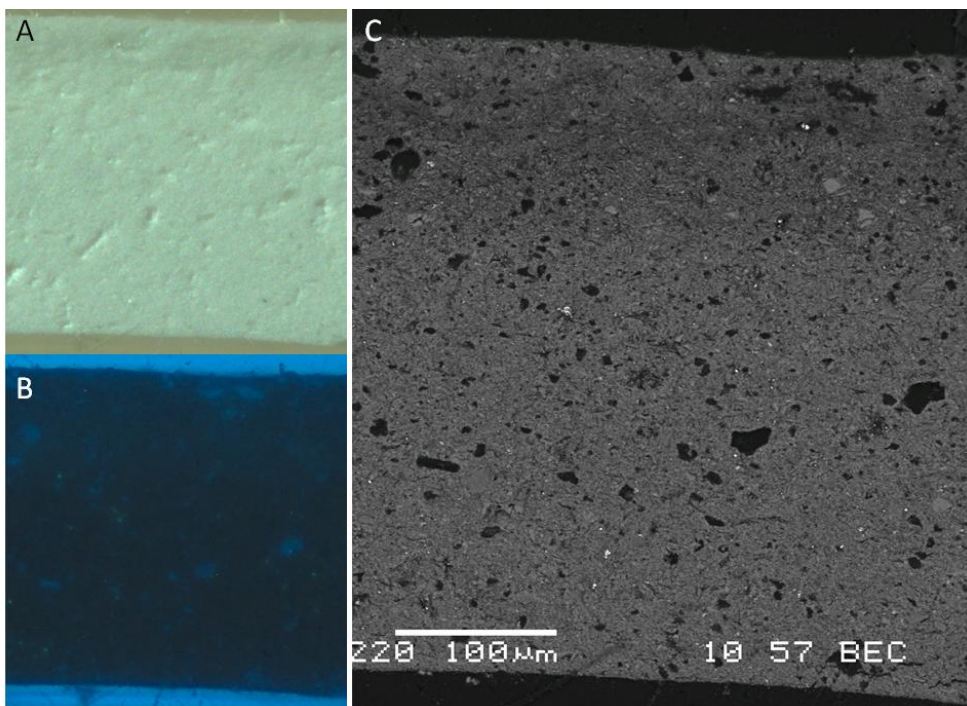
Figure 3.19 Ti/Zn safflower control with aluminium stearate 1998 cross-section optical images (A) visible and (B) UVF, and corresponding BSE image (C)
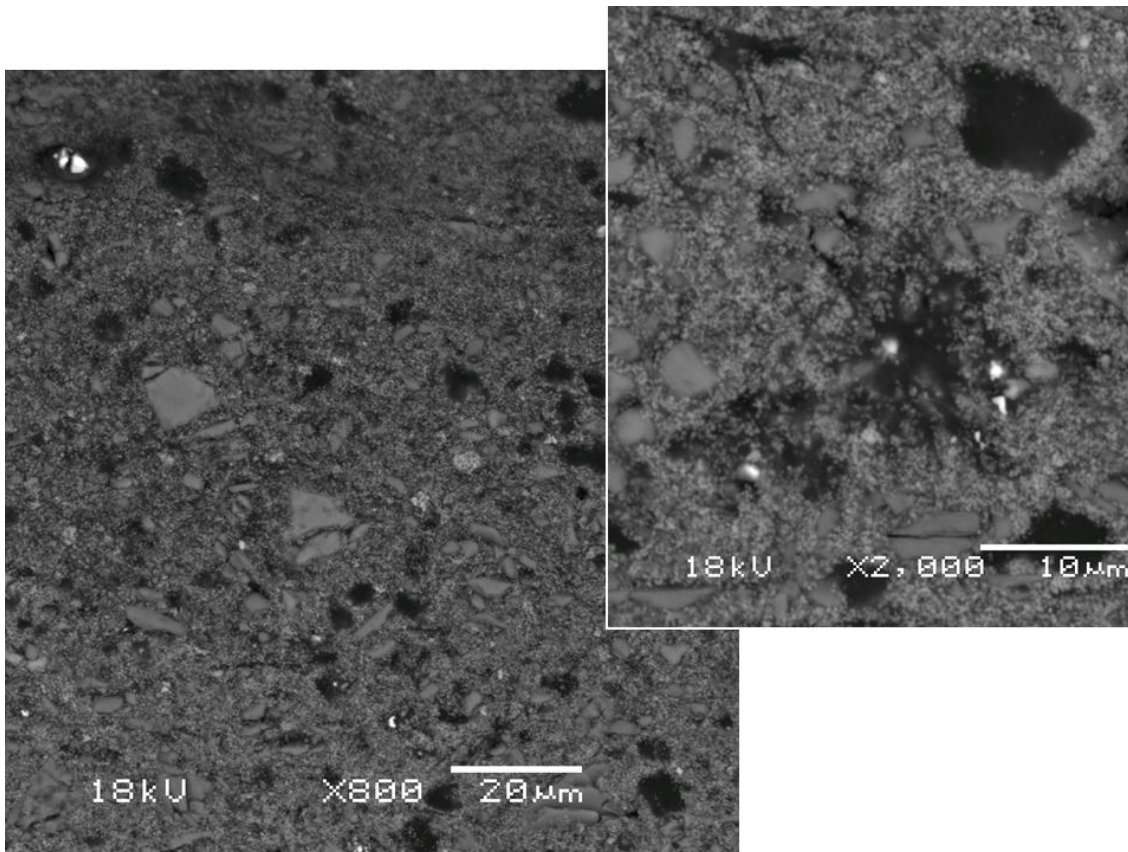
Figure 3.20 Ti/Zn safflower control with aluminium stearate 1998 cross-section image detail deriving from the top half of the paint film.

Titanium white pigment appears as extremely fine grey grains while zinc oxide is resolved as an occasional small, bright particle. Large grey particles are aluminium silicate extender. The higher magnification inset from an area in the bottom half of the paint film details several zinc oxide particles surrounded by areas of low particle density

Zinc oxide is visible as small white particles in the paint which occur in substantially lower concentration than the multitude of fine, grey titanium dioxide grains. This paint is formulated with a specified ratio of titanium dioxide to zinc oxide of 12:1 by weight (molar masses are very similar at 79.9 g/mol for titanium dioxide and 81.4 for zinc oxide). However, the apparent low coverage of zinc oxide particles may also reflect a reduction associated with zinc stearate formation. The higher magnification inset image in Figure 3.20 shows particles of zinc oxide at the centre of a region of low atomic density, consistent with an organic surround. Spot SEM-EDX measurement at the centre of the area confirms high carbon counts with lower Zn and Ti signals and traces of Al and Si.

Similar low atomic density regions are seen in Grumbacher Titanium white paint 1999. Spot EDX measurements from two such areas indicate some are aluminium based while others are zinc-based (Figure 3.21).
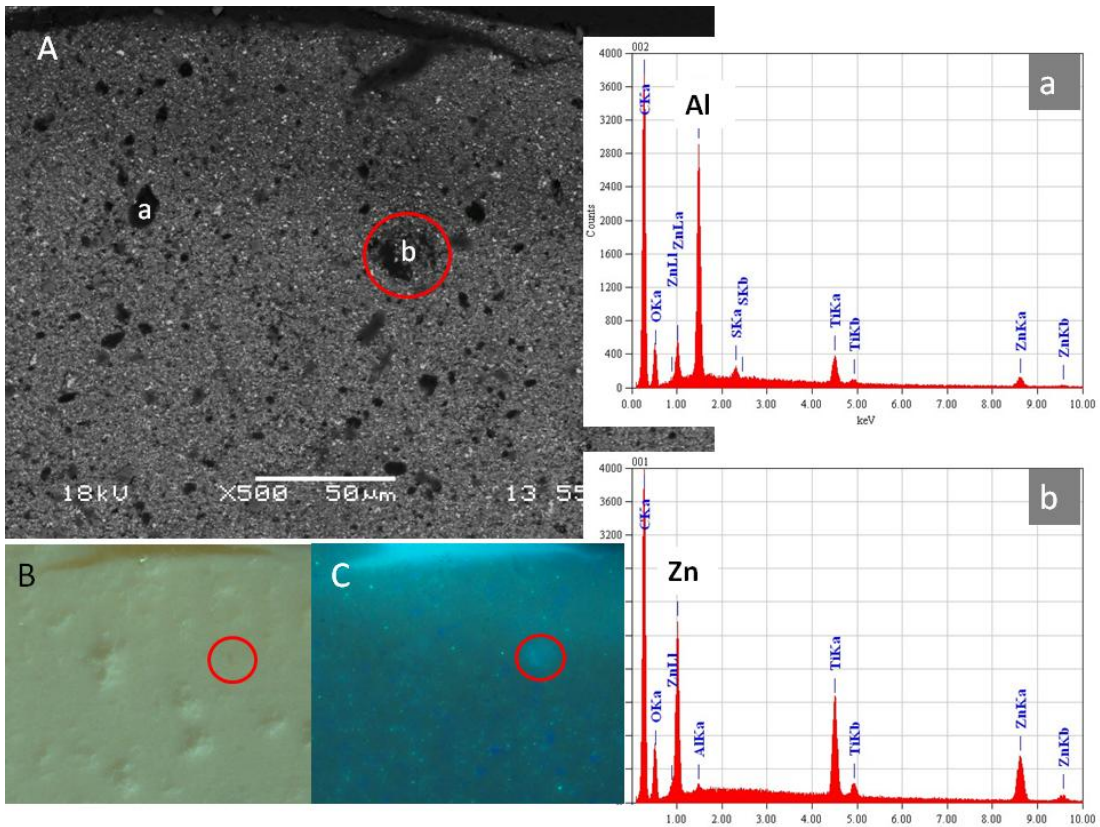
Figure 3.21 Grumbacher Titanium white 1999 cross-section BSE image detail (A) and corresponding optical images (B) visible and (C) UVF, with common circled feature. SEM-EDX spectra derive from spots designated (a-b)

Low density zinc-based regions typically have a less defined boundary with surrounding paint than comparable aluminium rich areas. The reduced atomic density of paint adjacent to zinc rich features (circled) may reflect localised saponification of zinc oxide. The area also appears more UV fluorescent than surrounding paint. A similar EDX signal derives from areas of reduced electron density towards the bottom of the paint film (Figure 3.22).
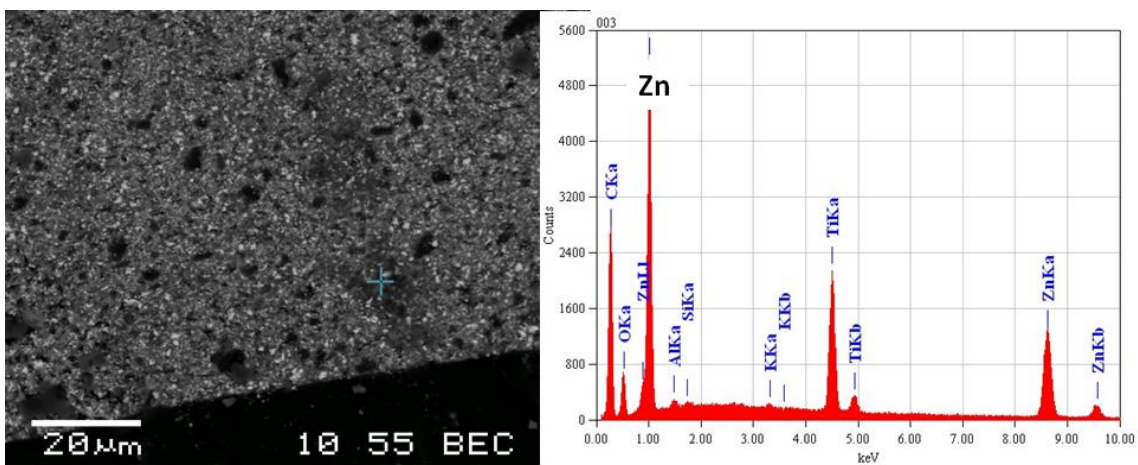
Figure 3.22 Grumbacher Titanium white 1999 cross-section BSE image detail showing bottom margin of paint film and SEM-EDX spectrum deriving from spot indicated

The reduced atomic brightness of these patches relative to the more general paint matrix is consistent with partial conversion of zinc oxide to zinc stearate; the incidence of patches in the lower margins of the paint film is also consistent with strongest zinc stearate signals recorded with ATR-FTIR at underside surfaces.

Cross-sections also enable visualisation of formulation changes such as that evident between 1978 and 1980 W&N Titanium paints (Figure 3.23). The later paint has a more perceptible fluorescent band at the top surface which corresponds to reduced carbonate absorption in ATR-FTIR spectra previously reported. W&N Titanium paint cast in 1999 appears very similar in cross-section (not shown). Other differences between the 1978 and 1980 castings include dispersed *ca* 10 μm fluorescent inclusions, magnesium carbonate and large amounts of barium sulfate in the later paints. The barium sulfate is evident as large white particles in the BSE image and its distribution appears consistent throughout, confirming the interpretation of ATR-FTIR spectra. SEM-EDX spot measurements and elemental mapping reveal the fluorescent masses as variously rich in C and Mg or Al and S (Figures 3.24-3.25).
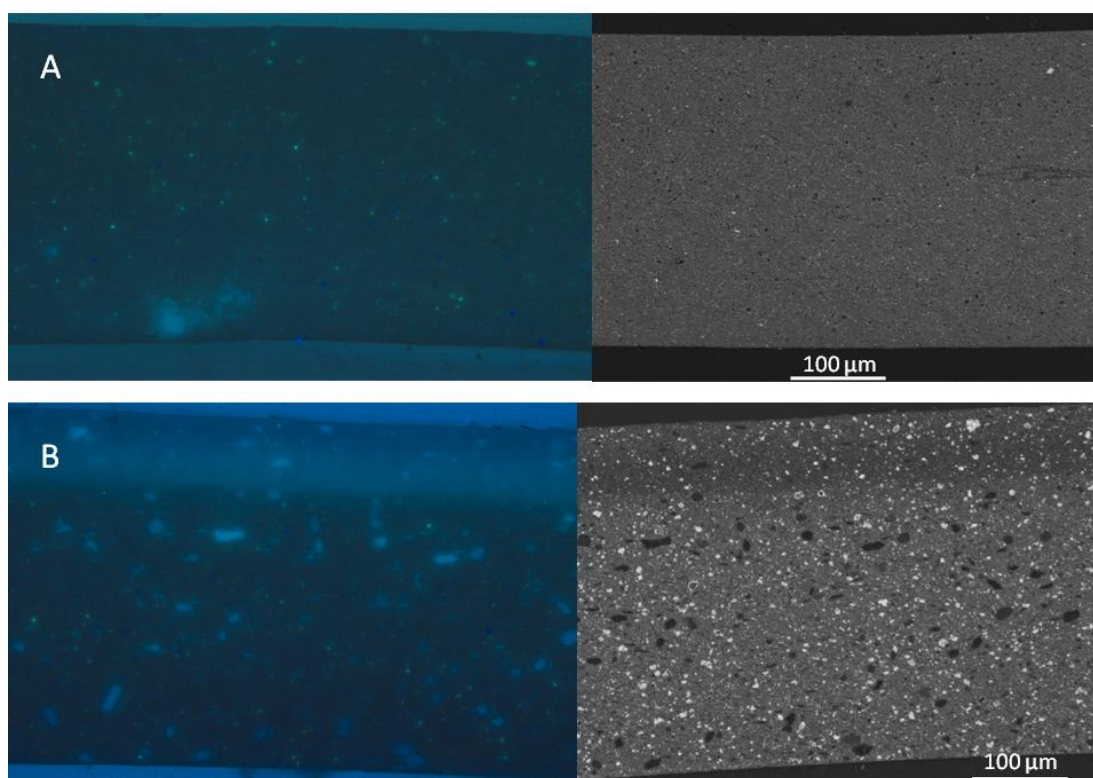
Figure 3.23 UVF (left) and BSE (right) cross-section images of W&N Ti white paints cast in (A) 1978 and (B) 1980 reflecting different formulations.

The later film has dispersed fluorescent inclusions and a higher proportion of high atomic mass fillers
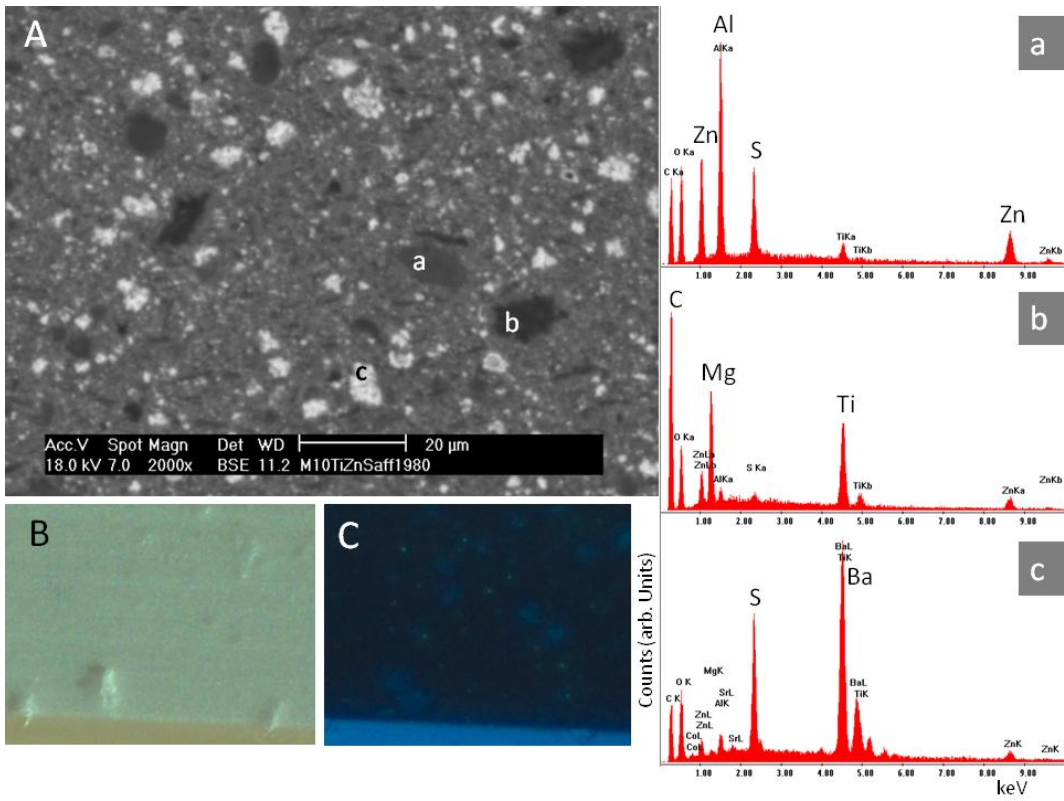
Figure 3.24 W&N Titanium white safflower 1980 cross-section details (A) BSE image; and corresponding optical images (B) visible and (C) UV fluorescence, with SEM-EDX spectra from points designated a-c
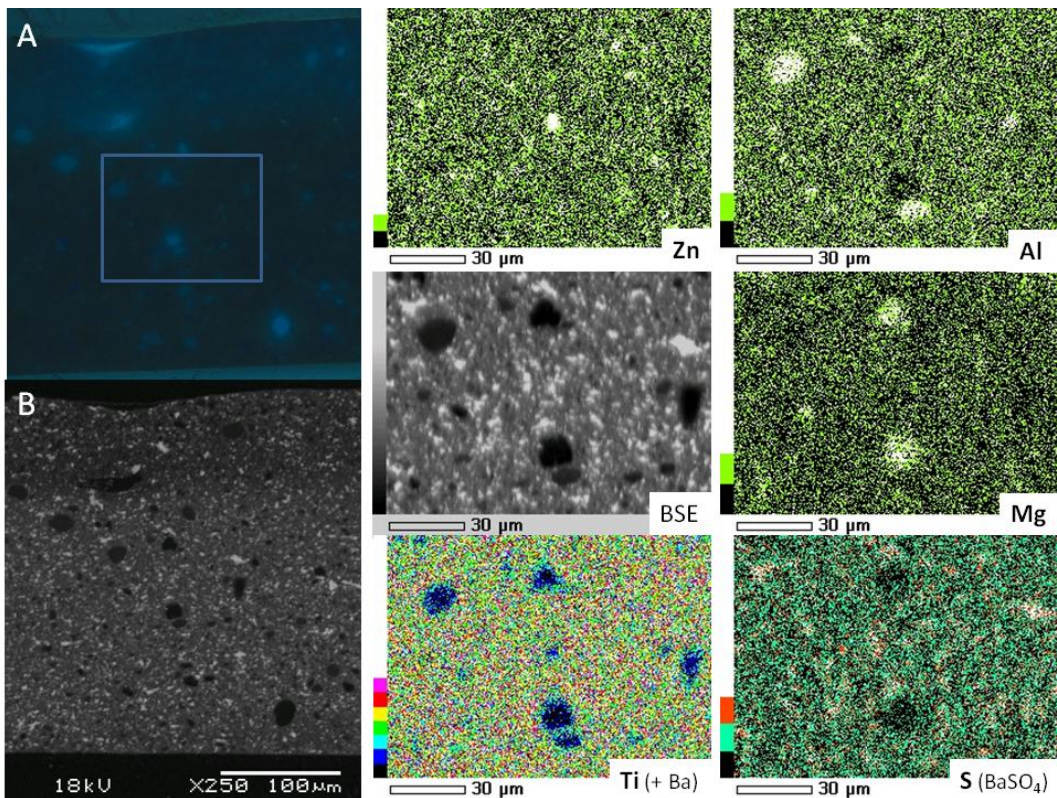
Figure 3.25 W&N Titanium white 1999 cross-section details (A) UV fluorescence image and (B) corresponding BSE image with SEM-EDX elemental maps obtained from boxed region

Although morphologically similar to aluminium-rich, low electron density masses present in the previous sample, no aluminium stearate has been used by W&N in formulating the paints included in this research (personal communication, Phil Jones, Group Innovation and Development Director, ColArt International Holdings Ltd, London, email 8 March 2011). It is possible these features correspond to magnesium stearate and alumina hydrate which, although not confirmed in the current samples, were used in formulating W&N Titanium white Artists' Oil Colour in the mid 1960s (personal communication, Ian Garrett, Technical Director W&N (retired), email 28 August 2013). In this scenario the presence of magnesium stearate does not appear to influence formation and segregation of zinc stearate in the same way as the aluminium counterpart.

In comparison, the low magnification BSE image of the earlier (1978) W&N Titanium white is relatively homogenous, with UV fluorescent sparkle characteristic of many zinc oxide containing paints. However at higher magnification small (*ca* 2 μm) dispersed low BSE intensity points are evident (Figure 3.26). These spots are carbon-rich with trace contributions from elements generally present in the paint, notably Ti, Zn, Ca and Mg with traces of Al, Si and Cl. Elemental distribution across the paint more generally is shown by SEM-EDX maps in Figure 3.27.
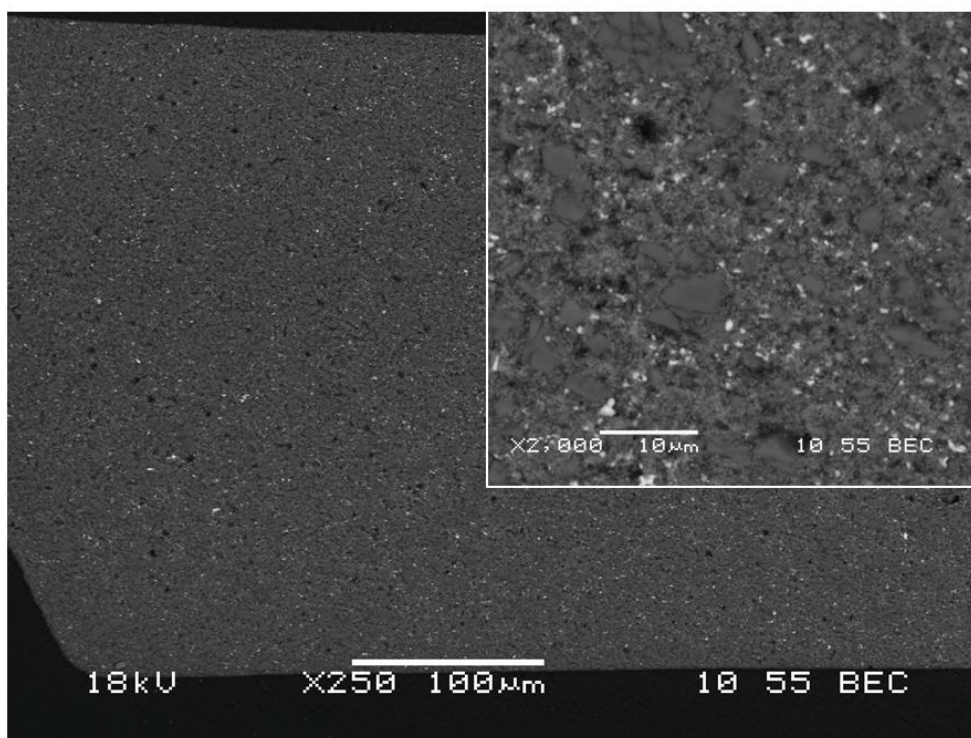
Figure 3.26 W&N Titanium white 1978 cross-section BSE image and higher magnification detail (inset).

Bright white particles in the inset image are zinc oxide with occasional larger particles of barium sulfate (the latter discernible at low magnification). Titanium dioxide appears as a multitude of very fine grey particles, while large grey particles are dolomite (calcium magnesium carbonate). Small low atomic contrast 'holes' are carbon-rich
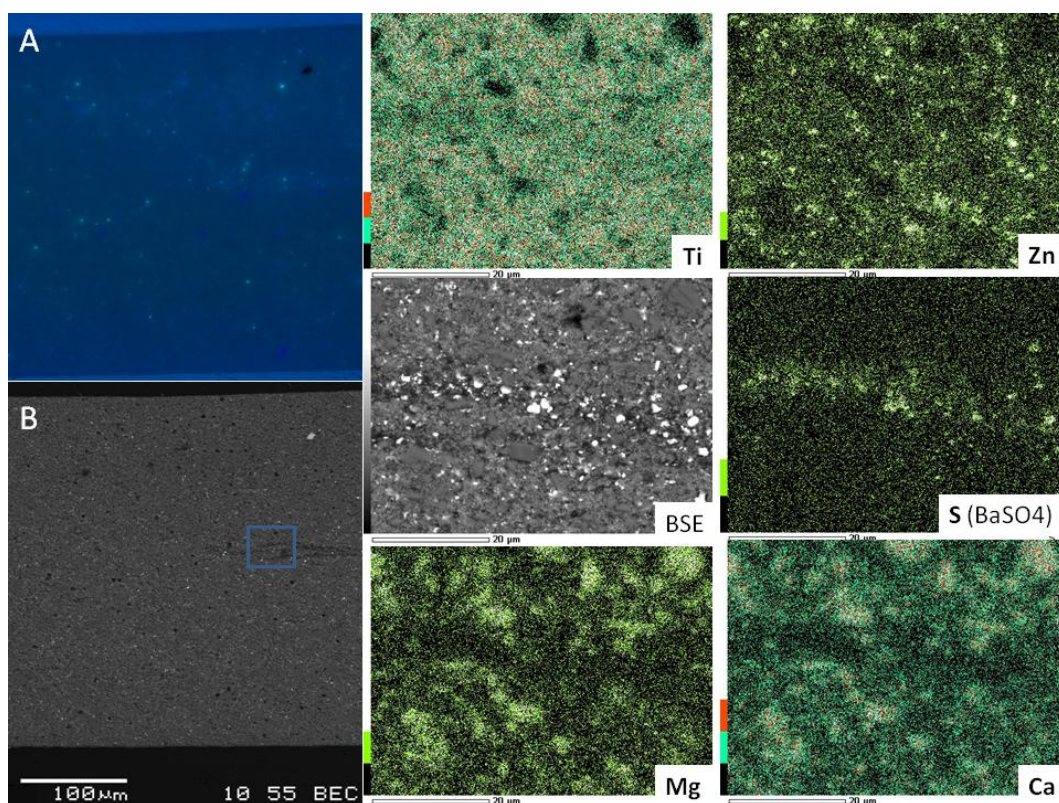
Figure 3.27 W&N Titanium white 1978 cross-section details (A) UV fluorescence image and (B) corresponding BSE image with SEM-EDX elemental maps obtained from boxed region.

The mapped area features an unusual vein of barium sulfate but is otherwise indicative of the paint film

The anomalous behaviour of this sample in recording strong underside zinc stearate FTIR absorption is attributed in published work to the likely inclusion of aluminium hydroxide (aluminium 'hydrate') in the formulation. However there is less evidence for its presence in the 1978 paint than in later W&N formulations described above. A feature of the early W&N paint not present in later titanium whites from W&N or other manufacturers is a high proportion of dolomite. Dolomite has been used by W&N in their *Winton* Titanium white oil paint in conjunction with hydrogenated castor oil (HCO), an alternative rheology modifier to stearates (personal communication, Ian Garrett, Technical Director W&N (retired), email 20 September 2013). HCO principally comprises glycerides of 12-hydroxystearic acid and stearic acid (Maskaev et al. 1971) and its presence could explain both the small carbon-rich masses and the higher stearic acid concentration available for soap formation in this paint than comparable paints without HCO.

Gamblin Titanium white 1999 in cross-section also features a fluorescent upper margin but maximum fluorescence occurs just below the exposed surface. Elemental maps show a corresponding high intensity of carbon and low titanium and calcium signals relative to adjacent paint. The reduction in zinc signal through the same band is less pronounced (Figure 3.28).
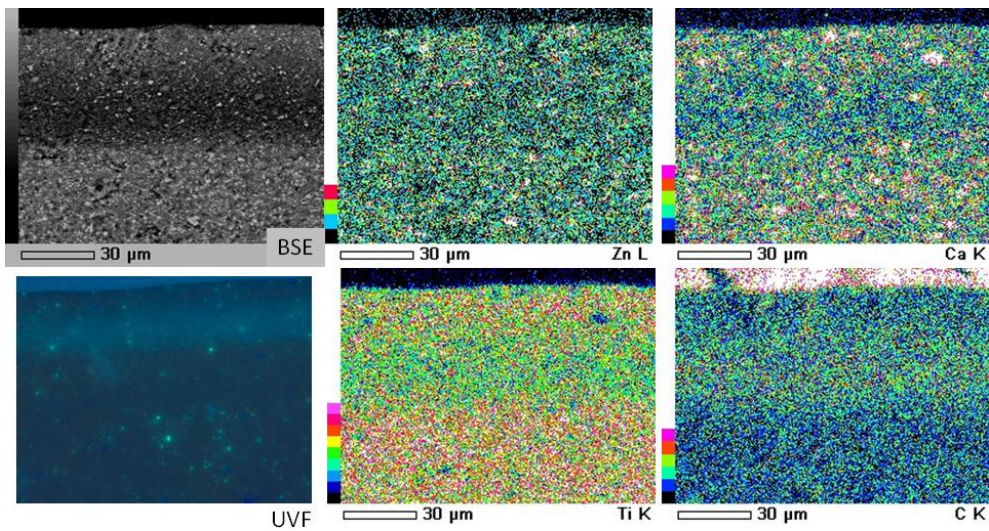
Figure 3.28 Gamblin Titanium white 1999 cross-section UVF image detail and higher magnification BSE image with SEM-EDX elemental maps

3.5.2.1.3 Naples yellow hue paints

UVF cross-section images of Naples yellow hue paints suggest Gamblin and Grumbacher formulations incorporate more zinc oxide than W&N counterparts. This is supported by SEM-EDX analysis. Differences in fluorescence apparent in cross-sections from the range of Naples yellow hue paints are shown in Figure 3.29.
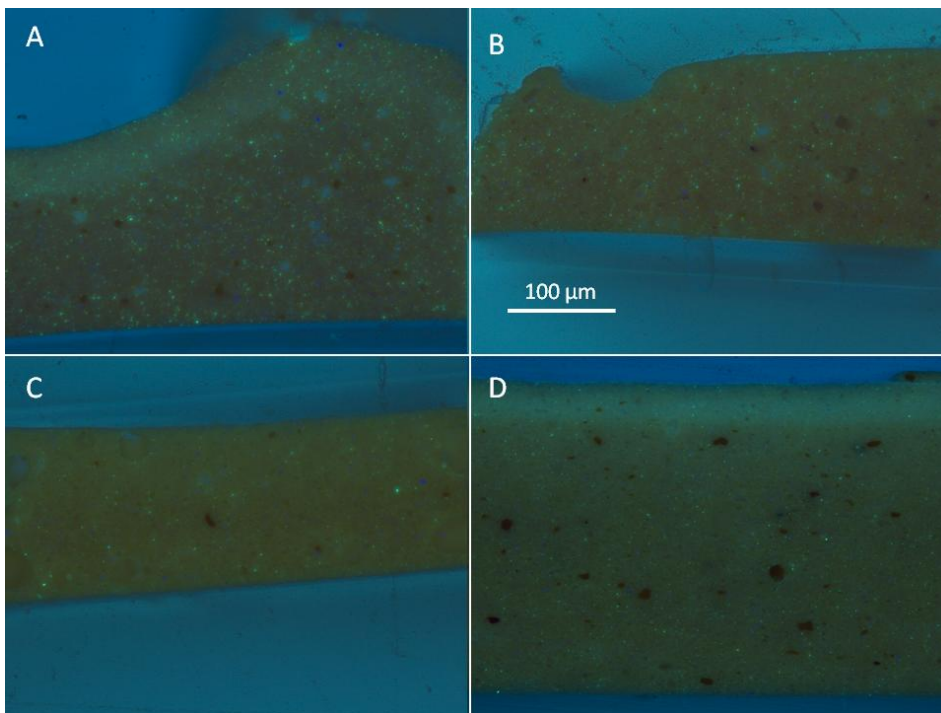
Figure 3.29 UVF cross-section images of Naples yellow hue paint films

(A) Gamblin 1999, (B) Grumbacher 1999, (C) W&N 1999 and (D) W&N 1978. The characteristic fluorescent sparkle of zinc white suggests the proportion of zinc oxide present is highest in the Gamblin and Grumbacher paints, with lower amounts in the W&N varieties

Grumbacher paint is substantially pigmented with zinc oxide with small amounts of high tinting strength yellow pigment. Gamblin paint is similarly based but differs in incorporating significant amounts of chalk (calcium carbonate) which features strongly in FTIR spectra and elemental maps (Figure 3.30). In this example the UV fluorescent surface band clearly corresponds to reduced pigment density and may reflect settling in the course of film formation. The prevalence of calcium becomes apparent, including its association with large UV fluorescent masses dispersed within the paint. At higher magnification calcium and zinc are seen to dominate in divergent areas of the paint film (Figure 3.31). The presence of titanium is also indicated among more general zinc oxide-based passages and may be linked to dark purple flecks visible in UVF images (Figure 3.32).
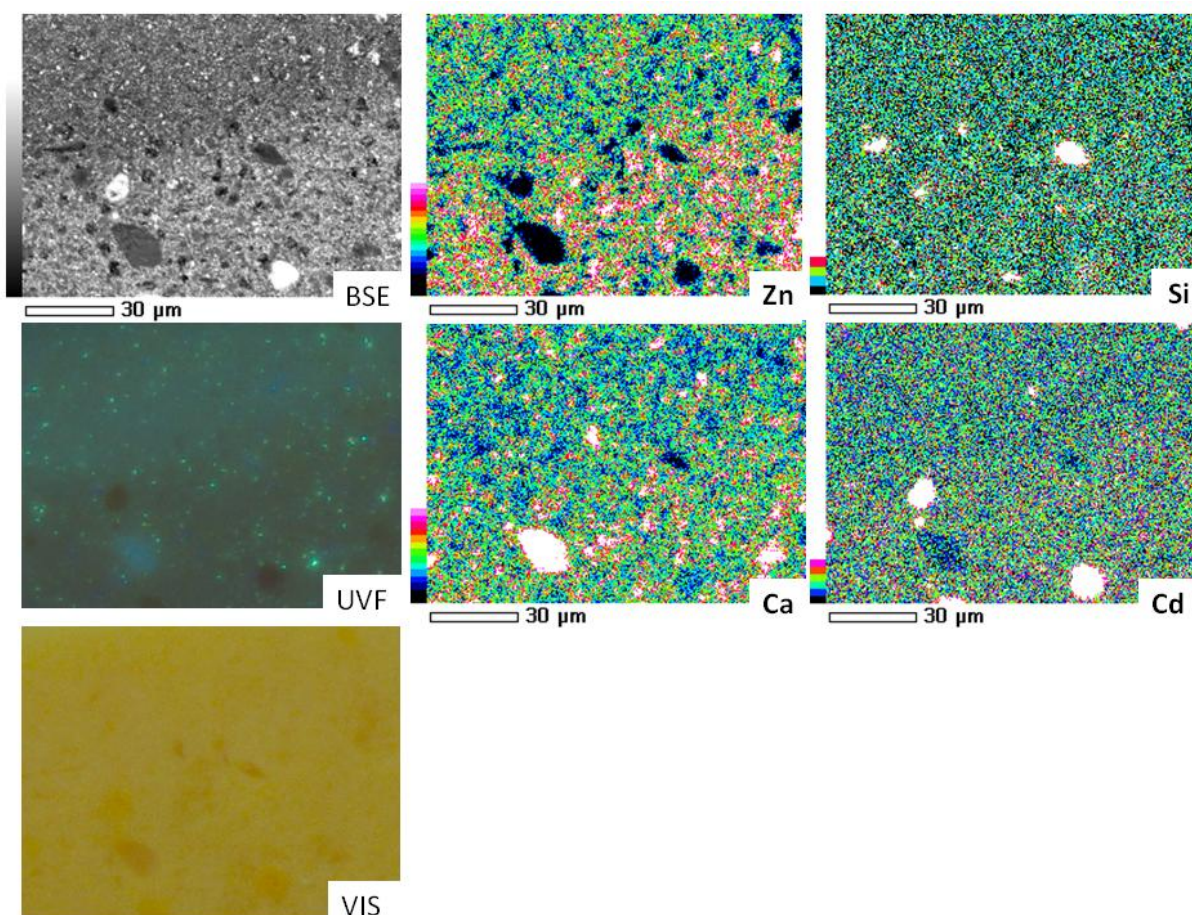
Figure 3.30 Cross-section image details (upper margin) and corresponding elemental maps of Gamblin Naples yellow hue 1999. The mapped region includes the boundary between UV fluorescent surface band and bulk film
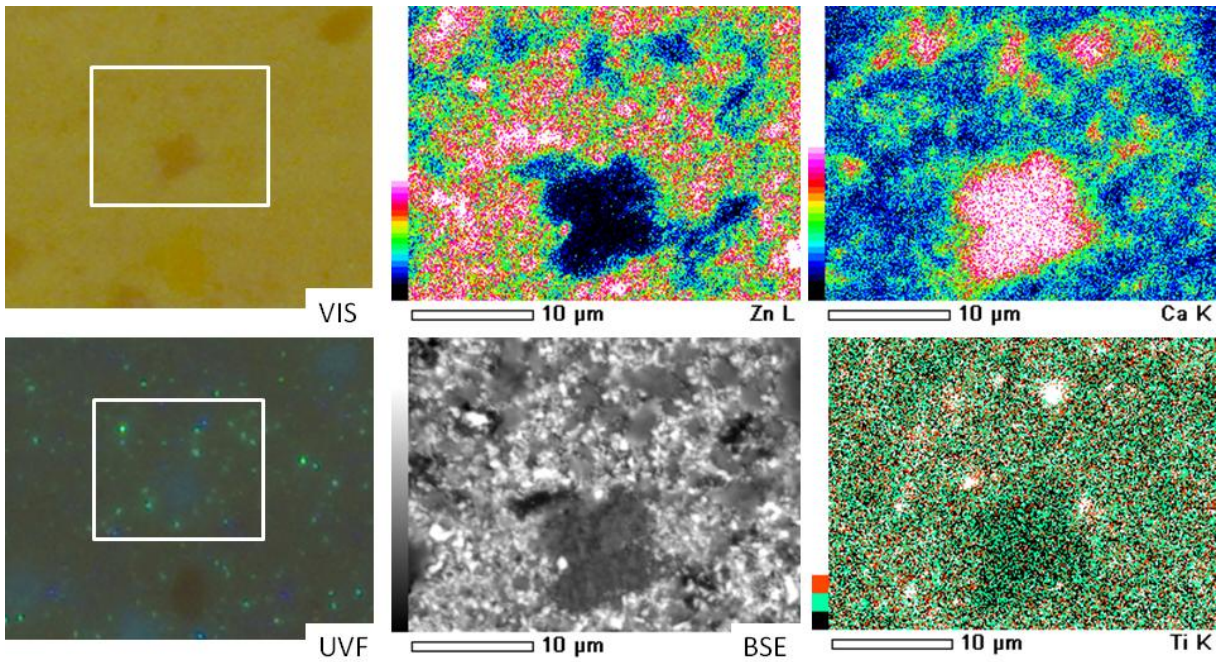
Figure 3.31 Gamblin Naples yellow hue 1999 cross-section optical image details with box denoting area of corresponding BSE image and elemental maps
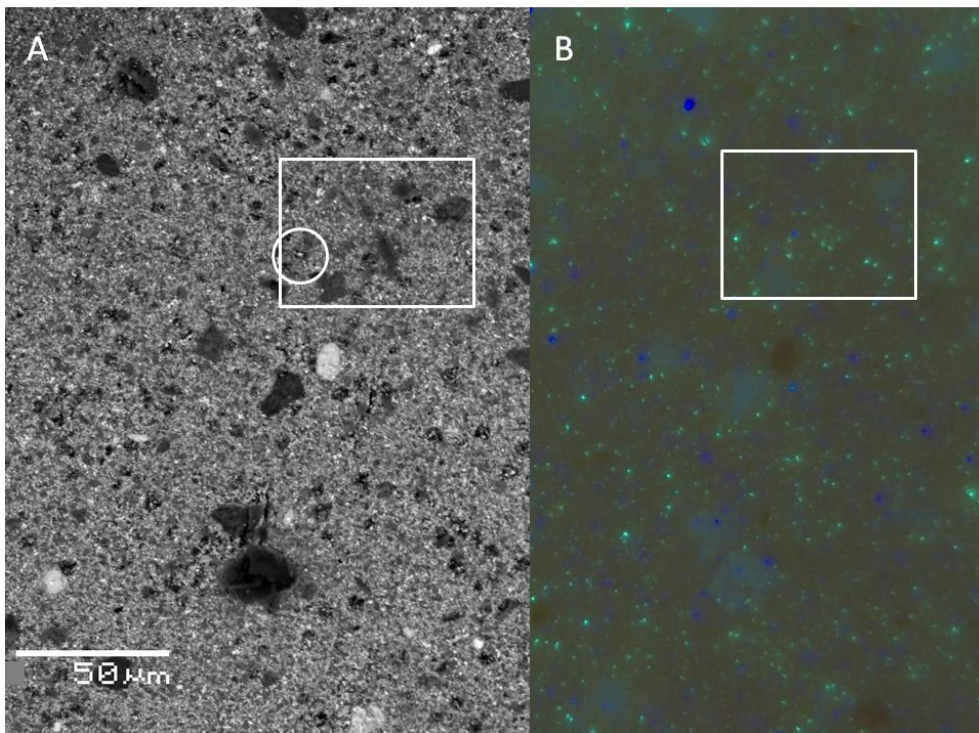
Figure 3.32 Gamblin Naples yellow hue 1999 cross-section image details (A) BSE and (B) UVF of corresponding area.

UV fluorescent sparkles and purple flecks in the optical image are difficult to correlate to features in BSE but the latter may relate to the incidence of titanium (dioxide?) among general zinc oxide-based pigmentation. Box denotes area detailed in Figure 34

111

Distinctive features visible in the UVF image including the purple flecks and 'characteristic' zinc white 'sparkle' are difficult to correlate with morphology revealed in BSE images. However, some distinctive (bright) micron-sized zinc-based particles surrounded by carbon-rich halos are apparent (Figure 3.33).
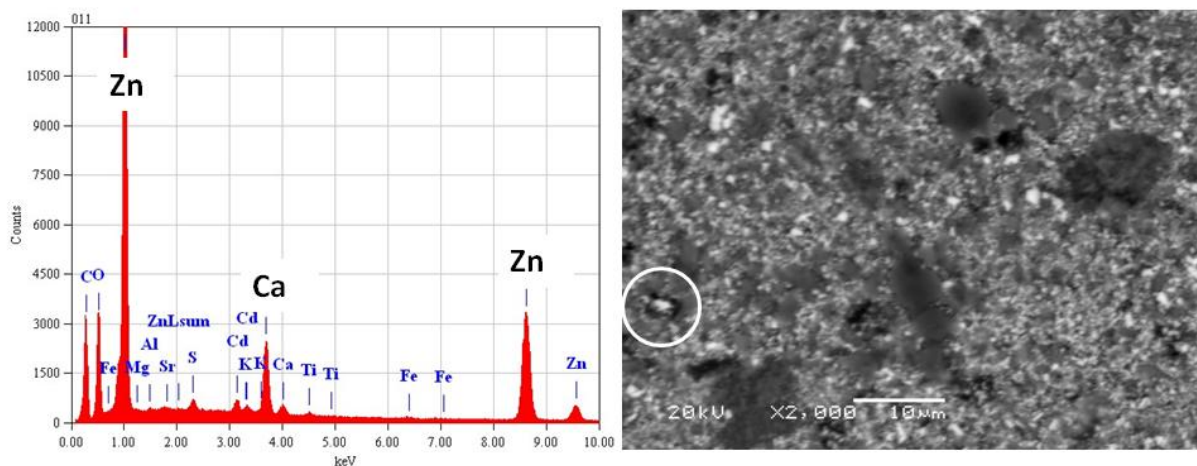
Figure 3.33 Gamblin Naples yellow hue 1999 cross-section BSE image detail of area denoted in Figure 3.32 and spot SEM-EDX spectrum obtained from the feature circled

Spot SEM-EDX spectra obtained from these features consistently indicate the presence of calcium in association with zinc. The incidence of calcium invites reference to the function of calcium driers in paint formulations. Calcium driers are used to increase the efficiency of surface driers; they preferentially adsorb onto pigment or filler surfaces where their higher alkalinity enables formation of relatively stable salts with acid groups, freeing surface driers from complexation and subsequent loss of catalytic activity (Soucek et al. 2012). By competing for formation of fatty acid complexes, calcium driers reduce mobility of carboxylates with which they coordinate (Mallégol et al. 2000c). Although no driers were used in formulating Gamblin Naples yellow hue (R. Gamblin, personal communication, email 21 September 2013), it is intriguing that calcium is detected in close association with zinc-based particles in paint with moderate general carboxylate absorption despite a high concentration of zinc oxide.

Also evident in the BSE image in Figure 3.33 are morphologically unresolved features of low electron density which appear to sit on the polished cross-section surface. A more pronounced example occurs in W&N Flake white 1999 (Figure 3.34).
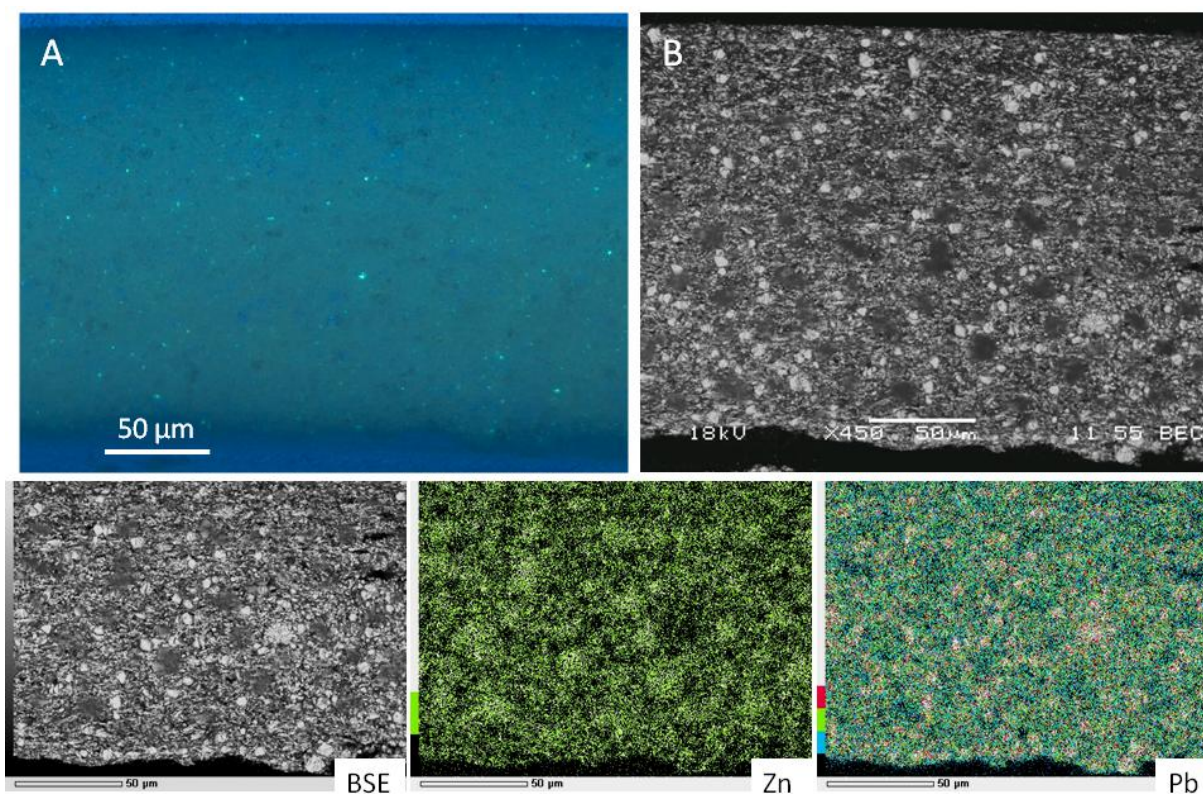
Figure 3.34 W&N Flake white 1999 cross-section images (A) UVF and (B) BSE with elemental map details from the bottom half of the cross-section

Unusual circular regions of reduced electron density occur across the lower half of the cross-section. Elemental mapping indicates zinc counts are high in correlation with these areas. A higher magnification detail is shown in Figure 3.35. The circular features appear to overlie the cross-section surface, possibly having emerged from within the microstructure under vacuum in the SEM. Spot EDX measurements indicate a higher relative lead signal in these areas than is apparent in zinc rich areas near the top surface, consistent with a contributing signal from underlying paint. In fact the high atomic contrast of lead white particles can be resolved beneath some of the surface-lying features. Lower pigment density arising from settling in the upper margin of paint films may accommodate the mobile soap phase within the microstructure more readily than within the film bulk, and it is likely the phase is present in lower concentration in upper margins.
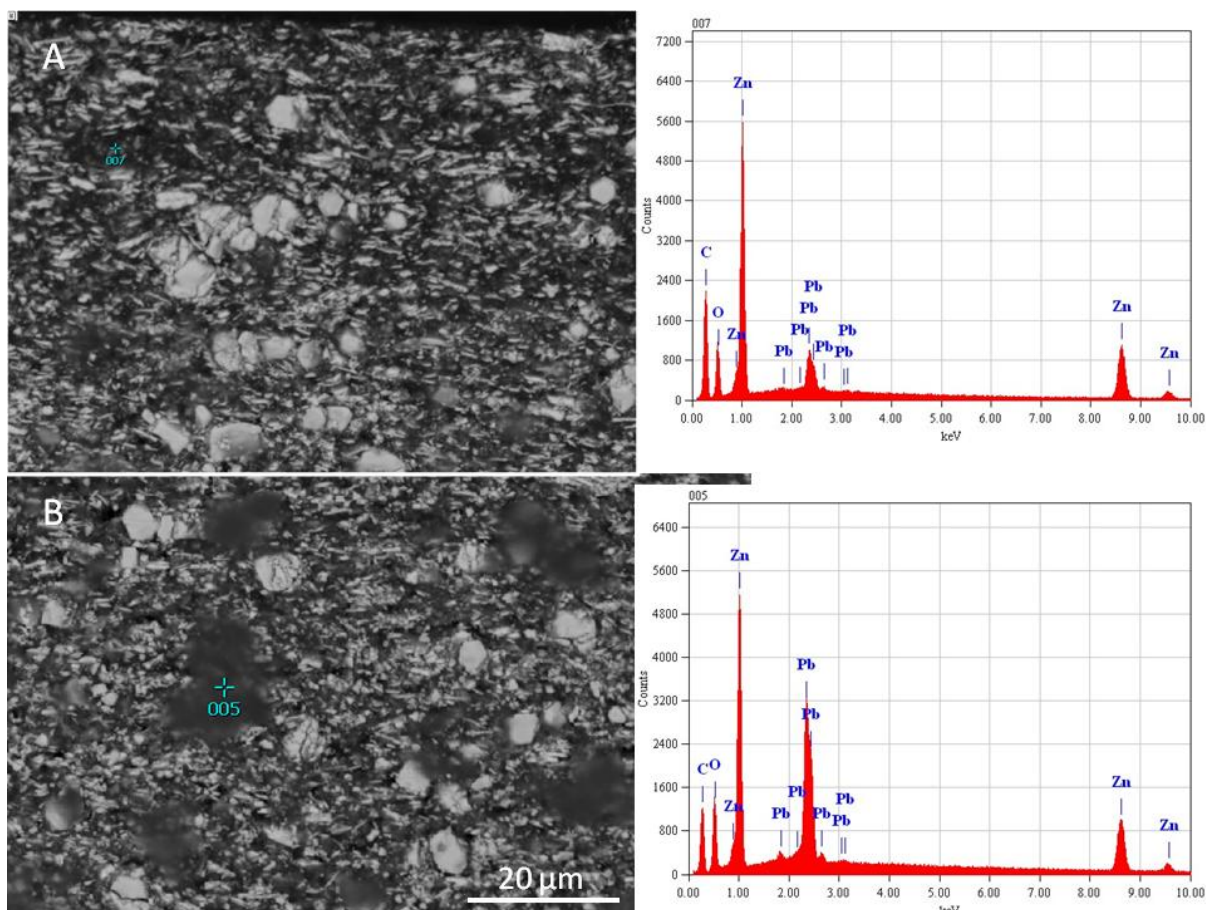
Figure 3.35 W&N Flake white 1999 cross-section image details and SEM-EDX spot measurements from the points indicated (A) upper margin and (B) film centre.

The higher Pb signal in (B) is consistent with a zinc-based soap phase overlying the paint having emerged from within the microstructure. The same phase in (A) by comparison remains contained within the film

3.5.2.2 SR-FTIR

Chemical maps were produced by integrating absorbance intensities corresponding to specific functional groups within the carboxylate region. Each SR-µFTIR map uses the full colour spectrum to indicate increments in absorption intensity, and graduations may represent widely varying values in different maps, requiring individual scale bars for comparison of relative intensities. This is distinct from full spectrum elemental maps where each colour refers to a consistent X-ray count and more colours equate to higher counts than monochrome maps recorded simultaneously.

Figures 3.36 and 3.37 show maps and spectra obtained from two soybean paints with aluminium stearate, one pigmented only with zinc oxide and the other with zinc oxide as a minor component in combination with titanium white.
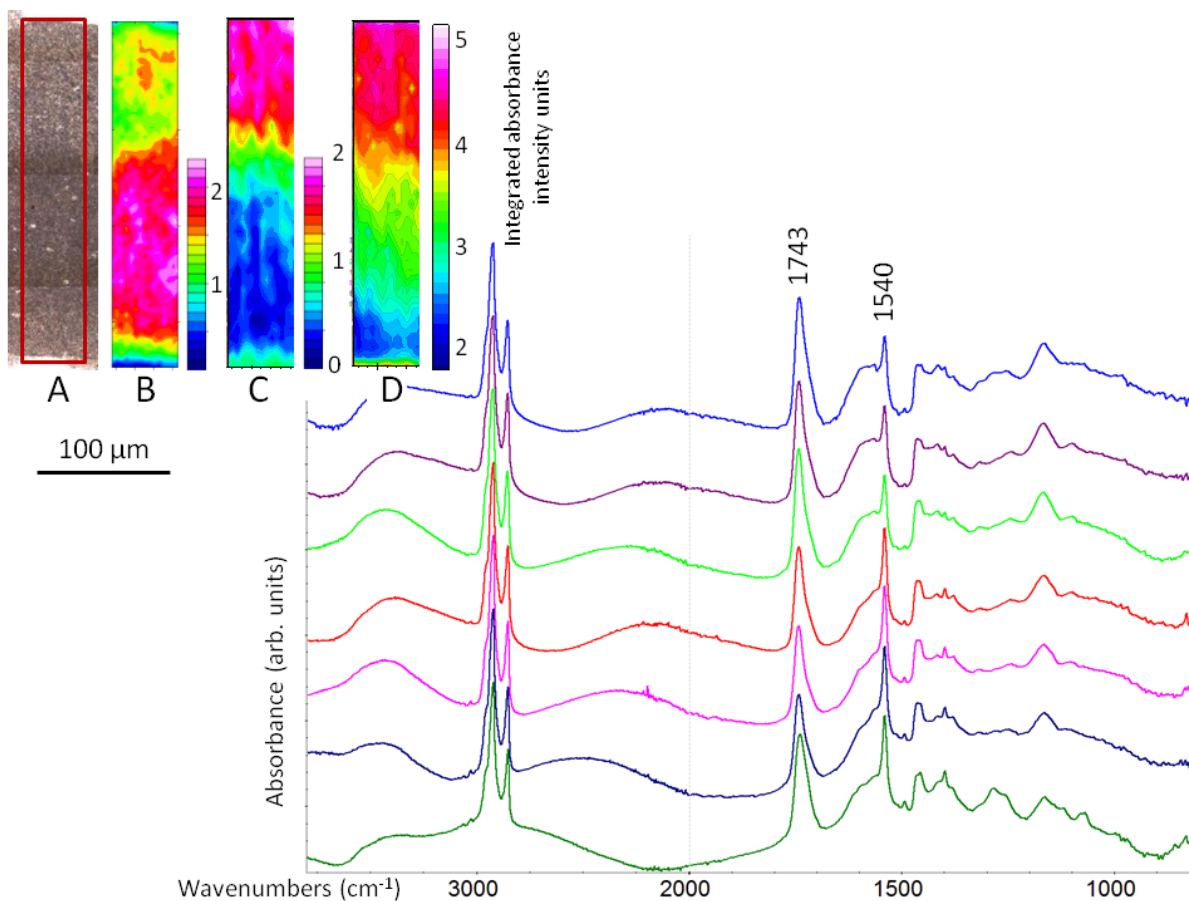
Figure 3.36 Zinc oxide soybean control with aluminium stearate 1998 thin-section detail

(A) optical image with box denoting area of SR-µFTIR integrated absorption intensity maps (B) 1525-1555 (C) 1555-1630 and (D) 1720-1760 cm^{-1}, and individual spectra extracted from points along a line spanning top to bottom through the sample

In keeping with published results, SR-µFTIR integrated absorption intensity maps show highest concentration of zinc stearate in the bottom half of both paint films. However, spectra extracted from the zinc oxide-based paint (Figure 3.36) show less variation across film thickness than the paint with titanium white, and a defined peak at 1540 cm^{-1} indicates zinc stearate is present throughout, a consistency not evident in comparable paints based on other oils with aluminium stearate. The distribution of zinc stearate in the zinc oxide soybean control is graduated through the film. Maps and extracted spectra show an inverse correlation between zinc stearate intensity and oil ester carbonyl absorption intensity; the ester carbonyl peak at 1743 cm^{-1} is more intense than the 1540 cm^{-1} asymmetric carboxylate peak in the upper half of the paint film, while the reverse applies in spectra obtained from lower in the film. The most intense carbonyl absorption and broad carboxylate absorption centred *ca* 1590 cm^{-1} correspond to the relatively transparent and UV fluorescent band evident at the surface of the paint in cross-section. No individual spectra with

characteristic aluminium stearate absorptions were observed, consistent with the absence of associated features in BSE images noted previously.
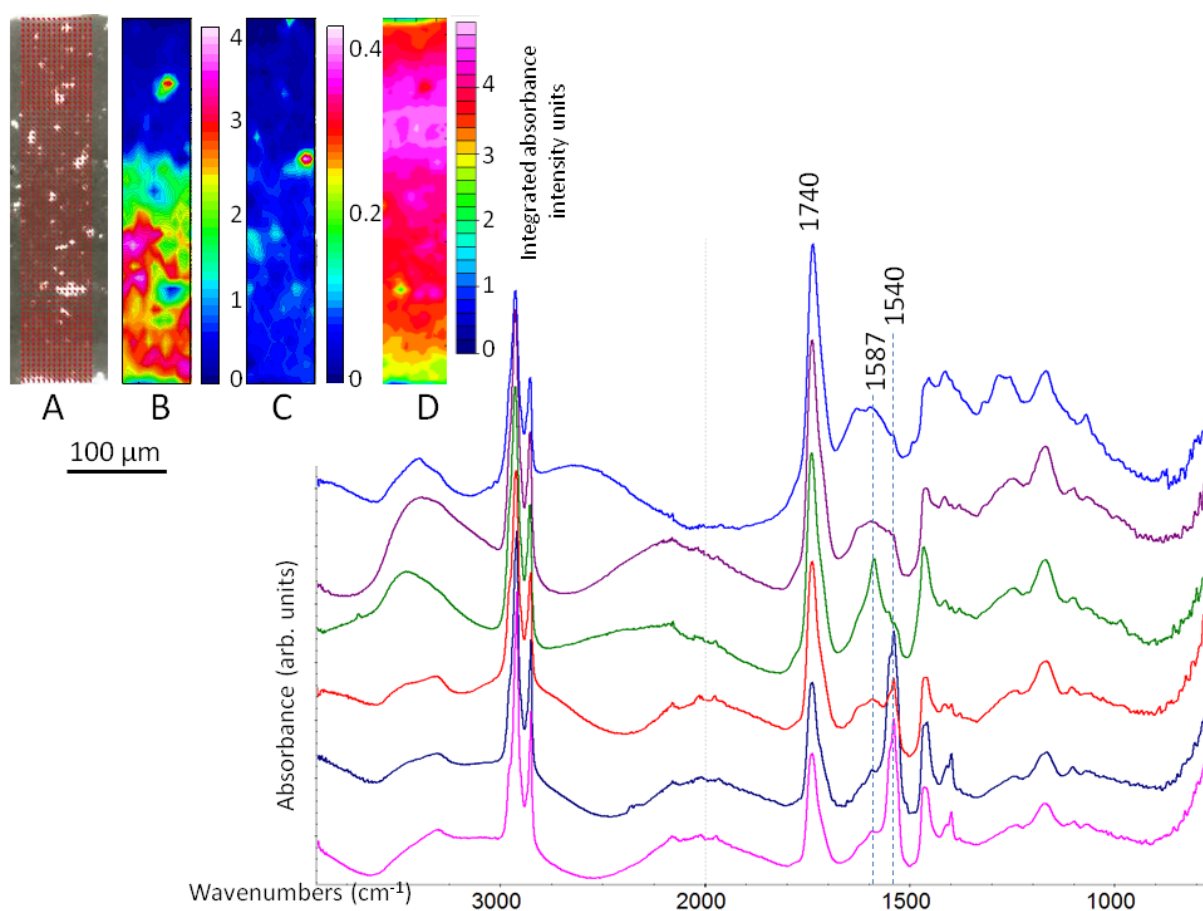
Figure 3.37 Speedball titanium white soybean paint with zinc oxide and aluminium stearate 1981 thin-section detail

(A) optical image with grid denoting area of SR-µFTIR integrated absorption intensity maps (B) 1525-1555 (C) 1580-1600 and (D) 1720-1760 cm^{-1}, and individual spectra extracted from points along a line spanning top to bottom through the sample

In contrast, greater variation occurs through film thickness in spectra extracted from SR-µFTIR integrated absorption intensity maps from the soybean paint formulation with titanium dioxide and zinc oxide (Figure 3.37). Zinc stearate is again concentrated in the lower half of the paint film, but is largely absent from the upper margins and there is a clear distinction between spectra deriving from upper and lower zones. The strong 1540 cm^{-1} peak is also less defined than in the previous sample, and forms a split peak in some spectra as discussed in published work. A further difference is the incidence of defined regions of aluminium stearate indicated both by hotspots in the integrated absorption intensity map 1580-1600 cm^{-1} and by characteristic spectra extracted from these points (green trace). Ester carbonyl absorption is typically strong and the ester triplet centred

ca 1170 cm^{-1} appears intact throughout film thickness although, as for the previous sample, the peak at 1740 cm^{-1} is significantly reduced towards the protected underside of the paint where zinc stearate absorption intensity is strongest.

A similar pattern is also seen in SR-µFTIR maps from a linseed-based paint with aluminium stearate which additionally contains large amounts of barium sulfate (Figure 3.38).
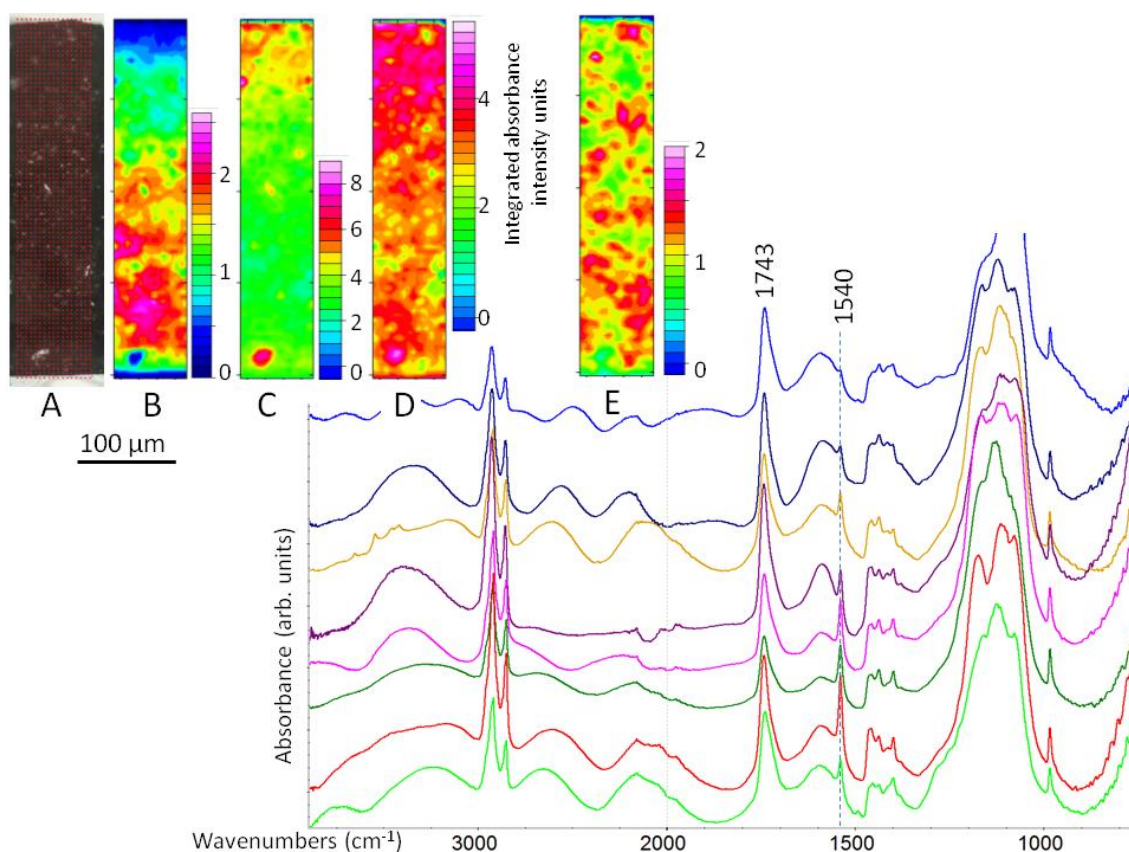
Figure 3.38 Colorlab titanium white linseed paint with zinc oxide, barium sulfate and aluminium stearate 1981 thin-section detail

(A) optical image with grid denoting area of SR-µFTIR integrated absorption intensity maps (B) 1530-1555 (C) 1555-1640 (D) 1730-1760 and (E) 970-995 cm^{-1}, and individual spectra extracted from points along a line spanning top to bottom through the sample

Zinc oxide is present in the paint at a ratio of 1:5:10 by weight with titanium dioxide and barium sulfate. Despite its low concentration significant levels of zinc stearate are again seen to have formed and accumulated in the lower half of the paint film. Strong broad carboxylate absorption is also apparent in the upper margin, over which a peak at 1587 cm^{-1} (v_a COO$^-$ aluminium stearate) is sometimes discernible within localised hotspots. The highest intensity ester carbonyl absorption in the upper margin corresponds to a UV fluorescent surface band (optical image not shown).

However, the integrated absorption intensity map for the sulfate S-O bending vibration at 984 cm^{-1} suggests a relatively consistent distribution of barium sulfate with no indication of pigment settling, supported by BSE images and elemental maps (not shown).

This can be compared to a titanium dioxide/zinc oxide pigmented paint (12:1 by weight) formulated with safflower oil and aluminium stearate supplemented with aluminium silicates in place of barium sulfate (Figure 3.39).
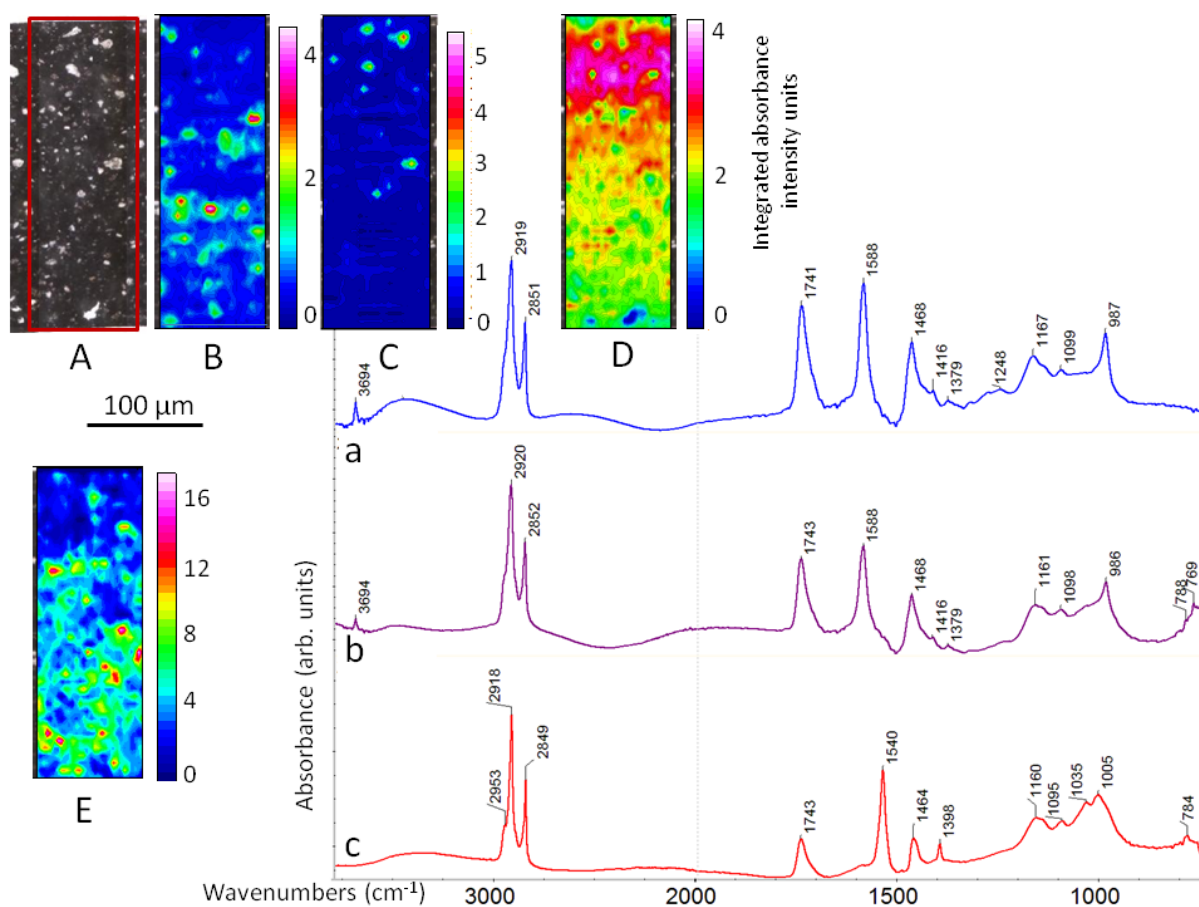
Figure 3.39 Titanium white safflower control with zinc oxide, Al silicates and aluminium stearate 1998 thin-section detail

(A) optical image with box denoting area of SR-µFTIR integrated absorption intensity maps (B) 1530-1555 (C) 1575-1605 (D) 1730-1760 and (E) 980-1055 cm^{-1}, and individual spectra extracted from hotspots in (C) (a) top and (b) centre and from (B) (c) centre

Mapping of the Si-O stretch 980-1055 cm^{-1} indicates settling of silicates has occurred in this paint and the oil ester carbonyl peak *ca* 1740 cm^{-1} is noticeably more intense in the upper margin. Less zinc stearate is evident than in previous samples consistent with the low proportion of zinc oxide in combination with lower reactivity of safflower oil, however small intense concentrations are present

notably in the lower two thirds of the paint film. Aluminium stearate hotspots feature in the centre and upper margin of the paint and correlate to transparent features in the optical thin-section image. Spectra extracted from hotspots in the maps for v_a COO$^-$ zinc stearate and v_a COO$^-$ aluminium stearate show the zinc stearate to be associated with a reduction in the ester carbonyl peak, consistent with formation *in situ*. The two spectra deriving from aluminium stearate hotspots retain strong C=O intensity with consistent relative peak heights between C=O and v_a COO$^-$ regardless of whether occurring near the exposed paint film surface or from deeper within the layer. However, the contribution from Al-O (987 cm^{-1}) and O-H (3694 cm^{-1}) vibrations appears marginally stronger in spectrum (a) derived from closer to the surface, consistent with more advanced (exposure related) hydrolysis.

This same paint also gives insight into the incidence of split v_a COO$^-$ peaks discussed in published work in relation to soybean-formulated paint. Figure 3.40 shows a detail from the centre of the mapped area in the previous figure and corresponding integrated absorption intensity maps for peaks indicative of zinc stearate and aluminium stearate. Hotspots in the aluminium stearate map correlate well with features evident in the optical image. Spectra extracted from points along a line extending from a zinc stearate hotspot show how the sharp v_a COO$^-$ peak at 1540 cm^{-1} progressively broadens and then splits beyond the periphery of the hotspot. Closer inspection of the green trace at the centre of extracted spectra reveals a peak at 1588 cm^{-1} (v_a COO$^-$ aluminium stearate) which coincides with a low level hotspot in map B. This suggests that the split v_a COO$^-$ peak may arise from mixed carboxylate structures which prevent compact molecular packing. This scenario is similar to the suggestion that small amounts of oil and free fatty acids may affect the structure of zinc soaps and influence spectra in this way (Helwig et al. 2014). It is known that impurities may dramatically affect chain packing (Akanni et al. 1992). Peak splitting has also been observed in zinc stearate monolayers during *in situ* acidification experiments, attributed to conformational disorder at pH 6.1 and further intensified by pH 5.75 (Simon-Kutscher et al. 1996).
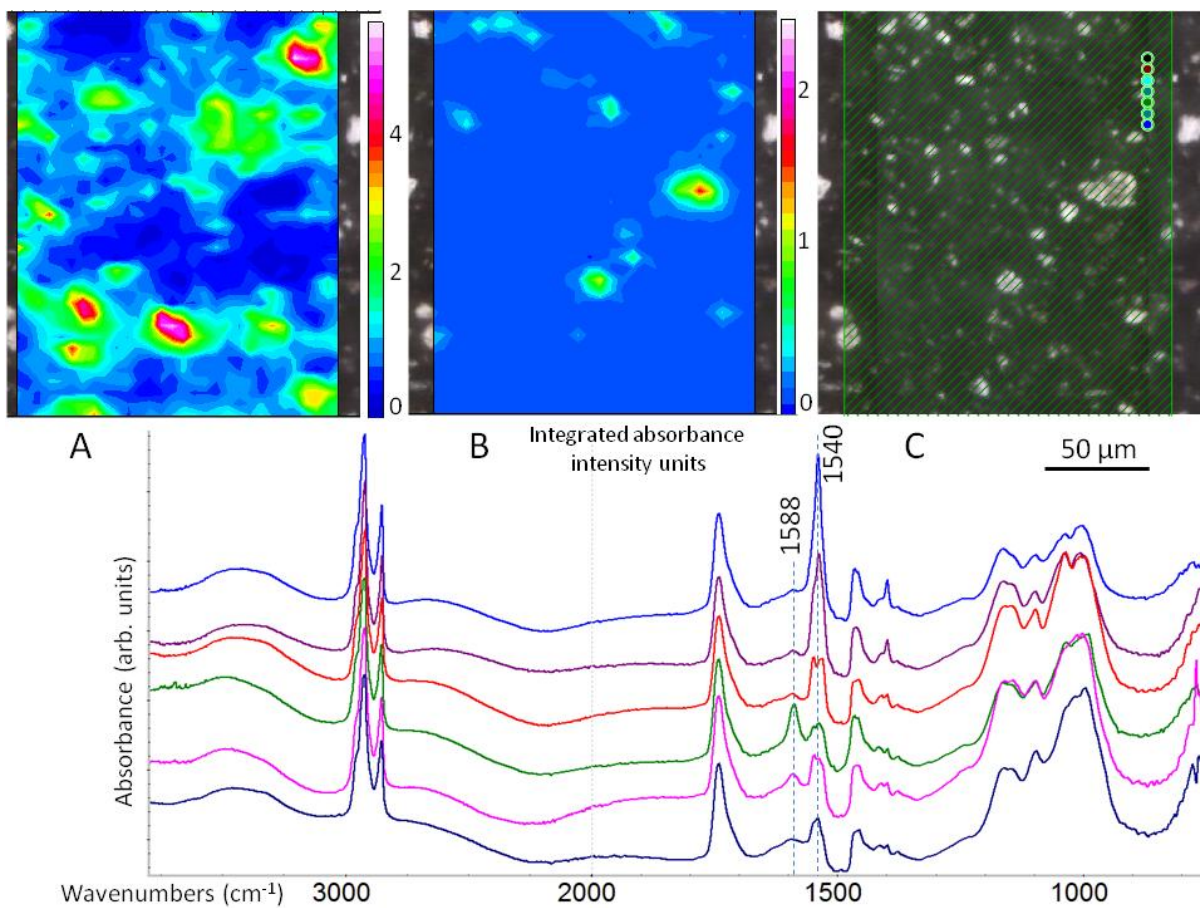
Figure 3.40 Titanium white safflower control with zinc oxide, Al silicates and aluminium stearate 1998 thin-section detail across centre of map area shown in Figure 3.39

SR-µFTIR integrated absorption intensity maps (A) 1525-1555 and (B) 1580-1600 cm⁻¹ and (C) corresponding optical thin-section detail with overlaid map area and circles designating positions of spectra extracted top to bottom

High quality SR-µFTIR maps from lead white paints were more elusive because of the difficulty in obtaining intact thin-sections. An early attempt is shown in Figure 3.41 where some resin infiltration is apparent at the perimeter of the sample. Resin infiltration occurred in some samples embedded in epoxy resin cured at elevated temperature (60°C) and was less evident in subsequent cross-sections with use of room temperature cured polyester. In this instance however infiltration may have assisted microtoming by consolidating an otherwise extremely brittle paint.

The spectral sequence in Grumbacher Flake white 1978 is similar to zinc oxide soybean control paint with aluminium stearate. Spectra at all levels through the film include a defined peak at 1540 cm⁻¹ which intensifies through the lower half. Spectra from the extremities of the film are not presented because of strong epoxy contamination, however no general broad carboxylate absorption without the 1540 cm⁻¹ side peak are apparent in contrast to ATR-FTIR spectra from the exposed film surface.
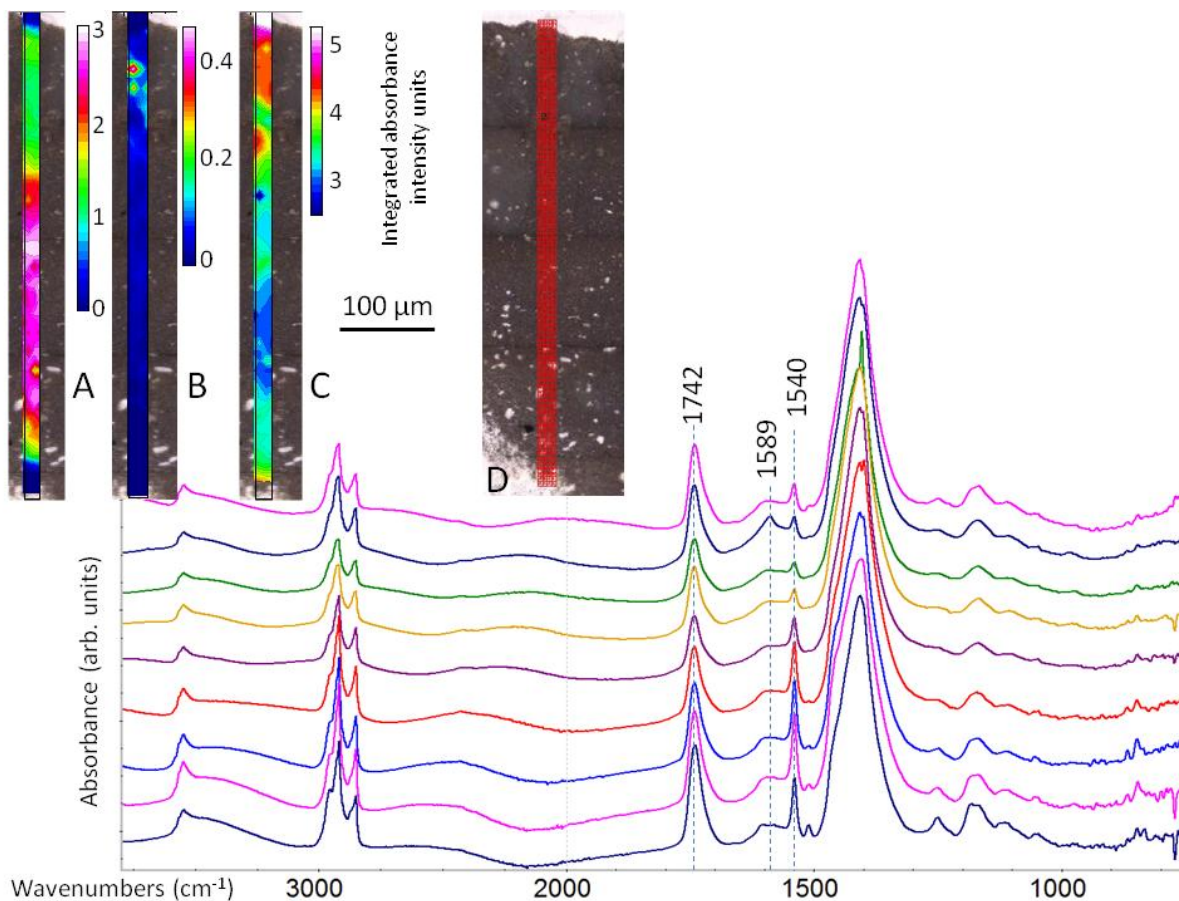
Figure 3.41 Grumbacher Flake white linseed 1978 thin-section detail

SR-µFTIR integrated absorption intensity maps (A) 1525-1555, (B) 1580-1600, (C) 1730-1760 cm^{-1}, (D) corresponding optical thin-section detail with overlaid map grid and individual spectra extracted from points along a line spanning top to bottom through the sample excluding extremities. The small peak at 1510 cm^{-1} reflects some resin infiltration in spectra closest to the sample periphery

The strong zinc stearate absorbance is accompanied by very low residual aluminium stearate, observed only in a small area towards the film surface. While the mapped area covers only a narrow band of the sample, it does appear that substantial conversion of aluminium stearate to zinc stearate has occurred in the paint where zinc oxide is a secondary component. This sample is among the oldest in the reference group so it is expected that reactions of interest will be more advanced than in younger films. It should also be noted that the specified ratio of basic lead carbonate to zinc oxide of 20:1 represents a molar ratio closer to 2:1 given the substantially higher molar mass of the lead pigment, so the proportion of zinc oxide in the paint is higher than might at first be thought.

SR-µFTIR maps of a second lead white-based commercial paint of the same film age are shown in Figure 3.42, in this case in a formulation with barium sulfate and without aluminium stearate.

Viable thin-sections were not obtained so spectra were acquired directly from the embedded sample using an ATR objective.
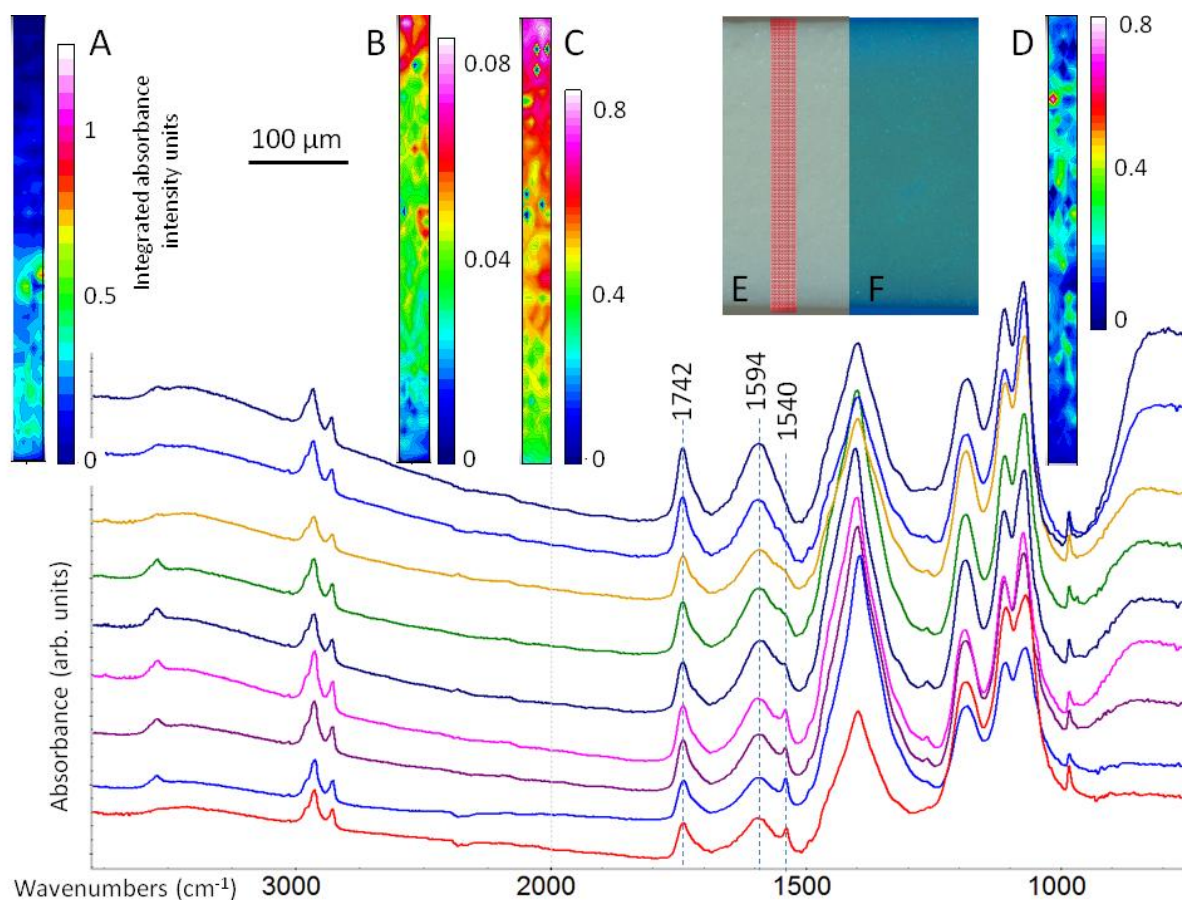
Figure 3.42 Winsor and Newton Flake white linseed 1978 thin-section detail

ATR SR-µFTIR integrated absorption intensity maps (A) 1525-1555, (B) 1580-1600, (C) 1730-1760, (D) 970-995 cm⁻¹ and individual spectra extracted from points along a line spanning top to bottom through the sample; optical cross-section details (E) visible image with overlaid map grid and (F) corresponding UVF image

SR-µFTIR spectra from the cross-section give a clearer indication of the presence of zinc stearate in the lower margin of the paint film than was apparent with ATR-FTIR spectra directly from the underside surface. The spectral sequence indicates a more moderate carboxylate concentration gradient than is apparent in the previous sample, with no zinc stearate evident in the upper margin. As with previously described titanium and zinc oxide-based paints, the small 1540 cm⁻¹ side peak corresponds to reduced ester carbonyl intensity. Barium sulfate absorbs strongly in individual spectra but general distribution is difficult to infer from the SR-µFTIR map given its narrow band of coverage. More conclusive is that over three decades, zinc stearate has formed in paint with zinc oxide as a secondary pigment where the only known source of stearic acid derives from the oil medium itself.

3.6 Concluding remarks

FTIR spectroscopy of reference paint films has shown that zinc carboxylate distribution within a paint film is influenced by additional components present in combination with zinc oxide, in this case by aluminium stearate as an original component of the paint. Stearic acid concentration and availability is increased by the inclusion of aluminium stearate both through its presence in free form in industrial grades, and as a consequence of the high susceptibility of aluminium stearate to hydrolysis. Paints which contain hydrogenated castor oil are likely to be similarly affected. The influence of aluminium stearate on zinc saponification is more significant than either different pigment combinations or oil types present in association with zinc oxide.

Substantial differences in IR absorption spectra obtained from exposed and protected surfaces in paint film draw-downs containing aluminium stearate were revealed by the use of ATR-FTIR measurements, most notably a broad COO^- stretching frequency at the exposed top surface in contrast to a strong, defined peak at 1540 cm^{-1} characteristic for zinc stearate at the underside. The pronounced difference in carboxylate absorption observed in ATR-FTIR spectra acquired from the two surfaces of a single paint film has not previously been reported. The PET substrate involved may influence specific distribution tendencies, however the observed trend for polar and non-polar carboxylates to separate is significant. Specific aluminium stearate absorptions were not evident in ATR-FTIR spectra but were discerned within individual SR-µFTIR spectra obtained from some paint cross-sections. Aluminium stearate is typically retained in these paints as dispersed, UV-fluorescent, low electron density features visible in the microstructure, most commonly within the upper half of the paint film.

SR-µFTIR mapping revealed gradients in metal carboxylate distribution and preferential concentrations of C_{16}/C_{18} chain saturated zinc carboxylates within lower margins of paints incorporating aluminium stearate. In zinc oxide-containing paints without aluminium stearate or another potential source of stearic acid such as hydrogenated castor oil, carboxylate absorption is broad with more subtle variation through film thickness. Moderate levels of zinc stearate were discerned towards the bottom of the oldest lead-based paint formulated without aluminium stearate (W&N) which had not been predicted with surface measurements.

Correlation of BSE images and SR-µFTIR maps suggests small dispersed concentrations of zinc stearate derive from less well defined regions of paint microstructure. Saponification of zinc oxide is indicated by localised areas of relatively low pigment density and reduced atomic brightness within BSE images. These zinc-based regions have a less defined boundary with surrounding paint than comparable aluminium rich areas, allowing differentiation between soaps present as original

components and those forming *in situ*. This distinction is supported by SR-µFTIR where only spectra dominated by characteristic zinc stearate carboxylate absorptions are accompanied by reduced ester carbonyl absorption consistent with conversion from the acid. The highest incidence of low BSE density zinc-based regions occurs in the lower margin of paint films in association with the strongest zinc stearate FTIR signals. The emergence of a low atomic density zinc-based phase from within the microstructure of some cross-sections under vacuum pressure is consistent with a mobile zinc stearate phase.

Different oils have some influence on zinc stearate formation. In zinc oxide-based soybean control paint with aluminium stearate, zinc stearate occurs throughout the film. The highest concentration is still found in the lower margin but as part of a general concentration gradient rather than the more pronounced separation typically apparent in films with other oils or in other soybean paints when zinc oxide is a secondary component. It is significant that this young zinc white soybean control film retains no visibly defined areas of aluminium stearate in cross-section (including in BSE images), suggesting a rapid conversion to zinc stearate. In contrast, multiple aluminium stearate hotspots are evident in the cross-section of the comparable young safflower control film where substantially less zinc stearate has formed. Both safflower and soybean oils are classed as semi-drying and share a triglyceride composition dominated by linoleic acid ($C_{18:2}$), so it is interesting that a marked difference in reactivity is demonstrated. Efflorescence on the soybean oil paint film surface suggests fatty acid release occurs readily in this formulation which would facilitate formation of soap molecules unattached to the cross-linked oil network. Paints based on the two semi-drying oils also share a localised incidence of spectra with split carboxylate frequencies and other subtle spectral differences revealed by SR-µFTIR. The split carboxylate peaks in spectra otherwise characteristic of zinc stearate are tentatively assigned to zinc stearate where variations in orientation, conformation and packing in the molecular lattice occur due to hydration, acidification, or to the presence of 'impurities' including other soaps, oil or acid structures.

Patterns of zinc stearate distribution do not appear strongly affected by pigment combinations whether through combination with titanium dioxide, barium sulfate, calcium or magnesium carbonates, or aluminium silicates. It is possible the presence of lead white has a more significant influence based on the incidence of zinc stearate revealed by SR-µFTIR spectra in early W&N Flake white paint, although the additional film age may also play a role; no equivalent zinc or titanium-based paints without added aluminium stearate have been as comprehensively analysed for comparison. The most obvious consequence of pigment combinations is to reduce the total amount of zinc oxide present, exemplified by the variety of Naples yellow hue formulations. However, while this may mean formation of less zinc stearate and zinc carboxylates more broadly, the

accumulation of zinc stearate in the lower half of paint films is a persistent pattern in formulations with aluminium stearate or those believed to contain hydrogenated castor oil. UV-fluorescent surface bands sometimes but not consistently correspond with pigment settling, with carbonates (Mg and Ca) and silicates apparently more susceptible than barium sulfate. In these instances ester carbonyl and/or broad metal carboxylate absorption may also be relatively intense as a consequence of higher localised medium concentration. The possible influence of calcium ions from chalk or in the form of added driers in stabilising fatty acid complexes remains to be further investigated.

Artist oil paint draw-downs from the SMCI reference collection have enabled comprehensive investigation of paint films with direct relevance to paints likely to be encountered in twentieth century paintings using analytical techniques applicable to unique samples. Observations from control paints have assisted interpretation of more complex commercially produced paints. Hypotheses initiated here will be considered further in the following chapter by examining component interactions under further simplified conditions. Uncertainty over the relevance of the migration and distribution of zinc carboxylate phases observed in paints applied to PET substrates will be addressed in subsequent chapters with reference to case studies from samples from paintings. The optical, spectral and microstructural characteristics documented in oil-based reference paint films containing zinc oxide helps inform understanding surrounding formation of zinc stearates and palmitates in paintings.

3.7   References

Akanni MS, Okoh EK, Burrows HD, Ellis HA (1992) The thermal behaviour of divalent and higher valent metal soaps: a review. *Thermochim Acta* 208:1-41

Helwig K, Poulin J, Corbeil M-C, Moffatt E, Duguay D (2014) Conservation issues in several 20th-century Canadian oil paintings: the role of zinc carboxylate reaction products. In: van den Berg KJ, Burnstock A, de Tagle M et al. (eds) *Issues in Contemporary Oil Paint*. Springer International Publishing, Switzerland, p Chapter 11. In press. doi:10.1007/978-3-319-10100-2__11

Mallégol J, Lemaire J, Gardette J-L (2000c) Drier influence on the curing of linseed oil. *Prog Org Coat* 39:107-113. doi:10.1016/S0300-9440(00)00126-0

Maskaev AK, Man'kovskaya NK, Lend'el IV, Fedorovskii VT, Simurova EI, Terent'eva VN (1971) Preparation of 12-hydroxystearic acid, the raw material for plastic greases. *Chem Technol Fuels Oils* 7 (2):109-112. doi:10.1007/bf00718698

Simon-Kutscher J, Gericke A, Hühnerfuss H (1996) Effect of bivalent Ba, Cu, Ni, and Zn cations on the structure of octadecanoic acid monolayers at the air-water interface as determined by external Infrared reflection-absorption spectroscopy. *Langmuir* 12 (4):1027-1034. doi:10.1021/la950731q

Soucek MD, Khattab T, Wu J (2012) Review of autoxidation and driers. *Prog Org Coat* 73 (4):435-454. doi:http://dx.doi.org/10.1016/j.porgcoat.2011.08.021

Standeven H (2011) *House paints, 1900-1960: history and use*. Research in Conservation. Getty Conservation Institute, Los Angeles

4 Model system

4.1 Abstract

Paintings are complex structures where physical and chemical properties are determined by many variables. Model experiments were designed to support observations made in paint films by means of investigating specific component interactions under controlled conditions. A selection of zinc oxide particles is characterised using TEM, diffraction, surface area measurement and FTIR techniques. The rationale and protocol for the choice of toluene solvent model is provided. Results establish the rapidity of reaction between zinc oxide pigment and stearic acid and include the significant finding that zinc stearate also forms readily in the presence of aluminium stearate as the sole source of stearic acid. The resulting precipitates are characterised with FTIR and optical microscopy. Comprehensive analysis of the product formed specifically with reaction of zinc oxide and stearic acid is undertaken using FTIR, Raman, XRD, and SAXS and SEM imaging with EDX analysis and confirms the presence of zinc oxide particles surrounded by a mass of zinc stearate in characteristic bilayer structures, replicating morpholgies observed in backscatter electron images in samples from paintings. Saponification involves a volume increase and zinc stearate effectively plays an emulsifying role enabling zinc oxide/carboxylate complexes to swell within the available space. Extrapolation of solvent model observations and interfacial tension measurements to published research involving synthesis of layered basic zinc soaps in biphasic systems suggests equilibrium changes caused by increasing concentration of stearic acid or temporary ionisation of carboxylate moieties drives mobility and favours heterogeneous nucleation and crystal growth of layered zinc soaps at interfaces. The presence of layered basic zinc salts in paintings is suggested by work presented in Chapter 5

Aspects of this work centred on the significance of aluminium stearate as a stearic acid source for zinc stearate formation were presented in association with results from reference paint film studies at the invitation of the Scientific Committee and organisers for Issues in Contemporary Oil Paint symposium, 28-29 March 2013, Amersfoort, The Netherlands. Peer-reviewed contributions have been published in a book of proceedings and include the paper: Osmond, G 2014. Zinc white and the influence of paint composition for stability in oil-based media. In: van den Berg KJ, Burnstock A, de Tagle M et al. (eds) *Issues in Contemporary Oil Paint*, Springer International Publishing, Chapter 18 pp 263-281.

4.2   Introduction and scope

The variety and complexity of paint formulations and unique characteristics of individual paintings makes it difficult to elucidate mechanisms underlying observed deterioration phenomena. Paint formulation, individual artistic practice and the myriad environmental conditions to which each painting may have been exposed will all influence ageing properties and may individually or collectively be significant factors for progression of deterioration. For actual paintings additional limitations to investigations are imposed by the restricted capacity for sampling and the size of samples which can be taken. This complexity makes it extremely difficult to isolate key determinants and processes.

Previous research applied to the deterioration phenomenon under investigation has largely focussed on the paintings themselves. Despite extensive characterisation, no fundamental mechanism to explain the cause of zinc soap aggregation has been determined using this approach. Drawing on expertise within the Australian Institute for Bioengineering and Nanotechnology (AIBN), we aimed for a complementary approach whereby model systems would be used to greatly reduce and control the possible variables and enable specific interactions to be investigated using a range of analytical techniques.

The initial model concept proposed producing a polymer to function as a matrix within which interactions and diffusion behaviour of selected reactants could be examined. While linseed oil might be considered the obvious choice for the matrix, the chemistry of linseed oil is itself highly variable and complex. Various studies have substituted m/ethyl esters of fatty acids to represent linseed oil in paint studies (Hancock et al. 1989; Muizebelt and Nielen 1996; van Gorkum and Bouwman 2005). However, previous studies investigating formation of metal soaps have found that methyl esters of applicable saturated fatty acids are relatively stable (Elm 1957; Boon et al. 2007) and so might not yield the intended results. Another major limitation of linseed oil as the matrix is the long time frame over which reactions of interest take place and the techniques by which interactions were intended to be analysed. Although FTIR is a useful technique for both liquid and solid samples, the most meaningful analysis able to be directly correlated to study of paint samples incorporates spatially resolved data such as may be obtained by mapping a film in cross-section. The intended techniques of SEM-EDX and SR-µFTIR are both ideally suited to producing high resolution and location specific data applicable to individual samples. Yet these techniques require a sample of sufficient cohesion and hardness to microtome or polish in cross-section – unlikely to be achieved under ambient conditions in a reasonable timeframe with a linseed oil or fatty acid ester model.

A proposed alternative to the linseed oil matrix was a synthetic polymer based on butyl acrylate with an average molecular weight in the vicinity of that of the cross-linked triglyceride oligomeric structures present in typical mature oil paint films (Mw 3000-6000 based on a hexamer of glycerol with 3 x C_{18} fatty acid chains being the largest analytically determined (Muizebelt and Nielen 1996; van der Weerd et al. 2005)). To achieve this, significant time was devoted to acquiring the skills necessary for controlled radical polymerisation and characterisation, and to obtaining predictable and reproducible results. Polymerisation of butyl acrylate alone did not achieve the requisite hardness; copolymerisation with styrene was undertaken to increase the glass transition temperature. Ultimately, difficulties in the tailoring of the polymer to achieve properties suitable for pigment dispersion and film formation were compounded by the unsuitability of the model polymer for the intended sampling and characterisation techniques. A particularly significant limitation was the strong infrared absorption of the copolymer in the carboxylate region which would preclude meaningful monitoring by that technique of acid to carboxylate conversion within the intended reactants. It is possible that if a suitable polymer had been readily available then this approach to a model system may have been viable. However, the process of optimal polymer synthesis itself proved beyond the scope of the current study and is left for possible future investigations. In preference a simpler solvent based model was applied within which component interactions could be investigated. This decision precluded application of the model for spatially resolved investigations but produced results within practical timescales which were compatible with FTIR techniques, providing some continuity with paint film studies.

Model systems will always remain open to challenge on the parameters on which they are based and the extent to which results are representative of interactions occurring in more complex systems. For example, a solvent model bears less resemblance to a mature paint system than a model based on higher molecular weight matrix, and largely precludes study of diffusion behaviour. Solutions are also highly dynamic systems, and even small differences in polarity of the solvent system may substantially influence coordination behaviour and thus chemical reactivity (van der Kerk 1972), and reactions will occur more rapidly than in the solid state. However, these conditions offer some advantages in allowing for accelerated testing. As paintings conservators we are concerned with potential changes which may occur in paint films over decades or centuries which are difficult to replicate in the laboratory. The solvent model provides an opportunity to observe the fundamental interaction of carboxylate ions with the oxide particle. The formation and behaviour of the resulting zinc soap may also give insight into possible mechanisms of transport and aggregation to complement data obtained from analysis of more complex paint systems and paint samples from actual works of art.

This chapter presents the rationale for model selection and includes comprehensive analysis of the product formed specifically from reaction between zinc oxide and stearic acid within the model. In response to the results of reference paint film studies described in Chapter 3, the reactivity of zinc oxide in the presence of aluminium stearate is further investigated. Experiments involving interfacial tension measurements within the model attempt to elucidate further detail about the interaction between zinc oxide and stearic acid and the mechanism of zinc stearate formation.

4.3   Choice of model and its characterisation

4.3.1 Solvent selection

A solvent was sought for use in model experiments which would demonstrate an affinity for (and by extension have similar cohesive forces to) a representative paint film. Similar to the range of solvents used for a study into stearic acid crystallisation (Garti et al. 1980), preliminary trials combining zinc oxide and stearic acid were conducted in solvents ranging from aliphatic (*n*-hexane) to polar (ethanol), ketone (acetone) and aromatic (toluene). Observations over several days showed an increase in the volume of solids in all solvents but most notably in the toluene and ethanol systems. Stirring produced a suspension of the fine white solids which settled quickly in the ethanol and n-hexane, and was most stable in the toluene.

In addition to trials, potential solvents were evaluated using published solubility parameters in correlation with graphic models charting oil paint film solubility according to swelling response to specific solvents. This is similar to the concept by which non-vaporisable polymers are assumed to have equivalent solubility parameters to a solvent or mixture of solvents in which they readily dissolve or which produces the greatest swelling (Rudin 1999). Attempts to understand and classify solvent sensitivity of paint films has been of long term interest to conservators who aim to minimise disruption of original materials during surface cleaning treatments.

4.3.1.1 *Review of solubility classification theory*

Thorough reviews of applicable solubility classification theory are provided in papers by Burke and Phenix, (Burke 1984; Phenix 2002b). This work is not repeated in detail here but is used to reference key developments which have facilitated graphic representation of solubility. In the 1930s Joel Hildebrand categorised solvents by a single number derived from the cohesive energy density or pressure of a liquid. This value came to be known as the Hildebrand solubility parameter δ_o. Charles Hansen expanded this concept in the 1960s by assigning a value to three contributing forces

(dispersion, polar and hydrogen bonding), known as Hansen's solubility parameters, which relate to δ_o according to the following equation:

$$\delta_o{}^2 = \delta_d{}^2 + \delta_p{}^2 + \delta_h{}^2$$

In 1968 Jean Teas introduced fractional parameters mathematically derived from Hansen values to facilitate graphic representation on a triangular chart. The contribution of each of the three forces is calculated as a percentage of δ_o:

e.g. $f_d = \delta_d / (\delta_d + \delta_p + \delta_h)$ x 100%

The Hildebrand and Hansen solubility parameters and Teas fractional parameters for the solvents under consideration as simplified paint system models are shown in Table 4.1, alongside the values for linseed oil, stearic acid and oleic acid.

Table 4.1 Hildebrand and Hansen solubility parameters (δ) (SI units δ(MPa)$^{\frac{1}{2}}$) and Teas fractional parameters (f) for the solvents under consideration as simplified paint system models.

The values for linseed oil, stearic acid and oleic acid are included for comparison where known. Based on figures quoted in Burke (1984)

Solvent	Dispersion		Polarity		H-bonding		Hildebrand solubility parameter
	δ_d	f_d	δ_p	f_p	δ_h	f_h	δ_o
toluene	18.0	80	1.4	7	2.0	13	18.2
n-hexane	14.9	100	0	0	0	0	14.9
ethanol	15.8	36	8.8	18	19.4	46	26.2
acetone	15.5	47	10.4	32	7.0	21	19.7
linseed oil		66		17		17	
stearic acid	16.4	65	3.3	14	5.5	24	17.6
oleic acid	14.3	62	3.1	13	14.3	22	15.6

4.3.1.2 *Review of peak oil paint swelling representations*

There have been systematic attempts since the 1950s to define the solubility region of aged oil paint films based on sensitivity of reference paint films to specific solvents or solvent mixtures classified according to solubility parameter (Stolow 1957; Feller et al. 1971; Hedley 1980). Despite the well documented limitations of representing solubility using fractional solubility parameters (Stavroudis

and Blank 1989) and of extrapolating broader relevance from the results of studies based on limited variables (Phenix 2002b), the system of triangularly plotting solubility remains a useful model for visualising predicted and observed solubility behaviour. As research has evolved, the solubility area in which 'typical' oil paint films are considered to be at significant risk of swelling has expanded beyond a single zone, and attempts have also been made to introduce contours based on measured degrees of swelling to account for the observed complexity (Phenix 2002b, a, 2013).

Each of the solvents under consideration in the current study as a model for ageing oil paint can be plotted according to its fractional solubility parameters against a chart of oil paint swelling (Figure 4.1).
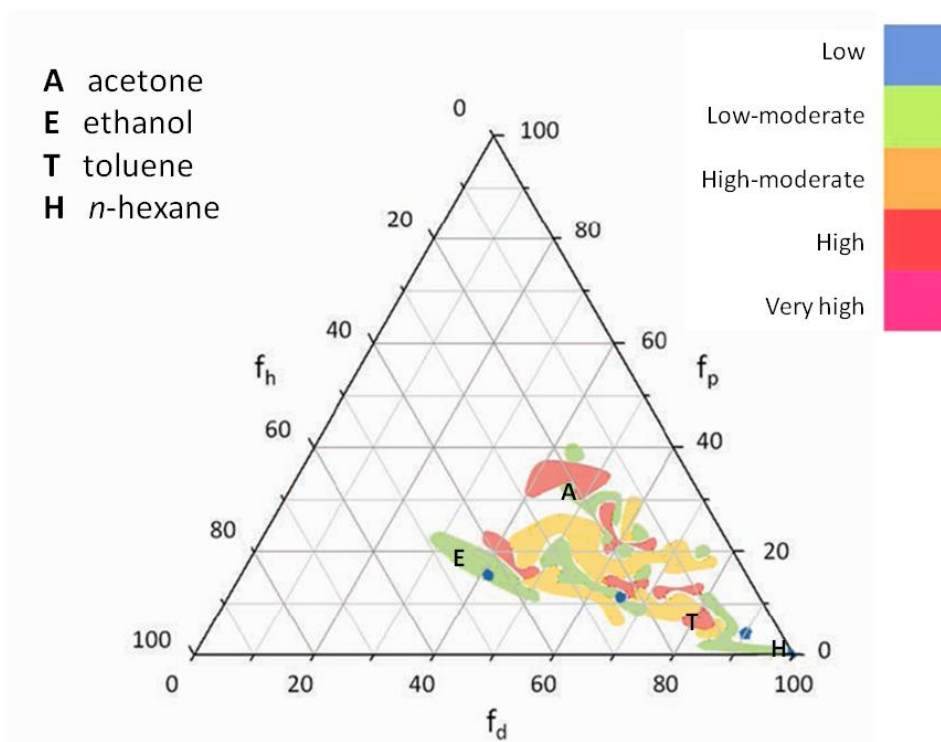
Figure 4.1 Plot of representative oil paint film swelling response to solvents using the Teas system of fractional solubility parameters.

Based on the work of Phenix (2012-2013), toluene is located in the high swelling region while acetone, ethanol and *n*-hexane are categorised as low-moderate or low swelling solvents. Image adapted from (Phenix 2013)

Solvents which overlie the peak swelling region are assumed to have comparable intermolecular forces to a 'typical' painting. Based on the work of Phenix (Phenix 2002a) toluene is in the category of high-moderate swelling for a representative paint film (10 year old lead white and yellow ochre in linseed oil), while acetone and ethanol are in the low-moderate range and *n*-hexane is an outlier. The sensitivity of the representative paint film to toluene was also consistent between light- and

dark-aged paint samples, indicating the solvent has high swelling potential for paint films of varying states of oxidation.

On the basis of solubility classification and the results of trial experiments, toluene was selected as the most appropriate solvent for use as a model for paint. Results reflect toluene's capacity for interaction with both aliphatic and polar moieties and its potential to model at some level the complex chemical environment of an oil paint.

4.3.2 Zinc oxide selection

Zinc oxide pigment samples were obtained from a leading artists' pigment supplier, Kremer Pigmente (Germany) (ZnO 99.8 % min.), and from the stocks of a local industrial paint producer (Wattyl Paints, Rocklea) using Australian supplied pigment (Umicore White seal, ZnO 99.8% min.). Kremer Pigmente is also the source of zinc oxide used in the formulation of control paints discussed in Chapter 3. Two further samples of nano-sized zinc oxide not specifically produced for the paint pigment market were sourced from MK Impex Corp. (Canada) to provide a more reproducible and consistent grade of particle for use in model experiments (MKN-ZnO-030, ZnO 99.9% pure, APS: 30 nm 30 nm; and MKN-ZnO-050L, ZnO 99.9% pure, APS: 50-150 nm). Potential candidates with average particle size closer to that found in typical paint grade pigment were excluded because of wider particle size distributions which would unnecessarily complicate quantification and interpretation of results. Structural and chemical characteristics of pigment particles were studied by high resolution transmission electron microscopy (HRTEM) and selected area electron diffraction (SAED). EDX surveys were used to confirm particle compositions. Each of the studied samples was found to comprise zinc oxide of Wurtzite structure.

TEM images of the Kremer, Umicore and MKN 30 nm samples are shown in Figure 4.2. The Kremer pigment in particular includes particles of highly variable size and shape including many which are distinctly acicular. Umicore pigment appears more regular and nodular in shape although still elongated in one dimension. The Umicore pigment is specified as high purity French Process zinc oxide. The two grades of nano zinc oxide were similarly shaped, however the product with the purportedly larger mean particle size (50 nm) had actual mean primary particle sizes closer to 5 nm. Table 4.2 details particle sizing and specific surface measurements undertaken using Low Angle Laser Light Scattering (LALLS) and Brunauer-Emmett-Teller (BET) respectively. Specific surface measurement confirmed the MKN 50L product had a significantly higher surface area than the 30 nm sample, commensurate with particle sizes indicated by TEM. The anomalous LALLS results can be explained by the strong aggregating tendencies of the dry pigment samples, ultrasonic dispersion notwithstanding.
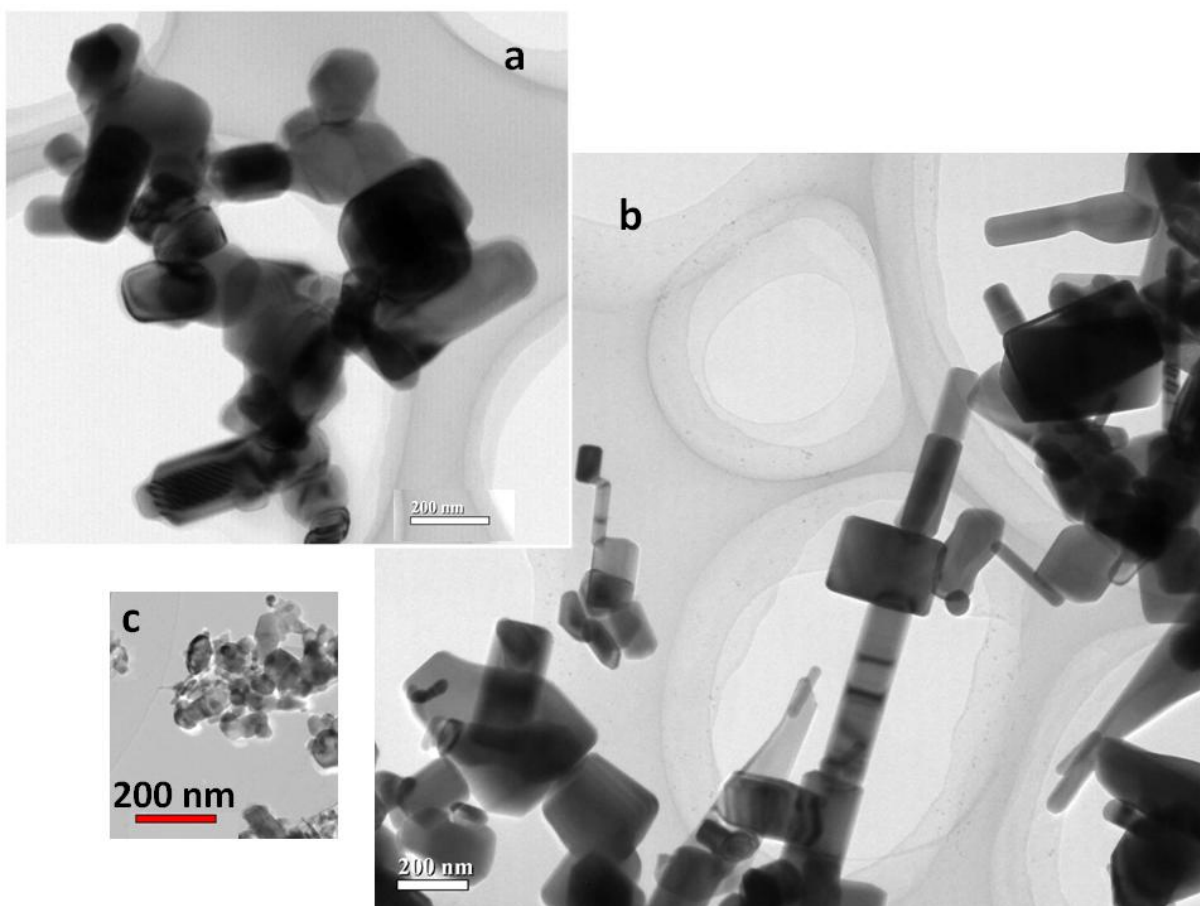
Figure 4.2 TEM images of zinc oxide shown at equivalent magnification (a) Umicore 'White seal' (b) Kremer Pigmente 46300 (c) MKN-ZnO-030 (images: Yanan Guo and John Drennan)

Table 4.2 Particle sizing (LALLS) and specific surface area (BET) measurements of zinc oxide samples.

LALLS results reflect the aggregated state of the pigment. Specific surface area measurements are commensurate with primary particle sizes observed with TEM

ZnO	Particle diameter range d(0.1) – d(0.9) (10-90 percentiles) (µm)	Median particle diameter d(0.5) (µm)	Volume weighted mean D[4,3] (µm)	Specific surface area (m²/g)
Kremer 46300	0.7-5.0	1.6	2.6	5.5-6.5 (TDS specified)
Umicore White seal	0.7-3.2	1.5	2.1	3.5-10.5 (TDS specified)
MKN 30	1.0-9.8	3.6	4.6	16.6 (measured)
MKN 50L	2.5-22.3	9.5	11.2	52 (measured)

The MKN 50L sample was rejected on the basis of particle size. Of the remaining tested pigment samples TEM images indicated MKN 30 nm zinc oxide had the most consistent particle size and shape (Figure 4.3). A tight particle size distribution was considered important for the model zinc oxide in order to minimise the effect of particle size as a variable within experiments. Consistent particle size and shape would also enable meaningful comparison of changes at individual particle level with TEM in the course of experiments. For this reason MKN 30 nm zinc oxide was selected for use in the model experiments despite its significantly smaller mean primary particle size than typical paint grade zinc oxide. Industrial paint literature refers to primary particle sizes of 0.25-1 µm (Princen and Devena-Peplinski 1964), while modern French Process zinc oxide has surface areas typically ranging between 2.5-12 m^2/g (International Zinc Association 2009). Mid twentieth century research categorised fine French Process pigment as being 'very reactive' as a consequence of its high surface area (Morley-Smith 1950). The International Zinc Association (2009) advocates zinc oxide with a specific surface area of 5 m^2/g as the preferred 'standard' for paint, corresponding to maximum opacity. The enhanced surface activity likely to accompany the larger surface area (16 m^2/g) of the selected 30 nm sample was in this case considered to have some advantage in reducing the time required for reactions of interest to proceed. However, to ensure that comparable interactions would occur using paint grade zinc oxide, some experiments were conducted simultaneously using Kremer zinc white pigment.
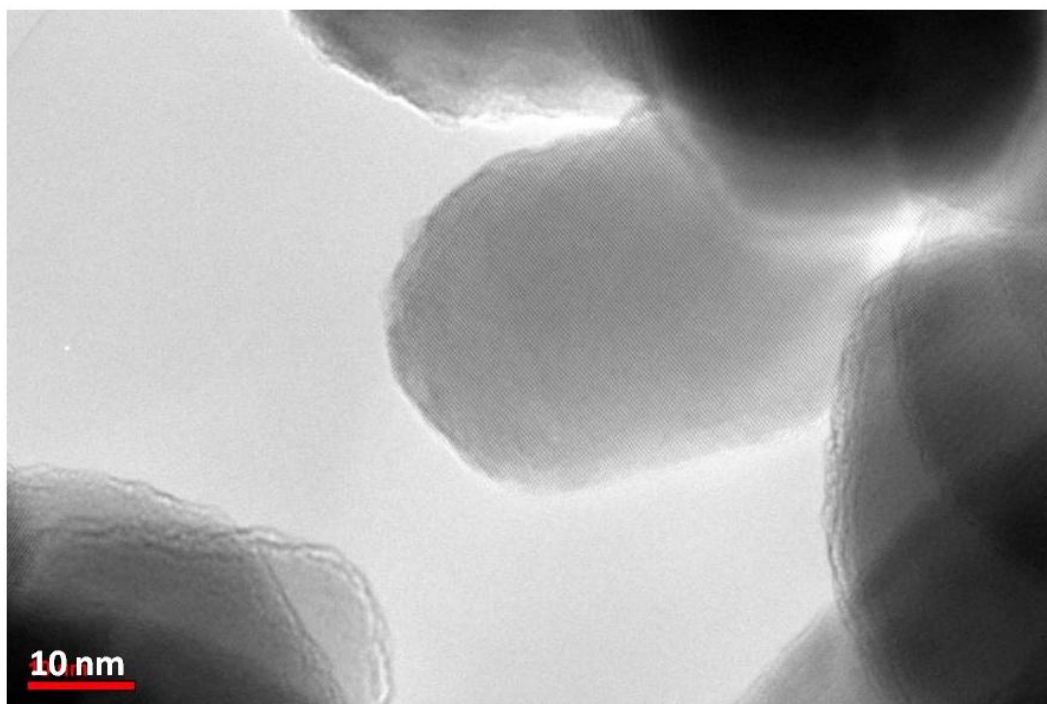
Figure 4.3 High magnification TEM image of MKN-ZnO-030 (440,000x) selected for use in solvent models, showing characteristic particle size and shape (image: John Drennan)

4.3.2.1 *Surface activity of zinc oxide powders*

Zinc oxide has a reactive surface arising from electrostatic instability in its two polar surfaces terminating in Zn and O atoms respectively, Zn-OZn and O-ZnO (Wöll 2007). It is well known that reactivity is influenced by the conditions under which pigment is stored, for example Hansen and Klauss found that zinc oxide and palmitic acid did not react in a carefully dried system but that this changed with the smallest additions of water, and the results of the experiment more generally were hampered by comparison of pigment samples with differing and unknown storage histories particularly with regard to moisture exposure (Hansen and Klauss 1971). Slight variations in water content were found to outweigh other variables in the exotherm of the reaction determined using differential thermal analysis.

FTIR spectra for the selected Kremer and MKN zinc oxide pigment samples are shown in Figure 4.4.
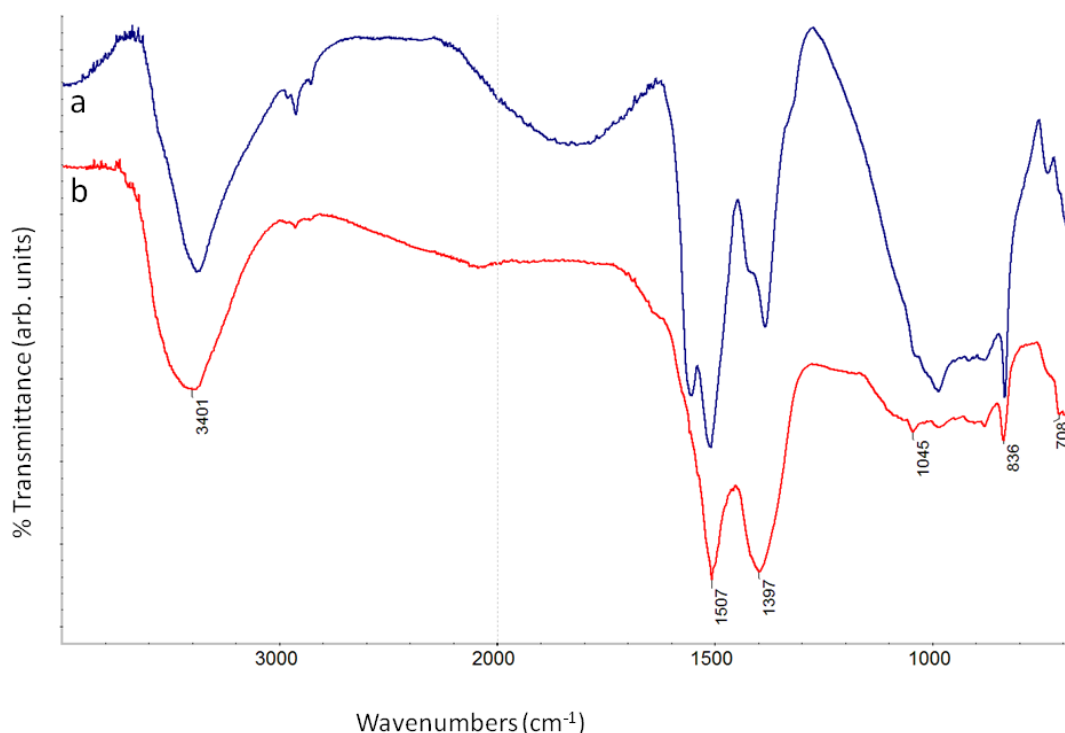
Figure 4.4 FTIR spectrum showing carbonate absorptions present in zinc oxide samples

(a) Kremer and (b) MKN 30 nm: CO_3^{2-} v_3 doubly degenerate antisymmetric stretch (1507, 1397 cm^{-1}) v_1 symmetric stretch (1045 cm^{-1}) v_2 bending mode (836 cm^{-1}) v_4 in phase bending (708 cm^{-1}). The split v_3 frequencies evident in the Kremer sample likely relate to greater crystallinity and different types of interactions between carbonate oxygens with zinc atoms and OH groups

Pure zinc oxide does not absorb IR in the range 600-4000 cm^{-1}, however as Figure 4.4 clearly shows, the two zinc oxide pigment samples have not recorded featureless spectra in this region. Both incorporate strong broad OH stretching at 3400 cm^{-1}, two prominent bands *ca* 1500 and 1380 cm^{-1} and a small sharp peak at 836 cm^{-1}. Zinc oxide is known to slowly absorb carbon dioxide from the air so that stored zinc oxides will contain zinc carbonate (H.W. 1925; Oil and Colour Chemists' Association 1966; Kühn 1986). This is similar to the process by which galvanised metals form a passive protective layer of zinc carbonate via a zinc hydroxide intermediate (Eq. 4.1). Relative humidity cycles are involved, where the carbonate forms from the hydroxide upon drying (Eq. 4.2) (Zhang 1996).

$$ZnO + H_2O \rightarrow Zn(OH)_2 \qquad\qquad [4.1]$$

$$5Zn(OH)_2 + 2CO_2 \rightarrow Zn_5(CO_3)_2(OH)_6 + 2H_2O \qquad\qquad [4.2]$$
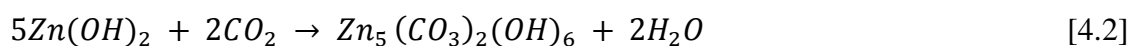
As suggested by the reaction sequence above, zinc carbonate is commonly a mixture of the carbonate and the hydroxide (Jackson 1998). The dominant absorption bands in the FTIR spectra of the zinc oxide samples shown in Figure 4.4 can be assigned to basic zinc carbonate, including v_3 CO_3^{2-} doubly degenerate asymmetric stretch (1507, 1397 cm^{-1}), v_1 CO_3^{2-} symmetric stretch (1045 cm^{-1}), v_2 CO_3^{2-} bending mode (836 cm^{-1}) and v_4 CO_3^{2-} in phase bending (708 cm^{-1}) (Musić et al. 2002). Differences in the spectra of the two zinc oxide samples include a notable splitting of the v_3 CO_3^{2-} asymmetric stretch vibrations in the Kremer sample indicating different types of interactions between carbonate oxygens with zinc atoms and OH groups (Musić et al. 2002).

Characteristic carbonate and hydroxide+carbonate binding energies were also detected on the MKN sample with the surface sensitive technique of X-ray photoelectron spectroscopy (XPS) (results not shown). However, XRD of the bulk pigment did not give any indication for the presence of either zinc carbonate or hydrozincite (Figure 4.5), suggesting carbonate formation may be amorphous and/or comprise a minor phase at the surface. The Kremer pigment had been stored locally for a substantially longer period (approximately 7 years) than the MKN (17 months), with an unknown history prior to acquisition for both. Carbonates are inferred to have formed from the zinc oxide in the course of storage.
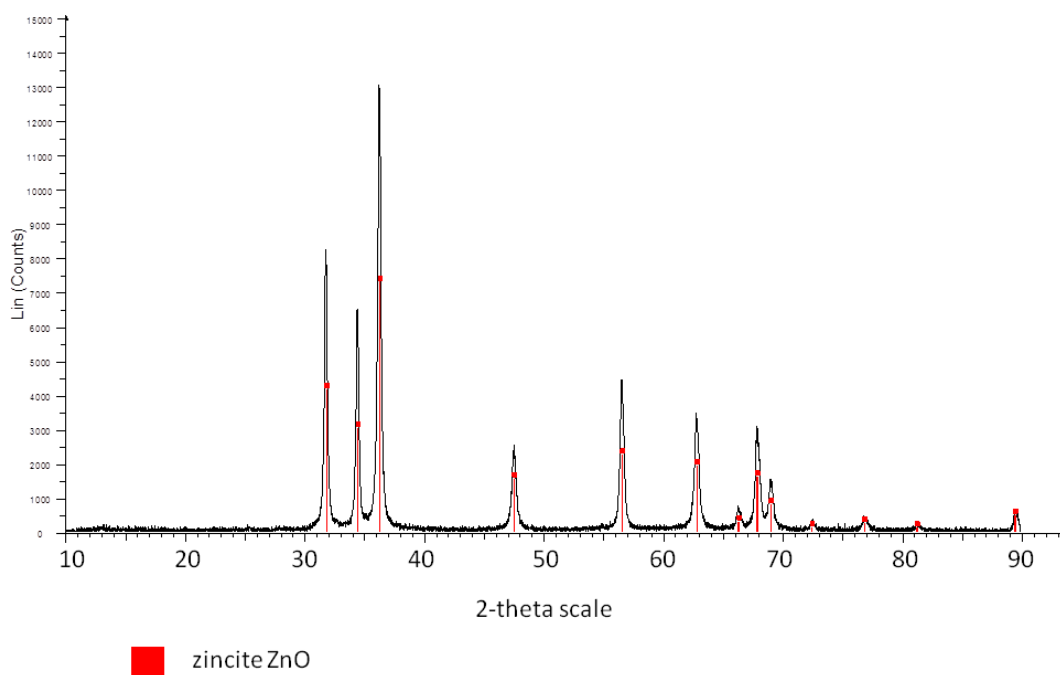
Figure 4.5 Assigned XRD pattern for MKN 30 nm ZnO after domestic storage for 17 months.

There is no indication of the zinc carbonate or hydrozincite observed with FTIR and XPS. Carbonate formation appears to be below the detection limit of the technique and is most likely limited to the surface of the oxide particles

Surface conversion of zinc oxide to zinc hydroxide in the presence of moisture may additionally facilitate saponification in the presence of fatty acids (FA), a reaction which itself produces water (Eq. 4.3).

$$Zn(OH)_2 + 2HFA \rightarrow ZnFA_2 + 2H_2O \qquad [4.3]$$

Similarly, hydrozincite, the principal hydroxycarbonate, although insoluble in water, is only stable within pH range 5.5-7 (Graedel 1989) and will be vulnerable to acids present or forming in oil-based paints. Saponification of basic zinc carbonate produces dissolved bicarbonate anions (Eq. 4.4) with potential for continuing reaction.

$$Zn_5(CO_3)_2(OH)_6 + 10HFA \rightarrow 5ZnFA_2 + H_2CO_3 + 6H_2O \qquad [4.4]$$
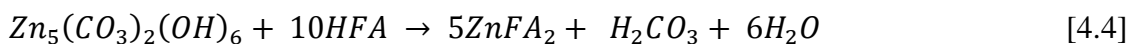
4.3.3 Stearic acid

Reagent grade stearic acid ≥95% (octadecanoic acid, $CH_3(CH_2)_{16}COOH$) was obtained from Sigma Aldrich and its composition confirmed with FTIR.

4.3.4 Zinc stearate

Zinc stearate [zinc octadecanoate, $Zn(C_{17}H_{35}COO)_2$] was synthesised and characterised as described in Chapter 2

4.3.5 Aluminium stearate

Reference paints containing aluminium stearate as an additive discussed in Chapter 3 suggest that aluminium stearate is a source of stearic acid which contributes to the formation of zinc stearate in paints containing zinc oxide. Commercial grades of aluminium stearate are known to frequently be mixtures of aluminium stearate and palmitate and to contain a percentage of free fatty acid (McBain and McClatchie 1932; Coe et al. 1948; Gray and Alexander 1948; Lower 1982); aluminium stearate as a potential source of stearic acid has been discussed in the conservation literature based on this as well as its susceptibility to hydrolysis (Tumosa 2001; Burnstock et al. 2007). Aluminium stearate was synthesised for use in an iteration of the solvent model as a substitute for stearic acid.

Aluminium stearate was synthesised from a sodium stearate intermediate and aqueous solution of aluminium sulphate hexadecahydrate ($Al_2(SO_4)_3 \cdot 16H_2O$ Fluka Purum p.a. $\geq 95.0\%$ (KT)) at 3:1 stoichiometric ratio using the modified double-decomposition technique described by Corkery (Corkery 2004) and further expanded in his PhD thesis (Corkery 1998). This technique was selected over the one-step precipitation method described for the synthesis of soaps of lead, copper and zinc (Corbeil and Robinet 2002) based on the results of FTIR of trial product obtained using each method. Sodium stearate was first produced based on techniques outlined by Corbeil (Corbeil and Robinet 2002). In summary, stearic acid and 1M sodium hydroxide were combined at 1:1 stoichiometry in a round bottomed flask with stirrer and heated in an oil bath at 70 °C for 1 hour before filtering and sequential rinsing/filtering with ethanol and warm water. FTIR was used to confirm the composition of the sodium soap, characterised by a sharp asymmetric COO$^-$ vibration at 1558 cm^{-1} and the absence of an acid carbonyl peak at 1703 cm^{-1}.

Five grams of the resulting sodium stearate was mixed to a paste with 25 mL of ethanol before being combined with 250 mL of water in a glass flask with stirrer and heated in an oil bath to 60 °C. An aqueous aluminium salt solution was then prepared by dissolving 11.5 g of aluminium sulfate hexadecahydrate in 250 mL of warm water. The sodium soap mixture was added to the aluminium sulfate solution while stirring (Corkery 1998) and maintained at 60 °C for 30-60 minutes. The resulting mixture was cooled, vacuum filtered and rinsed with warm water. The solids were then loosened in 50/50 acetone/dichloromethane, filtered and dried.

Corkery's analysis of his own soap syntheses (Corkery 1998) describes how the affinity for oxygen of basic metals such as aluminium is so high that over a large pH range an anionic carboxylate group cannot generally replace a covalently bound hydroxyl group, so the resulting soap will be basic. He, and various preceding studies have concluded that it is very difficult to produce a true aluminium tristearate, and the composition of the synthesised aluminium soap is more typically the

monobasic (distearate) soap, some di-basic soap and aluminium hydroxide Al(OH$_3$) (McBain and McClatchie 1932; Gray and Alexander 1948; Pilpel 1963). This is assumed to be indicative of the aluminium stearate synthesised here. Unreacted fatty acid is also likely to be retained in the soap in small percentages, evidenced by a peak at *ca* 1700 cm^{-1} in FTIR spectra from each of the aluminium soap variants produced. Corkery (1998) used a strontium soap of myristic acid to determine that IR is sensitive to the acid form at approximately 3 wt% (*cf* approximately 0.3 wt% using XRD).

Transmission FTIR of multiple samples from each batch of aluminium stearate synthesised was used to confirm the presence of the intended soap, the absence of the sodium stearate intermediary and the introduced aluminium salt, as well as to ascertain the extent of any free acid. A single batch was selected for use in the model experiments based on a well defined asymmetric COO$^-$ peak (1587 cm^{-1}), relatively small C=O peak (1701 cm^{-1}) and no discernible CH$_2$ progression bands which are prominent in the acid (Figure 4.6). The COO$^-$ absorption in the synthesised soap is sharper than a reference spectrum for aluminium stearate (Thermo Electron Corporation 1991-1994), with a significantly lower OH absorption.
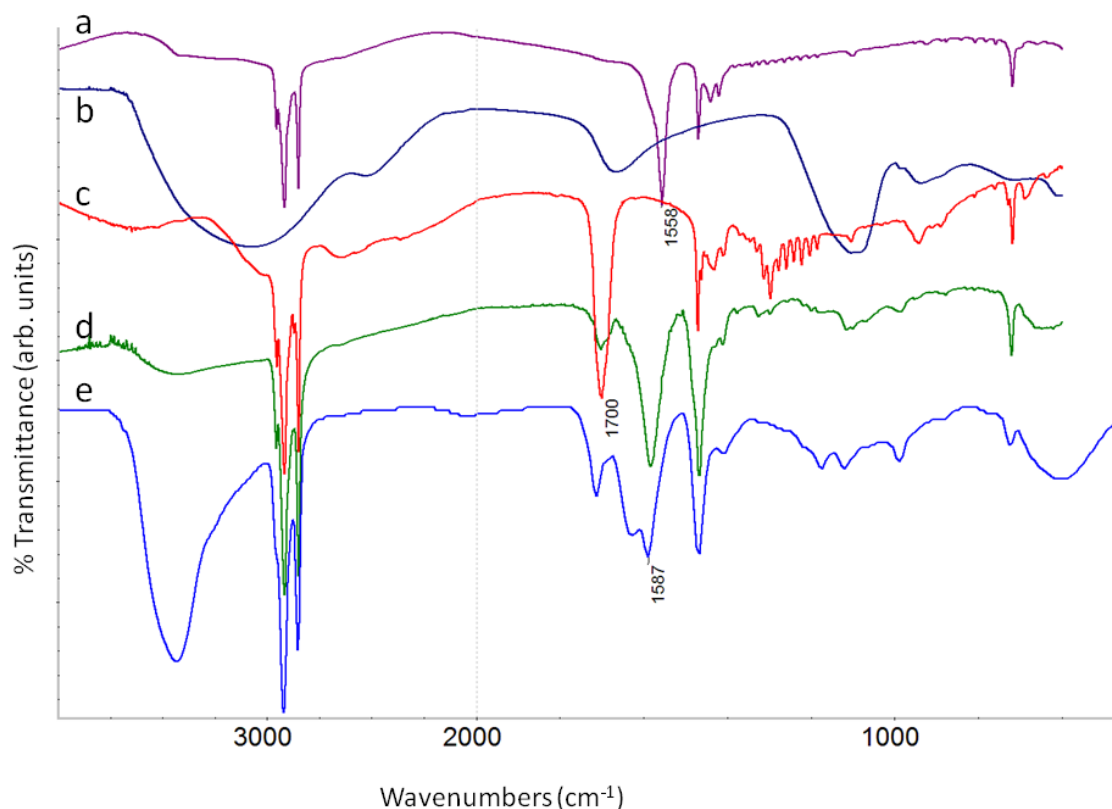
Figure 4.6 FTIR spectra of reactants and products in aluminium stearate synthesis

(a) sodium stearate intermediary (COO$^-$ 1558 cm^{-1}), (b) aluminium sulfate hexadecahydrate, (c) stearic acid, (d) aluminium stearate as synthesised, (e) reference spectrum for aluminium stearate (#2470 Coatings Technology 1991-1994). The synthesised soap retains a small acid C=O peak *ca*. 1700 cm^{-1} but shows no other contribution from reactants. The asymmetric COO$^-$ peak at 1587 cm^{-1} is sharper and OH vibrations less than in the aluminium stearate reference spectrum

The retention of some stearic acid in the synthesised product was considered acceptable in the current study as it is likely to reflect the industrial grades of aluminium stearate typically used in paint production. Additional FTIR analysis was undertaken of the aluminium stearate 5 months after synthesis. The resulting spectrum is shown in Figure 4.7. Interestingly, new peaks are apparent at 984 and 3690 cm^{-1} indicative for Al-O and O-H bonds respectively. This had occurred during ambient storage of the solid in a sealed glass vial and demonstrates the susceptibility of the aluminium soap to hydrolysis with attendant release of free stearic acid (Eq. 4.5).

$$AlSt_2OH + H_2O \rightarrow AlSt(OH)_2 + StH \qquad [4.5]$$
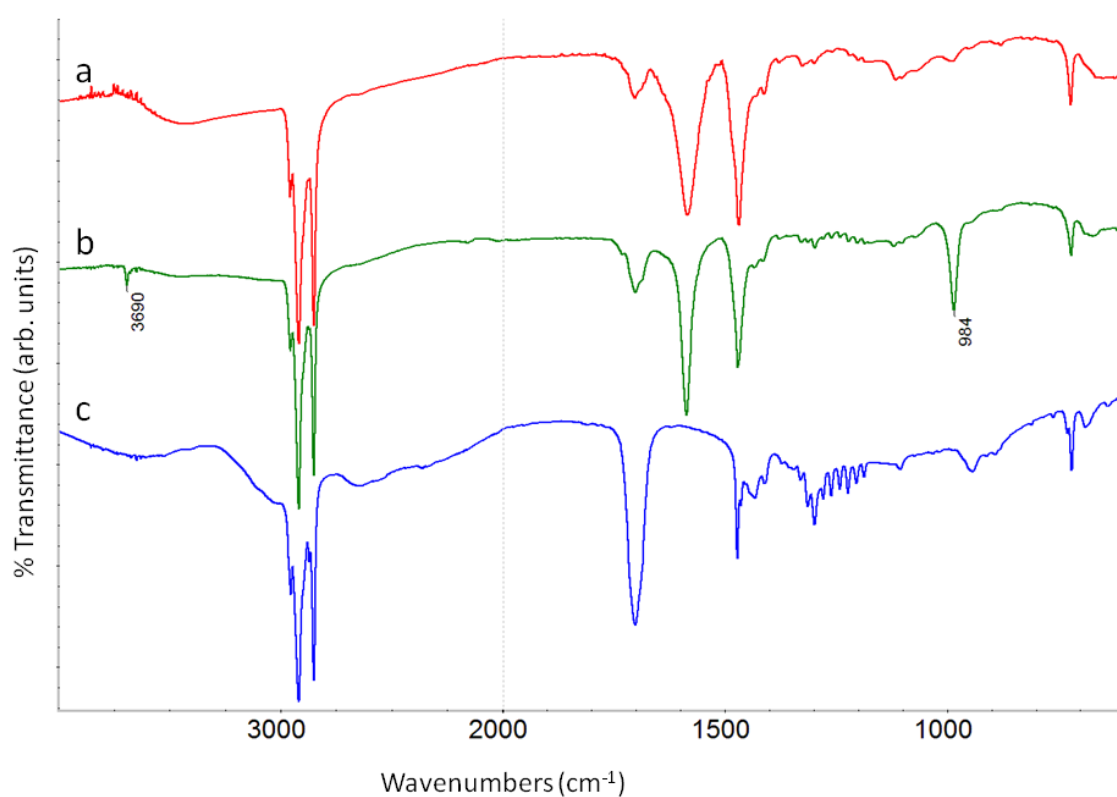
Figure 4.7 FTIR spectra illustrating hydrolysis tendency of aluminium stearate

(a) aluminium stearate as synthesised, (b) aluminium stearate 5 months after synthesis, (c) stearic acid (reference). The appearance of Al-O (984 cm^{-1}) and O-H (3690 cm^{-1}) bond vibrations in (b) is accompanied by the emergence of discernible CH$_2$ progression bands between 1150-1350 cm^{-1} consistent with release of stearic acid

4.4   Experimental

Instrumental methods uniquely applicable to this chapter are detailed here. Additional experimental conditions are provided in Chapter 2.

4.4.1 Transmission electron microscopy

The structural and chemical characteristics of zinc oxide particles were studied by high resolution transmission electron microscopy (HRTEM) in a FEI Tecnai F20 microscope operated at 200 kV, equipped with a Gatan CCD camera and energy dispersive X-ray spectroscopy (EDX). Composition of the particles was determined based on extensive EDX surveys of several particles for each sample. HRTEM images and selected area electron diffraction (SAED) were acquired to confirm the type of crystal polymorphs. Images were processed using Gatan Digital Micrograph (Version 3.9.1) and EDX results using ES Vision software (Version 4.0.172).

Pigment samples were prepared by evaporation of an ethanolic dispersion of the powders on copper mesh grids coated with perforated carbon film.

4.4.2 Particle sizing

Low Angle Laser Light Scattering was undertaken with a Malvern Mastersizer 2000 with Hydro 2000MU Accessory. Samples were dispersed in water with ultrasound but without dispersant

Brunauer-Emmett-Teller specific surface area measurements (BET method) were performed using a Micromeritics Gemini II 2370 Surface Area Analyzer. The samples were dried and degassed at 90 °C in a Micromeritics Flow Prep 060 module. The Gemini II 2370 performs fully automatic analysis in ultra-high purity nitrogen (99.9995), collects data and performs calculations to obtain the BET surface area.

4.4.3 Powder X-ray diffraction

Samples were analyzed in a Bruker D8 Advanced MKII X-ray Diffractometer in Bragg-Brentano geometry, equipped with a copper anode source (40 kV and 40 mA) and a LynxEye multi-pixel detector.

Measurements for ZnO powders were conducted from $2\theta = 5°$ to $80°$ in $0.020°$ increments at 1.25 s/increment. Selected samples were remeasured from $2\theta = 10°$ to $90°$ in $0.010°$ increments at 77 s/increment Midphase solids were measured from $2\theta = 5°$ to $80°$ in $0.020°$ increments at 39 s/increment. The powder patterns were compared with database patterns (Powder Diffraction File, Release 2012) using the EVA Evaluation Package.

4.4.4 Fourier transform infrared spectroscopy

Spectra were acquired using a Nicolet 5700 FTIR spectrometer and Continuum microscope. Solids were applied to a single diamond window of a micro-compression cell and flattened using a stainless steel roller. Samples were analysed in transmission mode. Data was collected using Omnic 7 software over wavenumber range 4000-600 cm^{-1}. Spectra are the sum of 64 scans at a resolution

of 4 cm^{-1}. Spectra obtained were interpreted and compared to published or personal reference spectra and are shown in transmission with an offset scale (arbitrary units) and x-axis split at 2000 cm^{-1}.

4.4.5 Raman spectroscopy

Raman spectroscopy was undertaken using a Renishaw inVia Raman Microscope. The microscope is a Leica DM2500M with 50X reflected light illuminated objectives, and a trinocular head with colour video camera. A Renishaw 514 nm laser with 50 mW nominal power at the source was calibrated on a silicon standard. The spatial resolution for the 50× objective is 2 μm. The spectrometer is a Near Infrared enhanced, deep depletion charge-couple device (CCD) array detector with 576 x 384 pixels and Peltier cooling, and fitted with Rayleigh edge filters and an 1800 lines per mm dispersive grating. Data was collected using Windows based Raman environment software WiRE version 3.0. Spectra were obtained with extended scans (3200-100 cm^{-1}) and 10 s dwell time at 50% laser power for samples on glass slides and 10% laser power with pin hole inserted for samples on silicon wafer, following bleaching at 10% power to 'exhaust' fluorescence.

4.4.6 Scanning electron microscopy

Samples from solvent models were dropped onto silicon wafers and dried for scanning electron microscopy (SEM) and energy dispersive X-ray (EDX) analysis using instrumentation detailed in Chapter 3. Samples were examined in low vacuum (1 Pa) at 15 kV accelerating voltage. Backscatter electron images were captured. EDX of points of interest on the specimen were acquired in spot mode.

4.4.7 Small angle X-ray scattering

Small angle X-ray scattering (SAXS) measurements were collected on an Anton Paar SAXSess instrument. The system uses a sealed X-ray tube (Cu, K$_\alpha$ 1.54 nm), a Kratky camera (i.e. line collimation) and a CCD detector. Dilutions of the suspended midphase were prepared to give an approximate Zn^{2+} concentration of 1.0 x 10^{-2} and 2.5 x 10^{-3} M. The process of dilution disrupted the suspension and caused solids to settle. Samples were introduced into a 1 mm silicon capillary at room temperature. Data was collected over a q-range of 0.07-0.5 A^{-1}. The data were reduced and normalised using standard procedure after collection of background, scattering from the solvent and transmission.

4.4.8 Drop analysis

Drop analysis was conducted using a Dataphysics OCA 20 optical contact angle measuring device. A dosing needle (SNC 165/119) was connected to a 500 μL Hamilton gastight syringe over a PTFE dosing tube with electronic software controlled dosing unit.

Dynamic contact angle measurements were obtained using the captive drop method; surface and interfacial tension was determined from the contours of a 30 or 50 µL pendent drop dispensed into the ambient phase contained in a glass cell (Dataphysics GC10). Drop shapes were captured with halogen lighting and CCD video camera with resolution 768 x 576 pixels. The data was collected with dynamic tracking and constant timing at 5 s intervals and processed using SCA22 software.

4.5 Preparation of the models

4.5.1 Controls in toluene

The solubility of the zinc oxide, stearic acid and zinc stearate individually in toluene at room temperature was determined as follows. A saturated solution of each was prepared by stirring an excess of the solid into 100 mL of toluene, stirred over 24 hours. The quantity of dissolved solids was calculated gravimetrically by evaporating toluene from known decanted volumes of supernatant and vacuum drying, enabling the solids to be weighed and the results averaged. The solubility of zinc oxide over several weeks remained below detection limits by this method.

Stearic acid solubility was determined as 42 g/L, or 0.15 M.

Zinc stearate solubility at room temperature was calculated at 1.1 g/L (0.0017 M), however the subsequent detection of residual stearic acid in the synthesised soap means a contribution reflecting the presence (and solubility) of stearic acid cannot be excluded. A 1948 study of zinc stearate solubility in toluene found negligible solubility below 75 °C (Martin and Pink 1948).

4.5.2 Zinc oxide and stearic acid

Zinc oxide (MKN and Kremer) and stearic acid were combined in toluene in different stoichiometric ratios as shown in Table 4.3. Models range from stearic acid (HSt) in excess to zinc oxide in excess according to Eq. 4.6

$$ZnO + 2HSt \rightarrow ZnSt_2 + H_2O \qquad\qquad [4.6]$$

Zinc oxide and aluminium stearate were also combined in toluene with a slight excess of zinc oxide assuming the aluminium stearate is predominantly in the form of aluminium stearate monohydrate and given indicative reactions represented by Eqs. 4.7-4.8

$$ZnO + AlSt_2OH + HSt \rightarrow ZnSt_2 + AlSt(OH)_2 \qquad\qquad [4.7]$$

$$ZnO + AlSt_2OH + H_2O \rightarrow ZnSt_2 + Al(OH)_3 \qquad\qquad [4.8]$$
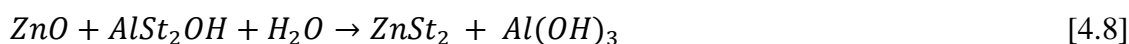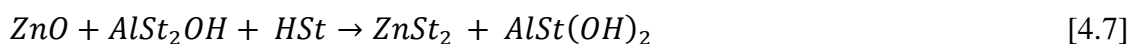
Table 4.3 details the conditions for each model (A-D). Solids were weighed and added to a vial containing a measured volume of toluene. In each case the concentration of stearic acid was within the solubility limit. Various repeats of models A and B were prepared including iterations with both MKN and Kremer zinc oxide.

Vials were capped with Teflon liners and for models A, B and D each vial was manually shaken before being left to stand. Five minutes after mixing, and subsequently at intervals extending from minutes to hours and then days, each solution was again shaken and a drop pipetted from the vial onto a glass slide to dry for in-situ optical microscopy and Raman microspectroscopy, and sampling of solids for transfer to a diamond cell for transmission FTIR spectroscopy. For Model A larger samples were taken from solvent mixtures at 1 hour and 10 weeks and centrifuged for 5 mins at 8000 rpm to separate solids and supernatant; drops from the latter were also pipetted onto glass slides. Solids were set aside for XRD analysis.

Table 4.3 Solvent models prepared to investigate stearic acid (HSt)/zinc oxide interactions

Solvent model		ZnO:HSt by weight	ZnO:HSt molar	Agitation	Analysis undertaken
$A^{(i)}$	stearic acid in excess	1:10	1:3	manually shaken only on mixing and at sampling points	OM FTIR SEM-EDX Raman XRD
$B^{(i)}$	ZnO in excess	1:1	3:1	manually shaken only on mixing and at sampling points	OM FTIR Raman
C	ZnO in excess	1:5	2:3	mechanically stirred 4hr (day 1)+30mins (day 2) then stagnant	OM FTIR SEM-EDX XRD SAXS
D	possible small excess ZnO	1:6 ($AlSt_2OH$)	5:4	manually shaken only on mixing and at sampling points	OM FTIR

[i] Models prepared with both MKN and Kremer ZnO. Other models use MKN only

For Model C, mixtures were stirred for 4 hours before being left stagnant overnight, then stirred for a further 30 min the following day, forming a pronounced 'midphase' of suspended solids (Figure 4.8).
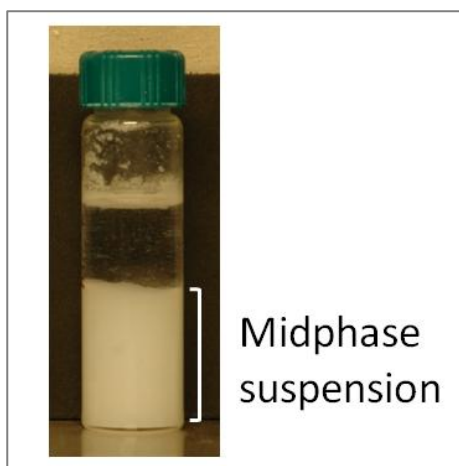
Figure 4.8 Representative toluene model vial image indicating the suspension of solids formed in the solvent – designated the 'midphase'

At 24 hours samples of the supernatant were collected for SAXS analysis. At 1 month drops were pipetted onto a silicon wafer for SEM imaging and EDX analysis, and dilutions of the suspended midphase were prepared for SAXS.

4.5.3 Drop analysis

Drop-shape experiments with solvent models were attempted as a means of obtaining further information about the interaction between zinc oxide and stearic acid, specifically regarding surface activity and micellar organisation of the acid/soap molecules. Additionally there was potential to observe behaviour of zinc stearate molecules under varying conditions, including concentration, pH (arising from dissolved CO_2) and polarity, and in the presence of mixed carboxylate species or metal ions in addition to zinc.

Drop analysis, or optical contact angle measurement, uses the dependency of interfacial elasticity (Gibb's elasticity) on the absorption of surfactant at an interface, determined by increasing the area of the interface and measuring the gradual decrease in interfacial tension (IFT) as drop size increases. Information about how zinc stearate molecules configure within the toluene model was sought for potential insight into related processes of migration and aggregation contributing to deterioration in paintings.

The planned experiments required baseline determinations of surface tension of a drop of toluene in air and with varying concentrations of stearic acid in toluene. However, the fast evaporating nature of toluene necessitated the substitution of MilliQ water for air as the ambient phase. Unfortunately, this was also far from straight forward and ultimately the properties of toluene as a model proved unsuitable for the intended drop-shape experiments. Pursuit of more effective methods for investigating the proposed interactions is left for future research. However, visual observations of importance were noted and are referred to in section 4.5.2.

4.6 Results

Over the experimental time frame of several months, the initial small, settled volume of solids in individual vials containing zinc oxide and stearic acid was observed to increase significantly and to take on a suspended form, termed the 'midphase'. A small volume of clear solvent was apparent above, with a white surface skin similar in consistency to the 'settled' midphase below. For stagnant models A and B, this was most apparent with MKN zinc oxide and stearic acid in excess (Figure 4.9) limited changes were observed for Kremer models over the same time frame.
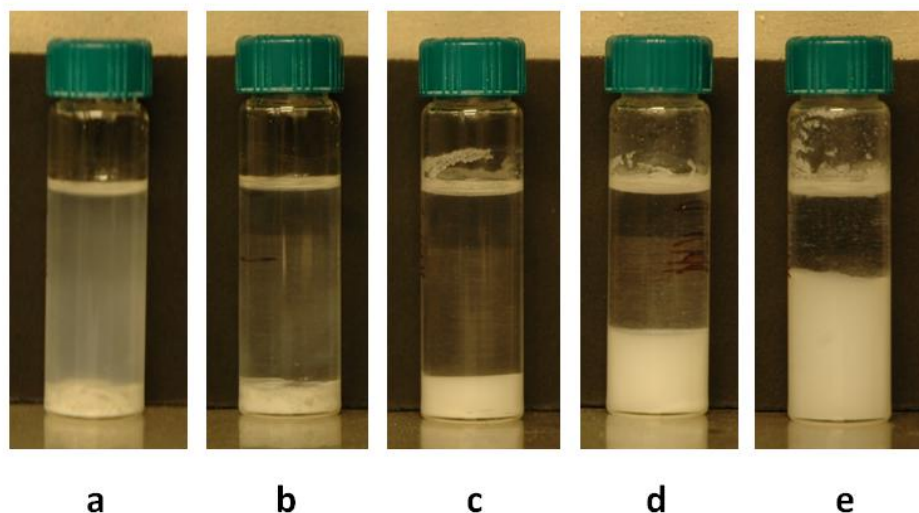
Figure 4.9 Vials containing zinc oxide (MKN) and stearic acid combined in toluene (Model A: stearic acid in excess). Vial (a) 30 mins after mixing, (b) 3 days, (c) 12 days, (d) 7 weeks, (e) 8 weeks

The most rapid change occurred with stirring (model C, MKN zinc oxide). Initial stirring produced fine white solids at the bottom of the vial with a clear solvent fraction above. A short period of stirring the following day led to a rapid and significant volume increase in the midphase, producing a thick, white, stable suspension. In the interest of accelerating timelines, the results discussed below refer to solvent models prepared with MKN zinc oxide unless specified otherwise.

4.6.1 Optical, FTIR and Raman analysis of dried droplets

4.6.1.1 Zinc oxide and stearic acid

Microscopy and FTIR analysis of droplets applied to glass slides sampled from model A (stearic acid in excess) shows the presence of stearic acid in two crystal arrangements: flat diamond-shaped platelets at the centre of the dried droplet, and spherical clusters which typically crystallise at the perimeter (Figure 4.10).
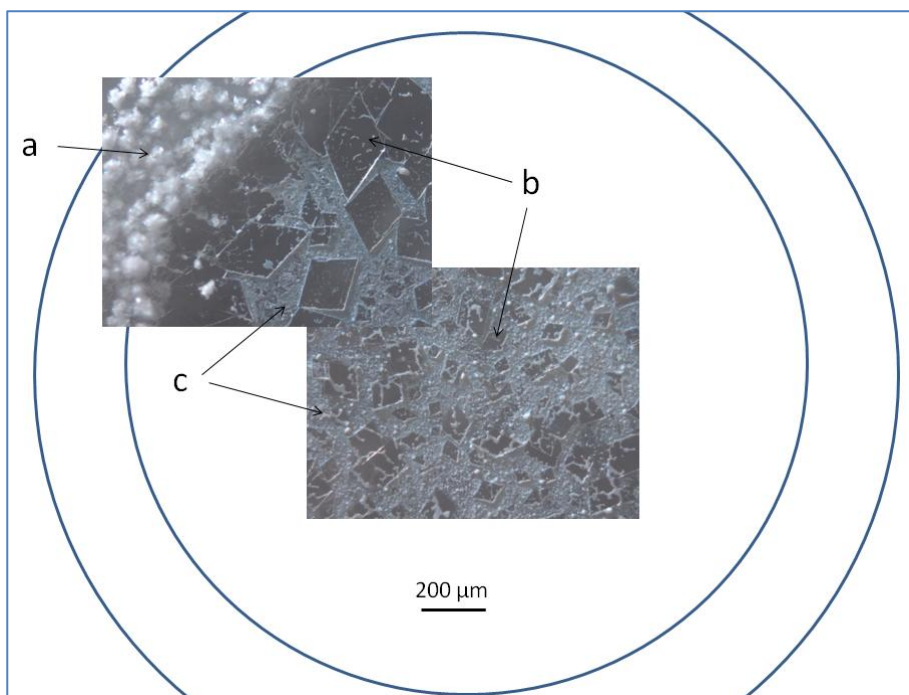
Figure 4.10 Droplet schematic with superimposed images from Model A (stearic acid in excess) sampled at 3 hr.

Two crystal arrangements of stearic acid, (a) spherical clusters and (b) diamond shaped platelets are apparent with zinc stearate (c) occupying the space between diamond platelets at the centre of the droplet
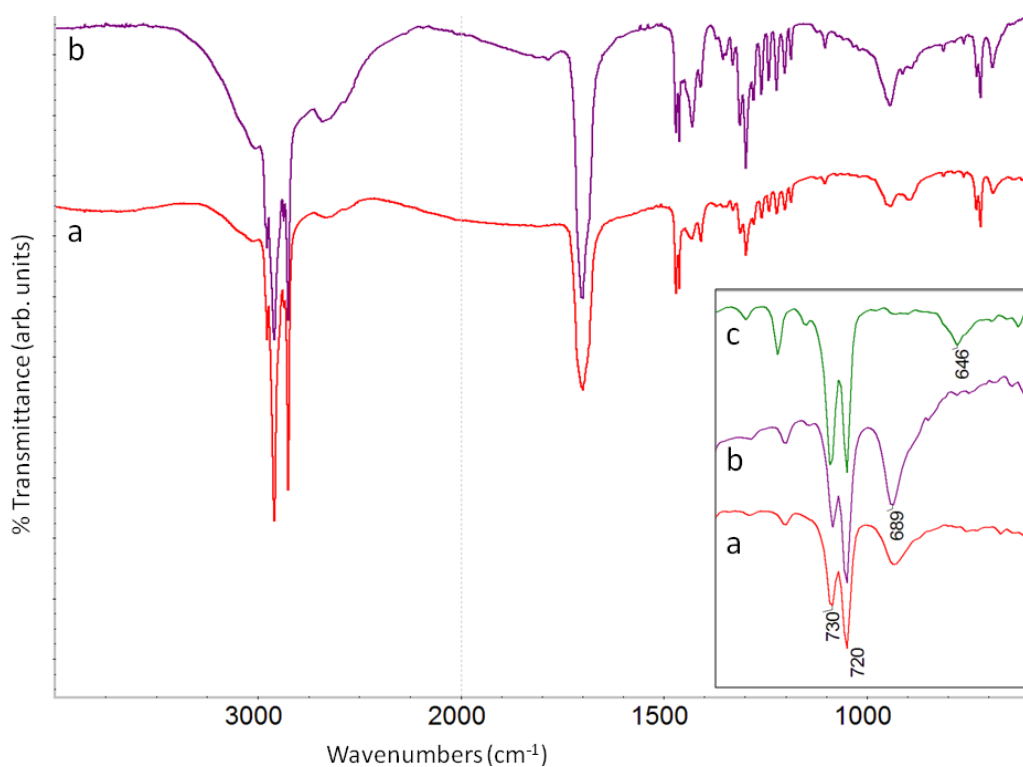
Figure 4.11 FTIR spectra of (a) spherical cluster and (b) diamond platelet stearic acid crystals sampled from Model A at 24 hr.

Inset detailing peak frequencies 600-800 cm^{-1} shows both have δ OCO at 689 cm^{-1} characteristic of E form (all-trans) crystals. A spectrum detail of B form (gauche conformer) stearic acid (c) with δ OCO at 646 cm^{-1} is included for reference

Stearic acid attributions were determined using FTIR with spectra shown in Figure 4.11. Despite the different physical appearance, both crystal types were determined as E form based on the presence of an OCO in-plane deformation peak at 689 cm^{-1} (Kaneko et al. 1999). This peak indicates an all-trans conformation. The alternative B form crystal is characterised by vibration at 646 cm^{-1} produced by a gauche conformer bond near the carboxylate group (Kaneko et al. 1999) (Figure 4.11 inset).

The two E form crystal arrangements are evident in dried droplets sampled from both a stearic acid/toluene control, as well as in mixtures of the acid in combination with zinc oxide. They were also apparent in samples from the clear solvent fraction, particularly when sampled within a few hours of mixing. Supernatant obtained from model A after a number of weeks contained significantly less dissolved stearic acid, consistent with progressive reaction to form insoluble zinc stearate (Figure 4.12).
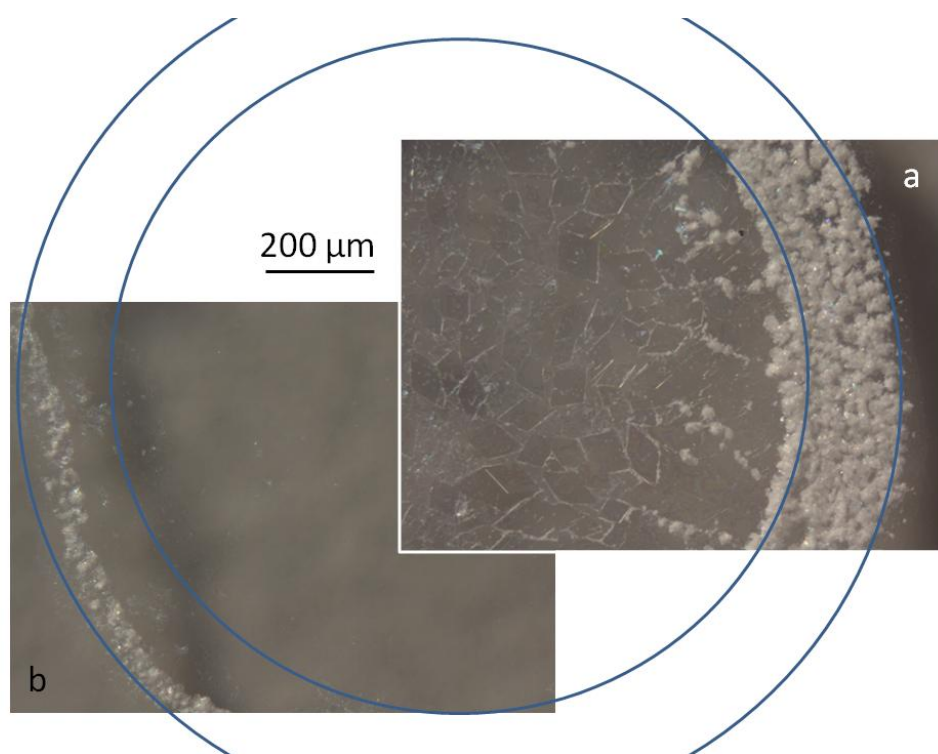
Figure 4.12 Droplet schematic with superimposed images comparing dissolved solids crystallised from model A centrifuged supernatant

(a) 1 hour after mixing and (b) 10 weeks after mixing. A marked reduction in stearic acid over time corresponds with formation of insoluble zinc stearate

In droplets obtained from solids and supernatant as shown in Figure 4.15, zinc stearate dries as a fine, white, almost waxy substance which encrusts and occupies space between stearic acid crystal

platelets. The close physical association of the soap with stearic acid crystals made the zinc stearate difficult to sample from the slides for transmission FTIR without fatty acid contamination. This is reflected in spectra which are typically dominated by features of stearic acid but with additional carboxylate peaks at 1541 and 1399 cm^{-1} reflecting contributions from the soap (Figure 4.13).
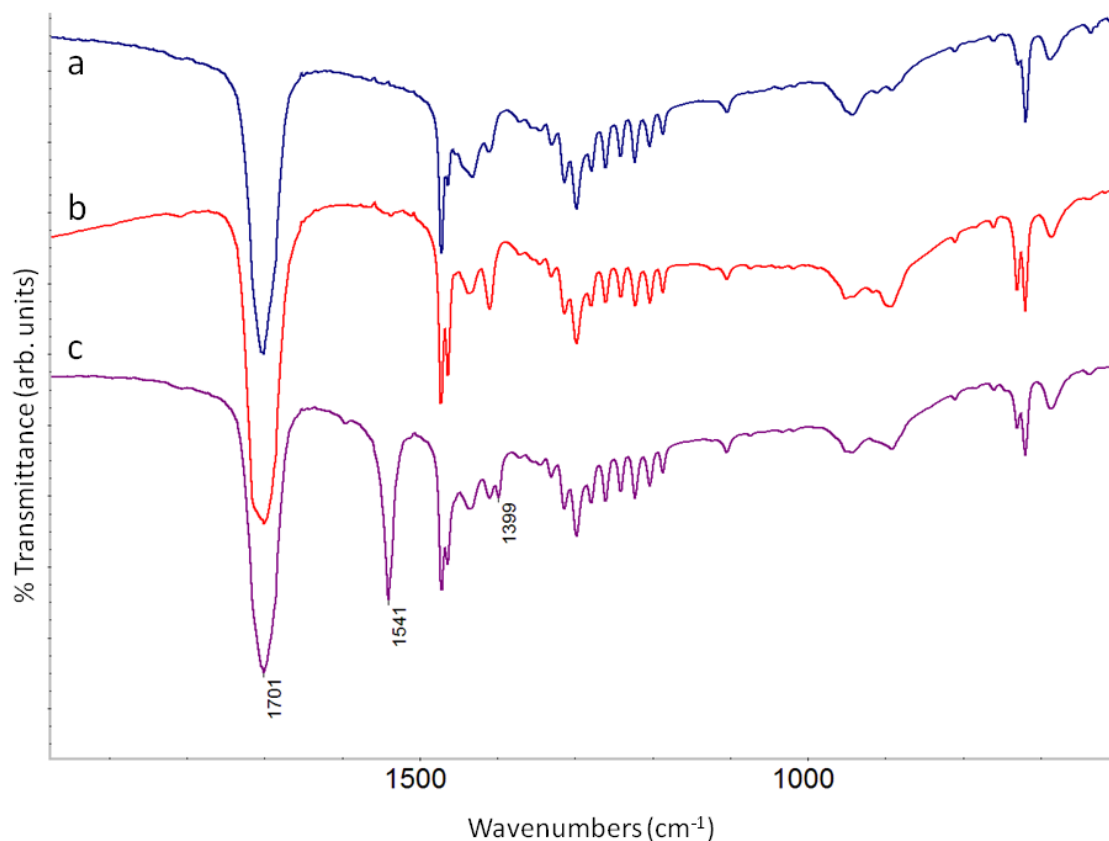
Figure 4.13 FTIR spectra collected from (a) stearic acid control, (b) crystals at the Model A 24 hr droplet perimeter and (c) solids at the soap dominated inner region of the droplet.

Stearic acid vibrations dominate each including (c) which reflects the difficulty in physically separating zinc stearate from stearic acid crystals deposited from toluene droplets on glass. Zinc stearate COO⁻ peaks are also present in (c) at 1541 and 1399 cm^{-1}

Raman spectroscopy was able to distinguish the zinc stearate *in situ* by its characteristic peak at 950 cm^{-1} (Robinet and Corbeil 2003) and differences in the relative intensities of peaks between 1400-1500 cm^{-1} in comparison to the acid (Figure 4.14). Raman also detected small amounts of zinc oxide in association with the soap, distinguished by a peak at 438 cm^{-1} (Goienaga et al. 2011). The presence of zinc oxide diminished over time for models with stearic acid in excess.

Droplets sampled from Model B with zinc oxide in excess indicate that available stearic acid reacts very quickly to form zinc stearate, even with minimal agitation. Microscopic images of dried droplets are shown in Figure 4.15.
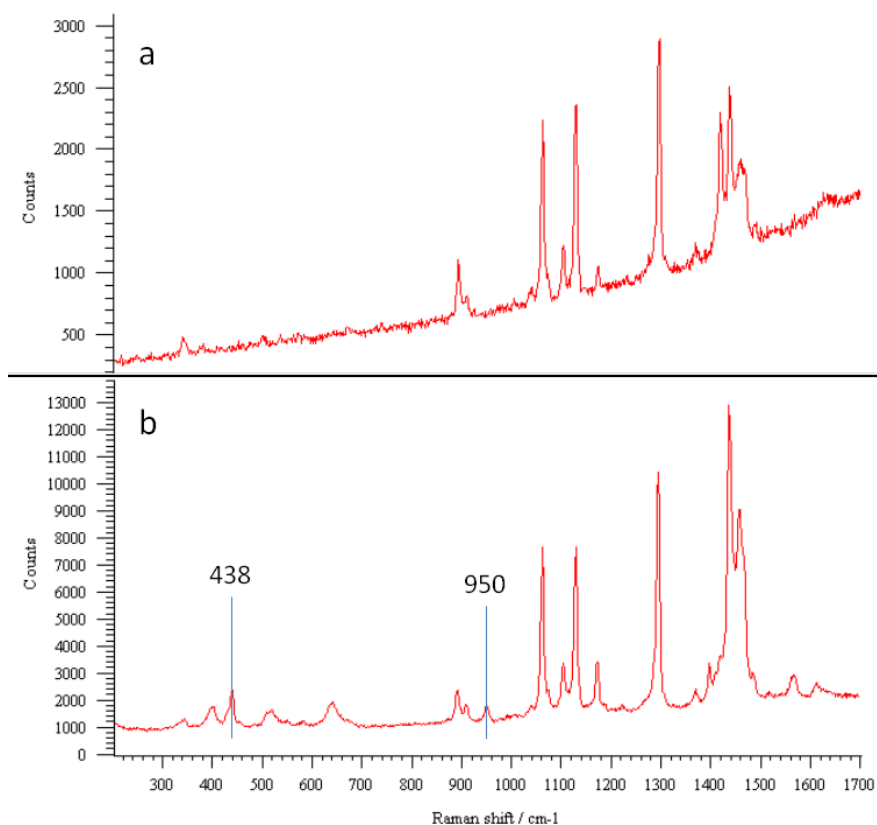
Figure 4.14 Raman spectra obtained *in situ* from solids crystallised from toluene on glass slides: (a) stearic acid control; (b) the waxy white solid adjacent to a stearic acid platelet from Model A at 24 hr.

Although the acid and soap forms have many peaks in common, the soap is distinguished by the peak at 950 cm^{-1} in addition to showing differences in the peaks between 1400 and 1500 cm^{-1}. Spectrum (b) is characteristic of zinc stearate with a contribution from zinc oxide (characteristic peak 438 cm^{-1})
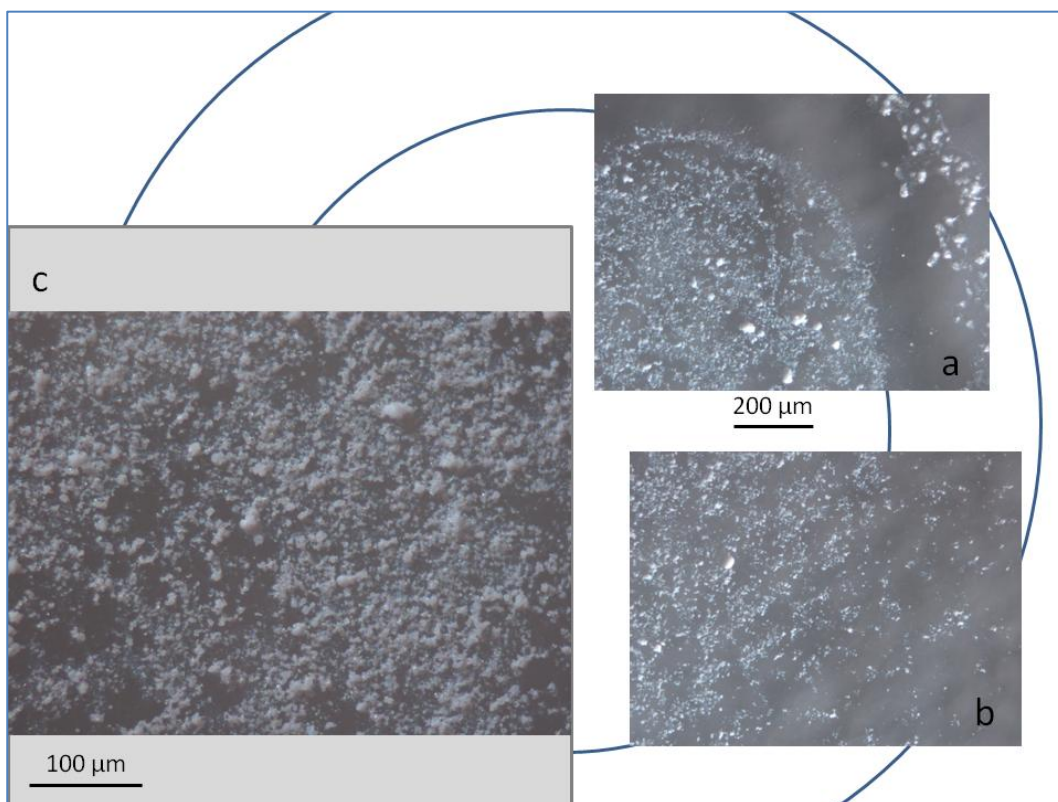
Figure 4.15 Droplet schematic with superimposed images from Model B (ZnO in excess) sampled at A: 3 hr and B: 24 hr showing a rapid reduction in the perimeter ring of stearic acid over time.

Inset (C) shows higher magnification detail from centre of droplet sampled at 24 hr; fine, irregular aggregates of a waxy solid are distributed across the droplet with no visible stearic acid crystals.

151

The perimeter ring of spherical stearic acid crystal clusters apparent in the early samples has greatly diminished after 3 hours and is no longer present at 24 hours. Fine, irregular aggregates of a waxy solid are distributed across the centre of the same droplets, becoming the only solid evident in the droplet sampled at 24 hours. The FTIR spectrum of this substance is consistent with that for zinc stearate, while Raman additionally indicates the presence of zinc oxide (Figure 4.16).
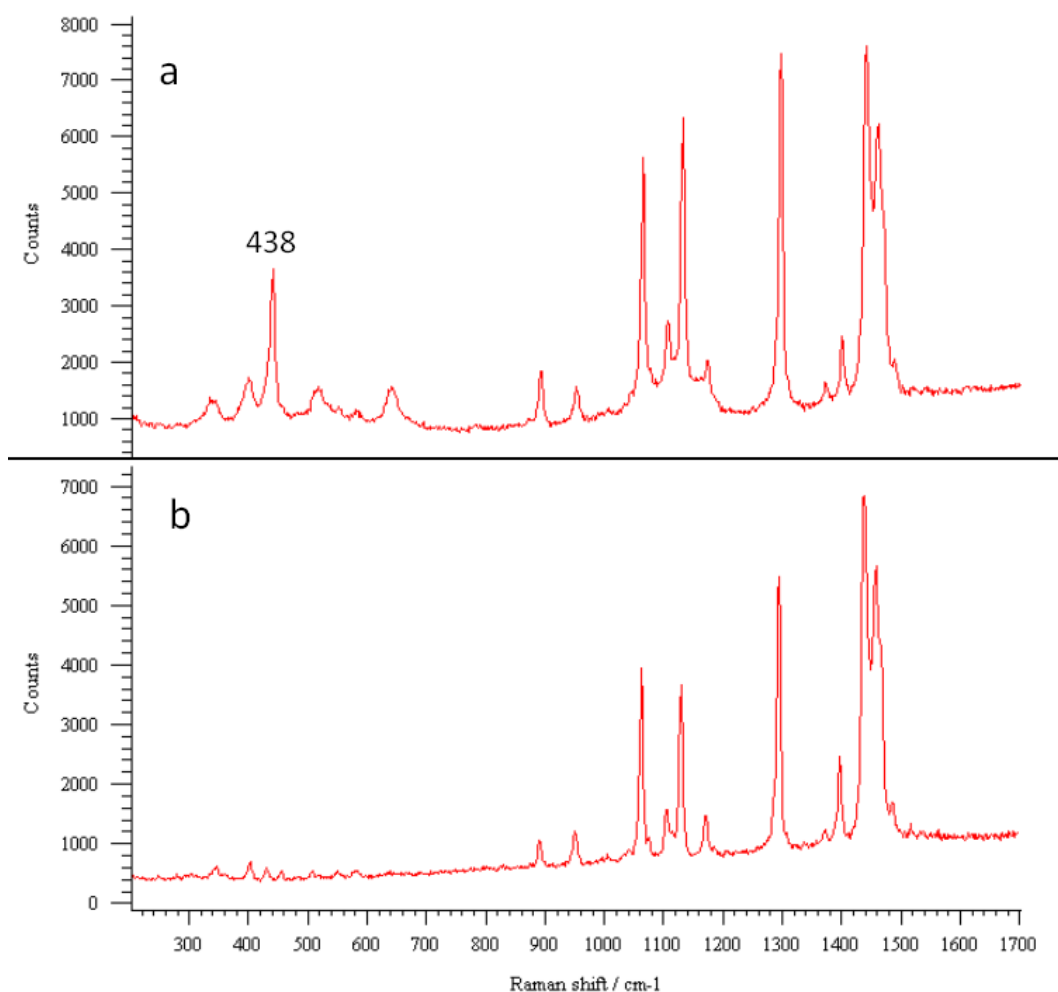
Figure 4.16 Raman spectra obtained from (a) model B after 30 mins showing strong contribution from zinc oxide in addition to zinc stearate; (b) model A after 10 weeks where zinc oxide is no longer consistently associated with the soap

In the comparable model prepared with Kremer zinc oxide (in excess) a similar progression is indicated but over significantly extended timelines. Unreacted stearic acid remains evident 17 months after mixing, with the sampled droplet and FTIR spectra similar to that observed in the MKN model at 3 hours (Figure 4.17).
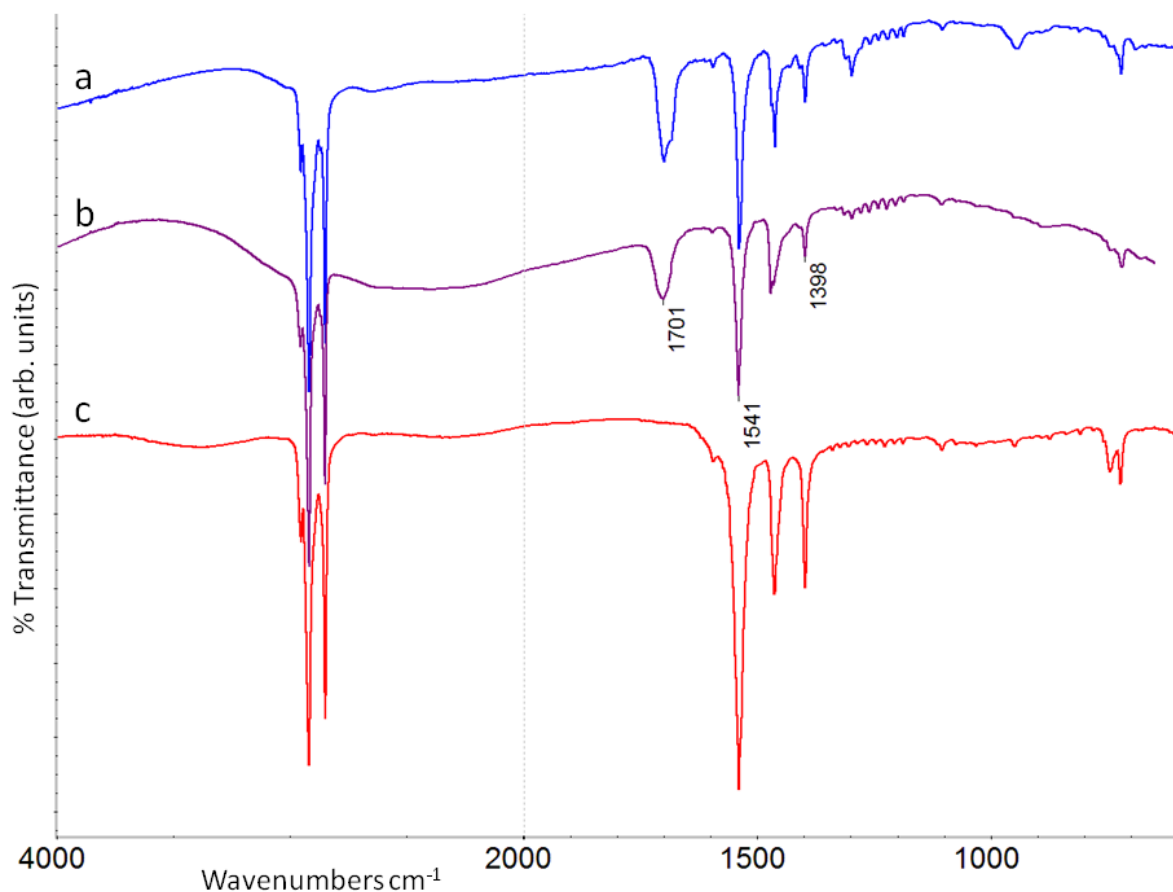
Figure 4.17 FTIR spectra for Model B (zinc oxide in excess) prepared with (a) MKN 30 nm zinc oxide at 3 hr and (c) 24 hr; and (b) Kremer zinc oxide artists' pigment at 17 months.

The 3 hr MKN and 17 month Kremer spectra are similar and incorporate peaks characteristic of both stearic acid (1701 cm^{-1}) and zinc stearate (1541 and 1398 cm^{-1}). After 24 hr no stearic acid is evident in the MKN model

4.6.1.2 Zinc oxide and aluminium stearate

Image details of droplets sampled from model D (aluminium stearate) over 24 hours are shown in Figure 4.18. There is little to visually distinguish the dried solids as each droplet comprises irregularly sized white lumps. However, after as little as 15 minutes FTIR analysis indicates formation of zinc stearate has commenced with the appearance of the characteristic COO$^-$ peak at 1541 cm^{-1} (Figure 4.19). This is accompanied by the disappearance of the small C=O acid peak in the spectrum suggesting that initially zinc stearate is formed by reaction with the most readily available free acid, a reaction producing water. In droplets sampled after 1 hour, a fine perimeter ring dries separately to the bulk which FTIR shows to principally comprise stearic acid. Solids sampled from the centre of the same drop contain both zinc and aluminium stearate along with peaks for Al-O/OH bonds indicating hydrolysis of aluminium stearate is occurring in the model.

153
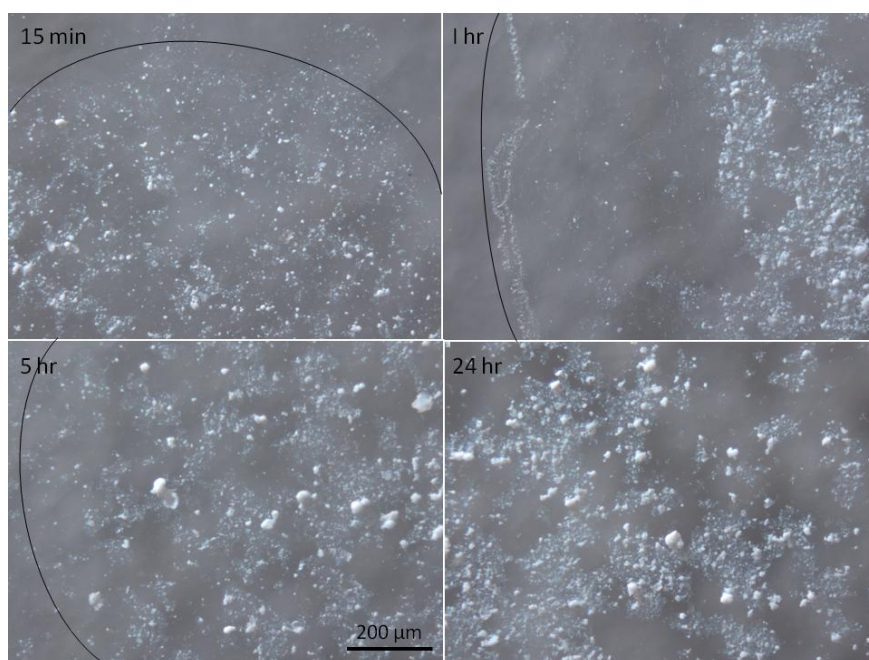
Figure 4.18 Droplet image details showing solids obtained from Model D aluminium stearate/ZnO/toluene mix with arcs denoting droplet perimeter.

At 15 min the solids are a mix of aluminium and zinc stearate, at 1 hr a small amount of stearic acid is present and crystallises at the perimeter of the droplet. By 5 hours pure zinc stearate is observed in some spectra and negligible acid is apparent. After 24 hours the centre of the droplet (shown) is predominantly zinc stearate with both aluminium and zinc soaps present at the perimeter
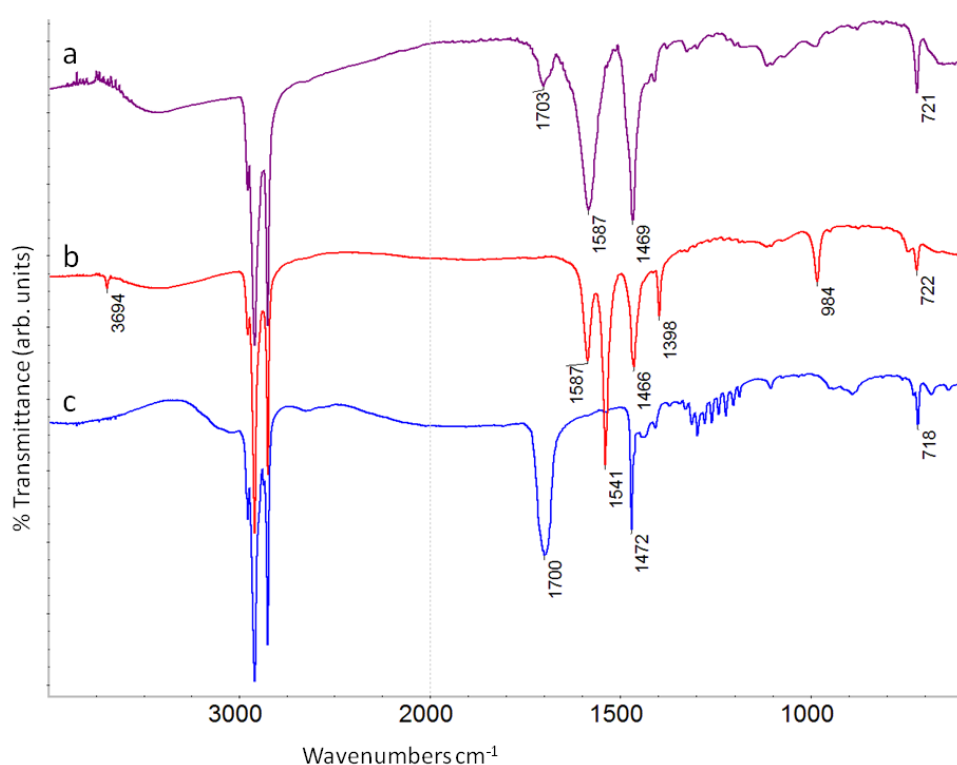
Figure 4.19 FTIR spectra from model D

The initial acid carbonyl peak (1703 cm^{-1}) in the aluminium stearate reagent (a) has after 1 hr been replaced by carboxylate peaks for zinc stearate at 1541 and 1398 cm^{-1} and Al-O/OH bonding vibrations (984/3694 cm^{-1}) (b). Corresponding release of stearic acid is indicated by spectrum (c) taken from a fine perimeter ring of crystals in the 1 hr droplet, consistent with hydrolysis occurring in the model

154

After 5 hours it is possible to obtain a trace for pure zinc stearate from the centre of the droplet although some spectra retain a contribution from the aluminium soap. Spectra reflecting pure stearic acid are obtained from crystals at the perimeter of the droplet. By 24 hours there is little evidence of stearic acid; within each crystallised droplet, the purest zinc stearate phase is found at the centre, while spectra from the perimeter solids indicate a mixture of zinc and aluminium soaps and Al-O/OH vibrations (Figure 4.20). Insoluble gel lumps have also formed in the toluene that have a tendency to adhere to the sides of the glass vial following agitation. These have a similar composition with stronger Al-O contribution consistent with indicative reaction Eq. 4.9

$$2ZnO + 3AlSt_2OH + 2H_2O \rightarrow 2ZnSt_2 + 2AlSt(OH)_2 + Al(OH)_3 \qquad [4.9]$$
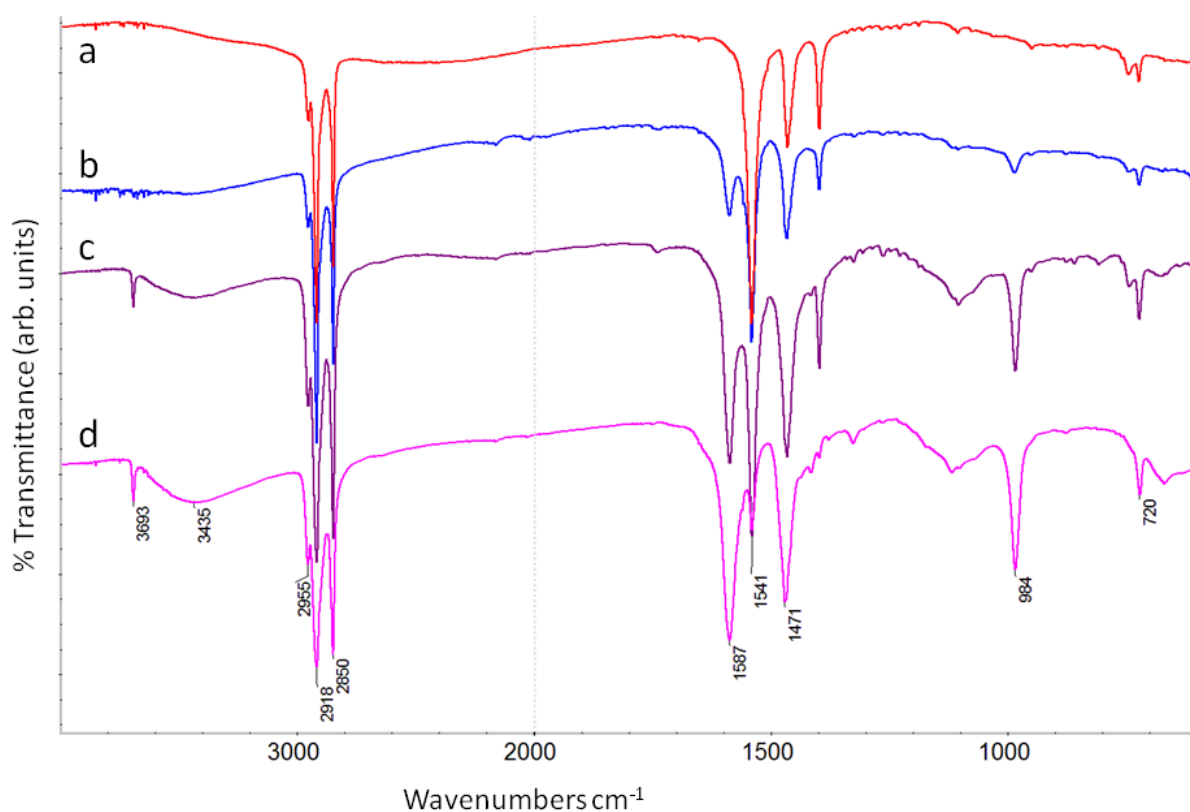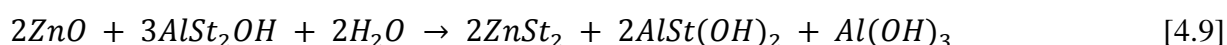
Figure 4.20 FTIR spectra from Model D after 24 hrs

No further stearic acid is evident. Zinc stearate (1541 cm^{-1}) predominates (a) but is found in combination with aluminium stearate (1587 cm^{-1}) towards the perimeter of the drop (b) with increasing evidence of Al-O/OH (984/3693 cm^{-1}) at the perimeter (c). Insoluble gel lumps sampled from the walls of the vial appear largely to comprise aluminium stearate/hydroxide with traces of zinc stearate (d)

The zinc stearate spectra obtained with FTIR from each solvent system and from the synthesised reference have constant ΔCOO^- of 143 cm^{-1} (Figure 4.21). This indicates a bridging bidentate

coordination to the zinc ion (Ishioka et al. 2000). The CH_2 bands also consistently fall at 2918 and 2848 cm^{-1}, characteristic of highly compact trans-zigzag conformation of acyl chains packed parallel with each other (Sakai and Umemura 2002). In studies of zinc stearate monolayers on water such low absolute values of v_a CH_2 and v_s CH_2 peak intensities are taken to suggest a tilting from perpendicular, attributable to crystal growth in 2 or 3D (Sakai and Umemura 2008).
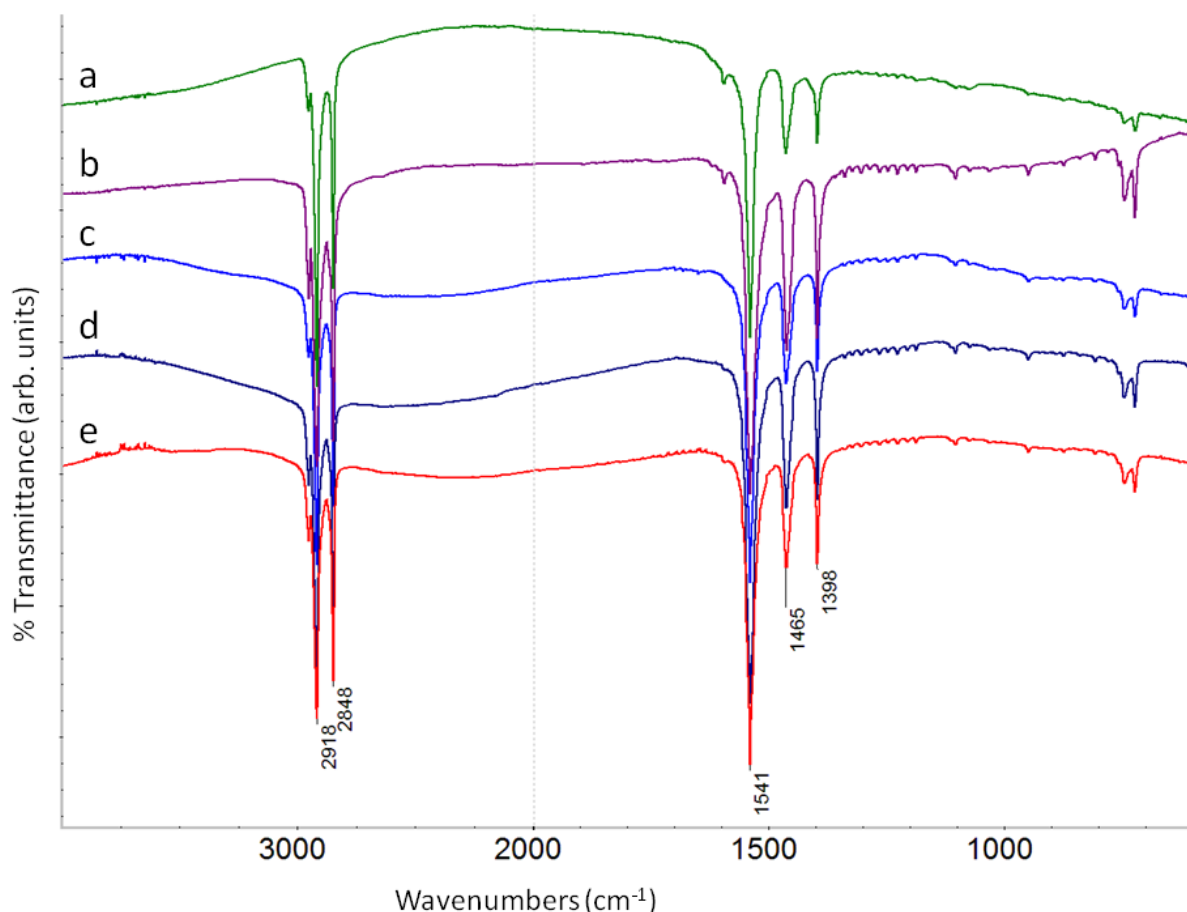
Figure 4.21 FTIR spectra of zinc stearate sampled from solvent systems

Consistent absolute CH_2 and COO^- values (ΔCOO^- 143 cm^{-1}) indicate compact packing of acyl chains and bridging bidentate coordination to the zinc ion. This is the case with Model B, ZnO in excess sampled at (a) 30 minutes or (b) 24 hours after mixing, (c) Model D, stearic acid delivered in the form of aluminium stearate (d) Model A, stearic acid in excess after 10 weeks, and (e) for the synthesised zinc stearate reference

4.6.2 Scanning electron microscopy and X-ray analyses

Backscatter electron images of solids crystallised from a droplet of model C supernatant after 4 weeks show characteristic diamond shaped platelets of stearic acid with some distinctive flower like structures along the crystal edges (Figure 4.22). Although these clusters of platelike particles appear remarkably similar to layered basic zinc salts intercalated with carboxylate ions (Inoue and

156

Fujihara 2010, 2011), in this instance no zinc is detected. EDX spectra are dominated by carbon with some silicon from the substrate which supports an assignation of stearic acid for both crystal structures, consistent with Raman and FTIR analysis. There is no indication of zinc oxide or zinc stearate.
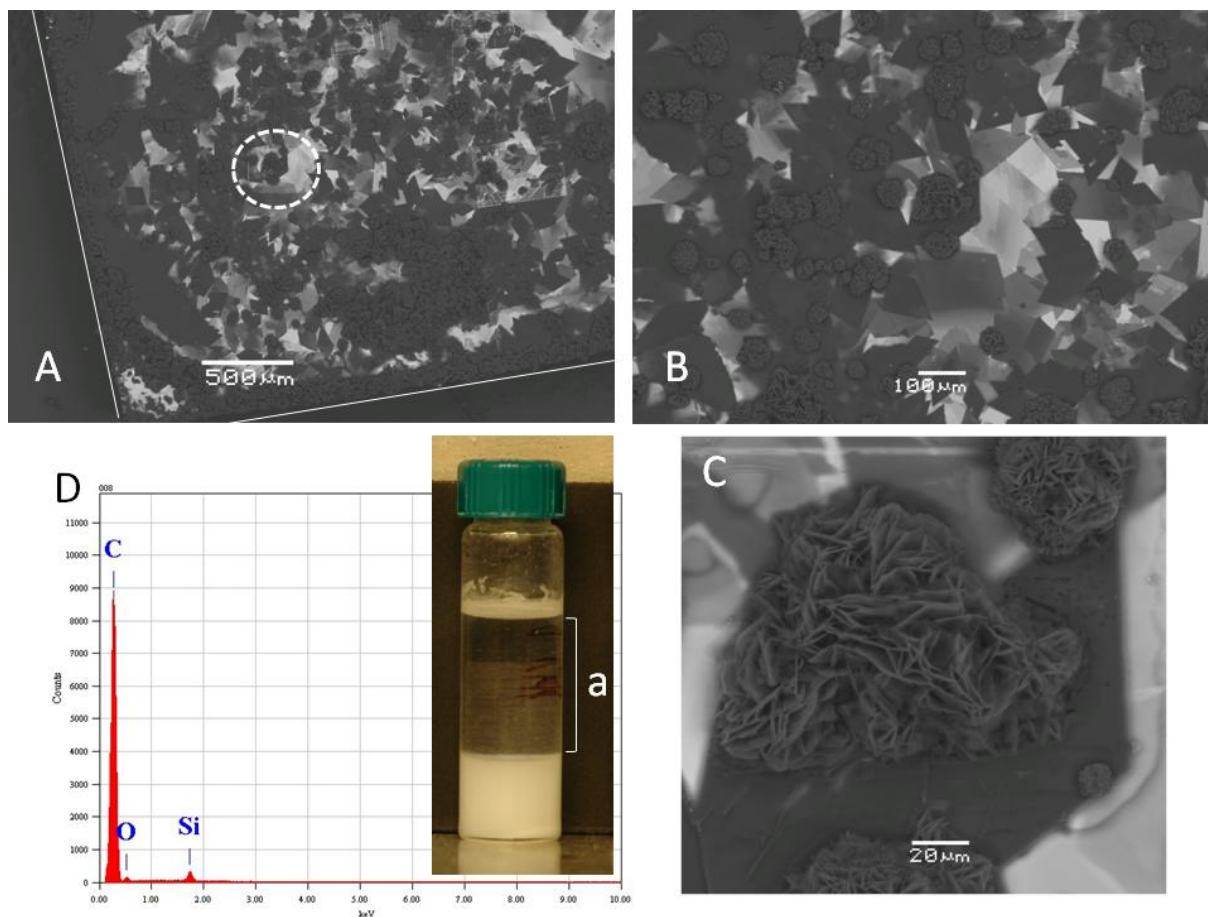
Figure 4.22 Backscatter electron images and corresponding EDX spectrum for solids crystallised from solvent Model C supernatant

(a) applied to Si wafer at 4 weeks (indicative vial image). Perimeter of wafer and droplet shown in low magnification image (A) includes locator of feature at centre of higher magnification images (B and C). No zinc is detected in the diamond shaped platelets or clusters of stacked sheets, consistent with the assignation of stearic acid for both structures as indicated by FTIR and Raman analysis (BSE images and EDX analysis: Kim Sewell)

BSE images of a droplet sampled from the suspended midphase of the same model at 4 weeks show nano scale bright spots surrounded by an amorphous substance of lower electron density (Figure 4.23). These features give a consistent EDX signal for zinc and are taken to be zinc stearate with zinc oxide particles at the centre, consistent with the Raman results reported above. A relatively small amount of clustered stearic acid is visible near the perimeter of the drop, amongst which both zinc oxide and zinc stearate are found. No diamond platelets of stearic acid are apparent.
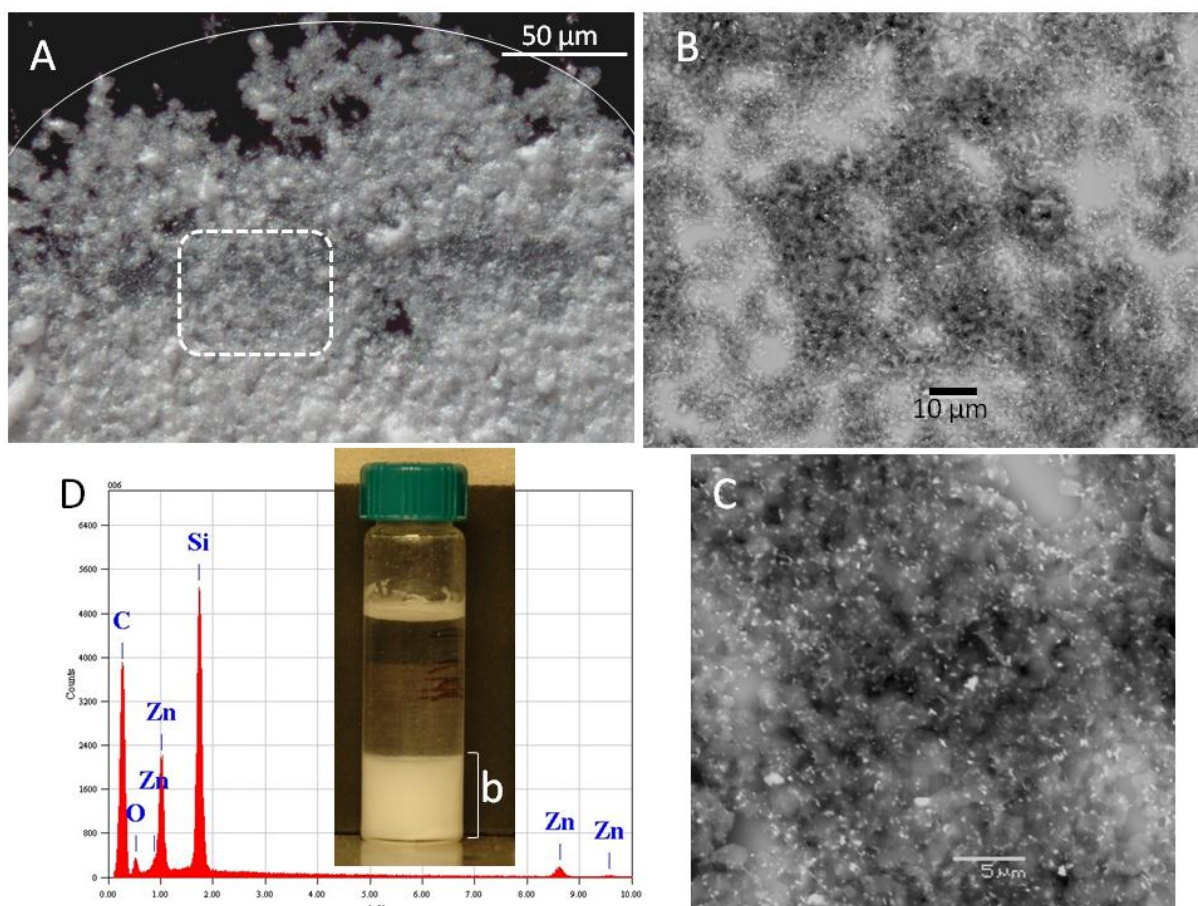
Figure 4.23 Optical and backscatter electron images and corresponding EDX spectrum for midphase solids (b) sampled from solvent Model C applied to Si wafer at 4 weeks (indicative vial image).

Perimeter of droplet shown in optical image (A) includes approximate locator of zone featured in BSE image (B) and higher magnification detail (C). In BSE image (C) the fine white solids appear as a mass of amorphous globules within which numerous bright spots are evident; the atomic contrast and Zn signal are consistent with the presence of zinc oxide and zinc stearate as indicated by Raman analysis (BSE images and EDX analysis: Kim Sewell)

Further corroboration of these assignments was obtained with small-angle X-ray scattering (SAXS) and powder X-ray diffraction (XRD). Although FTIR of solids crystallised from the solvent phase did indicate a trace amount of dissolved or finely dispersed zinc stearate, SAXS of supernatant following centrifuging did not detect any variation from a stearic acid/toluene control. The assigned X-ray diffraction pattern obtained from dried sediment following centrifuging is shown in Figure 4.24. This confirms the presence of both zinc stearate and zinc oxide, with no evidence for stearic acid. SAXS of dilutions of the suspended midphase prepared without centrifuging also scattered strongly showing a crystalline like order with a series of 00*l* reflections and a d-spacing of 4.2 nm. This series of reflections is consistent with those observed in the XRD pattern (Figure 4.24). Although angles below 5° 2θ were not measured in the XRD analysis, published diffraction data for zinc stearate assigns a d-spacing of 4.248 nm to the first order of XRD long spacing at 2.413 2θ,

(Corbeil and Robinet 2002), consistent with the d-spacing indicated by SAXS. This value is not unique to zinc stearate as it is similar for various metal soaps with comparable length of carbon chain and bridging structure, however it does support the attribution of zinc stearate to the suspended midphase in the model.
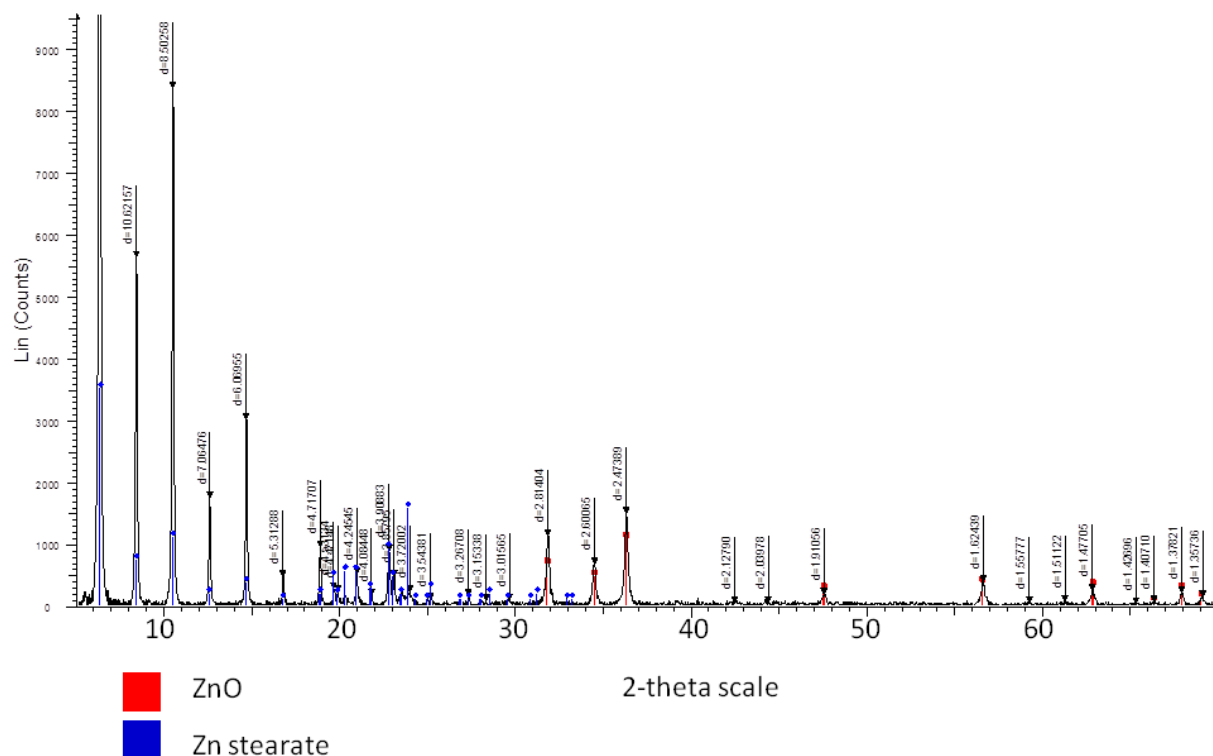
Figure 4.24 Assigned X-ray diffraction pattern of dried sediment following centrifuging of Model A. Both zinc stearate and zinc oxide are detected, with no evidence of stearic acid

4.6.3 Drop analysis

A baseline measurement of interfacial tension (IFT) for a drop of toluene in water was attempted by dispensing a 30 μL pendent drop of toluene into the ambient water phase. However, over the course of repeat measurements, the slight solubility of toluene in water resulted in a progressive decrease in drop size, consistent with loss to the ambient phase. Subsequent IFT measurements were therefore undertaken with the ambient phase comprising water pre-saturated with toluene, including an excess to compensate for evaporation over the experimental timeframe. As such, a clear layer of toluene could be seen on the surface of the water in the cuvette. Pre-saturation stabilised the toluene drop volume, however it was still not possible to produce a flat baseline for the toluene reference for reasons that were not able to be determined. The most stable plot obtained gave an approximate IFT of 35.2 mN/m. This is within the realm of published values of IFT for toluene in water at room temperature: 36-37 mN/m between pH 6-8 (Saien and Akbari 2006) and 33-35 mN/m determined with phases reversed (Alpbaz et al. 1988). Of these, the lowest value was obtained as here using the

(captive) pendent drop method, while higher values were determined as a factor of the volume at which buoyancy caused a fully formed drop to detach from the capillary.

Although a sloping baseline for the IFT of a drop of toluene in water indicates a problem with the experimental methodology, experiments were continued by introducing stearic acid into the toluene phase. Drop-shape analysis and interfacial tension measurements were recorded for a concentrated solution of stearic acid in toluene (1.5×10^{-1} M) and at concentrations of 1.0×10^{-1}, 1.0×10^{-2} and 1.0×10^{-3} M using pre-saturated water as the ambient phase. IFT measurements as a function of time are shown in Figure 4.25.
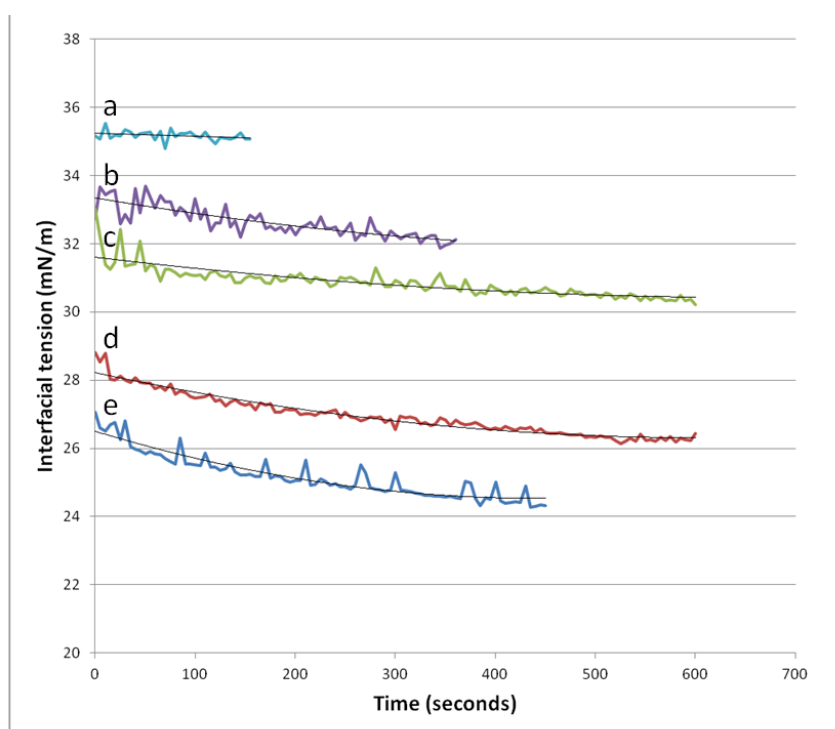
Figure 4.25 Interfacial tension measurements for stearic acid/toluene captive drop solutions in water (a) toluene reference, and stearic acid at molar concentrations of (b) 1.0×10^{-3} (c) 1.0×10^{-2} (d) 1.0×10^{-1} (e) 1.5×10^{-1} (saturated solution) showing a reduction in IFT as stearic acid concentration increases but with no stable values obtained

Individual plots show a progressive reduction in IFT over time at all concentrations. The IFT appears to be levelling off after approximately 7-10 minutes depending on concentration, however the readings did not stabilise and continued to decrease over timeframes extended to more than 30 min (results not shown). IFT is shown to be lower with increasing stearic acid concentration, indicating there is activity at the toluene/water interface. The instability of IFT over time may relate to dynamic interfacial activity where progressive ionisation of carboxyl groups increases the pH in

the ambient phase and results in continuing molecular reorganisation at the interface (Sundberg et al. 2009). Passage of stearic acid through the aqueous phase and dynamics at the water/air interface were evidenced by crystallisation around the rim of the glass cuvette and along the exterior of the stainless steel dispensing needle. However, the presence of toluene dissolved within or on the surface of the aqueous phase complicates interpretation of this behaviour and may have contributed to stearic acid transport and crystallisation following evaporation at the surface. Irrespective of cause, stearic acid mobility and crystallisation necessitated frequent replacement of the ambient phase reinforcing the unsuitability of the methodology for the intended purpose within the solvent model. For this reason, experiments did not progress to consider the influence of the presence of zinc ions or other variables. Observations do, however, demonstrate the interfacial activity of stearic acid and its capacity to move through a medium in which it has limited solubility, characteristics which would facilitate reaction with zinc oxide and soap formation in paintings.

4.7   Discussion

Zinc stearate formed in the solvent model is indicated by vibrational spectroscopic and X-ray data to conform to characteristic metal soap structure. The collective X-ray data suggests zinc stearate in the solvent models has a bilayered structure where zinc ions are arranged in planes between extended stearate chains in the *all-trans* state (Vold and Hattiangdi 1949; Öztürk and Balköse 2005; Corkery 2008). The polar metal-organic carboxylate framework layer for metal soaps generally is formed by 1D or 2D coordination polymers, determined by the ionic radius and coordination style of the metal (Corkery 2008). Room temperature zinc(II) *n*-alkanoates with chain lengths of between 4 and 20 carbons are understood to have individual zinc atoms tetrahedrally coordinated to oxygen atoms from four different carboxylate groups with each ligand forming a bidentate bridge with two tetrahedral zinc atoms (Taylor and Ellis 2007). The positioning of CH_2 vibrations in FTIR spectra indicates very close molecular packing, consistent with the small ionic or covalent radius of the zinc atom (Sakai & Umemura 2008) together with van der Waals interactions between the long straight stearate chains (Kanicky & Shah 2002).

Zinc stearate formed *in situ* in toluene has a different physical consistency to that where pre-synthesised zinc stearate was added to the solvent. Both zinc oxide and zinc stearate are essentially insoluble in toluene, but when the soap forms *in situ* via reaction between the oxide and dissolved stearic acid, a relatively stable 'midphase' suspension results. Raman spectroscopy and SEM imaging indicate a close association between the zinc stearate and residual oxide (when in excess) in the midphase, while unreacted stearic acid is contained in the supernatant. The initial formation

of zinc stearate as monolayers or lamellar soap structures centred on oxide particles is one possible explanation for this. Metal soaps in organic solvents have been described previously as behaving analogously to aqueous surfactant solutions, enabling dispersion of otherwise insoluble compounds (Pilpel 1963); changes in the mechanical properties of the system were explained by micelles expanding to ensure coverage, thereby accommodating additional soap molecules and sometimes changing shape. More recent consideration of the swelling capacity of metal soap structures has centred on solvent interaction at the hydrophobic interface between adjacent aliphatic chains (Corkery and Hyde 1996). Each molecular layer contains a single polar sheet running through the headgroups, sandwiched by two aliphatic layers as shown in Figure 4.26. Solvent interaction between layers may be sufficient to support the observed suspension.
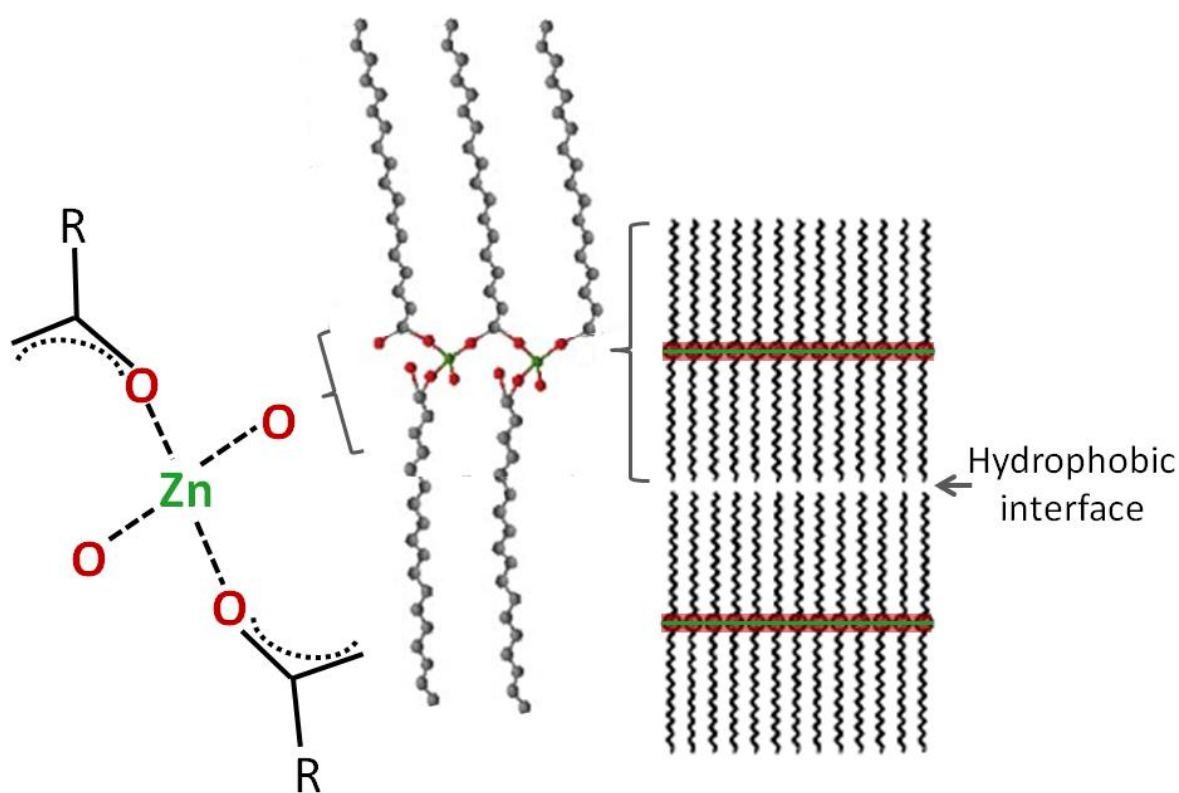
Figure 4.26 Simplified schematic representation of zinc stearate splayed chain bilayer structure.

The polar headgroup is contained in a single plane surrounded by hydrophobic chains. Lamella structures form via van der Waals bonds with a hydrophobic interface (adapted from (Corkery and Hyde 1996; Nelson et al. 2011)

The generous enveloping of zinc oxide particles by zinc stearate seen in BSE images of the midphase would appear to isolate residual oxide from continued reaction with available fatty acid. A similar phenomenon is discussed in relation to zinc stearate synthesis via fusion between molten

stearic acid and zinc oxide (Gönen et al. 2005); the initial fast reaction produced a shell of zinc stearate around zinc oxide particles which slowed the reaction, however stirring over time was found to increase yields. This echoes the dramatic midphase volume increase observed in solvent Model C subjected to vigorous stirring after initial zinc stearate formation, a process effectively disrupting the forces binding zinc stearate to oxide particles. As zinc stearate molecules detach and aggregate, more of the oxide is exposed to potential reactants, enabling the process of zinc stearate formation and zinc oxide dissolution to continue. Aggregation of zinc stearate is thermodynamically favourable and stirring accelerates the process beyond that occurring under stagnant ambient conditions. The availability and accessibility of zinc ions as a rate limiting step is further supported by the greatly reduced reaction rate apparent in models produced with Kremer pigment which have a significantly smaller surface area than MKN 30 nm zinc oxide. The kinetics driving ongoing formation of zinc stearate in a paint film will of course vary but will be determined by the inherent properties of the paint formulation in combination with environmental factors influencing changes in film chemistry over time. Damaging aggregation or crystal growth will occur when this configuration is energetically more favourable than the equivalent 'suspension'. Conditions which disrupt the equilibrium in a system have potential to renew reactivity and may have consequences for the ongoing stability of paintings where a source of both zinc and stearate ions remain.

Availability of stearic/palmitic acids in a painting is also critical for the formation of the corresponding zinc soap. Drop-shape experiments give some insight into possible mechanisms for stearic acid migration contributing to formation and distribution of zinc stearate despite the instability of the experimental model. In the toluene/water model, stearic acid has limited solubility in the ambient water phase but was shown to be highly mobile nonetheless, demonstrating activity at the toluene/water interface and moving readily from the toluene drop to crystallise at the water/air/glass interface in the model cell. The possible influence of toluene dissolved in the water phase has been mentioned, but this does not discount relevance to the complex conditions encountered in paintings. pH-induced dissociation of surface carboxyl groups has been shown to be significant for influencing phase distribution of C_{18} fatty acids between water and lipophilic colloidal phases in extractives from softwoods (Sundberg et al. 2009). In stearic acid monolayers different carboxylate ion-dipole interactions above and below the acid dissociation constant (pKa) have been shown to influence the distance between stearate chains, with crystallisation occurring when protonated stearic acid arranges itself into oligomers or clusters and is expelled from water in order to minimise the total energy of the system (Kanicky and Shah 2002). Stearic acid has high pKa but this does not preclude temporary ionisation at the toluene/water interface; in the presence of zinc ions, these mobile carboxylate ions would react readily leading to zinc soap crystal growth.

Similarly, many oil-based paints produce a gradual source of carboxylate ions in the course of ageing, available to react with zinc ions in paintings containing zinc oxide. Transient free acid states have been observed in paint reconstructions in the presence of basic lead carbonate pigment using solid state NMR (Verhoeven et al. 2006). In effect this may replicate the principle of biphasic synthesis systems where one phase acts as a gradual supplier of components that are hard to dissolve in the other phase (Inoue and Fujihara 2010), discussed further below. The absence of zinc in drop-shape experiments using the toluene/stearic acid/water model leads to stearic acid crystallisation at the air interface, a phenomenon also familiar in paintings manifesting as fatty acid efflorescence.

Mobility of stearate ions is again in evidence in solvent models with aluminium stearate. The finding that aluminium stearate as the sole source of stearic acid in combination with zinc oxide can result in formation of zinc stearate as effectively as free stearic acid is a novel one. Although the susceptibility of aluminium stearate to hydrolysis is well known, it has not previously been demonstrated that ion exchange will occur so readily - zinc stearate effectively replacing the aluminium soap. The applicability of zinc stearate formation observed in the toluene model to reactions likely to occur in oil-based paint is validated by the investigation of reference paint films discussed in Chapter 3 where strong zinc stearate concentrations are detected in paints with aluminium stearate but are largely absent in comparable paints without the additive.

Explanations for observed differences in zinc carboxylate distribution in paints may be assisted by reference to recent research into controlled production of zinc oxide nanostructures via formation of layered basic zinc soap precursors (Inoue and Fujihara 2010, 2011). This process uses a biphasic system to deliver C_7-C_{12} carboxylic acids under controlled concentration conditions in xylene to an aqueous phase containing zinc ions and a progressive source of hydroxyl ions, where the layered soap forms. Based on the principle of distribution equilibrium of solutes between two liquid phases, continuous transport of carboxylic acids from the xylene phase to the aqueous phase without mixing produces a crystalline solid precipitate, in this case a layered zinc hydroxide compound intercalated with carboxylate chains (basic zinc carboxylate of brucite type structure). Heterogeneous nucleation and subsequent layered crystal growth occurs preferentially on the internal wall of the glass container in the aqueous phase. Continuous transport of hydrophobic organic species through the liquid-liquid interface leads to higher yields of the layered basic zinc salts in a biphasic system than is possible with precipitation in a single liquid phase (Inoue and Fujihara 2010). As carboxylic acid chain length increases, the distribution ratio of the carboxylic acids between xylene and water and the pKa also both increase, meaning longer chain acids prefer to remain in the xylene phase. A higher concentration of longer chain carboxylic acid in the xylene is therefore necessary to deliver

sufficient concentration to the aqueous phase (Inoue and Fujihara 2011). Conversely, high concentrations of short chain carboxylic acids increase precipitation of zinc carboxylates in the xylene phase. This gives a possible explanation for how differing fatty acid profiles in paints might influence the formation and distribution of zinc soaps.

Although the tightly controlled conditions of zinc oxide nanostructure synthesis is a long way from the arbitrary and highly variable conditions encountered in paintings, the potential relevance of biphasic crystal growth mechanisms is strengthened by preliminary findings reported in the following chapter which suggest the presence of layered basic zinc soap structures in a sample from a painting. It is also apparent from results presented in Chapter 3 that having a relatively high concentration of longer (C_{16} and C_{18}) chain fatty acids in a paint film drives a different distribution pattern to that observed in paints with low stearic acid levels. Many zinc oxide-containing paints form soaps which remain dispersed throughout the film, characterised using FTIR by a general, broad carboxylate absorption reflecting a range of relatively polar zinc soaps and low concentrations of zinc stearate or palmitate. The distribution of these soaps is proposed to equate to precipitation of short chain carboxylic acids in the 'phase of origin' (Inoue and Fujihara 2011). If, however, the concentration of stearic acid is high, as in the presence of aluminium stearate or following significant exposure related hydrolysis, then the equilibrium distribution principle favours transfer of longer chain carboxylate ions to a second phase. As illustrated in the case of paints with added aluminium stearate, this translates to a high localised concentration of zinc stearate. And as zinc carboxylates crystallise through heterogeneous nucleation on the glass walls in biphasic models, in paintings this might occur at cracks, at interfaces between layers, or possibly at the surface of pigment particles. It is energetically favourable for the typical zinc stearate bilayer structures to aggregate, and increasingly so as the paint film oxidises over time. The dense packing which is also possible given the straight splayed chain structure and strong van der Waals interactions between the long hydrocarbon chains can only further encourage aggregation to accommodate the volume increase which accompanies continuing conversion of zinc oxide to zinc stearate.

4.8   Conclusion

Processes occurring in unique paintings over decades or longer are difficult to replicate experimentally. The solvent model has provided useful insight into some of the complex variables governing formation and aggregation behaviour of zinc stearate in paintings. This chapter considers the relatively simple interactions between zinc oxide and stearic acid, and the properties of stearic

acid itself within a toluene model and uses results to assist interpretation of complex paint film chemistry. The underlying chemistry is perhaps unsurprising, however the parallels drawn with paint film saponification are novel. This work contributes evidence and important new ideas to support hypotheses for causes of associated deterioration in paintings.

In summary:

Toluene was chosen, through a systematic process, as a solvent system in which to model soap formation. This model can be expanded to examine additional variables in future work and the approach taken to select the model introduces a protocol from which further experiments can be based.

A series of zinc oxide particles have been characterised. During the history of zinc oxide in painting formulations, the source and properties of available pigment has and continues to vary. There are clear indications that some forms of zinc oxide are more reactive than others and will influence the processes of soap formation. Results reaffirm the significance of particle size for reactivity of zinc oxide with stearic acid, and demonstrate the extreme rapidity with which saponification can occur under favourable ambient conditions. Stored zinc oxide pigment samples were found to have basic zinc carbonate surface functionality from adsorbed CO_2 and H_2O which may increase sensitivity to acids in paints. Availability of stearic acid will determine the extent of zinc stearate formed, however the accessibility of zinc ions in the oxide appears to be a rate limiting step. There is potential to reproduce experiments using a wider selection of characterised zinc oxide pigment samples.

Aluminium stearate has been synthesised and FTIR spectra recorded. A common additive in paint formulations, aluminium stearate has been demonstrated here to be a source of stearic acid to react with zinc oxide. FTIR is a key tool in determining the progression of the formation of zinc soaps. Under ambient conditions the free acid typically found in aluminium stearate reacts first, followed by stearic acid spontaneously released from the aluminium soap via hydrolysis. The reaction proceeds until a majority of aluminium stearate has been replaced by zinc stearate. Residual aluminium stearate becomes increasingly polar as hydroxyl groups displace stearate chains and insoluble gel lumps of aluminium hydroxide form. Reactions in the model using nano-grade zinc oxide appear to replicate reactions occurring longer term in paint films produced with artist-grade pigment.

Zinc stearate and zinc oxide are essentially insoluble in toluene but zinc stearate formed *in situ* in the model from reaction between zinc oxide and stearic acid establishes a stable suspension of the

soap and oxide. Correlation of molecular conformation and structural assembly data obtained with FTIR and XRD with results of optical and spatially resolved SEM-EDX and Raman analysis suggests oxide particles are surrounded by zinc stearate in characteristic splayed-chain bilayer structures. The aliphatic layers of adjacent assemblies form a hydrophobic interface which supports interaction with the toluene. The midphase suspension in toluene appears to model broad dispersion of zinc soaps apparent in many zinc oxide-containing paints and provides an indicator of the morphologies that can result.

Stearic acid has been shown to be active and mobile at the interface between toluene and water phases. Passage of stearic acid through the aqueous phase was likely facilitated by the small amount of toluene dissolved in the water but may also involve dynamic interfacial activity and temporary ionisation. In the presence of zinc oxide it is feasible this would lead to heterogeneous nucleation and crystal growth of zinc soaps, while in the model without zinc it resulted in crystallisation of stearic acid at the water/air/glass interface - similar to fatty acid efflorescence observed in paintings. Interfacial activity is governed by the principle of equilibrium distribution of solutes and is strongly influenced by the conditions prevailing in adjacent phases. 'Phases' in a paint film are not so easily defined, however equilibrium in a painting (both within and between layers) will shift gradually over time or may be influenced suddenly by applied or fluctuating external environmental conditions. Extrapolation of distribution patterns reported for controlled biphasic systems together with carboxylate distribution patterns observed in reference paint films suggest high concentrations of longer chain carboxylic acids will favour zinc stearate assembly in a separate region to shorter chain, more polar zinc carboxylates. Aggregation of zinc stearate is energetically favourable and the straight chain splayed structure of molecules is compatible with dense packing, enabling volume increases to be more efficiently accommodated within a solid-state system. Applied energy or disruption of the equilibrium in a system has the potential to renew reactivity with consequences for the ongoing stability of paintings where a source of both zinc and stearate ions remain.

4.9   References

Alpbaz M, Bilgesu O, Tutkum O (1988) The measurement of interfacial tension by drop-weight method. *Commun Fac Sci Univ Ank Serie B* 34:103-112

Boon JJ, Hoogland F, Keune K (2007) Chemical processes in aged oil paints affecting metal soap migration and aggregation. In: Mar Parkin H (ed) *AIC Paintings Specialty Group Postprints*, Providence, Rhode Island, 16-19 June 2006. AIC, pp 16-23

Burke J (1984) Solubility parameters: theory and application. *The AIC Book and Paper Group Annual* 3:13-58

Burnstock A, van den Berg KJ, de Groot S, Wijnberg L (2007) An investigation of water sensitive oil paints in twentieth century paintings. In: Learner T, Smithen P, Krueger JW, Schilling MR (eds) *Modern Paints Uncovered*, Tate Modern, London, 16-19 May 2006. The Getty Conservation Institute, pp 177-188

Coe RH, Mysels KJ, Smith GH (1948) Bound and free acid in aluminum soap prepared by precipitation. *Journal of Colloid Science* 3 (4):293-302. doi:10.1016/0095-8522(48)90016-6

Corbeil MC, Robinet L (2002) X-ray powder diffraction data for selected metal soaps. *Powder Diffr* 17 (1):52-60. doi:10.1154/1.1431950

Corkery RW (1998) *Artificial biomineralisation and metallic soaps*. PhD thesis, Australian National University, Canberra

Corkery RW (2004) A variation on Luzzati's soap phases. Room temperature thermotropic liquid crystals. *PCCP* 6:1534-1546. doi:10.1039/B315595C

Corkery RW (2008) Metal organic framework (MOF) liquid crystals. 1D, 2D and 3D ionic coordination polymer structures in the thermotropic mesophases of metal soaps, including alkaline earth, transition metal and lanthanide soaps. *Current Opinion in Colloid and Interface Science* 13:288-302

Corkery RW, Hyde ST (1996) On the Swelling of Amphiphiles in Water. *Langmuir* 12 (23):5528-5529. doi:10.1021/la960794o

Elm AC (1957) Reevaluation of the function of pigments in paints. *Official Digest* (April):351-385

Feller RL, Stolow N, Jones E (1971) *On picture varnishes and their solvents*. The Press of Case Western Reserve University, Cleveland

Garti N, Wellner E, Sarig S (1980) Stearic acid polymorphs in correlation with crystallization conditions and solvents. *Kristall und Technik* 15 (11):1303-1310. doi:10.1002/crat.19800151112

Goienaga N, Arrieta N, Carrero JA, Olivares M, Sarmiento A, Martinez-Arkarazo I, Fernández LA, Madariaga JM (2011) Micro-Raman spectroscopic identification of natural mineral phases and their weathering products inside an abandoned zinc/lead mine. *Spectrochimica Acta Part A: Molecular and Biomolecular Spectroscopy* 80 (1):66-74. doi:http://dx.doi.org/10.1016/j.saa.2011.01.032

Gönen M, Balköse D, İnal F, Ülkü S (2005) Zinc Stearate Production by Precipitation and Fusion Processes. *Industrial & Engineering Chemistry Research* 44 (6):1627-1633. doi:10.1021/ie049398o

Graedel TE (1989) Corrosion Mechanisms for Zinc Exposed to the Atmosphere. *J Electrochem Soc* 136 (4):193C-203C. doi:10.1149/1.2096868

Gray VR, Alexander AE (1948) Studies on Aluminum Soaps. II. The Composition, Structure, and Gelling Properties of Aluminum Soaps. *The Journal of Physical and Colloid Chemistry* 53 (1):23-38. doi:10.1021/j150466a003

H.W. (1925) *Notes on the durability and manipulation of zinc paints*. The decorator and painter for Australia and New Zealand, vol 1 October. Bishop Bros., Sydney

Hancock R, Leeves N, Nicks P (1989) Studies in autoxidation. I: The volatile by-products resulting from the autoxidation of unsaturated fatty acid methyl esters. *Prog Org Coat* 17 (3):321-336

Hansen CM, Klauss HC (1971) Mechanism of paint seeding. *Industrial and Engineering Chemistry Product Research and Development* 10 (2):189-192

Hedley G (1980) Solubility parameters and varnish removal a survey. *The Conservator* 4 (1):12-18. doi:10.1080/01410096.1980.9994931

Inoue S, Fujihara S (2010) Synthesis of Inorganic−Organic Layered Compounds Using Immiscible Liquid−Liquid Systems under the Distribution Law. *Langmuir* 26 (20):15938-15944. doi:10.1021/la1028542

Inoue S, Fujihara S (2011) Liquid−Liquid Biphasic Synthesis of Layered Zinc Hydroxides Intercalated with Long-Chain Carboxylate Ions and Their Conversion into ZnO Nanostructures. *Inorg Chem* 50 (8):3605-3612. doi:10.1021/ic1025729

International Zinc Association (2009) *Commercial grades of zinc oxide*. International Zinc Association. http://www.znoxide.org/commercial_grades.html. Accessed 7 June 2010

Ishioka T, Maeda K, Watanabe I, Kawauchi S, Harada M (2000) Infrared and XAFS study on structure and transition behaviour of zinc stearate. *Spectrochimica Acta Part A* 56:1731-1737

Jackson KDO (1998) A guide to identifying common inorganic fillers and activators using vibrational spectroscopy. *The Internet Journal of Vibrational Spectroscopy (wwwijvscom)* 2 (3):article no. 6

Kaneko F, Tashiro K, Kobayashi M (1999) Polymorphic transformations during crystallization processes of fatty acids studied with FT-IR spectroscopy. *J Cryst Growth* 198-199 (Part 2):1352-1359

Kanicky JR, Shah DO (2002) Effect of Degree, Type, and Position of Unsaturation on the pKa of Long-Chain Fatty Acids. *J Colloid Interface Sci* 256 (1):201-207. doi:10.1006/jcis.2001.8009

Kühn H (1986) Zinc white In: Feller RL (ed) *Artists' pigments* vol 1. Cambridge University Press, pp 169-186

Lower ES (1982) The properties of aluminium stearate and its uses in the coatings and allied industries. *Pigm Resin Technol* 11 (2):13-18

Martin EP, Pink RC (1948) 354. The solubility of zinc soaps in organic solvents. *Journal of the Chemical Society (Resumed)*:1750-1755

McBain JW, McClatchie WL (1932) The probable non-existence of normal tribasic aluminum soaps such as aluminum tripalmitate. *J Am Chem Soc* 54:3266-3268. doi:10.1021/ja01347a504

Morley-Smith CT (1950) The development of anti-chalking French Process zinc oxides. *Journal of the Oil & Colour Chemists' Association* 33:484-501

Muizebelt WJ, Nielen MWF (1996) Oxidative Crosslinking of Unsaturated Fatty Acids Studied with Mass Spectrometry. *J Mass Spectrom* 31 (5):545-554. doi:10.1002/(sici)1096-9888(199605)31:5<545::aid-jms329>3.0.co;2-1

Musić S, Popović S, Maljković M, Dragčević D (2002) Influence of synthesis procedure on the formation and properties of zinc oxide. *J Alloys Compd* 347 (1-2):324-332

Nelson PN, Ellis HA, Taylor RA (2011) Odd–even alternation in a homologous series of Zn (II) n-alkanoates. *J Mol Struct* 986 (1–3):10-15. doi:http://dx.doi.org/10.1016/j.molstruc.2010.11.014

Oil and Colour Chemists' Association (ed) (1966) *Pigments, dyestuffs and lakes*, vol Part Six. Paint technology manuals. Chapman and Hall for the Oil and Colour Chemists' Association, London

Öztürk S, Balköse D (2005) *Preparation and Characterization of Metal Soap Nanofilms*. İzmir Institute of Technology, İzmir,

Phenix A (2002a) Building Models: Comparative swelling powers of organic solvents on oil paint and the cleaning of paintings. *V&A Conservation Journal* 40 (Spring)

Phenix A (2002b) The Swelling of Artists' Paints in Organic Solvents. Part 2, Comparative Swelling Powers of Selected Organic Solvents and Solvent Mixtures. *Journal of the American Institute for Conservation* 41 (1):61-90

Phenix A (2013) Effects of organic solvents on artists' oil paint films: swelling. In: Mecklenburg MF, Charola EA, Koestler RJ (eds) *New insights into the cleaning of paintings: Proceedings from the Cleaning 2010 International Conference, Universidad Politécnica de Valencia and Museum Conservation Institute*. Smithsonian Institution Scholarly Press, Washington DC pp 69-76

Pilpel N (1963) Properties of Organic Solutions of Heavy Metal Soaps. *Chem Rev* 63 (3):221-234. doi:10.1021/cr60223a001

Princen LH, Devena-Peplinski M (1964) Effect of particle size on the mutual flocculation between zinc oxide and titanium dioxide. *Journal of Colloid Science* 19 (9):786-797

Robinet L, Corbeil MC (2003) The characterization of metal soaps. *Stud Conserv* 48 (1):23-40

Rudin A (1999) *Polymer science and engineering*. 2nd edn. Academic Press, London

Saien J, Akbari S (2006) Interfacial Tension of Toluene + Water + Sodium Dodecyl Sulfate from (20 to 50) °C and pH between 4 and 9. *Journal of Chemical & Engineering Data* 51 (5):1832-1835. doi:10.1021/je060204g

Sakai H, Umemura J (2002) Evaluation of molecular structure in Langmuir monolayers of zinc stearate and zinc 12-hydroxystearate by IR external reflection spectroscopy. *Colloid Polym Sci* 280 (4):316-321. doi:10.1007/s003960100581

Sakai H, Umemura J (2008) Evaluation of structural change during surface pressure relaxation in Langmuir monolayer of zinc stearate by infrared external reflection spectroscopy. *Colloid Polym Sci* 286 (14):1637-1641. doi:10.1007/s00396-008-1939-2

Stavroudis C, Blank S (1989) Solvents & sensibility. *WAAC Newsletter* 11 (2):2-10

Stolow N (1957) The action of solvents on drying oil films, parts I & II. *J Oil Colour Chem Assoc* 40:377-402, 488-499

Sundberg A, Strand A, Vähäsalo L, Holmbom B (2009) Phase Distribution of Resin and Fatty Acids in Colloidal Wood Pitch Emulsions at Different pH-Levels. *J Dispersion Sci Technol* 30 (6):912-919. doi:10.1080/01932690802646249

Taylor RA, Ellis HA (2007) Room temperature molecular and lattice structures of a homologous series of anhydrous zinc(II) n-alkanoate. *Spectrochimica Acta Part A: Molecular and Biomolecular Spectroscopy* 68 (1):99-107. doi:http://dx.doi.org/10.1016/j.saa.2006.11.007

Thermo Electron Corporation (1991-1994) *Coatings Technology FT-IR spectral reference library*. Thermo Electron Corporation,

Tumosa CS (2001) A brief history of aluminum stearate as a component of paint. *WAAC Newsletter* 23 (3)

van der Kerk GJM (1972) Organozinc coordination chemistry and catalytic effects of organozinc coordination compounds. *Pure Appl Chem* 30 (3-4):389-408. doi:10.1351/pac197230030389

van der Weerd J, van Loon A, Boon JJ (2005) FTIR studies of the effects of pigments on the aging of oil. *Stud Conserv* 50 (1):3-22

van Gorkum R, Bouwman E (2005) The oxidative drying of alkyd paint catalysed by metal complexes. *Coord Chem Rev* 249:1709-1728. doi:10.1016/j.ccr.2005.02.002

Verhoeven MA, Carlyle L, Reeddijk J, Haasnoot JG (2006) Exploring the application of solid-state Nuclear Magnetic Resonance to the study of the deterioration of paintings. In: Boon JJ, Ferreira ESB (eds) *Reporting highlights of the De Mayerne Programme*. Netherlands Organisation for Scientific Research (NWO), The Hague, pp 34-42

Vold RD, Hattiangdi GS (1949) Characterization of Heavy Metal Soaps by X-Ray Diffraction. *Industrial & Engineering Chemistry* 41 (10):2311-2320. doi:10.1021/ie50478a056

Wöll C (2007) The chemistry and physics of zinc oxide surfaces. *Prog Surf Sci* 82:55-120. doi:10.1016/j.progsurf.2006.12.002

Zhang XG (1996) *Corrosion and electrochemistry of zinc*. Plenum Press, New York

5 Zinc oxide-centred deterioration in 20th century Vietnamese paintings by Nguyễn Trọng Kiệm (1933-1991)

5.1 Abstract

Five paintings dated between 1963 and 1980 by Vietnamese artist Nguyễn Trọng Kiệm (1933-1991) in Witness Collection are investigated through study of paint cross-sections. Zinc oxide is dominant in all paintings and has strongly influenced their ageing. Widespread flaking and structural instability is an ongoing concern. The presence of unusual zinc and sulphur containing lumps in one early work has been investigated previously and the proposed mechanism of formation is reassessed. Paint samples are analysed using FTIR and examined in cross-section using optical microscopy, scanning electron microscopy with energy dispersive X-ray analysis, and synchrotron Fourier transform infrared microspectroscopy. X-ray microdiffraction is applied to one sample. Of particular interest are the presence of zinc carboxylates, zinc carbonate and zinc sulphate as products of deterioration. Preferential dissolution of zinc oxide over other pigment types including lead white and lithopone is observed in backscatter electron images, interpreted in conjunction with elemental and FTIR analysis. Structural consequences are indicated for inter- and intra-layer stability of affected paints. The hot, humid conditions and pollution levels in Vietnam coupled with paints containing zinc oxide of different grades and the presence of unpigmented medium or size layers are all significant factors in the current condition of these paintings.

A substantial body of work in this chapter has been published and is included as section 5.2:

Osmond G, Ebert B, Drennan J. 2014. Zinc oxide-centred deterioration in 20th century Vietnamese paintings by Nguyễn Trọng Kiệm (1933-1991). *AICCM Bulletin*, 34: 4-14

My contributions to the paper include experiment design, preparation and analysis of samples, data interpretation, pattern recognition and preparation of the manuscript and figures, refined in conjunction with contributing authors. B Ebert provided paint samples, images and details of paintings and contextual information. J Drennan was the project spokesperson for synchrotron beamtime and was responsible for supervision and critical review of the text.

5.2 Introduction

Previous chapters have investigated the reactivity of zinc oxide and aspects of zinc stearate formation in reference paints or model systems. This chapter makes important connections between the findings discussed in preceding work and actual deterioration observed in paintings. A case study of five paintings by Vietnamese artist Nguyễn Trọng Kiệm (1933-1991) is presented. Critical to this has been the support of Bettina Ebert, Senior Paintings Conservator at Asiarta Foundation, Malaysia. Ebert initially investigated deterioration in Kiệm's paintings as part of her own post graduate research within the University of Northumbria Conservation program. Her current employment involves responsibility for collections care and conservation of the Witness Collection, a comprehensive collection of modern and contemporary Vietnamese art, including paintings by Kiệm, among which are two works investigated at Northumbria. My focus on zinc oxide-centred deterioration of oil-based paints and Ebert's ongoing involvement with Witness collection provided an opportunity to further research the puzzling and problematic deterioration evident in Kiệm's paintings.

The conservation of vast collections of cultural heritage deriving from the Asia Pacific region is of growing interest among the international conservation community, exemplified by strong participation in Thailand during 2012 at the 3rd APTCCARN Meeting on The Conservation of Material Culture in Tropical Climates. Of particular concern for paintings conservators are challenges posed by artists using western approaches to painting while resident in environments far removed from the European origins of those practices. Pioneering work has been undertaken by Dr Nicole Tse, post doctoral fellow attached to the present Linkage Project. Tse's own PhD research specifically addressed questions about the production and conservation of Southeast Asian paintings created using Western art materials and techniques (Tse 2008). Twentieth century Vietnamese art was strongly influenced by academic techniques introduced via French colonial instructors at l'Ecole des Beaux-Arts de l'Indochine (EBAI), established in 1925.

Kiệm's work came to conservation attention following detailed investigation of two paintings during successive research projects at the University of Northumbria. The art historical interpretation, technical analysis and conservation treatment of these paintings are described in the resulting theses (MacMillan 2007; Ebert 2008) and feature in a number of subsequent publications (Singer et al. 2009; Ebert et al. 2011). A thorough introduction to Kiệm and the context for his painting career in North Vietnam during the mid twentieth century is provided by MacMillan (2007), and informs much of the background information included here.

Nguyễn Trọng Kiệm began his artistic career in Vietnam in the early years of anti-colonial revolution. Despite training at the Resistance School of Fine Arts (1949-1954), his teacher, Tô Ngọc Vân, and other instructors came from EBAI and so taught their students traditional French techniques (Nguyen Tran Minh and Tran Thi Minh Man 2008). Artists were encouraged to join the independence movement by becoming "national art workers", joining propaganda teams and painting idealised nationalistic compositions.

For a large part of Kiệm's career until the end of the war in 1975, there was no art market in Vietnam. State sponsored exhibitions were the only official means of showing artworks and participation also gave artists access to what were otherwise very limited supplies of painting materials. The majority of Kiệm's artistic production conformed to Government policy; he taught until his death at the Industrial Fine Art University in Hanoi where socialist realism remained the official style, and his work was regularly selected for national exhibition. However, Kiệm was also interested in experimenting with Western modern styles and he participated in the unofficial art scene which revolved around studios and cafes (MacMillan 2007).

This chapter investigates samples from five of Kiệm's 'unofficial' paintings dated between 1963 and 1980 which now form part of Witness Collection. The opportunity is taken to reconsider the mechanism attributed to formation of unusual zinc-based lumps causing dramatic deterioration in one of the paintings previously investigated at the University of Northumbria. Investigation has been done without first hand assessment of the paintings, and reference to their physical condition relies on images and documentation provided by a third party. Each of the paintings is physically fragile and prone to flaking and all incorporate substantial amounts of zinc oxide and reaction products related to the reactivity of that pigment. FTIR of paint fragments is used in conjunction with optical microscopy and scanning electron microscopy with energy dispersive X-ray analysis of embedded samples in cross-section from each painting. Metal stearate distributions within selected samples are resolved with cross-sectional mapping acquired via synchrotron FTIR microspectroscopy. XRD microdiffraction is applied to one sample to identify crystalline phases from single spot analyses and linear maps.

5.3 Zinc oxide-centred deterioration in 20th century Vietnamese paintings

This postprint is included with kind permission from AICCM in partnership with Maney. The final publication is available at www.maneyonline.com.

Osmond G, Ebert B, Drennan J (2014) Zinc oxide-centred deterioration in 20th century Vietnamese paintings by Nguyễn Trọng Kiệm. *AICCM Bulletin* 34:4-14

Zinc oxide centred deterioration in 20th century Vietnamese paintings by Nguyễn Trọng Kiệm (1933-1991)

Gillian Osmond, Bettina Ebert and John Drennan

Abstract

Five paintings dated 1963-1980 by Vietnamese artist Nguyễn Trọng Kiệm (1933-1991) in Witness Collection are investigated through study of paint cross-sections. Zinc oxide predominates in all paintings and has strongly influenced their ageing. Widespread flaking is an ongoing concern. Unusual zinc and sulphur containing lumps in one early work have been investigated previously and the mechanism of formation is reassessed. Paint samples are examined using optical microscopy, scanning electron microscopy with energy dispersive x-ray analysis, x-ray microdiffraction and FTIR techniques. Of key interest are zinc carboxylates, basic zinc carbonate and zinc sulphates as products of deterioration. No evidence is found to support the presence of crystalline zinc sulphate. Layered basic zinc salts incorporating carboxylate, carbonate and sulphate moieties are proposed as an alternative. Hot, humid conditions and pollution levels in Vietnam coupled with paints containing zinc oxide of different grades and the presence of unpigmented medium or size layers are significant factors in the condition of these paintings.

Keywords

Paintings conservation, zinc white, zinc oxide, zinc soap, Nguyễn Trọng Kiệm, zinc sulphate, zinc carbonate

Introduction

The paintings of Nguyễn Trọng Kiệm (1933-1991) have come to recent conservation attention following detailed investigation of two 1963 works during successive research projects at University of Northumbria. Technical analysis and conservation treatment of these paintings are described in the resulting theses (MacMillan 2007; Ebert 2008) and feature in subsequent publications (Singer et al. 2009; Ebert et al. 2011).
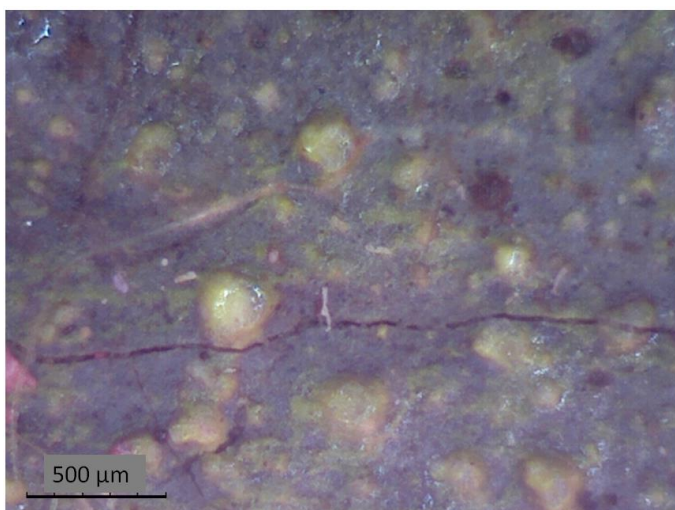
Figure 1 *Portrait of my wife* magnified surface detail showing white lumps emerging through paint

The majority of Kiệm's artistic production conformed to North Vietnamese government policy; he taught at the Hanoi Industrial Fine Art University where socialist realism remained the official style. However, Kiệm also experimented with Western modern approaches. Five of Kiệm's 'unofficial' paintings dated 1963-1980 are discussed here, including a review of previously investigated white, zinc based aggregates in *Portrait of my wife* which disrupt individual layers and the surface (**Figure 1**). Although an emerging body of evidence links zinc based lumps to zinc soaps formed by reactivity of zinc white pigment in oil-based media (Noble & Boon 2007), investigation of lumps in Kiệm's painting reveals differences to incidences of zinc carboxylate aggregation and remineralisation reported to date.

Previous research identified two zinc white paints present in the painting based on distinct particle size and ultraviolet fluorescence (UVF) properties. In *Portrait of my wife*, lumps only occur in bright green fluorescent layers, indicative of Direct Process zinc oxide, primarily within body paint (Ebert et al. 2011). The authors concluded that zinc sulphate heptahydrate crystals had formed in situ from direct conversion of underbound zinc oxide exposed to sulphurous pollution. However, this hypothesis contradicts the lower reactive surface area and superior paint stability associated with Direct Process zinc oxide (Morley-Smith 1950). The postulate also differs from conclusions regarding formation of growths in old master paintings where mineralised masses are attributed to precipitation from lead soap intermediaries (Higgitt et al. 2003; Keune & Boon 2007).
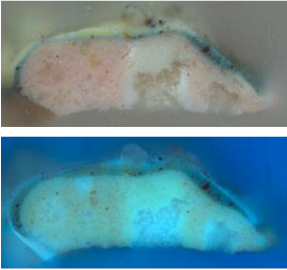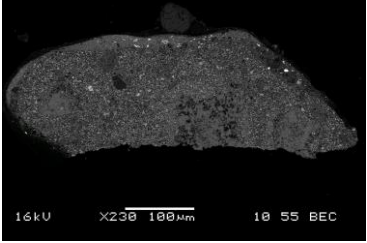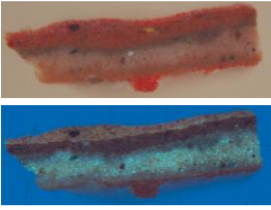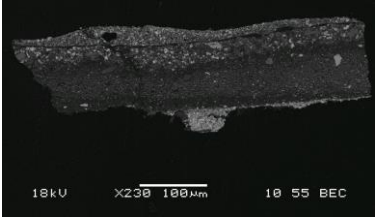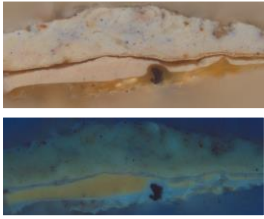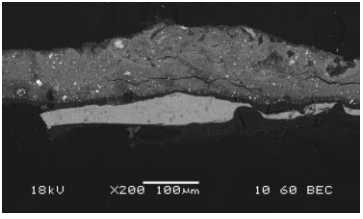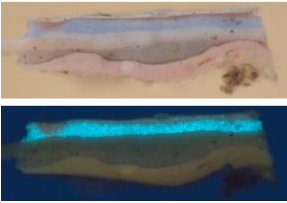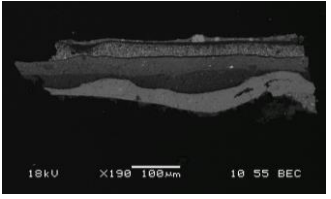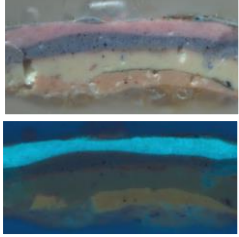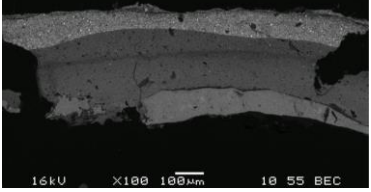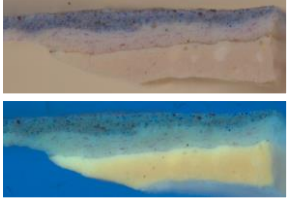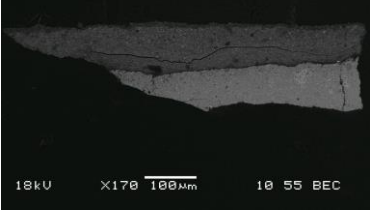
In Kiệm's paintings precipitation may have occurred within zinc soaps, just as zinc carbonate has been characterised within aggregates in paintings (Keune 2005). Precipitation of zinc sulphate from zinc soap aggregates was thought unlikely in Kiệm's painting based on low zinc and carbon concentrations within masses, and negligible depletion of zinc from surrounding paint (MacMillan 2007; Ebert et al. 2011). However, this does not preclude a zinc soap intermediary if reaction between zinc and fatty acids occurred early in the life of the paint. The current study reconsiders the mechanism attributed to lump formation through investigation of another sample with comparable features from the same painting, in addition to samples from other paintings by Kiệm. These include a second work from 1963 and three post-war paintings from 1979-1980. While only one painting exhibits the distinctive deterioration originally investigated, all paintings incorporate substantial amounts of zinc oxide and associated products related to pigment reactivity.

Overview of paintings and samples

Paint samples were obtained from 5 paintings by Kiệm currently in Witness Collection. Samples included several from the two 1963 paintings taken previously by MacMillan, which were not investigated at that time.

Samples were prepared as cross-sections and examined using optical microscopy (OM), scanning electron microscopy with energy dispersive x-ray analysis (SEM-EDX) and synchrotron Fourier transform infrared microspectroscopy (SR-μFTIR). Where possible, fragments from samples prior to embedding were analysed with conventional FTIR microspectroscopy. One sample was investigated using x-ray microdiffraction (μXRD). **Table 1** details the paintings and cross-sections.

Table 1. Images and cross-sections of paintings by Nguyễn Trọng Kiệm. Cross-sections are shown as visible, UVF and BSE images

Painting	Title/date	Cross section top: visible light bottom: UV fluorescence	Backscatter electron image
	Portrait of the artist's wife 1963		
	Portrait of a student 1963		
	Hàng Giấy street scene 1978		
	Children playing at the beach 1980		
	Staring out game 1980		
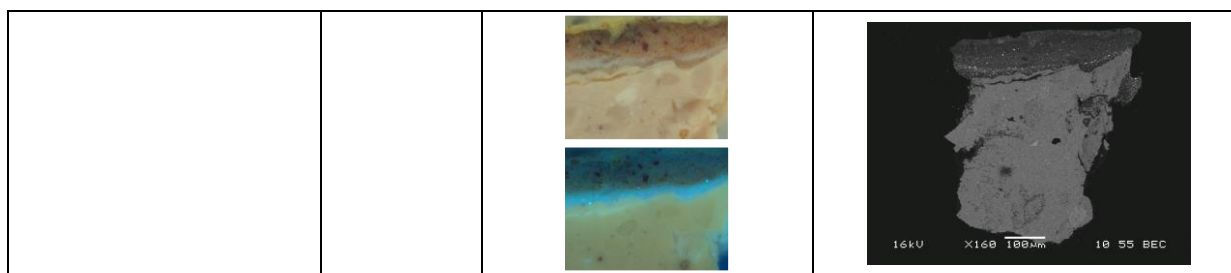
Results and discussion

Painting materials

Cross-sections show a conventional layer structure, in keeping with Kiệm's French colonial training. Animal glue sizing and a single ground layer are evident in *Hàng Giấy*, supporting a friend's recollection that Kiệm used linseed oil mixed with a 'white powder' (Bùi Quang Ánh 2012). All paintings examined have grounds based on lithopone, a precipitated pigment averaging 70% barium sulphate, 30% zinc sulphide and 1-2% zinc oxide. Grounds from both early works include FTIR markers for oil (fatty acids) and protein, while those of *Hàng Giấy* and *Staring out game* are more consistent with straight oil. Previously reported gas chromatography-mass spectrometry (GC-MS) analysis of the 1963 grounds suggests a possible casein/oil emulsion (Ebert et al. 2011).

Paint layers in all works are consistent with oil, although extensive hydrolysis is indicated by FTIR. An unusually small ester carbonyl peak is rivalled by absorption typical of free fatty acids. Metal carboxylate absorption is strong, frequently including a defined peak indicative of zinc stearate/palmitate (1541 cm^{-1}) (**Figure 2**). SR-μFTIR cross-section mapping suggests hydrolysis is most extreme at the exposed painting surface (**Figure 3**).

Paint samples contain a range of white pigments, probably reflecting Kiệm's difficulty in obtaining paints. Zinc oxide is ubiquitous, but in both 1963 paintings it occurs in different particle sizes alone and in mixtures with lead white, barium sulphate and chalk. Post-war paintings also include zinc white with and without lead white. A fluorescent sparkle typical of many paints containing zinc white in cross-sections viewed with UV light is not consistently observed. Kiệm disliked zinc white because of its tendency to harden in the tube (Nguyễn Trần Minh & Trần Thị Minh Man 2008). However, his stated preference for titanium white (ibid) is not borne out by analysis, with titanium detected only occasionally. This is consistent with limited availability and expense.
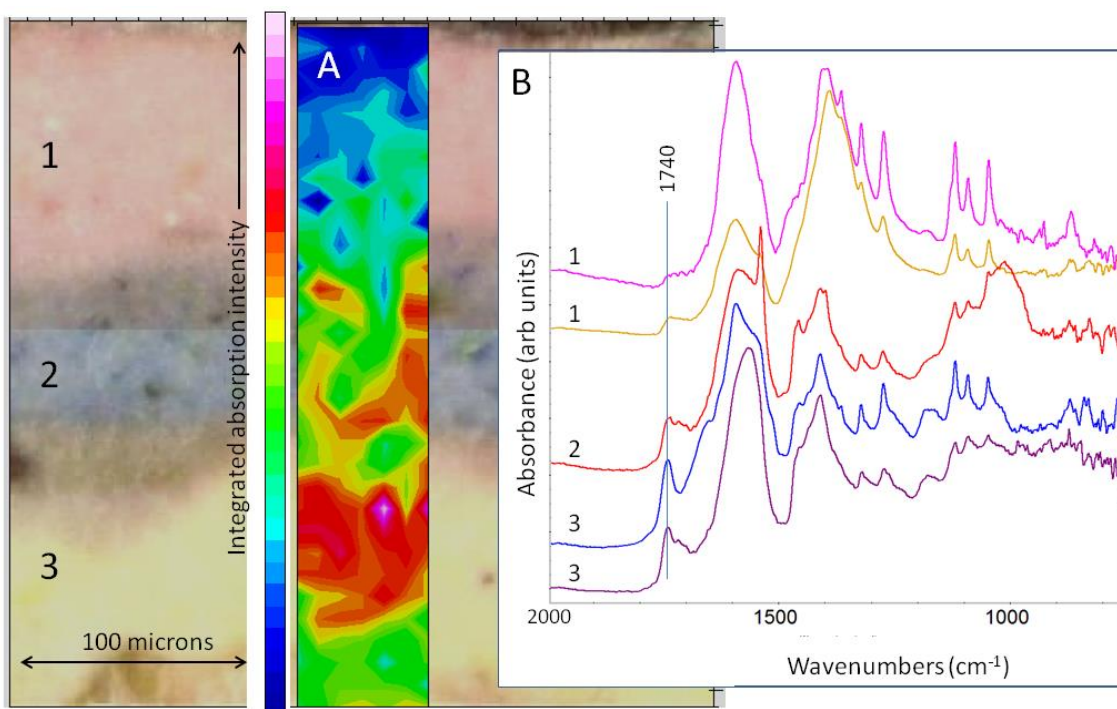
Figure 2 *Hàng Giấy* FTIR spectrum. The carbonyl peak for oil (1737 cm^{-1}) is rivalled by the carboxylic acid peak (1713 cm^{-1}). v_a COO$^-$ (1541 cm^{-1}) zinc stearate/palmitate dominates the spectrum
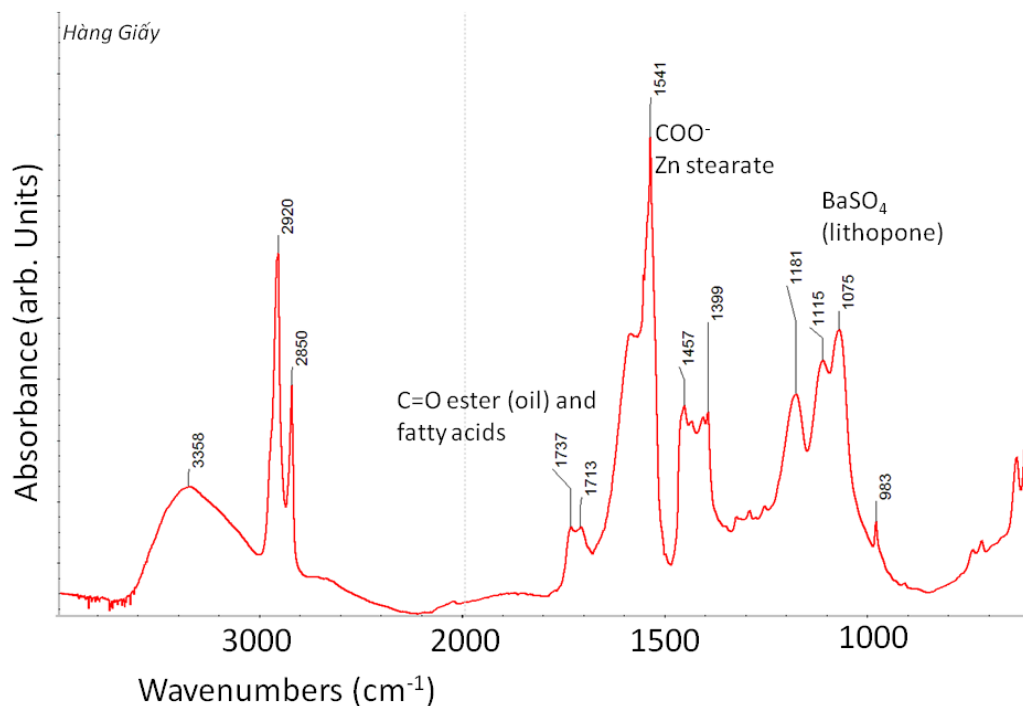
Figure 3 *Children playing at the beach* cross-section ATR SR-µFTIR. A: integrated absorption intensity map for oil ester carbonyl peak (1730-1755 cm^{-1}) plotted over the top three zinc oxide-based paint layers and B: spectra extracted from layers 1-3 numbered top to bottom. Reduced intensity of the 1740 cm^{-1} peak to virtually zero at the upper surface is consistent with exposure-related hydrolysis. Pink paint (layer 1) includes lead white and zinc oxide

Coloured pigmentation varies across paintings but mineral pigments dominate rather than paints based on extenders with modern dyes, supporting recollections by Kiệm's family that he used reputable artists' tube paints wherever possible. Ultramarine blue and zinc yellow appear frequently. War period works include cadmium selenium red, cadmium yellow, viridian, chrome yellow, Prussian blue, various iron-based colours and clay fillers. Cobalt green and an organic red in paint otherwise dominated by zinc oxide and silicates occur in *Portrait of my wife*. *Hàng Giấy* incorporates Naples yellow (lead antimonate), unusual for a modern paint formulation. *Staring out game* contains cobalt violet. *Children playing at the beach* includes a pigment with aluminium, cobalt and chromium, possibly cobalt aluminate blue spinel.

These findings are broadly consistent with compositions of period tube paints obtained from studios of Kiệm's North Vietnamese Army artist contemporaries (MacMillan 2007), principally paints manufactured by Farbenfabrik Nerchau, East Germany. MacMillan's analysis found the medium was characteristically raw linseed oil. Zinc stearate was also frequently identified but whether it originates as an additive or following reactions with zinc oxide is uncertain (no white paints were studied).

Review of deterioration in 'Portrait of my wife'

The paint sample investigated from *Portrait of my wife* includes large translucent and white masses with distinctive appearance in backscatter electron (BSE) images (**Figure 4**). EDX spectra are dominated by zinc but associated with different proportions of carbon, oxygen and sulphur (**Figure 5**).
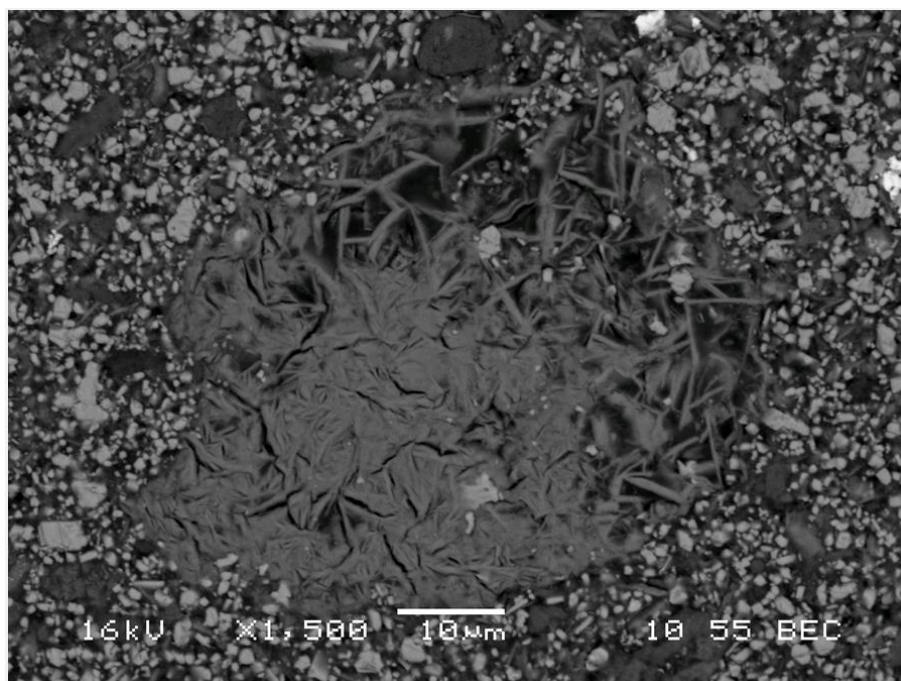
Figure 4 *Portrait of my wife* BSE cross-section image detail. The distinctive mass has consistent appearance to inclusions previously attributed to zinc sulphate heptahydrate
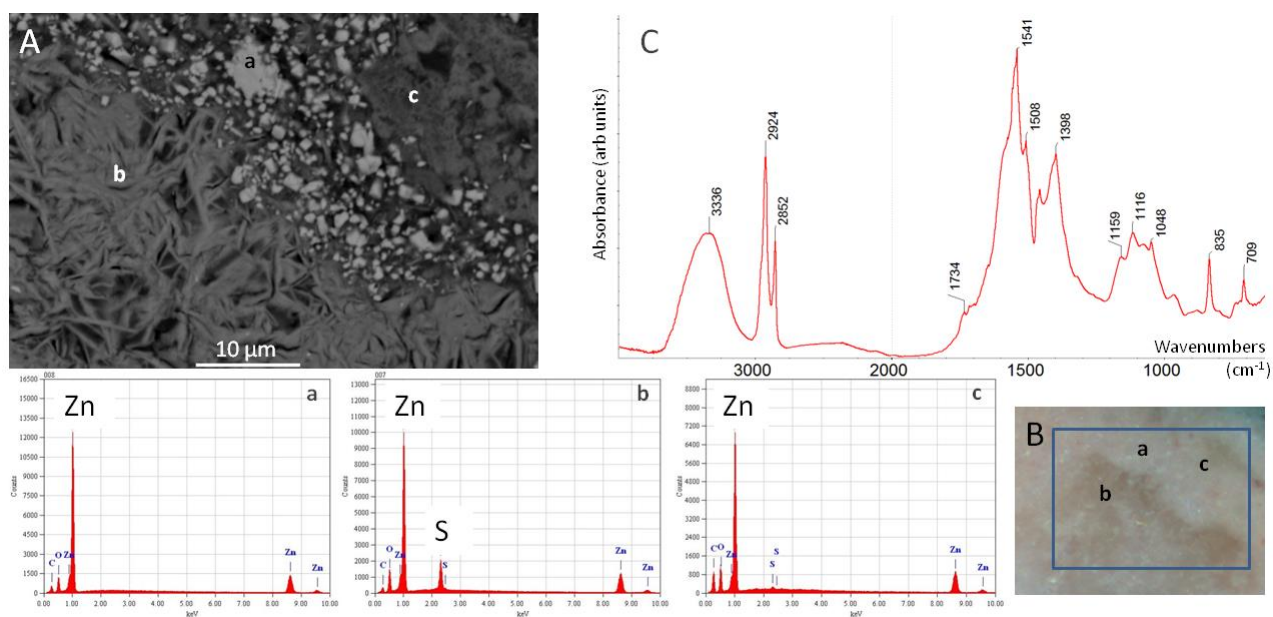
Figure 5 *Portrait of my wife* cross-section detail, A: BSE image and B: corresponding optical image. EDX spectra obtained from points designated suggest contribution from (a) zinc oxide; (b) zinc/sulphur compound; (c) zinc compound. C: transmission FTIR spectrum incorporates peaks characteristic of zinc stearate/palmitate, basic zinc carbonate and sulphates

Despite limitations of SEM-EDX for quantitative analysis of heterogeneous samples, observed relative peak heights for different features in the sample are reasonably consistent and imply correlation with the microstructure. ZAF-corrected standardless quantitative analysis suggests there is too little sulphur and oxygen relative to zinc to confirm the presence of zinc sulphate. This does not preclude zinc sulphate being present among other zinc-based compounds.

An FTIR spectrum of paint from the sample shows contributions from sulphates (1048, 1116, 1165 cm^{-1}) and basic zinc carbonate (3340, 1380, 1048, 1508, 835 cm^{-1}) in addition to strong metal carboxylate absorption, notably zinc stearate (1541, 1399 cm^{-1}) (Figure 5C). Zinc oxide has no absorption signal between 600-4000 cm-1. Despite problems mapping the cross-section with SR-µFTIR, it was possible to extract some well resolved individual spectra (**Figure 6**). These show strong association between zinc carboxylates and basic zinc carbonate. No clear zinc sulphate spectra are observed. In addition to carboxylate absorption c. 1540-1550 cm^{-1}, many spectra contain a strong peak at 1596 cm^{-1} related to an unusual recurring spectral pattern (Figure 6b). A comparable spectrum has recently been attributed to zinc lactate (Helwig et al. 2013). The same series of peaks are evident in spectra from *Children playing at the beach* (Figure 3).
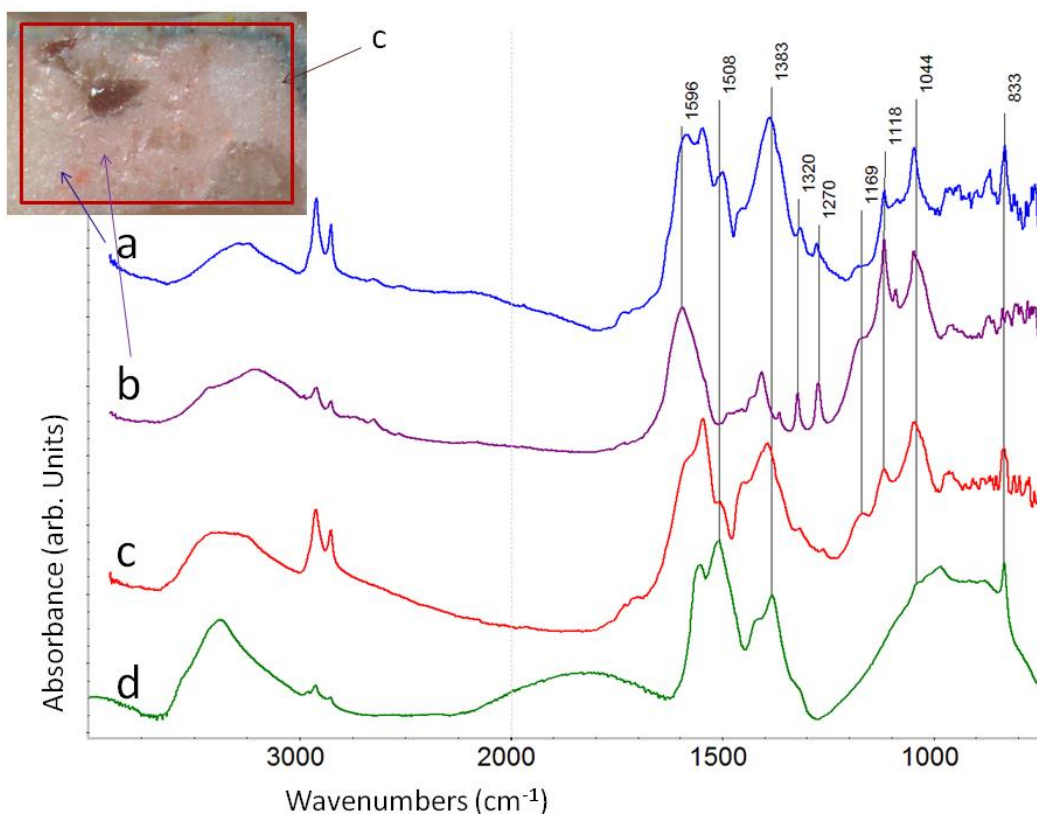
Figure 6 *Portrait of my wife* ATR SR-µFTIR spectra extracted from individual 5x5 µm points of the cross-section (a-c) show strong association between zinc carboxylates (1520-1620 cm^{-1}) and basic zinc carbonate (1508, 1383, 1044, 833 cm^{-1}). For reference, transmission spectrum (d) shows basic zinc carbonate absorptions in Kremer zinc white pigment reflecting surface conversion of the oxide in storage. No clear zinc sulphate spectra are resolved although sulphates may contribute to absorption 1000-1170 cm^{-1}, notably in spectrum (c). Strong carboxylate absorption at 1596 cm^{-1} relates to an unusual recurring spectral pattern (b) tentatively attributed to zinc lactate

Clarification on sample composition was sought using µXRD on the same cross-section from *Portrait of my wife*. Again, despite the coincidence of zinc and sulphur in large masses, no crystalline zinc sulphate was detected (Hay 2012). The predominant crystalline component in the sample is zinc oxide. An unattributed peak at 32.8° 2θ was also recorded. Subsequent investigation revealed this peak is a consistent feature, (100) plane, of layered basic zinc salts with brucite-type zinc hydroxide structure (Inoue & Fujihara 2011). Unfortunately the geometry of the µXRD instrument precludes collection of diffraction data for lower angle peaks from small paint cross-sections which are the strongest diffracting planes for these structures. However the possibility of such compounds forming in-situ seems feasible. Significantly, carboxylate, carbonate and sulphate ions can all be accommodated within OH layers forming stable layered basic zinc salts (Hofmeister & Platen 1992). This scenario could explain apparent contradiction between µXRD results implying an absence or low density of zinc sulphate, and SEM imaging and EDX analysis revealing large zinc and sulphur containing masses with distinctive morphology. Layered basic zinc salts might also account for sulphates inferred by characteristic FTIR peaks within typically complex spectra, and the close association of zinc based carboxylates and carbonates revealed with individual SR-µFTIR spectra.

Sources of sulphur in zinc white pigment stock

A possible explanation for the presence of zinc/sulphur compounds is use of low purity zinc oxide in impasto body paint. Previous research linked deterioration to paints with Direct Process zinc oxide (Ebert et al. 2011). Manufacture of Direct Process zinc oxide produces sulphur dioxide (SO_2), and complex sulfites and sulphates form on the pigment surface (Brown 1957). SO_2 pollution in Vietnam means it is also possible sulphur compounds formed in dry pigment stock prior to paint production. Zinc oxide has an active surface and conversion to carbonate or sulphide readily occurs on ambient storage (Kühn 1986). Relative humidity cycles are implicated in this process, via a zinc hydroxide intermediate. Review of an FTIR spectrum produced by MacMillan (2007, p.107) from white body paint in *Portrait of my wife* indicates strong contribution from basic zinc carbonate in addition to zinc carboxylates (and sulphates). This interpretation is supported by BSE images, EDX analysis and FTIR of current sample material. FTIR of Kremer zinc white pigment stored in a closed jar in benign laboratory conditions for 7 years similarly registers basic zinc carbonate absorptions (Figure 6d). Carbonate was not present in sufficient quantity to be detected with powder x-ray diffraction, suggesting formation is superficial. However, in conditions of sustained high humidity potential exists for continued conversion of zinc oxide to carbonate or sulphate. Different exposure histories of pigment stock prior to paint production may explain the incidence of sulfate deterioration in one paint more than another. Use of lower quality pigment or paint stock for underlying textural effect is plausible for an artist struggling to obtain his preferred painting materials.
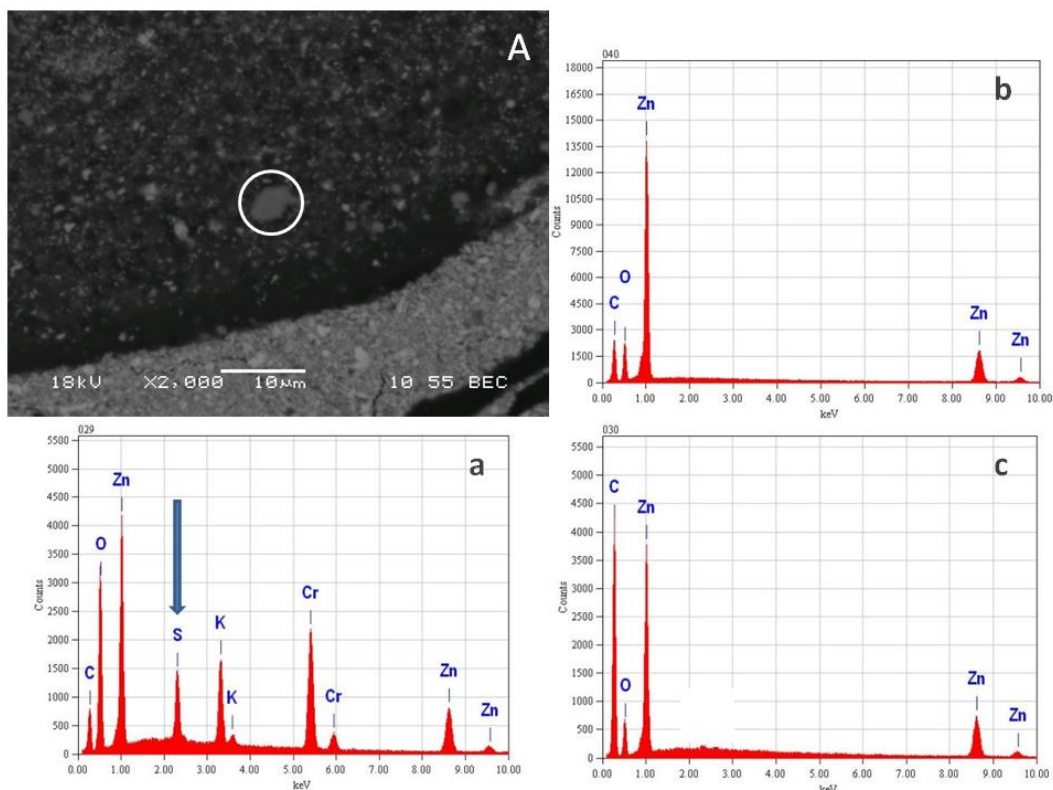
Figure 7 *Children playing at the beach* cross-section BSE image detail. (a) EDX spectrum obtained from a discoloured particle of zinc potassium chromate pigment (circled) contains sulphur consistent with exposure to SO_2 at high RH. There is negligible evidence of sulphur in surrounding zinc white paint in either (b) low carbon or (c) high carbon regions

This does not diminish the argument that Kiệm's paintings have been exposed to warm, humid, polluted environments. Sulphur detected using SEM-EDX in discoloured zinc potassium chromate pigment in *Children playing at the beach* (**Figure 7**) is consistent with deterioration of zinc yellow in paint films exposed to SO_2 at high RH (Casadio et al. 2011). However, despite evidence of SO_2 exposure, there is negligible indication of sulphur in surrounding paint or having affected zinc white pigment in Kiệm's paintings. This may be explained by reactivity of zinc oxide with fatty acids in oil-based media

Zinc carboxylate formation

Formation of zinc soaps as a precursor to development of zinc sulphate lumps in Kiệm's paintings was previously discounted on the basis of elemental mapping indicating consistent levels of zinc within and outside masses (Singer et al. 2009; Ebert et al. 2011). While free fatty acids progressively reacting with zinc oxide particles over time is one possible scenario, the assumption that all soap formation occurs this way oversimplifies conditions under which metal soaps develop in paintings. Keune and Boon (2007) describe a variety of lead soap aggregates in paintings and conclude that although reaction of lead ions and fatty acids to form lead soaps is straight forward, the conditions under which it occurs are complex and multifaceted. Soap formation occurring during early drying will manifest differently to that developing in a mature paint system. Zinc oxide is more reactive with fatty acids than lead white and may be more likely to replicate lead soap formation attributable to reactive lead acetate in nineteenth century paintings. Soaps are likely to form quickly or even before paint application, particularly in warm, humid conditions favouring hydrolysis of ester bonds in oils. Paints pigmented with zinc oxide have high permeability to water vapour (Suryanarayana 1970), while thermal degradation favours release of saturated fatty acids (Schilling et al. 1999). Soaps formed by reaction of zinc oxide with saturated monocarboxylic acids are not connected to the paint network and may mobilise and progressively aggregate as their concentration increases. As paint oxidises and becomes more polar, the longer-chain saturated zinc carboxylates, zinc stearate and palmitate, become less compatible with the paint matrix and are most likely to form a separate phase. In this scenario there is less reason to expect depleted concentration of zinc ions in paint immediately surrounding aggregates, just as lead soaps attributable to the presence of lead acetate can explain lead soap aggregates within otherwise intact lead white paint films (Keune & Boon 2007).

Rapid saponification in Kiệm's 1963 paintings is supported by high oleic acid levels detected previously using GC-MS (MacMillan 2007). Oleic acid ordinarily oxidises early in oil film drying and it is unusual for significant levels to remain in a mature painting. However, similar findings were made in mid-20th century works with zinc white-based underlayers (Rogala et al. 2010; Maines et al. 2011). Zinc soap structures were proposed to lock-up fatty acids and limit cross-linking reactions; high residual oleic acid levels imply this occurred early. Availability of free fatty acids in Kiệm's paintings stems from extensive oil hydrolysis as indicated by FTIR. Fatty acid carboxylate chains initially attach via zinc ions at the pigment surface, forming a soap layer. This layer was found to restrict oxygen absorption in zinc oxide-containing paints (Nicholson 1940). Rapid soap formation surrounding pigment particles would limit opportunity for in-situ conversion of zinc oxide to zinc sulphate in *Portrait of my wife*.

Dissolution of zinc oxide particles

Soap formation in Kiệm's paintings is further supported by particle morphology visible in BSE images. Individual pigment particles are discernible and differences in zinc oxide distinguished between layers. Indistinct particle morphology in localised areas suggests partial dissolution of zinc oxide associated with soap formation.

White paint adjacent to preparatory layers in *Staring out game* contains large particles of lead white mixed with small particles of zinc oxide; the latter have almost disappeared from the lower margin of this layer, while lead white remains intact (**Figure 8**). This occurs adjacent to an unpigmented layer, and a similar phenomenon is apparent adjacent to the ground in *Portrait of a student*. In *Children playing at the beach* size or unpigmented layers are present between zinc oxide-based paint and lithopone-based retouching and ground layers. In these instances pigment dissolution is visible in zinc oxide-based layers while lithopone remains intact (**Figure 9**). Elemental mapping also indicates zinc is present in the unpigmented layer, suggesting localised formation and migration of zinc soaps.
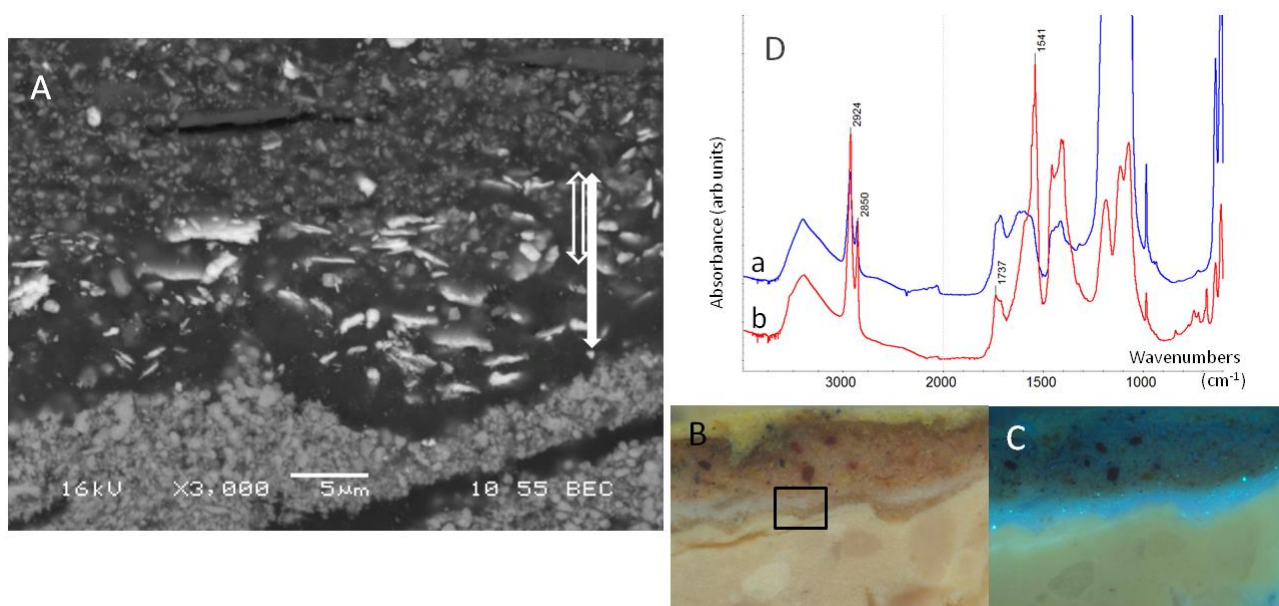
Figure 8 *Staring out game* cross-section details A: BSE and corresponding B: visible and C: UVF images. White paint above the ground (solid marker) shows intact lead white (bright plate-like particles in BSE) and zinc oxide (small grey particles). Zinc oxide is visible in the top half (open marker) but is largely absent from the lower margin. Conversion of zinc oxide to zinc stearate is suggested by transmission FTIR spectra (D) obtained from the lithopone ground: (a) spectra are dominated by $BaSO_4$ with small, broad carboxylate absorption and (b) strong Zn stearate signal (1541 cm^{-1}) likely derives from saponification in the layer above

SEM-EDX and FTIR of ground layers are consistent across Kiệm's later paintings. Barium sulphate in lithopone dominates IR spectra, and there are modest ester carbonyl peaks and broad metal carboxylate absorption. Some FTIR spectra from a ground sample in *Staring out game* include additional features from lead white. Lead derives from adjacent paint and a strong zinc stearate signal in this spectrum but not others suggests the soap also derives from above (Figure 8D). Reduced definition of zinc oxide particles in BSE images, depleted zinc counts in elemental maps

and the strong zinc stearate signal in specific FTIR spectra all support the premise that zinc stearate concentration is high adjacent to unpigmented layers. Unpigmented layers in Kiệm's paintings are a potential source of fatty acids or, in the case of hygroscopic glue size, a source of water contributing to oil hydrolysis, increasing opportunities for zinc soap formation. Apparent dissolution of zinc oxide in adjacent layers is evident with finer particle size zinc white and larger particle size zinc white mixed with lead white; it occurs whether unpigmented layers are above or below zinc oxide-containing paint. Proximity to a fatty acid source appears more critical than layer sequence, pigment combination or zinc oxide particle size.
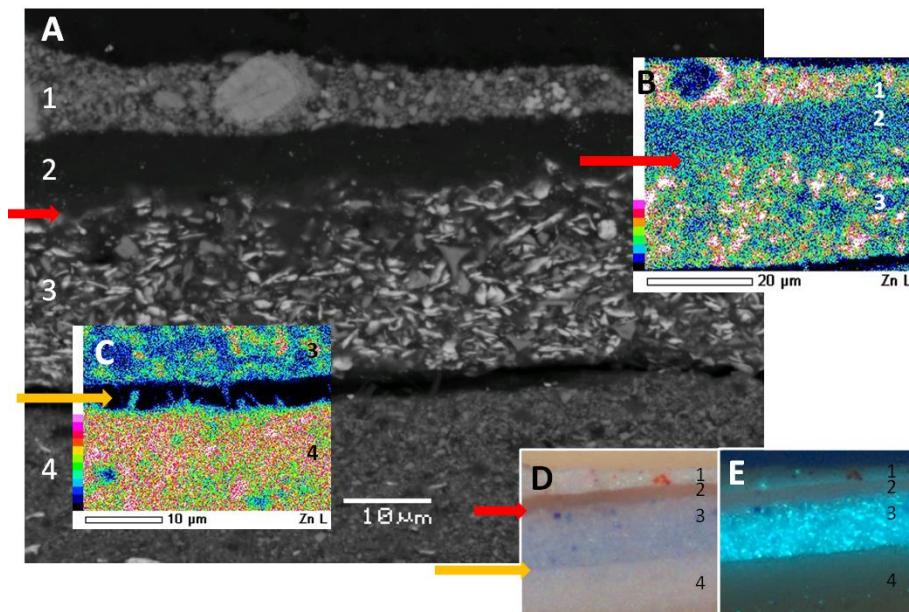
Figure 9 *Children playing at the beach* cross-section details A: BSE image with overlaid elemental distribution maps for zinc (B and C) and corresponding visible (D) and UVF(E) images. Lithopone-based retouching (1) is above a size or medium rich layer (2); the top of layer 3 (lead white and zinc oxide) shows visible pigment dissolution (red arrow), while zinc sulphide-containing lithopone above remains intact. Layer 2 appears unpigmented but zinc is detected with elemental mapping (B), possibly deriving from saponification in layer 3. Zinc is associated with low electron density features (C) bridging layers 3 and 4 (yellow arrow), suggesting zinc soaps at the interface; the layers have separated under vacuum in the SEM

The tendency for zinc white-based paints and Kiệm's paintings to crack and flake may be linked to soap formation. All the paintings in this study have required consolidation, and individual paint samples were susceptible to cracking during SEM. Elemental maps detect zinc in features bridging two separated zinc white-containing layers (Figure 9C). These features have low electron density and morphology which distinguishes them from zinc oxide pigment, and may reflect zinc soaps at the interface. Zinc stearate and palmitate have long, straight hydrocarbon chains which are not readily accommodated within oxidised paint. For this reason these soaps have a tendency to phase separate and potentially concentrate at interfaces as demonstrated for paint films cast on PET film (Maor and Murray 2008; Osmond et al. 2012). Accumulation of zinc soaps between layers may contribute to instability. Kiệm's paintings, furthermore, have layers which crack internally (**Figure 10**). BSE images and EDX analysis show cracks in regions with relatively low electron density, high carbon concentration and indistinct particle morphology consistent with localised zinc soap formation; reduced cohesive strength evident in affected paint supports the hypothesis that zinc soap structures limit cross-linking reactions resulting in brittle paint (Rogala et al. 2010).
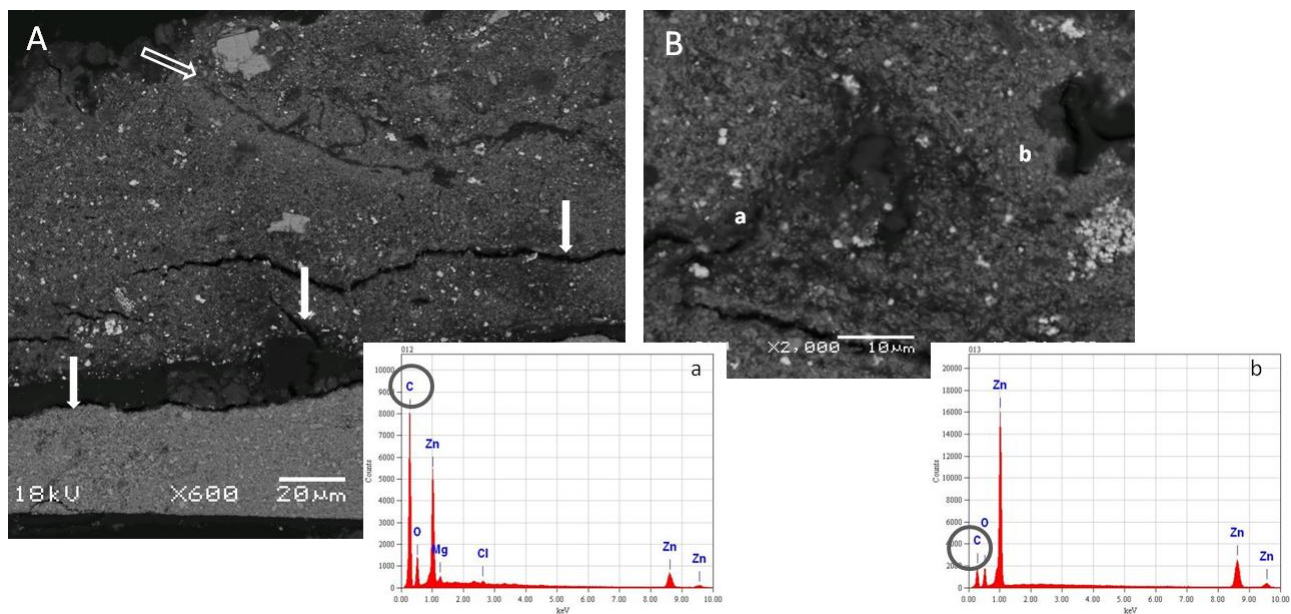
Figure 10. *Hàng Giấy* BSE cross-section image details A: cracks in the lower margin and at interface with ground (solid markers) have opened under vacuum in the SEM. By contrast, the top crack (open arrow) is pre-existing. At higher magnification (B), darker regions of lower electron density and indistinct particle morphology near cracks (a) have higher carbon counts in EDX spectra compared to surrounding paint (b) suggesting localised zinc soap formation and reduced cohesive strength

Conclusion

Paint samples from five paintings by Nguyễn Trọng Kiệm allow investigation of a variety of deterioration mechanisms occurring in zinc oxide-based paint layers. The paintings have been exposed to warm, humid conditions which have inevitably accelerated deterioration, and significant chemical and structural deterioration is evident even in more recent works.

However, the presence of unusual large zinc and sulphur containing masses in *Portrait of my wife* appears atypical for Kiệm's paintings. The painting's experimental nature and strong correlation of zinc and sulphur in layers uniquely used to achieve impasto make it plausible that sulphur compounds were present in pigment stock prior to paint mixing. Supporting evidence includes shared history with a second work produced the same year without impasto which is not affected, and indications of SO_2 exposure in other paintings without comparable deterioration. Furthermore, new data suggests morphologically distinct features in samples from the painting may reflect formation of layered basic zinc salts incorporating carboxylate, carbonate and sulphate species, a hypothesis requiring further investigation.

The condition of more recent paintings by Kiệm appears influenced by his incorporation of unpigmented layers. Whether as a direct source of fatty acids or as hygroscopic layers facilitating hydrolysis of proximate oil media, adjacent zinc oxide pigment has frequently reacted away. Formation of zinc soaps is suggested by the analytical data, with structural consequences apparent.

Zinc oxide is unquestionably a reactive pigment and formation of sulphates and carbonates during production or in dry pigment stocks, in addition to rapid soap formation with fatty acids in oil-based media all have implications for the current condition of these paintings.

Experimental

Cross-section preparation

Samples were embedded in polyester resin (Volksglas, MEKP), microtomed to expose a cross-section and polished with Micro- Mesh™ (12000 grit) where required.

Optical Microscopy (OM)

Leica DMLP microscope with N plan objectives; EL6000 light source with mercury short arc reflector lamp and Leica 'A' filter (excitation range BP 340-380, suppression BP 425) for UVF.

Fourier Transform Infrared Spectroscopy (FTIR)

Nicolet 5700 FTIR spectrometer and Continuum microscope. Paint scrapings flattened using a stainless steel roller on a diamond window for analysis in transmission mode. Data collected using Omnic 7 software over wavenumber range 4000-600 cm^{-1}. Spectra are the sum of 64 scans at 4 cm^{-1} resolution, shown in absorbance units.

Synchrotron Fourier Transform Infrared Microspectroscopy (SR-μFTIR)

Infrared Microspectroscopy beamline, Australian Synchrotron: Bruker Hyperion 2000 microscope with 250 μm tip germanium ATR crystal and LN2-cooled narrow-band MCT detector coupled to Vertex V80v FTIR spectrometer. Cross-sections analysed following custom defined grid points using 20x20 μm apertures and 10 μm steps corresponding to 5x5 μm aperture and 2.5 μm steps on the sample. Spectra are the sum of 32 scans at 4 cm^{-1} resolution over wavenumber range 3800-750 cm^{-1}. Chemical maps show absorbance intensity as a function of an integrated area under a spectral band defined by the two frequency points after subtraction of the local baseline defined by the same two points.

Scanning Electron Microscopy (SEM)

Samples carbon coated with JEOL JEE-4X vacuum evaporator. Imaging and EDX analysis using JEOL JSM-6460 LA thermionic emission SEM. EDX spectrometer with SiLi crystal, approximate resolution 130 eV, polymer light element windows and matrix correction software (JEOL Analysis Station V3.8). Samples examined in high vacuum mode at 16 or 18 kV accelerating voltage. BSE images captured. EDX acquired in spot mode or full spectrum x-ray mapping of larger regions.

X-ray Microdiffraction (μXRD)

Bruker General Area Diffraction Detector System, utilising CuKα radiation from a conventional long fine focus tube operating at 40mA, 40kV. Emergent beam focussed with crossed mirror optics to a parallel high-brilliance source, directed through collimating pinholes to the sample surface. Bruker "Hi-Star" area detector enabled sampling of a segment of approximately 40 degrees of the diffracted Debye cones. Measurements made using a collimated beam of 100 μm diameter. Variable counting times up to 2400 seconds for each recorded spot. Two linear maps along the length of the sample measured 18 patterns at 50 μm spacings giving an overlap of 50 μm. Crystalline phases identified using Bruker EVA software with ICDD Powder Diffraction File database.

Acknowledgements

References

Brown, HE 1957, *Zinc oxide rediscovered*. New York: New Jersey Zinc Company.

Bùi Quang Ánh 2012, [Notes from interview between Bettina Ebert and Bùi Quang Ánh, HCMC, May 2012].

Casadio, F, Xie, S, Rukes, S, Myers, B, Gray, K, Warta, R, et al. 2011, 'Electron energy loss spectroscopy elucidates the elusive darkening of zinc potassium chromate in Georges Seurat's 'A Sunday on La Grande Jatte-1884". *Analytical and Bioanalytical Chemistry* vol. 399(9), pp. 2909-2920.

Ebert, B 2008, *Volume II: A scientific investigation into the degradation processes of zinc-based paints*. MA thesis, Northumbria University, Newcastle.

Ebert, B, MacMillan Armstrong, S, Singer, B, & Grimaldi, N. 2011. 'Analysis and conservation treatment of Vietnamese paintings'. *Preprints of the ICOM Committee for Conservation 16th Triennial Meeting*, Lisbon.

Hay, D. (2012). *XRD microdiffraction study of paint flake for University of Queensland and Queensland Art Gallery Conservation, 29 August 2012*. Melbourne: CSIRO Materials Science and Technology.

Helwig, K, Corbeil, MC, Moffatt, E, & Poulin, J. 2013. 'Using analysis to shed light on conservation issues in 20th century Canadian oil paintings'. *Issues in contemporary oil paint*, 28-29 March 2013, Amersfoort, The Netherlands, pp.79-80.

Higgitt, C, Spring, M, & Saunders, D 2003, 'Pigment-medium interactions in oil paint films containing red lead or lead-tin yellow'. *National Gallery Technical Bulletin* vol. 24, pp. 75-95.

Hofmeister, W, & Platen, HV 1992, 'Crystal Chemistry and Atomic Order in Brucite-related Double-layer Structures'. *Crystallography Reviews* vol. 3(1), pp. 3-26.

Inoue, S, & Fujihara, S 2011, 'Liquid−Liquid Biphasic Synthesis of Layered Zinc Hydroxides Intercalated with Long-Chain Carboxylate Ions and Their Conversion into ZnO Nanostructures'. *Inorganic Chemistry* vol. 50(8), pp. 3605-3612.

Keune, K 2005, *Binding medium, pigments and metal soaps characterised and localised in paint cross-sections*. PhD thesis, University of Amsterdam, Amsterdam.

Keune, K, & Boon, JJ 2007, 'Analytical imaging studies of cross-sections of paintings affected by lead soap aggregate formation'. *Studies in Conservation* vol. 52(3), pp. 161-176.

MacMillan, S 2007, *A report on two paintings on canvas by Vietnamese artist Nguyen Trong Kiem (1933-1991) dated 1963*. MA thesis, Northumbria University, Newcastle.

Maines, CA, Rogala, D, Lake, S, & Mecklenburg, MF 2011, 'Deterioration in Abstract Expressionist paintings: analysis of zinc oxide paint layers in works from the collection of the Hirshhorn Museum and Sculpture Garden, Smithsonian Institution'. *MRS Symposia Proceedings* vol. 1319, pp. 275-284.

Maor, Y, & Murray, A. (2008). 'Delamination of Oil Paints on Acrylic Grounds'. *MRS Symposia Proceedings* vol. 1047, pp. 127-136.

Morley-Smith, CT 1950, 'The development of anti-chalking French Process zinc oxides'. *Journal of the Oil & Colour Chemists' Association* vol. 33, pp. 484-501.

Nguyễn Trần Minh, & Trần Thị Minh Man 2008, [Interview transcript with Nguyễn Trọng Kiệm's family included as Appendix 1 in MacMillan 2007].

Nicholson, DG 1940, 'Drying of Linseed Oil Paint Effect of Acidity upon Rate of Oxygen Absorption'. *Industrial & Engineering Chemistry* vol. 32(9), pp. 1259-1261

Noble, P, & Boon, JJ. 2007, 'Metal soap degradation of oil paintings: aggregates, increased transparency and efflorescence'. *AIC Paintings Specialty Group Postprints* vol. 19, pp. 1-15

Osmond, G, Boon, JJ, Puskar, L, & Drennan, J 2012, 'Metal stearate distributions in modern artists' oil paints: surface and cross-sectional investigation of reference paint films using conventional and synchrotron infrared microspectroscopy'. *Applied Spectroscopy* vol. 66(10), pp. 1136-1144.

Rogala, D, Lake, S, Maines, C, & Mecklenburg, M 2010, 'Condition problems related to zinc oxide underlayers: examination of selected Abstract Expressionist paintings from the collection of the Hirschhorn Museum and Sculpture Garden, Smithsonian Institution'. *Journal of the American Institute for Conservation* vol. 49(2), pp. 96-113.

Schilling, MR, Carson, DM, & Khanjian, H, P. (1999). 'Gas chromatographic determination of the fatty acid and glycerol content of lipids. IV. Evaporation of fatty acids and the formation of ghost images by framed oil paintings'. *Preprints of the ICOM Committee for Conservation 12th Triennial Meeting,* pp. 242-247.

Singer, B, MacMillan, S, Grimaldi, N, & Brown, J 2009, 'Analysis of Vietnamese oil paintings affected by sulphur dioxide pollution'. In S Lee & NN Huy (Eds.), *Essays on Modern and Contemporary Vietnamese Art*, Singapore: Singapore Art Museum, pp. 68-74.

Suryanarayana, NP 1970, 'Critical pigment volume concentration of some oxide pigments'. *Journal of the Colour Society* vol. 9(2), pp. 2-6.

5.4 Supplementary information

Table images from published work are reproduced in larger format for clarity with additional figures and text as supporting information.

5.4.1 *Portrait of my wife* 1963

Portrait of my wife (Figure 5.1), painted in 1963, is the painting most discussed and referred to in publications arising from investigations undertaken at University of Northumbria and continued in the present research.
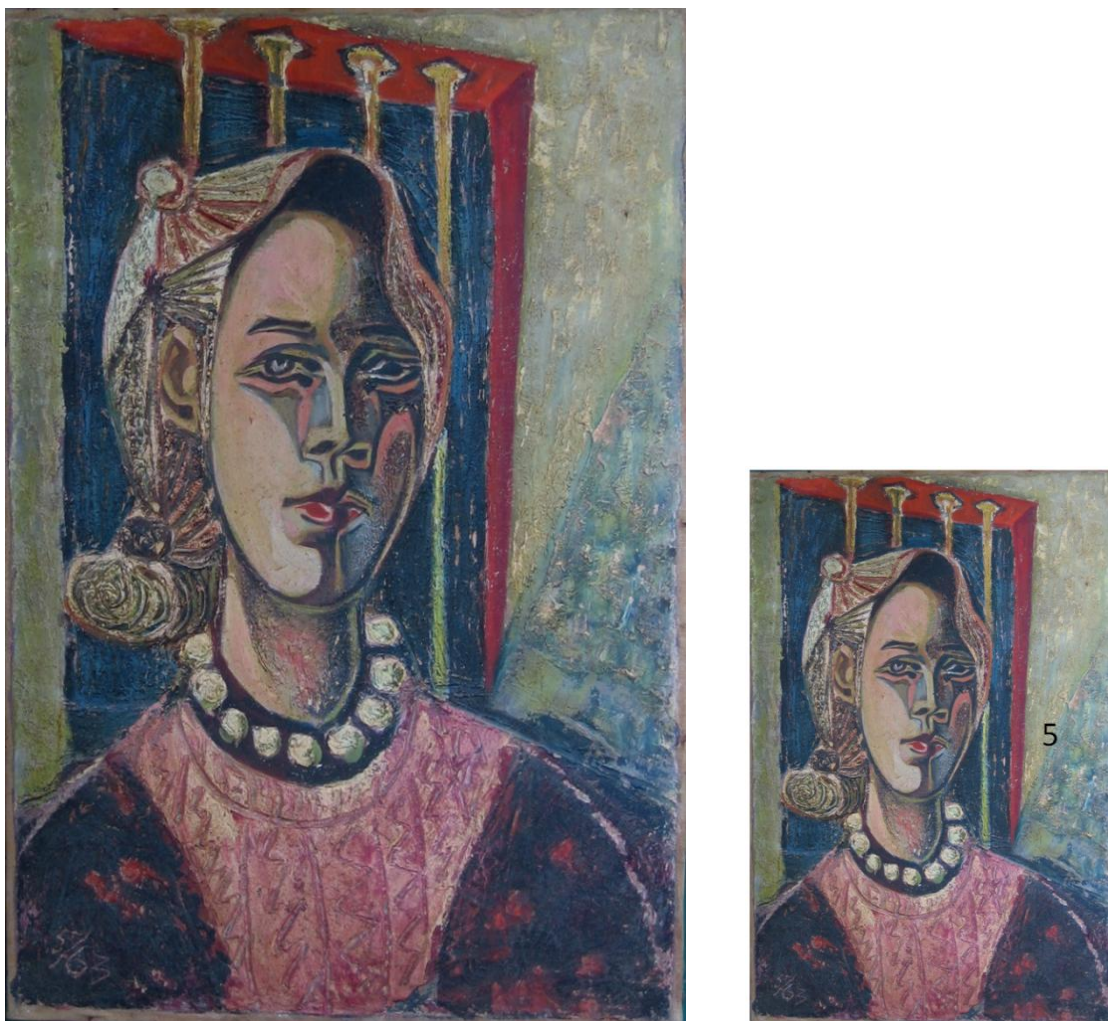
Figure 5.1 Nguyễn Trọng Kiệm, *Portrait of my wife* **1963, oil on canvas, 57 x 38 cm. Witness Collection. The source location of sample #5 is indicated in the small offset image**

A number of paint samples were obtained in the course of previous work (MacMillan 2007) but were not embedded or investigated at that time, and were kindly made available for the present study. Sample #5 derives from the background of the painting at centre right and is shown in cross-section in Figure 5.2. The sample comprises broken fragments of pale green and dark blue-green paint over an underlying layer of pinkish impasto.
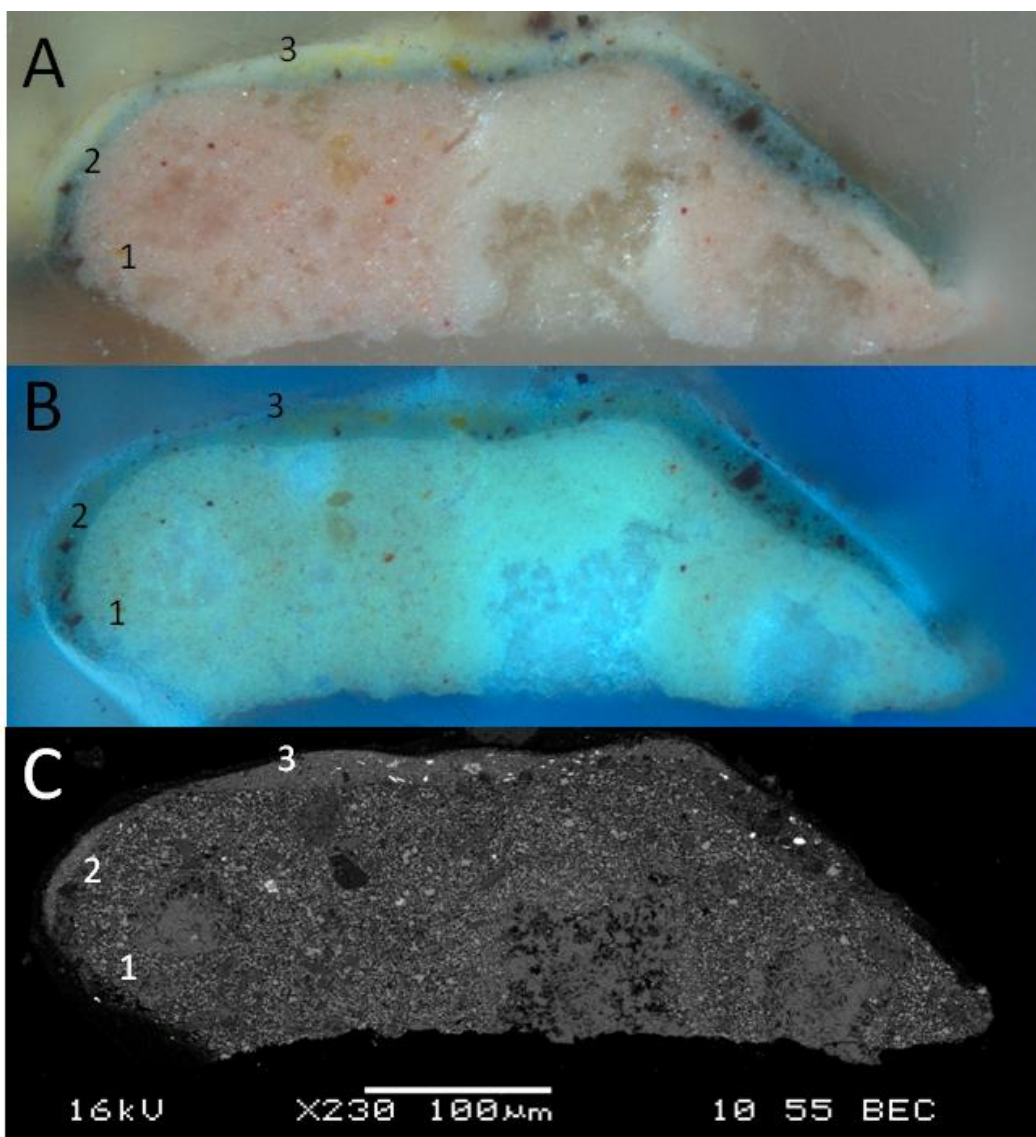
Figure 5.2 *Portrait of my wife* **1963 sample #5 cross-section optical images (A) visible and (B) UVF, and (C) corresponding BSE image. Numbers correspond to layers described in the text**

Surface paint layers and impasto separated from underlying layers on sampling, so the cross-section does not include the ground. Layer 1 is pink and white paint based on coarse particle size zinc oxide; red pigment has not been characterised. Layer 2 comprises a thin blue zinc oxide-based paint (fine particle size) with Prussian blue and traces of lead; large brown particles have not been characterised but spot SEM-EDX produces generally low counts with zinc and carbon present alongside various trace elements. Layer 3 is a thin pale zinc oxide-based paint (fine particle size) with cadmium sulfide yellow. The distinctive zinc and sulfur containing masses discussed in published work occur in layer 1. A higher magnification detail from this layer is shown in Figure 5.3.
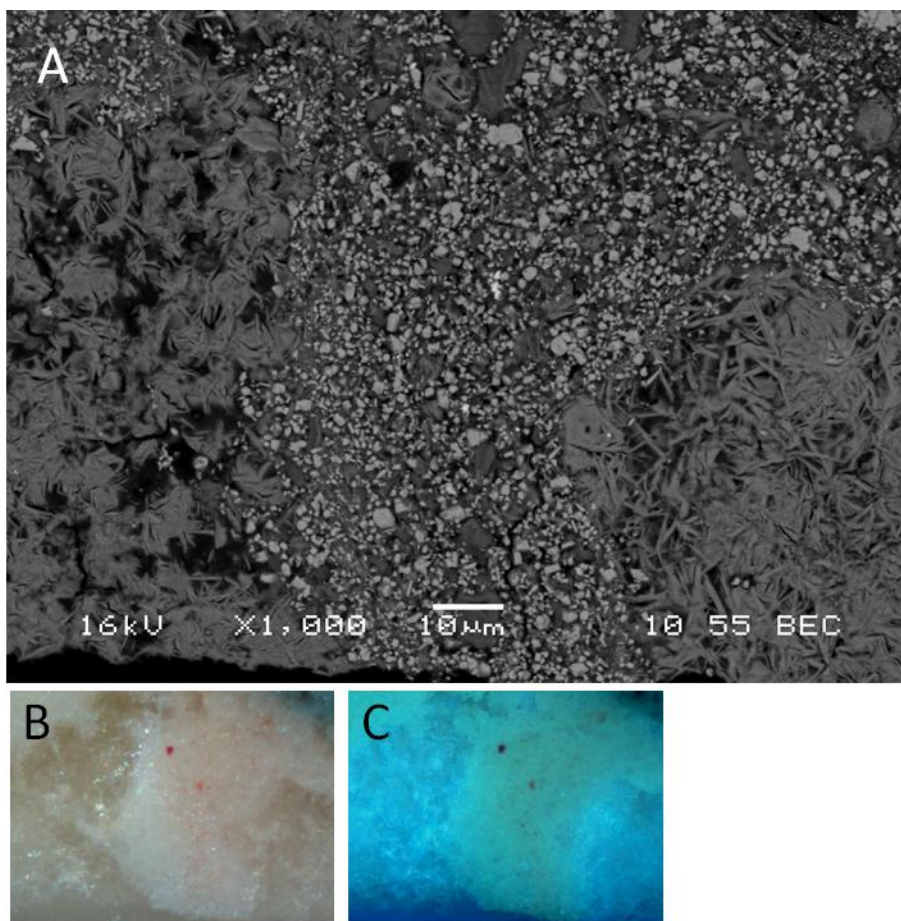
Figure 5.3 *Portrait of my wife* **#5 cross-section image detail from the right half of layer 1 detailing the boundary between pink and white paint (A) BSE and corresponding optical images (B) visible and (C) UVF**

Both pink and white regions of layer 1 can be seen from the BSE image to comprise a mixture of bright zinc oxide particles and mid-density grey particles. Particles are more closely packed in white paint, while pink paint appears to have a higher incidence of larger grey particles. The 'fibrous' structure of the large zinc and sulfur containing masses is more tufted in white paint and with more open space than occurs in the comparable feature located within pink paint, possibly coinciding with increased transparency in the optical image. It is not clear whether compression or deformation of paint surrounding the masses has occurred as might be expected with *in situ* growth, although visible lumps are known to be present on the painting surface.

Elemental maps of a detail at the top left end of the cross-section are shown in Figure 5.4. SEM-EDX elemental maps show the clear association of sulfur with the morphologically distinctive feature located at bottom right of the cross-section detail (in addition to being present in small particles of cadmium sulfide yellow). Carbon concentration is low through the centre of the large mass but increases towards the perimeter where the apparently crystalline network is more open. Another mass contained within this sample is detailed in Figure 5.5.
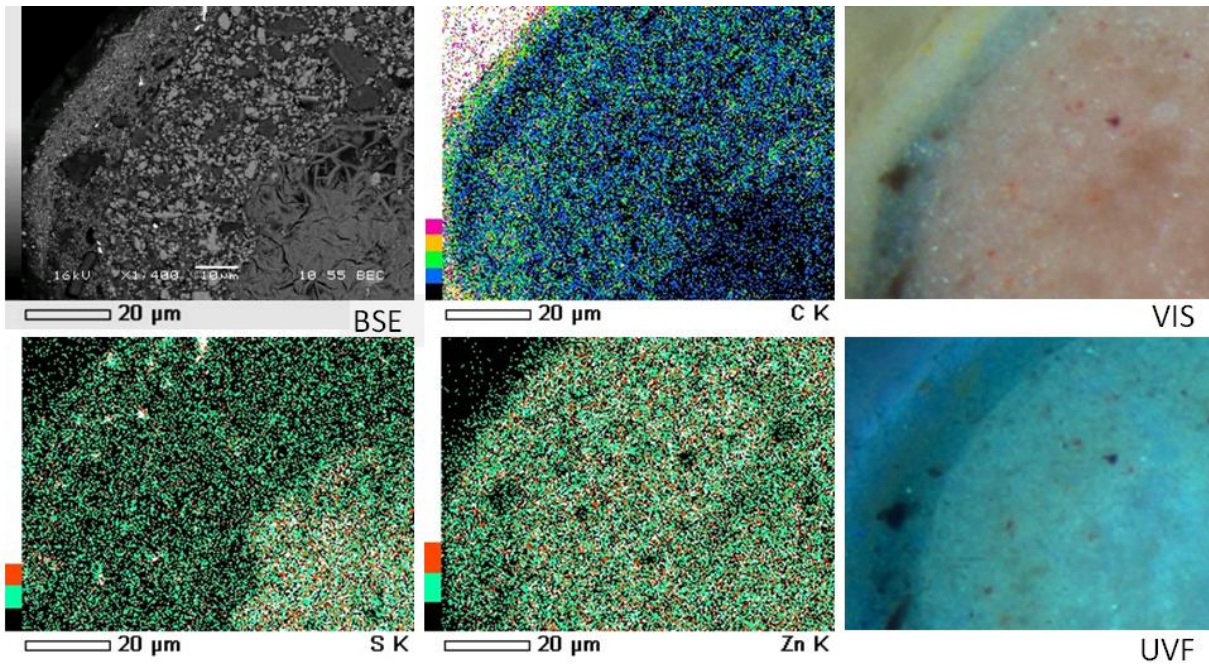
Figure 5.4 *Portrait of my wife* **#5 cross-section image detail and corresponding SEM-EDX maps for carbon, sulfur and zinc showing a clear association of sulfur with the morphologically distinctive feature at bottom right**
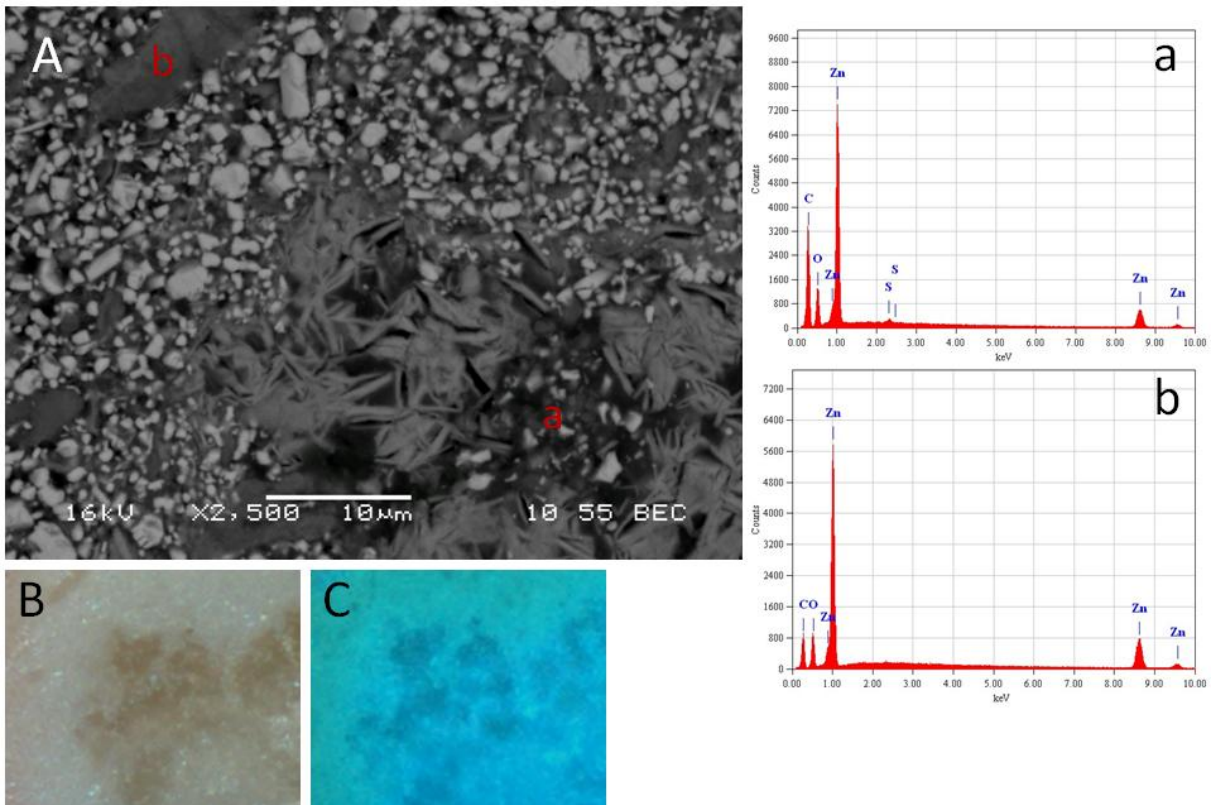
Figure 5.5 *Portrait of my wife* **#5 cross-section image detail from the top of the large mass located at the centre of layer 1 (A) BSE and corresponding optical images (B) visible and (C) UVF and SEM-EDX spectra obtained from the points designated (a and b)**

194

The sulfur-containing mass appears as an assemblage of tufted elongated particles. In the surrounding paint, coarse, irregularly sized particles of zinc oxide are the brightest and most prevalent component evident in the BSE image, interspersed with similar grey particles of lower atomic density. An SEM-EDX spectrum obtained from an unusually large grey particle indicates it comprises only zinc, oxygen and carbon. A pigmented region (a) within the periphery of the distinctive sulfur containing mass has similar elemental composition but with lower counts, a higher proportion of carbon and a trace of sulfur. This is consistent with the lower density of bright zinc oxide pigment particles in this area relative to the surrounding paint, and the reduced definition of smaller particles. The increased transparency evident in optical images supports the possibility that this may reflect partial saponification of zinc oxide pigment (Noble et al. 2005).

The elemental and morphological distinction between zinc-based components in the paint is illustrated at higher magnification in Figure 5.6.
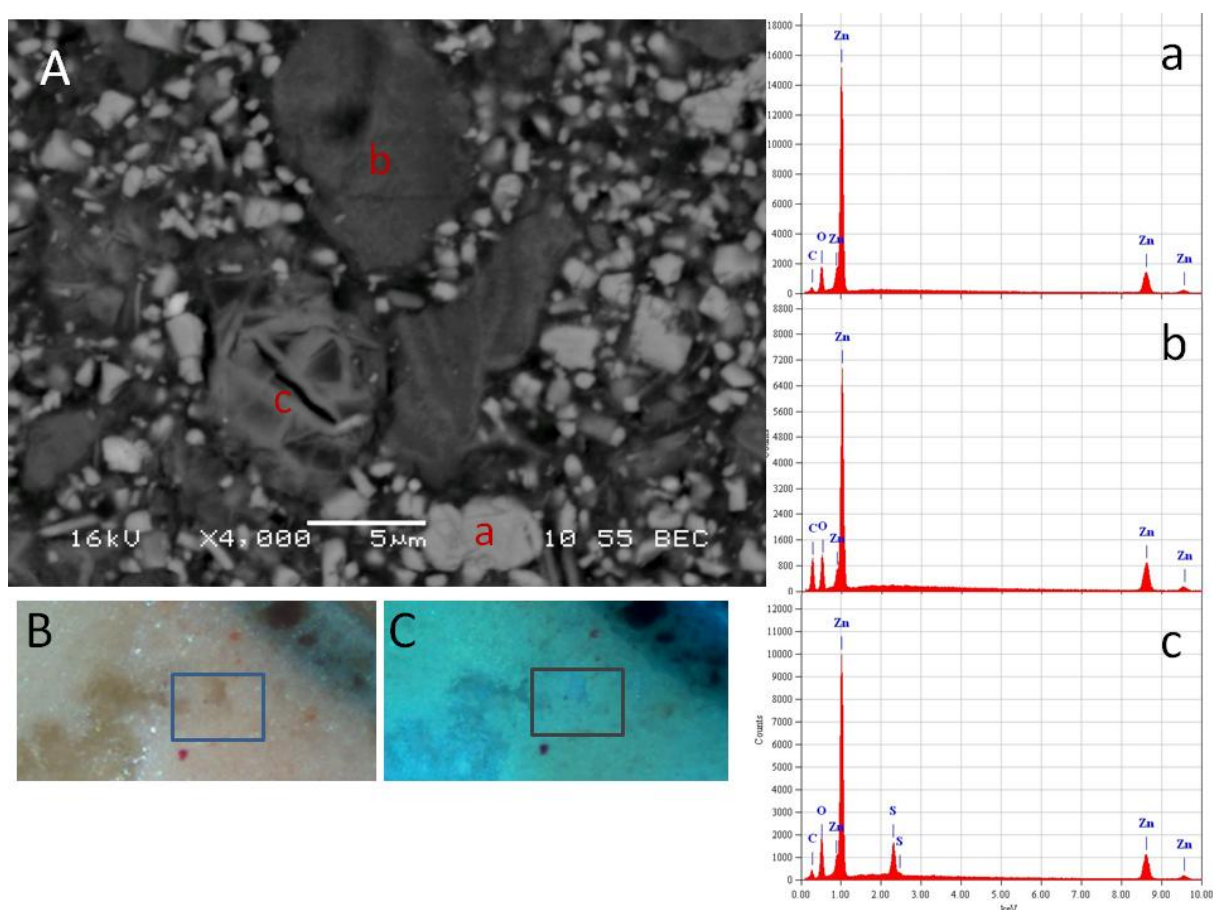
Figure 5.6 *Portrait of my wife* **#5 cross-section image detail from layer 1 (A) BSE and optical images (B) visible and (C) UVF with the box detailing the area captured by the BSE image, and SEM-EDX spectra obtained from the points designated (a-c)**

SEM-EDX spectra from spots indicated in the BSE image in Figure 5.6 compare measurements obtained from three white or translucent particles representing (a) zinc oxide pigment, (b) lower BSE density zinc-based compound and (c) a zinc/sulfur compound. The presence of basic zinc carbonate in Kiệm's paintings and the predisposition for its formation in zinc oxide pigment stock is discussed in published work. It remains to be confirmed whether the mid-density particles present in the paint layer reflect the presence of zinc hydroxide or basic zinc carbonate. FTIR spectra with hydroxide and carbonate features obtained from the painting using both conventional and synchrotron based instrumentation are shown in Figure 5.7.
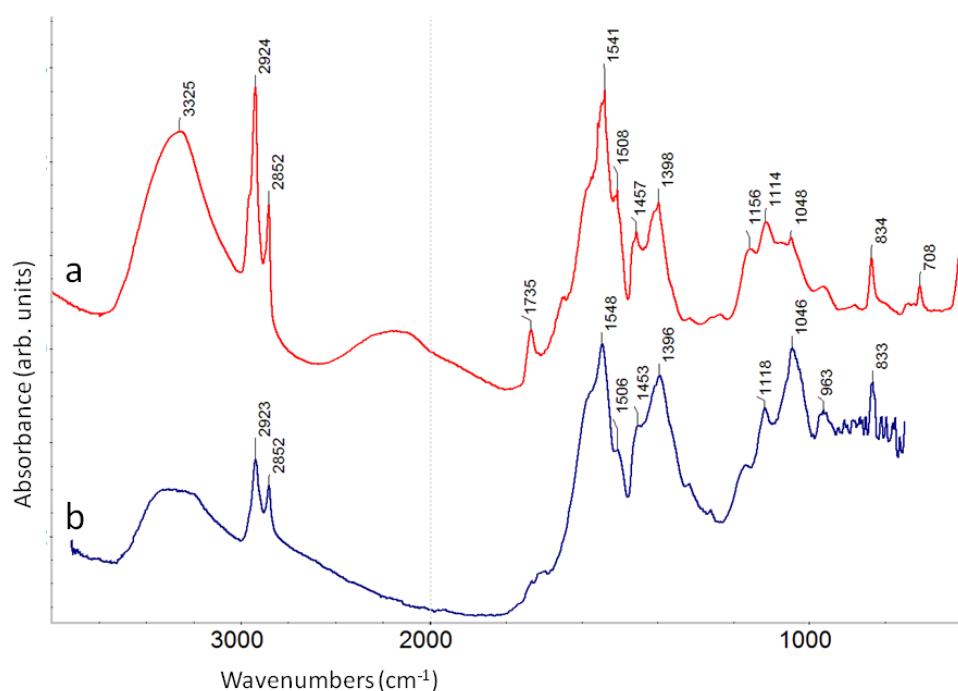
Figure 5.7 *Portrait of my wife* **#5 spectra obtained via (a) conventional FTIR microscopy from a scraping rolled onto a diamond window and measured in transmission mode prior to embedding of the sample and (b) ATR SR-µFTIR from the embedded sample on the polished cross-section surface**

The conventional FTIR instrument measures absorption through a relatively large aperture (100 x 100 µm) and consequently its spectrum may incorporate features reflecting a range of constituents. In comparison the synchrotron source spectrum derives from a 5x5 µm spot on the cross-section surface. SR-µFTIR therefore has greater potential to laterally resolve spectral variation across the analysis area, and features emphasised within individual spectra may assist in discriminating components in complex formulations. The SR-µFTIR spectrum illustrated in Figure 5.7 was selected for its resemblance to the conventionally obtained spectrum and because it does not emphasise unusual components evident in many other extracted spectra, which will be discussed later. Both featured spectra include strong underlying contribution from basic zinc carbonate (3325,

1508, 1380, 1048 and 834 cm^{-1}) (Jackson 1998) in addition to zinc carboxylate absorptions (v COO^{-} zinc stearate/palmitate at 1541 and 1398 cm^{-1} in the conventional spectrum) and CH absorptions at 2923, 2852 and 1457 cm^{-1}. The oil medium contributes to CH stretching and ester carbonyl absorption at 1735 cm^{-1}, broadened to lower wavenumber by the presence of fatty acids (Meilunas et al. 1990; van der Weerd et al. 2005). This peak is typically low or non-existent in most spectra from the painting suggesting a high degree of hydrolysis and likely saponification in the paint. Peaks between 950 and 1200 cm^{-1} may reflect the presence of various sulfate species, for example vibrations at 1158, 1056, and 987 cm^{-1} have been assigned to zinc oxide with adsorbed sulfate with monodentate bonding coordination (Wu et al. 2011).

Although the presence of sulfates is suggested by FTIR spectra, and elemental mapping confirms the association of zinc and sulfur within the morphologically distinctive masses, conclusive characterisation remains elusive. Spot SEM-EDX measurement obtained from a large mass in layer 1 is compared with measurement from the zinc and sulfur containing lithopone ground from another of Kiệm's paintings in Figure 5.8.
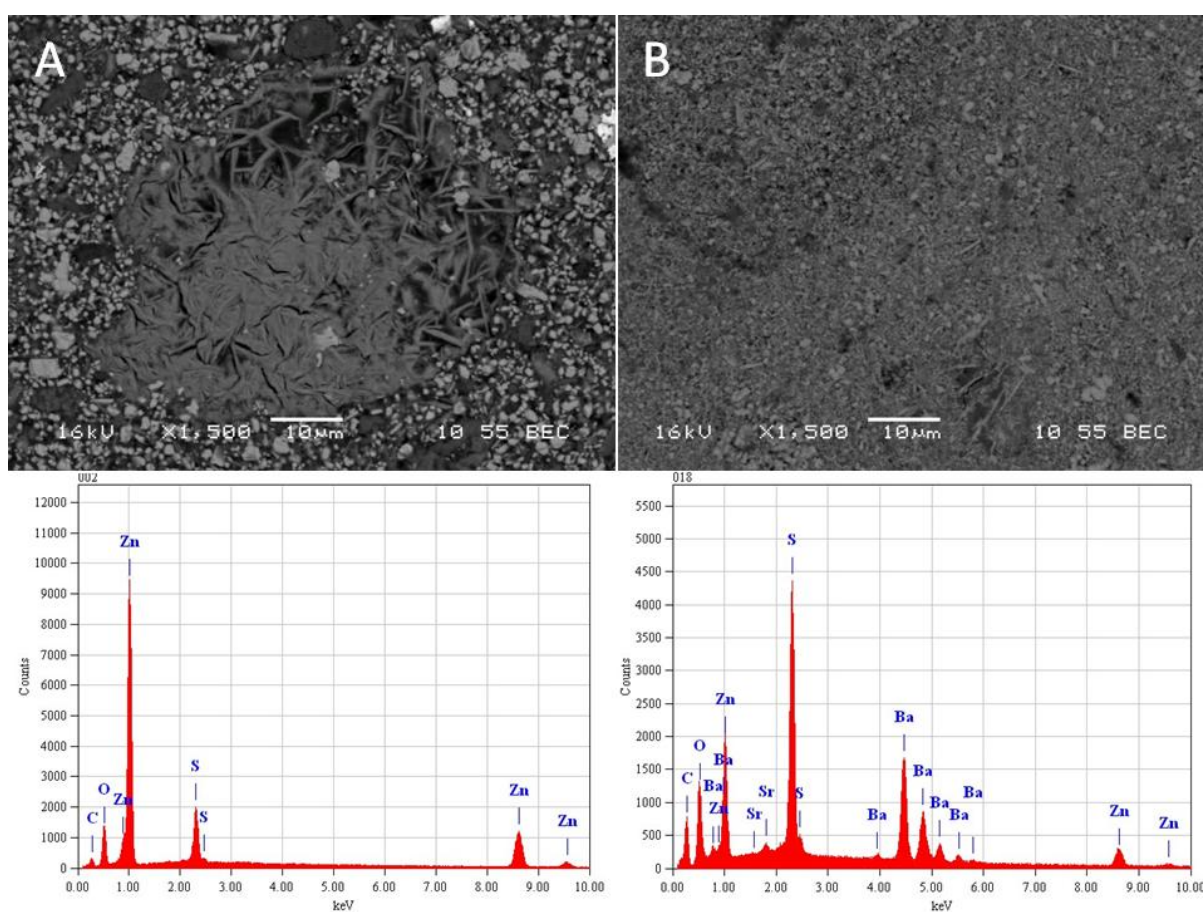
Figure 5.8 *Portrait of my wife* **#5 cross-section BSE image detail (A) and SEM-EDX spot measurement spectrum from within the distinctive apparently crystalline mass contained within layer 1.**

For comparison BSE image detail (B) and corresponding SEM-EDX spectrum derive from the lithopone ground layer in another of Kiệm's paintings (*Hàng Giấy* 1978)

The SEM-EDX spectrum obtained from the mass located in pink paint at the left end of layer 1 in *Portrait of my wife* #5 contains zinc, sulfur, oxygen and carbon only. ZAF-corrected standardless quantitative analysis suggests the atomic ratio of zinc to sulfur and oxygen approximates 10:2:5. This contrasts with a theoretical ratio of 1:1:4(+) for zinc sulfate. Even allowing for substantial error given the complex and heterogeneous nature of the sample, these indicative proportions appear inconsistent with the presence of zinc sulfate at any state of hydration. For comparison, a representative spectrum obtained from the lithopone ground of *Hàng Giấy* (1978) is also presented. Lithopone is a co-precipitated pigment comprising approximately 70% barium sulfate, 30% zinc sulfide and 1-2% zinc oxide. In this instance the matrix-corrected quantitative analysis gives results much closer to those expected for lithopone, with an atomic ratio of barium to zinc and sulfur approximating 5:4:9, approaching theoretical atomic percentages of 12:15:27 (oxygen: 47). The implication of the anomalous quantitative result is that the distinctive zinc-based masses contained with *Portrait of my wife* #5 are only partially composed from compounds with sulfur.

Various attempts were made to clarify characterisation of the large masses in the paint sample. Raman spectroscopy (near infrared diode laser at 785 nm) unexpectedly caused considerable damage to the cross-section and was not pursued. The sample was resurfaced to remove evidence of laser damage in preparation for planned SR-μFTIR. It was not possible to obtain intact thin-sections from the cross-section, so SR-μFTIR experiments were undertaken using an ATR accessory. Unfortunately, most spectra obtained were of poor quality, with poor signal to noise ratio and few useful features. Spectra from some areas were also apparently contaminated by infiltration of embedding resin. Results prevented the assembly of meaningful integrated absorption intensity maps, however it was possible to extract some well resolved individual spectra. In addition to the SR-μFTIR spectrum included in Figure 5.7, sulfates, basic zinc carbonate and zinc lactate are also suggested by characteristic absorptions in spectra reproduced in published work. Despite these examples, it has frustratingly not been possible to associate sulfates specifically with the features of interest in the cross-section.

A final attempt to more conclusively characterise the sample was made using X-ray microdiffraction. Analysis was conducted at CSIRO Materials Science and Engineering, Melbourne (Hay 2012). An indexed overlay of XRD patterns obtained from a linear scan along the length (L-R) of the cross-section is presented in Figure 5.9.
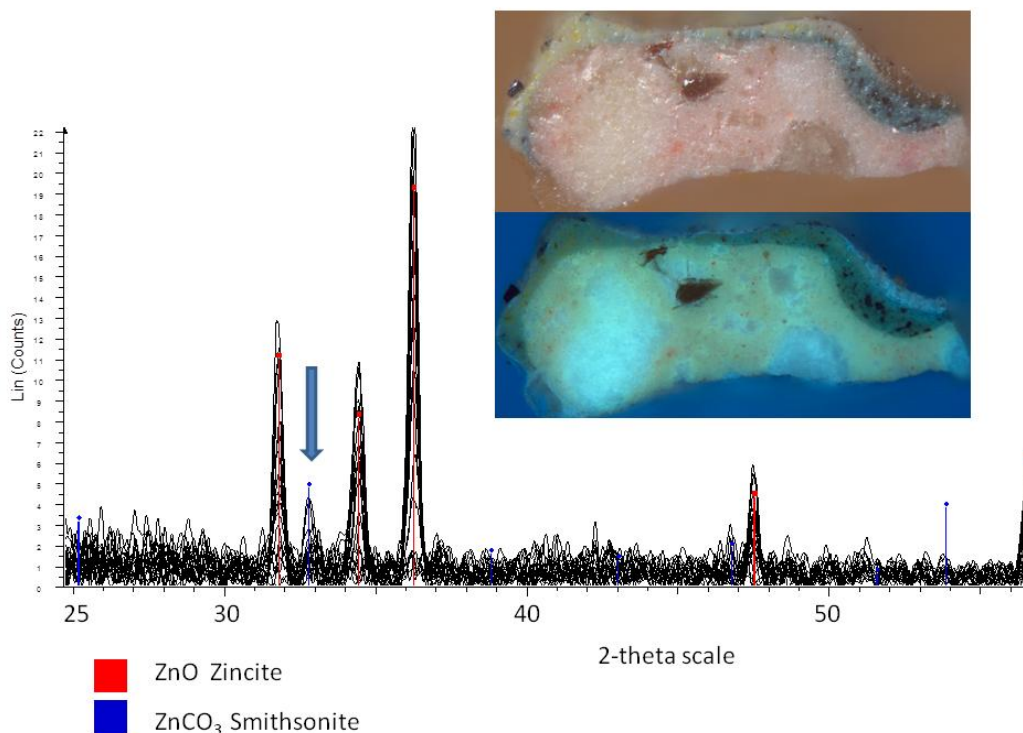
Figure 5.9 Indexed overlay of XRD patterns (2-theta range approximately 25° to 57°) from a scan along length (L-R) of *Portrait of my wife* #5 with surface presentation as shown in optical cross-section images.

Characteristic peaks for zinc oxide are present with an additional peak at 32.8° 2θ (blue arrow) of ambiguous assignment

XRD patterns from across the sample contain the characteristic peaks for zinc oxide with an additional peak at 32.8° 2θ present in some. Two linear scans obtained from upper and lower margins of the impasto layer gave similar results, suggesting the 100 micron spot size required to overcome extremely poor counting statistics did not resolve detailed differences within the distance range between the two scans, limiting potential for conclusive correlation with optical features. A peak at 32.8° 2θ is found in zinc carbonate, however, the absence of corresponding peaks makes assignment problematic. An alternative attribution is the (100) plane commonly found in layered basic zinc salts of brucite-type zinc hydroxide structure (Inoue and Fujihara 2011). Unfortunately however, as discussed in published work, it was not possible to confirm this assignment because the geometry of the XRD instrument precludes collection of diffraction data from lower angle peaks from small paint cross-sections which are the strongest diffracting planes for such structures. The presence of multifunctional zinc complexes is feasible as a consequence of zinc's d10 electron configuration capable of supporting a range of coordination modes (Zhang et al. 2013). No evidence of crystalline zinc sulphate was observed, although variation in the intensities of the diffracted zincite peaks along the length of the sample suggest that large circular masses within the impasto layer may be amorphous or composed of very small crystallites (Hay 2012).

5.4.2 *Portrait of a student* 1963

Paint samples were studied from a second painting by Kiệm from 1963, *Portrait of a student* (Figure 5.10). The condition of this work has been described previously (Ebert et al. 2011). A cross-section taken from the sitter's red dress is shown in Figure 5.11.
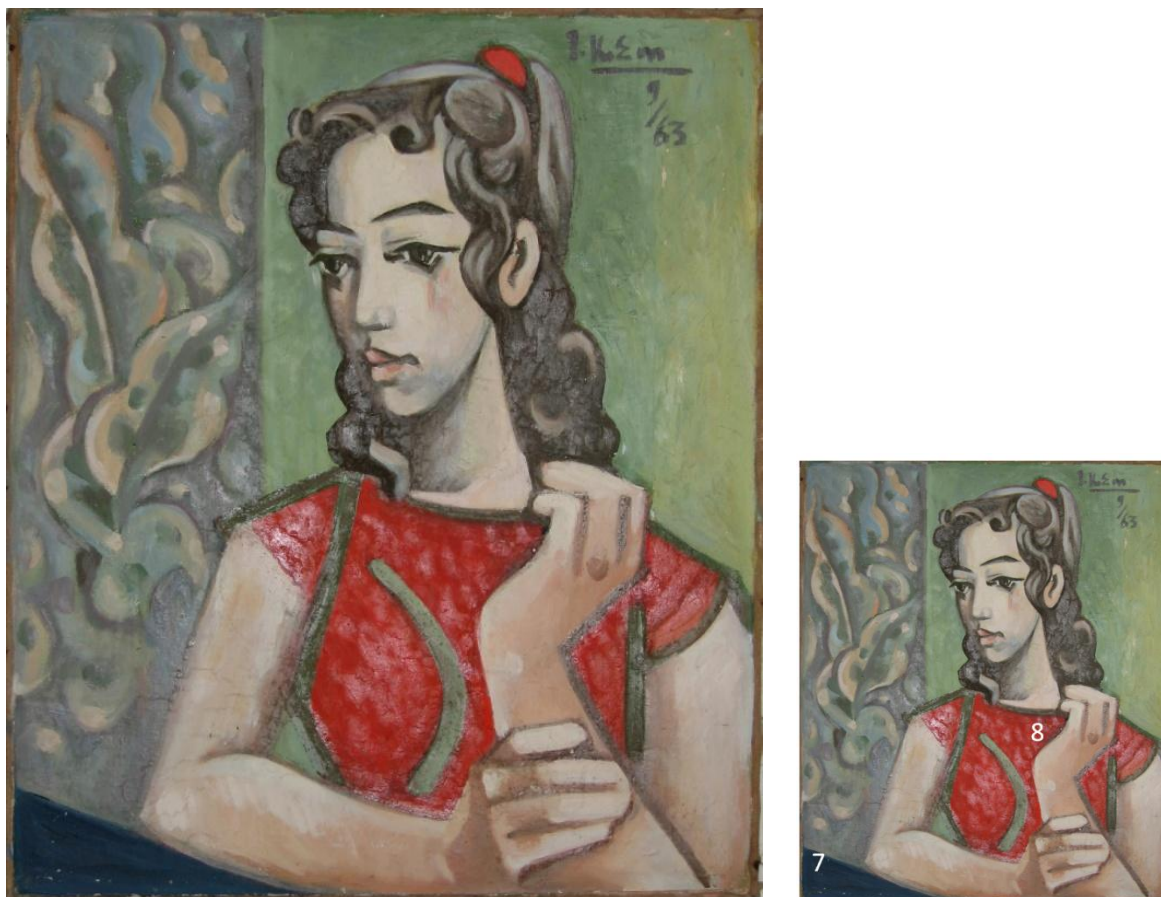
Figure 5.10 Portrait of a student 1963, oil on canvas, 53 x 45 cm. Witness Collection. The source location of samples is indicated in the small offset image

Sample #8 derives from red paint of matt appearance which had delaminated from the underlying ground. As a result, no ground is captured in the cross-section. Layer 1 includes cadmium selenium red plus barium sulfate and zinc, possibly as lithopone but also feasibly as zinc white mixed with cadmium red tube paint in which the barium sulfate exists as an extender (Burnstock et al. 2007). Layers 2-4 are zinc oxide-based with a trace of titanium white including a small unmixed area (also containing zinc) visible at the centre of the cross-section, and a variety of coloured pigmentation. Layer 5 comprises barium sulfate-based paint with cadmium selenium sulfide and iron-based reds, chrome yellow and clay filler. Layer 6 involves lithopone-based reworking applied over a thin unpigmented layer. It is unclear why the fluorescent sparkle of layer 3 is not apparent in layers 2 and 4 as the zinc oxide particles are not obviously different, as can be seen at higher magnification (Figure 5.12).
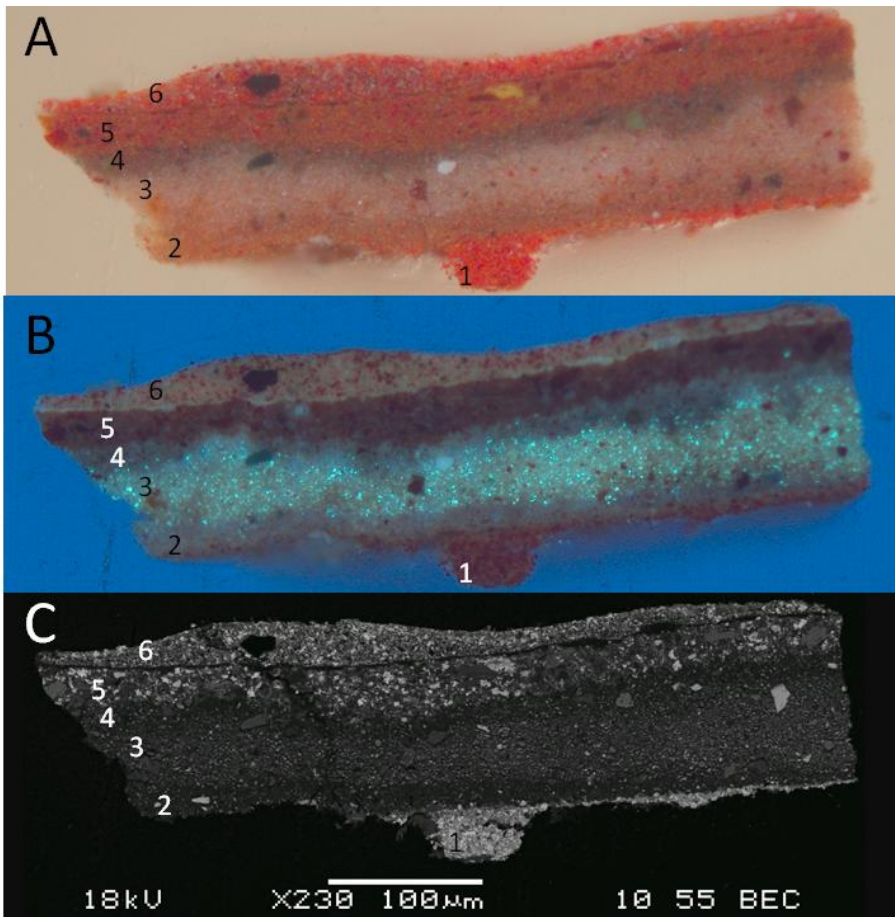
Figure 5.11 *Portrait of a student* **1963 sample #8 cross-section optical images (A) visible and (B) UVF, and (C) corresponding BSE image. Numbers correspond to layers described in the text**
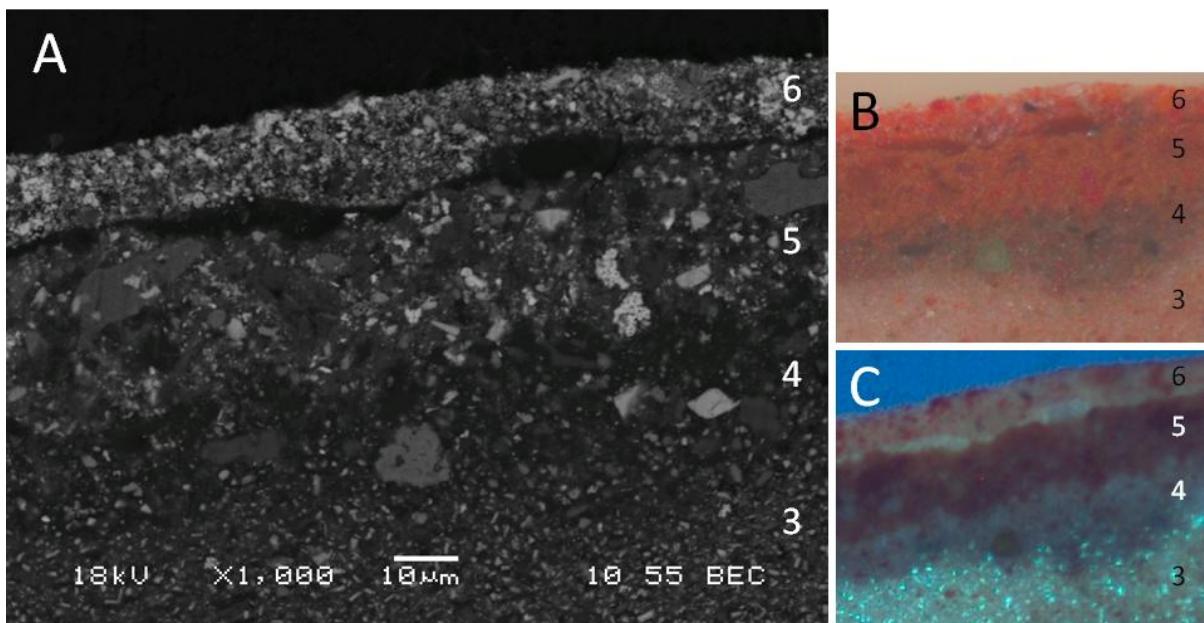
Figure 5.12 *Portrait of a student* **#8 cross-section image detail from the top of the right half of the sample (A) BSE and corresponding optical images (B) visible and (C) UVF.**

Layers 3 and 4 are both zinc oxide-based but only layer 3 exhibits the 'characteristic' UVF sparkle

In the BSE image it is apparent that layer 4 generally has greater pigment variety but lower pigment density than the more fluorescent layer beneath. Layer 4 also appears to have lower base zinc oxide particle concentration, possibly with a higher proportion of mid-density grey particles. More information is obtained through elemental maps shown in Figure 5.13.
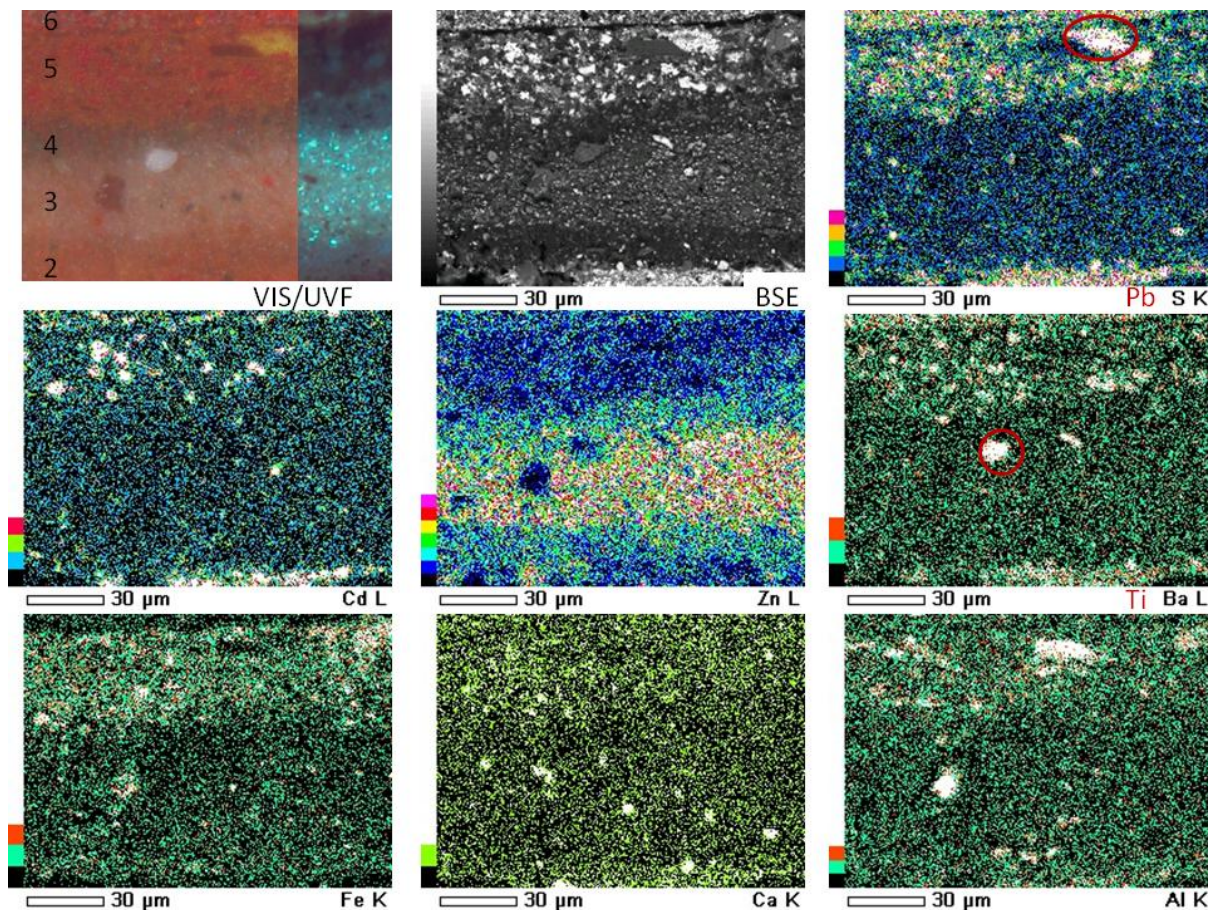
Figure 5.13 *Portrait of a student* **#8 cross-section optical and BSE image details and corresponding SEM-EDX maps for the elements shown. NB. Circled features highlight components detected by overlapping X-ray emission lines which do not reflect the intended element**

Elemental maps confirm that of the three zinc oxide-based layers (2-4), zinc counts are highest in the sparkly fluorescent paint (layer 3) but are also strong in the two adjoining brown layers which do not sparkle. Other maps indicate general pigment distribution which does not immediately assist with determining a reason for the differing fluorescence properties of the layers. A small circular region of titanium white is seen at the boundary between layers 3 and 4, detected in the Ba map because of an overlap of Ba L and Ti Kα lines. Spot SEM-EDX measurements suggest trace amounts of titanium are present in all three zinc oxide-based layers. Sulfur indicates the presence of cadmium red when cross referenced with the Cd map, as well as barium sulfate when cross referenced with the Ba map. An overlap of the S Kα X-ray line at 2.307 keV and Pb Mα line at 2.364 keV further results in the sulfur map detecting lead, notably present in chrome yellow (lead

chromate). No correlation is observed between the Zn and Ba maps in layers 2 or 5, strengthening the likelihood that barium sulfate is present in the cadmium red paint.

A second paint sample from *Portrait of a student* was investigated with the cross-section shown in Figure 5.14.
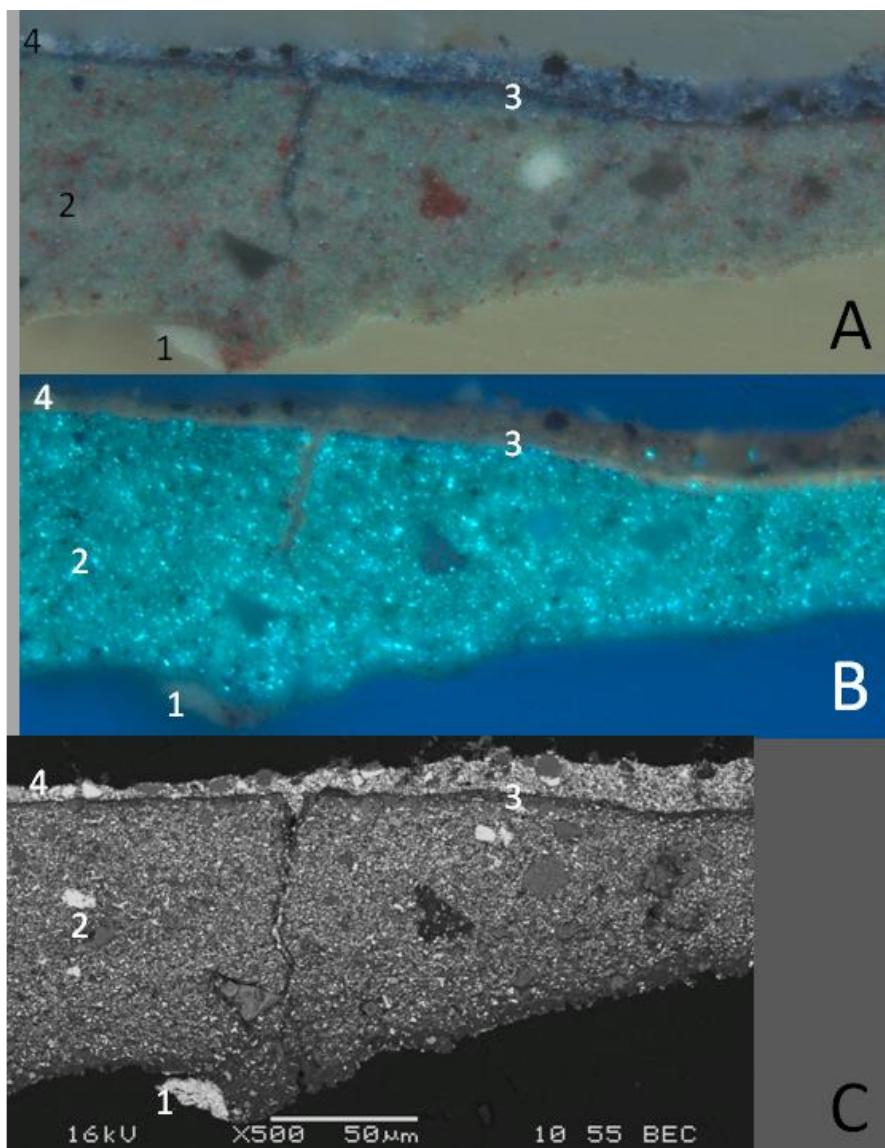
Figure 5.14 *Portrait of a student* **#7 cross-section images from blue paint, optical images (A) visible and (B) UVF, and (C) corresponding BSE image. Numbers correspond to layers described in the text**

Sample #7 derives from dark blue paint at the bottom left corner of the painting (Figure 5.10). It is dominated by an underlying layer of grey paint with strong UVF sparkle. A trace of the lithopone ground layer (1) is captured in the cross-section although the paint more generally separated from the ground at the time of sampling. Layer 2 is zinc oxide-based paint with complex pigmentation

including chalk based particles, iron-based red and a small area of unmixed titanium white which also contains zinc oxide, similar to that seen in the previous sample (#8). Layer 3 is a thin layer of zinc-based paint with a sodium aluminium silicate blue. Blue layer 4 comprises lithopone based reworking which has penetrated a crack in the original paint layers. Both blue layers have a similar orange autofluorescence, suggesting the blue pigment may be sodalite rather than ultramarine (Miser and Glass 1941). The interface between lithopone ground and paint layer 2 is detailed in Figures 5.15 and 5.16.
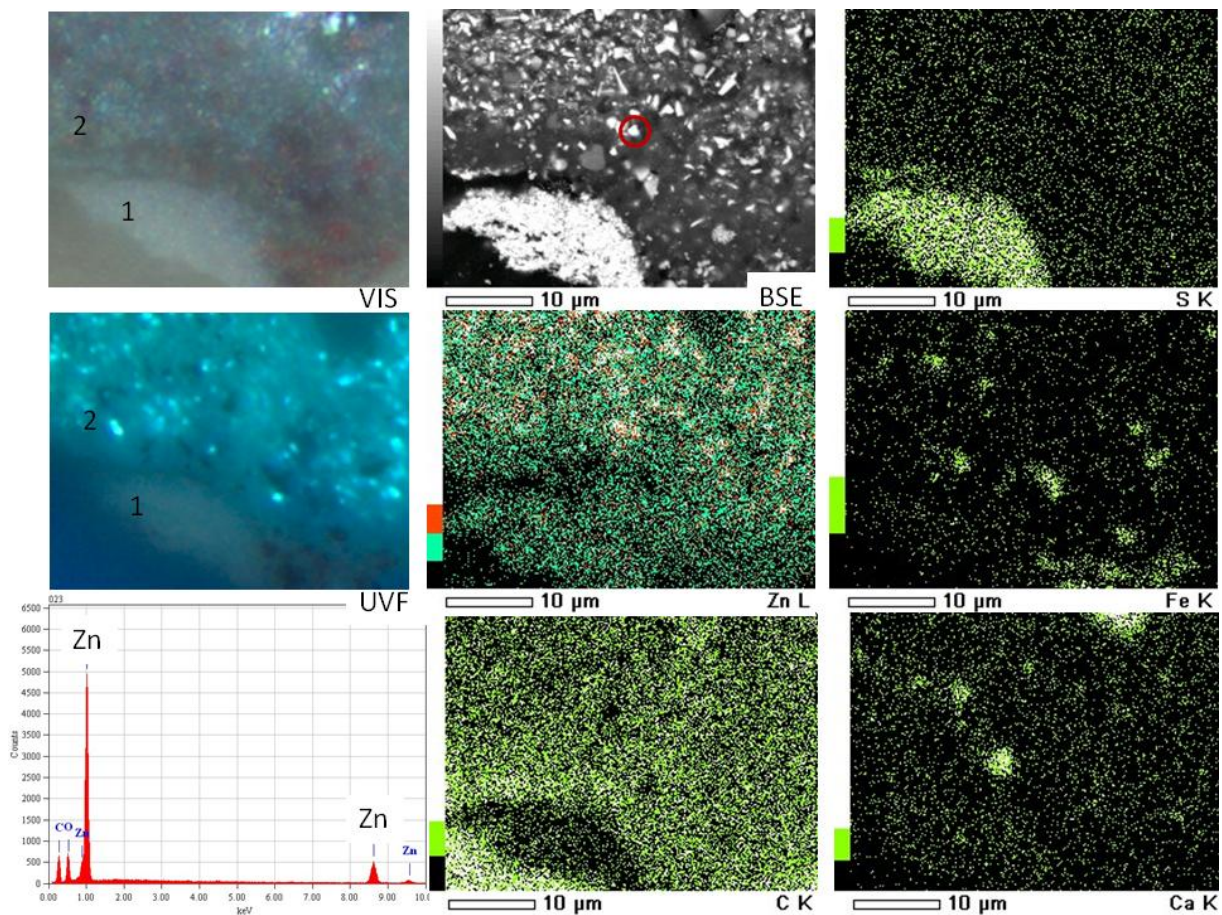
Figure 5.15 *Portrait of a student* **#7 optical and BSE image details of paint layer 2 adjacent to ground layer (1) with corresponding SEM-EDX maps for elements shown and an SEM-EDX spectrum obtained from the zinc oxide pigment particle circled**

The BSE image and sulfur map shown in Figure 5.15 clearly distinguish the lithopone ground. Iron based red and calcium-based particles are defined and correspond to dark points in the UVF image. Of particular interest is the relatively high carbon concentration adjacent to the ground layer (1) which coincides with reduced zinc oxide counts and fewer defined pigment particles in the paint. This BSE image detail is shown at larger scale in Figure 5.16.
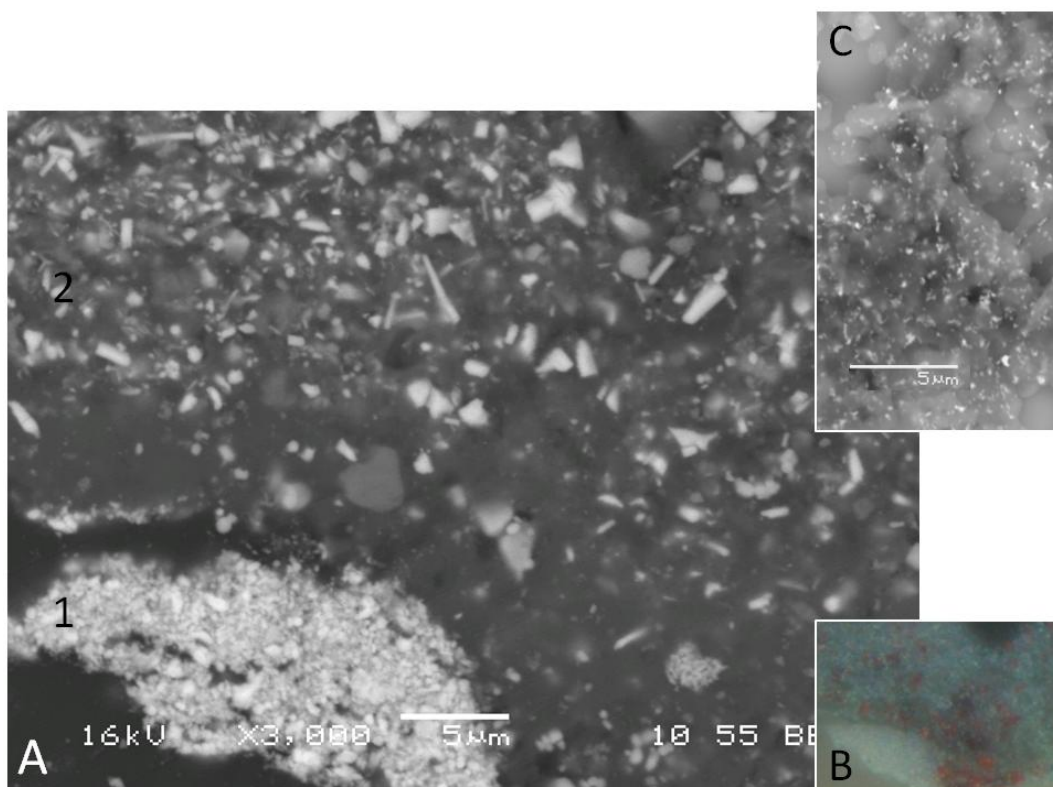
Figure 5.16 *Portrait of a student* **#7 (A) BSE detail and (B) corresponding optical image of the same area detailed in the previous figure.**

The inset BSE image (C) records solids obtained from a mixture of zinc oxide and zinc stearate in toluene. NB the initial particle size of zinc oxide in the toluene model is significantly smaller than that in the painting

Zinc oxide particles adjacent to the ground layer in BSE image (A) appear reduced in size and definition relative to those in the bulk of layer 2. Even fewer zinc oxide particles are discernible when iron and calcium based hotspots in the elemental maps (and with reference to the optical image (B)) are taken into account. The apparent morphology is similar to that observed in BSE image (C) of solids obtained following combination of zinc oxide (in excess) and stearic acid in toluene (see Chapter 4). Raman and XRD analysis of the precipitate sampled from the experimental model confirmed it as a mixture of zinc oxide and zinc stearate. It seems feasible that the bright particles of zinc oxide in the paint cross-section with indistinct boundaries and surrounded by a poorly defined mass of lower BSE density matter are similarly composed, reflecting partial saponification of the pigment. The two BSE images are shown at equivalent magnification, contrasting the relatively large particles of paint grade zinc oxide with the 30 nm zinc oxide particles used in the toluene model. BSE images have been similarly interpreted in relation to saponification of lead white pigment particles in samples from paintings (Keune et al. 2011).

No spatially correlated FTIR spectra were obtained from this painting however general spectra obtained from sample fragments are shown in Figure 5.17.
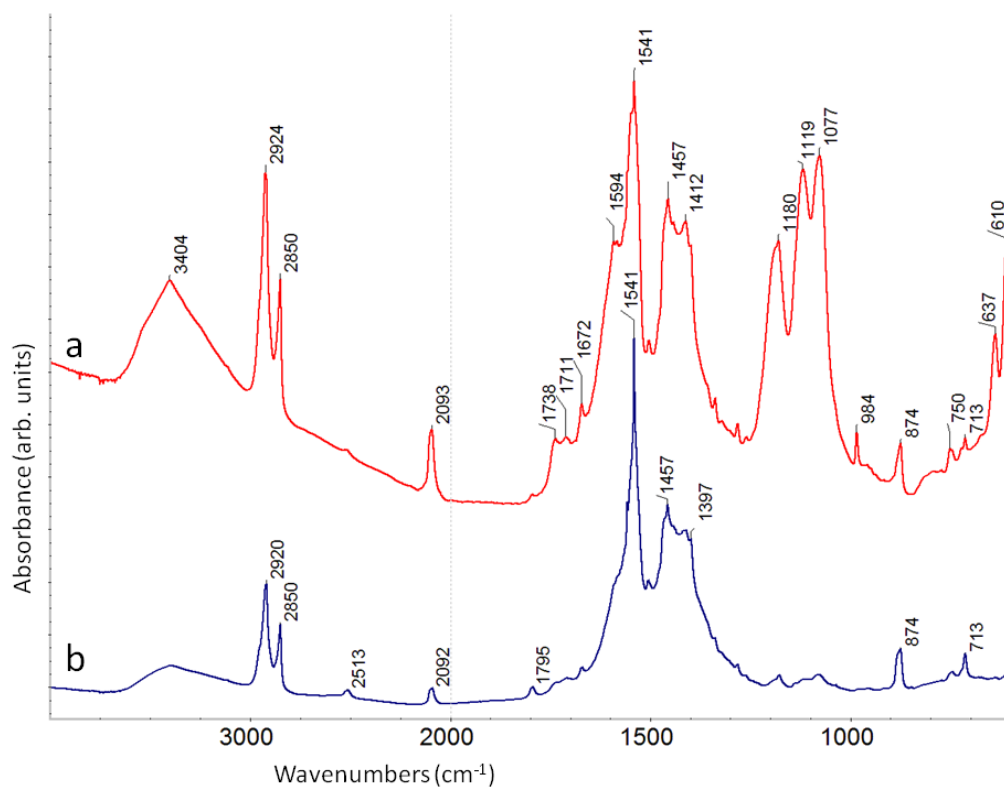
Figure 5.17 *Portrait of a student* **transmission FTIR spectra from fragments of green background paint**

Both spectra derive from green background paint sampled without ground. The presence of zinc stearate/palmitate is confirmed by dominant peaks at 1541, 1457 and 1397 cm^{-1} with broader carboxylate/OH absorption extending to 1630 cm^{-1}. Advanced hydrolysis and saponification of the oil medium is supported by the very small oil carbonyl ester peak at 1738 cm^{-1} and rival acid carbonyl absorption at 1711 cm^{-1}. Other features in the spectra include chalk (1430, 2513, 1795, 874 cm^{-1}) and barium sulfate (1180, 1119, 1077, 984, 637, 610 cm^{-1}) probably reflecting the inclusion of some lithopone (possibly artist reworking) in (a). Prussian blue is indicated by the peak at 2093 cm^{-1}.

The strong 1541 cm^{-1} signal in FTIR coupled with apparent zinc oxide dissolution adjacent to the ground layer may reflect a localised concentration of zinc carboxylates at the interface. This may, in turn play a role in the tendency for interlayer cleavage which sees paint readily separating from the preparatory ground in this painting.

5.4.3 *Hàng Giấy* 1978

In addition to the two paintings from 1963, samples from a number of post war paintings by Kiệm were investigated. *Hàng Giấy* from 1978 is shown in Figure 5.18. Its condition report describes numerous brown and semi-transparent circular growths pushing up through paint (Ebert 2011b). Paint sample #1 from the sky at top right is shown in Figure 5.19.

Figure 5.18 *Hàng Giấy* 1978, oil on canvas, 60 x 73 cm. Witness Collection. The source location of samples is indicated in the small offset image
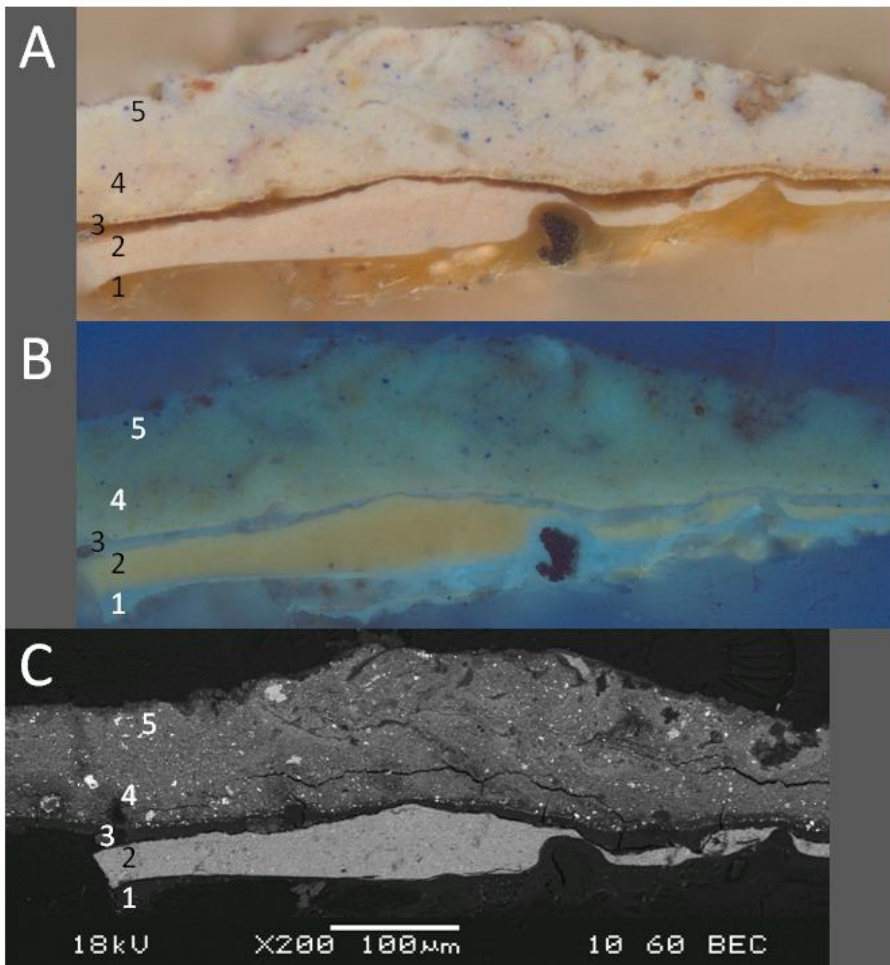
Figure 5.19 *Hàng Giấy* 1978 sample #1 cross-section from the sky at top right as optical images (A) visible and (B) UVF, and (C) corresponding BSE image. Numbers correspond to layers described in the text

The sample has two thick UV-fluorescent layers (1 and 3) characteristic of glue size either side of the lithopone ground (2). Layers 4-5 comprise zinc oxide-based paint layers applied wet-in-wet including pale hues of pink, blue and yellow. Pigmentation includes ultramarine blue and Naples yellow (lead antimonate). SEM-EDX indicates tin is frequently associated with lead and antimony based particles, suggesting the possibility the pigment was synthesised via a process using tin oxide (Dik et al. 2005). A higher magnification detail from the top right of the cross-section is shown in Figure 5.20.
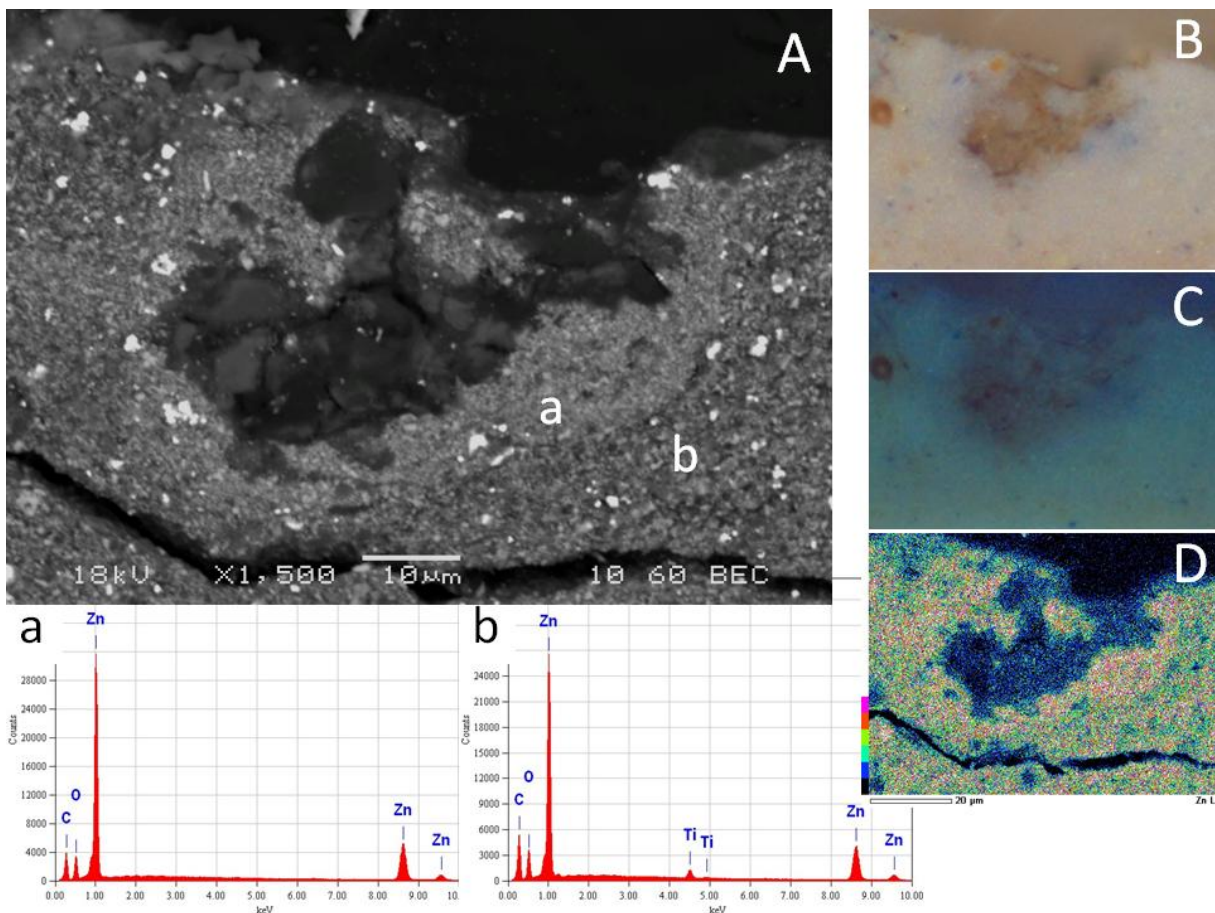
Figure 5.20 *Hàng Giấy* **#1 (A) BSE detail and corresponding optical images: (B) visible and (C) UVF, and (D) elemental map for zinc of yellow and blue paint mixed in layer 5, and SEM-EDX spectra obtained from spots in each of the two paints (a and b).**

The low atomic density mass at centre is clay based while bright white particles are lead antimonate (yellow)

The BSE image detail shows blue paint apparently prepared with a finer particle size and higher pigment density of zinc oxide than that used in yellow paint. Neither exhibits the distinctive UV-fluorescent 'zinc' sparkle. Spot SEM-EDX spectra from each colour additionally indicate a small amount of titanium is associated with yellow paint but not with blue. Review of the larger cross-

section images in Figure 5.19 and images in published work shows that blue paint has developed internal cracks or veins which are visible in optical images and have lower atomic contrast in BSE images. In contrast the yellow paint is susceptible to cracking under vacuum in the SEM, evidenced by the large crack through layer 4 which runs through patches of reduced atomic density in the lower margin of the layer. A detail of this cracking is shown in Figure 5.21.

Figure 5.21 *Hàng Giấy* **#1 (A) BSE detail and corresponding optical images: (B) visible and (C) UVF, and SEM-EDX spectra obtained from spots indicated (a-b).**

Zinc counts are high in areas with few defined zinc oxide particles adjacent to unpigmented layer 3

Indicators of saponification within zinc oxide-based paints in close proximity to potential reservoirs of fatty acids are discussed in relation to this cross-section in published work. The BSE image above also suggests preferential dissolution of zinc oxide particles is occurring in layer 4 adjacent to size layer 3 while bright particles of lead antimonate in the same zone remain intact. Strong zinc counts in areas with low particle definition are consistent with the presence of a zinc carboxylate phase. Zinc carboxylates are confirmed with FTIR spectra obtained from fragments of paint deriving from the same area of the painting (Figure 5.22).
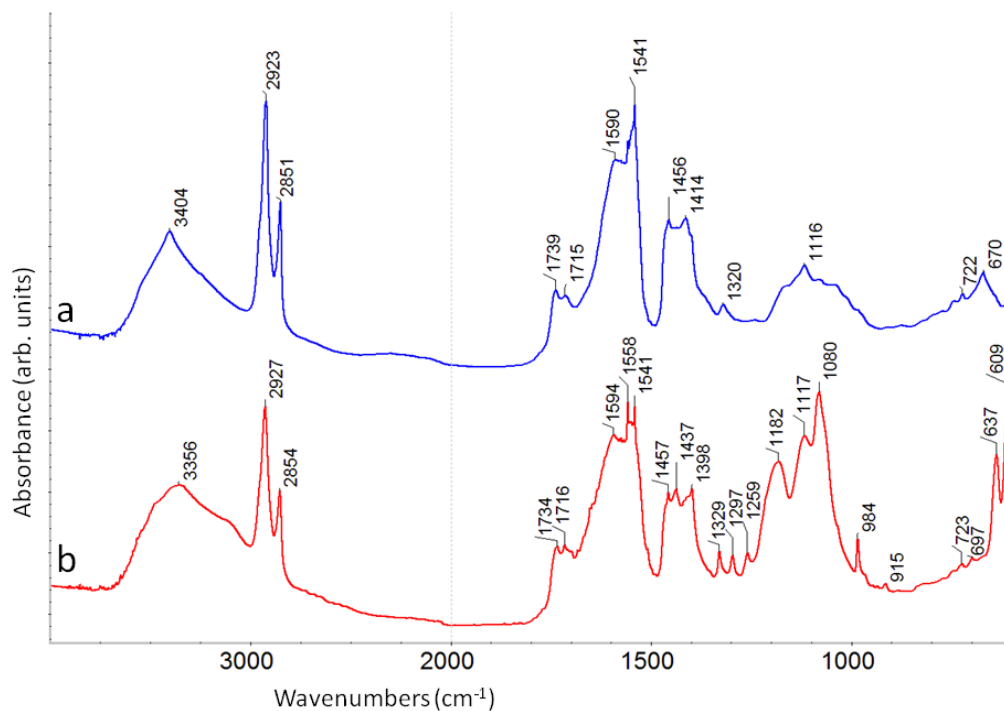
Figure 5.22 *Hàng Giấy* **#2 transmission FTIR spectra from unembedded fragments of (a) pale yellow/blue sky paint and (b) underlying ground**

Spectrum (a) is from an area of blue paint with mixed pigmentation possibly including Naples yellow (670 cm^{-1}) (van der Weerd et al. 2005). Absorptions *ca* 1116 cm^{-1} may reflect silicates (including possible blue pigment) or unassigned sulfates. Spectrum (b) derives from underlying lithopone ground with consequent barium sulfate absorptions. Zinc carboxylate absorptions are strong in both spectra including those characteristic of zinc stearate/palmitate, while (b) additionally incorporates a series of defined peaks and spectral features tentatively assigned to zinc lactate (discussed further in the following section). Hydrolysis of glycerol esters in the oil medium is again suggested by the defined acid carbonyl at 1715 cm^{-1} adjacent to the oil ester carbonyl at 1740 cm^{-1} together with OH (3400) and C-O (1319 cm^{-1}) stretching vibrations. No ester triplet is evident underlying or shouldering the respective silicate and sulfate bands.

Very similar spectral features are observed in sample #3 from paint obtained from the street awning at centre right of the painting (Figure 5.23).
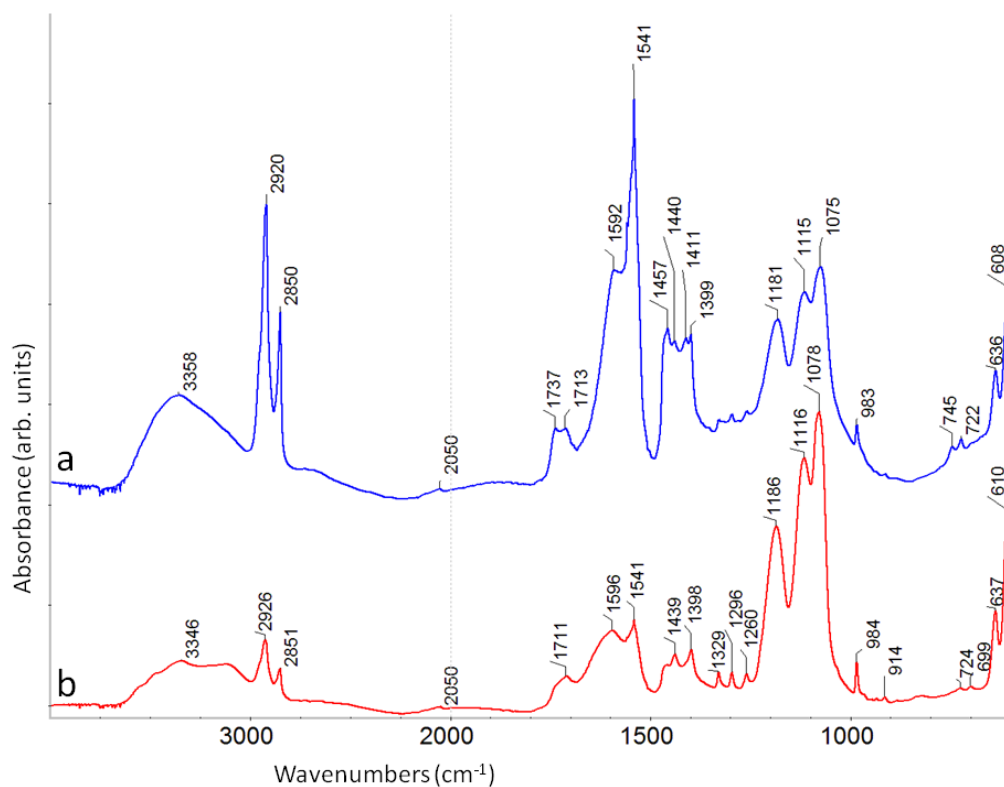
Figure 5.23 *Hàng Giấy* **#3 transmission FTIR spectra from unembedded fragments of pale blue/yellow paint**

Characteristic zinc stearate/palmitate absorptions are similarly dominant. Barium sulfate and acid carbonyl vibrations are generally present, and distinctive zinc lactate spectral features are apparent in paint as well as in the ground sample previously described.

In *Hàng Giấy* saponification in paint closest to the ground appears significant, periodically extending deep into the paint layer. A hygroscopic glue size layer between paint and ground is likely to have facilitated oil hydrolysis and subsequent reaction with zinc oxide pigment. Substantive intralayer cracking observed under vacuum is clearly linked to affected areas, suggesting apparent consequences of saponification for paint strength and cohesion.

5.4.4 *Children playing at the beach* 1980

Children playing at the beach (Figure 5.24) has suffered extensive losses with active flaking paint. Significant retouching is evident in perimeter margins, applied over an earlier surface coating (Ebert 2011a). Two paint samples are discussed here. Sample #3 derives from the beach at centre right from an area of unstable paint and is shown in cross-section in Figure 5.25.
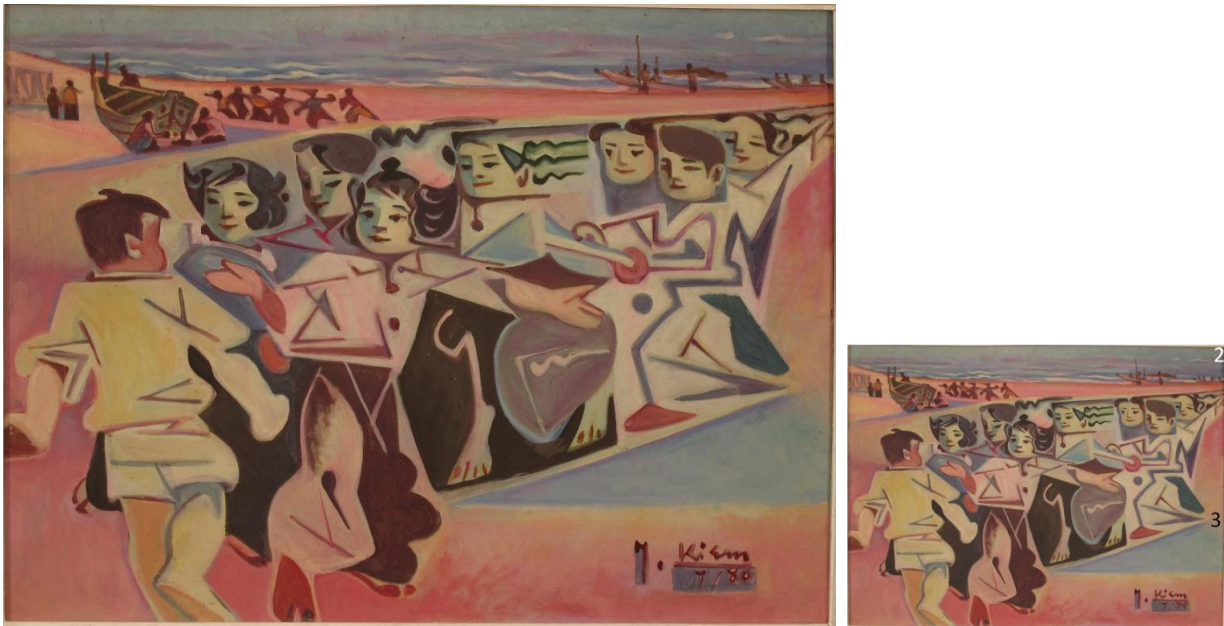
Figure 5.24 *Children playing at the beach* **1980, oil on canvas, 72.3 x 97 cm. Witness Collection. The source location of samples is indicated in the small offset image**
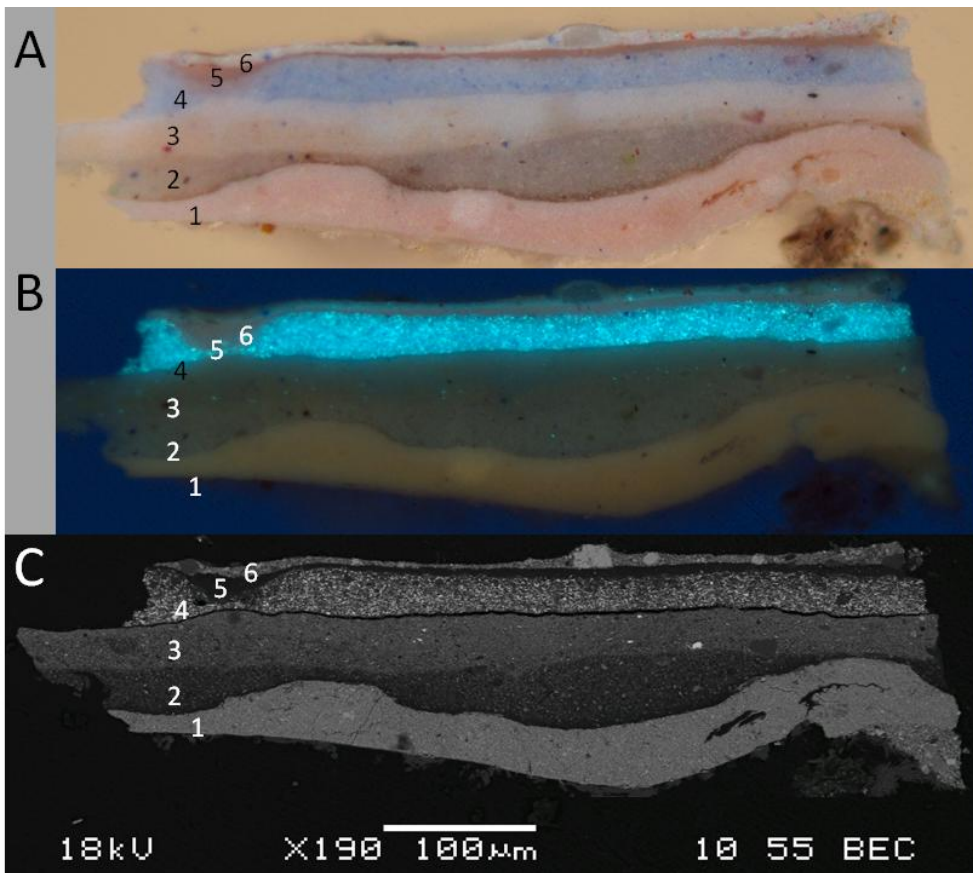
Figure 5.25 *Children playing at the beach* **1980 sample #3 cross-section as optical images (A) visible and (B) UVF, and (C) corresponding BSE image. Numbers correspond to layers described in the text**

212

The cross-section includes a lithopone ground (layer 1), two zinc oxide-based paint layers – one grey (2) and one white (3), a lead white and zinc oxide-based paint with cobalt-based blue (4); an unpigmented layer (5) and lithopone-based reworking (6). Layers 3 and 4 have separated under vacuum in the SEM, and the indicators for an accumulation of zinc carboxylates at this interface are discussed in published work.

Optical image details and elemental maps from an area within layers 1 and 2 are shown in Figure 5.26.
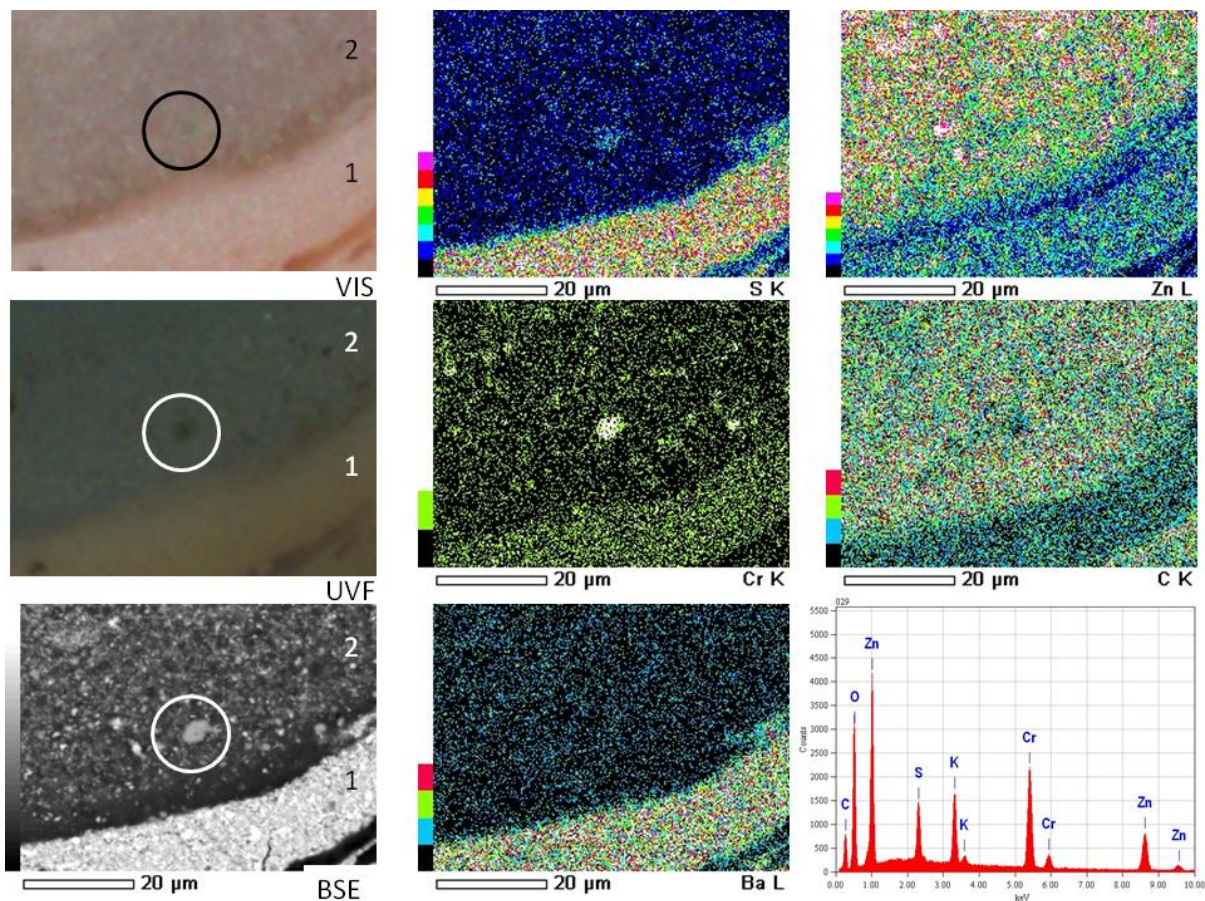
Figure 5.26 *Children playing at the beach* **#3 cross-section optical and BSE image details with corresponding SEM-EDX maps for elements shown and an SEM-EDX spectrum obtained from a discoloured particle of zinc yellow (circled)**

Elemental maps show that in addition to sulfur concentrated with barium in the lithopone ground, a sulfur hotspot coincides with a discoloured zinc potassium chromate pigment particle in layer 2. This is confirmed by a spot SEM-EDX spectrum. Sulfur has been linked to deterioration observed in zinc yellow pigment ($K_2O \cdot 4ZnCrO_4 \cdot 3H_2O$) in oil paint exposed to sulfur dioxide at 90% relative humidity (Casadio et al. 2011). Electron energy loss spectroscopy measurements determined that the pigment surface of samples which turned olive green contained mostly the altered species Cr(III). Elemental mapping gives no indication of sulfur uptake in surrounding zinc oxide-based paint.

A second sample from the top right corner of sky in *Children playing at the beach* is shown in Figure 5.27.
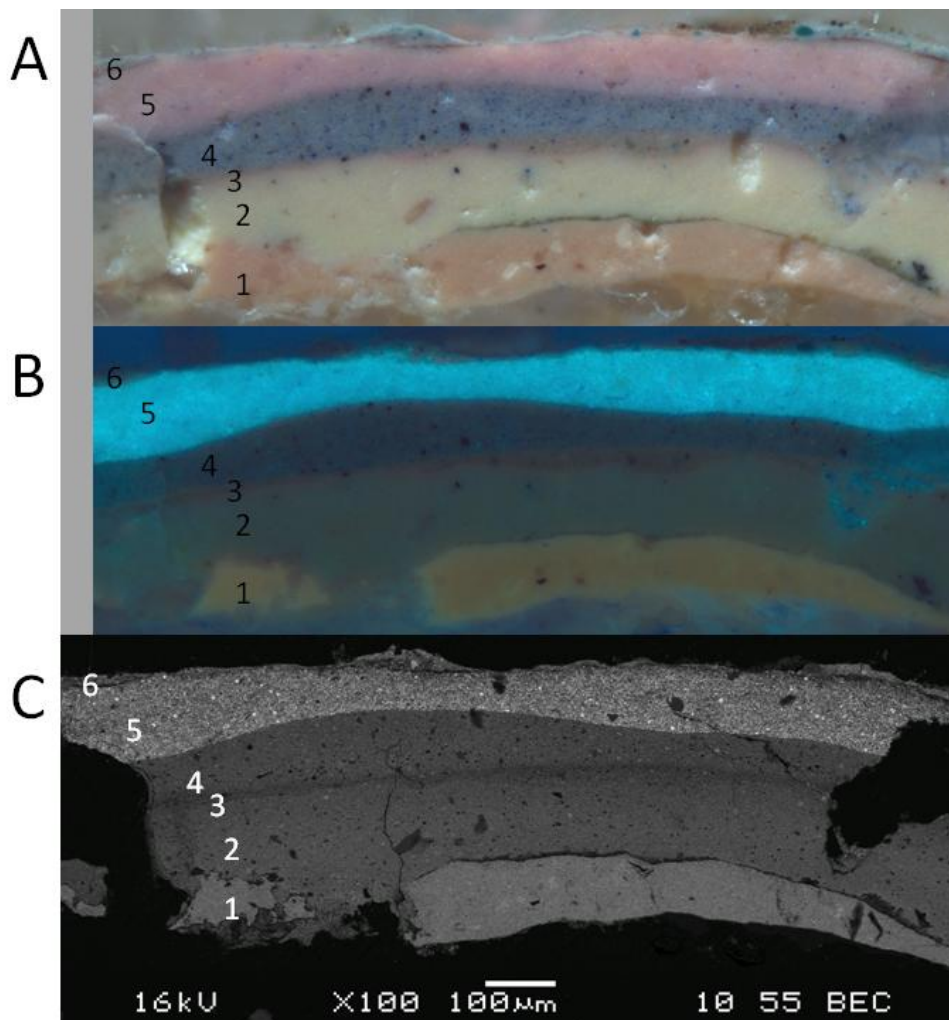
Figure 5.27 *Children playing at the beach* sample #2 from top right corner sky cross-section as optical images (A) visible and (B) UVF, and (C) corresponding BSE image. Numbers correspond to layers described in the text

At first glance the structure of sample #2 is very similar to the previous one, with lithopone ground, several zinc oxide-based paint layers, a single layer combining lead white and zinc oxide, and lithopone based reworking. Both samples include blue paint layers, however, whereas in sample #3 blue paint coincided with the lead white-containing layer, in the present example, blue paint is zinc oxide-based while pink paint additionally incorporates lead. In both samples the lead-containing paint is the uppermost original paint layer and has a strong UV-fluorescent sparkle in contrast to the layers below without lead. The sequencing suggests Kiệm may have substituted his white paint for later stages of working, either consciously or by necessity.

In addition to lead white and zinc oxide, pink paint in layer 5 incorporates occasional aluminium silicate particles. Layer 4 (blue) contains predominantly zinc oxide but also calcium sulfate. Layer 3

is thinly applied and includes zinc yellow, and white paint in layer 2 is zinc oxide-based, possibly with zinc stearate as an additive. A detail of layers 4 and 5 is shown in Figure 5.28.
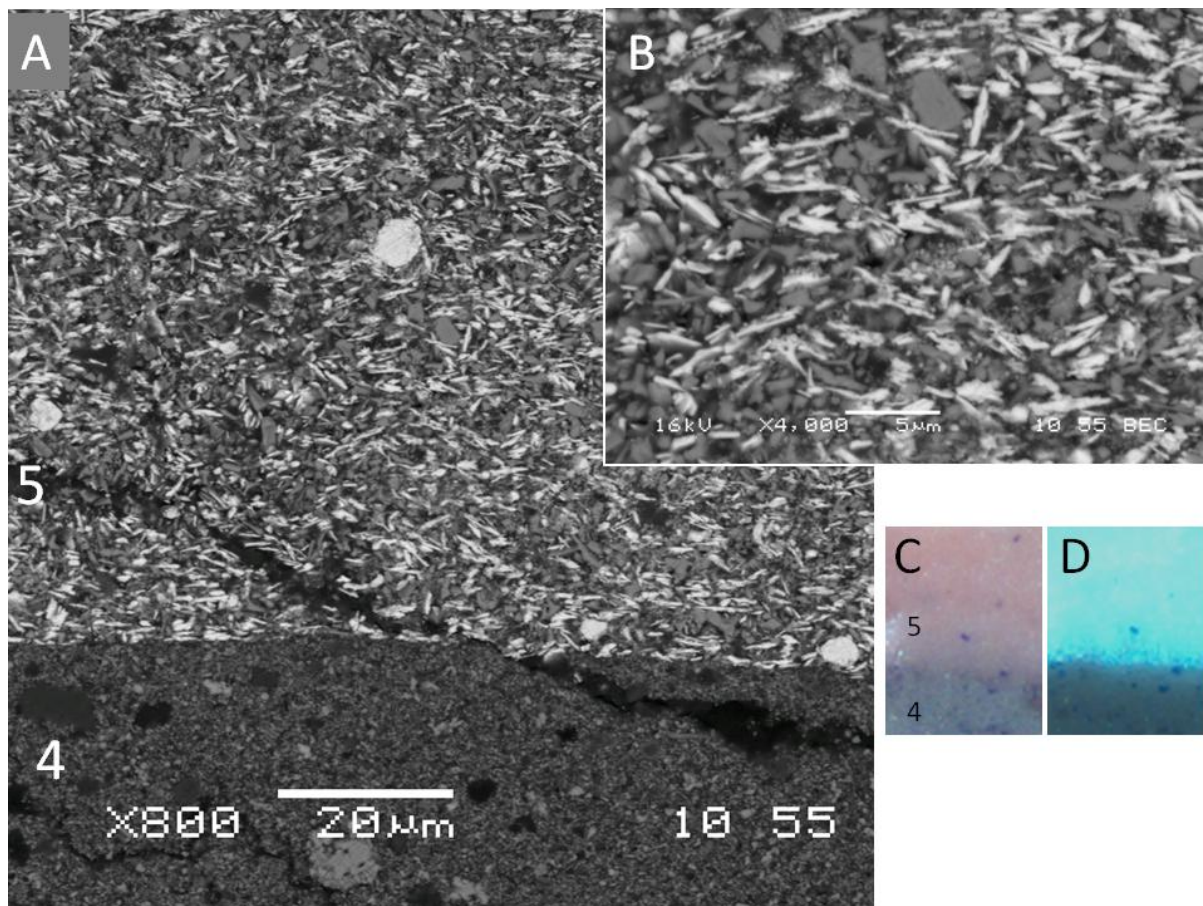
Figure 5.28 *Children playing at the beach* **#2 BSE image detail (A) with higher magnification inset (B) and optical images corresponding (A): (C) visible and (D) UVF**

The BSE detail of layers 4 and 5 illustrates the contrasting particle characteristics of zinc oxide in layers with and without lead. The distinctive bright platelets of lead white in layer 5 are interspersed with grey particles of zinc oxide which at higher magnification (inset) are seen to be highly variable in shape and size. Some twinning is apparent but no strongly acicular particles are evident. Zinc oxide in layer 4 is nodular and finer in size. Small regular 'voids' may reflect the incidence of zinc stearate as an original component. Another detail is shown in Figure 5.29. The SEM-EDX spectrum obtained from an area of low atomic density in layer 4 (a) shows zinc and carbon predominate. The defined boundaries of these areas suggest they may comprise an original component of the paint. Particles of gypsum are additionally present which differ only slightly in appearance from features attributed to added zinc stearate. Blue pigment particles are not immediately distinguishable in the BSE image and have unfortunately not been characterised. Similar features are apparent in layer 2 (Figure 5.30).
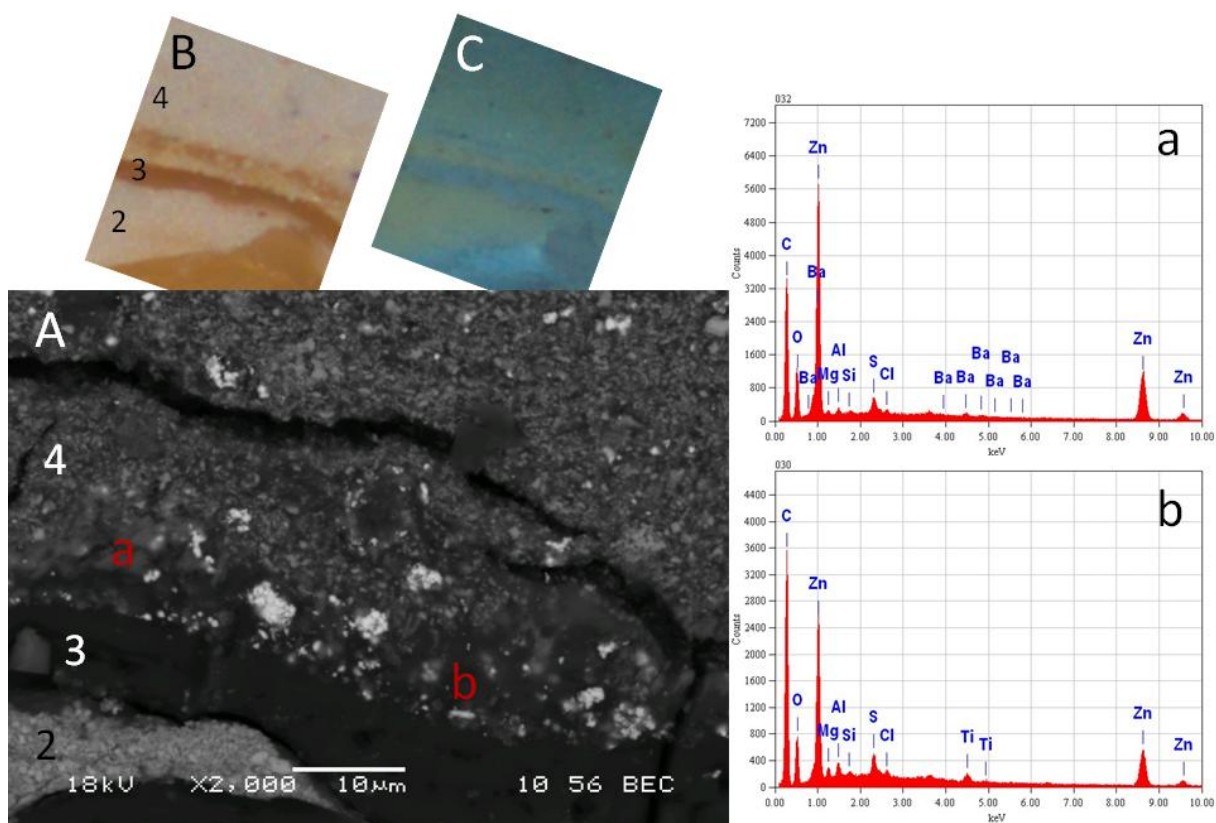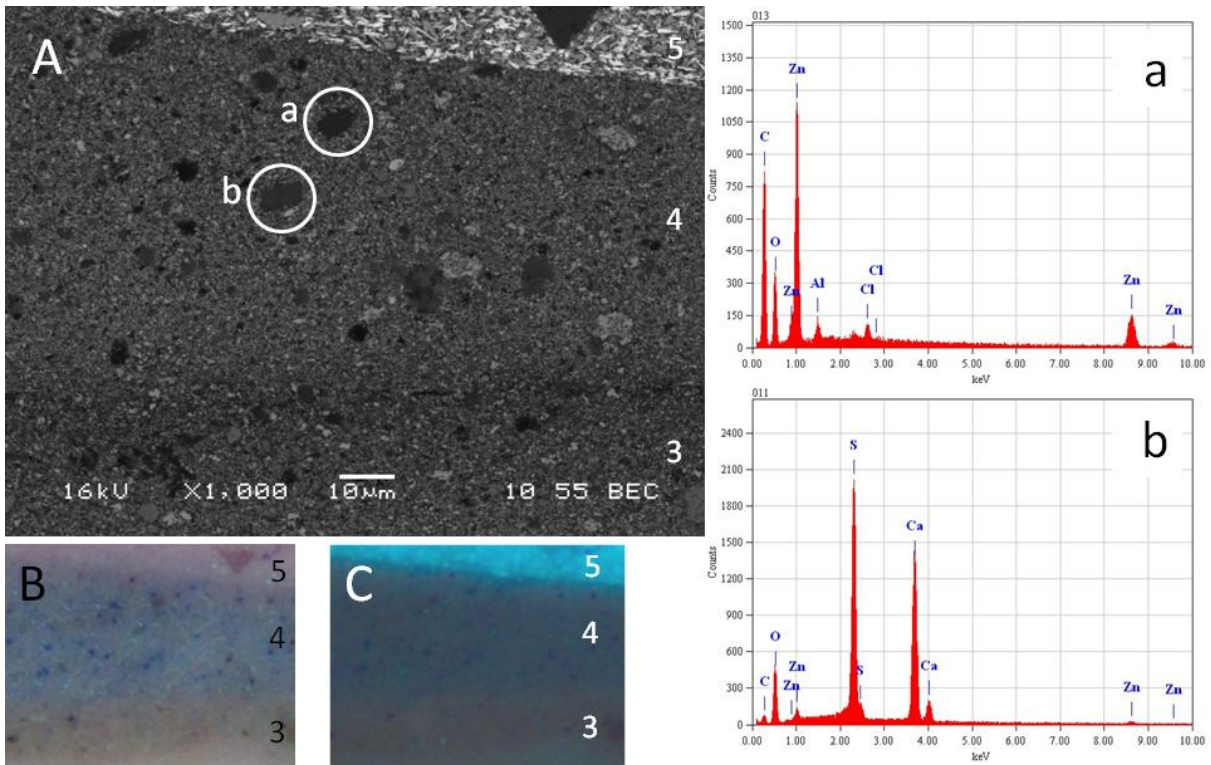
Figure 5.29 *Children playing at the beach* **#2 (A) BSE detail of layers 3-5 and corresponding optical images (B) visible and (C) UVF and SEM-EDX spectra obtained from spots indicated (a-b)**
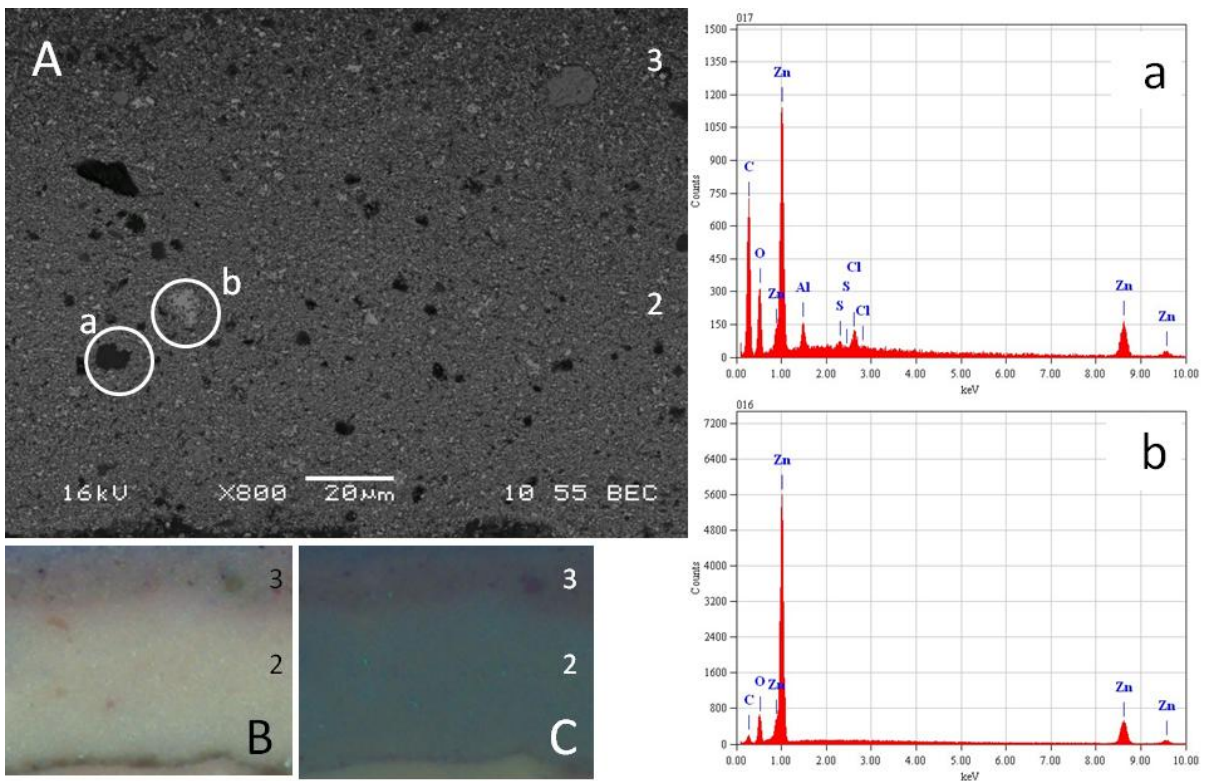
Figure 5.30 *Children playing at the beach* **#2 (A) BSE detail of layers 2 and 3 and corresponding optical images (B) visible and (C) UVF and SEM-EDX spectra obtained from spots indicated (a-b)**

The general characteristics of white paint are similar to those described for blue paint but without calcium sulfate. Comparable elemental composition, including trace elements, is indicated by SEM-EDX spectrum (a) from a defined area of low atomic density. Within the otherwise relatively homogeneous mix of zinc oxide, aggregated particles are seen in both layers. A band of lower atomic density occurs towards the top of Figure 5.30, seen more clearly in Figure 5.31.
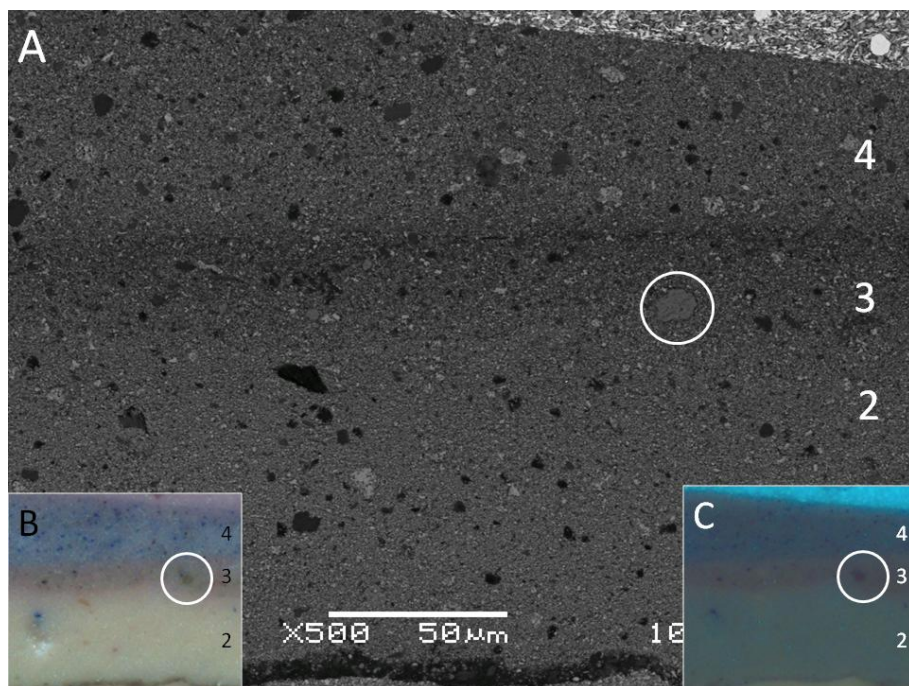
Figure 5.31 *Children playing at the beach* **#2 (A) BSE detail with corresponding optical images (B) visible and (C) UVF. A low atomic density band is evident at the top at layer 3. A discoloured particle of zinc yellow is circled to assist with correlation of the images**

The dark band evident in the BSE detail corresponds to the upper margin of layer 3. It is possible this relates to an accumulation of zinc carboxylates at the interface with layer 4 but remains to be confirmed. A potential separation is hinted at by a rupture within the dark band to the left of centre. A more pronounced band occurs at the interface between layer 2 and the lithopone ground which is dominated by zinc and carbon as seen in Figure 5.32. Significantly, no barium signal from the lithopone ground accompanies the strong zinc signal in the spot SEM-EDX spectrum obtained from the band, suggesting the interaction volume of the electron beam does not extend substantially into adjacent layers. Rather it seems feasible that preferential dissolution of zinc oxide has occurred at the interface. It is not clear from lower magnification cross-section images if this band reflects a discontinuous unpigmented layer between ground and paint, and its appearance in BSE images and lack of UV fluorescence distinguish it from the pronounced layer apparent in *Hàng Giấy* sample #1.
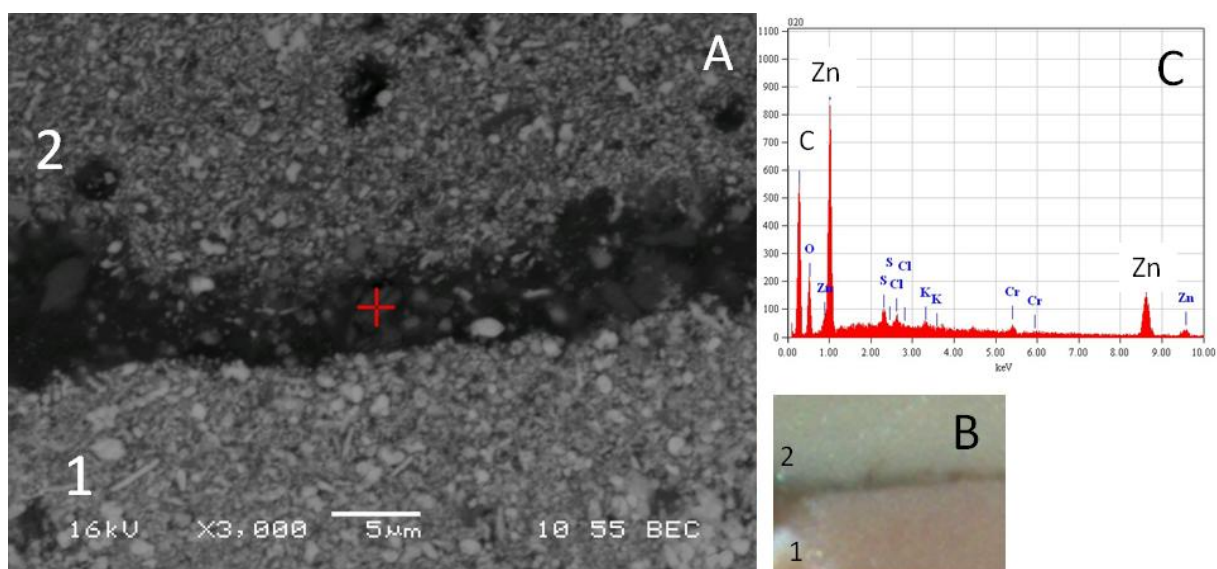
Figure 5.32 *Children playing at the beach* **#2 (A) BSE detail at the interface of ground and paint with corresponding optical image (B) and SEM-EDX spectrum (C) obtained from the spot indicated**

Further characterisation of the sample was attempted using ATR SR-µFTIR. A selection of integrated absorption intensity maps are shown in Figure 5.33.
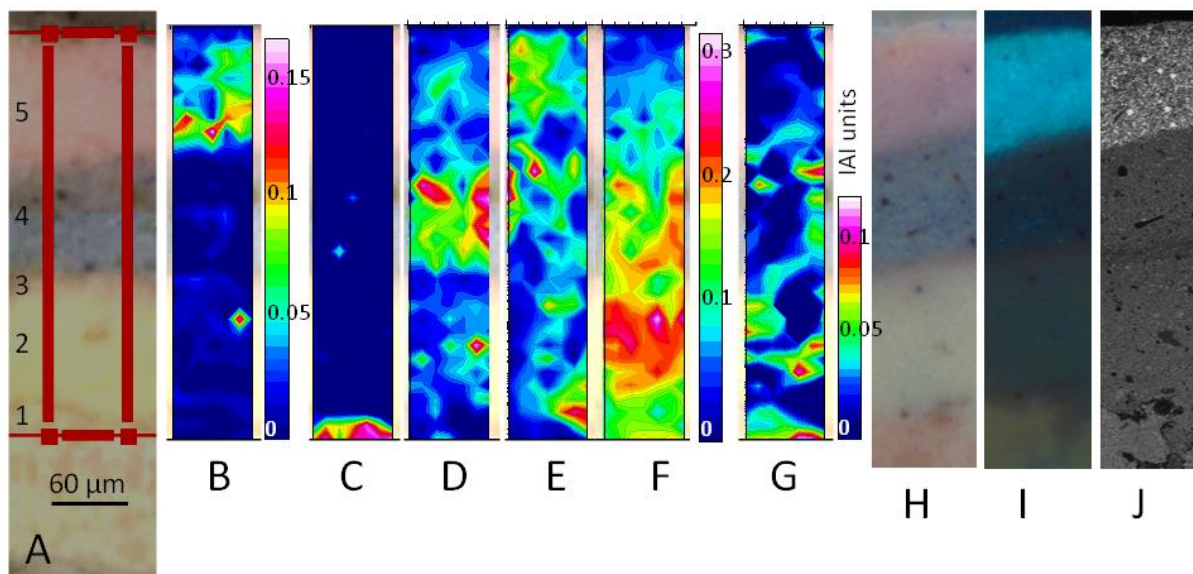
Figure 5.33 *Children playing at the beach* **#2 (A) optical cross-section image detail with box denoting ATR SR-µFTIR map area and corresponding integrated absorption intensity maps for wavenumber ranges (B) 3515-3550 (basic lead carbonate); (C) 1050-1095 (barium sulfate in lithopone); (D) 1530-1550 (zinc stearate/palmitate); (E) 1260-1285 (zinc lactate); (F) 1730-1755 (oil ester carbonyl); (G) 1690-1725 cm^{-1} (carboxylic acid carbonyl).**

H-J are indicative optical and BSE images and do not correspond exactly to the surface presentation captured in maps. NB. The dark band at the top of layer 4 (blue) in (A) is attributable to variable exposure in the automated image capture mosaic and should not be confused for layer 3 located between blue and white paint

Unfortunately there is little to immediately distinguish the interface between paint and ground, and the area of interest around layer 3 is also not well represented within the mapped region of the cross-section and is not spectrally distinguished from layer 2. Zinc stearate/palmitate is most strongly associated with layer 4 (map D). The oil ester carbonyl absorption is strongest in layer 2 and decreases progressively towards the sample surface (map F), possibly reflecting exposure related hydrolysis as discussed in published work. As expected, the basic form of lead carbonate is found across layer 5 as indicated by the intensity of the peak at 3535 cm^{-1} (map B). The integration of this peak also captures the presence of a gypsum particle in layer 2 but avoided more numerous overlapping peaks than an integration of the major carbonate absorption ca 1400 cm^{-1}. Indicative spectra extracted from hotpots in selected maps are shown in Figures 5.34-5.39.
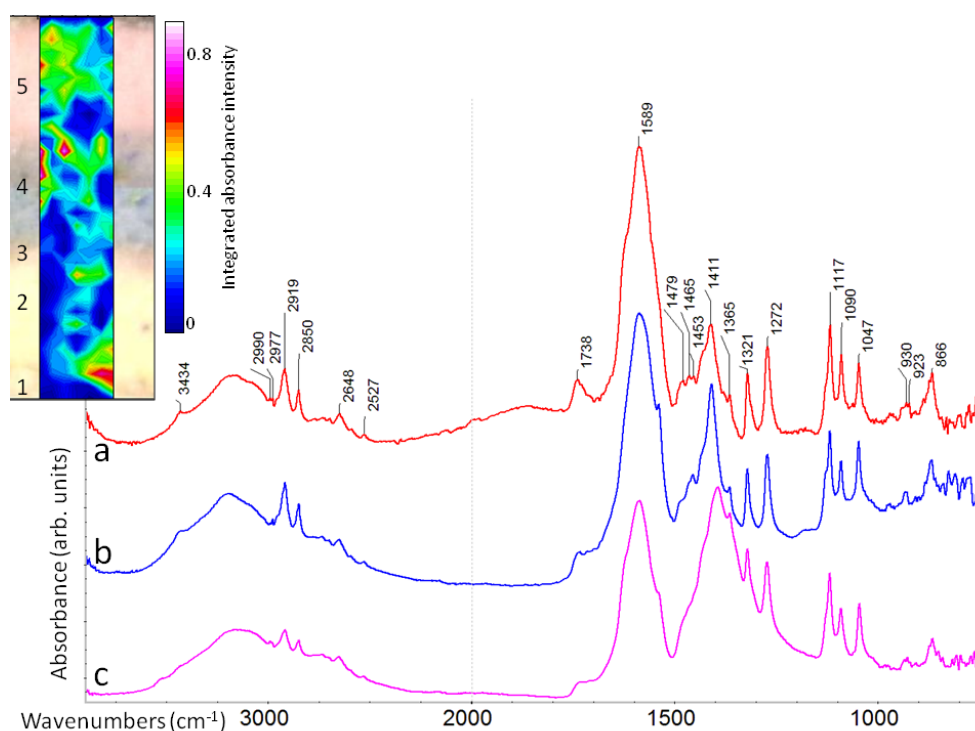
Figure 5.34 *Children playing at the beach* **1 #2 ATR SR-µFTIR integrated absorption intensity map (E) 1260-1285 cm^{-1} and spectra from hotspots extracted from (a) layer 2 - white; (b) layer 4 - blue; (c) layer 5 - pink paint, the latter including carbonate absorption centred 1395 cm^{-1} masking underlying peaks.**

Spectral shape and peak positions are very similar to those assigned to zinc lactate

The integrated peak at 1260-1285 cm^{-1} corresponds to a small, sharp peak recurring as one of a series in many spectra from this painting. The 1272 cm^{-1} peak was selected for integration in preference to the strongest vibrations at 1589 and 1411 cm^{-1} to avoid overlap with carbonate and carboxylate vibrations deriving from other components in the painting, enabling the spatial distribution to be better resolved. Initial attempts at characterising the distinctive spectrum proved elusive until a connection was made with recent analysis of mid 20th century Canadian paintings,

attributing a very similar spectrum to the incidence of zinc lactate (Helwig et al. 2014). A spectrum from Kiệm's painting is compared with a zinc lactate trihydrate reference spectrum in Figure 5.35.
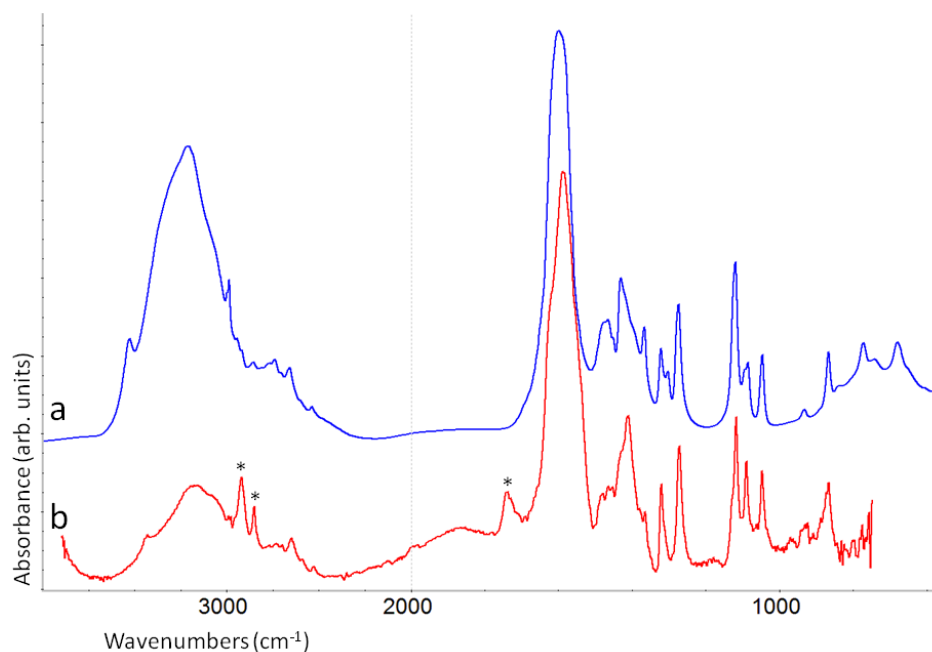
Figure 5.35 (a) Commercial zinc lactate trihydrate transmission FTIR spectrum (courtesy Kate Helwig, Canadian Conservation Institute) and (b) ATR SR-µFTIR spectrum extracted from *Children playing at the beach #2* (white paint). Asterisked peaks are additional, attributed to the oil medium

Zinc lactate is a water-soluble short chain carboxylate salt, zinc 2-hydroxypropanoate. The incidence of zinc lactate reported here varies from that documented by Helwig et al (2014) in the sense that it occurs in multiple layers throughout the painting rather than as a disfiguring surface phenomenon. The high incidence of zinc oxide in Kiệm's painting invites the hypothesis that zinc lactate has formed *in situ* following reaction with lactic acid ($CH_3CH(OH)COOH$), but this remains speculative. No obvious explanation for a source of lactic acid or zinc lactate is provided and is left for future research.

Zinc lactate absorptions are also apparent in association with some spectra from hotspots in the integrated absorption intensity map indicative for zinc stearate/palmitate (Figure 5.36). The strongest 1540 cm^{-1} absorbance is concentrated in blue paint. Spectra extracted from hotspots in other layers also include characteristic zinc stearate/palmitate COO^- peaks at 1540 and 1399 cm^{-1} in combination with zinc lactate absorptions (a and b). Spectrum (c) taken from white paint additionally includes sulfate peaks at 1137, 1047 and 983 cm^{-1} which correlate well to monodentate SO_4^{2-} vibrations reported at zinc oxide surfaces (Wu et al. 2011). In each of the extracted spectra oil ester carbonyl absorption at 1740 cm^{-1} is broadened by adjacent carbonyl peaks indicative of fatty acids. Integration of the acid carbonyl peak region is shown in Figure 5.37.
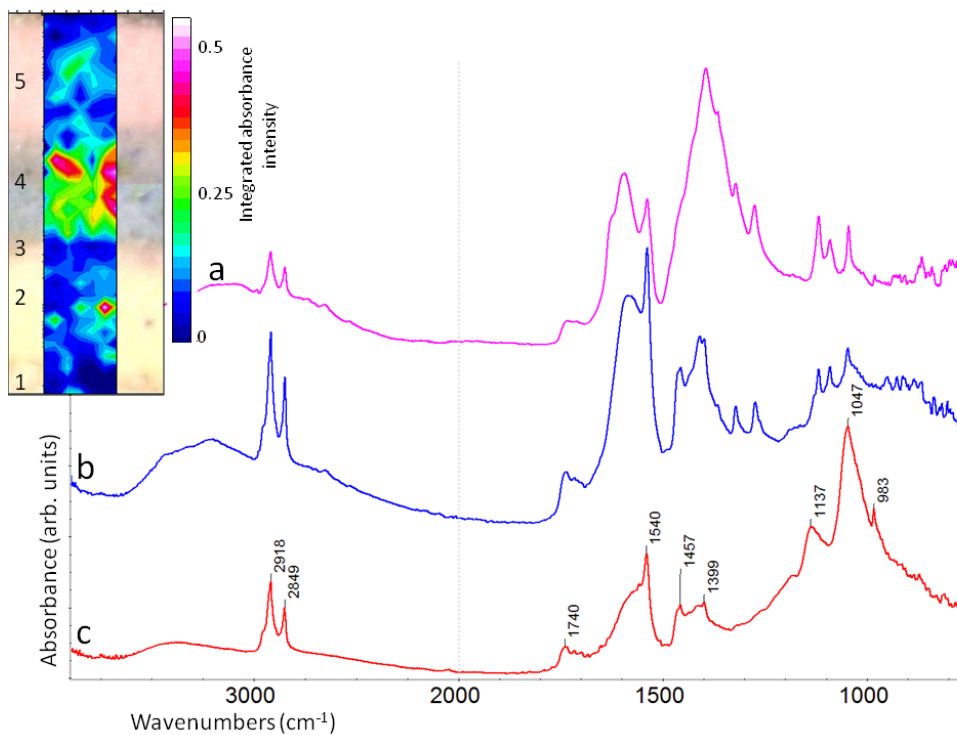
Figure 5.36 *Children playing at the beach* **#2 ATR SR-µFTIR integrated absorption intensity map (D) 1530-1550 cm^{-1} (v_{as} COO$^-$ zinc stearate/palmitate 1540 cm^{-1}) and spectra extracted from hotspots in (a) layer 5 - pink; (b) layer 4 - blue; (c) layer 2 – white paint**
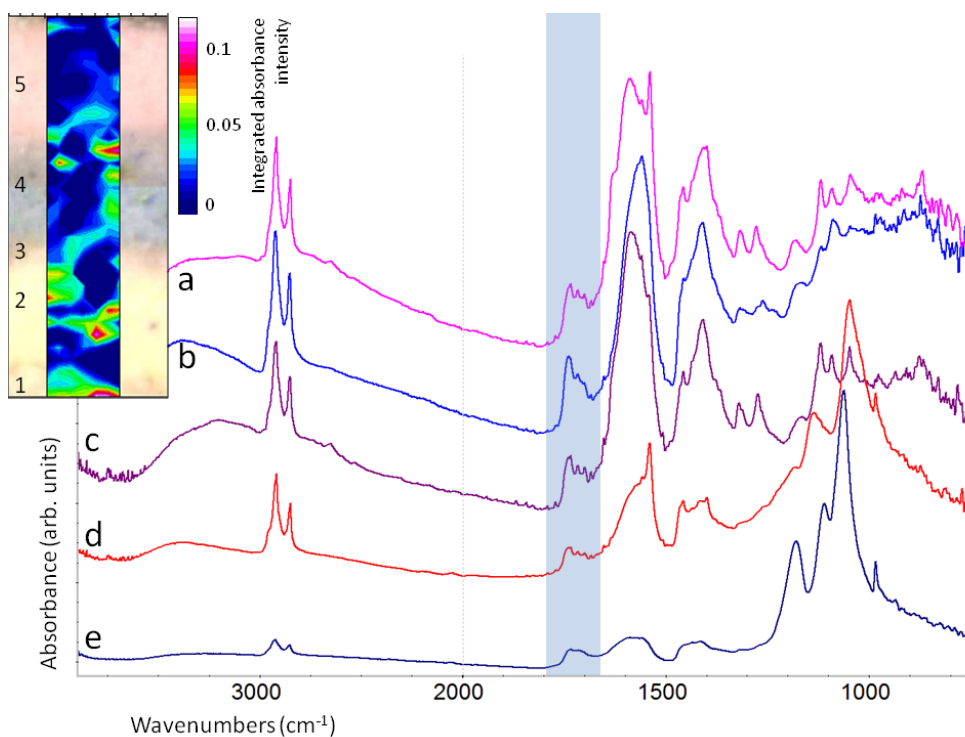
Figure 5.37 *Children playing at the beach* **#2 integrated absorption intensity map (G) 1690-1725 cm^{-1} and spectra extracted from hotspots in (a) layer 4 - blue; (b-d) layer 2 - white paint; (e) layer 1 - lithopone ground.**

Shaded band corresponds to carbonyl absorption

Spectra extracted from hotspots in the acid carbonyl map typically include a reproducible series of peaks adjacent to the oil ester carbonyl in paint layers but these are less defined in the lithopone ground. The carbonyl and carboxylate region is shown in more detail in Figure 5.38.
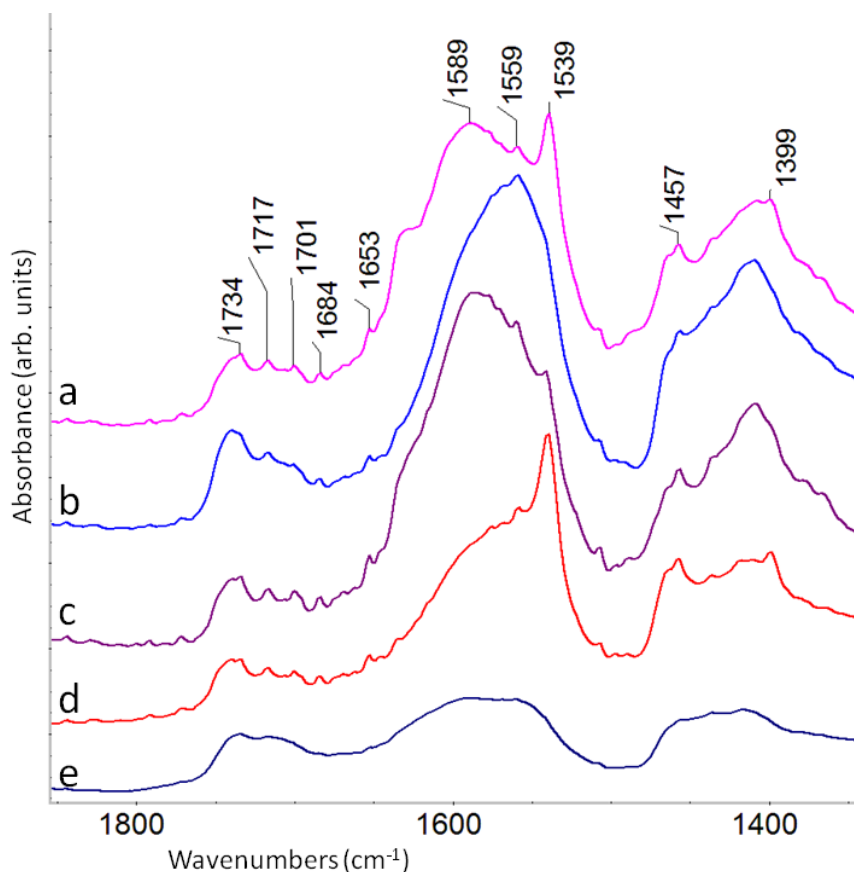
Figure 5.38 *Children playing at the beach* **#2 ATR SR-µFTIR spectral details from previous figure with annotated peak positions 1350-1800 cm^{-1} from (a) blue paint; (b-d) white paint; (e) lithopone ground.**

A reproducible series of C=O acid peaks occurs adjacent to the oil ester carbonyl in paint layers

The acid carbonyl peaks occur at consistent wavenumbers but further analysis is required to ascertain the specific acids represented. Absorption in the range 1500-1650 cm^{-1} is variable in association, which although primarily attributable to zinc soaps, suggests coordination of zinc to a range of carboxylate moieties.

The presence of barium sulfate within the lithopone ground is illustrated by integration of the sulfate peak centred 1065 cm^{-1} (Figure 5.39).
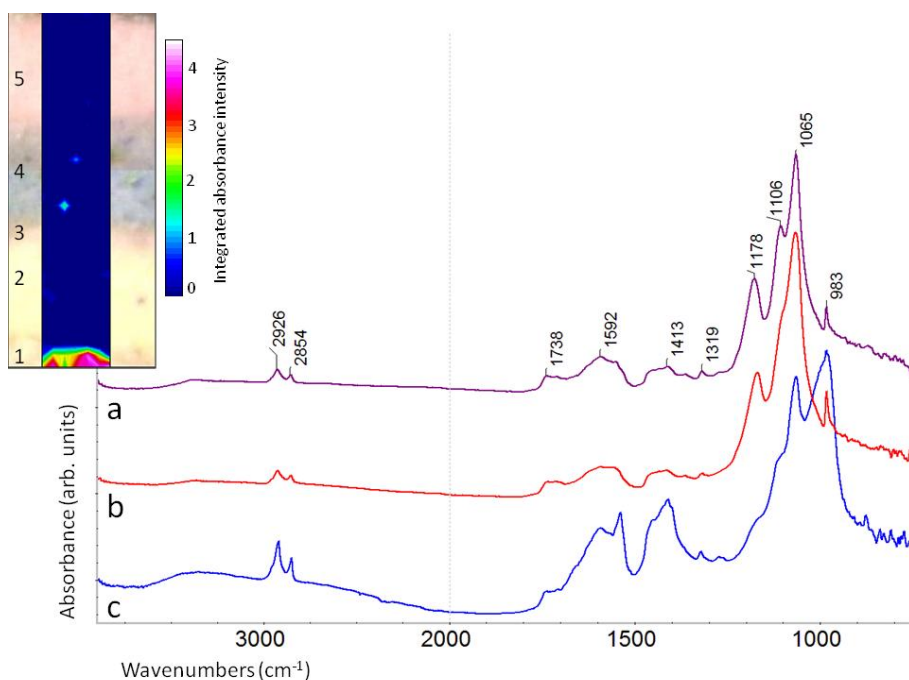
Figure 5.39 *Children playing at the beach* #2 ATR SR-µFTIR integrated absorption intensity map (C) 1050-1095 cm^{-1} and spectra extracted from hotspots in layer 1 - lithopone ground (a-b) and (c) layer 4 - blue paint

Spectra extracted from layer 1 are consistent, while a different peak configuration is associated with a small hotspot located in blue paint layer 4 (spectrum c). In this case the assignment is not certain but may reflect silicate absorptions, possibly a blue pigment particle. A similar spectrum is derived from the blue mineral Riebeckite, a sodium iron magnesium silicate hydroxide (Philadelphia Museum of Art 2007).

In addition to the indications of BSE images and conventional FTIR of samples from *Children playing at the beach*, ATR SR-µFTIR mapping enables more spatially resolved data to be obtained from a cross-section. Interrogation of individual spectra extracted from maps is an important part in interpreting results and ensuring integrations are meaningful. Zinc stearate is observed to be concentrated in blue zinc oxide-based paint and individual spectra confirm it is also present in white paint, consistent with the observation of defined zinc and carbon-rich areas of low atomic density in both layers. The close association of different carboxylates such as zinc lactate and zinc stearate/palmitate is another interesting finding, as is the unusual incidence of zinc lactate apparently distributed through all layers in the painting.

5.4.5 *Staring out game* 1980

The final painting discussed in this chapter dates from 1980 and is shown in Figure 5.40. Drying cracks and age cracks are generally noted with some associated paint loss (Ebert 2011c). Sample #2, taken from the foreground centre-bottom edge, is shown in cross-section in Figure 5.41.

Figure 5.40 *Staring out game* **1980, oil on canvas, 74.6 x 94.2 cm. Witness Collection. The source location of samples is indicated in the small offset image**
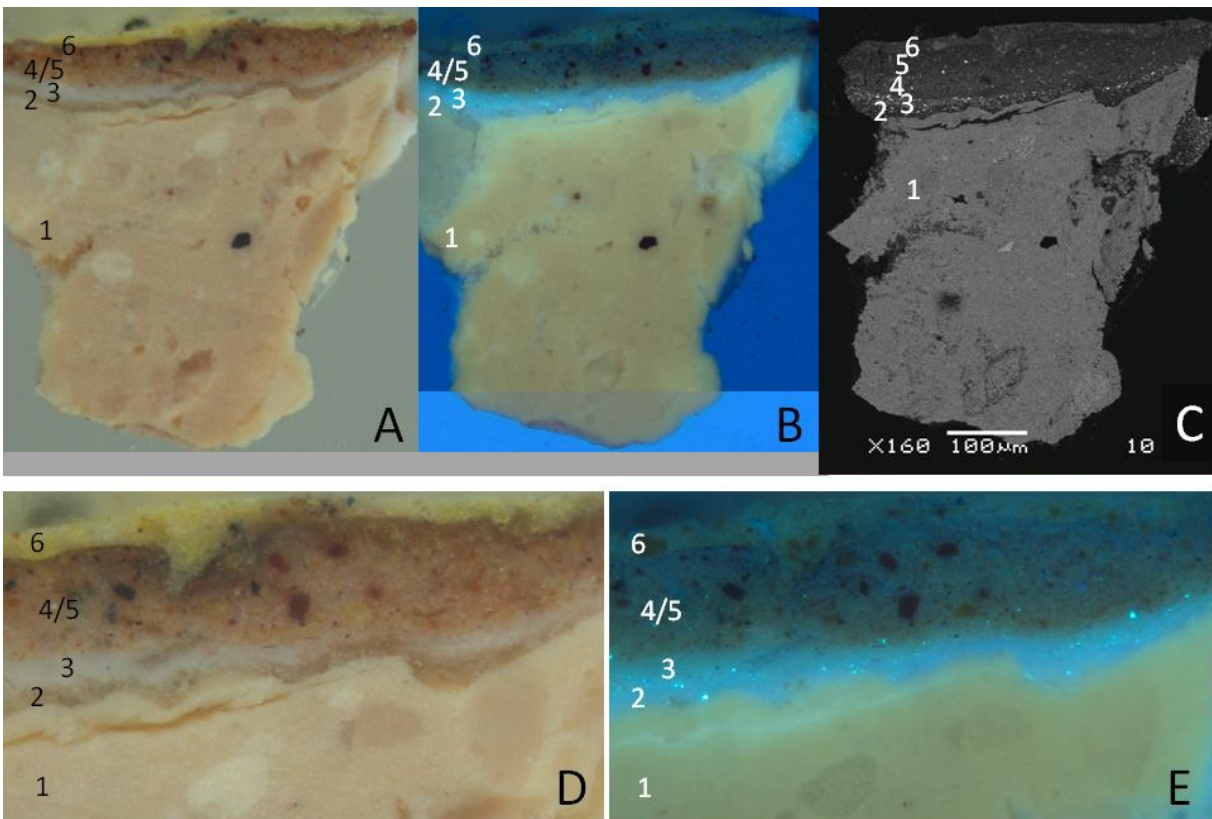
Figure 5.41 *Staring out game* **1980 sample #2 cross-section from foreground bottom edge as optical images (A) visible and (B) UVF, and (C) corresponding BSE image, and higher magnification optical image details (D and E). Numbers correspond to layers described in the text**

The sample incorporates a thick lithopone ground layer (1) to which it appears an unpigmented layer (2) has been applied. A thin white layer (3) containing zinc oxide and lead white pigment is discussed in terms of preferential zinc oxide dissolution in published work. This layer is UV-fluorescent with some sparkling particles. Layers 4-6 are all zinc oxide-based paint with varying coloured pigmentation. The incidence of both lead white and zinc oxide in a single layer of white paint suggests the combination occurs within a commercial formulation rather than arising from an artist mix. This can be more confidently supposed than from the same mixture occurring in coloured paint, for example zinc and lead white containing layers within *Children playing at the beach*, as zinc oxide is frequently found in coloured paint formulations and may not necessarily derive from the white paint with which it is mixed.

A second paint sample from *Staring out game* is shown in Figure 5.42, sourced from an area of blue sky.
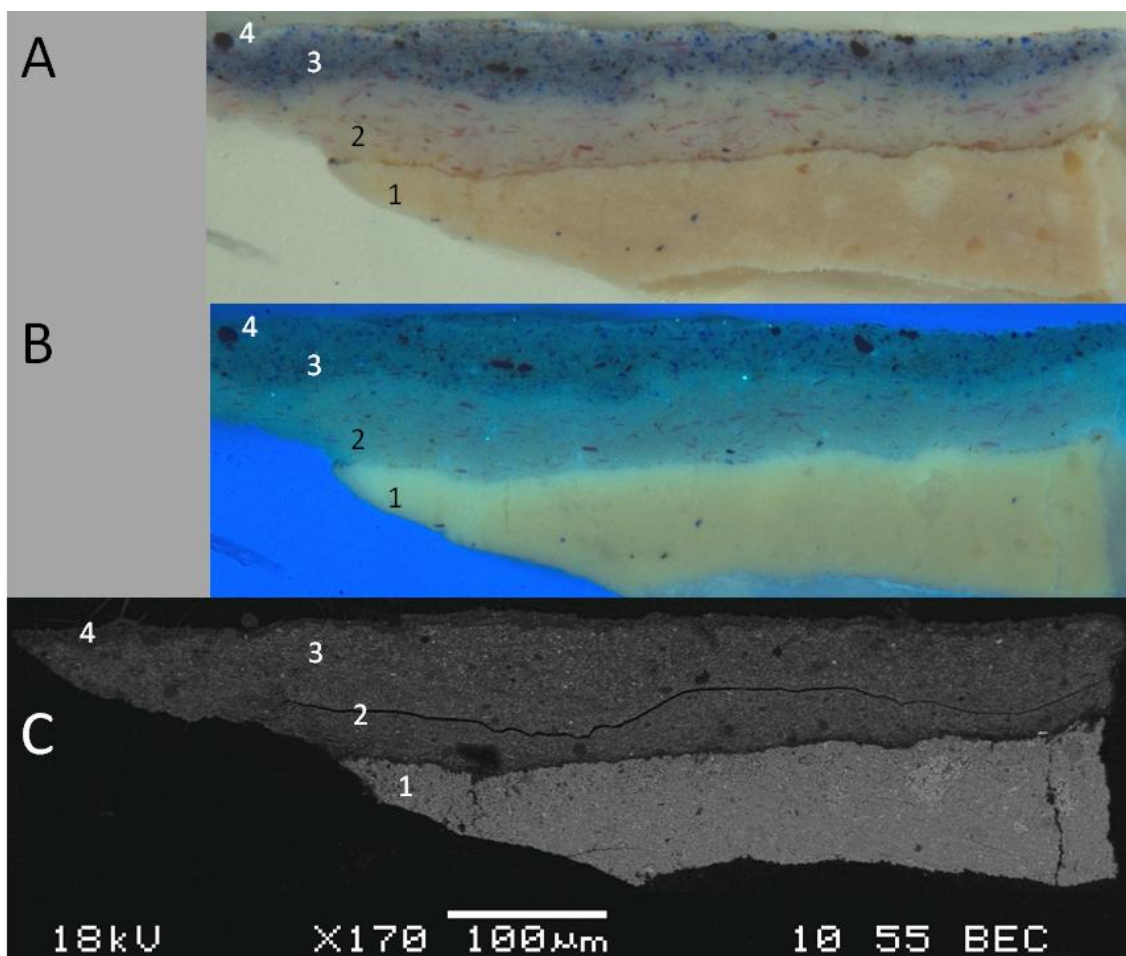
Figure 5.42 *Staring out game* **sample #3 cross-section from deep blue sky at top left as optical images (A) visible and (B) UVF, and (C) corresponding BSE image. Numbers correspond to layers described in the text**

The structure of sample #3 is relatively simple with a lithopone ground (1) and two zinc oxide-based paint layers (2-3). In the BSE image a thin, dark pigmented surface layer (4) is also apparent and does not appear to contain zinc oxide or any base pigment. This layer is not clearly resolved in optical images except possibly as a greyish surface lightening. A thin unpigmented layer may additionally be present between ground and paint. Cobalt violet (cobalt(II) phosphate, $Co_3(PO_4)_2$) is found in all paint layers with additional bone black (calcium phosphate, $Ca_3(PO_4)_2$) and a sodium aluminium silicate blue in layer 3. The possibility of added zinc stearate is suggested by the presence of defined circular features in layer 2 as shown in Figure 5.43.
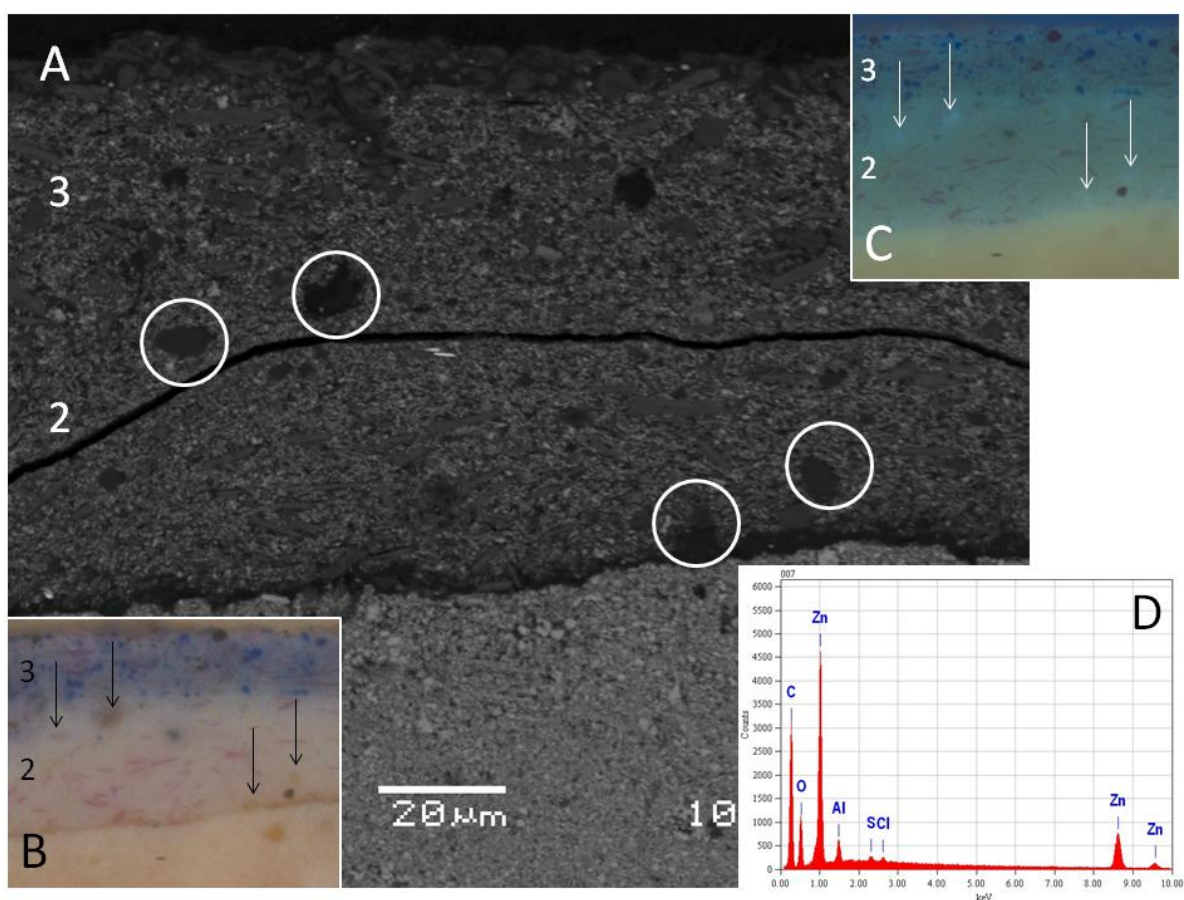
Figure 5.43 *Staring out game* **#3 (A) BSE detail with corresponding optical images (B) visible and (C) UVF and SEM-EDX spectrum (C) representative of those obtained from the features circled**

The circled features are dark in the visible image and fluorescent in UV. In the BSE image each area has low atomic density with a defined perimeter boundary and yields a consistent SEM-EDX spectrum dominated by zinc and carbon. Morphology suggests the zinc soap may be present as a paint additive.

A final cross-section from pink paint in *Staring out game* is discussed here, shown in Figure 5.44.
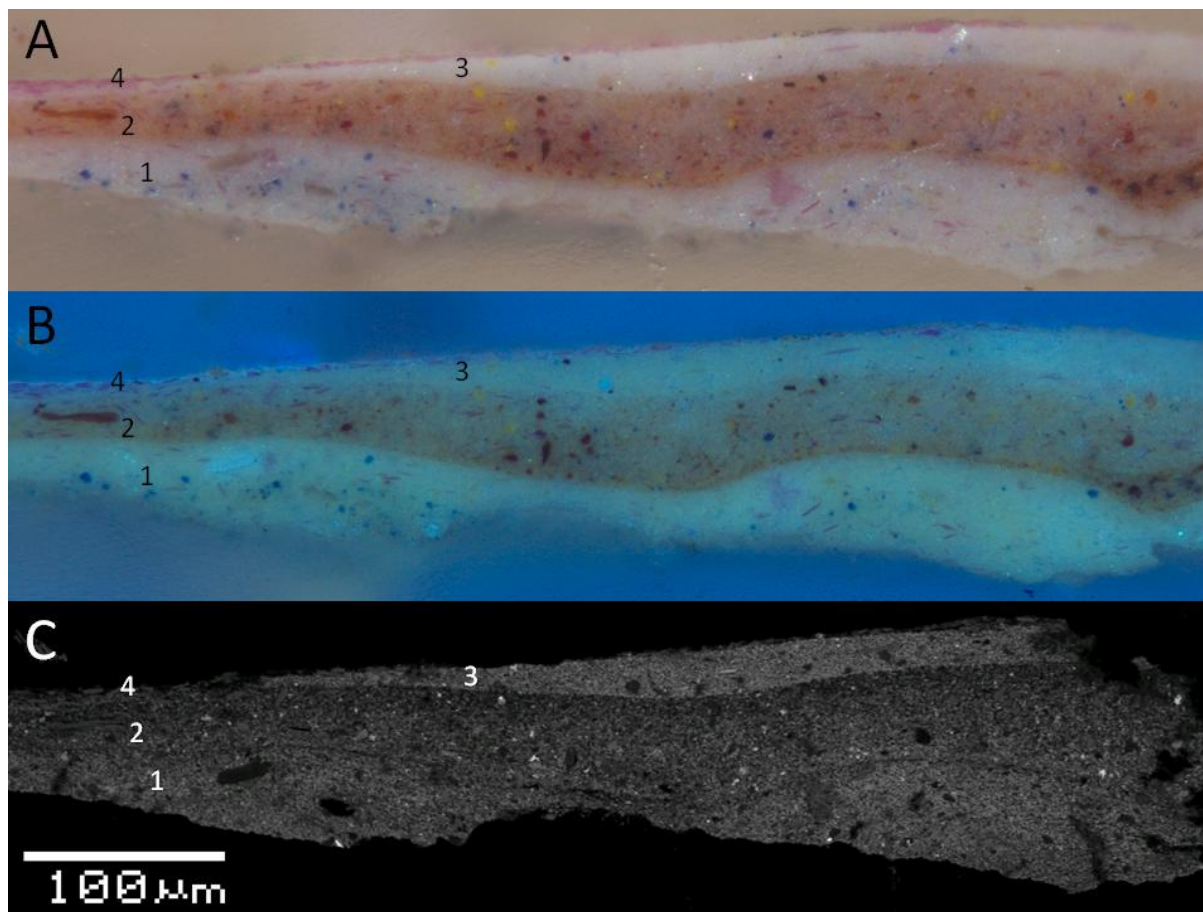
Figure 5.44 *Staring out game* sample #1 cross-section from dark pink stripe, upper left edge as optical images (A) visible and (B) UVF, and (C) corresponding BSE image. Numbers correspond to layers described in the text

No ground layer is present in sample #1. All paint layers (1-4) are zinc oxide-based; cobalt violet occurs throughout albeit in small amounts in layer 3 which is predominantly white. Pigmentation is variously complex including cadmium yellow and an iron-based red in layer 2. No lead white is evident; its absence in this white paint when compared to the mixture of lead and zinc whites in white paint in sample #2 confirms that Kiệm was using more than one preparation of white paint within a single painting. SEM-EDX elemental maps detailing upper layers from an area right of centre are shown in Figure 5.45.
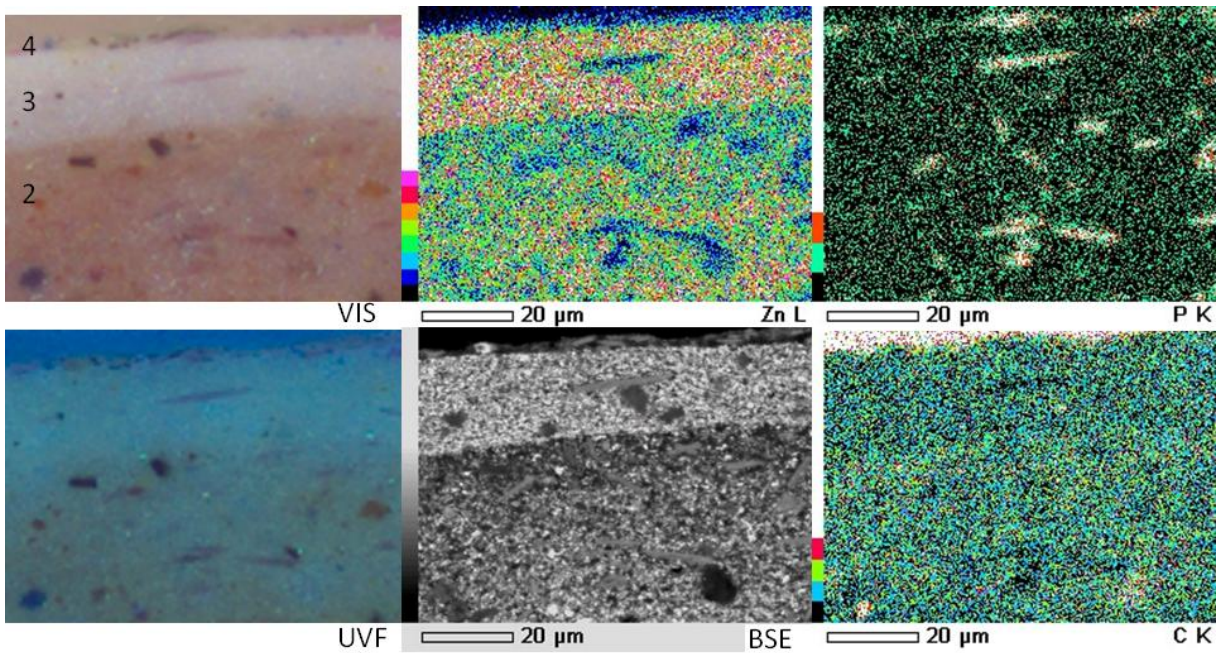
Figure 5.45 *Staring out game* **#1 cross-section detail of layers 2-3 as optical and BSE images with corresponding SEM-EDX maps for the elements shown**

The phosphorous map correlates closely to the cobalt map (not shown) and corresponds to distinctive elongated particles in the BSE and optical images. Zinc counts are strong in layers 2-3 but reduced in the upper margin of layer 2, coinciding with elevated carbon counts. A dark band is also seen in the BSE image (Figure 5.44) between layers 1 and 2, shown at higher magnification in Figure 5.46. Unlike the boundary between layers 2 and 3 above, this does not obviously correspond to reduced zinc or increased carbon counts and may in fact reflect the beginning of a physical separation.
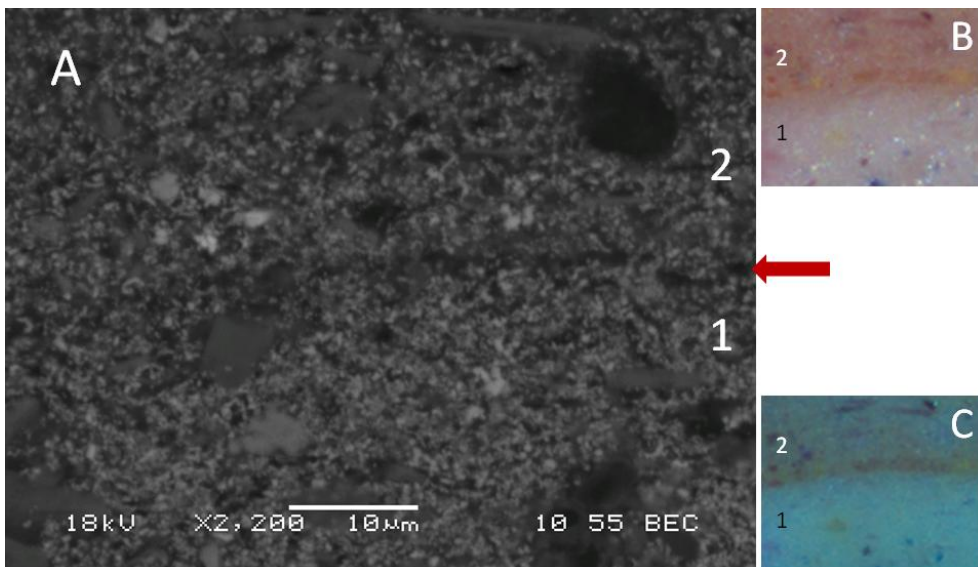
Figure 5.46 *Staring out game* **#1 cross-section detail of layers 2-3 (A) BSE with corresponding optical images (B) visible and (C) UVF. Arrow denotes possible physical separation between layers**

The FTIR spectrum obtained from a fragment of sample #1 prior to embedding is shown in Figure 5.47.
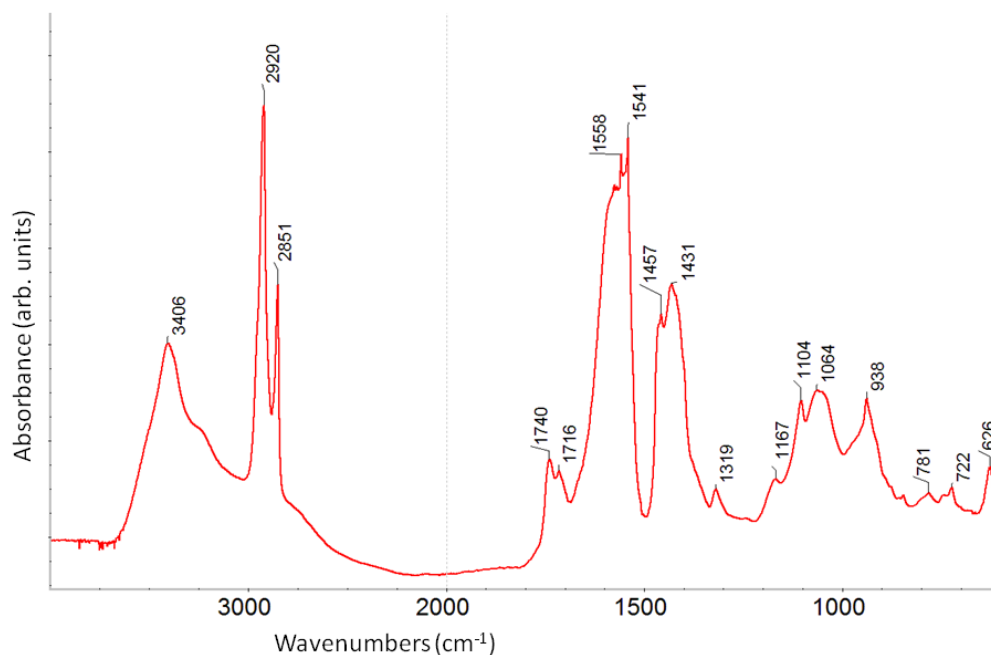
Figure 5.47 *Staring out game* **#1 transmission FTIR spectrum obtained prior to embedding**

Broad carboxylate absorption typical of zinc white-based paints dominates the spectrum between 1520 and 1630 cm^{-1}. A sharp peak at 1541 cm^{-1} projects above the broader absorption indicating the presence of zinc stearate/palmitate. Hydrolysis is again suggested by the defined acid carbonyl at 1716 cm^{-1} adjacent to the oil ester carbonyl at 1740 cm^{-1} together with OH (3400) and C-O (1319 cm^{-1}) stretching vibrations. Possible sulfates (1000-1200 cm^{-1}) may also contribute to strong OH absorption.

5.5   Concluding remarks

Paint samples from five paintings by Nguyễn Trọng Kiệm allow investigation of a variety of deterioration mechanisms occurring in zinc oxide-based paint layers. The paintings have been exposed to warm, humid conditions which have inevitably accelerated deterioration, and significant chemical and structural deterioration is evident even in more recent works. In FTIR spectra significant oil hydrolysis is indicated by typically low oil ester carbonyl absorption, simultaneously broadened by, or with defined acid carbonyl peaks and little evidence of ester C-O bands expected for intact triglyceride structures. The resultant release of fatty acids combined with a prevalence of zinc oxide in Kiệm's paintings translates to formation of zinc carboxylates, signalled strongly in FTIR.

Although painted by the one artist and to a significant extent conforming to traditional western approaches to painting, the restrictive and impoverished conditions in North Vietnam under which Kiệm produced these works limited his choice of materials and has almost certainly necessitated substitutions and compromise based on availability. Kiệm is said to have disliked zinc white, preferring titanium white for painting, but the five paintings examined here suggest the artist used whatever paint was available, with zinc white predominant. Samples variously include pure zinc white, lead white containing a substantial proportion of zinc oxide and zinc white to which a small amount of titanium white paint appears to have added, apparently mixed by the artist in some cases but potentially as a commercial preparation in others. Lithopone is also used on occasion, consistently for ground preparations but also in coloured paints, most notably in areas of later artist reworking. Paint layers combining lead and zinc whites are observed to sparkle under UV in two post-war paintings, while a sparkling layer in the earlier *Portrait of a student* does not contain lead. Variable zinc oxide particle characteristics including size and UV-fluorescence properties are evident across the range of Kiệm's paints both between and within individual samples. In several paints zinc stearate is conceivably present as an original constituent. Component variability will undoubtedly have influenced reactivity and degradation processes occurring in Kiệm's paintings.

Unusual large zinc and sulphur-containing masses which have formed in *Portrait of my wife* were not observed in samples from other paintings by Kiệm although caution is required in drawing conclusions from the limited number of cross-sections examined which have largely been interpreted without reference to the paintings themselves. However, the presence of a thick layer of body paint to impart texture in *Portrait of my wife* is not typical of Kiệm's work. The painting's experimental nature and strong correlation of zinc and sulphur in layers uniquely used to achieve impasto make it plausible that sulphur compounds were present in pigment stock prior to paint mixing, formed either during production or in dry pigment storage. Supporting evidence includes shared history with a second work produced the same year without impasto which is not affected, and indications of SO_2 exposure in other paintings, notably examples of sulfur-affected zinc yellow, without comparable deterioration. The presence of sulfates is inferred by characteristic IR absorptions but they occur within complex spectra which also variously include vibrations characteristic of zinc stearate/palmitate, zinc lactate and basic zinc carbonate. Significantly, X-ray diffraction data from an affected sample did not detect any crystalline zinc sulfate. However, an ambiguous peak at 32.8° 2θ may be attributable to the (100) plane of layered basic salts with brucite type zinc hydroxide structure. High and fluctuating relative humidity levels may cause repeat cycles of dissolution, diffusion and recrystallisation of water soluble salts including zinc sulfate, which offer a potential source of zinc and hydroxyl ions for reaction with carboxylic acids. Formation of

layered basic zinc salts incorporating carboxylate, carbonate and sulphate ligands could then account for morphologically distinct features in samples from the painting. Such multifunctional complexes are feasible given zinc's unoccupied valence shell orbitals, but the incidence of specific coordination structures requires further investigation.

Although such distinctive deterioration is not evident in each of Kiệm's paintings, all are structurally fragile. Detailed consideration of particle morphology revealed in backscatter electron images in conjunction with FTIR analysis does suggest a progressive loss of zinc oxide pigment which will influence current and future mechanical properties and stability of the paintings. Bright particles of zinc oxide in paint cross-sections with indistinct peripheral boundaries and surrounded by poorly defined masses of lower BSE density matter are frequently observed. Partial saponification of zinc oxide pigment is supported by comparison with control samples characterised as zinc oxide and zinc stearate in conjunction with FTIR analysis confirming the presence of metal carboxylates.

Further examples of zinc oxide reactivity are seen in Kiệm's paintings based on apparent preferential dissolution when present in mixtures with lead white, Naples yellow, chalk or iron based red pigment. In each case particles of zinc oxide have lost definition and atomic density in BSE images which is not evident in accompanying pigment types. This is most pronounced in paint adjacent to unpigmented layers with presumed capacity to act as reservoirs of water or fatty acids that facilitate saponification at the surface of proximate zinc oxide particles. When an unpigmented layer adjoins zinc oxide-based paint on one side and a lithopone layer on the other, the preferential dissolution is only apparent in the zinc oxide-based layer, irrespective of particle size or layer sequence. Conventional FTIR of paint fragments consistently indicates the presence of zinc carboxylates with zinc stearate/palmitate regularly dominating, evidenced by strong v_a COO$^-$ at 1540 cm^{-1}. Paints with multiple or extended regions of apparent dissolution appear more susceptible to cracking under vacuum in the SEM.

Dissolution of zinc oxide also appears to be favoured at the interface between two zinc oxide containing paint layers, and accompanying poor adhesion is suggested in at least one sample. Examples include paint where zinc oxide predominates in both layers and others where one layer incorporates zinc oxide in combination with lead white or lithopone. The absence of ground layers from a number of cross-sections, and the high incidence of flaking reported for Kiệm's paintings generally are further indicators of structural weakness at interfaces.

In some cases zinc stearate may derive from its possible inclusion in paint formulations based on the incidence of regular circular features rich in carbon and zinc with defined perimeter boundaries

dispersed across a particular paint layer, but this is not consistently indicated. Unfortunately only limited SR-μFTIR of Kiệm's samples was possible and has not confirmed this interpretation. In one sample a substantially stronger zinc stearate/palmitate signal is measured with SR-μFTIR in blue paint than white paint when both predominantly comprise zinc oxide and incorporate similar circular features with comparable elemental composition. The white paint records a more intense oil ester carbonyl absorption suggesting a lower rate of saponification in this layer than has occurred in blue paint; this in turn infers that *in situ* saponification may contribute proportionally more to overall carboxylate absorption in FTIR spectra than zinc stearate as a component in the formulation.

More surprisingly, zinc lactate also appears to feature strongly in FTIR spectra from a number of Kiệm's paintings. SR-μFTIR does not associate this specifically with any one layer or component, suggesting lactic acid may derive from the paint medium more generally.

The predominance of zinc oxide in Kiệm's paintings coupled with relatively extreme exposure history has contributed to notable deterioration within just a few decades. Useful case studies are provided by paintings incorporating zinc oxide with different particle properties and in different pigment combinations. The warm humid conditions prevalent in Vietnam favour oil hydrolysis, and analysis supports the premise of zinc carboxylates having developed in the early stages of film formation or perhaps even prior to paint application, with reaction continuing as further fatty acids are released. Zinc oxide is unquestionably a reactive pigment and formation of sulphates and carbonates during production or in dry pigment stocks, in addition to rapid soap formation with fatty acids in oil-based media all have implications for the current condition of these paintings.

5.6   References

Burnstock A, van den Berg KJ, de Groot S, Wijnberg L (2007) An investigation of water sensitive oil paints in twentieth century paintings. In: Learner T, Smithen P, Krueger JW, Schilling MR (eds) *Modern Paints Uncovered*, Tate Modern, London, 16-19 May 2006. The Getty Conservation Institute, pp 177-188

Casadio F, Xie S, Rukes S, Myers B, Gray K, Warta R, Fiedler I (2011) Electron energy loss spectroscopy elucidates the elusive darkening of zinc potassium chromate in Georges Seurat's 'A Sunday on La Grande Jatte-1884'. *Anal Bioanal Chem* 399 (9):2909-2920. doi:10.1007/s00216-010-4264-9

Dik J, Hermens E, Peschar R, Schenk H (2005) Early production recipes for lead antimonate yellow in Italian art. *Archaeometry* 47 (3):593-607. doi:10.1111/j.1475-4754.2005.00221.x

Ebert B (2008) *Volume II: A scientific investigation into the degradation processes of zinc-based paints together with art historical research* MA thesis, Northumbria University, Newcastle

Ebert B (2011a) *Examination report: Nguyễn Trọng Kiệm, Children playing at the beach, W06.8.61.*

Ebert B (2011b) *Examination report: Nguyễn Trọng Kiệm, Hàng Giấy, W06.8.59.*

Ebert B (2011c) *Examination report: Nguyễn Trọng Kiệm, Staring out game, W06.3.3.*

Ebert B, MacMillan Armstrong S, Singer B, Grimaldi N (2011) Analysis and conservation treatment of Vietnamese paintings. In: Bridgland J, Antomarchi C (eds) *Preprints of the ICOM Committee for Conservation 16th Triennial Meeting*, Lisbon, 2011. ICOM-CC, p 1305

Hay D (2012) *XRD Microdiffraction Study of Paint Flake for University of Queensland and Queensland Art Gallery Conservation, 29 August 2012*. CSIRO Materials Science and Technology, Melbourne

Helwig K, Poulin J, Corbeil M-C, Moffatt E, Duguay D (2014) Conservation issues in several 20th-century Canadian oil paintings: the role of zinc carboxylate reaction products. In: van den Berg KJ, Burnstock A, de Tagle M et al. (eds) *Issues in Contemporary Oil Paint*. Springer International Publishing, Switzerland, p Chapter 11. In press. doi:10.1007/978-3-319-10100-2__11

Inoue S, Fujihara S (2011) Liquid−Liquid Biphasic Synthesis of Layered Zinc Hydroxides Intercalated with Long-Chain Carboxylate Ions and Their Conversion into ZnO Nanostructures. *Inorg Chem* 50 (8):3605-3612. doi:10.1021/ic1025729

Jackson KDO (1998) A guide to identifying common inorganic fillers and activators using vibrational spectroscopy. *The Internet Journal of Vibrational Spectroscopy (wwwijvscom)* 2 (3):article no. 6

Keune K, van Loon A, Boon JJ (2011) SEM Backscattered-Electron Images of Paint Cross Sections as Information Source for the Presence of the Lead White Pigment and Lead-Related Degradation and Migration Phenomena in Oil Paintings. *Microsc Microanal* 17 (05):696-701. doi:10.1017/S1431927610094444

MacMillan S (2007) *A report on the art historical investigation, condition, technical examination and initial investigations into the conservation treatment of two paintings on canvas by Vietnamese artist Nguyen Trong Kiem (1933-1991) dated 1963; in conjunction with scientific investigation of various tube paints used by Vietnamese artists during the mid C20th, and the materials, degradation mechanisms and conservation issues regarding the two paintings*. MA thesis, Northumbria University, Newcastle

Meilunas R, Bentsen J, Steinberg A (1990) Analysis of aged paint binders by FTIR spectroscopy. *Stud Conserv* 35:33-51

Miser HD, Glass JJ (1941) Fluorescent sodalite and hackmanite from Magnet Cove, Arkansas. *Am Mineral* 26 (7):437-445

Nguyen Tran Minh, Tran Thi Minh Man (2008) *Interview transcript with Nguyen Trong Kiem's family included as Appendix 1 in MacMillan 2007*. interview transcript Hanoi

Noble P, van Loon A, Boon JJ (2005) Chemical changes in old master paintings II: darkening due to increased transparency as a result of metal soap formation. In: Verger I (ed) *Preprints of the ICOM Committee for Conservation 14th Triennial meeting*, The Hague, 12-16 September 2005. James and James, London, pp 496-503

Philadelphia Museum of Art (2007) *IMP00223 Riebeckite*. In: Price BA, Pretzel B (eds) Infrared and Raman Users Group spectral database. http://www.irug.org/

Singer B, MacMillan S, Grimaldi N, Brown J (2009) Analysis of Vietnamese oil paintings affected by sulphur dioxide pollution. In: Lee S, Huy NN (eds) *Essays on Modern and Contemporary Vietnamese Art*. Singapore Art Museum., Singapore, pp 68-74

Tse N (2008) *The characterisation of oil paintings in tropical southeast Asia*. PhD thesis, The University of Melbourne, Melbourne

van der Weerd J, van Loon A, Boon JJ (2005) FTIR studies of the effects of pigments on the aging of oil. *Stud Conserv* 50 (1):3-22

Wu C-M, Baltrusaitis J, Gillan EG, Grassian VH (2011) Sulfur Dioxide Adsorption on ZnO Nanoparticles and Nanorods. *The Journal of Physical Chemistry C* 115 (20):10164-10172. doi:10.1021/jp201986j

Zhang X, Xing N, Bai F, Wan L, Shan H, Hou Y, Xing Y, Shi Z (2013) Multi-functional d10 metal-organic materials based on bis-pyrazole/pyridine ligands supported by a 2,6-di(3-pyrazolyl)pyridine with different spanning flexible dicarboxylate ligands: synthesis, structure, photoluminescent and catalytic properties. *CrystEngComm* 15 (44):9135-9147. doi:10.1039/c3ce41213j

6 Zinc carboxylate formation in the paintings of E. Phillips Fox

6.1 Introduction

In 2011 the Queensland Art Gallery presented a significant Australian art exhibition, *Art, Life and Love: Ethel Carrick and E Phillips Fox*. The preparation of paintings for this exhibition fortuitously coincided with independent post graduate research into the materials and techniques of Phillips Fox being undertaken by Melbourne-based conservator, Catherine Nunn (Nunn 2012). These concurrent activities provided a rare opportunity to obtain and investigate samples from a range of the artist's paintings. Emanuel Phillips Fox (1865-1915) was a respected Australian artist who spent much of his career based in England and France. His paintings clearly show the influence of French late-Impressionist painting technique. Although it is not clear that Fox was consciously choosing to use zinc white over lead white paint either generally or for specific applications, his paintings do frequently include zinc oxide-based layers. In the course of Nunn's research she observed that various Fox paintings had developed an unusual granular texture with coarse lumps disrupting the image surface. The possibility that these lumps were attributable to zinc soap aggregates presented an obvious opportunity for collaboration, with Nunn providing samples from paintings she considered to be affected. Additional paint samples were sourced from Fox paintings within the Queensland Art Gallery collection. The range of paintings investigated reflects the availability of samples for analysis; although they all derive from the period 1900-1911, this does not necessarily imply works from this time are more susceptible than those from other periods of Fox's career. The start of the twentieth century saw Fox's return from Australia to Europe (England 1901-1905 and Paris 1905-1912) which Nunn (2012) has defined as Fox's mid-career oeuvre. Nunn's research has demonstrated that at this time Fox was consciously working to achieve a matt aesthetic involving use of thick, opaque paint layers applied across absorbent supports. Paintings with both commercial (oil) and artist (glue) prepared ground layers are represented. They include small works completed rapidly *en plein air*, large-scale studio compositions, and paintings with a range of conservation histories including both lined and unlined examples. The implications of painting technique, exposure history and the incidence of zinc oxide-based paint for the stability of Fox's paintings is the focus of this chapter.

6.2 Overview of paintings and samples

Samples from five mid-career paintings by Fox are represented in the current study, all painted on canvas supports. The two earliest works have commercial oil-ground layers. *Autumn showers* (c. 1900, Melbourne period) (Figure 6.1) has a double ground based on chalk and lead white, and *Untitled (Ploughing)* (not dated, Paris period?) (Figure 6.2) includes a zinc oxide-based priming.

Although many of Fox's paintings were painted on commercially prepared supports (Nunn 2012), the specific grounds of these two paintings are unusual among his oeuvre. *Autumn showers* is in a particularly poor state of preservation with widespread cracking. It has been wax-lined onto a solid support, and *Ploughing* has been consolidated with wax.

Figure 6.1 E. Phillips Fox (Australia; France, b.1865, d.1915) *Autumn showers* **1900, oil on canvas, 153 x 193 cm, Art Gallery of NSW, purchased 1900. Photo: AGNSW**

Figure 6.2 Fox, E. Phillips (1865-1915) *Untitled (Ploughing)***, not dated, oil on canvas, 46 x 38 cm. The University of Melbourne Art Collection, gift of Dr and Mrs Eric Stock 1989**

Bathing hour (c. 1909) (Figure 6.3) is a large format studio painting which was exhibited at the New Salon in 1912 (Goddard 2011). *Rocks and sea* c. 1911 (Figure 6.4) is a small work completed quickly during an extended Mediterranean painting trip (Nunn 2012). Despite their differences, both works have been painted on canvases hand-prepared using Fox's self-described combination of 'special size' and plaster of Paris (gypsum). This formulation produced an absorbent ground suited to Fox's preference for a matt aesthetic, but in the case of *Rocks and sea* would also have had practical benefits for working *en plein air* and transporting finished canvases en route by facilitating more rapid drying of paint (Nunn 2012). *Rocks and sea* is widely cracked and has been marouflaged onto a solid support, possibly using the heat-seal adhesive BEVA$^{®}$371 (Nunn, personal communication, email 29 June 2010). *Bathing hour* is unlined and in relatively good condition although the paint film is cracked, brittle and generally fragile with fragments prone to detachment.

Figure 6.3 E. Phillips Fox, *Bathing hour (L'heure du bain)* **c.1909, oil on canvas, 184 x 113 cm. Queensland Art Gallery collection, purchased 1946**
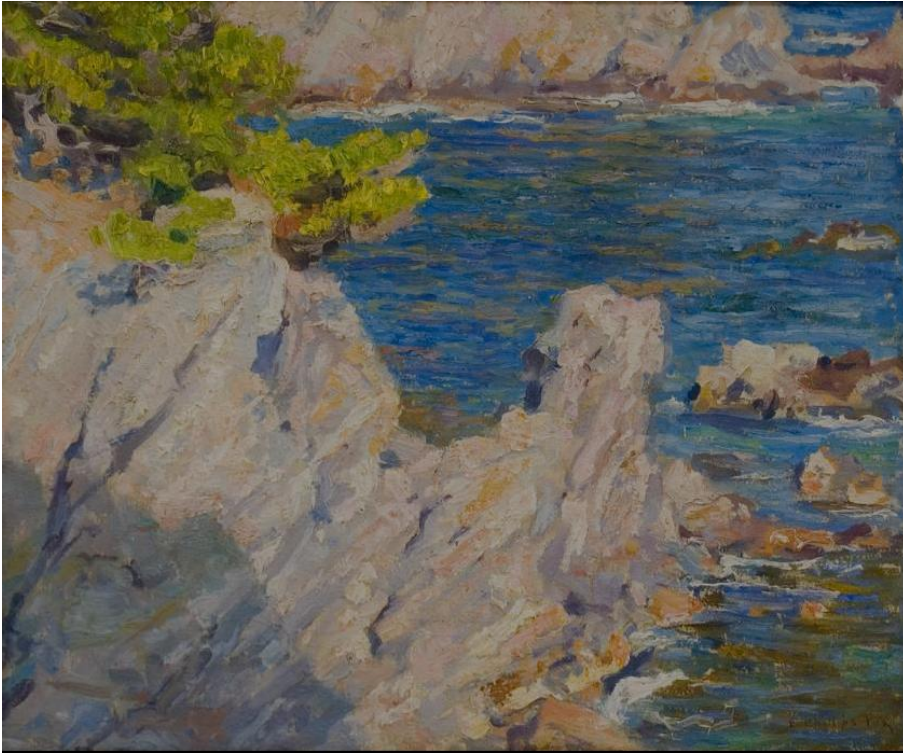
Figure 6.4 Fox, E. Phillips (1865-1915) *Rocks and sea* **c. 1911, oil on canvas, 36 x 44 cm. The University of Melbourne Art Collection, gift of Dr Samuel Arthur Ewing 1938**

Lamplight c. 1911 (Figure 6.5) is another large scale work painted in Paris for exhibition at the Royal Academy, London 1911 and the Paris Salon 1912. It has a commercial lead white-based oil ground. The painting was shipped to Australia in 1913 for exhibition in Melbourne and Sydney, and was donated to the University of Melbourne in 1939. It spent many years hanging in the Union Buffet, 'baking in the... sun due to a glass wall at the end of the Buffet' before receiving conservation treatment in the 1980s (Nunn 2008). Treatment included surface cleaning with Vulpex® (Nunn, personal communication, email 29 June 2010), a strongly alkaline anionic surfactant solution (aqueous potassium methyl cyclohexyl oleate).

Figure 6.5 Fox, E. Phillips (1865-1915) *Lamplight* **c. 1911, oil on canvas, 188.5 x 229.5 cm. The University of Melbourne Art Collection, gift of Mrs E. Phillips Fox 1939**

Nine paint samples from the five paintings were obtained and prepared as cross-sections. Where possible, fragments from the same samples prior to embedding were analysed with conventional FTIR microspectroscopy in transmission mode. Cross-sections were examined using optical microscopy and SEM-EDX, and ATR-FTIR was applied to large features evident in some of the samples. Thin-sections were taken from a selection of samples for the purpose of SR-µFTIR in transmission mode. Unfortunately it was not possible to obtain viable thin-sections in every case, so ATR-SR-µFTIR was alternatively undertaken on the embedded block-face of samples.

6.3   Results

6.3.1 *Autumn Showers* c. 1900

Unusually for the group of Fox's paintings investigated here and also among the much larger range considered by Nunn (2012), *Autumn showers* is painted on a commercial double oil ground based on chalk and lead white. The paint sample discussed here derives from the sky (Figure 6.6).

Figure 6.6 E. Phillips Fox, *Autumn showers* c. 1900 with number denoting the source location of paint sample #1

6.3.1.1 FAS#1

Optical and BSE images of sample FAS#1 are shown in Figure 6.7 and at higher magnification in Figure 6.8 - with layers numbered.
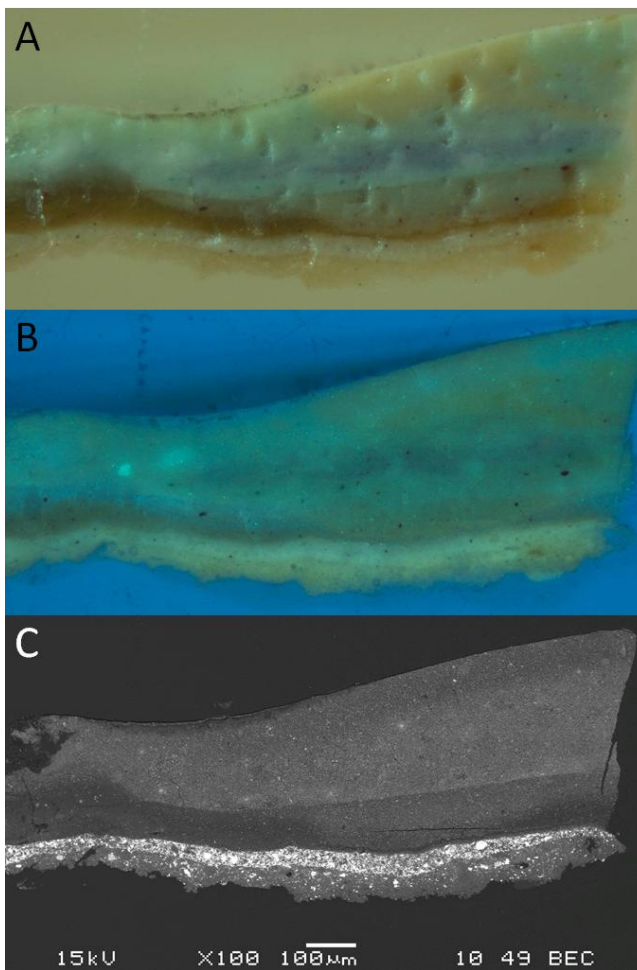
Figure 6.7 *Autumn showers* cross-section FAS#1: (A) visible, (B) UVF and (C) BSE images
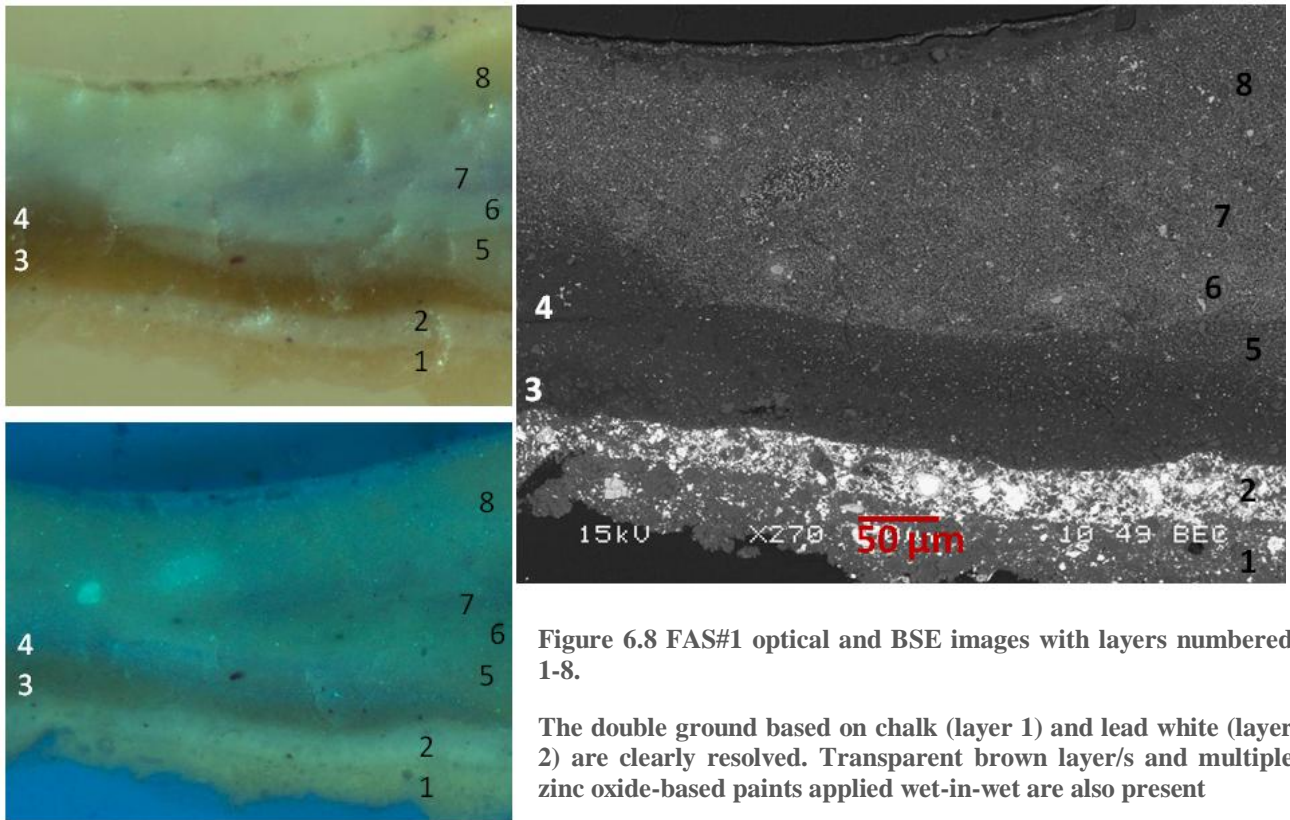
Figure 6.8 FAS#1 optical and BSE images with layers numbered 1-8.

The double ground based on chalk (layer 1) and lead white (layer 2) are clearly resolved. Transparent brown layer/s and multiple zinc oxide-based paints applied wet-in-wet are also present

The double ground is readily distinguished - layer1 predominantly chalk and layer 2 predominantly lead white with a trace of barytes. Beyond this the sample stratigraphy is difficult to precisely determine. Above the ground is a transparent brown layer (3) which has a discontinuous lighter-hued, more UV-fluorescent upper region (4). This variation is less obvious in BSE images but at higher magnification it appears layer 4 may contain more defined pigment particles. Layer 5 is only present at the right half of the cross-section and has a similar pale-brown appearance in visible light to layer 4 but lacks the general blue fluorescence and has noticeably higher electron density in BSE images (Figure 6.9). Layers 6-8+ are applied wet-in-wet or as colours mixed on the brush, variably green, purple-blue and yellow, with little to distinguish them in BSE apart from slightly lower electron density at the top margin at right which corresponds with increased autofluorescence. A dirty varnish layer is also present. All paint layers are dominated by zinc oxide and have characteristic fluorescent sparkle. Coloured pigmentation is sparse, including emerald green (copper arsenate), terre verte (green earth), red-brown iron oxide and Prussian blue. Yellow pigmentation has not been characterised. The transparent brown layer (3) contains a small amount of lead, (possibly as a drier) and a few particles of calcium sulfate, with traces of magnesium and aluminium additionally detected by SEM-EDX (Figure 6.9).
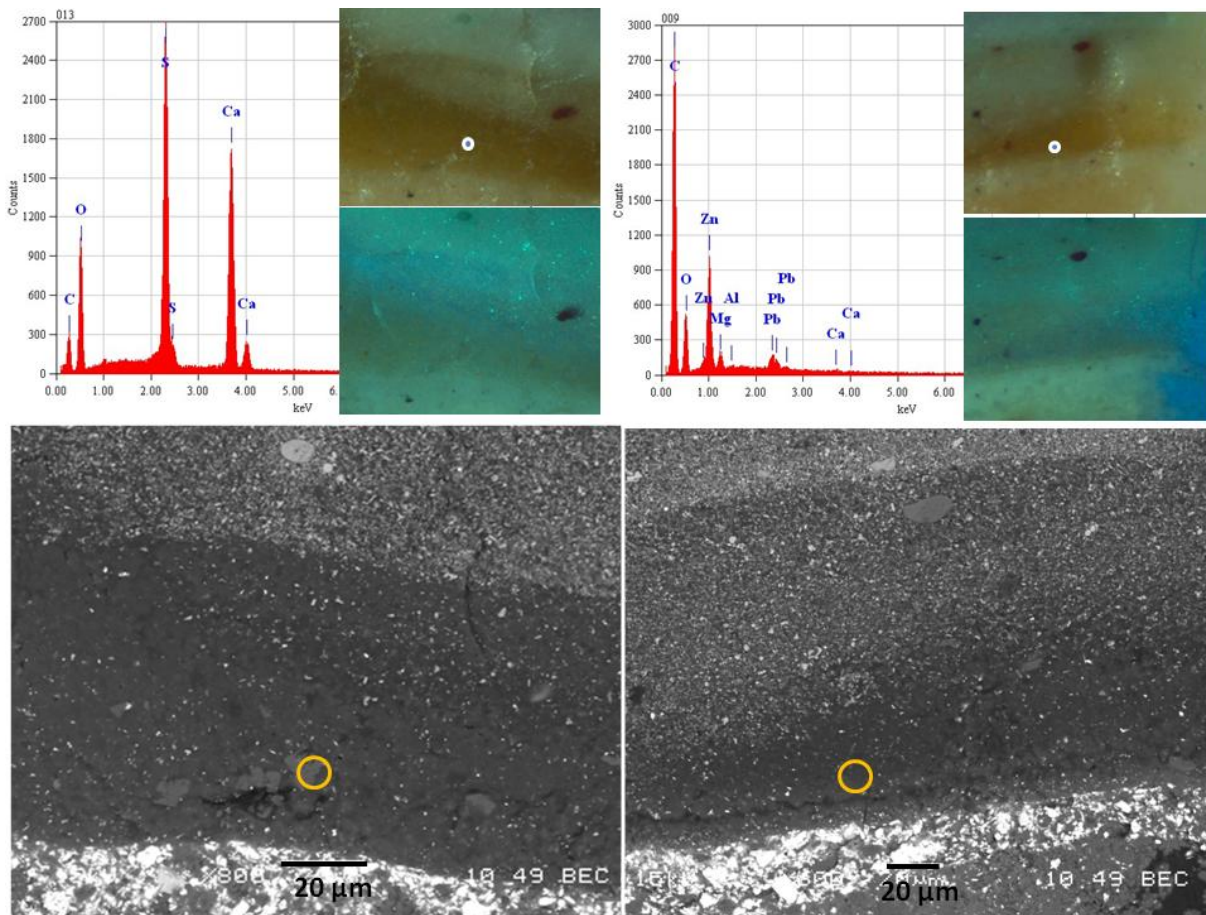
Figure 6.9 FAS#1 BSE and corresponding optical image details with circles denoting location of point EDX spectra taken from two areas of the yellowed 'toning' layer 3.

The left spectrum indicates some calcium sulfate is present in the layer. The right spectrum from a more fluorescent area shows predominantly zinc and carbon with traces of lead, magnesium, aluminium and calcium

Round white fluorescent aggregates, some with darker centres are evident in all paint layers. The cross-section surface is also dimpled, consistent with localised erosion in the course of polishing or microtoming. This suggests some parts of the sample are softer than the surrounding paint. At higher magnification, BSE images show the distinctive morphology of fluorescent features comprising relatively dispersed pigment particles of high average atomic brightness without the smaller, mid-tone particles which dominate more generally (Figure 6.10).
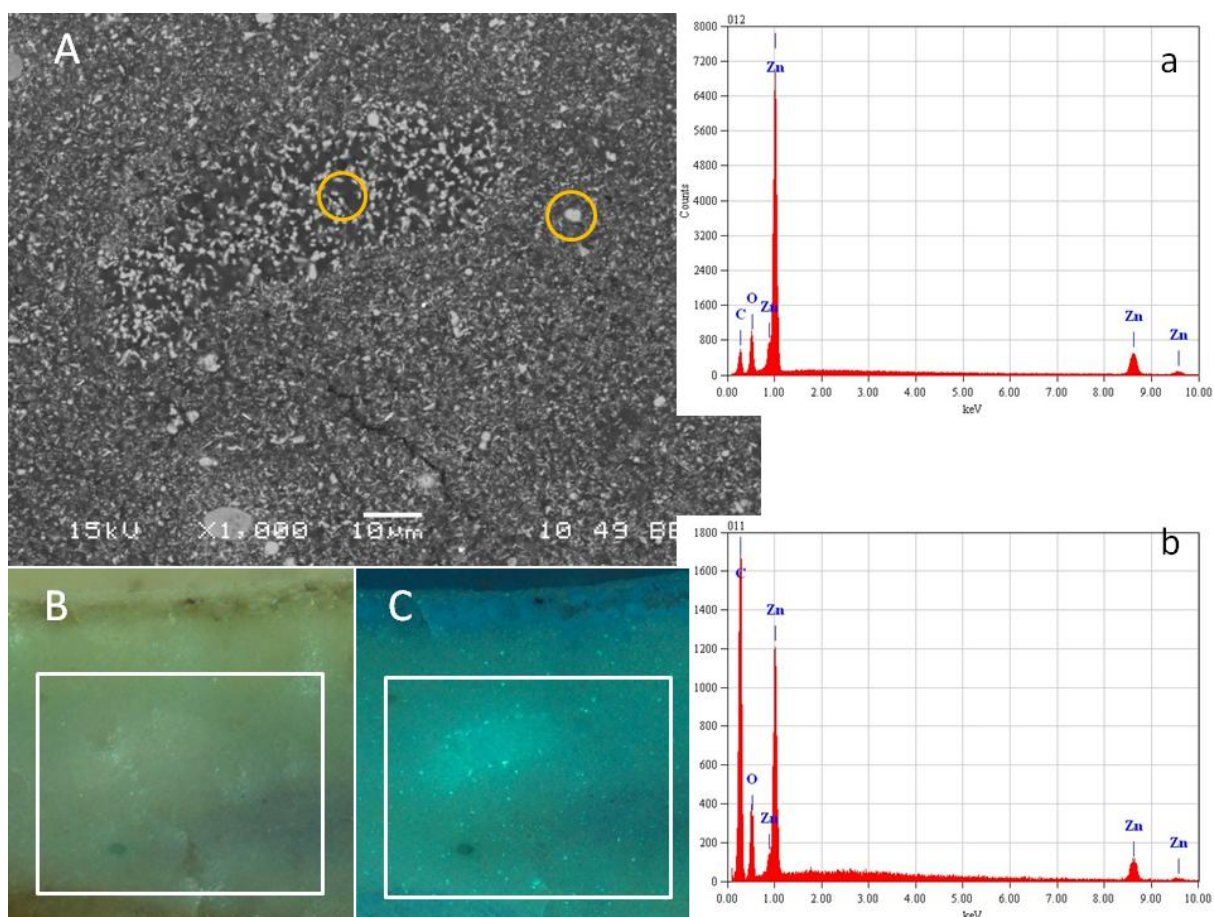
Figure 6.10 FAS#1 BSE image (A) and corresponding visible (B) and UVF (C) images with box denoting area of BSE detail.

EDX spectra obtained from the circled points show the high zinc counts and low carbon derived from a large zinc oxide pigment particle (a) compared to the high carbon and reduced zinc counts obtained from an area of lower particle density within a fluorescent white mass present in the top paint layer

Conversely, a whitish circular feature with an optically more transparent and UV-absorbent centre has morphology suggesting *in situ* crystal growth (Figure 6.11). An EDX spectrum obtained from the large central particle is dominated by zinc and is physically similar to crystals observed in *Ploughing* #3, discussed in more detail below, and characterised as basic zinc carbonate. Unfortunately it has not been possible to confirm this assignment in the case of FAS#1 as this feature was not retained following thin-sectioning for SR-µFTIR.

243
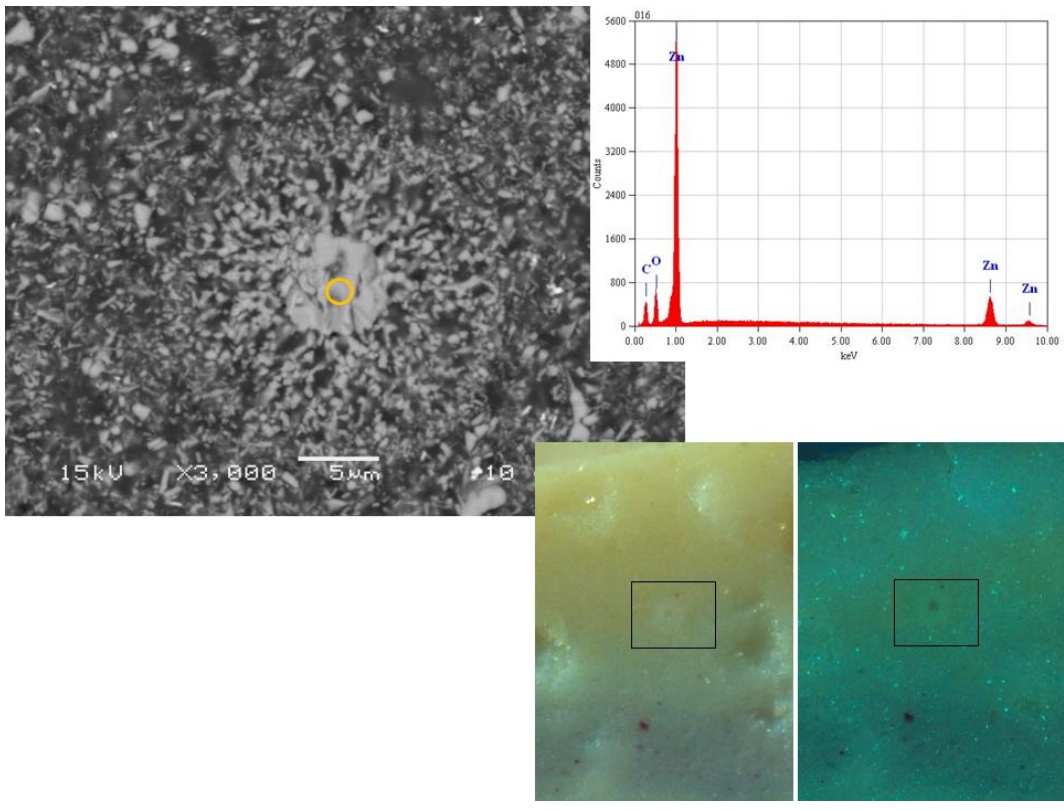
Figure 6.11 FAS#1 BSE image detail from boxed area in corresponding optical images, and EDX spectrum from the spot designated. The unusual circular feature shown has morphology suggesting *in situ* crystal growth.

Elemental composition at the centre (circled) is dominated by zinc. Optical images show the feature occurs within yellow layer 8 but appears white itself with a darker, more UV-absorbent centre than surrounding paint
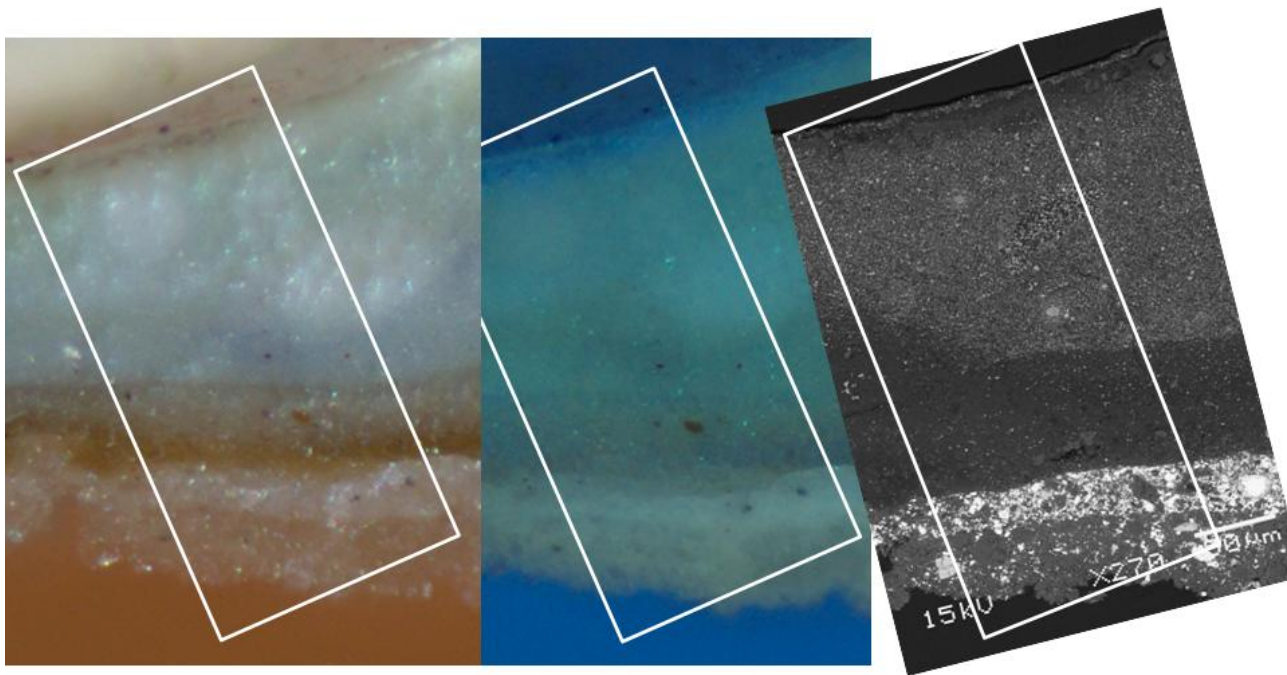
Figure 6.12 FAS#1 optical and BSE image details with boxed area denoting region mapped with SR-µFTIR.

The surface presentation for BSE varies slightly from that mapped as it predates final microtoming

Thin-sections taken from the sample unfortunately weren't viable, so the embedded block-face was used for ATR SR-µFTIR, with a slightly different presentation surface to that documented in BSE images (Figure 6.12). Spectra were acquired across a 7x16 grid with 20 µm aperture and step size corresponding to 5x5 µm² aperture on the sample. Test measurements with the ATR crystal produced a number of indentations in the sample surface which interfered with subsequent spectral acquisition from these areas, however good quality data was obtained otherwise. Spectra extracted from a line extending top to bottom along the left hand side of the map grid are shown in Figure 6.13.
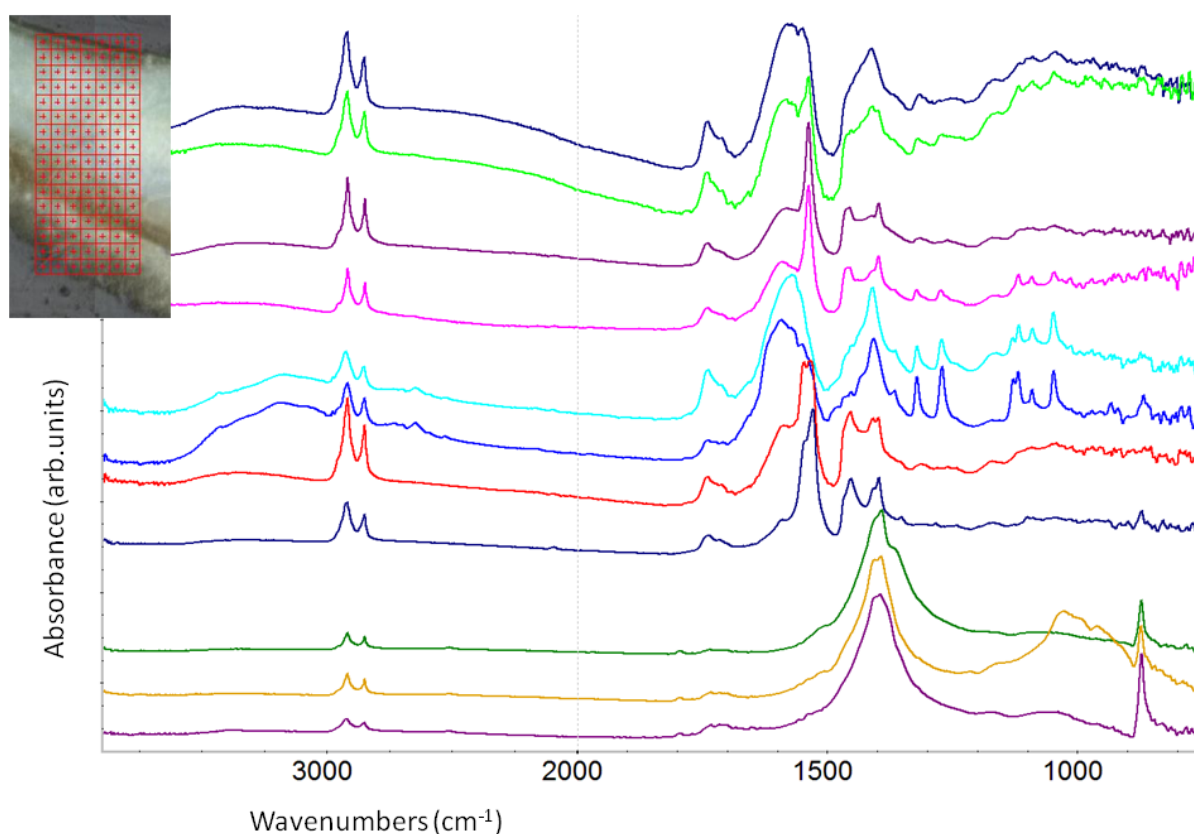
Figure 6.13 FAS#1 ATR SR-µFTIR spectra from a line extending top to bottom along the left hand side of the map grid (inset image) showing variation through the layers of the painting

The main paint layer comprising various pale hues applied wet-in-wet has carboxylate absorption ranging from a broad peak centred *ca* 1575 cm^{-1} at the upper margin, sharp peaks at 1538 and 1398 cm^{-1} in the centre, characteristic of zinc stearate/palmitate, and broad absorption centred *ca* 1590 cm^{-1} near the boundary with the toning layer. The toning layer itself includes peaks indicative of zinc stearate/palmitate and possibly zinc oleate, while the ground layers are dominated by carbonate absorption both from the chalk and lead white components, with sulfate traces. With the exception of the ground layers which show almost no absorption linked to oil or other organic media, ester

carbonyl peaks at 1740 cm^{-1} are small and broad with a strong shoulder c. 1712 cm^{-1} indicative of free fatty acids.

Integrated absorption intensity maps clarify the location of different components within the sample (Figure 6.14).
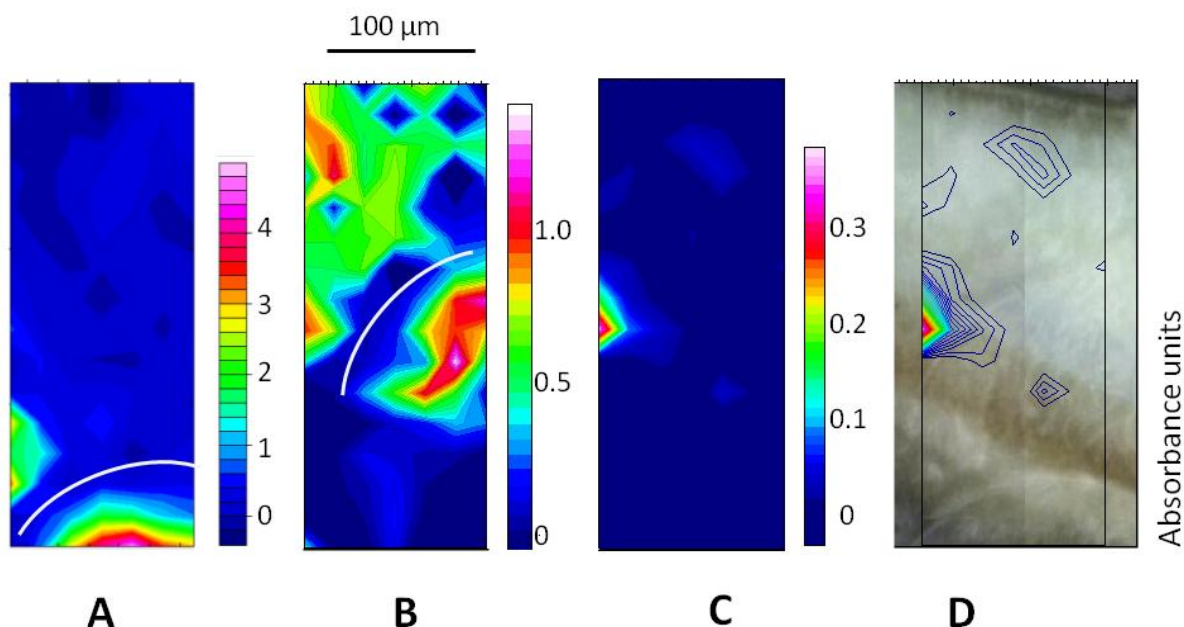
Figure 6.14 FAS#1 ATR-SR-µFTIR integrated absorption intensity maps (A) 835-890 (chalk); (B) 1560-1620 (COO$^-$ broad); (C) and (D) 1260-1280 cm^{-1} (zinc lactate).

Chalk is contained in the ground and broad carboxylate absorption is distributed through the zinc oxide-based paint layers but incorporates two distinct spectral patterns including one assigned to zinc lactate. Absorption intensity plotted as contour lines superimposed over the sample image (D) places the zinc lactate adjacent to the transparent brown layer. White lines overlaid in A and B indicate gaps in the data arising from indents in the sample surface

Map A shows the presence of chalk in the ground layers based on integration of the characteristic carbonate peak at 870 cm^{-1}, while map B plots the intensity of broad carboxylate absorption over wavenumber range 1560-1620 cm^{-1}, distributed through the zinc oxide-based paint layers. Individual spectra extracted from hotspots in map B reveal that two distinct spectral patterns are captured by the more general plot of broad carboxylate absorption (Figure 6.15).
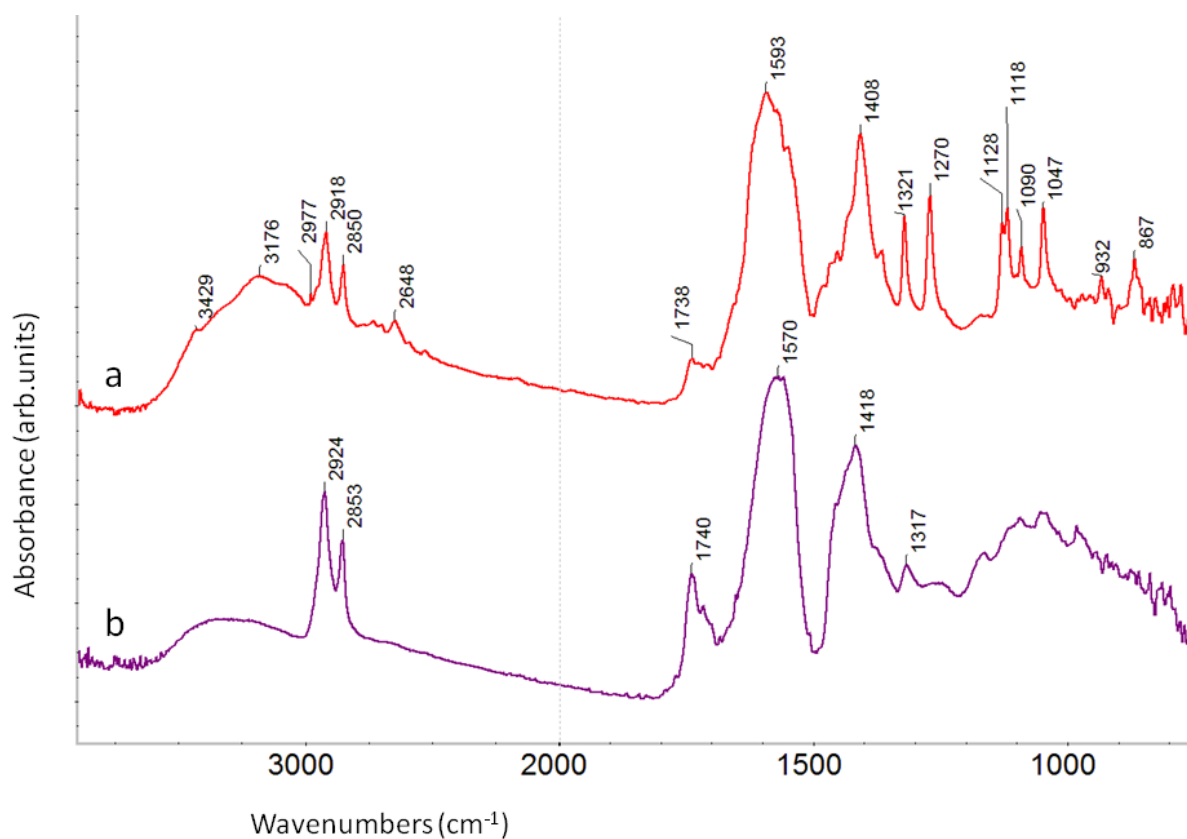
Figure 6.15 Comparison of two spectra extracted from FAS#1 incorporating broad COO⁻ absorption.

In spectrum (a) accompanying features suggest the presence of zinc lactate. Spectrum (b) is more typical of that associated with 'generic' zinc oxide oil paint

A small number of spectra include a series of distinctive sharp peaks in the fingerprint region and additional detail in the spectrum above 2600 cm^{-1} which aligns closely to that attributed to zinc lactate (Helwig et al. 2014). An integrated absorption intensity map for one of these peaks (1270 cm^{-1}) reveals this spectrum corresponds to a small feature at the left edge of the mapped region (Figure 6.14C and D). This area occurs at the interface between paint and the transparent brown layer, however, there are no obvious distinguishing optical characteristics, and its source is unclear.

The suggested presence of zinc oleate in *Autumn showers* is another uncertainty. Although there is evidence to support unusually high levels of oleic acid in zinc oxide-based paints (Rogala et al. 2010; Maines et al. 2011), the presence of the soap form has not been conclusively demonstrated and the likelihood for its existence in mature paints is an open question. Integrated absorption intensity maps show the overlapping spatial and spectral relationship of spectra assigned to zinc stearate/palmitate and zinc oleate (Figure 6.16).
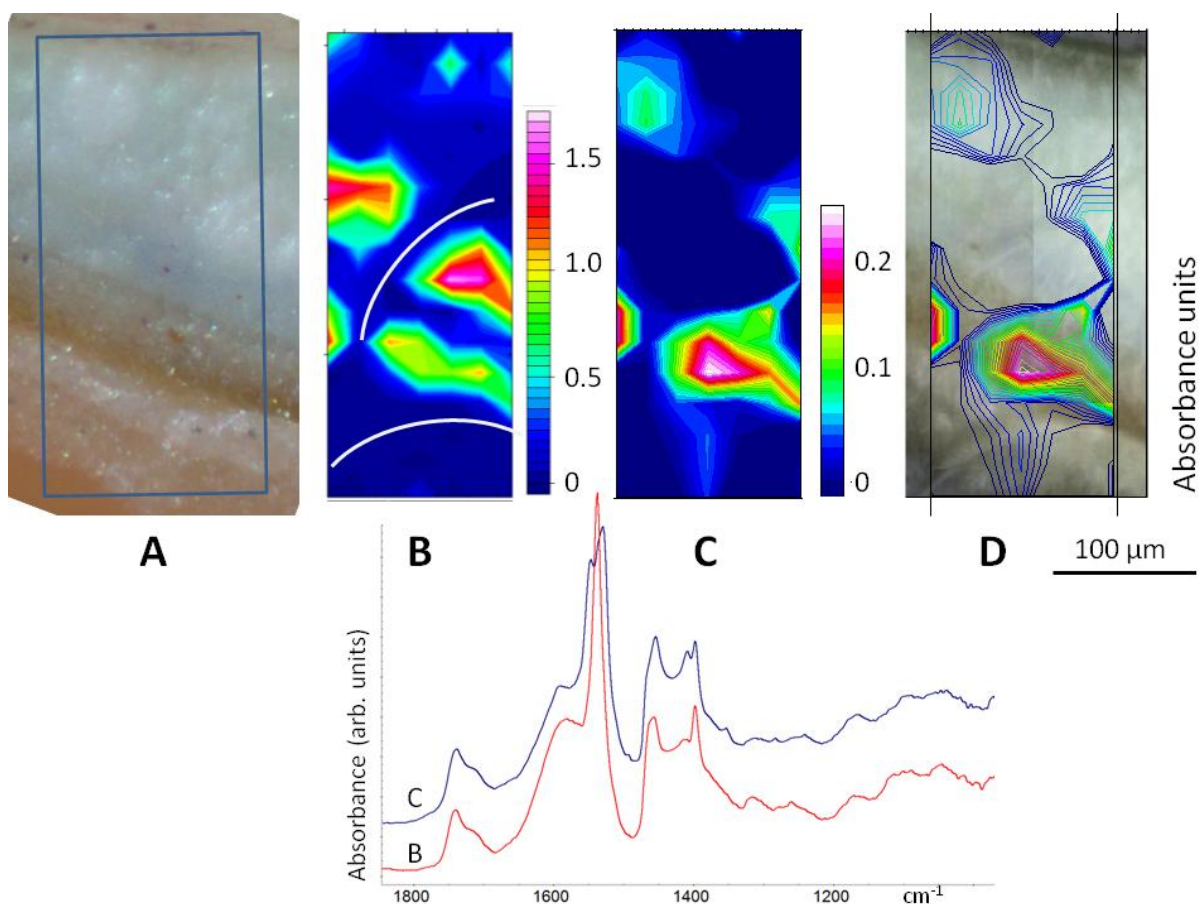
Figure 6.16 FAS#1 detail as optical image (A) with box denoting area shown in ATR SR-µFTIR integrated absorption intensity maps (B) 1550-1520 cm^{-1} (v_a COO$^-$ 1540 zinc stearate/palmitate and 1526 zinc oleate) and (C and D) 1543-1560 cm^{-1} (v_a COO$^-$ 1548 zinc oleate).

Map (D) plots intensity as contour lines superimposed over the sample image and shows 'zinc oleate' to be concentrated in the transparent brown layer with smaller amounts contained in circular white masses in the main body of paint. Spectra extracted from hotspots in (B) and (C) show single and split COO$^-$ peaks for the zinc soap are concentrated in blue paint and the transparent brown layer respectively. White lines overlaid in (B) indicate gaps in the data arising from indents in the sample surface

Mapping over wavenumber range 1550-1520 cm^{-1} encompasses both v_a COO$^-$ zinc stearate/ palmitate (1540 cm^{-1}) and zinc oleate (1526 cm^{-1}) (B), while a narrow integration to isolate the second v_a COO$^-$ peak for zinc oleate at 1548 cm^{-1} indicates the split peak spectra are associated with the transparent brown layer, with smaller amounts contained in circular white masses in the main body of paint (C/D). Spectra extracted from hotspots in map B show zinc stearate to be in highest concentration in (Prussian) blue paint. Split v COO$^-$ and δ CH$_2$ peaks do appear to correspond to those characterised for zinc oleate (Robinet and Corbeil 2003), however, it is more difficult to assign the lower frequency peaks given typical overlap and masking by other components in the paint. There is also variation in the higher frequency peaks in comparison to a zinc oleate reference spectrum, including the absence of a peak at 3002 cm^{-1} expected from the CH stretch from a carbon-carbon double bond (Figure 6.17).
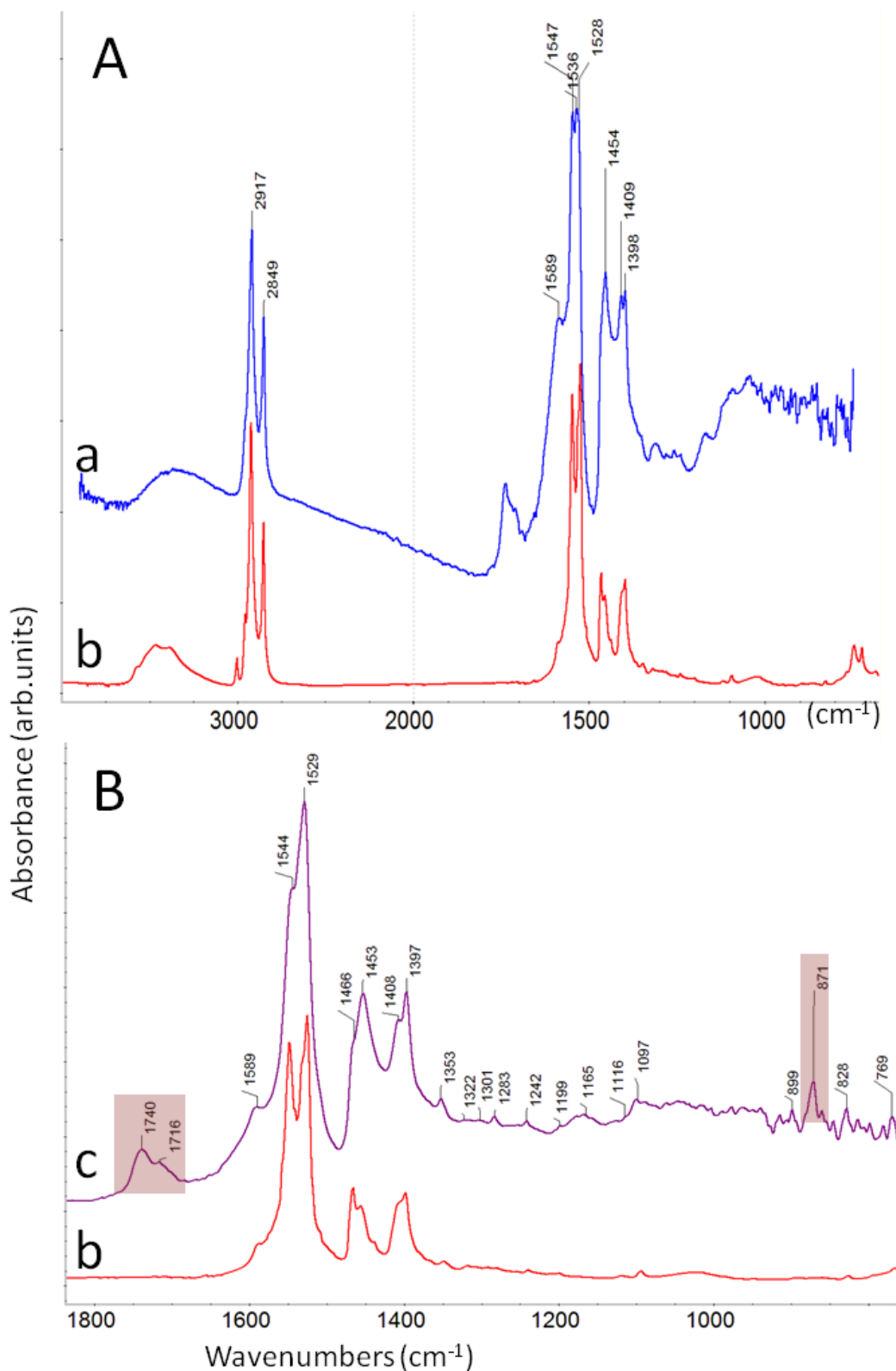
Figure 6.17 FAS#1 ATR SR-µFTIR spectra (a) and (c) extracted from hotspots in map Figure 10C (layer 3) compared to transmission FTIR zinc oleate reference spectrum (b).

COO⁻ and CH_2 doublets (1547/1528 1467sh/1454 1409/1398 cm⁻¹) characteristic of zinc oleate are present but without a C=C-H peak at *ca* 3002 cm⁻¹. A second spectrum detailed in (c) shows peaks at or within a few wavenumbers of the peaks characterised for zinc oleate. Highlighted peaks at 1740 and 1716 cm⁻¹ relate to carbonyl bonds in the oil medium including carboxylic acids (oleic acid 1712 cm⁻¹). The peak at 871 cm⁻¹ is a carbonate (chalk) peak

It is possible the split COO⁻ peaks may instead reflect variations in molecular conformation of the more typical saturated zinc soaps such as zinc stearate or palmitate (Helwig et al. 2014), although closer inspection of one sample spectrum with more defined lower-frequency features does align well with methylene and C-C progression bands characteristic of zinc oleate (Robinet and Corbeil 2003; Barman and Vasudevan 2006a) (Figure 6.17B). Ultimately, mass spectrometry is required to confirm the fatty acid composition, and attribution is the subject of ongoing research.

6.3.2 *Untitled (Ploughing)* not dated

Untitled (Ploughing) is another painting with a commercial ground preparation, in this instance an oil-based zinc white layer, unusual among Fox's work. A sample of blue paint was obtained, deriving from the location indicated in Figure 6.18.
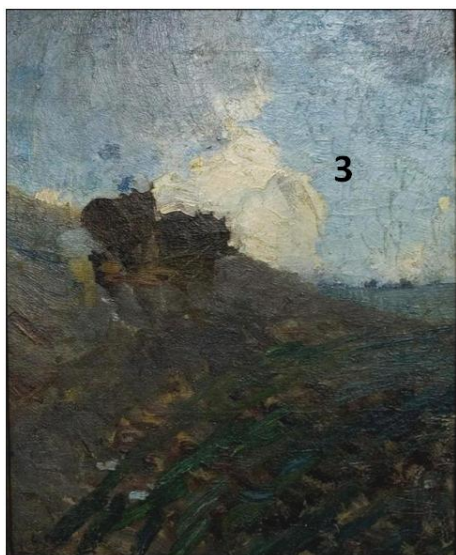
Figure 6.18 E. Phillips Fox, *Untitled (Ploughing)*, not dated, with number denoting the source location of paint sample FP#3

6.3.2.1 *FP#3*

Sample FP#3 has a simple structure including a thin ground layer and blue paint comprising zinc white and Prussian blue (Figure 6.19). A large white area is also present in the cross-section and may be unmixed white paint or possibly a large zinc-based mass which has developed within blue paint, contributing to the granular texture observed in the painting (Nunn 2012). The ground layer and adjacent blue and white paint layers have the same elemental composition, all dominated by zinc, carbon and oxygen with a few Fe/K/Al/Mg silicate particles in both ground and paint. The blue colorant is the intense Prussian blue pigment, ferric ferrocyanide, present in low concentration but readily detected with FTIR due to characteristic C≡N vibrations at 2090 cm⁻¹. Although the

ground and blue paint layers have very similar UV-fluorescence, BSE images and elemental maps show the ground has lower pigment density and is richer in carbon (Figure 6.20).
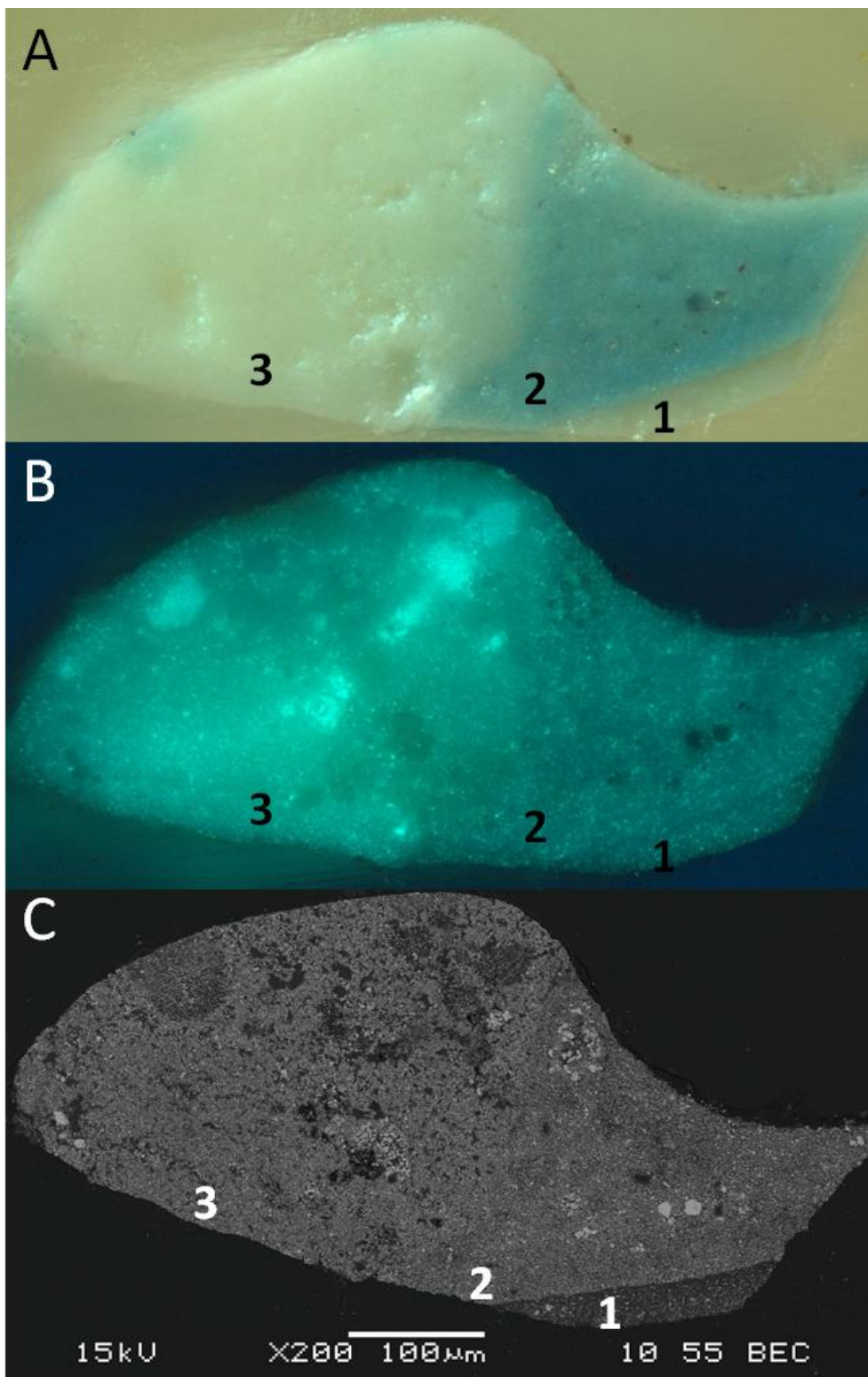
Figure 6.19 *Untitled (Ploughing)* **cross-section FP#3: (A) visible (B) UVF and (C) BSE images showing ground layer (1), blue paint (2) and white paint (3)**
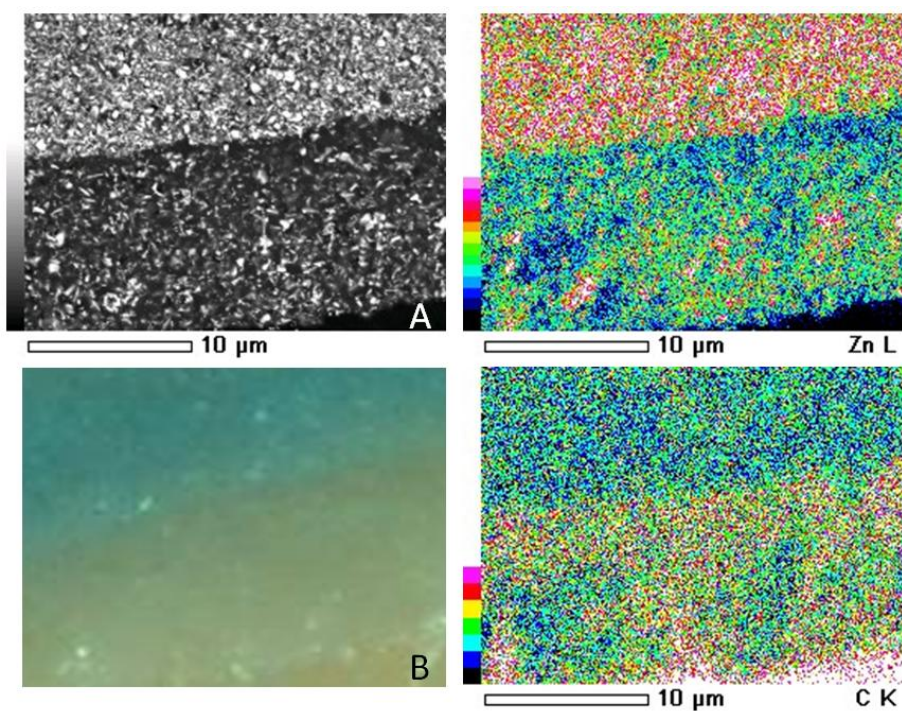
Figure 6.20 FP#3 BSE detail (A) with corresponding optical image (B) and elemental maps for zinc and carbon spanning the boundary between zinc oxide-based ground and blue paint layers.

Elemental composition of the two layers is the same, however, zinc concentration is lower and carbon counts higher in the ground
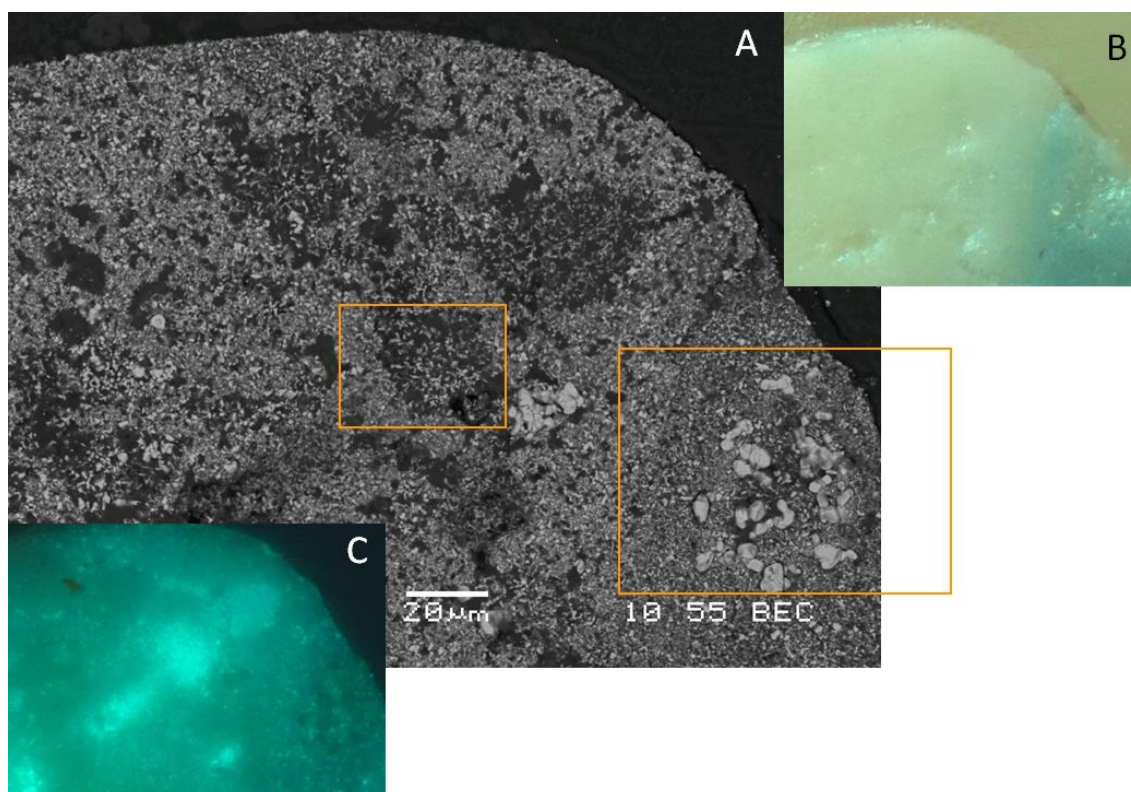
Figure 6.21 FP#3 BSE image detail (A) and corresponding optical images (B) visible and (C) UVF showing unusual morphological features occurring in the paint within both white and blue areas.

Boxes denote regions detailed in subsequent figures

252

Backscatter electron images reveal a variety of unusual morphological features (Figure 6.21). In white paint circular regions of low electron density are filled with dispersed needle-like crystals; these same regions are brightly UV-fluorescent (Figure 6.22).
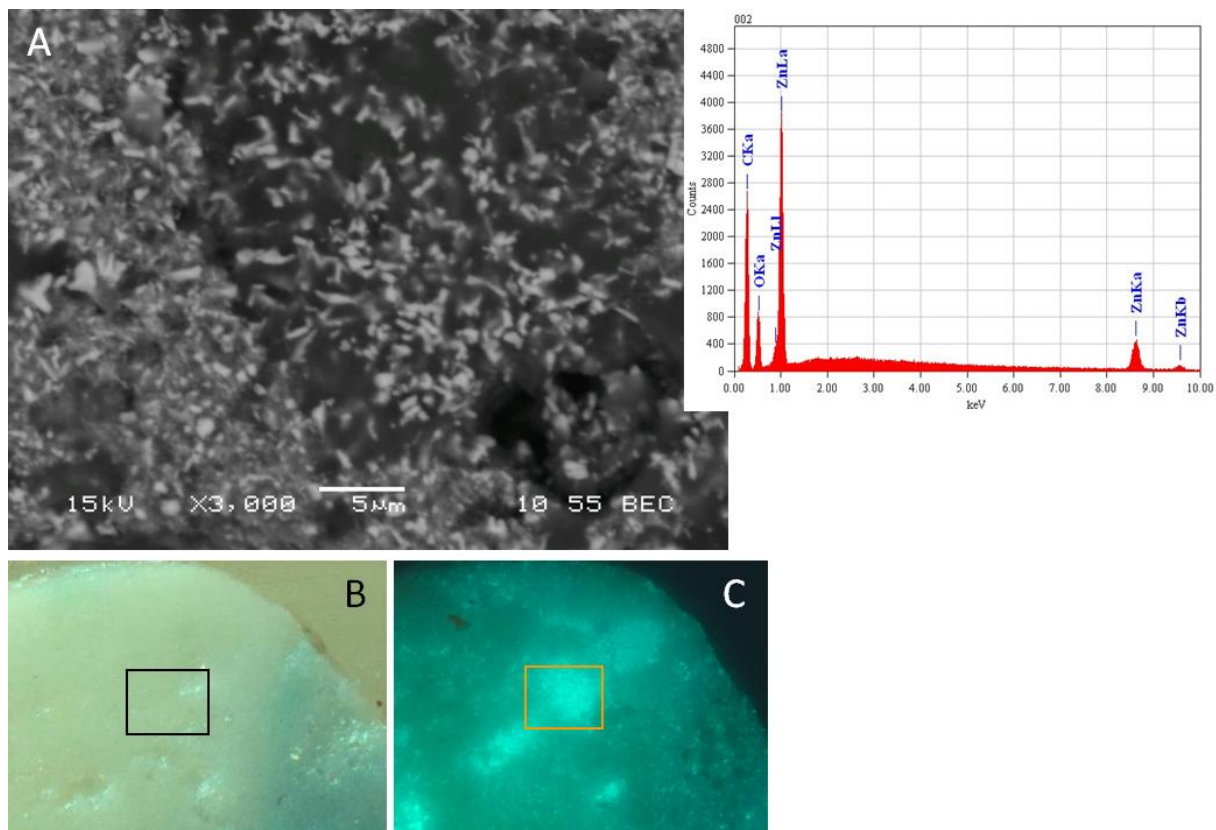
Figure 6.22 FP#3 BSE image detail from white paint (A), corresponding area denoted with box in optical images (B) visible and (C) UVF, and EDX spectrum from the brightly UV-fluorescent region in the optical image.

This area has high carbon counts and acicular particles appear dispersed within an amorphous medium such as might occur with dissolution of small nodular zinc oxide particles accompanying formation of zinc carboxylates

Within some of these regions and also in localised areas of blue paint there is reduced UV-fluorescence and the area appears translucent-white where relatively large white hexagonal crystals appear to have emerged (Figure 6.23). EDX spot measurements show zinc predominates in these crystals with very high counts.
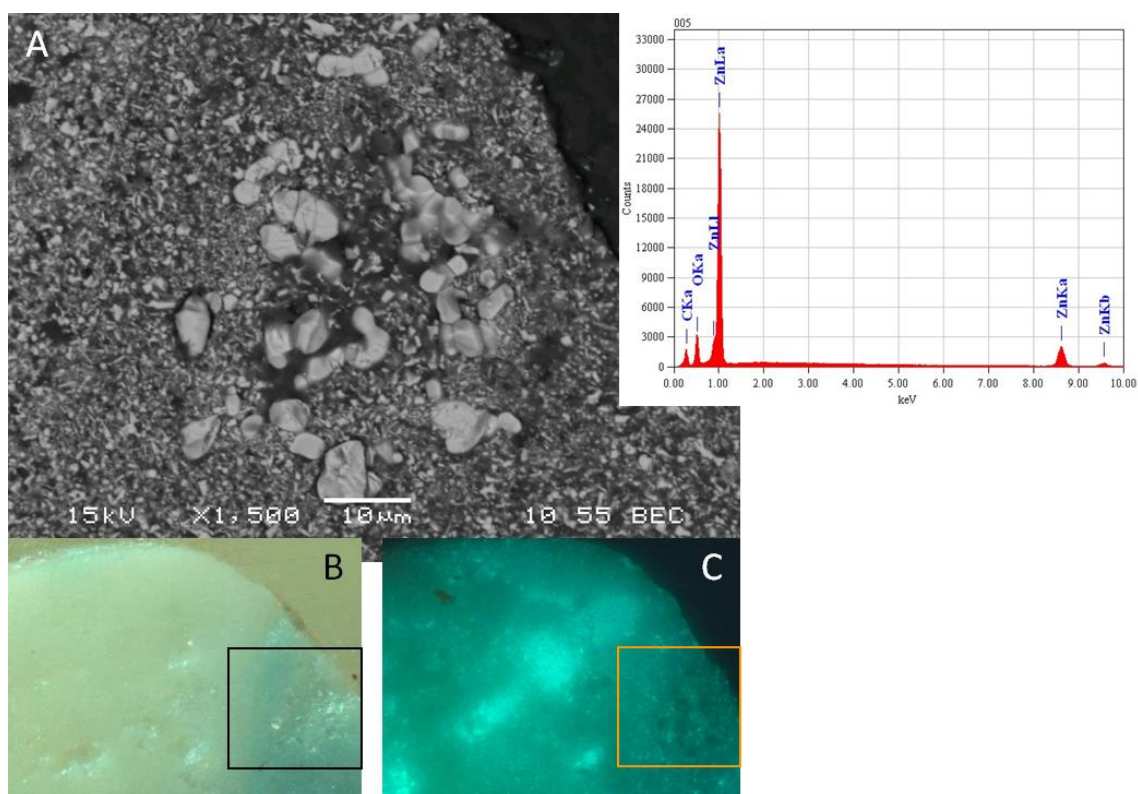
Figure 6.23 PF#3 BSE image detail from blue paint (A)

Corresponding area denoted with box in optical images (B) visible and (C) UVF, and EDX spectrum from one of the white crystals apparently emerging from within an area of low electron density in the sample. In the optical image this area appears as a translucent-white mass within the blue paint and has reduced UV-fluorescence

Further information is obtained by means of SR-μFTIR. Precise correlation of SR-μFTIR data with features observed in BSE images is difficult because the surface presentation was altered slightly between analyses by removal of thin-sections. The thin-sections obtained were not viable for transmission experiments, so mapping was performed in ATR mode on the surface of the embedded sample using a 7x23 grid with 20 μm aperture and step size. An integrated absorption intensity map for the characteristic Prussian blue absorption shows the correlation with blue paint in the cross-section (Figure 6.24). SR-μFTIR maps also show zinc stearate/palmitate to be in highest concentration in blue paint, while white paint contains broader carboxylate absorption, sometimes tending to a triangular shaped peak centred at 1592 cm^{-1} (Figure 6.25), discussed further in subsequent samples. The possibility that zinc stearate is present as an original component in blue paint would be a logical assumption to make based on these results; the first patent application for use of zinc (and aluminium) stearates as aids to grinding pigments and preventing settling or separation of pigment from oil dates to 1920 (Tumosa 2001), five years after Fox's death, although earlier use of aluminium salts has been described in late nineteenth century treatises (Carlyle 2001) making its deliberate addition to the paint possible but difficult to confirm.
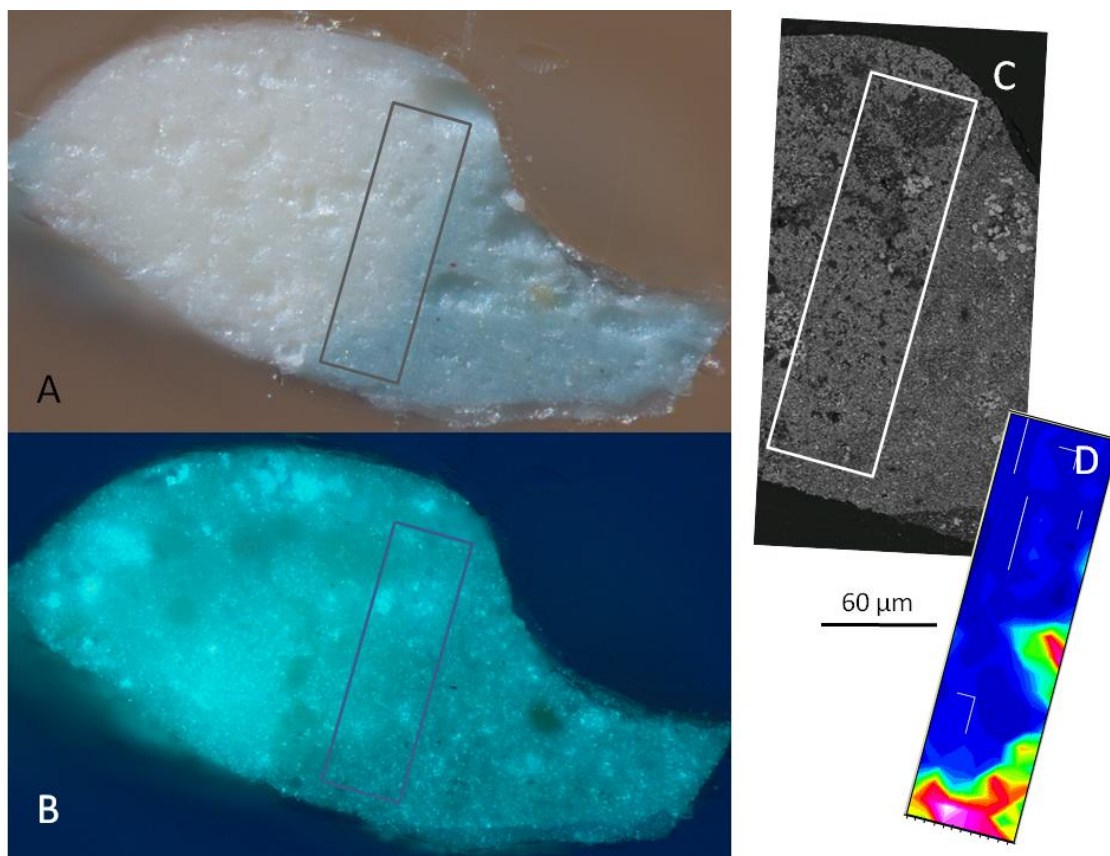
Figure 6.24 FP#3 optical images (A) visible light and (B) UVF, and corresponding BSE detail (C) with box denoting area mapped with ATR SR-µFTIR. Integrated absorption intensity map over wavenumber range 2075-2110 cm^{-1} (D) corresponds to Prussian blue pigment in blue paint
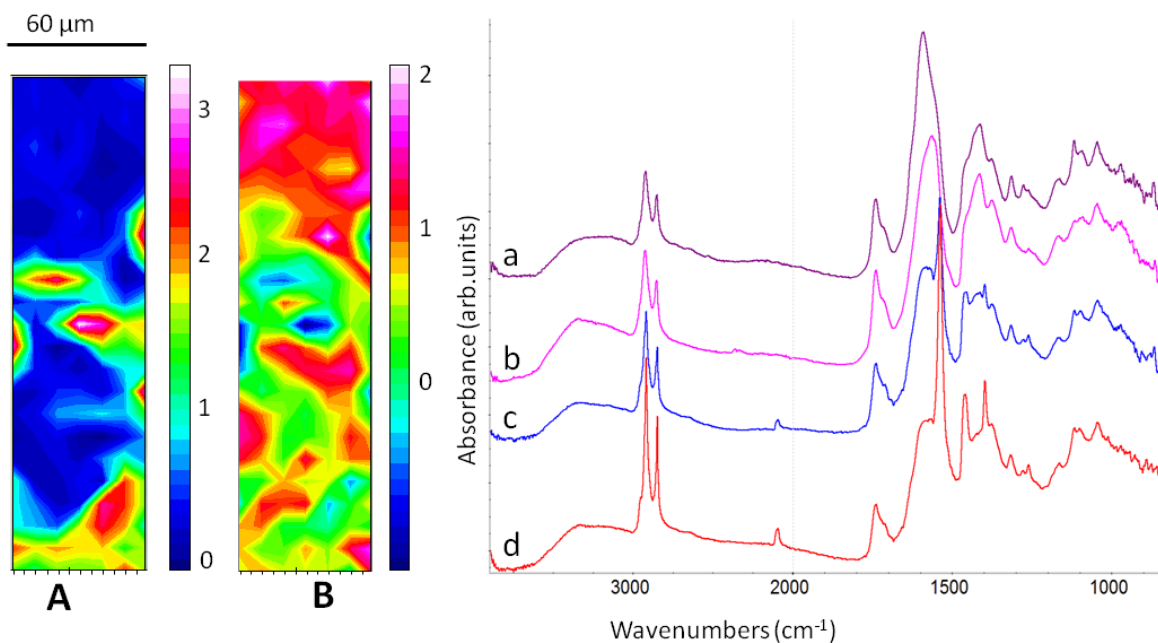
Figure 6.25 FP#3 ATR SR-µFTIR absorption intensity maps integrated over wavenumber range (A) 1520-1560 (zinc stearate/palmitate) and (B) 1550-1620 cm^{-1} (broad COO$^-$+OH).

Zinc stearate/palmitate is primarily associated with blue paint. Extracted spectra show a range of carboxylate peaks including (a) centred at 1592 cm^{-1}, (b) more typically broad, rounded peak shape; and (c-d) broad absorption with a sharp strong peak at 1540 and v_s COO$^-$ 1399 cm^{-1} also clearly visible over the background absorption

Other spectra extracted from the sample include features characteristic of basic zinc carbonate. Integration of the peak 810-845 cm^{-1} suggests high intensity carbonate absorption is broadly associated with areas of the paint with altered morphology, including the distinctive large crystals observed in BSE images. A series of spectra extracted from a line through a carbonate hotspot shows high concentrations of zinc stearate/palmitate immediately adjacent and the features of zinc stearate and basic zinc carbonate represented within a single spectrum (Figure 6.26). The close association of soap and carbonate species in combination with the morphology observed in BSE images suggests the basic zinc carbonate may have crystallised within localised concentrations of zinc stearate/palmitate. The zinc carboxylates appear to have formed by reaction of the small, nodular particles of zinc oxide present in the paint.
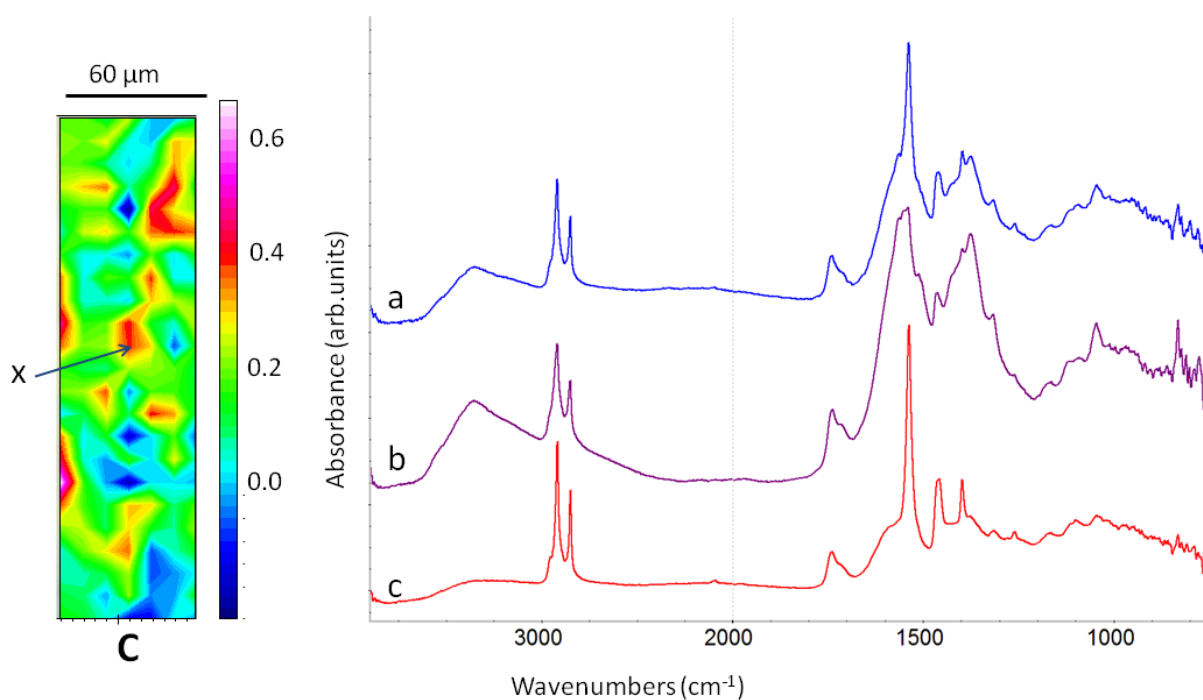
Figure 6.26 FP#3 ATR SR-µFTIR absorption intensity map integrated over wavenumber range 810-845 cm^{-1} (basic zinc carbonate).

Spectra extracted from a line through the area indicated with arrow (x) show a transition from sharp zinc stearate peaks (c) to basic zinc carbonate (b) and then a spectrum with features of both (a) confirming intimate association. Spectrum (c) has a tiny peak for Prussian blue (2090 cm^{-1}) deriving from the boundary between the white and blue layers

Another interesting feature of this sample revealed by SR-µFTIR includes two defined points within the mapped area where IR spectra contain a distinct C=O doublet (Figure 6.27). The second carbonyl peak at 1715 cm^{-1} suggests there is high local concentration of free fatty acid. Zinc stearate/palmitate also appears to be present based on a strong peak at 1540 cm^{-1}. Absorption intensity maps are very similar whether the integration occurs on the acid carbonyl peak at 1715 or

the sharp peak at 1200 cm^{-1}. The latter is present with a second peak at 1183 cm^{-1} and these have not as yet been attributed. The two hotspots in the map have no obvious correlation with physical features in the sample.
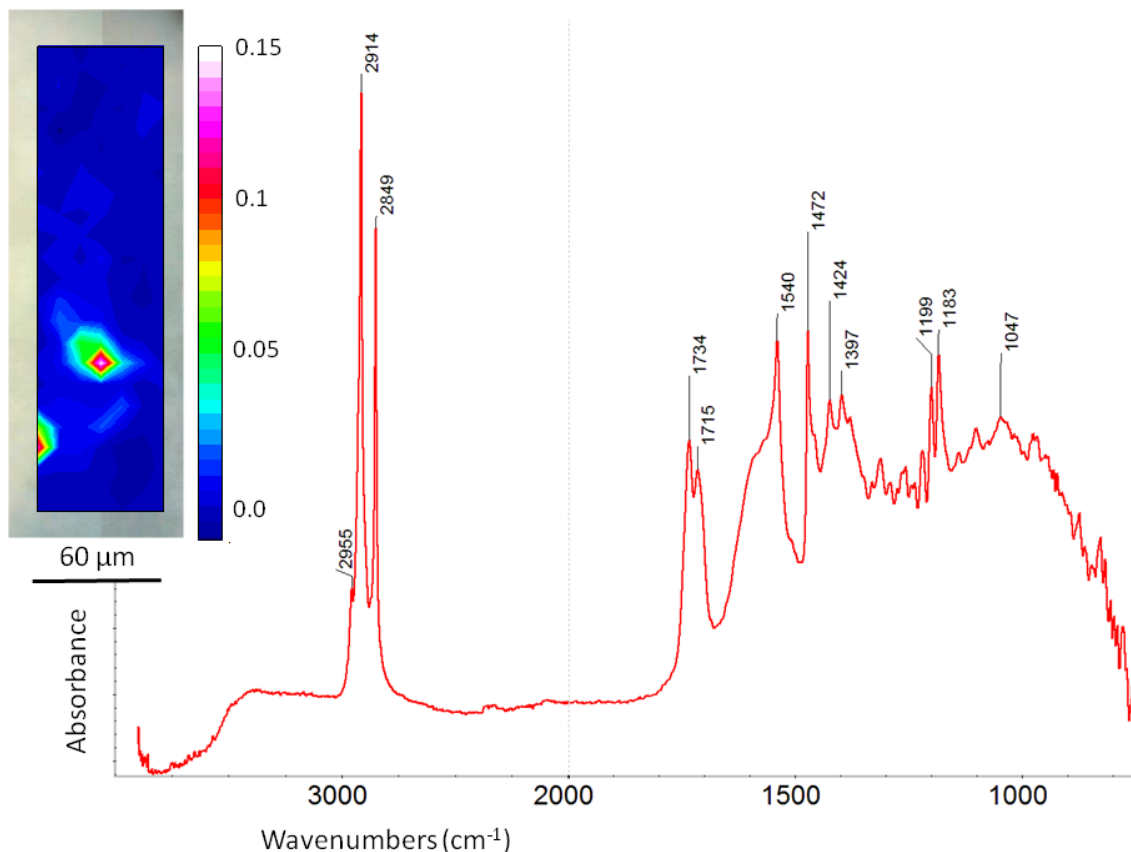
Figure 6.27 FP#3 integrated absorption intensity map for 1190-1205 cm^{-1} (a similar map is obtained by integrating the peak centred at 1715 cm^{-1}) and spectrum extracted from hotspot showing indicative spectrum.

The second carbonyl peak at 1715 cm^{-1} may indicate high local concentration of free fatty acid

6.3.3 *Bathing hour* c.1909

Bathing hour is a large studio painting dating from Fox's Paris period, painted on an absorbent ground hand prepared with calcium sulfate (probably Plaster of Paris) and some form of animal glue ('special size'). Three samples are discussed here deriving from the locations indicated in Figure 6.28.

Figure 6.28 E. Phillips Fox, *Bathing hour (L'heure du bain)* **c.1909 with numbers denoting the source location of paint samples**

6.3.3.1 FBH#3

Sample FBH#3 is taken from the centre of the painting from an area of sand in sunlight. Over the partial ground layer, three or more zinc oxide-based paint layers are evident comprising pale-blue among various light-hued yellow-pink layers (Figure 6.29). The boundaries between the layers are not defined suggesting paint has been applied wet-in-wet. The paint has a fluorescent sparkle under UV and various circular masses are apparent which either fluoresce very brightly or have a more UV-absorbent purple appearance. SEM-EDX shows zinc, carbon and oxygen to be dominant in the paint, with chlorine also associated. Coloured pigmentation is principally vermilion and cadmium yellow, both sulfide pigments of mercury and cadmium respectively. Small amounts of earth/clay fillers comprising iron, silicon, potassium and magnesium are also detected. The ground contains calcium and sulfur.
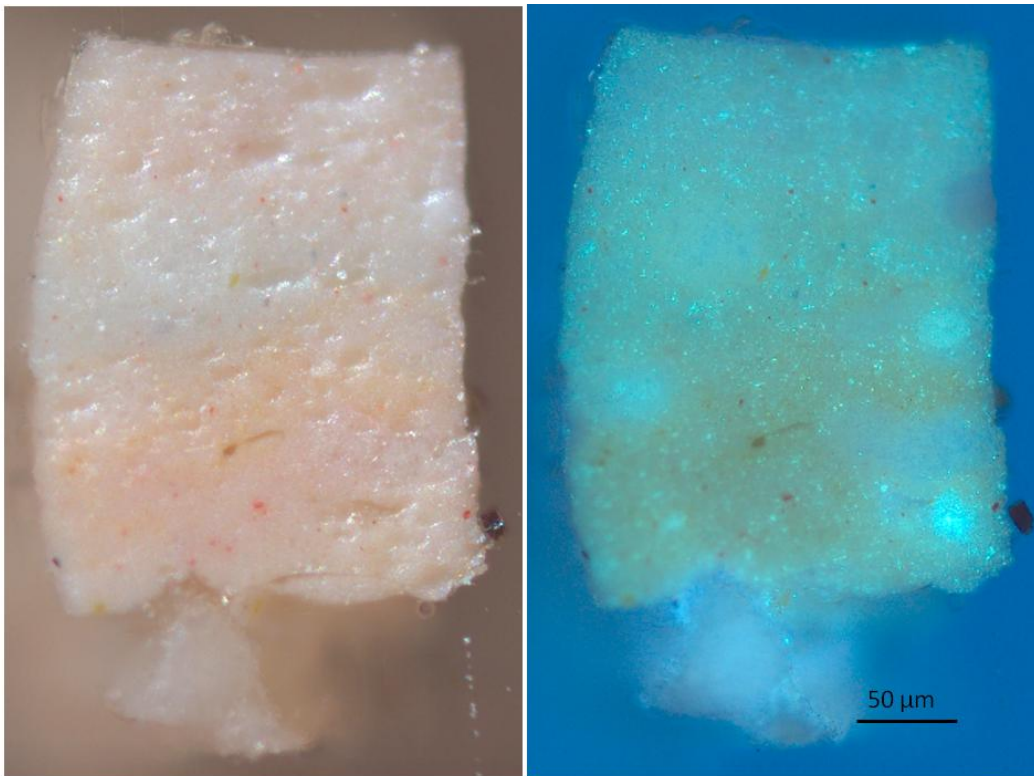
Figure 6.29 *Bathing hour* **cross-section FBH#3 visible and UVF images**

An area spanning the paint layers near the right edge of the sample was mapped with ATR SR-µFTIR (Figure 6.30).
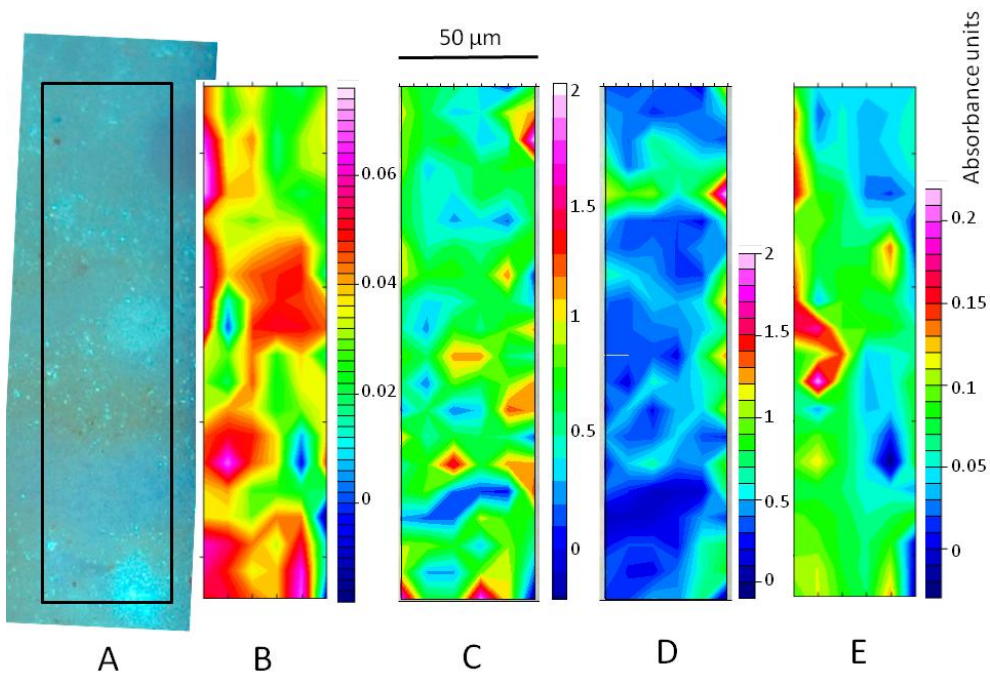
Figure 6.30 FBH#3 ATR SR-µFTIR absorption intensity maps from area designated in optical UVF image (A) integrated over wavenumber range (B) 1700-1718 (carboxylic acids); (C) 1560-1620 (carboxylates - broad including zinc lactate); (D) 1520-1560 (carboxylates - zinc stearate) and (E) 3675-3705 cm^{-1} (kaolinite)

Integrated absorption intensity maps are of limited interest due to surface irregularity and variable spectral quality. It is also the case that zinc oxide is the predominant pigment which has negligible IR absorption in the 600-4000 cm^{-1} range, and nor do the sulfide pigments vermilion and cadmium yellow. As a result, carboxylate soaps and silicates are the most discernible features in IR spectra. Map B appears to show a correlation between high carboxylic acid concentration (1703-1718 cm^{-1}) and brightly fluorescent features in the sample. This also seems to occur in the vicinity of coloured pigment particles. Figure 6.31 shows a spectrum (b) extracted from a brightly fluorescent area which contains strong general carboxylate absorption typical for zinc oxide in oil, and relatively intense C-H (2852, 2922) and C=O oil (1739) and free acid (1714 cm^{-1}) peaks.
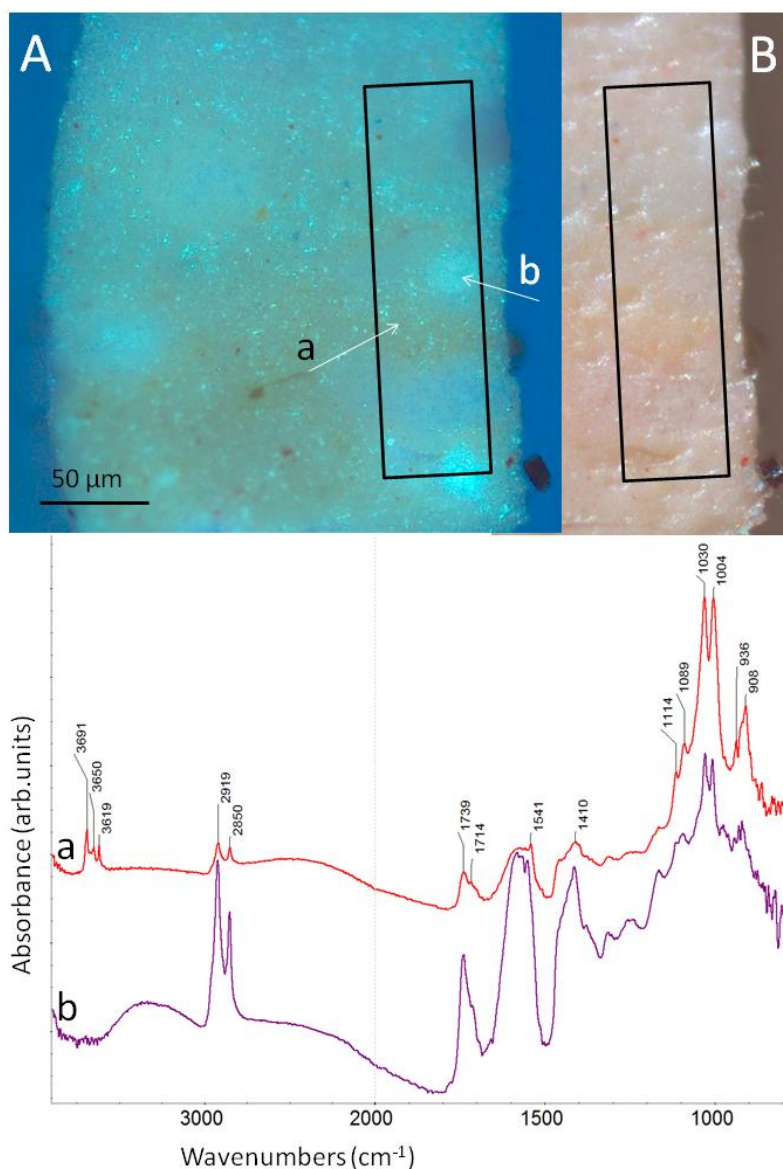
Figure 6.31 FBH#3 optical image details (A) UVF and (B) visible with box denoting ATR SR-μFTIR map area and spectra extracted from locations indicated (a) kaolinite hotspot and (b) UV-fluorescent hotspot.

(a) typical kaolinite absorptions are accompanied by broad carboxylate absorption with a small 1541 cm^{-1} side peak (zinc stearate); (b) stronger general carboxylate absorption accompanies more intense oil and free acid peaks; silicate peaks are also apparent

Silicate peaks are also present; it is possible ultramarine blue (a sodium aluminium silicate) is present in the sample although no blue pigment is obvious at the indicated area, and the dominance of zinc in EDX spectra prevents detection of sodium because of overlapping X-ray emission lines. Spectrum (a), from a hotpot in Figure 6.30E, also incorporates silicate peaks but with water of crystallisation (>3600 cm^{-1}) characteristic of kaolinite (3691, 3619, 1114, 1030, 1004 and 908 cm^{-1}), accompanied by broad carboxylate absorption with a small 1541 cm^{-1} side peak. Other points in the sample produce spectra with a strong sharp carboxylate peak at 1541 cm^{-1} indicative of zinc stearate, or a broad-based pointed peak centred *ca* 1590 cm^{-1} with corresponding peaks tentatively assigned to zinc lactate (Figure 6.32).
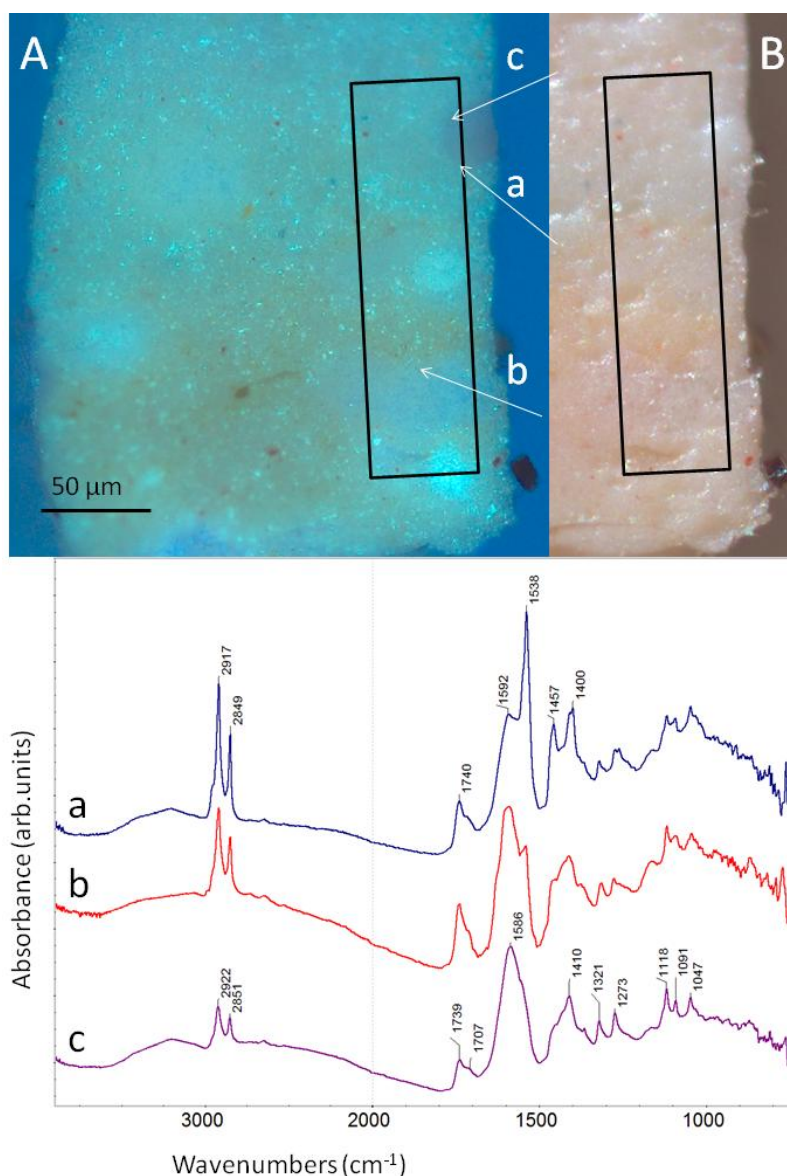
Figure 6.32 FBH#3 optical image details: (A) UVF and (B) visible, with box denoting ATR SR-µFTIR map area and spectra extracted from locations indicated with dominant absorptions indicative of (a) zinc stearate (c) zinc lactate and (b) a combination of the two

Examples of both broad-based carboxylate peaks can be found adjacent to the purple UV-absorbent feature at upper right of the mapped region but it is difficult generally to associate specific absorptions with physical features in the sample, particularly given the variable quality of spectra.

Backscatter electron imaging reveals interesting sample morphology. This sample was one of the first studied and was examined uncoated under low vacuum conditions but at higher beam voltage than subsequent samples. Optical images taken of the sample after investigation reveal charring from the electron beam on the sample surface incurred during EDX (Figure 6.33). This particular surface presentation also features circular masses with low fluorescence in layer 4 versus a prevalence of more brightly fluorescent masses in paint layers 2-3. Both types occur in close proximity as shown in a detail from the centre left region of the sample at the boundary of layers 3 and 4 (Figure 6.34). EDX spectra obtained from spot measurements from the points circled show zinc, carbon and oxygen to be the predominant elements, with chlorine also consistently detected.
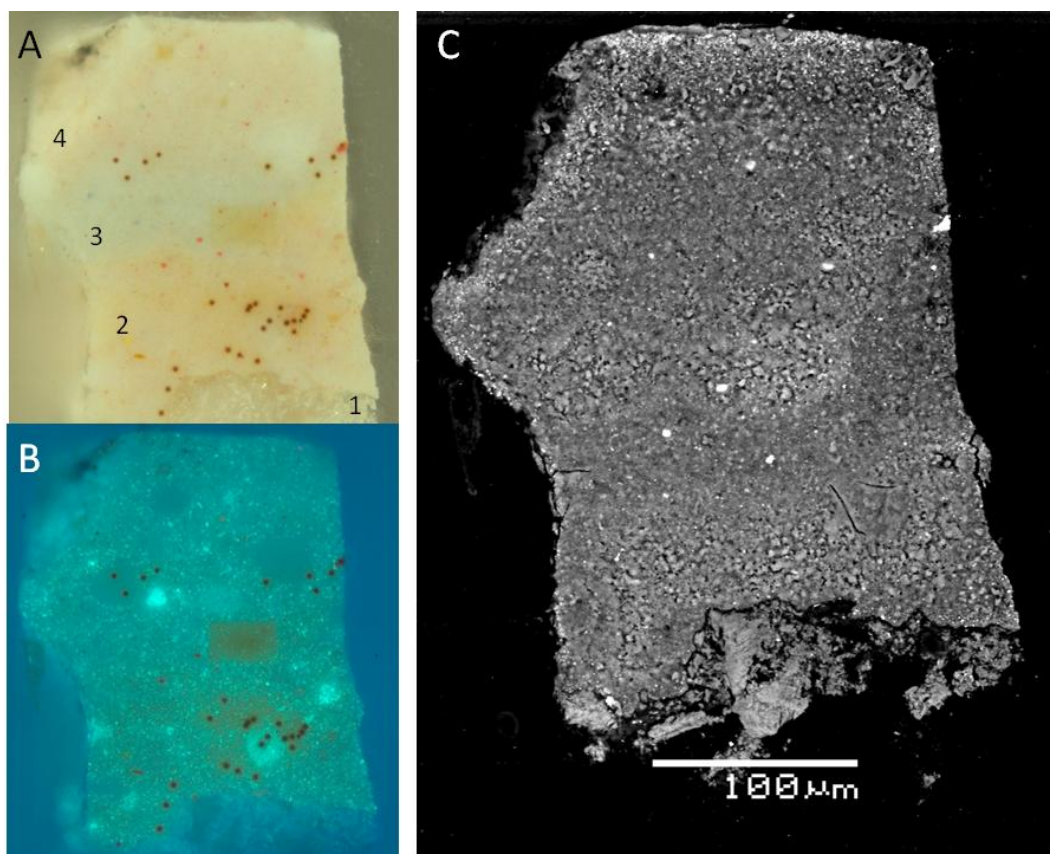
Figure 6.33 FBH#3 showing the surface presentation applicable for SEM imaging and elemental analysis, optical images: (A) visible and (B) UVF, and (C) BSE image.

The dark spots and rectangular shapes visible in the optical images reflect surface charring from the electron beam incurred in the course of EDX
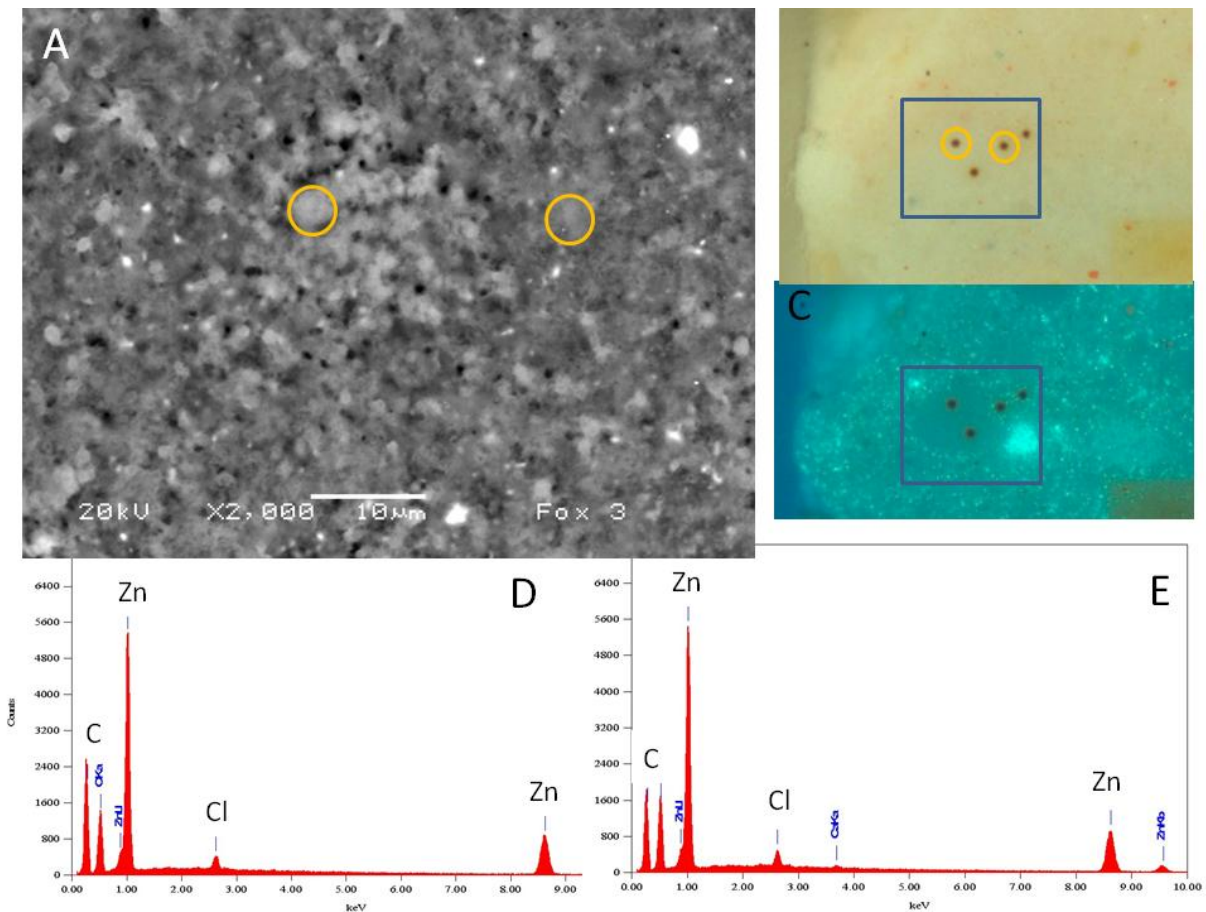
Figure 6.34 FBH#3 BSE detail (A) from area denoted in optical images (B) and UVF (C) at the boundary of layers 3 and 4.

Spectra from spot EDX points circled show zinc, carbon and oxygen to be the predominant elements, with chlorine also a consistent component. Spectra are very similar from both within (D) and outside (E) the circular UV-absorbent feature with minor variation in the ratio of carbon to oxygen

Spectra are very similar from both within and beyond the UV-absorbent feature with a slightly higher ratio of carbon to oxygen inside. The brightly fluorescent feature is not obviously distinguishable in BSE images. A BSE image detail from layer 2 shows an unusual circular feature which does not appear to correlate to the brightly UV-fluorescent region or any particular feature in optical images (Figure 6.35); the circular zone has an amorphous appearance seemingly as if a 'skin' has formed on the cross-section surface. Small ruptures are evident in the 'skin' in the BSE image detail, apparently at the boundary between UV-fluorescent and surrounding regions. Spectra from EDX spot measurements (circled) show zinc, carbon and oxygen to again be the predominant elements, with chlorine also once more a consistent component. X-ray counts are higher from the UV-fluorescent region (D) while trace elements are more evident in the spectrum from outside this area (E), including sulfur, calcium, iron, aluminium and silicon.
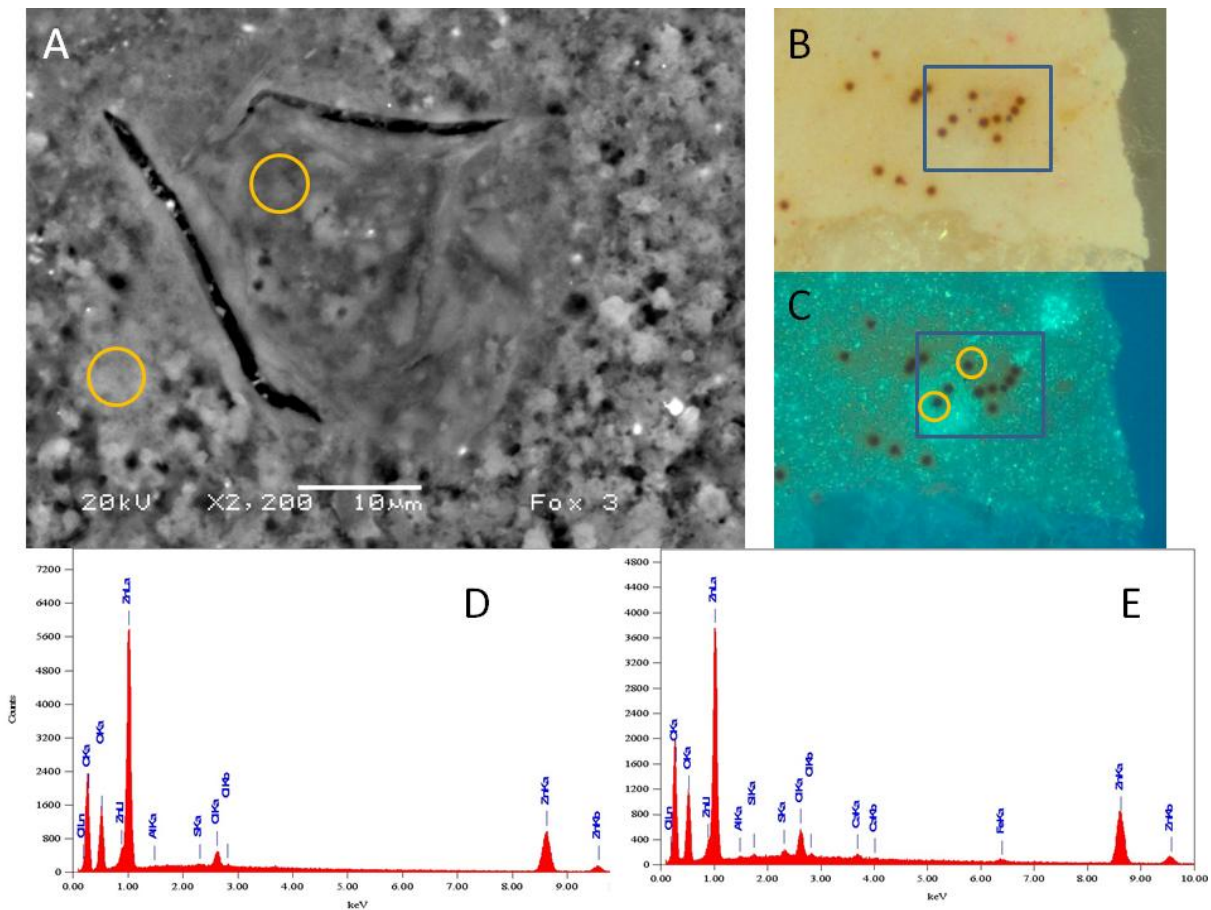
Figure 6.35 FBH#3 BSE detail (A) from area in layer 2 as denoted in optical images: (B) visible and (C) UVF.

EDX spectra from spots circled show zinc, carbon and oxygen to predominate, with chlorine also present. The amorphous circular feature evident in the BSE image does not correlate with the brightly fluorescent feature in UVF; the ruptures apparent in (A) appear to occur at the boundary between fluorescent and surrounding regions. X-ray counts are higher from the UV-fluorescent region (D) while trace elements are more prevalent in the spectrum from outside this area (E)

The consistent detection of chlorine in EDX measurements from FBH#3 is curious and is not repeated in analysis of the other two samples from this painting described below, nor generally observed in features from the other paintings. FBH#3 is the only sample investigated uncoated under low vacuum conditions (and higher beam current) in this study and so the results may not be directly comparable.

6.3.3.2 FBH #4

Sample FBH#4 derives from the green-blue sea at upper left of the painting. It contains a single paint layer with only a trace of ground at the lower left of the cross-section (Figure 6.36). Investigation of the sample was limited to SEM imaging and EDX analysis.
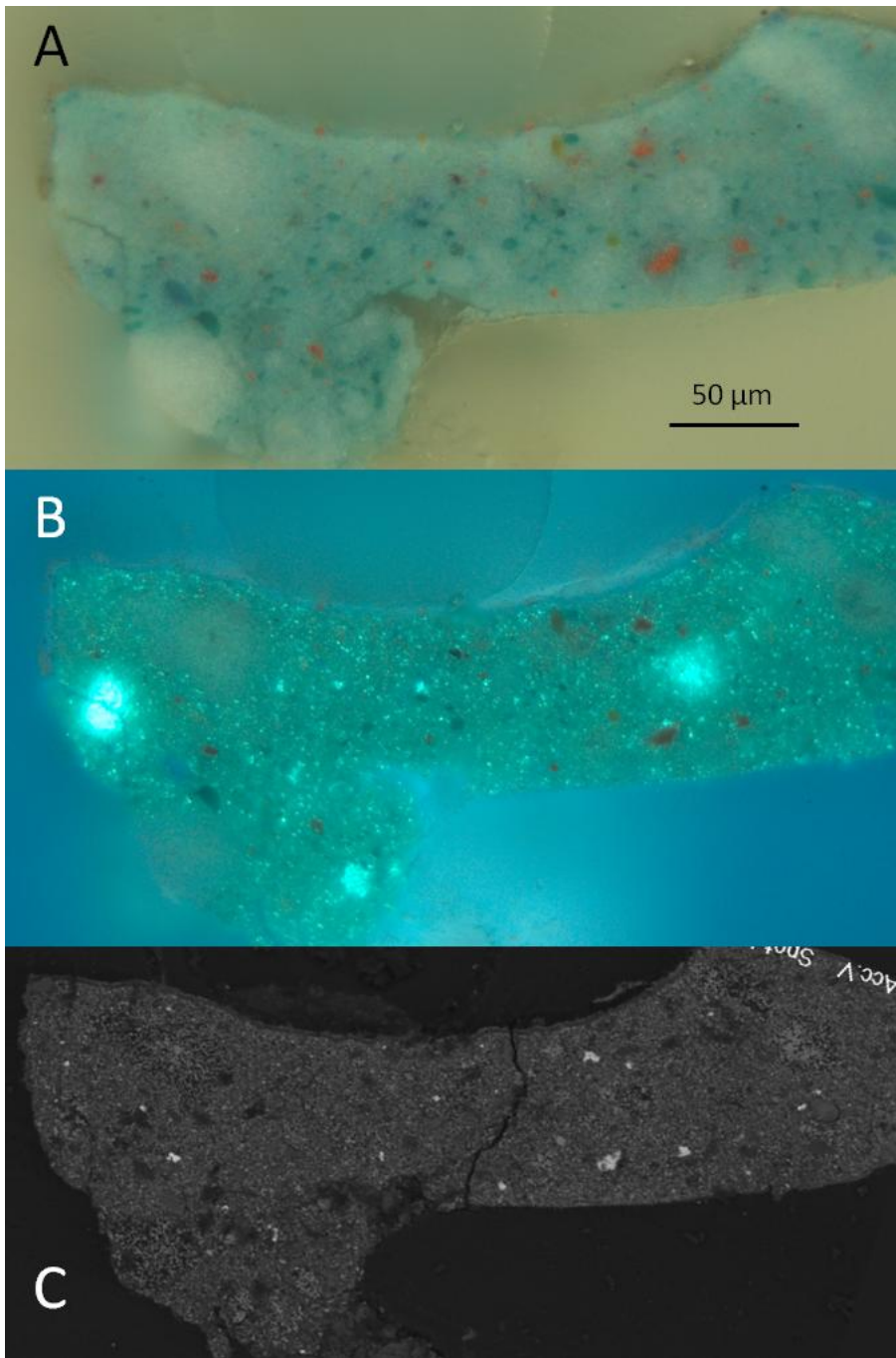
Figure 6.36 *Bathing hour* **cross-section FBH#4: (A) visible (B) UVF and (C) BSE images**

The paint layer contains complex pigmentation including vermilion, cadmium yellow, viridian and cobalt blue. Intensity of colour is greater than FBH#3 although the paint is again based on zinc oxide. White circular inclusions are present throughout the cross-section and include both UV-fluorescent and absorbent regions consistent with the previous sample. All are based on zinc, carbon and oxygen, with varying proportions of carbon (Figure 6.37).
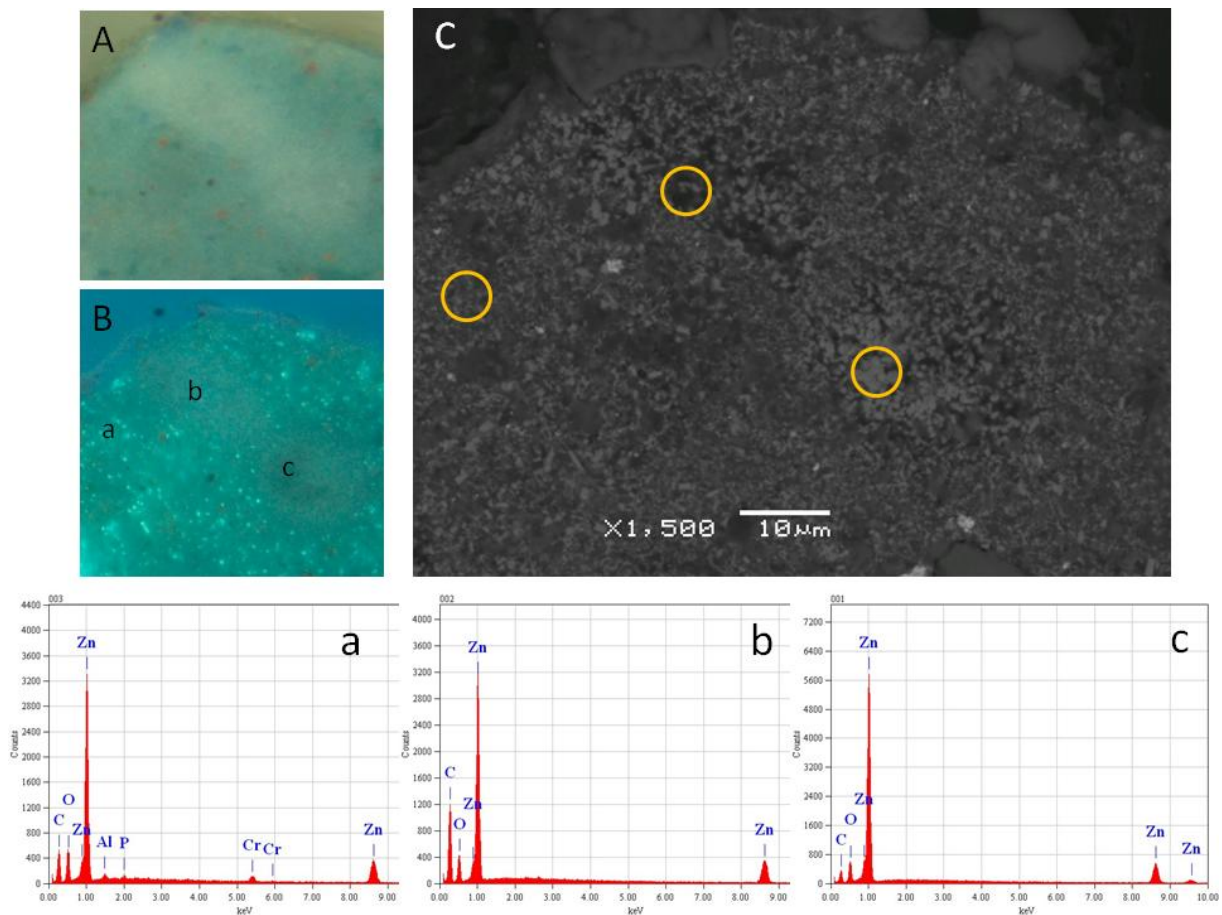
Figure 6.37 FBH#4 optical (A) visible and (B) UVF, and (C) BSE image details and spot EDX spectra from points designated

(a) intact paint with UV-fluorescent sparkle (b) white mass with open structure in BSE and (c) white mass with denser structure and lower UV-fluorescence. Zinc, carbon and oxygen predominate in each case with varying proportions of carbon, and zinc counts are highest in (c)

Spectrum (a) obtained from 'intact' paint exhibiting a dispersed UV-fluorescent sparkle has lower carbon counts than spectrum (b) from a white mass with lower density structure in the BSE image, but higher carbon counts than spectrum (c) from an optically similar area which appears more densely mineralised in the BSE image. Zinc counts are also highest from spot (c). In another part of the sample two white masses with very distinct UV-fluorescence are not readily distinguishable in BSE images but brighter fluorescence is associated with higher carbon counts (Figure 6.38).
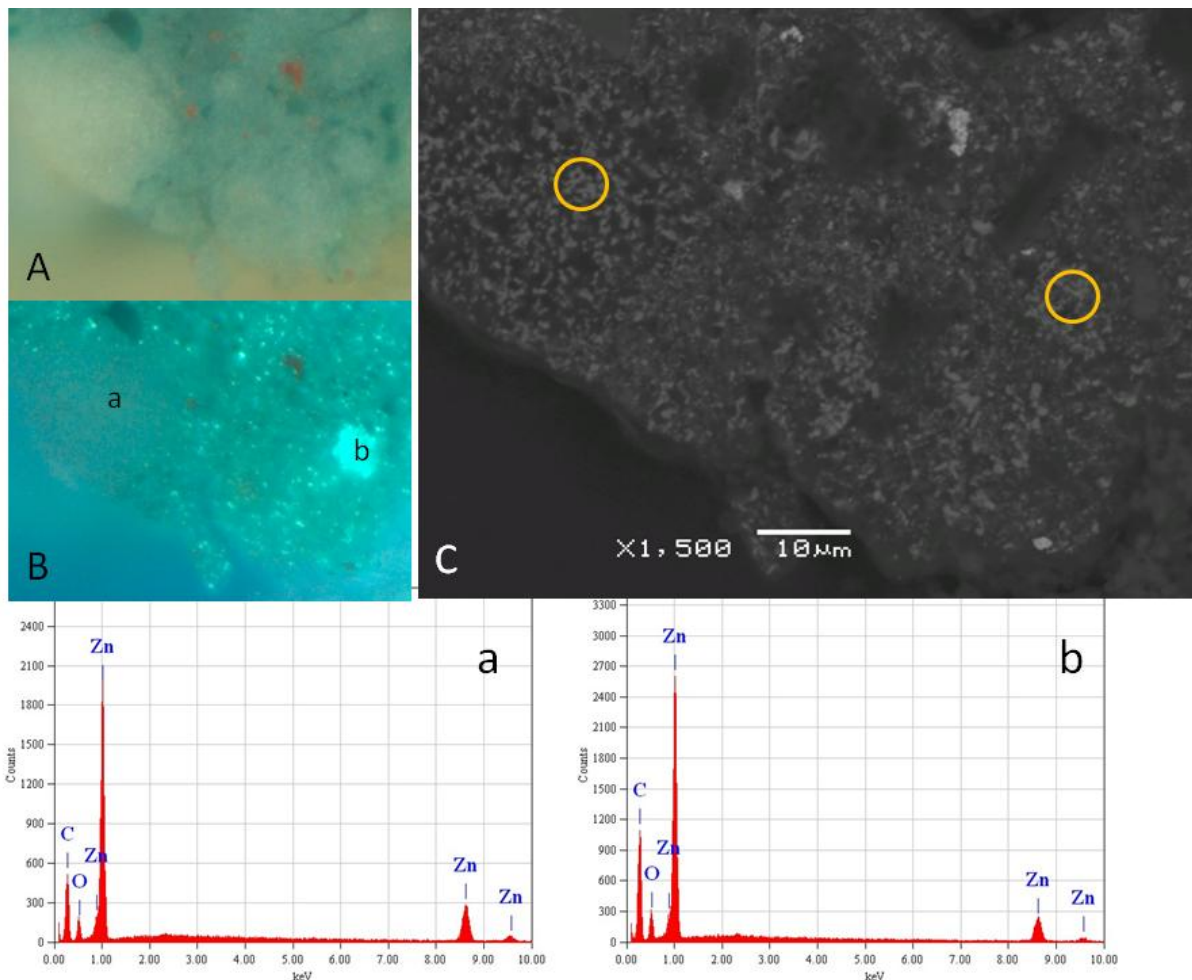
Figure 6.38 FBH#4 optical: (A) visible and (B) UVF, and (C) BSE image details and spot EDX spectra from points designated

(a) white mass with low UV-fluorescence and (b) white mass with bright UV-fluorescence. Both regions comprise zinc, carbon and oxygen while carbon is in higher proportion in the fluorescent zone. There is little to distinguish the areas in BSE

6.3.3.3 FBH#1

Sample FBH#1 derives from the mother's dress which has been painted over the background sand. The sample has been examined with a number of surface presentations reflecting procedures undertaken on different occasions. Visible stratigraphy includes the ground layer (1), pink paint with some yellow traces (2), a warm grey-blue paint layer (3) and a surface coating (Figure 6.39). Elemental analysis shows the consistent presence of zinc oxide-based paint with aluminium silicate traces. Pigmentation includes vermilion, iron earth-based red/brown, cobalt blue and cadmium sulfide (with zinc). A chromium based pigment is also apparent. Layer 2 has a relatively dense, evenly pigmented appearance in BSE images, punctuated by bright particles of vermilion (mercuric sulfide). Small particles of high atomic brightness are more numerous throughout layer 3 and within veins of yellow paint in layer 2, again reflecting the incidence of mercury but also lead (of uncertain form, primarily in yellow paint) (Figure 6.40).

267
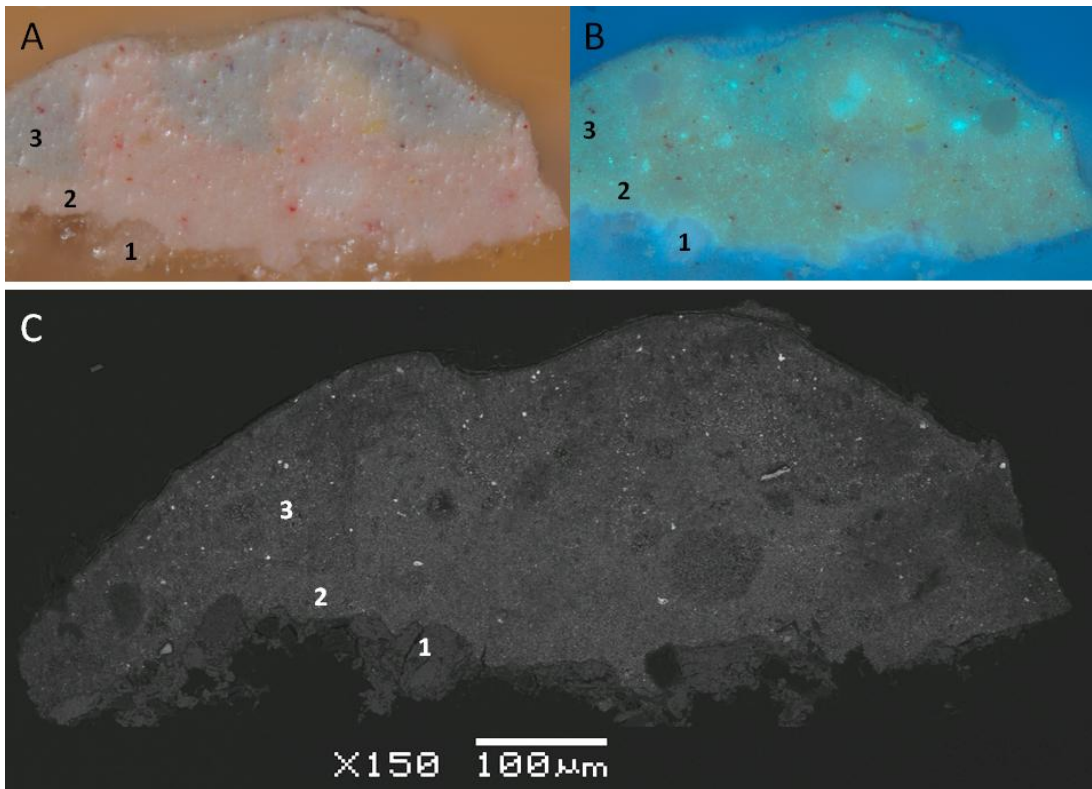
Figure 6.39 *Bathing hour* **cross-section FBH#1**

(A) visible (B) UVF and (C) BSE images showing surface presentation applicable to SEM imaging and spot EDX measurements. Ground layer (1), pink paint (with yellow) (2) and blue paint (3)
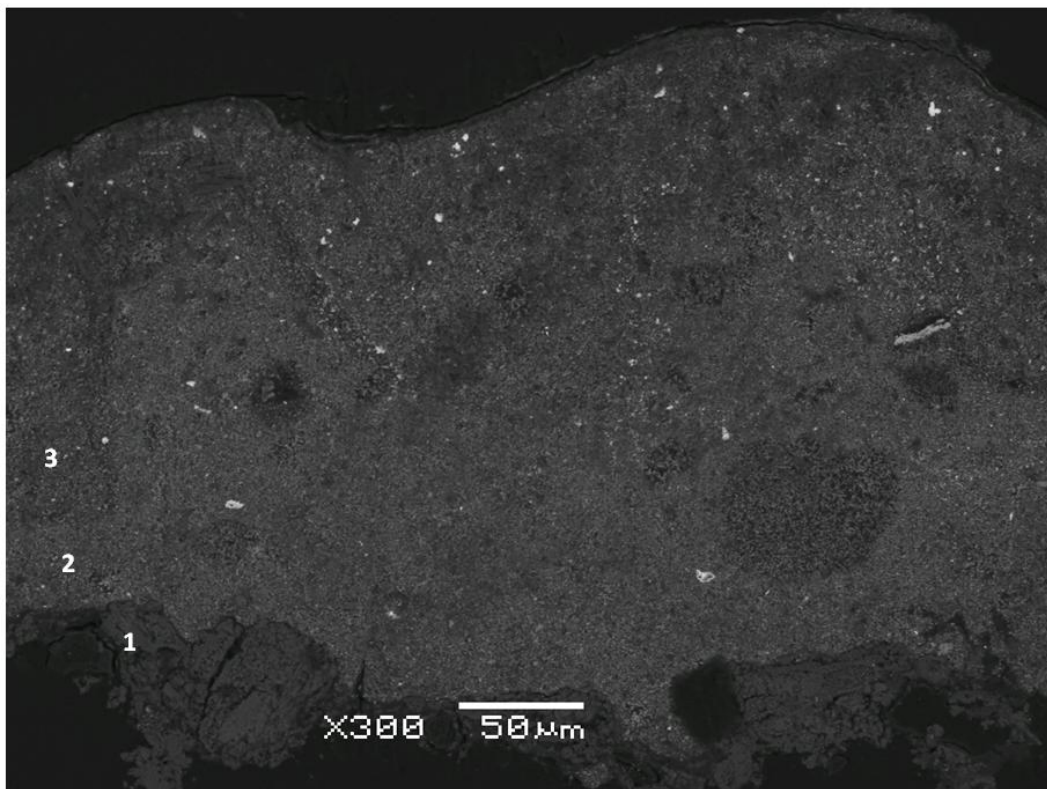
Figure 6.40 FBH#1 BSE image detail. Layer 2 has a relatively dense, evenly pigmented appearance but is also more disrupted by large circular features with a comparatively open morphology

Typical round, whitish masses with variable UV-fluorescence and atomic density occur in both paint layers, but most obviously in layer 2. As with previous samples, these masses are dominated by zinc, carbon and oxygen. Fluorescent regions appear to have proportionally higher carbon counts relative to the surrounding paint (Figure 6.41). Another feature within layer 2 which is almost indistinguishable from the previous fluorescent example based on the EDX spectrum and appearance in BSE images has more even, subdued UV-fluorescence and opaque white appearance in optical images (Figure 6.42).
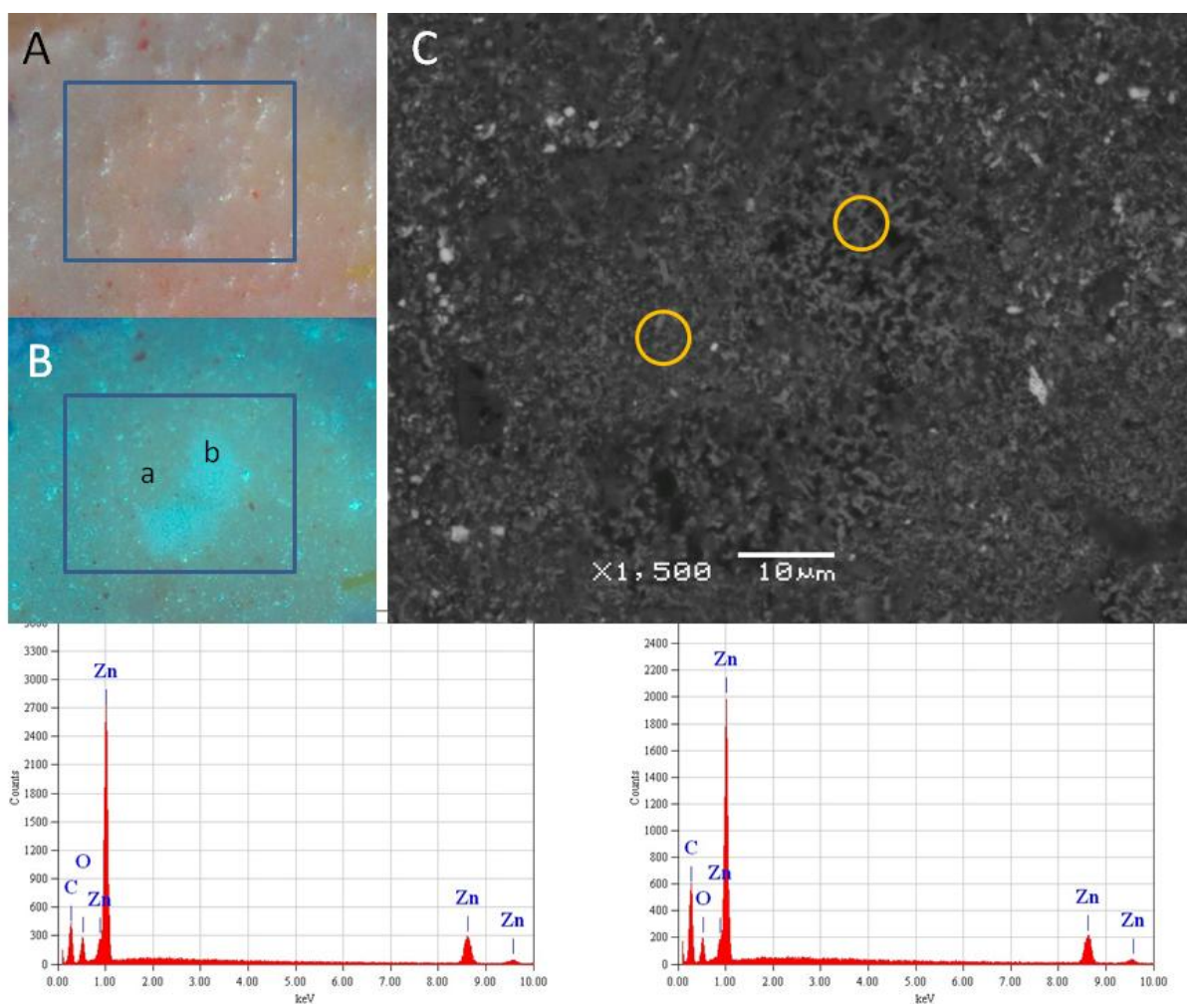
Figure 6.41 FBH#1 Optical (A) visible (B) UVF, and (C) BSE image details and spot EDX spectra from points designated in layer 2 in an area adjacent to yellow paint representing (a) intact paint with UV-fluorescent sparkle and (b) UV-fluorescent mass with open structure in BSE.

Zinc, carbon and oxygen predominate with a higher proportion of carbon in the fluorescent region
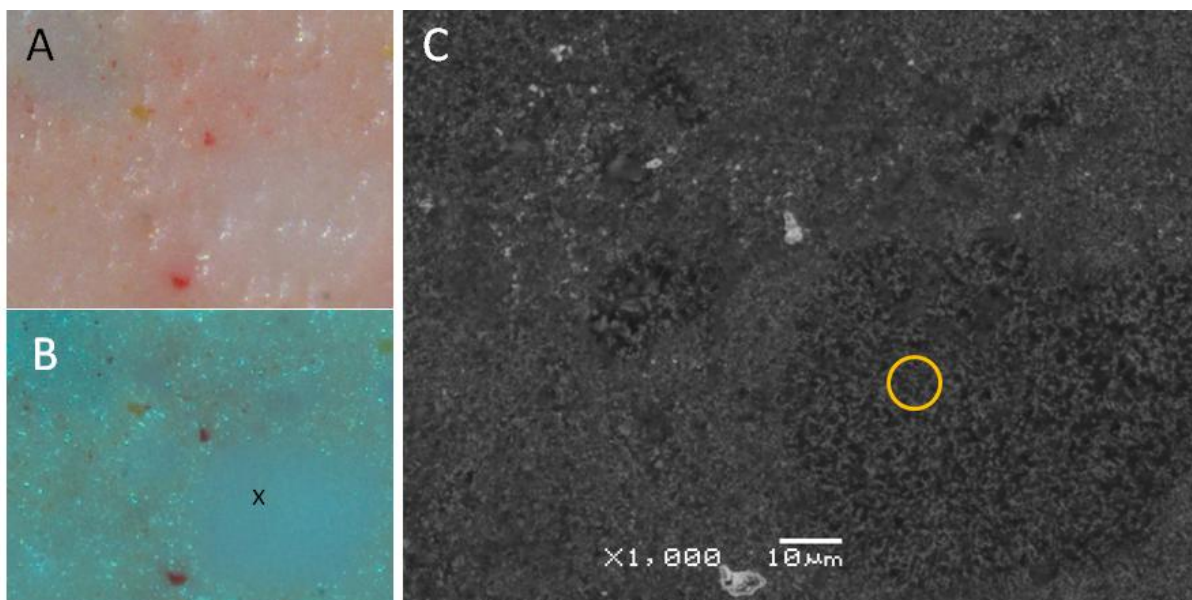
Figure 6.42 FBH#1 Optical (A) visible (B) UVF, and (C) BSE image details and spot EDX spectrum from a large feature with homogeneous low-level UV-fluorescence in layer 2.

The EDX spectrum and appearance in BSE images are very similar to that shown in the previous figure. The feature is opaque white in visible light
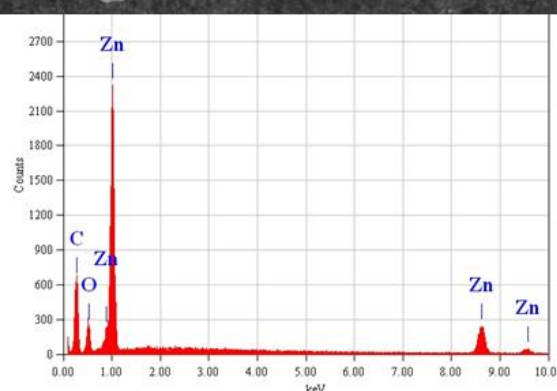
Interesting information regarding these circular masses is obtained through elemental mapping. Unfortunately this was undertaken with a different surface presentation, meaning it was not possible to make a direct correlation with the BSE image details presented above.

An elemental map spanning ground layer 1, paint layer 2 and part of layer 3 shows zinc is generally in high concentration in the paint (Figure 6.43). Three circular masses in layer 2 with distinctive appearance in BSE images have particularly high zinc concentration at the centre in contrast to depleted levels at the periphery where BSE density is low. The high density centres correspond to reduced UV-fluorescence. This is similar to a feature observed in *Autumn showers* FAS#1 (Figure 6.11) where a mineralised centre is proposed to have crystallised from within a carboxylate soap phase.
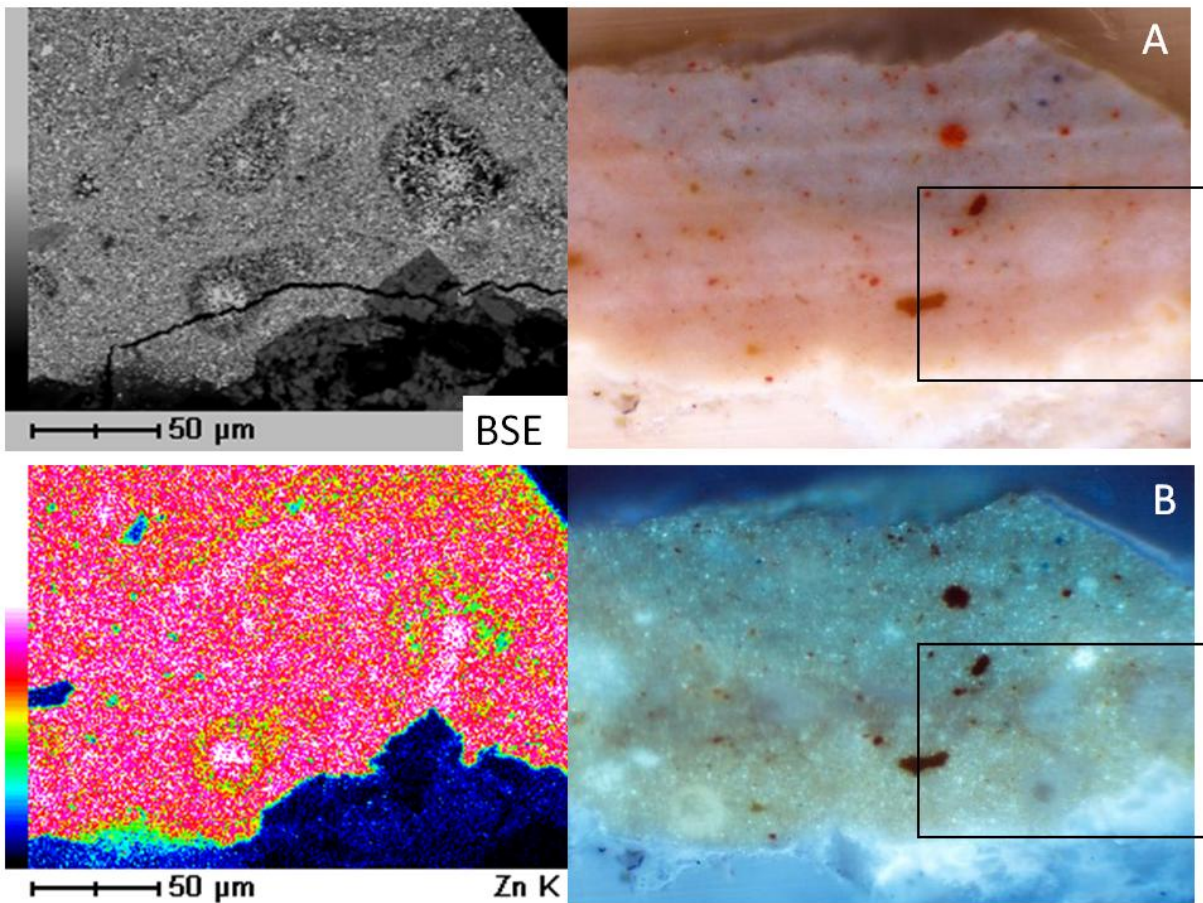
Figure 6.43 FBH#1 Optical images of surface presentation applicable to EDX maps (A) visible and (B) UVF, with boxed area corresponding to BSE image detail and elemental map for zinc.

Zinc is in high concentration throughout the paint layers and particularly at the centre of circular masses, contrasting with depletion of zinc at the periphery where BSE density is low. The high density centres correspond to reduced UV-fluorescence

Elemental mapping also suggests zinc concentration in layer 2 is reduced at the interface with the glue and plaster-based ground layer.

Elemental maps for various elements within the same region of FBH#1 highlight the composition and distribution of different particles across layers of the sample (Figure 6.44). The sulfur map reflects sulfur in various forms including as sulfate with calcium and as sulfide with mercury and cadmium (as vermilion and cadmium yellow); however it also reflects traces of lead due to an overlapping peak in the emission spectrum. Sulfur (and lead) in all forms is noticeably absent from within the three circular features of interest.
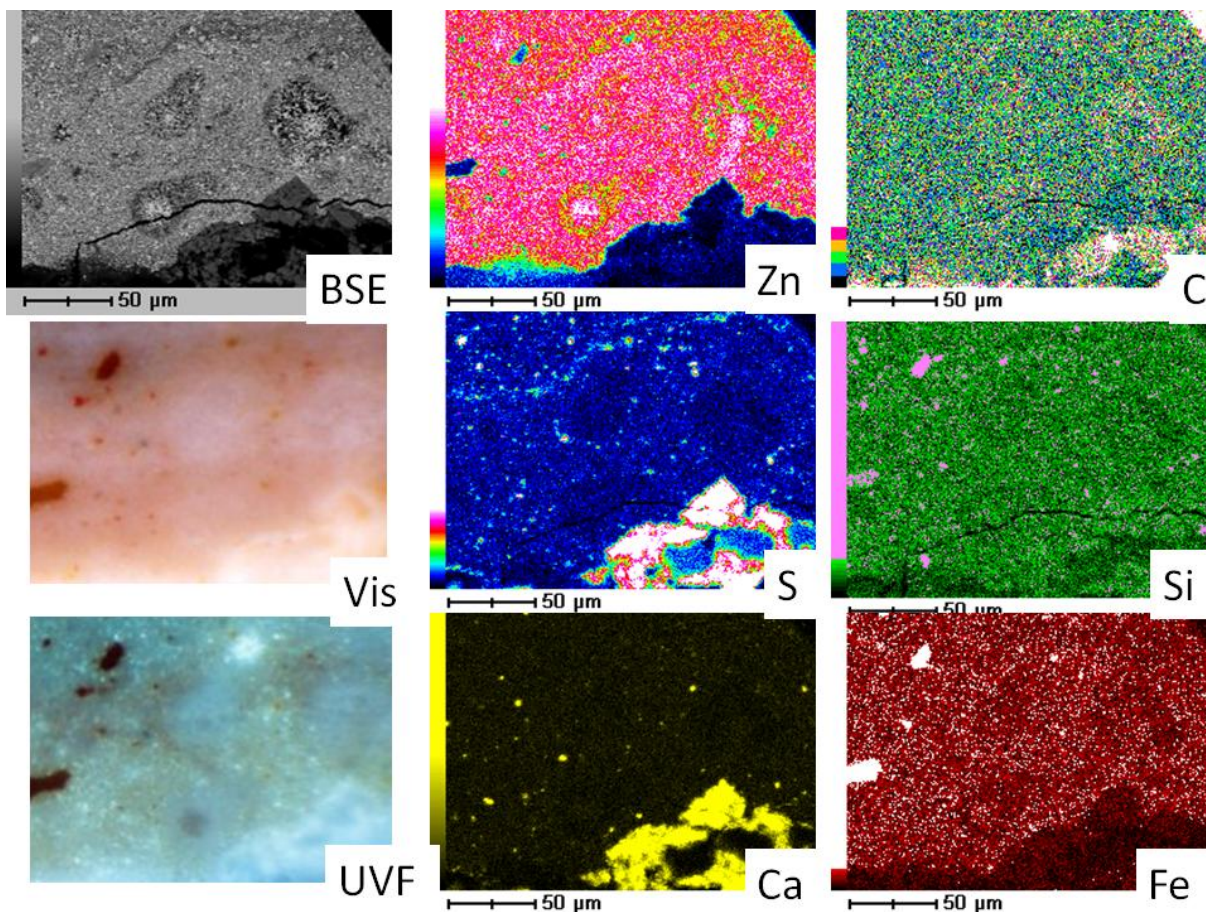
Figure 6.44 FBH#1. BSE and optical image details with corresponding elemental maps

Distributions are shown for zinc, calcium (as calcium sulfate), sulfur (as sulfate with calcium, sulfide with mercury and cadmium (not shown) as vermilion and cadmium yellow, and also reflecting traces of lead detected by peak overlap), and Si (with Al - not shown - as fillers) or with Fe (as coloured earth pigments)

6.3.4 *Rocks and Sea* c. 1911

Rocks and sea was produced in the course of an extended Mediterranean painting trip and is likely to have been painted *en plein air*. It has an absorbent ground - hand-prepared with plaster of Paris and 'special size'. Two samples are included in this study, deriving from the locations indicated in Figure 6.45.

Figure 6.45 E. Phillips Fox *Rocks and sea* c. 1911 with numbers denoting the source location of paint samples

6.3.4.1 FRS#3
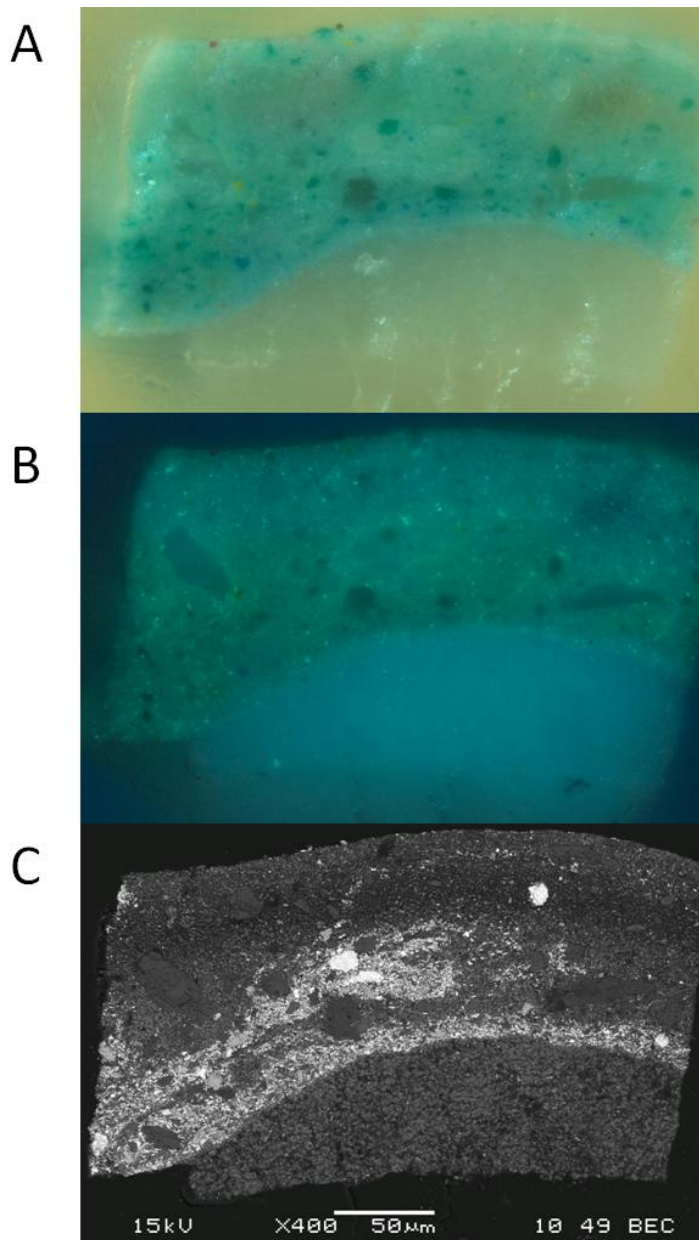
Figure 6.46 *Rocks and sea* cross-section FRS#3: (A) visible, (B) UVF and (C) BSE images

This sample derives from the crest of a wave and comprises two green paint layers applied wet-in-wet over a thin blue layer (Figure 6.46). The blue paint and lower green layer are lead white-based, with zinc oxide-based green paint uppermost. A thick transluscent-white and UV-fluorescent layer underlies the paint and is believed to be a large mass which has formed in the paint. No ground layer is evident in the cross-section and in fact the orientation of this sample isn't certain.

Elemental mapping of an area of the cross-section encompassing both lead- and zinc-based paint layers illustrates the presence of large chromium-based green pigment particles (viridian), cobalt blue, cadmium yellow and large colourless fillers, predominantly calcium sulfate in zinc-based paint and barytes in lead-based paint (Figure 6.47). Carbon counts are higher in the zinc-based layers and the top of the map area coincides with a low electron density band in the BSE image (Figure 6.46) which runs through the centre of the top layer.
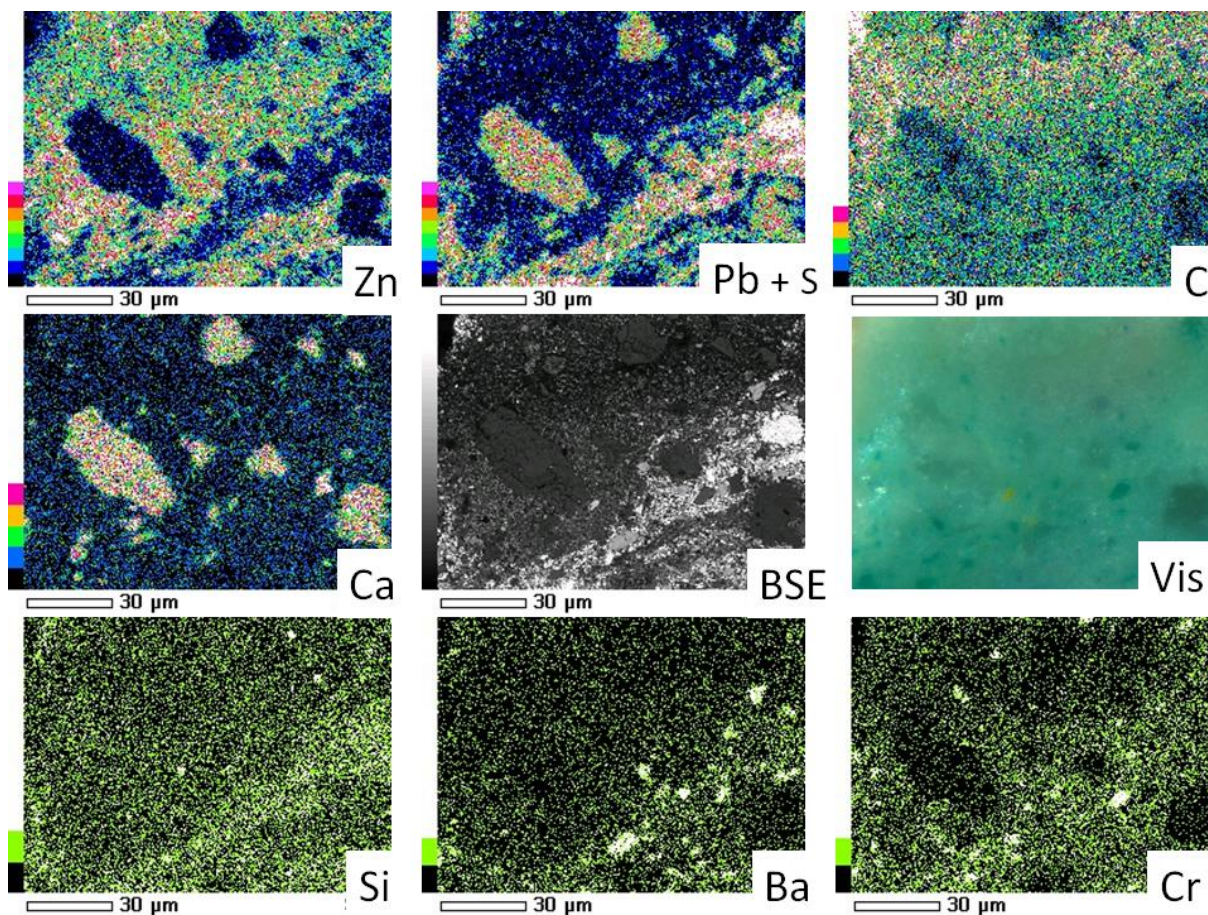
Figure 6.47 FRS#3 SEM-EDX maps for elements indicated with corresponding BSE and optical images. Cr corresponds to viridian pigment.

In zinc-based paint carbon levels are highest and zinc intensity reduced at the upper part of the layer. The lead peak overlaps with sulfur so that the lead map reflects the presence of calcium sulfate particles (see Ca map) in addition to lead white pigment

A second elemental map bridging the interface between the translucent-white mass and paint shows that carbon counts are highest in the white mass and that zinc (with oxygen) is the only other element to register above background levels (Figure 6.48).
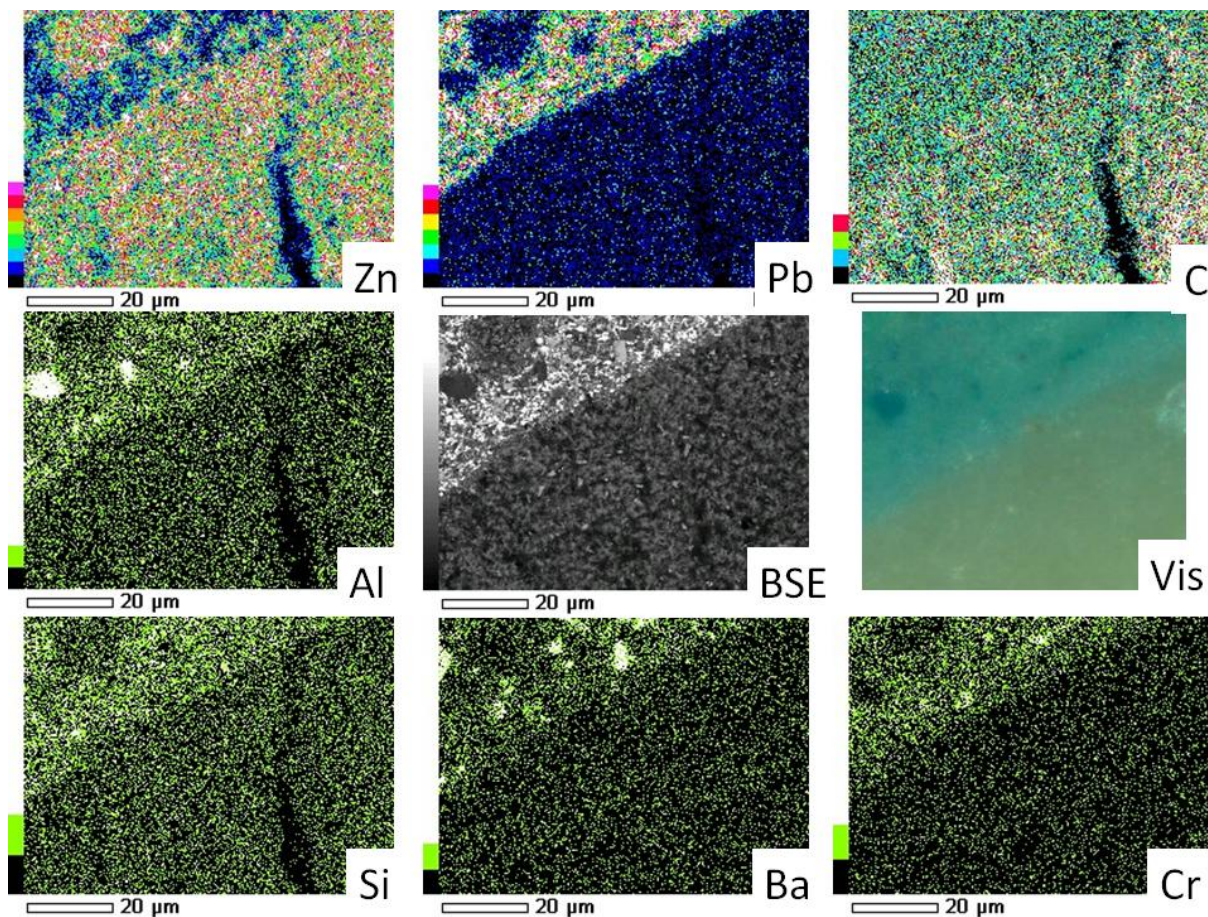
Figure 6.48 FRS#3 SEM-EDX maps for elements indicated with corresponding BSE and optical images.

Al corresponds to cobalt blue pigment. Carbon levels are highest in the translucent-white mass across the bottom half of the map area, and zinc is the only other element detected above background levels in the same region

At higher magnification, BSE images show this white mass is composed from small bright particles among numerous needle-shaped clusters of lower atomic density (Figure 6.49). An EDX spectrum from the region confirms that zinc, carbon and oxygen are the only elements detected. The small bright particles are likely to comprise zinc oxide which is distributed among another zinc-based compound, possibly a zinc carboxylate.
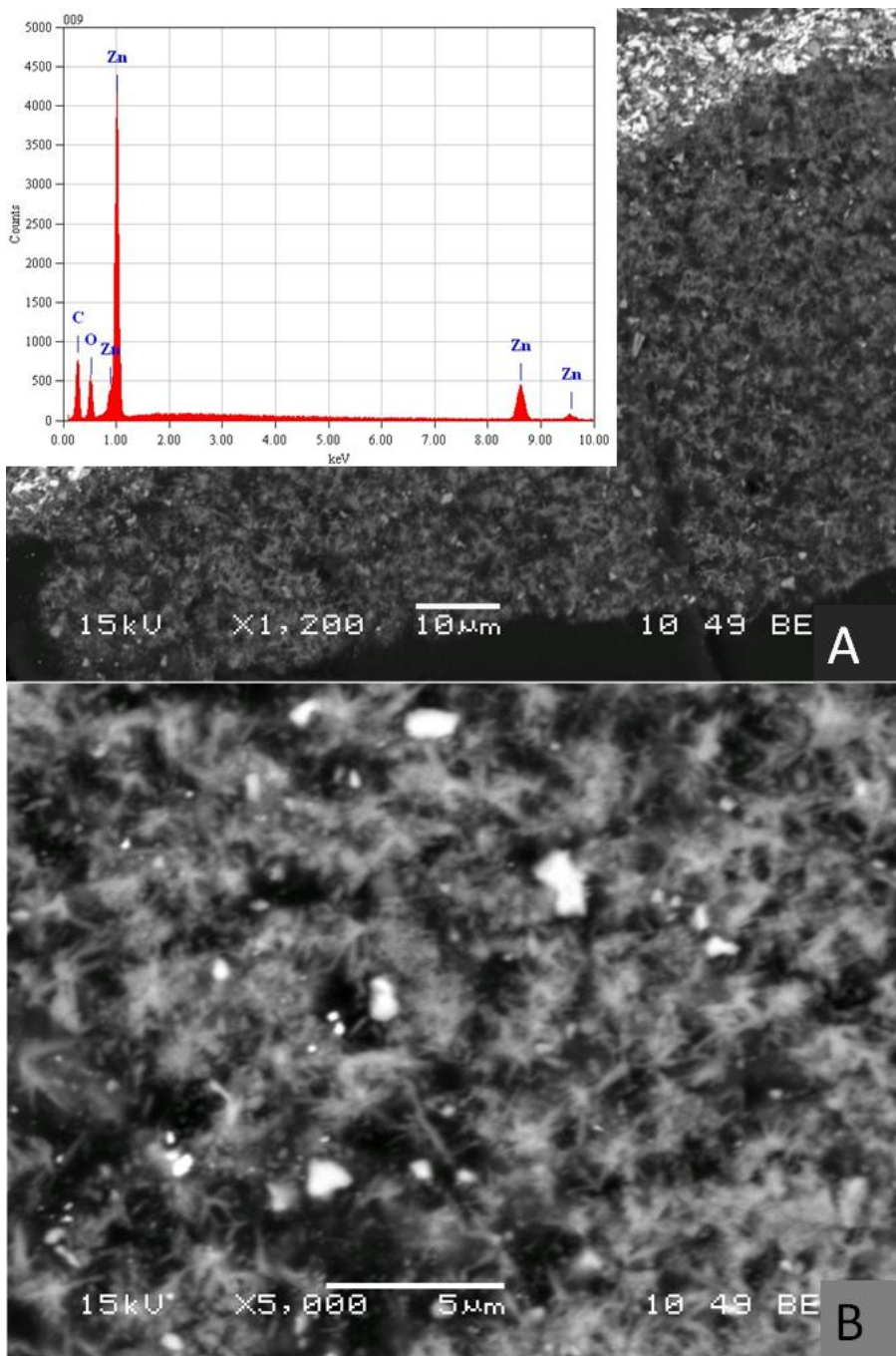
Figure 6.49 FRS#3 BSE image detail (A) of area mapped in Figure 6.48 and higher magnification detail from the translucent-white mass (B)

Particles of zinc oxide are surrounded by needle like crystals of another zinc-based compound. An EDX spectrum from the mass (inset) detects only zinc, carbon and oxygen

Conventional ATR-FTIR microscopy - with the ATR crystal positioned in contact with the white mass - produced a spectrum with strong carboxylate absorption but which does not appear characteristic of zinc stearate. A spectrum obtained from the same paint sample prior to embedding includes similar unattributed carboxylate absorptions (Figure 6.50). There appear to be underlying

basic zinc carbonate absorptions contributing to both spectra including peaks at *ca* 3380, 1510, 1380 and 832 cm^{-1}.
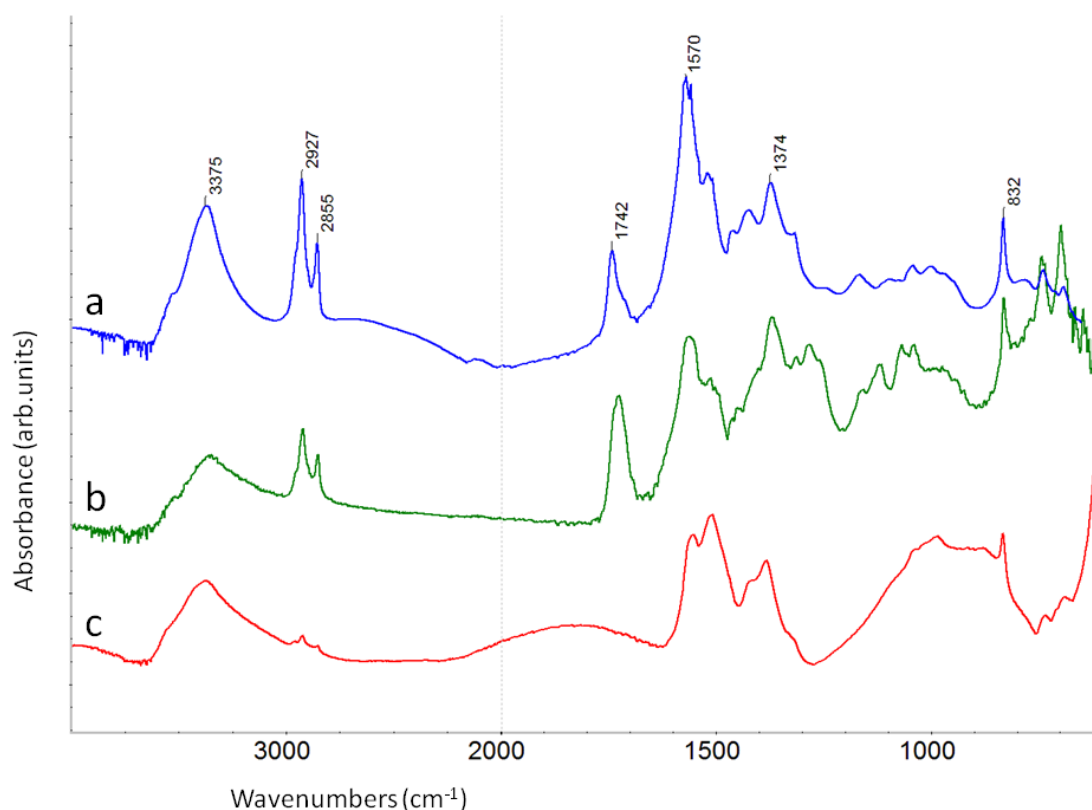
Figure 6.50 FRS#3: comparison of FTIR spectra obtained via (a) transmission prior to embedding and (b) ATR on the surface of the embedded cross-section with the ATR crystal positioned on the large white mass.

Transmission spectrum (c) shows indicative carbonate absorptions observed on the surface of a modern zinc oxide pigment sample (Kremer) which may be contributing to broad peaks *ca* 3380, 1510 and 1380 and at 832 cm^{-1} in the sample. The white mass contains strong carboxylate absorption but not specifically zinc stearate

Other spectra recorded prior to embedding reflect more general, broad COO$^-$ absorption very typical of zinc white-based oil paint (not shown). Clarification was sought by means of SR-µFTIR mapping of a thin-section obtained from the sample across a 14x34 grid with 5x5 µm^2 aperture and 5 µm step size. The synchrotron spectra are of high quality but the thin-section itself may not have been complete and it is difficult to determine its orientation and relationship to optical and BSE images. It is possible that the large aggregate of interest was not retained in the thin-section. Individual spectra representing a range of components occur across the mapped area (Figure 6.51). Integration of characteristic peaks among the representative spectra show that zinc stearate/palmitate is concentrated in two small masses within the mapped area (Figure 6.52).
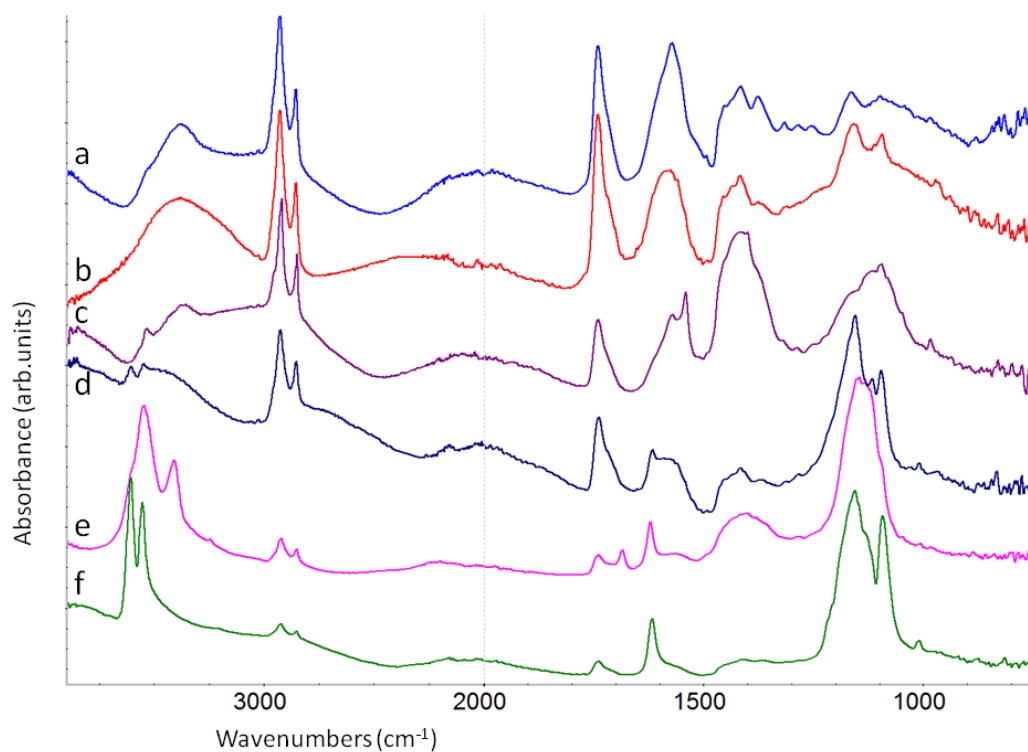
Figure 6.51 FRS#3 range of extracted transmission SR-µFTIR spectra.

Characteristic peaks include (c) 1540 cm^{-1} (zinc stearate/palmitate) with lead white and barytes; (b) broad zinc carboxylate absorption very characteristic of zinc white oil paint; (e) gypsum (CaSO$_4$.2H$_2$O); (f) plaster (calcium sulfate hemihydrate) and (a) triangular peak centred at 1572 cm^{-1} (unattributed)
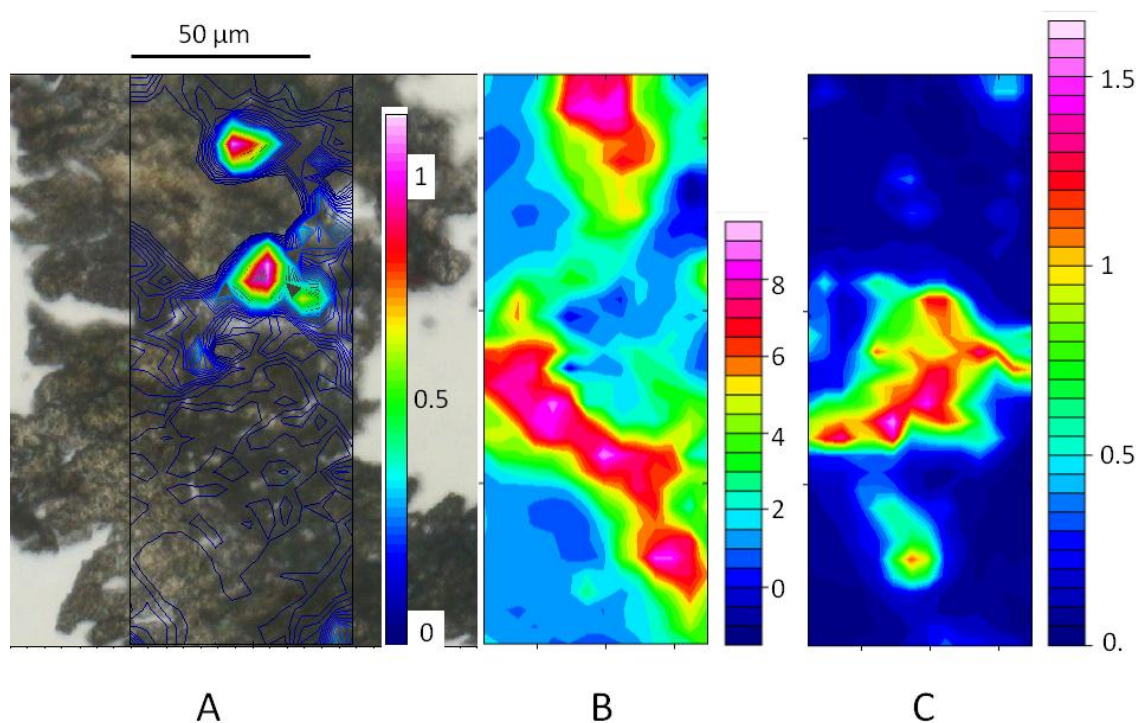
Figure 6.52 FRS#3 partial thin-section detail (A) showing region mapped using SR-µFTIR with overlaid integrated absorption intensity map for 1530-1555 cm^{-1} (zinc stearate/palmitate).

Maps of the same area are shown in (B) 1380-1460 (lead white) and (C) 1610-1635 cm^{-1} (calcium sulfate as hemi and dihydrate). The orientation of the thin-section relative to cross-section images is unclear

Zinc stearate/palmitate more generally is not in high concentration, and spectra extracted from the two high-intensity points show it occurs in association with other substances including lead white and gypsum (Figure 6.53). Spectra also show an apparent carboxylate doublet at 1540 and 1573 cm^{-1}. This carboxylate doublet is found in calcium stearate (Ferreira et al. 2011) but other corresponding peaks are not evident. Closer examination of the spectra in Figure 6.50 suggests this second peak relates to a separate carboxylate species. It occurs with a series of small reproducible peaks between 1200 and 1350 cm^{-1} which, when integrated, is shown to occupy a localised area of the mapped sample (Figure 6.54).
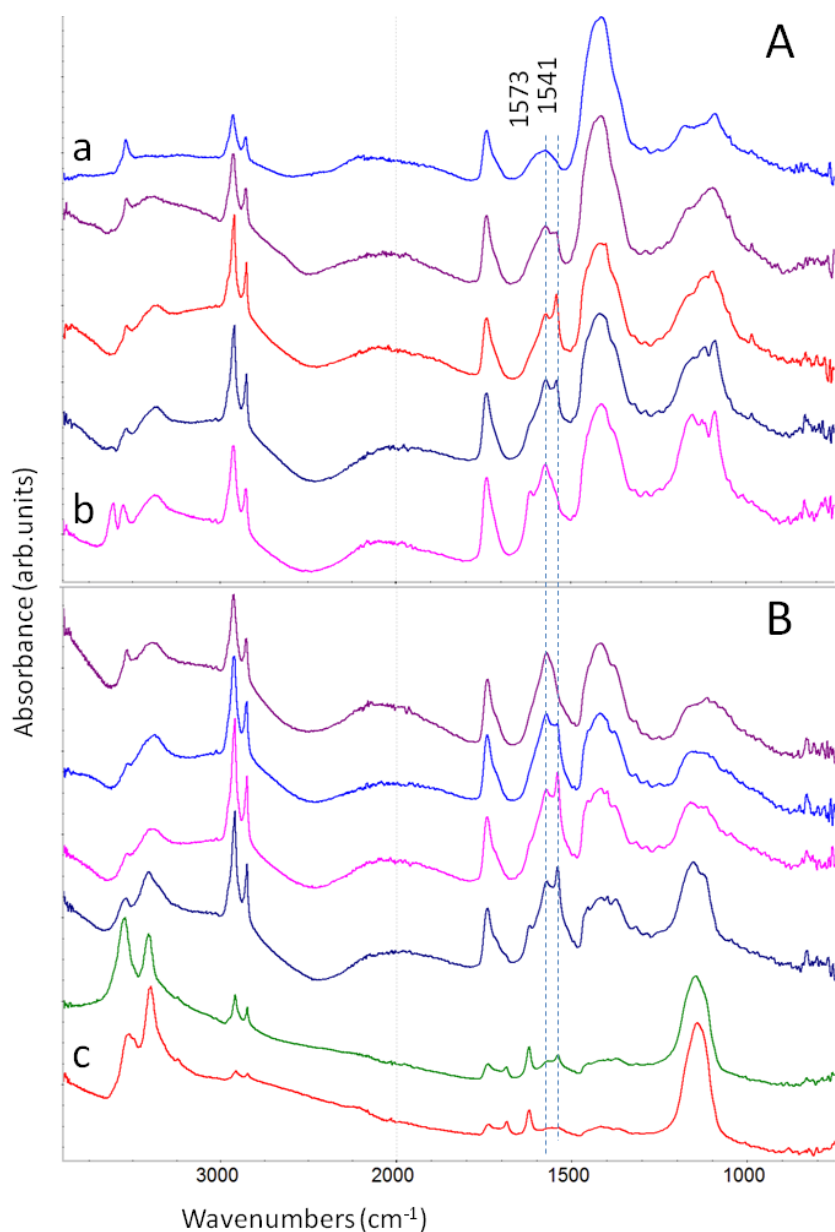
Figure 6.53 FRS#3 SR-µFTIR spectra extracted from a line through each of the two 1540 cm^{-1} hotpots.

A peak at 1573 is present with the strongest 1541 cm^{-1} absorption but this appears to relate to a distinct carboxylate species. Other spectral features reflect contributions from adjacent components including (a) lead white (b) calcium sulfate hemihydrate and (c) gypsum (calcium sulfate dihydrate)
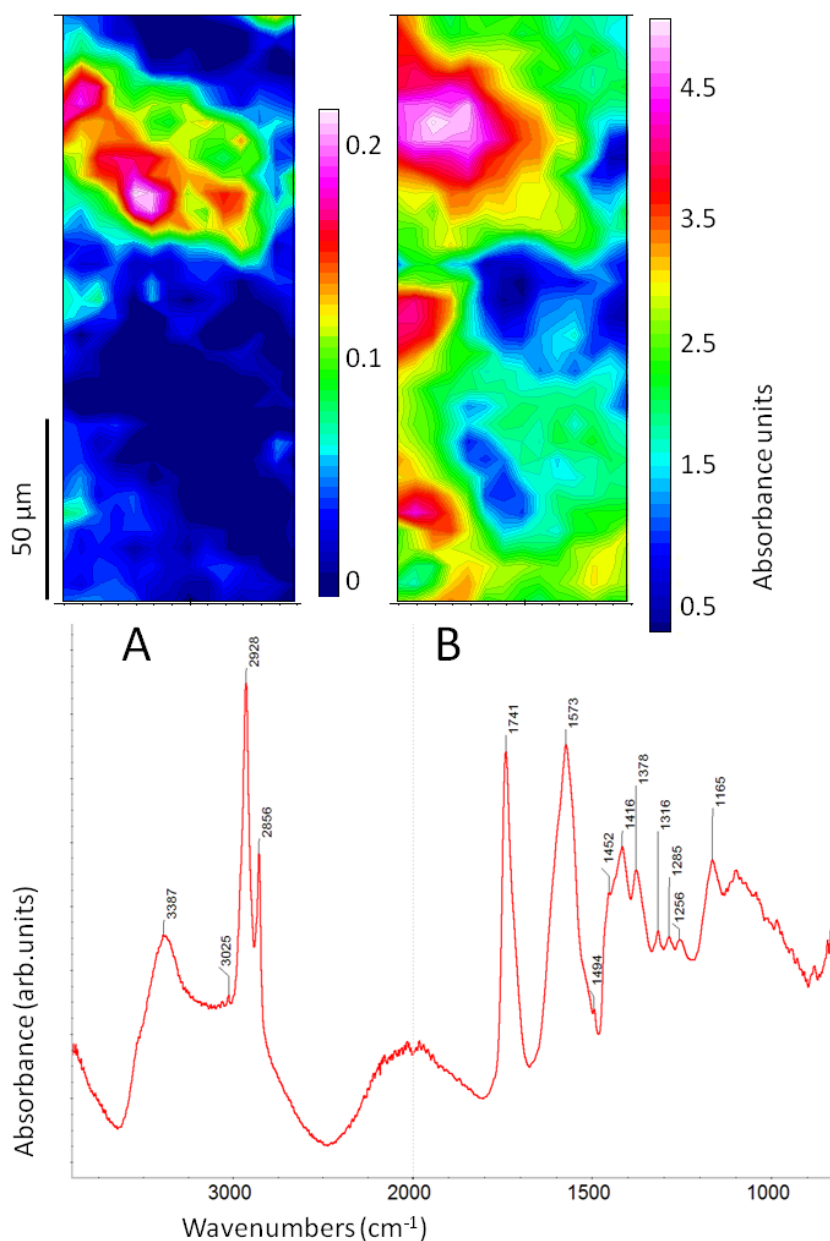
Figure 6.54 FRS#3 SR-µFTIR integrated absorption intensity maps for (A) 1306-1330 and (B) 1710-1760 cm^{-1}.

A spectrum extracted from the hotspot in map A is typical of the region with a pointed carboxylate peak at 1573 cm^{-1} and a series of reproducible peaks as annotated. Map B suggests a possible correlation with strong ester carbonyl absorption

The 'triangular' COO$^-$ peak shape echoes that of zinc lactate although at 1573 cm^{-1} is lower than that seen in the paintings previously discussed, and with different peak positions for the peak series at lower wavenumbers; the spectral complexity at higher wavenumbers surrounding C-H stretching vibrations associated with zinc lactate is also absent, and the carbonyl intensity is significantly stronger. Spectral features also bear similarities to those assigned to zinc formate in another recent painting study (Keune and Boevé-Jones 2014), but again with sufficient inconsistency to make this an unlikely attribution.

The absence of basic zinc carbonate spectra from SR-µFTIR mapping does suggest that the large mass of primary interest in this sample did not survive the process of thin-section preparation, unfortunately preventing capture of high resolution, spatially resolved spectra. The precise composition is left open to speculation, however the morphology evident in BSE images combined with elemental composition and the general finding of basic zinc carbonate in association with complex carboxylates does not exclude the possibility of layered basic zinc salts as tentatively identified and discussed in relation to Kiệm's paintings (Chapter 5). Ultimately, FRS#3 is a sample of very complex composition, including calcium sulfate in different hydration states, lead white, barium sulfate and a range of coloured pigments, making it one of the more difficult to interpret.

6.3.4.2 FRS#2

Sample FRS#2 derives from the pale yellow rock at the centre left edge of the painting (Figure 6.55).
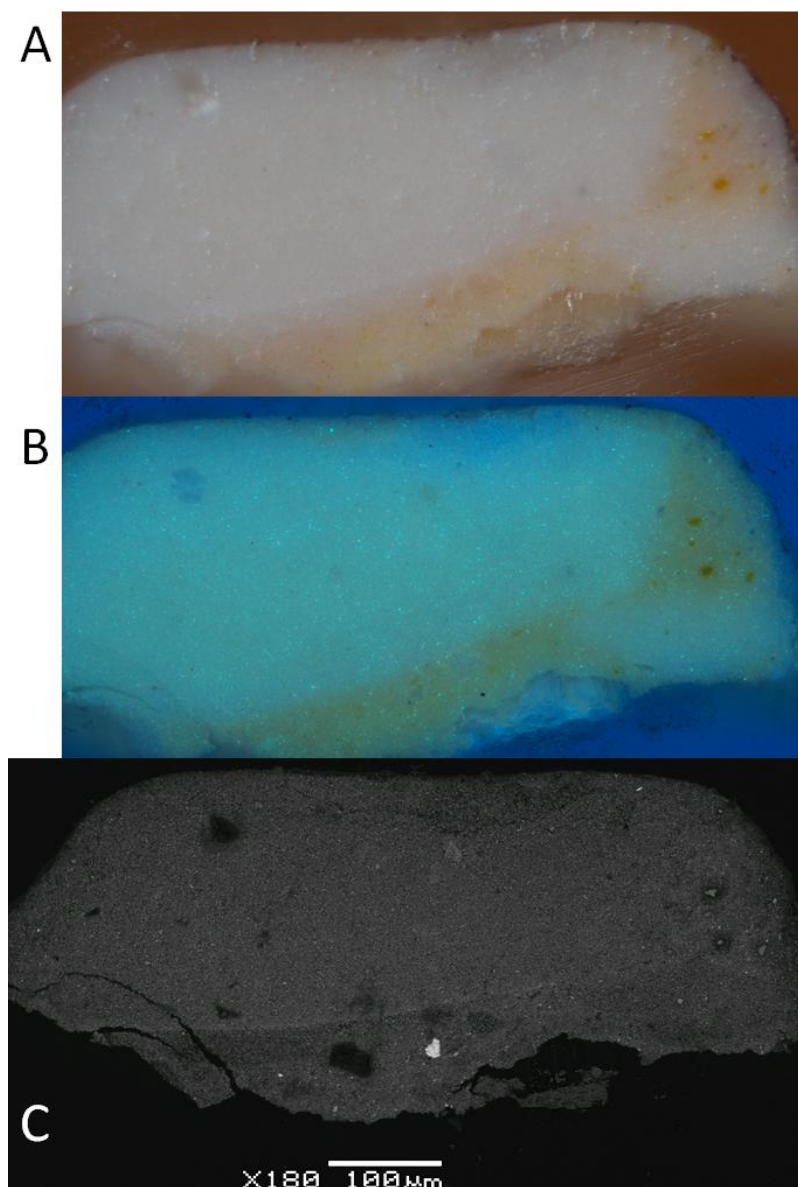
Figure 6.55 *Rocks and sea* cross-section FRS#2: (A) visible, (B) UVF and (C) BSE images

The sample has a simple structure comprising intermixed white and yellow paint layers over a trace of the calcium sulfate-based ground. It is interesting that at a previous stage of investigation the sample presentation appeared more as a single-coloured paint layer incorporating circular white masses consistent with those seen in samples from *Bathing hour*. The surface presentation shown in Figure 6.55 correlates to that used for SEM-EDX and SR-μFTIR.

Both white and coloured passages appear similar in BSE images, the yellow paint having slightly lower electron density, possibly indicative of higher medium content. Both paints have a comparable UV-fluorescent sparkle and predominantly comprise zinc oxide. Yellow pigment particles are cadmium sulfide, and yellow paint also includes some small dispersed lead-based particles which in one instance occur as a mass of aggregated pigment (Figure 6.56); this incomplete mixing suggests the lead-based pigment is not present as a commercially incorporated component of the paint. A few particles of gypsum are also evident.
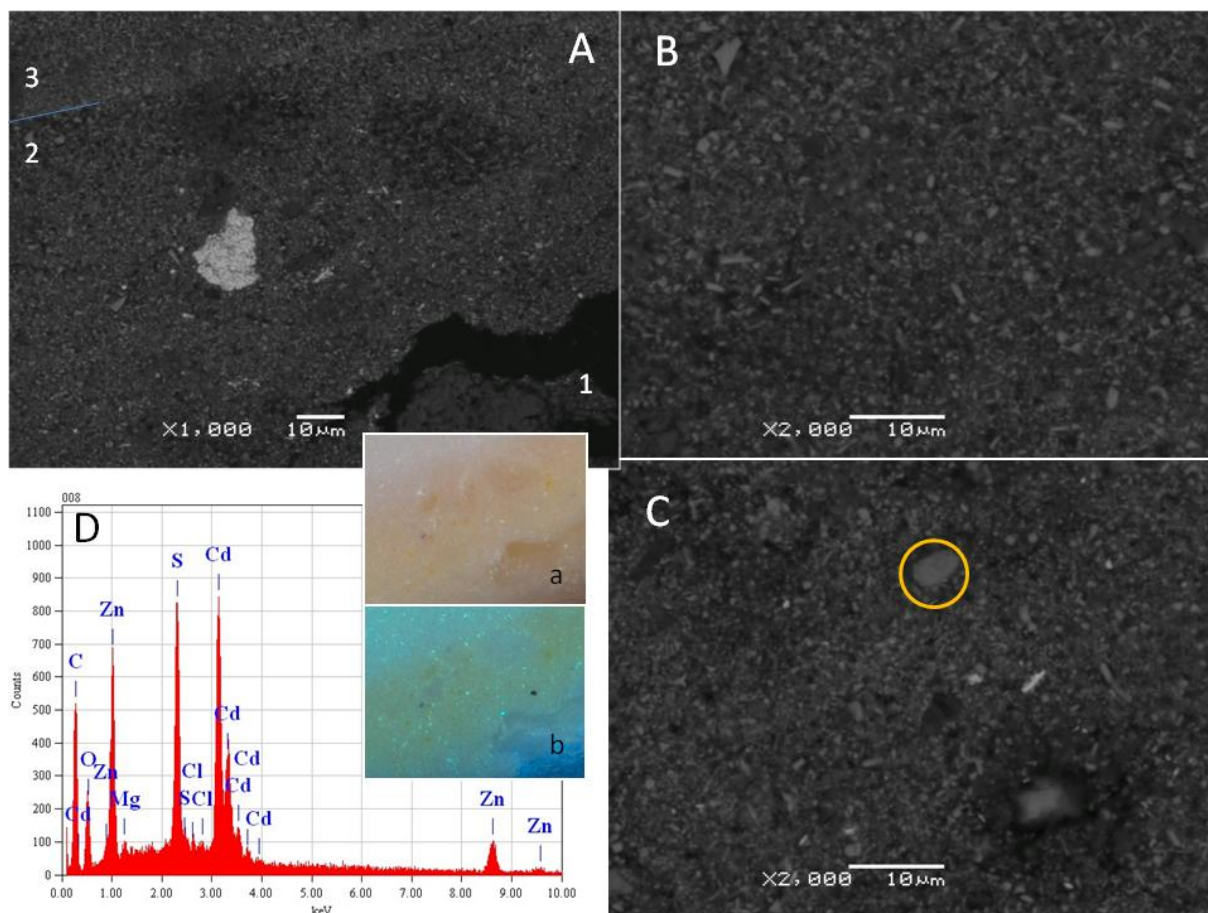
Figure 6.56 FRS#2 (A) BSE image detail showing (1) ground layer, (2) yellow and (3) white paint layers with corresponding optical images (a) visible and (b) UVF.

Higher magnification BSE image details from white (B) and yellow (C) paint layers show the similar morphologies in general zinc oxide-based pigmentation. Lead-based particles with high atomic brightness are present in layer 2. An EDX spectrum (D) obtained from the circled particle in yellow paint (C) shows elemental composition consistent with cadmium sulfide with contribution from the surrounding matrix high in zinc and carbon

The most prominent cadmium yellow particles have a low density halo in BSE images. EDX associates high zinc, carbon, oxygen and traces of magnesium with these regions, in addition to cadmium and sulfur. Magnesium is not otherwise detected in the general paint matrix. SR-µFTIR mapping of a thin-section (10x35 grid with 5x5 µm^2 aperture and 5 µm step size) shows strong carboxylate absorption centred at 1540 cm^{-1} in the vicinity of cadmium yellow pigment (Figure 6.57). An obvious question surrounding this finding is whether the carboxylate formed may in fact comprise a cadmium soap rather than zinc, as has been attributed to paint reconstructions combining cadmium yellow in linseed oil (Mazzeo et al. 2008). Cadmium stearate does include a v_a COO$^-$ peak at 1540 cm^{-1} similar to zinc stearate, however this occurs as part of a doublet with a second peak at 1601 cm^{-1} and v_s COO$^-$ at 1414 cm^{-1} (Mesubi 1982); shorter chain (C$_{16-6}$) cadmium carboxylates have peaks at 1547-1548 and 1408-1411 cm^{-1} (ibid), and all have a very different and less defined shape than the spectrum for zinc stearate/palmitate.
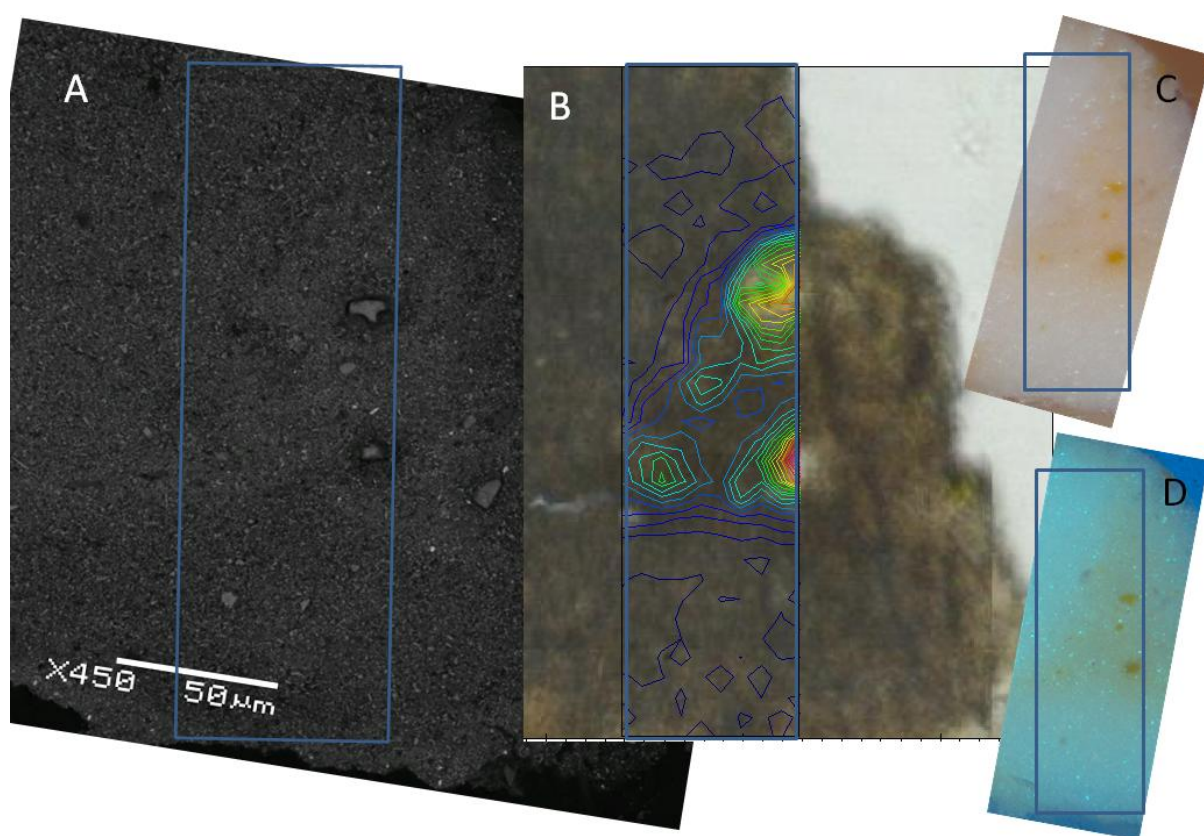
Figure 6.57 FRS#2 BSE detail (A), thin-section detail (B) and corresponding cross-section images visible (C) and UVF (D) with box denoting region mapped using SR-µFTIR.

Prominent particles of cadmium yellow are visible in the wedge of coloured paint at the centre of the mapped area. The contour lines overlying the thin-section (B) relate to SR-µFTIR absorption intensity at 1540 cm^{-1}, discussed in more detail below

Individual spectra extracted from 1540 cm^{-1} hotspots in the sample are characteristic for zinc stearate/palmitate, and a reduction in electron density is evident in the surrounding zinc oxide-based paint, consistent with localised conversion of zinc oxide to zinc stearate. The highest intensity 1541 cm^{-1} absorption is also clearly associated with a reduced C=O ester peak at 1741 cm^{-1} and a shift in C-H stretching vibrations to lower frequencies, all consistent with oil hydrolysis and saponification of fatty acids (Figure 6.58).
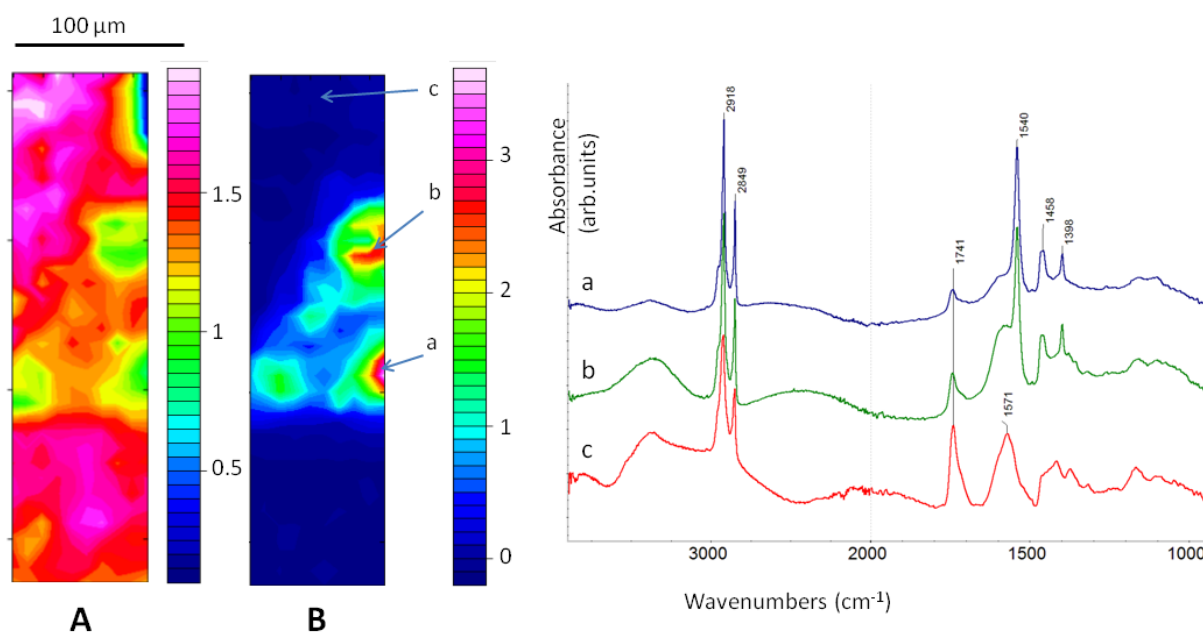
Figure 6.58 FRS#2 transmission SR-μFTIR integrated absorption intensity maps for (A) 1730-1760 and (B) 1530-1555 cm^{-1}, and spectra extracted from the points designated showing inverse intensity relationship between oil ester carbonyl absorption (1741 cm^{-1}) and carboxylate absorption (v_a COO$^-$ zinc stearate/palmitate) at 1540 cm^{-1}.

Map B and spectra (a) and (b) show zinc stearate/palmitate is concentrated in yellow paint around particles of cadmium sulfide. Carboxylate absorption in spectrum (c) from white paint has a quite different pointed peak centred at 1571 cm^{-1} which occurs in combination with strong absorption at 1741 cm^{-1}

Pronounced zinc stearate/palmitate absorption is also associated with other discrete particles in the yellow paint characteristic of gypsum, CaSO$_4$.2H$_2$0 (Souza and Derrick 1995) (Figure 6.59). Interestingly, the ester carbonyl peak at 1742 cm^{-1} is still strong in these areas possibly reflecting the high oil absorbency of gypsum. Additional areas of reduced electron density in yellow paint are visible in BSE images without obvious cadmium or calcium based particles at the centre. These similarly comprise zinc, carbon and oxygen (without apparent magnesium) and appear slightly more transparent with brighter UV-fluorescence than adjacent paint. These characteristics are more in keeping with features observed in samples from *Bathing hour*. Unfortunately no such areas were included in the SR-μFTIR map area, precluding comparison of spectra with those from the more obvious areas of saponification surrounding particles of cadmium yellow and gypsum.
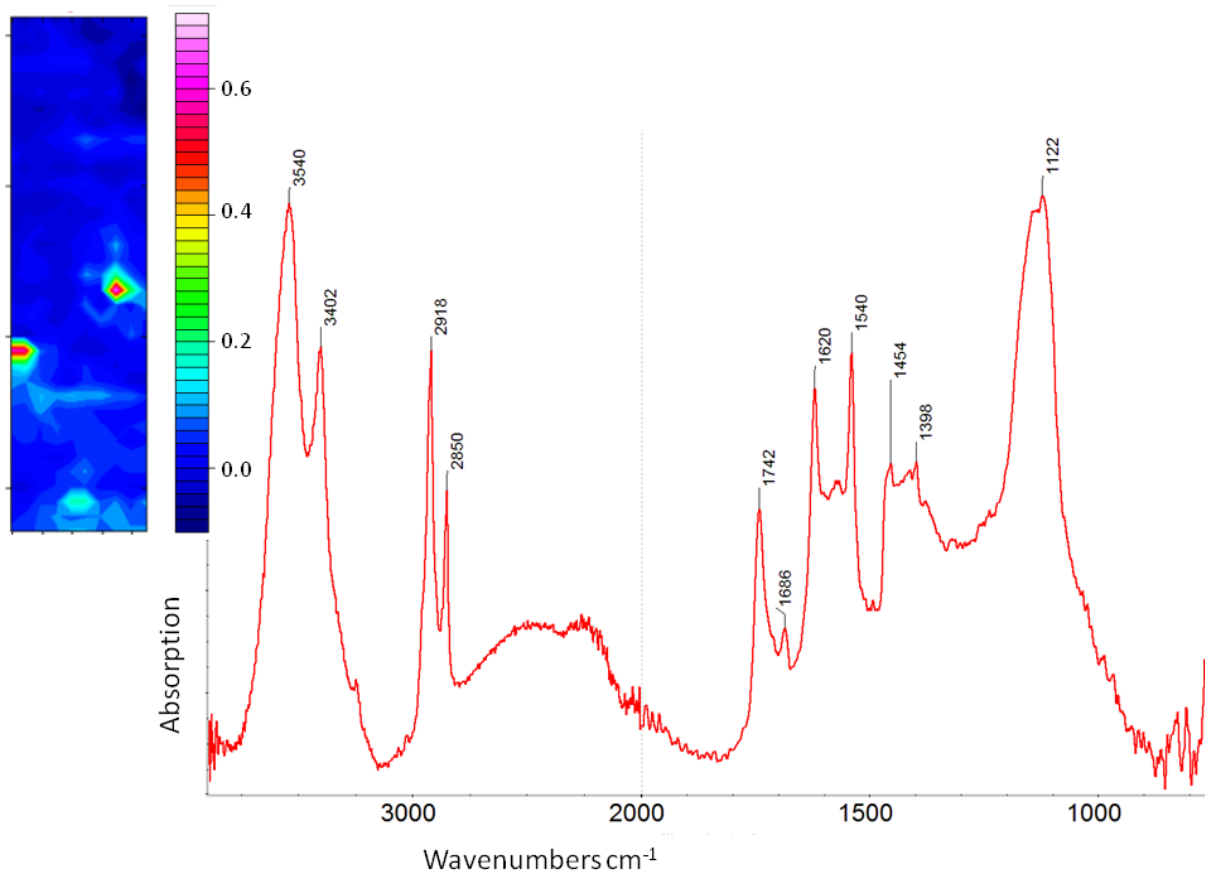
Figure 6.59 FRS#2 transmission SR-µFTIR integrated absorption intensity map 1610-1630 cm⁻¹ and spectrum extracted from high intensity spot showing characteristic absorption of gypsum (CaSO₄.2H₂O) (3540 3402 1686 1620 1122 cm⁻¹) in close association with zinc stearate/palmitate (2918 2850 1540 1454 1398 cm⁻¹). The oil ester carbonyl peak is also strong at 1742 cm⁻¹

The rounded, broad carboxylate peak centred at 1582 cm⁻¹ associated with yellow paint more generally is very typical of zinc oxide-based oil paint. However, in the white paint also based on zinc oxide, carboxylate absorption produces a more triangular peak shape centred at 1571 cm⁻¹, similar to that observed in a region of FRS#3 (Figure 6.54) although without two of the three small, well resolved peaks between 1250-1320 cm⁻¹. In both examples the triangular carboxylate peak is associated with higher wavenumber CH_2 stretch vibrations (c 2926 and 2855 cm⁻¹) and without a pronounced shoulder at 2953 cm⁻¹ in comparison to that observed in yellow paint (2918 and 2849 cm⁻¹). The higher wavenumber of CH_2 stretch vibrations coupled with a strong ester carbonyl peak at 1741 cm⁻¹ suggests hydrolysis and saponification of the oil medium has occurred to a lesser extent in white paint. One possible explanation is the use of different oils in the formulation of the white and yellow paints; linseed oil is commonly avoided in white paints because of its tendency to discolour – a characteristic which is less critical for yellow paint. Poppy and walnut oils were frequently used alternatives to linseed for applications where yellowing was to be avoided, the former gaining increasing popularity during the nineteenth century (Carlyle 2001). The linseed oil

285

substitutes invariably comprise lower levels of the triply-unsaturated linolenic acid, resulting in slower drying tendencies and possibly different processing or modifications in paint production. Fatty acid analysis which would assist determination of the oils present in each of the paints is beyond the scope of this study, so observed differences in the two layers remains qualitative. Of course, in addition to potential variation in the composition and fatty acid profiles of the two painting mediums, the possibility that additional metal ions present in yellow paint may have influenced reactivity must also be considered.

6.3.5 *Lamplight* c. 1911

Lamplight is a large-scale salon piece painted in Paris on a commercial lead-based oil ground. It was shipped to Australia in 1913 and donated to the University of Melbourne in 1939. For many years it was displayed in less than ideal conditions including periods exposed to direct sun entering through a glass wall. The conservation history includes surface cleaning with a strongly alkaline surfactant. Two samples are included in this study, deriving from the locations indicated in Figure 6.60.

Figure 6.60 E. Phillips Fox *Lamplight* c. 1911 with numbers denoting the source location of paint samples

6.3.5.1 *FL#2*

Sample FL#2 derives from an area of blue-green shadow over a pink background curtain. Four layers are evident including a thin lead-based priming (1), the red background paint (2) and two grey-green paint layers (3 and 4) (Figure 6.61). Layer 4 contains various small, white circular

masses and one large mass (5) which has deformed the layer causing a perceptible lump in the painting surface. The sample has complex pigmentation and unfortunately did not sustain thin-sectioning for SR-µFTIR mapping, so conventional FTIR of fragments prior to embedding, and of the embedded section are reported in association with SEM imaging and elemental analysis.
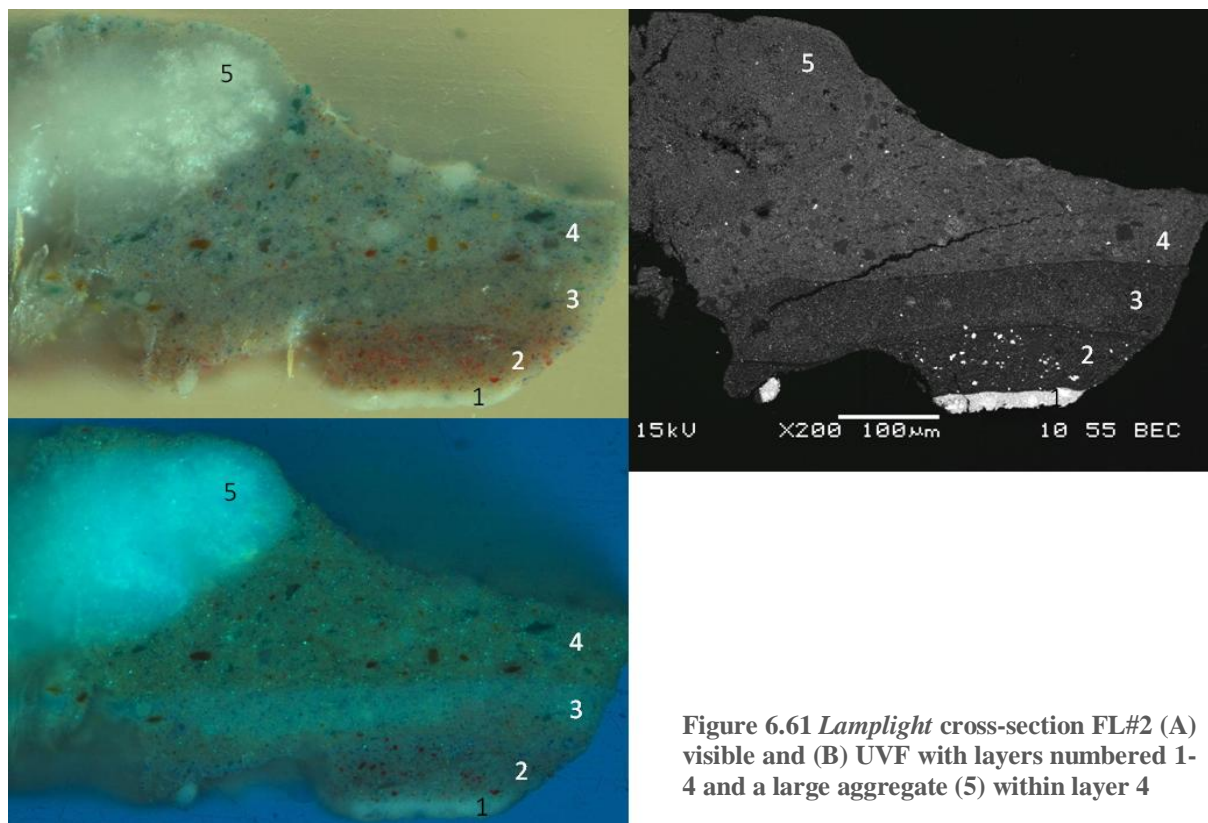
Figure 6.61 *Lamplight* **cross-section FL#2 (A) visible and (B) UVF with layers numbered 1-4 and a large aggregate (5) within layer 4**

Elemental mapping indicates all layers other than the ground are zinc-based, with aluminium silicates including kaolinite and a number of coloured earth pigments also widely distributed in the paint as represented by the silicon map (Figure 6.62). This includes an unusual uncharacterised arsenic-containing yellow-brown pigment. Green pigment in layers 3 and 4 is chromium-based, characteristic of viridian, with a small amount of cadmium yellow also present.
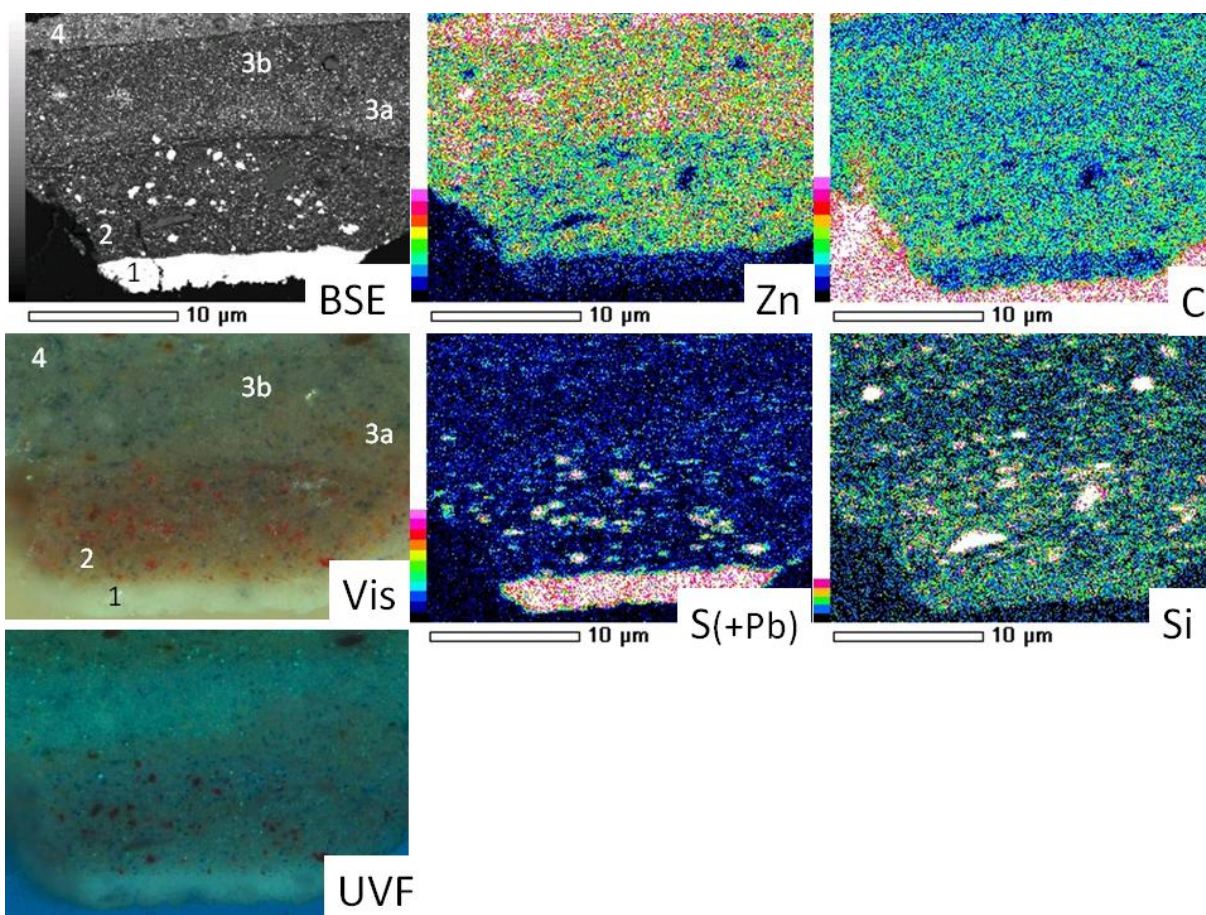
Figure 6.62 FL#2 elemental maps for the region shown in visible, UVF and BSE images.

Zinc is present in all layers other than the ground, in highest concentration in layer 4. Aluminium silicates including kaolinite and probably terre verte are also widely distributed in the paint as shown by the Si map. The sulfur map indicates the presence of the red pigment vermilion (mercuric sulfide) in layer 2 but also lead white in layer 1 due to an overlap of the Pb and S X-ray lines. Layer 3 is possibly two layers applied wet in wet with 3a having less green pigmentation and higher zinc counts, while 3b is more UV-fluorescent

Zinc is in highest concentration in layer 4 and lowest in layer 2. The sulfur map reflects the presence of the red pigment vermilion (mercuric sulfide) in layer 2 but due to a peak overlap of the Pb Mα1 X-ray line with the S Kα1 peak used to produce the map, the sulfur map also detects lead white (basic lead carbonate) which forms the basis of the priming (layer 1). Layer 3 is possibly two layers applied wet-in-wet, with 3a having less green pigmentation and higher zinc counts, while 3b is more UV-fluorescent. At higher magnification it appears the fluorescence corresponds to lower pigment density in the BSE image where particles have a perceptible dark halo (Figure 6.63). Small circular masses are present here too, but not in the less fluorescent margin. A thin, dark band separating layers 3 and 4 is apparent in the BSE image but not the optical images, and similarly between layers 2 and 3, and between the ground and paint layer 2. Elemental mapping of an area from the large mass within green paint (denoted '5' in Figure 6.61) shows the region predominantly comprises zinc and carbon, with a few bright lead-based grains (Figure 6.64).
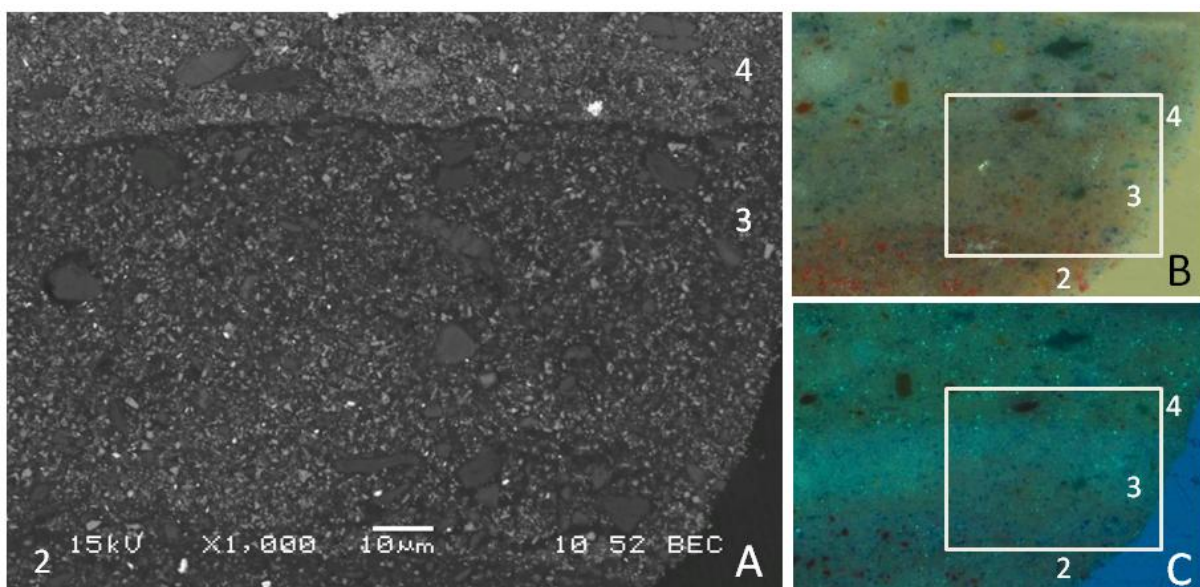
Figure 6.63 FL#2 (A) BSE detail of layer 3 and interface with layer 4, with corresponding visible (B) and UVF (C) details with box denoting imaged area.

A distinct boundary between the layers is evident in the BSE image but not in the optical images. Fluorescence in layer 3 corresponds to lower electron and particle density in the BSE image
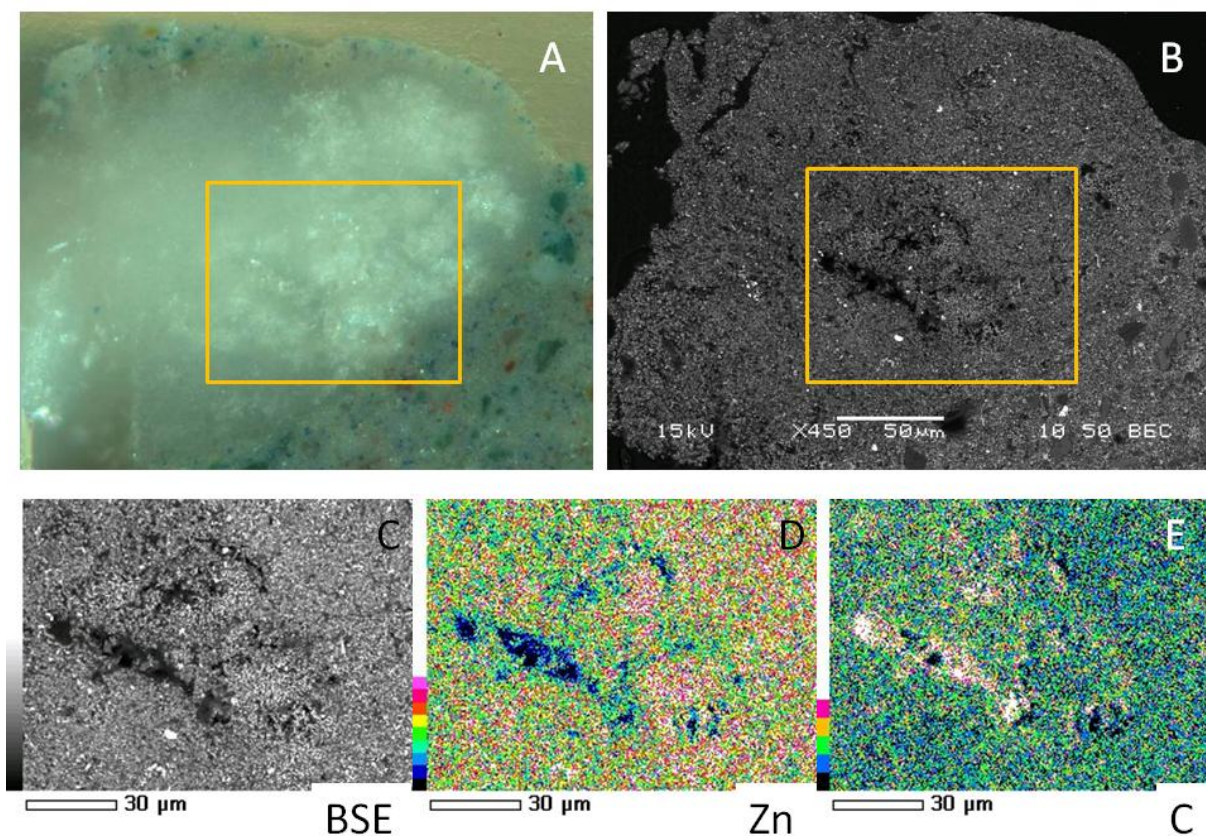
Figure 6.64 FL#2 elemental maps within the large mass adjacent to intact green paint in the region denoted by boxes in the (A) optical and (B) BSE images show the region predominantly comprises zinc (D) and carbon (E), with a few lead-based grains evident as bright white spots in the BSE image (C) (map not shown)

Zinc is generally abundant but particularly through the right half of the mapped area where the mass is relatively opaque. Optical transparency within the mass is associated with lower particle density and elevated carbon counts; at higher magnification it can be seen that the areas richest in carbon correlate with areas where particles are absent or poorly defined, in some cases accompanied by ruptures in the mineralised matrix (Figure 6.65).
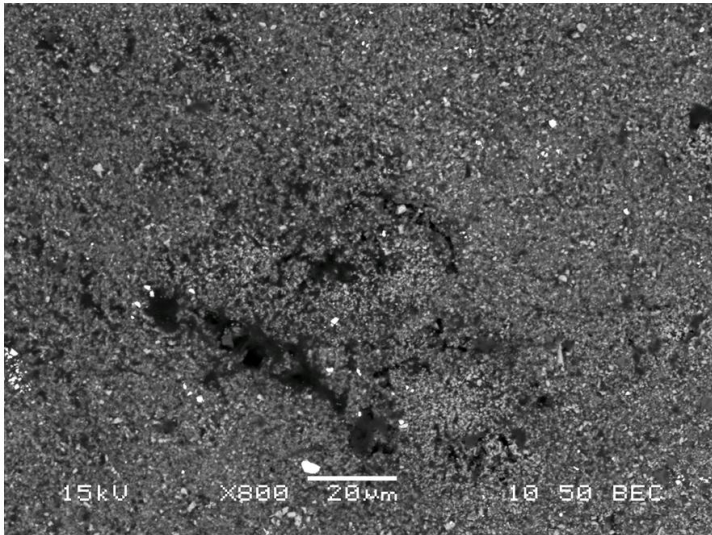
Figure 6.65 FL#2 BSE detail of area mapped in Figure 6.64

The areas richest in carbon correlate to features with low electron density where particles are absent or poorly defined, in some case accompanying ruptures in the surrounding matrix

Smaller circular masses within layer 4 have similar elemental composition to the large mass and a more open morphology in BSE images than the surrounding paint (Figure 6.66).
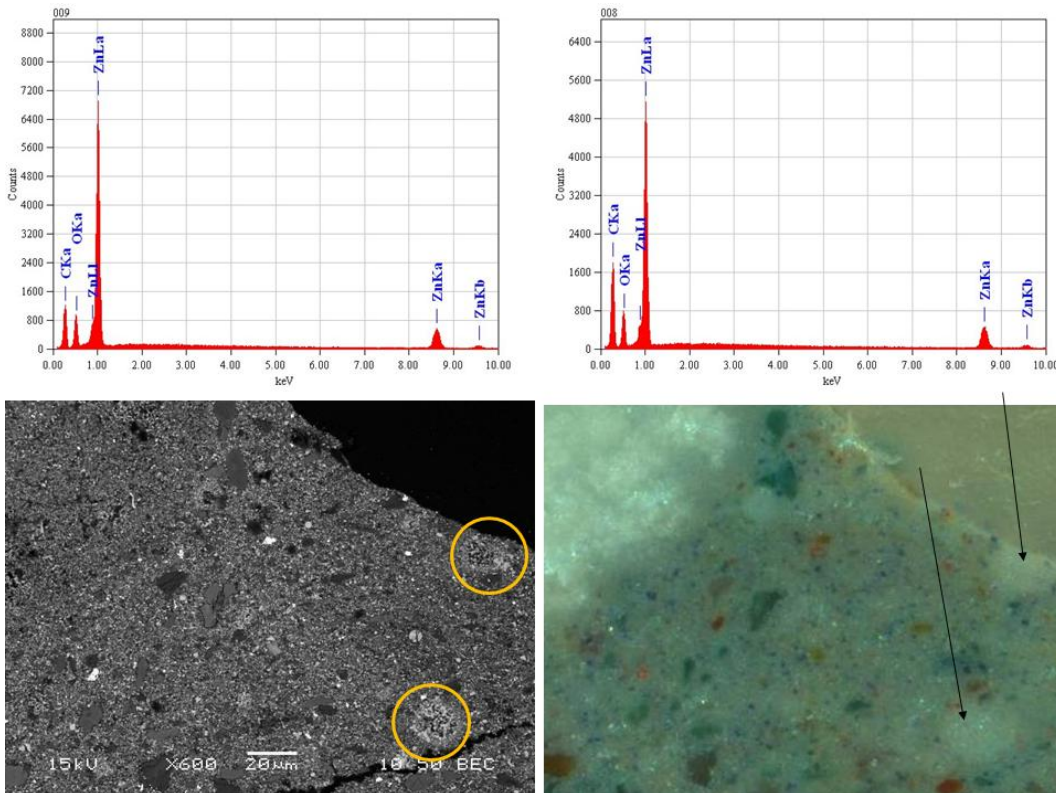
Figure 6.66 FL#2 BSE and optical image details show the distinctive appearance in BSE of circular white masses present in the paint (circled). Spot EDX measurements detect only zinc, carbon and oxygen

ATR-FTIR spectra obtained from the largest white mass (5) suggest a combination of zinc stearate and basic zinc carbonate (Figure 6.67). A spectrum obtained from green paint also includes a sharp peak at 1540 cm^{-1} suggesting zinc stearate/palmitate is present throughout, although with broader accompanying carboxylate absorption than within the white mass. The broad carboxylate peak typical of zinc oxide-based oil paints predominates in transmission spectra obtained from fragments of the sample prior to embedding and also reflects the widespread presence of silicates and kaolinite in particular.
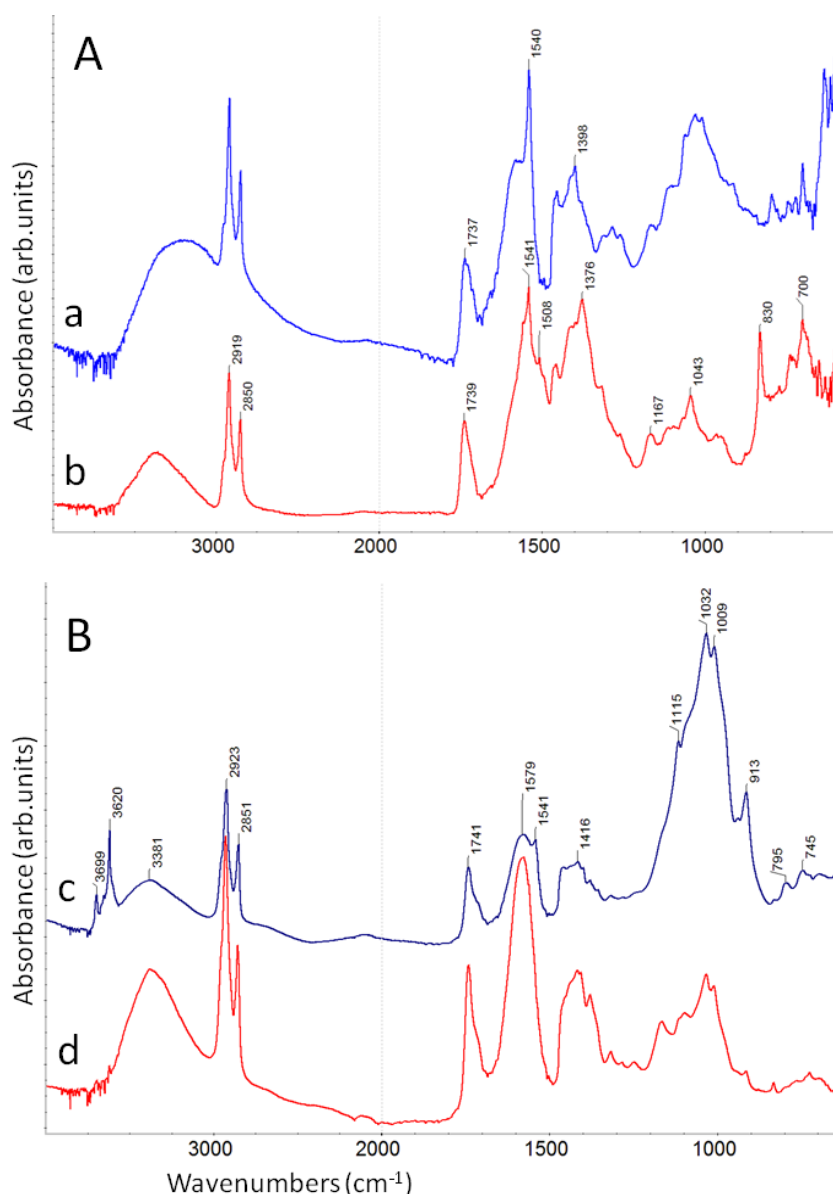
Figure 6.67 FL#2 FTIR spectra obtained (A) using ATR from the surface of the embedded cross-section and (B) in transmission mode from sample fragments prior to embedding.

The ATR crystal was positioned on (a) green paint and (b) the large translucent-white mass. The sharp peak at 1540 cm^{-1} apparent in both ATR spectra indicates zinc stearate/palmitate is present throughout. In the white mass the zinc carboxylate peaks are accompanied by strong absorptions for basic zinc carbonate (3360, 1508, 1376, 1043 and 830 cm^{-1}). Transmission spectra are dominated by broad carboxylate absorption (1579 cm^{-1}) and kaolinite (3699, 3620, 1115, 1032, 1009, 913 cm^{-1}). The small side peak at 1541 cm^{-1} characteristic of zinc stearate/palmitate is strongest in association with kaolinite (c)

6.3.5.2 FL#3

Sample FL#3 derives from the pink cushion and includes the ground and two paint layers (Figure 6.68). Detailed investigation with optical and electron microscopies, including elemental analysis has been undertaken. FTIR analysis was limited to conventional transmission experiments using fragments prior to embedding of the sample.
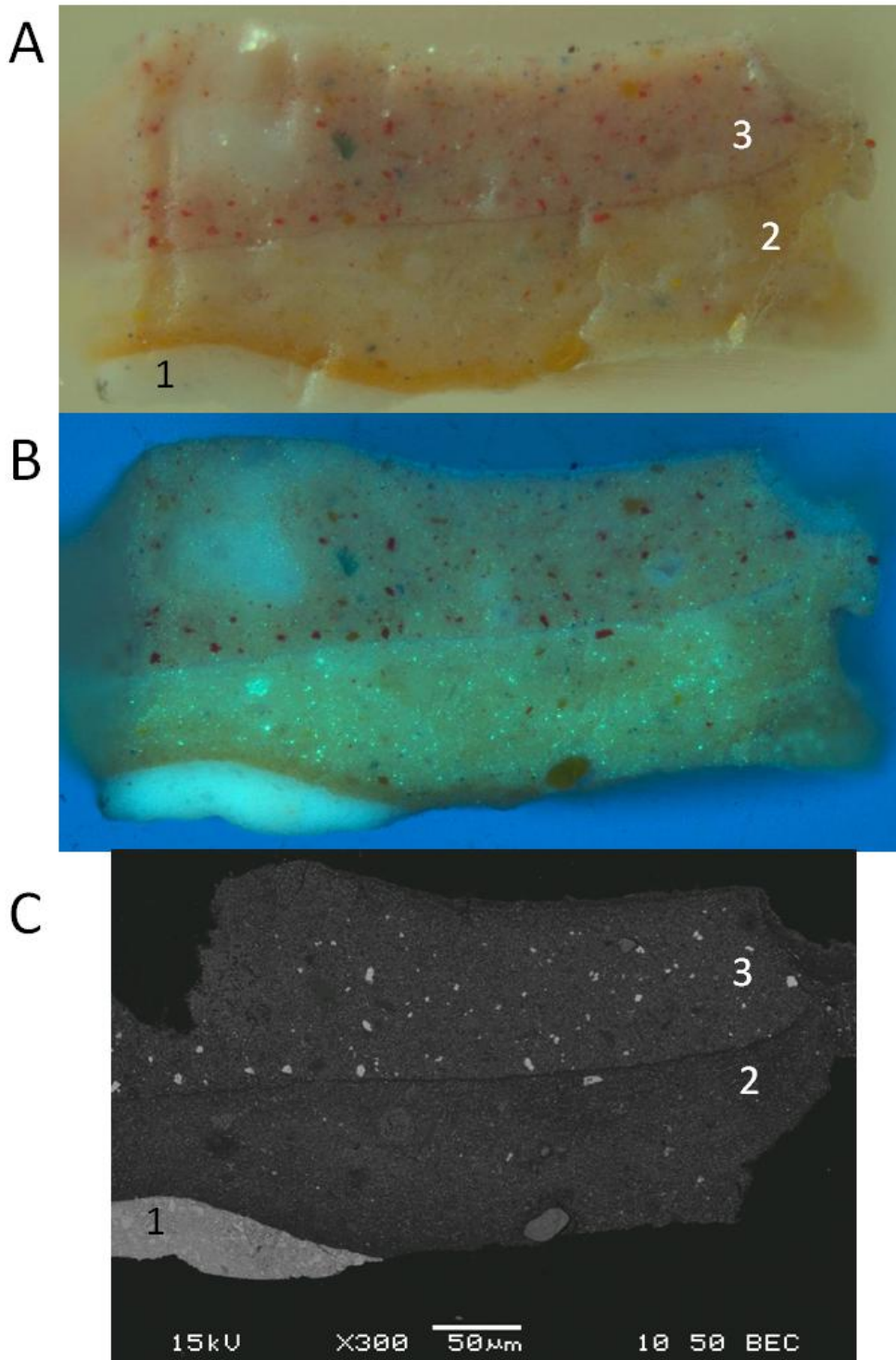
Figure 6.68 *Lamplight* **cross-section FL#3: (A) visible (B) UVF and (C) BSE images with (1) lead ground, (2) yellow and (3) pink paint layers**

The lead ground layer is consistent with FL#2, and two zinc oxide-based paint layers are present, both pigmented with varying proportions of vermilion and cadmium yellow to produce pink and yellow layers respectively. A UV-fluorescent sparkle is more evident in layer 2 than layer 3 despite the apparent similarity in base pigmentation. A dark band between the two layers is apparent in BSE images, similar to those observed in #2, however in this case the band is also visible in optical images, appearing UV-fluorescent and dark in visible light. Conversely, the reduced pigment density apparent in the most intense yellow band adjacent to the ground layer (1) has reduced UV-fluorescence. It is possible this intense yellow layer has been applied separately to the rest of layer 2, although an extremely large particle of cadmium sulfide at one end of the band does appear to belong to the bulk layer when viewed in UV (Figure 6.69). The low electron density halo surrounding the cadmium yellow particle in the BSE image echoes that assigned to zinc stearate/ palmitate in FRS#2.
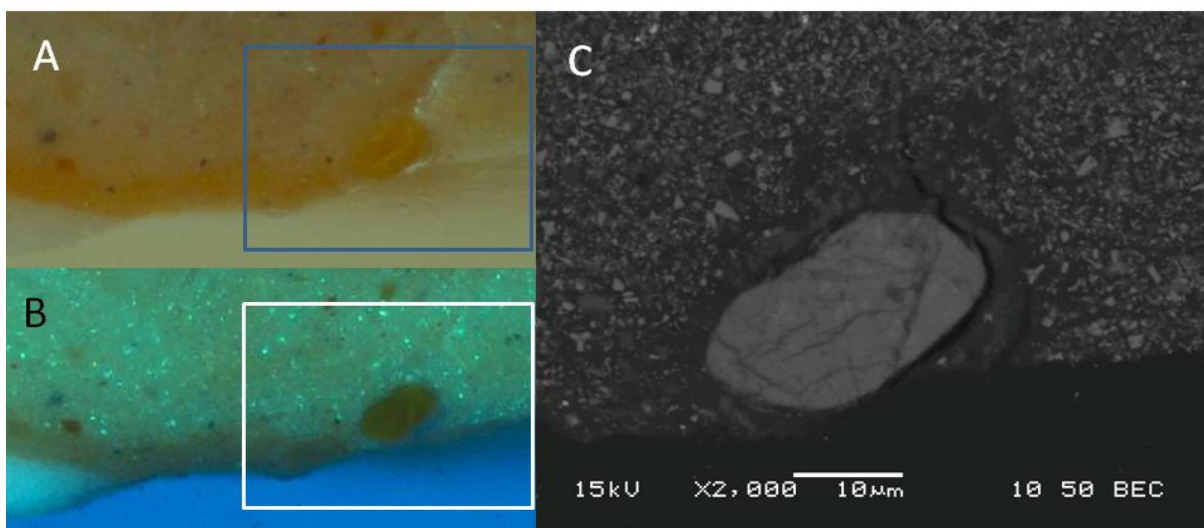
Figure 6.69 FL#3 detail showing large particle of cadmium yellow at the bottom of layer 2.

It is not clear if the intense yellow band adjacent to the ground is part of layer 2 or applied separately. The large yellow pigment particle appears to belong to the yellow band in the visible light image (A) but not in the UVF image (B) where it is surrounded by paint with fluorescence characteristic of the bulk layer above. The BSE image (C) reveals an absence of defined zinc oxide particles immediately surrounding the cadmium sulfide pigment

White circular masses similar to those evident in FL#2 are distributed through both layers (Figure 6.70). These primarily contain zinc, carbon and oxygen. This is also the case for a larger mass in layer 3 however one spectrum from this region additionally shows sulfur to be present in low concentration (Figure 6.71).
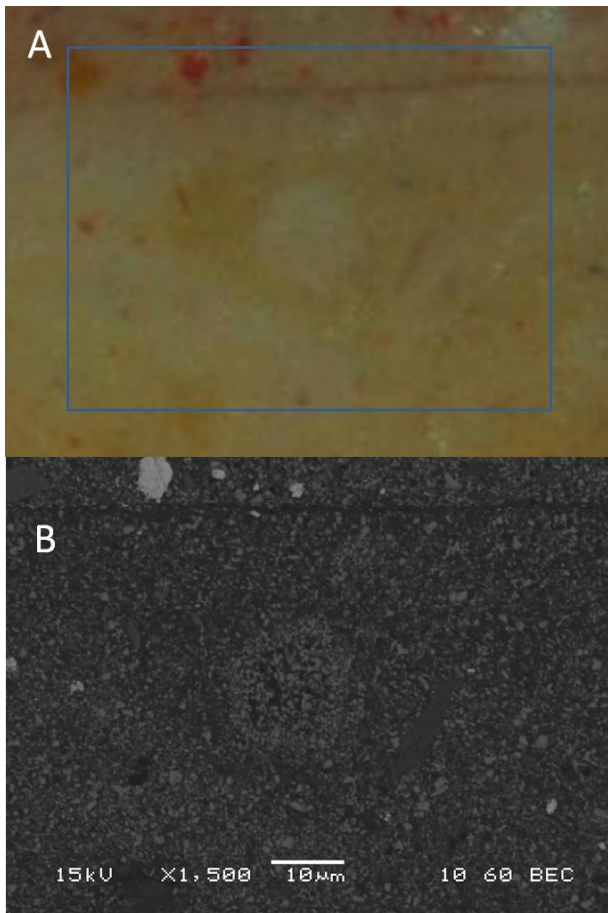
Figure 6.70 FL#3 optical image detail (A) and BSE image of boxed region (B) showing circular feature in layer 2 associated with opaque white/reduced yellow colouration.

Morphology is similar to features observed in FL#2
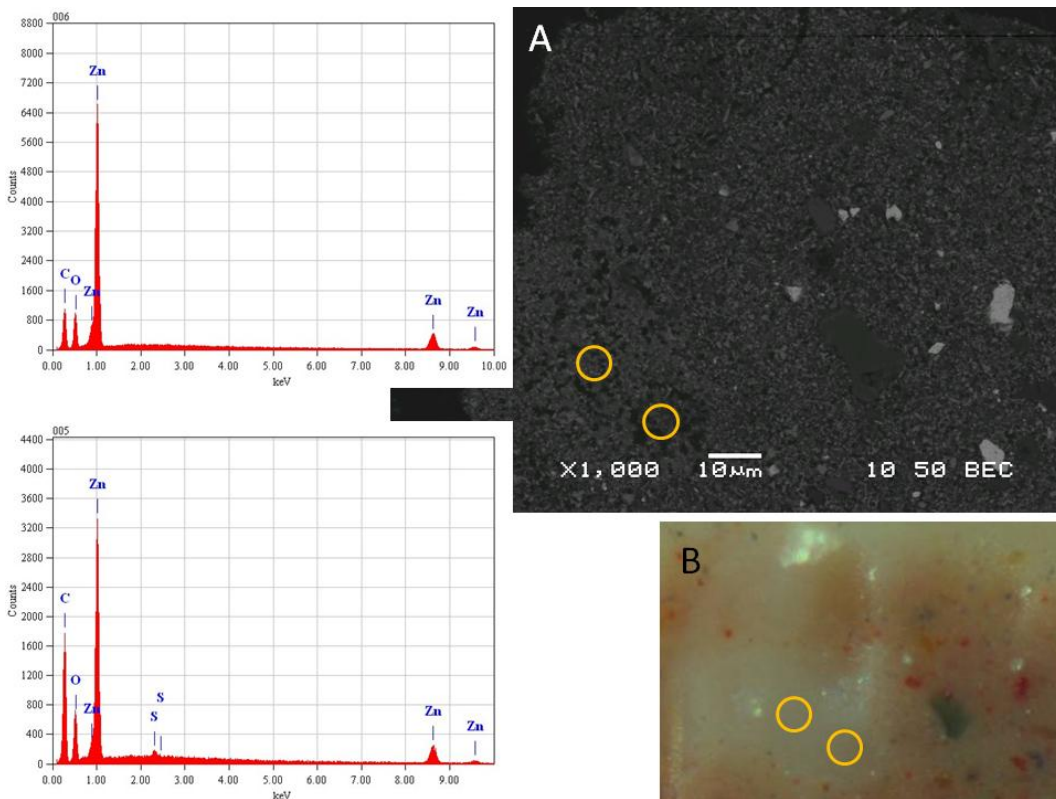
Figure 6.71 FL#2 BSE (A) and corresponding optical image detail (B) showing zinc-based aggregate in layer 3.

Spot EDX measurements from the points circled indicate the presence of zinc, carbon and oxygen. A trace of sulfur is additionally detected in the region of lowest electron density

Another circular feature in layer 2 with lower electron density in BSE and reduced opacity in optical images is based on the same three elements, however trace amounts of mercury, sulfur and magnesium are additionally detected (Figure 6.72). The mercury and sulfur are likely to derive from vermilion pigment, although vermilion is not prominent in this layer. Magnesium appears in many spot measurements from pigment particles in layer 3, often in association with potassium, aluminium and silicon. In this case the presence of magnesium silicate (talc) is a possible attribution. The low electron density feature in the BSE image has poorly defined pigment particles and similar morphology to the intense yellow band at the bottom of the layer.
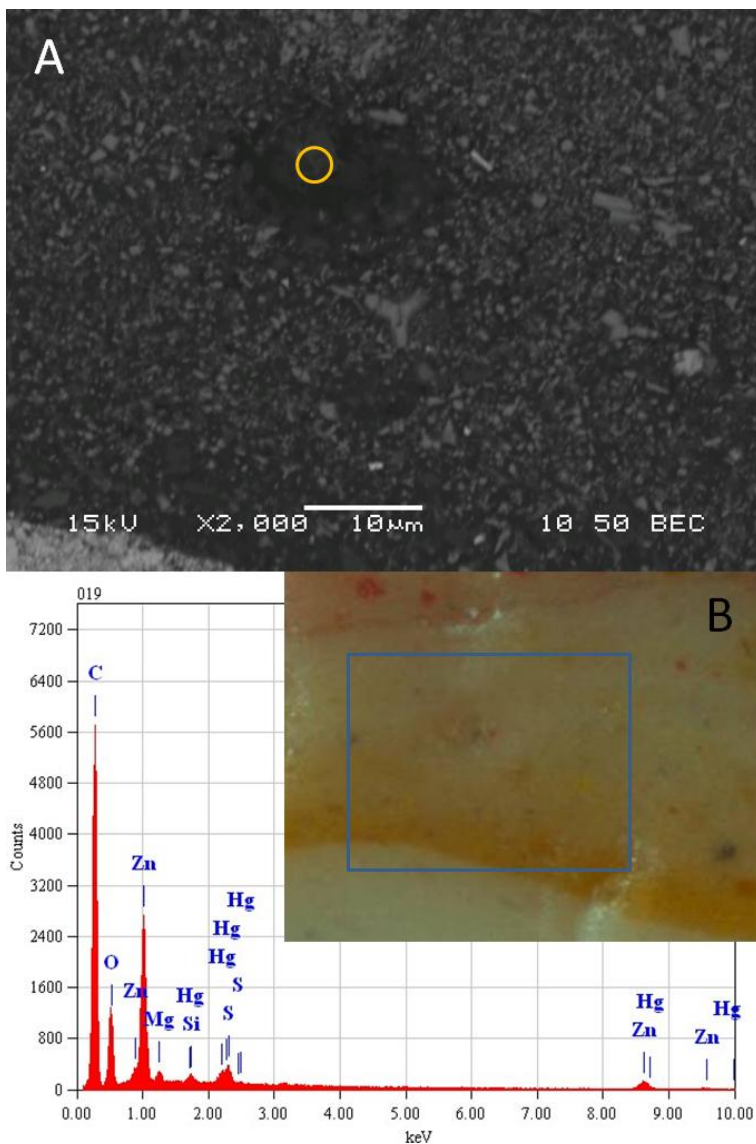
Figure 6.72 FL#3 BSE image detail (A) and optical image with box denoting corresponding detail (B).

Relatively large particles of twinned (tripod-shaped) acicular zinc oxide are evident among the more prevalent smaller, nodular particles comprising layer 2. An area of lower atomic brightness without defined pigmentation corresponds to a feature with reduced opacity in the optical image. The EDX spectrum obtained at the point circled shows carbon, zinc and oxygen to be the principle components

No spatially resolved FTIR data has been obtained for FL#3. Transmission spectra obtained from fragments prior to embedding reveal a strong ester carbonyl peak with broad carboxylate absorption and no discernible peak at 1540 cm^{-1}. There is a strong silicate contribution including kaolinite, evidence of bone/ivory black and some possible sulfate absorptions (Figure 6.73).
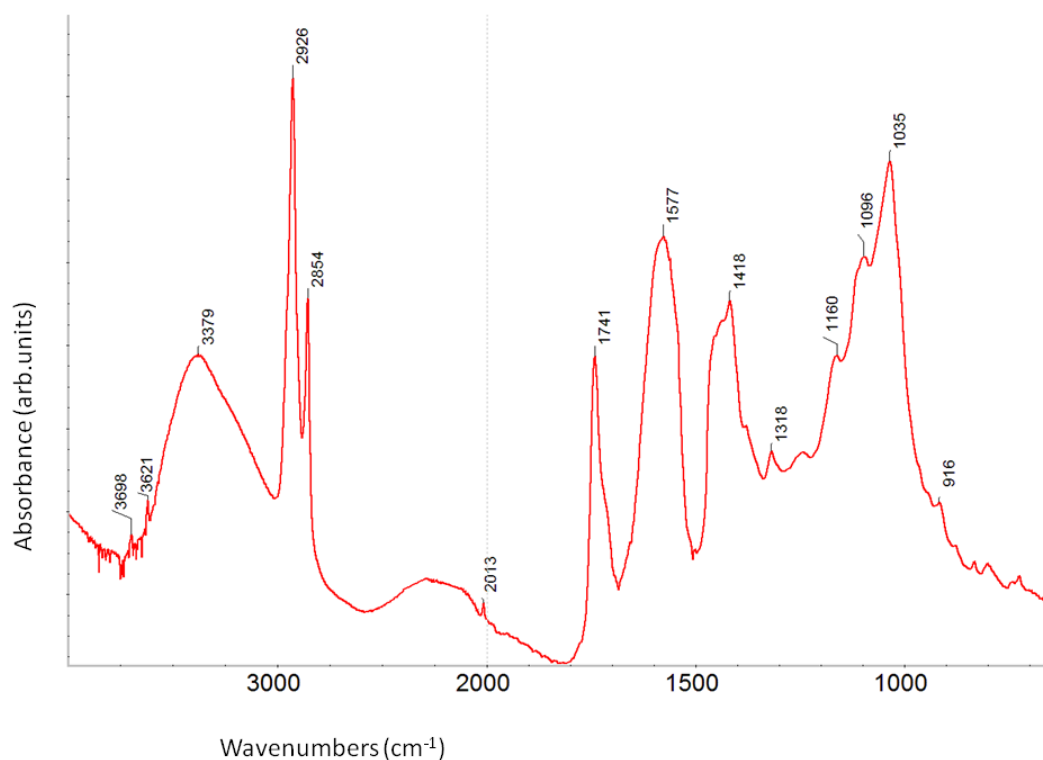
Figure 6.73 FL#3 transmission FTIR spectrum showing strong ester carbonyl and broad carboxylate absorption at (1741 and 1577 cm^{-1} respectively).

Pigment contributions include ivory/bone black (2013, *1455/1418*, 1035 cm^{-1}), overlapping silicate peaks including kaolinite (3698, 3621, *1116*, 1035, *1009*, 916 cm^{-1}) and possible sulfate absorption (1160, 1096 cm^{-1}). Italics indicate peaks underlying the dominant absorption bands

6.4 Discussion and conclusion

This study of Fox's paintings includes samples taken from formal studio works through to rapidly executed sketches produced outdoors. Most appear to have been completed in France and the majority date from around the end of first decade of the twentieth century. All are painted in oils on canvas but a range of ground preparations are represented including commercial lead and zinc-based oil grounds (lean and rich respectively) through to artist-applied preparatory layers of plaster and size. All are predominantly painted with zinc white-based layers with lead-based paint only apparent in *Rocks and sea* or occasionally as a minor addition. The provenance of most of the featured paintings includes a period in private ownership prior to entry to museum collections, and

they have variable environmental and conservation histories. A majority have been consolidated or structurally reinforced with wax or resin-based materials applied using heat, suggesting a propensity for cracking and instability.

Exposure environments where known also include some harsh conditions both at the time of production as in the case of *Rocks and sea* which was transported with Fox and his wife during their extended Mediterranean tour, through to *Lamplight* which was displayed in the passage of direct sun and radiant heat over many years. *Bathing hour* appears to have experienced the least intervention over time but has spent decades in the subtropical Brisbane environment following its acquisition by the Queensland Art Gallery in 1946 and prior to the provision of museum standard conditions in 1982. However, in comparison to the paintings of Kiệm (Chapter 5), the oil medium appears relatively intact based on the intense ester carbonyl peak present in many spectra, so soap formation does not appear to be attributable to extensive oil hydrolysis in the same way.

While some of Fox's paintings do include size-based ground layers, they do not (with the exception of *Autumn showers*) include thick, unpigmented interlayers with potential to act as moisture reservoirs as seen in Kiệm's paintings. *Autumn showers*, as the exception, does have a diminished oil ester carbonyl peak in association with relatively strong general carbonyl absorption characteristic of free fatty acids; in samples from other paintings this only occurs in localised instances. The medium-rich layer in *Autumn showers* includes strong carboxylate absorption characteristic of zinc stearate/palmitate and a closely related substance, possibly zinc oleate or a disordered arrangement of zinc stearate/palmitate, while distinctive IR spectra assigned to zinc lactate are also associated with adjacent paint. More localised examples of an acid/ester carbonyl doublet include small points within *Ploughing* FP#3 (distinctive accompanying spectral features have not been characterised) and circular UV-fluorescent regions in *Bathing hour* FBH#3 possibly associated with coloured pigment particles.

The influence of specific pigments, fillers or metal ions on the reactivity of zinc oxide and fatty acids remains of interest but inconclusive. Zinc stearate/palmitate levels are clearly higher in some paints than others, notably Prussian blue (this is also apparent in the paintings of Kiệm discussed in Chapter 5). This initially invites the conclusion stearates are present as a paint additive until the discrepancy in dates with respect to Fox's work and accepted dates of introduction of stearates as paint modifiers makes this an uncertain scenario. Prussian blue is a pigment with high oil absorbency. Eighteenth and nineteenth century treatises describe it as a colour which 'grows fat' during storage - prepared paints effectively coagulating within a week so as to become unusable (Carlyle 2001). This property suggests an inherent interaction between pigment and oil. A potential

link between iron-containing pigments and oil-hydrolysis has previously been hypothesised but had not translated to carboxylate formation (Mazzeo et al. 2008). Lower ester carbonyl absorption does appear to accompany the sharp zinc stearate peaks in both *Ploughing* and *Autumn showers* suggesting the possibility that the ferrocyanide pigment catalyses hydrolysis of the oil thereby increasing availability of fatty acids.

Localised zinc stearate formation is also evident adjacent to cadmium yellow particles, convincingly illustrated in *Rocks and sea* by means of SR-µFTIR integrated absorption intensity maps allowing spatially resolved correlation of data at high resolution, and similarly apparent in *Lamplight* (FL#3). *Rocks and sea* furthermore contains localised concentration of zinc stearate/palmitate in association with particles of gypsum, although without an apparent diminution of ester carbonyl absorption. Other observations include the association of trace elements with some of the more obvious white or translucent carboxylate-based masses present in samples from Fox's paintings. This includes tiny lead-based particles present within the large white mass dominating green paint in *Lamplight* FL#2, and traces of mercury, sulfur and magnesium detected within a small mass developing in FL#3 from the same painting, or chlorine in the case of *Bathing hour* BH#3. While interesting, the presence of trace elements is not a consistent finding across all paintings and no definitive patterns can be described across the range of results presented here.

More consistent among the paintings discussed in this study is the presence of distinctive, typically circular features evident in cross-sections based exclusively or predominantly on zinc, carbon and oxygen irrespective of the composition of the paint in which they occur, other than a common base of zinc oxide. The large white mass present in green paint in *Lamplight* FL#2 seems clearly to have emerged *in situ*, deforming the layer within which it is contained. Smaller features typically have reduced opacity and higher UV-fluorescence than the general paint, and lower electron and particle density in BSE images. In the case of *Ploughing*, the defined particles present in these regions have a relatively acicular shape while more numerous smaller, nodular particles of zinc oxide evident in adjacent paint appear to have preferentially reacted away. Circular features in samples also show a tendency to erode in the course of microtoming or polishing for cross-section preparation, indicating a hardness differential. Both observations are consistent with localised saponification of zinc oxide, producing softer regions within the aged paint.

Other areas in a majority of the cross-sections include relatively opaque white circular masses, often with reduced UV-fluorescence. BSE images show the presence of larger, higher atomic brightness particles within a dark amorphous region. The particles are larger than the general zinc oxide pigmentation, although again only zinc, carbon and oxygen are detected. The most dramatic

example occurs in *Ploughing* where large hexagonal rod and rock shaped crystals have formed a white mass within the blue paint, and to a lesser extent in white paint. An isolated crystal with very similar appearance is documented in *Autumn showers* at the centre of a circular feature, the morphology suggesting growth has drawn on ions from the surrounding area. This is supported by elemental mapping of comparable features in *Bathing hour* (BH#1) which shows high zinc concentration at the centre of an area with a zinc-depleted periphery. Basic zinc carbonate has been identified in association with the features in *Ploughing* together with high zinc stearate/palmitate concentration, and is implied in the other two instances. Although zinc carbonate has been proposed to mineralise at the centre of zinc carboxylate aggregates previously in paintings of Vincent van Gogh (Keune 2005), the spectra obtained on which conclusions were based are of low resolution. It was not possible to confirm the presence of zinc carbonate suspected to have mineralised at the centre of small (<10 μm) zinc carboxylate aggregates due to the limited spatial resolution of the conventional source FTIR instrument using reflectance imaging. SR-μFTIR has superior capabilities enabling improved correlation of spectra with optical and elemental data to assist interpretation of the microstructure. The assignment of basic zinc carbonate in *Ploughing* in the current study is more secure than previous case studies and adds detail to understanding of the relationship between zinc stearate/palmitate and basic zinc carbonate.

Basic zinc carbonate absorptions are additionally evident within the large white masses present in *Lamplight* and *Rocks and sea* (FRS#3) in association with strong carboxylate absorption although not specifically zinc stearate in the latter. In *Bathing hour* (FBH#4) a range of circular features with varying ratios of carbon to zinc appears to represent different stages of saponification and remineralisation accompanied by an increase or decrease in UV fluorescence respectively.

The heavily affected nature of sample FBH#4 from *Bathing hour* is interesting given it involves a single paint layer applied directly to the plaster and glue-based ground. Sample FBH#1 from the same painting similarly shows the paint layer closest to the ground to be more disrupted by circular masses than subsequent layers. Although the affected layers in the two samples are both pink in hue, one is pigmented with vermilion while the other contains more iron and cadmium-based particles. This suggests proximity to the gypsum-based ground may be more significant than pigment combination. Fox's 'plaster and size' canvas preparation is inherently more likely to absorb moisture than an oil-based priming, which may favour hydrolysis reactions in oil which has been absorbed from the paint above. Fatty acids released over time are then free to react with zinc oxide in adjacent paint, a scenario supported by elemental maps in FBH#1 showing reduced zinc counts in paint at the interface with the ground. *Bathing hour* is the only painting in this study which was not selected on the basis of obvious texture change at the painting surface, although similar processes

are clearly taking place within the paint. Exposure to humid summers over many years is likely to have been a factor in the condition of *Bathing hour*, although apparently benign conditions otherwise may have helped it avoid so far the development of more dramatic lumps and obvious surface deterioration.

It is interesting to compare cross-sections with the largest aggregates, while keeping in mind that the samples provided comprise only a microscopic fragment from the applicable painting and it is impossible to know how representative each may be of the structure as a whole. The composition of large UV-fluorescent masses within *Rocks and sea* and *Lamplight*, while both dominated by zinc, carbon and oxygen, produce different FTIR spectra. Morphology apparent in BSE images also appears distinct at first glance, however the mass in *Rocks and sea* FRS#3 has been imaged at substantially higher magnification revealing clusters of tiny, needle-shaped crystals which are not resolved at the lower magnification used to acquire images of *Lamplight* FL#2. The distinction between masses and adjacent paint is also more dramatic in *Rocks and sea* as a consequence of the presence of lead in intact paint providing atomic contrast not found in *Lamplight* where all layers are based on zinc oxide. It is, however, the case that the mass in *Lamplight* FL#2 produces FTIR spectra with strong basic zinc carbonate and zinc stearate/palmitate absorptions which are not evident in spectra obtained from the comparable feature in *Rocks and sea*. Given similar elemental composition, the different carboxylate structures suggest fatty acid profiles vary between the two paintings. This may reflect differences in the original paint mediums but also possibly different environmental histories favouring distinct reaction pathways.

Another interesting and recurrent finding in Fox's paintings is the apparent incidence of zinc lactate. Characteristic SR-µFTIR spectra were obtained from white features in *Autumn showers*, *Ploughing* and *Bathing hour*, while a different but possibly similarly-structured salt is suggested in spectra from *Rocks and sea*. Although not specifically identified in the current study, its presence also cannot be ruled out in *Lamplight* given the absence of high resolution synchrotron data for this painting. Zinc lactate has only recently been linked to deterioration of zinc oxide-based paints in the form of a disfiguring surface deposit (Helwig et al. 2014) and there are no known incidences of its presence within paint layers as reported here and in the preceding chapter. The possible sources of lactic acid are unclear but all point to the complex composition and multiple potential interactions which may occur within individual paintings.

6.5   References

Barman S, Vasudevan S (2006a) Contrasting Melting Behavior of Zinc Stearate and Zinc Oleate. *The Journal of Physical Chemistry B* 110 (2):651-654. doi:10.1021/jp055814m

Carlyle L (2001) *The artist's assistant: oil painting instruction manuals and handbooks in Britain 1800-1900 with reference to selected eighteenth-century sources*. Archetype Publications, London

Ferreira ESB, Boon JJ, Stampanoni M, Marone F (2011) Study of the mechanism of formation of calcium soaps in an early 20th-century easel painting with correlative 2D and 3D microscopy. In: Bridgland J, Antomarchi C (eds) *Preprints of the ICOM Committee for Conservation 16th Triennial Conference*, Lisbon, 2011. ICOM-CC p1604

Goddard A (2011) *Art, love and life: Ethel Carrick and E Phillips Fox*. Queensland Art Gallery/Gallery of Modern Art, Brisbane

Helwig K, Poulin J, Corbeil M-C, Moffatt E, Duguay D (2014) Conservation issues in several 20th-century Canadian oil paintings: the role of zinc carboxylate reaction products. In: van den Berg KJ, Burnstock A, de Tagle M et al. (eds) *Issues in Contemporary Oil Paint*. Springer International Publishing, Switzerland, p Chapter 11. In press. doi:10.1007/978-3-319-10100-2__11

Keune K (2005) *Binding medium, pigments and metal soaps characterised and localised in paint cross-sections*. PhD thesis, University of Amsterdam, Amsterdam

Keune K, Boevé-Jones G (2014) It's surreal: zinc-oxide degradation and misperceptions in Salvador Dali's *Couple with clouds in their heads*, 1936. In: van den Berg JDJ, Burnstock A, de Tagle M et al. (eds) *Issues in contemporary oil paint*. Springer International Publishing, Switzerland, p Chapter 19. In press. doi:10.1007/978-3-319-10100-2__19

Maines CA, Rogala D, Lake S, Mecklenburg MF (2011) Deterioration in Abstract Expressionist paintings: analysis of zinc oxide paint layers in works from the collection of the Hirshhorn Museum and Sculpture Garden, Smithsonian Institution. *Materials Research Society Proceedings* 1319:275-284. doi:10.1557/opl.2011.733

Mazzeo R, Prati S, Quaranta M, Joseph E, Kendix E, Galeotti M (2008) Attenuated total reflection micro FTIR characterisation of pigment-binder interaction in reconstructed paint films. *Anal Bioanal Chem* 392 (1-2):65-76. doi:10.1007/s00216-008-2126-5

Mesubi MA (1982) An infrared study of zinc, cadmium, and lead salts of some fatty acids. *J Mol Struct* 81:61-71

Nunn C (2008) The making of *Lamplight* (c. 1911): a preliminary study of the methods and materials of Emanuel Phillips Fox. *AICCM Bulletin* 31:15-27

Nunn C (2012) *The matt aesthetic and the art of E. Phillips Fox*. MA thesis, University of Melbourne, Melbourne

Robinet L, Corbeil MC (2003) The characterization of metal soaps. *Stud Conserv* 48 (1):23-40

Rogala D, Lake S, Maines C, Mecklenburg M (2010) Condition problems related to zinc oxide underlayers: examination of selected Abstract Expressionist paintings from the collection of the Hirschhorn Museum and Sculpture Garden, Smithsonian Institution. *Journal of the American Institute for Conservation* 49 (2):96-113

Souza LAC, Derrick MR (1995) The use of FT-IR spectrometry for the identification and characterisation of gesso-glue grounds in wooden polychromed sculptures and panel paintings. *Materials Research Society Symposium Proceedings* 352:573-578

Tumosa CS (2001) A brief history of aluminum stearate as a component of paint. *WAAC Newsletter* 23 (3)

7   Conclusion

This thesis combines results from historical research of technological developments in zinc oxide pigment and paint production, simple experimental models, naturally aged reference paints and samples from actual paintings and contributes important new detail to the continuing study of zinc soap formation in paintings.

Developments and variety in zinc oxide pigment production and paint formulation mean that a range of properties can be expected in oil-based paints, with differing susceptibilities to saponification and associated deterioration. Correlation of BSE images, elemental analysis and synchrotron FTIR mapping of paint cross-sections provide compelling insight into zinc oxide-centred deterioration and zinc carboxylate formation. Zinc oxide particles in mixed pigment paints preferentially react ahead of lithopone, lead white and a range of coloured pigments. Paint layers with a mix of zinc oxide particle sizes indicate smaller, typically nodular particles react before larger or acicular particles. Formation of zinc stearate at the surface of zinc oxide particles in stagnant solvent models appears to morphologically replicate pigment particles surrounded by poorly defined, low atomic density masses in painting cross-sections. Early-stage *in situ* saponification is indicated by zinc-based regions with poorly defined boundaries, relatively low pigment density and reduced atomic brightness within BSE images. These characteristics may assist differentiation from stearates present as original components.

Fatty acid profiles are critical and different oils demonstrate varying reactivity. Reference paint films of comparable film age and pigment composition indicate linseed oil is more reactive than safflower. Pronounced fatty acid release is evident in soybean oil-based paints, translating to higher zinc stearate/palmitate concentrations than comparable films based on linseed or safflower oils, and may additionally lead to surface efflorescence. However the presence of additives such as aluminium stearate appears more significant for zinc stearate formation than pigment combinations or oil types. Aluminium stearate increases concentration and availability of stearic acid typically released through hydrolysis. Hydroxyl groups replace stearate chains to form relatively polar molecules of aluminium mono- or di-stearate or aluminium hydroxide. In a paint film, increasing concentration of zinc stearate encourages phase separation. Progressive reorganisation and aggregation of similar soap molecules is energetically favourable for C_{16} and C_{18} chain saturated zinc soaps as film chemistry increases in polarity with age. Heterogeneous nucleation and crystal growth may result, ultimately manifesting as lumps which disrupt the image surface. Basic zinc carbonate mineralisation within carboxylate aggregates is observed in the paintings of E Phillips Fox, while carbonate and sulfate functionality occurs in association with complex zinc carboxylates in FTIR spectra from Kiệm's paintings. Zinc lactate is characterised in samples from paintings by both profiled artists.

In some paintings zinc soap concentrations have developed at the interface between paint layers, particularly adjacent to layers with a source of fatty acids or where hygroscopicity may favour oil hydrolysis. Environmental conditions may accelerate hydrolysis or favour release of C_{16}/C_{18} fatty acids over C_9 diacids. Extreme hydrolysis is indicated in Kiệm's paintings, although some are little more than three decades old, and their condition will have been exacerbated by exposure to warm, humid conditions. Equally, more sudden equilibrium shifts arising from fluctuating environmental conditions or applied treatments may encourage mobility of zinc stearate. These influences may induce carboxylates to detach from the pigment surface, exposing further oxide to potential reaction and enabling the process of zinc stearate formation and zinc oxide dissolution to continue.

The complexity, enormous variety and long timescales of potential interactions occurring within unique paintings and even within reference paint films of relatively simple composition all underline that this research cannot possibly hope to have answered all outstanding questions surrounding the phenomenon of zinc carboxylate formation in paintings. It does, however, identify trends and contributes important new detail to assist interpretation of associated deterioration. Work presented in this thesis will support continuing study of pigment-medium interactions in paintings and the implications for their conservation.

7.1   Further research

Smithsonian Museum Conservation Institute reference paints collection: There is significant scope to continue investigation of paints obtained from SMCI. A relatively generous amount of each paint is available, enabling a broader range of analytical techniques to be applied than is possible in unique samples from paintings. Fatty acid analysis to support the FTIR and elemental analysis reported to date would strengthen interpretation. High resolution transmission and scanning electron microscopy methods offer potential for detailed examination of the environment around the reacting zinc oxide particles and the transition to zinc carboxylate.

Model system: The model system applied in this thesis could be readily reproduced to compare reaction rates of a wider range of well-characterised zinc oxide samples. At its simplest this may involve continuation of measurements of existing experiments involving Kremer artist pigment for longer term correlation with the reactivity of MKN 30 nm grade zinc oxide, but zinc oxide products with more subtle differences could equally be investigated, for example variations in amounts of adsorbed CO_2 or H_2O. The solvent model additionally lends itself to expansion to consider other variables including but not limited to the simultaneous presence of more than one acid type or more

than one type of metal ion. Longer term projects might include replicating model experiments in a triglyceride medium e.g. glyceryl tripalmitate, where the potential catalysing effect of different zinc oxide products or pigment combinations such as Prussian blue could be examined.

Zinc lactate: The recurring incidence of zinc lactate in paintings by Kiệm but also intriguingly in the very different Fox paintings invites investigation into possible sources of lactic acid. Unlike the only other known reported incidence of zinc lactate proposed to relate to reaction of the paint to pollutants, the distribution of zinc lactate throughout some of the case-studied paintings suggests the source may be the paint medium itself.

Layered basic zinc salts: Further work is required to confirm the existence and clarify possible structures of multifunctional zinc complexes within large aggregates, and to consider the feasibility that gradual changes occurring in paint films over time could account for this mechanism of formation.

Magnesium stearate: Investigation of magnesium stearate as a known paint additive in respected artist's paint formulations could be investigated in light of findings concerning the influence of aluminium stearate on zinc stearate formation.

Calcium ions: Research into the possible role of calcium ions from chalk or in the form of added driers as stabilisers through competition for formation of fatty acid complexes.

8 References

Ainsworth MW (2005) From Connoisseurship to Technical Art History: The Evolution of the Interdisciplinary Study of Art. *The Getty Conservation Institute Newsletter* 20 (1):4-10

Akanni MS, Okoh EK, Burrows HD, Ellis HA (1992) The thermal behaviour of divalent and higher valent metal soaps: a review. *Thermochim Acta* 208:1-41

Alpbaz M, Bilgesu O, Tutkum O (1988) The measurement of interfacial tension by drop-weight method. *Commun Fac Sci Univ Ank Serie B* 34:103-112

Barba C, san Andrés M, Peinado J, Báez MI, Baldonedo JL (1995) A note on the characterization of paint layers by transmission electron microscopy. *Stud Conserv* 40:194-200

Barman S, Vasudevan S (2006a) Contrasting Melting Behavior of Zinc Stearate and Zinc Oleate. *The Journal of Physical Chemistry B* 110 (2):651-654. doi:10.1021/jp055814m

Barman S, Vasudevan S (2006b) Melting of Saturated Fatty Acid Zinc Soaps. *The Journal of Physical Chemistry B* 110 (45):22407-22414. doi:10.1021/jp064306p

Barman S, Vasudevan S (2007) Mixed Saturated-Unsaturated Alkyl-Chain Assemblies: Solid Solutions of Zinc Stearate and Zinc Oleate. *The Journal of Physical Chemistry B* 111 (19):5212-5217. doi:10.1021/jp068675x

Barnett CE (1949) Physics and Chemistry of Pigments. *Industrial & Engineering Chemistry* 41 (2):272-279. doi:10.1021/ie50470a015

Beakes HL (1928) Settling of Pigments in House Paints. *Industrial & Engineering Chemistry* 20 (7):732-734. doi:10.1021/ie50223a020

Bell SH (1970) Zinc oxide hazing. *Paint and Varnish Production* April 1970:55-60

Boitelle R, van den Berg KJ (2005) A technical examination of Odilon Redon's paintings from the Bonger Collection, Van Gogh Museum. *ArtMatters: Netherlands technical studies in art* 3:66-81

Bomford D, Kirby J, Leighton J, Roy A (1990) *Art in the making: Impressionism*. National Gallery Publications Limited, London

Bonotto S, Bonner EF (1968) Effect of Ion Valency on the Bulk Physical Properties of Salts of Ethylene-Acrylic Acid Copolymers. *Macromolecules* 1 (6):510-515. doi:10.1021/ma60006a011

Boon J, Keune K, Learner T (2002a) Identification of pigments and media from a paint cross-section by direct mass spectrometric and microspectrometric techniques In: Vontobel R (ed) *Preprints of the ICOM Committee for Conservation 13th Triennial Meeting*, Rio de Janeiro, 2002. James and James, London, pp 223-230

Boon J, Keune K, Zucker J (2005) Imaging analytical studies of lead soaps aggregating in preprimed canvas used by the Hudson River School painter F.E. Church. *Microsc Microanal* 11 (Supplement 2):444-445

Boon J, van der Weerd K, Keune K, Noble P, Wadum J (2002b) Mechanical and chemical changes in Old Master paintings: dissolution, metal soap formation and remineralization processes in lead pigmented ground/intermediate paint layers of 17th century paintings. In: Vontobel R (ed) *Preprints*

of the ICOM Committee for Conservation 13th Triennial Meeting, Rio de Janeiro, 2002. James and James, London, pp 401-406

Boon JJ, Ferreira ESB (eds) (2006) *Reporting highlights of the De Mayerne Program, research program on molecular studies in conservation and technical studies in art history* NWO, The Hague

Boon JJ, Hoogland F, Keune K (2007) Chemical processes in aged oil paints affecting metal soap migration and aggregation. In: Mar Parkin H (ed) *AIC Paintings Specialty Group Postprints*, Providence, Rhode Island, 16-19 June 2006. AIC, pp 16-23

Boon JJ, Peulvé SL, van den Brink OF, Duursma MC, Rainford D (1997) Molecular aspects of mobile and stationary phases in ageing tempera and oil paint films. In: Bakkenist T, Hoppenbrouwers R, Dubois H (eds) *Early Italian paintings: techniques and analysis, Symposium*, Maastricht, 1996. Limburg Conservation Institute, pp 35-56

Boon JJ, van der Horst J (2008) Remarkably improved spatial resolution in SEM images of paint cross-sections after argon ion polishing. In: Townsend J, Doherty T, Heydenreich G (eds) *Preparation for painting: the artist's choice and its consequences*, London, 2007. Archetype Books, pp 42-49

Brown HE (1957) *Zinc oxide rediscovered*. New Jersey Zinc Company, New York

Browne FL (1955) Swelling of paint films in water III: Absorption and volumetric swelling of bound and free films from air of different relative humidities. *Forest Products Journal* 5:92-96

Browne FL (1956) Swelling of paint films in water VIII: Swelling of linseed oil paints in water and organic liquids. *Forest Products Journal* 6:312-318

Burke J (1984) Solubility parameters: theory and application. *The AIC Book and Paper Group Annual* 3:13-58

Burnstock A, van den Berg KJ, de Groot S, Wijnberg L (2007) An investigation of water sensitive oil paints in twentieth century paintings. In: Learner T, Smithen P, Krueger JW, Schilling MR (eds) *Modern Paints Uncovered*, Tate Modern, London, 16-19 May 2006. The Getty Conservation Institute, pp 177-188

Carlyle L (2001) *The artist's assistant: oil painting instruction manuals and handbooks in Britain 1800-1900 with reference to selected eighteenth-century sources*. Archetype Publications, London

Carlyle L, Witlox M (2005) Historically accurate reconstructions of artists' oil painting materials. In: Clarke M, Townsend J, Stijnman A (eds) *Art of the past: sources and reconstructions. Proceedings of the first symposium of the Art Technolgical Source Research study group*, Amsterdam, 2004. Archteype Publications Ltd, London, pp 53-59

Casadio F, Xie S, Rukes S, Myers B, Gray K, Warta R, Fiedler I (2011) Electron energy loss spectroscopy elucidates the elusive darkening of zinc potassium chromate in Georges Seurat's 'A Sunday on La Grande Jatte-1884'. *Anal Bioanal Chem* 399 (9):2909-2920. doi:10.1007/s00216-010-4264-9

Church AH (1915) *The chemistry of paints and painting*. Fourth edition, revised and enlarged edn. Seeley, Service & Co. Limited, London

Clarke M, Boon JJ (eds) (2003) *Molart: a multidisciplinary NWO Prioriteit project on molecular aspects on ageing in painted works of art. Final report and highlights 1995-2002*. FOM Institute AMOLF, Amsterdam

Clegg W, Little IR, Straughan BP (1988) Zinc carboxylate complexes: structural characterization of the mixed-metal linear trinuclear complexes $MZn_2(crot)_6(base)_2$ (M = Mn, Co, Ni, Zn, Cd, Mg, Ca, Sr; $crot^-$ = crotonate(1-); base = quinoline, 6-methylquinoline). *Inorg Chem* 27 (11):1916-1923. doi:10.1021/ic00284a020

Cocks EJ, Walters B (1968) *A history of the zinc smelting industry in Britain*. George G. Harrap & Co. Ltd., London

Coe RH, Mysels KJ, Smith GH (1948) Bound and free acid in aluminum soap prepared by precipitation. *Journal of Colloid Science* 3 (4):293-302. doi:10.1016/0095-8522(48)90016-6

Colombini A, Grauby O (2011) Morpholgy and chemical investigations of zinc soaps by scanning electron microscopy and transmission electron microscopy: case study of Picasso paintings. In: *From Can to Canvas. Early uses of housepaint by Picasso and his contemporaries in the first half of the 20th century (poster session)*, Marseille and Antibes, 25-27 May 2011.

Considine B (2005) Recent initiatives in technical art history. *The Getty Conservation Institute Newsletter* 20 (1):21-24

Corbeil MC, Helwig K, Poulin J (2011) *Jean Paul Riopelle: the artist's materials*. Getty Conservation Institute, Los Angeles

Corbeil MC, Robinet L (2002) X-ray powder diffraction data for selected metal soaps. *Powder Diffr* 17 (1):52-60. doi:10.1154/1.1431950

Corkery RW (1998) *Artificial biomineralisation and metallic soaps*. PhD thesis, Australian National University, Canberra

Corkery RW (2004) A variation on Luzzati's soap phases. Room temperature thermotropic liquid crystals. *PCCP* 6:1534-1546. doi:10.1039/B315595C

Corkery RW (2008) Metal organic framework (MOF) liquid crystals. 1D, 2D and 3D ionic coordination polymer structures in the thermotropic mesophases of metal soaps, including alkaline earth, transition metal and lanthanide soaps. *Current Opinion in Colloid and Interface Science* 13:288-302

Corkery RW, Hyde ST (1996) On the Swelling of Amphiphiles in Water. *Langmuir* 12 (23):5528-5529. doi:10.1021/la960794o

Cotte M, Checroun E, Mazel V, Sole VA, Richardin P, Taniguchi Y, Walter P, Susini J (2009) Combination of FTIR and X-rays synchrotron-based micro-imaging techniques for the study of ancient paintings. A practical point of view. *e-Preservation Science* 6:1-9

Cotte M, Checroun E, Susini J, Dumas P, Tchoreloff P, Besnard M, Walter P (2006) Kinetics of oil saponification by lead salts in ancient preparations of pharmaceutical lead plasters and painting lead mediums. *Talanta* 70:1136-1142. doi:10.1016/j.talanta.2006.03.007

Cotte M, Checroun E, Susini J, Walter P (2007) Micro-analytical study of interactions between oil and lead compounds in paintings. *Appl Phys A* 89:841-848. doi:10.1007/s00339-007-4213-4

Crook J, Learner T (2000) *The impact of modern paints*. Tate Gallery Publishing, London

Currie C, Smith J (1994) 'The Biglin brothers turning the stake boat' by Thomas Eakins: a technical study reveals surprising techniques. In: Real WA (ed) *AIC Paintings Specialty Group Postprints*, Nashville Tennessee, 10 June 1994. AIC, pp 18-23

Derrick M, Douza L, Kieslich T, Florsheim H, Stulik D (1994a) Embedding paint cross-section samples in polyester resins: problems and solutions *Journal of the American Institute for Conservation* 33:227-245

Derrick M, Stulik D, Landry J (1999) *Infrared spectroscopy in conservation science* The Getty Conservation Institute Los Angeles

Derrick MR, Doehne EF, Parker AE, Stulik DC (1994b) Some new analytical techniques for use in conservation. *Journal of the American Institute for Conservation* 33 (2):171-184

Diebold MP, Bettler CR, Mukoda DM (2003) Mechanism of TiO2/ZnO instability in latex paints. *J Coat Technol* 75 (942):29-36

Dik J, Hermens E, Peschar R, Schenk H (2005) Early production recipes for lead antimonate yellow in Italian art. *Archaeometry* 47 (3):593-607. doi:10.1111/j.1475-4754.2005.00221.x

Dredge P (1996) John Russell: a study of his Impressionist technique. In: Wallace S-A, Macnaughtan J, Parvey J (eds) *The articulate surface: dialogues on paintings between conservators, curators and art historians*, Canberra, 1-3 May 1992. The Humanities Research Centre, ANU and National Gallery of Australia, pp 265-277

Dredge P (2012) A history of Australian housepaint technology from the 1920s to the 1950s, with reference to its use by Australian artists, particularly Sidney Nolan. *AICCM Bulletin* 33:53-61

Dredge P, Schilling MR, Gautier G, Mazurek J, Learner T, Wuhrer R (2013) Lifting the Lids Off Ripolin: A Collection of Paint from Sidney Nolan's Studio. *Journal of the American Institute for Conservation* 52 (4):213-226

Ebert B (2008) *Volume II: A scientific investigation into the degradation processes of zinc-based paints together with art historical research* MA thesis, Northumbria University, Newcastle

Ebert B (2011a) *Examination report: Nguyễn Trọng Kiệm, Children playing at the beach, W06.8.61.*

Ebert B (2011b) *Examination report: Nguyễn Trọng Kiệm, Hàng Giấy, W06.8.59.*

Ebert B (2011c) *Examination report: Nguyễn Trọng Kiệm, Staring out game, W06.3.3.*

Ebert B, MacMillan Armstrong S, Singer B, Grimaldi N (2011) Analysis and conservation treatment of Vietnamese paintings. In: Bridgland J, Antomarchi C (eds) *Preprints of the ICOM Committee for Conservation 16th Triennial Meeting*, Lisbon, 2011. ICOM-CC, p 1305

Elm AC (1957) Reevaluation of the function of pigments in paints. *Official Digest* (April):351-385

Erhardt D, Tumosa CS, Mecklenburg MF (2005) Long-term chemical and physical processes in oil paint films. *Stud Conserv* 50 (2):143-150

Farquharson Boan R (1924) *The manufacture of mixed paints*. The Australasian Decorator and Painter, vol January 1. J.E. Bishop, Melbourne

Faubel W, Simon R, Heissler S, Friedrich F, Weidler PG, Becker H, Schmidt W (2011) Protrusions in a painting by Max Beckmann examined with confocal μ-XRF. *J Anal At Spectrom* 26 (5). doi:10.1039/C0JA00178C

Faucett PH (1943) Conserving oils in paints. *Paint, oil and chemical review* 105 (8):9-10

Feller RL, Stolow N, Jones E (1971) *On picture varnishes and their solvents*. The Press of Case Western Reserve University, Cleveland

Ferreira ESB, Boon JJ, Stampanoni M, Marone F (2011) Study of the mechanism of formation of calcium soaps in an early 20th-century easel painting with correlative 2D and 3D microscopy. In: Bridgland J, Antomarchi C (eds) *Preprints of the ICOM Committee for Conservation 16th Triennial Conference*, Lisbon, 2011. ICOM-CC p1604

Finnie W, Grant R, McColm K (1936) The adsorption of metallic driers by pigments. *American Paint Journal* 21 (8):7-10

Gardner HA (1917) *Paint researches and their practical application*. Press of Judd and Detweiler, Inc., Washington D.C.

Garti N, Wellner E, Sarig S (1980) Stearic acid polymorphs in correlation with crystallization conditions and solvents. *Kristall und Technik* 15 (11):1303-1310. doi:10.1002/crat.19800151112

Gautier G, Bezur A, Muir K, Casadio F, Fiedler I (2009) Chemical Fingerprinting of Ready-Mixed House Paints of Relevance to Artistic Production in the First Half of the Twentieth Century. Part I: Inorganic and Organic Pigments. *Appl Spectrosc* 63 (6):597-603. doi:10.1366/000370209788559584

Goddard A (2011) *Art, love and life: Ethel Carrick and E Phillips Fox*. Queensland Art Gallery/Gallery of Modern Art, Brisbane

Goienaga N, Arrieta N, Carrero JA, Olivares M, Sarmiento A, Martinez-Arkarazo I, Fernández LA, Madariaga JM (2011) Micro-Raman spectroscopic identification of natural mineral phases and their weathering products inside an abandoned zinc/lead mine. *Spectrochimica Acta Part A: Molecular and Biomolecular Spectroscopy* 80 (1):66-74. doi:http://dx.doi.org/10.1016/j.saa.2011.01.032

Gönen M, Balköse D, İnal F, Ülkü S (2005) Zinc Stearate Production by Precipitation and Fusion Processes. *Industrial & Engineering Chemistry Research* 44 (6):1627-1633. doi:10.1021/ie049398o

Goodall RA, Hall J, Sharer RJ, Traxler L, Rintoul L, Fredericks PM (2008) Micro-Attenuated Total Reflection Spectral Imaging in Archaeology: Application to Maya Paint and Plaster Wall Decorations. *Appl Spectrosc* 62 (1):10-16

Graedel TE (1989) Corrosion Mechanisms for Zinc Exposed to the Atmosphere. *J Electrochem Soc* 136 (4):193C-203C. doi:10.1149/1.2096868

Gray VR, Alexander AE (1948) Studies on Aluminum Soaps. II. The Composition, Structure, and Gelling Properties of Aluminum Soaps. *The Journal of Physical and Colloid Chemistry* 53 (1):23-38. doi:10.1021/j150466a003

Greathouse JA, Johnson KL, Greenwell HC (2014) Interaction of natural organic matter with layered minerals: recent developments in computational methods at the nanoscale. *Minerals* 4 (2):519-540. doi:10.3390/min4020519

H.W. (1925) *Notes on the durability and manipulation of zinc paints*. The decorator and painter for Australia and New Zealand, vol 1 October. Bishop Bros., Sydney

Hackney S, Ridge J, Townsend JH (2002) Pre-Raphaelite technique and its consequences. In: Vontobel R (ed) *Preprints of the ICOM-CC 13th Triennial Meeting*, Rio de Janeiro, 2002. James and James, London, pp 426-431

Hackney S, Townsend JH, Ridge J (2004) Pre-Raphaelite methods and materials. In: Townsend JH, Ridge J, Hackney S (eds) *Pre-Raphaelite painting techniques 1848-1856*. Tate Publishing, London, pp 51-75

Hancock R, Leeves N, Nicks P (1989) Studies in autoxidation. I: The volatile by-products resulting from the autoxidation of unsaturated fatty acid methyl esters. *Prog Org Coat* 17 (3):321-336

Hansen CM, Klauss HC (1971) Mechanism of paint seeding. *Industrial and Engineering Chemistry Product Research and Development* 10 (2):189-192

Harley RD (1970) *Artists' pigments c.1600-1835*. Butterworths and IIC, London

Haswell R, Zeile U, Mensch K (2008) Van Gogh's painting grounds: an examination of barium sulphate extender using analytical electron microscopy – SEM/FIB/TEM/EDX. *Microchimica Acta* 161 (3):363-369

Hay D (2012) *XRD Microdiffraction Study of Paint Flake for University of Queensland and Queensland Art Gallery Conservation, 29 August 2012*. CSIRO Materials Science and Technology, Melbourne

Heckel GB (1934) A century of progress in the paint industry. *J Chem Educ* 11 (9):487-493. doi:10.1021/ed011p487

Hedley G (1980) Solubility parameters and varnish removal a survey. *The Conservator* 4 (1):12-18. doi:10.1080/01410096.1980.9994931

Heeren R, Boon J, Noble P, Wadum J (1999) Integrating imaging FTIR and secondary ion mass spectrometry for the analysis of embedded paint cross-sections In: Bridgland J, Brown J (eds) *Preprints of the ICOM Committee for Conservation 12th Triennial Meeting* Lyon, 1999. James and James, London, pp 228-233

Heeren R, van der Weerd J, Boon J (2000) FTIR imaging spectroscopy for organic surface analysis of embedded paint cross-sections In: Fotakis C, Papazoglou TG, Kalpouzos C (eds) *Optics and lasers in biomedicine and culture: contributions to the Fifth International Conference on Optics within Life Sciences*, 1998. Springer, pp 179-182

Helwig K, Poulin J, Corbeil M-C, Moffatt E, Duguay D (2014) Conservation issues in several 20th-century Canadian oil paintings: the role of zinc carboxylate reaction products. In: van den Berg KJ, Burnstock A, de Tagle M et al. (eds) *Issues in Contemporary Oil Paint*. Springer International Publishing, Switzerland, p Chapter 11. In press. doi:10.1007/978-3-319-10100-2__11

Hermans JJ, Iedema PD (2014) Comment on the paper "Odd–even alternation in a homologous series of Zn(II) n-alkanoates" by P.N. Nelson, H.A. Ellis and R.A. Taylor [J. Mol. Struc. 986 (2011) 10–15]. *J Mol Struct* 1070 (0):43-44. doi:http://dx.doi.org/10.1016/j.molstruc.2014.04.026

Higgitt C, Spring M, Saunders D (2003) Pigment-medium interactions in oil paint films containing red lead or lead-tin yellow. *National Gallery Technical Bulletin* 24:75-95

Hochleitner B, Schreiner M, Drakopoulos M, Snigireva I, Snigirev A (2003) Analysis of paint layers by light microscopy, scanning electron microscopy and synchrotron induced X-ray micro-diffraction. In: *Proceedings of Art 2002*, Antwerp, Belgium, 2-6 June 2002.

Hoffmann E, Saracz A (1969) Weathering of Paint Films .I. Chalking Caused by Zinc Oxide in Latex Paints. *Journal of the Oil & Colour Chemists Association* 52 (2):113-132

Hoffmann E, Saracz A (1971) Weathering of paint films III. Influence of wavelength of radiation and temperature on the chalking of latex paints. *Journal of the Oil & Colour Chemists Association* 54:450-470

Hofmeister W, Platen HV (1992) Crystal Chemistry and Atomic Order in Brucite-related Double-layer Structures. *Crystallography Reviews* 3 (1):3-26. doi:10.1080/08893119208032964

Hoogland FG, van der Horst J, Boon JJ (2007) Liquefying oil paint in some late twentieth-century paintings. In: Learner TJS, Smithen P, Krueger JW, Schilling MR (eds) *Modern Paints Uncovered*, Tate Modern, London, 16-19 May 2006. The Getty Conservation Institute, pp 282-283

Iedema P, van Loon A, Keune K (2014) *PAinT - Paint alterations in time*. University of Amsterdam. http://www.s4a-paint.uva.nl/. Accessed 10 July 2014

Inoue S, Fujihara S (2010) Synthesis of Inorganic−Organic Layered Compounds Using Immiscible Liquid−Liquid Systems under the Distribution Law. *Langmuir* 26 (20):15938-15944. doi:10.1021/la1028542

Inoue S, Fujihara S (2011) Liquid−Liquid Biphasic Synthesis of Layered Zinc Hydroxides Intercalated with Long-Chain Carboxylate Ions and Their Conversion into ZnO Nanostructures. *Inorg Chem* 50 (8):3605-3612. doi:10.1021/ic1025729

International Zinc Association (2009) *Commercial grades of zinc oxide*. International Zinc Association. http://www.znoxide.org/commercial_grades.html. Accessed 7 June 2010

Ishioka T, Maeda K, Watanabe I, Kawauchi S, Harada M (2000) Infrared and XAFS study on structure and transition behaviour of zinc stearate. *Spectrochimica Acta Part A* 56:1731-1737

Jackson KDO (1998) A guide to identifying common inorganic fillers and activators using vibrational spectroscopy. *The Internet Journal of Vibrational Spectroscopy (wwwijvscom)* 2 (3):article no. 6

Jacobsen AE, Gardner WH (1941) Zinc soaps in paints: zinc oleates. *Ind Eng Chem* 33 (10):1254-1256

Jolly JH (1993) Materials flow of zinc in the United States 1850-1990. *Resources, Conservation and Recycling* 9 (1-2):1-30

Joseph E, Prati S, Sciutto G, Ioele M, Santopadre P, Mazzeo R (2010a) Performance evaluation of mapping and linear imaging FTIR microspectroscopy for the characterisation of paint cross sections. *Anal Bioanal Chem* 396 (2):899-910. doi:10.1007/s00216-009-3269-8

Joseph E, Ricci C, Kazarian SG, Mazzeo R, Prati S, Ioele M (2010b) Macro-ATR-FT-IR spectroscopic imaging analysis of paint cross-sections. *Vib Spectrosc* 53 (2):274-278

Kaneko F, Tashiro K, Kobayashi M (1999) Polymorphic transformations during crystallization processes of fatty acids studied with FT-IR spectroscopy. *J Cryst Growth* 198-199 (Part 2):1352-1359

Kanicky JR, Shah DO (2002) Effect of Degree, Type, and Position of Unsaturation on the pKa of Long-Chain Fatty Acids. *J Colloid Interface Sci* 256 (1):201-207. doi:10.1006/jcis.2001.8009

Kastens ML, Hansen FR (1949) Drier soap manufacture. *Ind Eng Chem* 41 (10):2080-2090. doi:10.1021/ie50478a008

Kemp F, Wise A, Hamilton B (2004) Re-inventing Diddy: The examination and treatment of a pastel drawing on paper by Grace Cossington Smith. In: *Collaboration and Connections: Postprints of the AICCM Paper, Books and Photographic Materials Special Interest Group Symposium* Sydney 1-4 April, 2004. AICCM, pp 115-124

Keune K (2005) *Binding medium, pigments and metal soaps characterised and localised in paint cross-sections*. PhD thesis, University of Amsterdam, Amsterdam

Keune K, Boevé-Jones G (2014) It's surreal: zinc-oxide degradation and misperceptions in Salvador Dali's *Couple with clouds in their heads*, 1936. In: van den Berg JDJ, Burnstock A, de Tagle M et al. (eds) *Issues in contemporary oil paint*. Springer International Publishing, Switzerland, p Chapter 19. In press. doi:10.1007/978-3-319-10100-2__19

Keune K, Boon JJ (2004) Imaging secondary ion mass spectrometry of a paint cross section taken from an early Netherlandish painting by Rogier van der Weyden. *Anal Chem* 76 (5):1374-1385. doi:10.1021/ac035201a

Keune K, Boon JJ (2007) Analytical imaging studies of cross-sections of paintings affected by lead soap aggregate formation. *Stud Conserv* 52 (3):161-176

Keune K, Hoogland F, Boon JJ, Peggie D, Higgitt C (2008) Comparative study of the effect of traditional pigments on artificially aged paint systems using complementary analytical techniques. In: Bridgland J (ed) *Preprints of the ICOM Committee for Conservation 15th Triennial Meeting* New Delhi, 2008. Allied Publishers Pvt Ltd, New Delhi, pp 833-842

Keune K, Hoogland F, Boon JJ, Peggie D, Higgitt C (2009) Evaluation of the "added value" of SIMS: A mass spectrometric and spectroscopic study of an unusual Naples yellow oil paint reconstruction. *Int J Mass spectrom* 284 (1-3):22-34. doi:10.1016/j.ijms.2008.10.016

Keune K, van Loon A, Boon JJ (2011) SEM Backscattered-Electron Images of Paint Cross Sections as Information Source for the Presence of the Lead White Pigment and Lead-Related Degradation and Migration Phenomena in Oil Paintings. *Microsc Microanal* 17 (05):696-701. doi:10.1017/S1431927610094444

Khandekar N (2003) Preparation of cross-sections from easel paintings *Reviews in Conservation* 4:52-64

Koller J, Burmester A (1990) Blanching of unvarnished modern paintings: a case study on a painting by Serge Poliakoff In: Mills JS, Smith P (eds) *Cleaning, retouching and coatings, Preprints of the contributions to the Brussels Congress*, 3-7 September 1990. IIC, London, pp 138-143

Kühn H (1986) Zinc white In: Feller RL (ed) *Artists' pigments* vol 1. Cambridge University Press, pp 169-186

Langley A, Burnstock A (1999) The analysis of layered paint samples from moden paintings using FTIR microscopy. In: Bridgland J, Brown J (eds) *Preprints of the ICOM Committee for Conservation 12th Triennial Meeting*, Lyon, 1999. James and James, London, pp 234-241

Lau D (2008) Conservation science in Australia: a space between places. In: Villis C, Ellem A (eds) *Paintings conservation in Australia from the nineteenth century to the present day: Connecting the past to the future. 11th AICCM Paintings Group Symposium*, National Gallery of Victoria, Melbourne 9-10 October, 2008. AICCM, pp 143-148

Lau D, Brunoro K, Varcoe-Cocks M (2007) Preliminary investigations into crystalline efflorescence on Australian and Indigenous paintings in the NGA and NGV collections - research in progress. In: Pagliarino A, Osmond G (eds) *Contemporary collections: AICCM National Conference*, Brisbane, 17-19 October 2007. AICCM, p 57

Lenz A, Selegård La, Söderlind F, Larsson A, Holtz PO, Uvdal K, Ojamäe L, Käll P-O (2009) ZnO Nanoparticles Functionalized with Organic Acids: An Experimental and Quantum-Chemical Study. *The Journal of Physical Chemistry C* 113 (40):17332-17341. doi:10.1021/jp905481v

Levin J, Considine B, Lechtman H, Stone R, Walch-von Miller K (2005) A discussion about technical studies in art history. *The Getty Conservation Institute Newsletter* 20 (1):11-16

Li C, Zhao B, Lu Y, Liang Y (2001) Microstructure and Ion Exchange in Stearic Acid Langmuir–Blodgett Films Studied by Fourier Transform Infrared-Attenuated Total Reflection Spectroscopy. *J Colloid Interface Sci* 235 (1):59-65. doi:10.1006/jcis.2000.7343

Lluveras-Tenorio A, Andreotti A, Bonaduce I, Boularand S, Cotte M, Roqué J, Colombini MP, Vendrell-Saz M (2012) Mass Spectrometric and Synchrotron Radiation based techniques for the identification and distribution of painting materials in samples from paints of Josep Maria Sert. *Chemistry Central Journal* 6. doi:http://dx.doi.org/10.1186/1752-153X-6-45

Lower ES (1982) The properties of aluminium stearate and its uses in the coatings and allied industries. *Pigm Resin Technol* 11 (2):13-18

MacMillan S (2007) *A report on the art historical investigation, condition, technical examination and initial investigations into the conservation treatment of two paintings on canvas by Vietnamese artist Nguyen Trong Kiem (1933-1991) dated 1963; in conjunction with scientific investigation of various tube paints used by Vietnamese artists during the mid C20th, and the materials, degradation mechanisms and conservation issues regarding the two paintings*. MA thesis, Northumbria University, Newcastle

Maines CA, Rogala D, Lake S, Mecklenburg MF (2011) Deterioration in Abstract Expressionist paintings: analysis of zinc oxide paint layers in works from the collection of the Hirshhorn Museum and Sculpture Garden, Smithsonian Institution. *Materials Research Society Proceedings* 1319:275-284. doi:10.1557/opl.2011.733

Mallégol J, Gardette J-L, Lemaire J (1999) Long-term behavior of oil-based varnishes and paints I. Spectroscopic analysis of curing drying oils. *J Am Oil Chem Soc* 76 (8):967-976. doi:10.1007/s11746-999-0114-3

Mallégol J, Gardette J-L, Lemaire J (2000a) Long-term behaviour of oil-based varnishes and paints. Fate of hydroperoxides in drying oils. *Journal of the Amercian Oil Chemists' Society* 77 (3):249-255. doi:10.1007/s11746-000-0041-5

Mallégol J, Gardette J-L, Lemaire J (2000b) Long-term behaviour of oil-based varnishes and paints. Photo- and thermooxidation of cured linseed oil. *Journal of the Amercian Oil Chemists' Society* 77 (3):257-263

Mallégol J, Gonon L, Lemaire J, Gardette J-L (2001) Long-term behaviour of oil based varnishes and paints 4. Influence of film thickness on the photooxidation. *Polym Degrad Stab* 72:191-197

Mallégol J, Lemaire J, Gardette J-L (2000c) Drier influence on the curing of linseed oil. *Prog Org Coat* 39:107-113. doi:10.1016/S0300-9440(00)00126-0

Maor Y, Murray A (2008) Delamination of Oil Paints on Acrylic Grounds. In: Vandiver PB, McCarthy B, Tykot RH, Ruvalcaba-Sil JL, Casadio F (eds) *Materials issues in art and archaeology VIII*, Boston, MA, Nov 26-28 2007. Materials Research Society, pp 127-136

Marques EF, Burrows HD, da Graça Miguel M (1998) The structure and thermal behaviour of some long chain cerium carboxylates. *Journal of the Chemical Society, Faraday Transactions* 94 (12):1729-1736

Marshbanks TL, Ahn DJ, Franses EI (1994) Transport and ion exchange in Langmuir-Blodgett films: water transport and film microstructure by attenuated total reflectance Fourier transform infrared spectroscopy. *Langmuir* 10 (1):276-285. doi:10.1021/la00013a041

Martin de Fonjaudran C, Nevin A, Piqué F, Cather S (2008) Stratigraphic analysis of organic materials in wall painting samples using micro-FTIR attenuated total reflectance and a novel sample preparation technique. *Anal Bioanal Chem* 392 (1):77-86. doi:10.1007/s00216-008-2111-z

Martin EP, Pink RC (1948) 354. The solubility of zinc soaps in organic solvents. *Journal of the Chemical Society (Resumed)*:1750-1755

The Mascot Smelting Works (1925). The decorator and painter for Australia and New Zealand, vol April 1. Bishop Bros., Sydney

Maskaev AK, Man'kovskaya NK, Lend'el IV, Fedorovskii VT, Simurova EI, Terent'eva VN (1971) Preparation of 12-hydroxystearic acid, the raw material for plastic greases. *Chem Technol Fuels Oils* 7 (2):109-112. doi:10.1007/bf00718698

Mazzeo R, Joseph E, Prati S, Millemaggi A (2007) Attenuated total reflection-fourier transform infrared microspectroscopic mapping for the characterisation of paint cross-sections. *Anal Chim Acta* 599 (1):107-117. doi:10.1016/j.aca.2007.07.076

Mazzeo R, Prati S, Quaranta M, Joseph E, Kendix E, Galeotti M (2008) Attenuated total reflection micro FTIR characterisation of pigment-binder interaction in reconstructed paint films. *Anal Bioanal Chem* 392 (1-2):65-76. doi:10.1007/s00216-008-2126-5

McBain JW, McClatchie WL (1932) The probable non-existence of normal tribasic aluminum soaps such as aluminum tripalmitate. *J Am Chem Soc* 54:3266-3268. doi:10.1021/ja01347a504

Mecklenburg MF (2008) *Meccanismi di cedimento nei dipinti su tela: approcci per lo sviluppo di protocolli di consolidamento - Failure Mechanisms in Canvas Supported Paintings: Approaches for Developing Consolidation Protocols*. I Talenti. Metodologie, tecniche e formazione nel mondo del restauro Il Prato, Padova

Mecklenburg MF, Tumosa CS, Erhardt D (2005) The changing mechanical properties of aging oil paints. In: Vandiver PB (ed) *Materials Issues in Art and Archaeology VII*, Boston, 2004. Materials Research Society pp 13-24

Mehrotra KN, Shukla RK, Chauhan M (1995) Spectroscopic and Conductometric Studies of Lanthanide Soaps. *Bull Chem Soc Jpn* 68 (7):1825-1831

Meilunas R, Bentsen J, Steinberg A (1990) Analysis of aged paint binders by FTIR spectroscopy. *Stud Conserv* 35:33-51

Mesubi MA (1982) An infrared study of zinc, cadmium, and lead salts of some fatty acids. *J Mol Struct* 81:61-71

Mills JS (1966) The gas chromatographic examination of paint media. Part I. Fatty acid composition and identification of dried oil films. *Stud Conserv* 11:92-107

Mills JS, White R (1987) *The organic chemistry of museum objects* Butterworths Series in Conservation and Museology. Butterworths, London

Miser HD, Glass JJ (1941) Fluorescent sodalite and hackmanite from Magnet Cove, Arkansas. *Am Mineral* 26 (7):437-445

Monico L, Van der Snickt G, Janssens K, De Nolf W, Miliani C, Dik J, Radepont M, Hendriks E, Geldof M, Cotte M (2011a) Degradation Process of Lead Chromate in Paintings by Vincent van Gogh Studied by Means of Synchrotron X-ray Spectromicroscopy and Related Methods. 2. Original Paint Layer Samples. *Anal Chem* 83 (4):1224-1231. doi:10.1021/ac1025122

Monico L, Van der Snickt G, Janssens K, De Nolf W, Miliani C, Verbeeck J, Tian H, Tan H, Dik J, Radepont M, Cotte M (2011b) Degradation Process of Lead Chromate in Paintings by Vincent van Gogh Studied by Means of Synchrotron X-ray Spectromicroscopy and Related Methods. 1. Artificially Aged Model Samples. *Anal Chem* 83 (4):1214-1223. doi:10.1021/ac102424h

Morley-Smith CT (1950) The development of anti-chalking French Process zinc oxides. *Journal of the Oil & Colour Chemists' Association* 33:484-501

Morley-Smith CT (1958) Zinc oxide - a reactive pigment. *Journal of the Oil & Colour Chemists' Association* 41 (January):85-97

Muizebelt WJ, Nielen MWF (1996) Oxidative Crosslinking of Unsaturated Fatty Acids Studied with Mass Spectrometry. *J Mass Spectrom* 31 (5):545-554. doi:10.1002/(sici)1096-9888(199605)31:5<545::aid-jms329>3.0.co;2-1

Mulvihill E (2012) *Analysing paint cross-sections with FTIR microspectroscopy: developing alternative sample preparation methodologies*. Minor Thesis, Master of Cultural Material Conservation, University of Melbourne, Melbourne

Musić S, Popović S, Maljković M, Dragčević D (2002) Influence of synthesis procedure on the formation and properties of zinc oxide. *J Alloys Compd* 347 (1-2):324-332

Nelson PN, Ellis HA, Taylor RA (2011) Odd–even alternation in a homologous series of Zn (II) n-alkanoates. *J Mol Struct* 986 (1–3):10-15. doi:http://dx.doi.org/10.1016/j.molstruc.2010.11.014

Nelson SM, Pink RC (1952) 322. Solutions of metal soaps in organic solvents. Part III. The aggregation of metal soaps in toluene, isobutyl alcohol, and pyridine. *Journal of the Chemical Society (Resumed)*:1744-1750

Nguyen Tran Minh, Tran Thi Minh Man (2008) *Interview transcript with Nguyen Trong Kiem's family included as Appendix 1 in MacMillan 2007*. interview transcript Hanoi

Nicholson DG (1940) Drying of Linseed Oil Paint Effect of Acidity upon Rate of Oxygen Absorption. *Industrial & Engineering Chemistry* 32 (9):1259-1261. doi:10.1021/ie50369a046

Noble P, Boon J, Wadum J (2002) Dissolution aggregation and protrusion: lead soap formation in 17th century grounds and paint layers. *Art Matters: Netherlands technical studies in art* 1:46-61

Noble P, Boon JJ (2007) Metal soap degradation of oil paintings: aggregates, increased transparency and efflorescence. In: Mar Parkin H (ed) *AIC Paintings Specialty Group Postprints*, Providence, Rhode Island, 16-19 June 2006. AIC, pp 1-15

Noble P, van Loon A, Boon JJ (2005) Chemical changes in old master paintings II: darkening due to increased transparency as a result of metal soap formation. In: Verger I (ed) *Preprints of the ICOM Committee for Conservation 14th Triennial meeting*, The Hague, 12-16 September 2005. James and James, London, pp 496-503

Noble P, Wadum J, Groen K, Heeren R, van den Berg KJ (2000) Aspects of 17th century binding medium: inclusions in Rembrandt's 'Anatomy lesson of Nicolaes Tulp'. In: *Art et chimie, La couleur, Actes du Congrès*, Paris, 1998. pp 126-129

Nunn C (2008) The making of *Lamplight* (c. 1911): a preliminary study of the methods and materials of Emanuel Phillips Fox. *AICCM Bulletin* 31:15-27

Nunn C (2012) *The matt aesthetic and the art of E. Phillips Fox*. MA thesis, University of Melbourne, Melbourne

O'Donoghue E, Johnson AM, Mazurek J, Preusser FD, Schilling MR, Walton MS (2006) Dictated by media: conservation and technical analysis of a 1938 Joan Miro canvas painting. In: Saunders D, Townsend J, Woodcock S (eds) *The object in context: Crossing Conservation Boundaries: Contributions to the Munich Congress*, 28 August - 1 September 2006. IIC, London, pp 62-68

O'Hanlon G (2007) *Zinc white: problems in oil paint*. Natural pigments LLC. www.naturalpigments.com/education/article.asp?ArticleID=127. Accessed 24 October 2011

Oil and Colour Chemists' Association (ed) (1966) *Pigments, dyestuffs and lakes*, vol Part Six. Paint technology manuals. Chapman and Hall for the Oil and Colour Chemists' Association, London

Ordonez E, Twilley J (1997) Clarifying the haze: efflorescence on works of art in WAAC Newsletter 20(1) 11pp reproduced from *Anal Chem* 69 (13):A416-A422

Osmond G, Keune K, Boon J (2005) A study of zinc soap aggregates in a late 19th century painting by R.G. Rivers at the Queensland Art Gallery. *AICCM Bulletin* 29:37-46

Otero V, Sanches D, Montagner C, Vilarigues M, Carlyle L, Lopes JA, Melo MJ (2014) Characterisation of metal carboxylates by Raman and infrared spectroscopy in works of art. *Journal of Raman Spectroscopy*:n/a-n/a. doi:10.1002/jrs.4520

Öztürk S, Balköse D (2005) *Preparation and Characterization of Metal Soap Nanofilms*. İzmir Institute of Technology, İzmir,

Phenix A (2002a) Building Models: Comparative swelling powers of organic solvents on oil paint and the cleaning of paintings. *V&A Conservation Journal* 40 (Spring)

Phenix A (2002b) The Swelling of Artists' Paints in Organic Solvents. Part 2, Comparative Swelling Powers of Selected Organic Solvents and Solvent Mixtures. *Journal of the American Institute for Conservation* 41 (1):61-90

Phenix A (2013) Effects of organic solvents on artists' oil paint films: swelling. In: Mecklenburg MF, Charola EA, Koestler RJ (eds) *New insights into the cleaning of paintings: Proceedings from the Cleaning 2010 International Conference, Universidad Politécnica de Valencia and Museum Conservation Institute*. Smithsonian Institution Scholarly Press, Washington DC pp 69-76

Philadelphia Museum of Art (2007) *IMP00223 Riebeckite*. In: Price BA, Pretzel B (eds) Infrared and Raman Users Group spectral database. http://www.irug.org/

Pilc J, White R (1995) The application of FTIR-microscopy to the analysis of paint binders in easel paintings *National Gallery Technical Bulletin* 16:73-84

Pilpel N (1963) Properties of Organic Solutions of Heavy Metal Soaps. *Chem Rev* 63 (3):221-234. doi:10.1021/cr60223a001

Pilz K (2005) *Zinc white*. Student report, University of Applied Sciences, Cologne,

Plater MJ, De Silva B, Gelbrich T, Hursthouse MB, Higgitt CL, Saunders DR (2003) The characterisation of lead fatty acid soaps in 'protrusions' in aged traditional oil paint. *Polyhedron* 22 (24):3171-3179. doi:10.1016/s0277-5387(03)00461-3

Pouyet E, Lluveras-Tenorio A, Nevin A, Saviello D, Sette F, Cotte M (2014) Preparation of thin-sections of painting fragments: Classical and innovative strategies. *Anal Chim Acta* 822 (0):51-59. doi:http://dx.doi.org/10.1016/j.aca.2014.03.025

Prati S, Rosi F, Sciutto G, Mazzeo R, Magrini D, Sotiropoulou S, Van Bos M (2012) Evaluation of the effect of six different paint cross section preparation methods on the performances of Fourier Transformed Infrared microscopy in attenuated total reflection mode. *Microchem J* 103 (0):79-89. doi:http://dx.doi.org/10.1016/j.microc.2012.01.007

Prati S, Sciutto G, Catelli E, Ashashina A, Mazzeo R (2013) Development of innovative embedding procedures for the analyses of paint cross sections in ATR FITR microscopy. *Anal Bioanal Chem* 405 (2-3):895-905. doi:10.1007/s00216-012-6435-3

Princen LH, Devena-Peplinski M (1964) Effect of particle size on the mutual flocculation between zinc oxide and titanium dioxide. *Journal of Colloid Science* 19 (9):786-797

Rimer B, Fiedler I, Miller M, Cunningham M, van den Berg J (1999) Investigation of fatty acid migration in alizarin crimson oil paint in two works by Frank Stella In: Wallace FA (ed) *AIC Paintings Specialty Group Postprints*, St. Louis, Missouri, 8-13 June 1999. AIC, pp 1-14

Rinse J (1967) Metal soaps. *American Paint Journal* (March 13):22-28

Rizzo A (2008) Progress in the application of ATR-FTIR microscopy to the study of multi-layered cross-sections from works of art. *Anal Bioanal Chem* 392 (1):47-55. doi:10.1007/s00216-008-2064-2

Robinet L, Corbeil MC (2003) The characterization of metal soaps. *Stud Conserv* 48 (1):23-40

Rogala D, Lake S, Maines C, Mecklenburg M (2010) Condition problems related to zinc oxide underlayers: examination of selected Abstract Expressionist paintings from the collection of the Hirschhorn Museum and Sculpture Garden, Smithsonian Institution. *Journal of the American Institute for Conservation* 49 (2):96-113

Roy A (1987) The materials of van Gogh's 'A cornfield, with cypresses'. *National Gallery Technical Bulletin* 11:50-59

Rudin A (1999) *Polymer science and engineering*. 2nd edn. Academic Press, London

Saien J, Akbari S (2006) Interfacial Tension of Toluene + Water + Sodium Dodecyl Sulfate from (20 to 50) °C and pH between 4 and 9. *Journal of Chemical & Engineering Data* 51 (5):1832-1835. doi:10.1021/je060204g

Sakai H, Umemura J (2002) Evaluation of molecular structure in Langmuir monolayers of zinc stearate and zinc 12-hydroxystearate by IR external reflection spectroscopy. *Colloid Polym Sci* 280 (4):316-321. doi:10.1007/s003960100581

Sakai H, Umemura J (2008) Evaluation of structural change during surface pressure relaxation in Langmuir monolayer of zinc stearate by infrared external reflection spectroscopy. *Colloid Polym Sci* 286 (14):1637-1641. doi:10.1007/s00396-008-1939-2

Salvin SB (1944) Influence of zinc oxide on paint molds. *Ind Eng Chem* 36:336-340

Sanyova J, Cersoy S, Richardin P, LapreÌ • vote O, Walter P, Brunelle A (2011) Unexpected Materials in a Rembrandt Painting Characterized by High Spatial Resolution Cluster-TOF-SIMS Imaging. *Anal Chem* 83 (3):753-760. doi:10.1021/ac1017748

Saunders D, Kirby J (2004) The effect of relative humidity on artists' pigments. *National Gallery Technical Bulletin* 25:62-72

Schilling MR, Carson DM, Khanjian H, P. (1999) Gas chromatographic determination of the fatty acid and glycerol content of lipids. IV. Evaporation of fatty acids and the formation of ghost images by framed oil paintings In: Bridgland J, Brown J (eds) *Preprints of the ICOM Committee for Conservation12th Triennial Meeting*, Lyon, 1999. James and James, London, pp 242-247

Schilling MR, Khanjian H, P. (1996) Gas chromatographic determination of the fatty acid and glycerol content of lipids I. The effects of pigments and aging on the composition of oil paints. In: Bridgland J (ed) *Preprints of the ICOM Committee for Conservation 11th Triennial meeting*, Edinburgh, Scotland. James and James, London, pp 220-227

Schilling MR, Mazurek J, Learner TJS (2007) Studies of modern oil-based artists' paint media by gas chromatography/mass spectrometry. In: Learner TJS, Smithen P, Krueger JW, Schilling MR (eds) *Modern paints uncovered*, Tate Modern, London, 16-19 May 2006. The Getty Conservation Institute, pp 129-139

Shekhter YN, Bogdanova TI, Teterina LN, Fuks IG, Zaslavskaya IR (1975) Polarity and functional properties of soaps of stearic acid. *Chem Technol Fuels Oils* 11 (9):734-737. doi:10.1007/bf00730325

Shimadzu Y, Keune K, van den Berg KJ (2008) The effects of lead and zinc white saponification on surface appearance of paint. In: Bridgland J (ed) *Preprints of the ICOM Committee for Conservation: Preprints of the 15th Triennial Meeting*, New Delhi, 22-26 September 2008. Allied Publishers Pvt Ltd, pp 626-632

Shimadzu Y, van den Berg KJ (2006) On metal soap related colour and transparency changes in a 19th century painting by Millais. In: Boon JJ, Ferreira ESB (eds) *Reporting Highlights of the de Mayerne Programme*. Netherlands Organisation for Scientific Research (NWO), The Hague, pp 43-52

Simon-Kutscher J, Gericke A, Hühnerfuss H (1996) Effect of bivalent Ba, Cu, Ni, and Zn cations on the structure of octadecanoic acid monolayers at the air-water interface as determined by external Infrared reflection-absorption spectroscopy. *Langmuir* 12 (4):1027-1034. doi:10.1021/la950731q

Singer B, Devenport J, Wise D (1995) Examination of a blooming problem in a collection of unvarnished oil paintings. *The Conservator* 19:3-9

Singer B, MacMillan S, Grimaldi N, Brown J (2009) Analysis of Vietnamese oil paintings affected by sulphur dioxide pollution. In: Lee S, Huy NN (eds) *Essays on Modern and Contemporary Vietnamese Art*. Singapore Art Museum., Singapore, pp 68-74

Sloggett R, Kyi C, Tse N, Tobin MJ, Puskar L, Best SP (2010) Microanalysis of artworks: IR microspectroscopy of paint cross-sections. *Vib Spectrosc* 53 (1):77-82

Smith G (2003) Infrared microspectroscopy using a synchrotron source for arts-science research *Journal of the American Institute for Conservation* 42:399-406

Soucek MD, Khattab T, Wu J (2012) Review of autoxidation and driers. *Prog Org Coat* 73 (4):435-454. doi:http://dx.doi.org/10.1016/j.porgcoat.2011.08.021

Souza LAC, Derrick MR (1995) The use of FT-IR spectrometry for the identification and characterisation of gesso-glue grounds in wooden polychromed sculptures and panel paintings. *Materials Research Society Symposium Proceedings* 352:573-578

Spring M, Ricci C, Peggie D, Kazarian S (2008) ATR-FTIR imaging for the analysis of organic materials in paint cross sections: case studies on paint samples from the National Gallery, London. *Anal Bioanal Chem* 392 (1):37-45. doi:10.1007/s00216-008-2092-y

Standeven H (2003) *The historical and technical development of gloss housepaints, with reference to their use by twentieth century artists*. PhD thesis, Royal College of Art, London

Standeven H (2011) *House paints, 1900-1960: history and use*. Research in Conservation. Getty Conservation Institute, Los Angeles

Stavroudis C, Blank S (1989) Solvents & sensibility. *WAAC Newsletter* 11 (2):2-10

Stolow N (1957) The action of solvents on drying oil films, parts I & II. *J Oil Colour Chem Assoc* 40:377-402, 488-499

Sundberg A, Strand A, Vähäsalo L, Holmbom B (2009) Phase Distribution of Resin and Fatty Acids in Colloidal Wood Pitch Emulsions at Different pH-Levels. *J Dispersion Sci Technol* 30 (6):912-919. doi:10.1080/01932690802646249

Suryanarayana NP (1970) Critical pigment volume concentration of some oxide pigments. *Journal of the Colour Society* 9 (2):2-6

Tachibana T, Kitazawa S, Takeno H (1970) Studies of Helical Aggregates of Molecules. II. The Sense of Twist in the Fibrous Aggregates from the Alkali Metal Soaps of Optically Active 12-Hydroxystearic Acid. *Bull Chem Soc Jpn* 43 (8):2418-2421

Taylor CJA, Marks S (eds) (1969) *Solvents, oils, resins and driers*, vol Part 2. Paint technology manuals, Second edition edn. Chapman and Hall on behalf of the Oil and Colour Chemists' Association, London

Taylor RA, Ellis HA (2007) Room temperature molecular and lattice structures of a homologous series of anhydrous zinc(II) n-alkanoate. *Spectrochimica Acta Part A: Molecular and Biomolecular Spectroscopy* 68 (1):99-107. doi:http://dx.doi.org/10.1016/j.saa.2006.11.007

Thermo Electron Corporation (1991-1994) *Coatings Technology FT-IR spectral reference library*. Thermo Electron Corporation,

Townsend J, Carlyle L, Khandekar N, Woodcock S (1995) Later nineteenth century pigments: evidence for additions and substitutions *The Conservator* 19:65-78

Townsend JH, Jones R, Stoner K (2007) Lead soap aggregates in sixteenth- and seventeenth-century British paintings. In: Mar Parkin H (ed) *AIC Paintings specialty group postprints*, Providence, Rhode Island, 16-19 June 2006. AIC, pp 24-32

Townsend JH, Keune K (2006) Microscopical techniques applied to traditional paintings. *infocus: Magazine of the Royal Microscopical Society* 1 (March):53-65

Tsang J, Cunningham R (1991) Some improvements in the study of cross sections. *Journal of the American Institute for Conservation* 30 (2):163-177

Tse N (2008) *The characterisation of oil paintings in tropical southeast Asia*. PhD thesis, The University of Melbourne, Melbourne

Tumosa CS (2001) A brief history of aluminum stearate as a component of paint. *WAAC Newsletter* 23 (3)

Tumosa CS, Erhardt D, Mecklenburg MF, Su X (2005) Linseed oil paint as ionomer: synthesis and characterization. In: Vandiver PB (ed) *Materials issues in art and archaeology VII*, Boston, Massachusetts, 2004. Materials Research Society, pp 25-31

Turner JHW, Kemp SG, Harson SE (1958) The function of aluminium complexes as structure modifiers for paint. *J Oil Colour Chem Assoc* 41 (11):769-779

van den Berg J, van den Berg K, Boon J (1999) Chemical changes in curing and ageing oil paints. In: Bridgland J (ed) *Preprints of the ICOM Committee for Conservation 12th Triennial Meeting, Lyon*. pp 248-253

van den Berg JDJ, van den Burg KJ, Boon JJ (2001) Determination of the degree of hydrolysis of oil paint using a two-step derivatisation method and on-column GC/MS. *Prog Org Coat* 41:143-155

van den Berg JDJ, Vermist ND, Carlyle L, Holčapek M (2004) Effects of traditional processing methods of linseed oil on the composition of its triacylglycerols. *J Sep Sci* 27:181-199. doi:10.1002/jssc.200301610

van den Berg JJD (2002) *Analytical chemical studies on traditional linseed oil paints*. PhD thesis, University of Amsterdam, Amsterdam

van der Kerk GJM (1972) Organozinc coordination chemistry and catalytic effects of organozinc coordination compounds. *Pure Appl Chem* 30 (3-4):389-408. doi:10.1351/pac197230030389

van der Snickt G, Dik J, Cotte M, Janssens K, Jaroszewicz J, de Nolf W, Groenewegen J, van der Loeff L (2009) Characterization of a degraded cadmium yellow (CdS) pigment in an oil painting by means of synchrotron radiation based X-ray techniques. *Anal Chem* 81 (7):2600-2610. doi:10.1021/ac802518z

van der Weerd J, Boon JJ, Gelddof M, Heeren RMA, Noble P (2002a) Chemical changes in old master paintings: dissolution, metal soap formation and remineralisation processes in lead pigmented paint layers of 17th century paintings. *Zeitschrift für Kunsttechnologie und Konservierung* 16:36-51

van der Weerd J, Brammer H, Boon JJ, Heeren RMA (2002b) Fourier Transform Infrared Microscopic Imaging of an Embedded Paint Cross-Section. *Appl Spectrosc* 56 (3):275-283

van der Weerd J, Gelddof M, van der Loeff LS, Heeren R, Boon J (2003) Zinc soap aggregate formation in 'Falling leaves (Les Alyscamps)' by Vincent van Gogh *Zeitschrift für Kunsttechnologie und Konservierung* 17 (2):407-416

van der Weerd J, Heeren RMA, Boon JJ (2004) Preparation methods and accessories for the infrared spectroscopic analysis of multi-layer paint films. *Stud Conserv* 49:193-210

van der Weerd J, van Loon A, Boon JJ (2005) FTIR studies of the effects of pigments on the aging of oil. *Stud Conserv* 50 (1):3-22

van Gorkum R, Bouwman E (2005) The oxidative drying of alkyd paint catalysed by metal complexes. *Coord Chem Rev* 249:1709-1728. doi:10.1016/j.ccr.2005.02.002

van Loon A (2008) *Color changes and chemical reactivity in seventeenth century oil paintings*. PhD thesis, University of Amsterdam, Amsterdam

Verhoeven MA, Carlyle L, Reeddijk J, Haasnoot JG (2006) Exploring the application of solid-state Nuclear Magnetic Resonance to the study of the deterioration of paintings. In: Boon JJ, Ferreira ESB (eds) *Reporting highlights of the De Mayerne Programme*. Netherlands Organisation for Scientific Research (NWO), The Hague, pp 34-42

Vold RD, Hattiangdi GS (1949) Characterization of Heavy Metal Soaps by X-Ray Diffraction. *Industrial & Engineering Chemistry* 41 (10):2311-2320. doi:10.1021/ie50478a056

Wang X, Rackaitis M (2009) Gelling nature of aluminum soaps in oils. *J Colloid Interface Sci* 331 (2):335-342. doi:10.1016/j.jcis.2008.11.032

Ware EE, Christman RE (1916) A study of the effect of storage on mixed paints. *Ind Eng Chem* 8 (10):879-883

Weiss J (1957) Organic aluminium compounds in drying oils. *J Oil Colour Chem Assoc* 40:863-879; 976-989

Wendt R, Wagner E (1954) Applications of fatty acids in metallic soaps. *J Am Oil Chem Soc* 31 (11):590-593

Williams RS (1988) Blooms, blushes, transferred images and mouldy surfaces: what are these distracting accretions on art works? In: *Proceedings of the 14th annual IIC-Canadian Group conference* Toronto, Canada, 27-30 May 1988. pp 65-84

Winter G, Whittem RN (1950) Fluorescence and photo-chemical activity of zinc oxides. *Journal of the Oil & Colour Chemists' Association* 33 (November):477-483

Wöll C (2007) The chemistry and physics of zinc oxide surfaces. *Prog Surf Sci* 82:55-120. doi:10.1016/j.progsurf.2006.12.002

Wu C-M, Baltrusaitis J, Gillan EG, Grassian VH (2011) Sulfur Dioxide Adsorption on ZnO Nanoparticles and Nanorods. *The Journal of Physical Chemistry C* 115 (20):10164-10172. doi:10.1021/jp201986j

Zhang X, Xing N, Bai F, Wan L, Shan H, Hou Y, Xing Y, Shi Z (2013) Multi-functional d10 metal-organic materials based on bis-pyrazole/pyridine ligands supported by a 2,6-di(3-pyrazolyl)pyridine with different spanning flexible dicarboxylate ligands: synthesis, structure, photoluminescent and catalytic properties. *CrystEngComm* 15 (44):9135-9147. doi:10.1039/c3ce41213j

Zhang XG (1996) *Corrosion and electrochemistry of zinc*. Plenum Press, New York

Zucker J (1999) From the ground up: the ground in 19th-century American pictures *Journal of the American Institute for Conservation* 38:3-20

Zucker J, Boon J (2007) Opaque to transparent: paint film defects in the work of Frederick Church and the Hudson River School. In: Mar Parkin H (ed) *AIC Paintings Specialty Group Postprints*, Providence, Rhode Island, 16-19 June 2006. AIC, pp 33-41

Zümbuhl S, Fuesers O (2006) The formation of protrusions in the later works of Alexej von Jawlensky. In: Saunders D, Townsend JH, Woodcock S (eds) *The object in context - crossing conservation boundaries: contributions to the Munich Congress (poster session)*, Munich, 28 August - 1 September 2006. IIC, p 309